

ORIGINAL FILE COPY

(1)

AGARD-R-774

AGARD-R-774

AD-A217 716

AGARD

ADVISORY GROUP FOR AEROSPACE RESEARCH & DEVELOPMENT

7 RUE ANCELLÉ 92200 NEUILLY SUR SEINE FRANCE

AGARD REPORT No.774

Special Course

on

Advances in Cryogenic
Wind Tunnel Technology

DTIC

ELECTE

JAN 30 1990

S B D

NORTH ATLANTIC TREATY ORGANIZATION



NORTH ATLANTIC TREATY ORGANIZATION
ADVISORY GROUP FOR AEROSPACE RESEARCH AND DEVELOPMENT
(ORGANISATION DU TRAITE DE L'ATLANTIQUE NORD)

AGARD Report No.774
SPECIAL COURSE
ON
ADVANCES IN CRYOGENIC WIND TUNNEL TECHNOLOGY

The material assembled in this book was prepared under the combined sponsorship of the Fluid Dynamics Panel, the von Kármán Institute and the Consultant and Exchange Program of AGARD and was presented as an AGARD Special Course at the von Kármán Institute, Rhode-Saint-Genèse, Belgium, on 5—9 June 1989

THE MISSION OF AGARD

According to its Charter, the mission of AGARD is to bring together the leading personalities of the NATO nations in the fields of science and technology relating to aerospace for the following purposes:

- Recommending effective ways for the member nations to use their research and development capabilities for the common benefit of the NATO community;
- Providing scientific and technical advice and assistance to the Military Committee in the field of aerospace research and development (with particular regard to its military application);
- Continuously stimulating advances in the aerospace sciences relevant to strengthening the common defence posture;
- Improving the co-operation among member nations in aerospace research and development;
- Exchange of scientific and technical information;
- Providing assistance to member nations for the purpose of increasing their scientific and technical potential;
- Rendering scientific and technical assistance, as requested, to other NATO bodies and to member nations in connection with research and development problems in the aerospace field.

The highest authority within AGARD is the National Delegates Board consisting of officially appointed senior representatives from each member nation. The mission of AGARD is carried out through the Panels which are composed of experts appointed by the National Delegates, the Consultant and Exchange Programme and the Aerospace Applications Studies Programme. The results of AGARD work are reported to the member nations and the NATO Authorities through the AGARD series of publications of which this is one.

Participation in AGARD activities is by invitation only and is normally limited to citizens of the NATO nations.



The content of this publication has been reproduced directly from material supplied by AGARD or the authors.

Accession For	
NTIS GRA&I	<input checked="" type="checkbox"/>
DTIC TAB	<input type="checkbox"/>
Unannounced	<input type="checkbox"/>
Justification	
By _____	
Distribution/	
Availability Codes	
Dist	Avail and/or Special
A-1	

Published November 1989

Copyright © AGARD 1989
All Rights Reserved

ISBN 92-835-0532-8



*Printed by Specialised Printing Services Limited
40 Chigwell Lane, Loughton, Essex IG10 3TZ*

PREFACE

The development and use of cryogenic wind tunnels is a major advance in aerodynamic testing. One advantage of cryogenic tunnels is their ability to achieve full-scale values of Reynolds number in tunnels of moderate size at reasonable operating pressure. Another important advantage is the ability to independently vary temperature, pressure, and speed. This lets us separate the effects of Reynolds number, aerolasticity, and Mach number.

Since 1980, the AGARD Fluid Dynamics Panel and the von Kármán Institute for Fluid Dynamics have sponsored three series of lectures on cryogenic wind tunnels. The lectures of this Special Course are, in many ways, updates of the lectures given in 1980 and 1985. These lectures reflect the progress made in building and using cryogenic tunnels in recent years.

The purpose of this Special Course is to address as specifically as possible the concerns we have today in trying to build and use cryogenic wind tunnels. It is designed for engineers and managers who wish to obtain in concentrated form the most up-to-date information on cryogenic wind tunnels. This course covers both the theory and practice of cryogenic wind tunnel design, operation, and use.

The course begins with a brief review of the development and early use of cryogenic tunnels. It then covers all aspects of the design and operation of cryogenic tunnels.

Among the areas covered are: cryogenic engineering and safety, properties of materials at cryogenic temperatures, tunnel design requirements, model design and construction, automatic tunnel control, data acquisition, data accuracy, flow visualization, productivity, and costs of models and operation.

Also covered is the status of cryogenic wind tunnel projects in AGARD countries and in the rest of the world.

This bound volume of lecture notes includes a transcription of a question and answer session held at the end of the Special Course.

R.A.Kilgore
Special Course Director

* * *

AVANT-PROPOS

Le développement et la mise en oeuvre des souffleries cryogéniques représentent un grand pas en avant pour la communauté d'essai aérodynamique. L'un des avantages des souffleries cryogéniques est leur capacité pour réaliser des nombres de Reynolds en vraie grandeur à des pressions d'utilisation raisonnables dans des souffleries de taille moyenne. Un autre avantage important est la possibilité de faire varier indépendamment la température, la pression et la vitesse. Il nous permet de séparer les effets du nombre de Reynolds, de l'aéroélasticité et du nombre de Mach.

Depuis 1980, le Panel AGARD de la Dynamique des Fluides et l'Institut von Kármán ont organisé trois cycles de conférences sur les souffleries cryogéniques. A bien d'égards, les communications présentées lors de ce cours spécial sont à considérer comme des mises à jour des conférences données en 1980 et en 1985. Ces communications reflètent les progrès réalisés récemment dans la construction et l'emploi des souffleries cryogéniques.

L'objet de ce cours spécial est d'examiner, de façon très précise, les questions qui nous préoccupent lorsque nous abordons la construction et la mise en oeuvre de telles souffleries. Il est destiné aux ingénieurs et aux décideurs qui veulent acquérir, sous forme condensée, les dernières informations sur les souffleries cryogéniques. Le cours couvre les aspects théoriques et pratiques de la conception, du fonctionnement et de l'emploi des souffleries cryogéniques.

Parmi les sujets traités on distingue: la technique cryogénique et la sécurité, les caractéristiques des matériaux aux températures cryogéniques, les spécifications de conception des souffleries, la conception et la construction des modèles, le contrôle automatique de la veine, l'acquisition des données, la précision de la mesure, la visualisation du flux, le rendement, et le coût des modèles et du fonctionnement.

Ce cours fait également le point de l'état d'avancement des projets de construction de soufflerie dans les pays membres de l'OTAN et dans le reste du monde.

Ce recueil des textes retranscrit les questions et réponses de la séance de clôture de ce cours spécial.

R.A.Kilgore
Directeur de cours spécial

SPECIAL COURSE STAFF

Special Course Director: Dr. R.A.Kilgore
Chief Scientist, TAD
Mail Stop 285
NASA Langley Research Center
Hampton, Virginia 23665-5225
United States

LECTURERS/AUTHORS

Mr X.Bouis
ETW GmbH
DLR/Res. Ctr Köln-Porz
Postfach 90 60 58
5000 Köln 90
Federal Republic of Germany

Dr G.Hefer
DLR/Inst. for Experimental
Fluid Dynamics
Bunsenstraße 10
3400 Göttingen
Federal Republic of Germany

Mr R.Kronen
DLR/Res. Ctr Köln-Porz
Postfach 90 60 58
5000 Köln 90
Federal Republic of Germany

Dr G.Viehweger
DLR/Res. Ctr Köln-Porz
Postfach 90 60 58
5000 Köln 90
Federal Republic of Germany

Dr J.P.Archambaud
ONERA-CERT
2 Ave. Belin
31055 Toulouse Cedex
France

Mr M.Bazin
ONERA/GME
BP 72
92322 Chatillon
France

Mr J.Christophe
ONERA/GME
BP 72
92322 Chatillon Cedex
France

Mr A.Mignosi
ONERA/CERT/DERAT
BP 4025
31055 Toulouse Cedex
France

Dr M.J.Goodyer
Dept. Aeron. & Astron.
University of Southampton
Southampton SO9 5NH
Hampshire
United Kingdom

Dr D.A.Wigley
17 Bassett Wood Drive
Southampton SO2 3PT
Hampshire
United Kingdom

Dr S.Balakrishna
Mail Stop 287
NASA Langley Research Center
Hampton, Virginia 23665-5225
United States

Mr W.E.Bruce
Head, High Reynolds Number
Aero Branch/Mail Stop 267
NASA Langley Research Center
Hampton, Virginia 23665-5225
United States

Ms A.T.J.Ferris
Mail Stop 238
NASA Langley Research Center
Hampton, Virginia 23665-5225
United States

Mr B.B.Gloss
Mail Stop 267
NASA Langley Research Center
Hampton, Virginia 23665-5225
United States

Mr P.L.Lawing
High Reynolds Number
Aero Branch/Mail Stop 267
NASA Langley Research Center
Hampton, Virginia 23665-5225
United States

Mr E.J.Ray
0.3-m Transonic Cryogenic Tunnel
Mail Stop 276
NASA Langley Research Center
Hampton, Virginia 23665-5225
United States

Ms M.S.William
Mail Stop 238
NASA Langley Research Center
Hampton, Virginia 23665-5225
United States

LOCAL COORDINATOR

Prof. M.Carbonaro
von Kármán Institute for Fluid Dynamics
Chaussée de Waterloo, 72
1640 Rhode-Saint-Genèse
Belgium

AGARD REPRESENTATIVE

Mr M.C.Fischer
Fluid Dynamics Panel Executive
AGARD
7 rue Ancelle
92200 Neuilly sur Seine
France

CONTENTS

	Page
PREFACE	iii
SPECIAL COURSE STAFF	iv
	Reference
INTRODUCTION TO CRYOGENIC WIND TUNNELS by M.J.Goodyer	1
THE NASA LANGLEY 0.3-METER TRANSONIC CRYOGENIC TUNNEL by E.J.Ray	2
THE US NATIONAL TRANSONIC FACILITY, NTF by W.E.Bruce, Jr. and B.B.Gloss	3
THE KRYO-KANAL-KÖLN (KKK): DESCRIPTION OF THE TUNNEL CONVERSION by G.Viehweger	4
AUTOMATIC CONTROL OF KKK by R.Kronen	5
THE EUROPEAN TRANSONIC WINDTUNNEL (ETW) by X.Bouis	6
THE CRYOGENIC INDUCTION TUNNEL T2 AT TOULOUSE by J.-P.Archambaud	7
THE CRYOGENIC LUDWIEG TUBE TUNNEL AT GÖTTINGEN by G.Hefer	8
OTHER CRYOGENIC WIND TUNNEL PROJECTS by R.A.Kilgore	9
CRYOGENIC ENGINEERING AND MATERIALS by D.A.Wigley	10
INSTRUMENTATION FOR CRYOGENIC WIND TUNNELS by M.Bazin	11
FUNDAMENTAL CONSIDERATIONS IN TESTING IN CRYOGENIC WIND TUNNELS by A.Mignosi	12
TEST TECHNIQUES FOR CRYOGENIC WIND TUNNELS by P.L.Lawing	13
FLOW VISUALIZATION IN THE CRYOGENIC WIND TUNNEL by M.J.Goodyer	14
MATERIALS AND TECHNIQUES FOR MODEL CONSTRUCTION by D.A.Wigley	15
SOME RECENT DEVELOPMENTS IN MATERIALS & TECHNIQUES FOR MODEL FABRICATION by D.A.Wigley	16
MODELS FOR CRYOGENIC WIND TUNNELS by P.L.Lawing	17
AUTOMATIC CONTROL OF CRYOGENIC WIND TUNNELS by S.Balakrishna	18
EXPERIENCE WITH STRAIN-GAGE BALANCES FOR CRYOGENIC WIND TUNNELS by M.S.Williams (Presented by Ed Bruce)	19

	Reference
STATUS REPORT ON CRYOGENIC BALANCES FOR THE US NTF by A.T.Ferris	20
SAFETY AND CRYOGENIC WIND TUNNELS by E.J.Ray	21
PRODUCTIVITY AND CRYOGENIC WIND TUNNELS by J.Christophe	22
ENERGY MANAGEMENT AND RECOVERY by P.L.Lawing	23
ROUND TABLE DISCUSSION AND CONCLUDING REMARKS All Lecturers; R.A.Kilgore, Moderator	24
BIBLIOGRAPHY	B

INTRODUCTION TO CRYOGENIC WIND TUNNELS

M.J. Goodyer
Department of Aeronautics and Astronautics
The University
Southampton SO9 5NH, U.K.

Summary

The cryogenic wind tunnel was conceived as a way of increasing Reynolds number in a wind tunnel while avoiding an increase in its size. This it does very effectively and with some other surprisingly beneficial effects. Important among these is a reduction of tunnel drive power and the ability for the first time in a wind tunnel test to identify the separate effects of Reynolds number, Mach number and dynamic pressure.

The lecture forms a brief introduction at the fundamental level highlighting some of the characteristics of cryogenic wind tunnels and their flows.

1. Background

This section has two parts, together forming a background on Osborne Reynolds and on wind tunnel testing. The first part is a brief description of the ideas and experiments which led Reynolds to describe the importance of the group of parameters which we now call the Reynolds number. In the second, for the benefit of those whose background has not involved a close association with the wind tunnel, there is an introductory description of the role it plays in aeronautics.

1.1 Osborne Reynolds, FRS

In one of his many contributions to the understanding of engineering science,^(1,2) this outstanding engineer pointed the way for introducing order to what had been a confusion of hydrodynamic phenomena. He examined the behaviour of internal flows, specifically the flow of water in channels varying in scale from pipe-sized to coastal estuaries. The word *scale* is deliberately introduced at this point because it raises an issue central to the cryogenic wind tunnel, which is the effect of *scale* on model performance. Continuing with this description of his work, for our purposes it is sufficient to look briefly at his pipe-flow experiments as a means of highlighting some of the significance of Reynolds number. A complicated variation of resistance to flow had been noted, pressure drop along a length of pipe varying in some circumstances in a very regular way as water velocity, but in other circumstances varying as a higher power, approaching the square of velocity. He noted that the division between these two behaviours was associated with a change in the nature of the flow between what we now call laminar and turbulent flow; and to introduce some order to the situation he set out to establish the conditions which would govern the transition from one flow regime to the other. Purely from physical reasoning he concluded that an expression which represented the ratio of inertia force present to the viscous force acting on a particular volume of fluid, would indicate the likely state of the flow. Figure 1 below shows the point where he first published⁽³⁾ the group of parameters which now honours his work by being called the Reynolds number. In this expression U is the mean velocity of the water, ρ its density, μ its viscosity and c the diameter of the pipe.

This is a definite relation of the exact kind for which I was in search. Of course without integration the equations only gave the relation without showing at all in what way the motion might depend upon it.

It seemed, however, to be certain, if the eddies were due to one particular cause, that integration would show the birth of eddies to depend on some definite value of

$$\frac{\rho U c}{\mu}$$

Figure 1. The first publication of the Reynolds Number expression?

His experiments established the numerical value of this dimensionless group above which the flow would experience the transition at which the eddies would appear. Further, by varying the parameter as much as he conveniently could, he showed that the transition occurred at the same value of Reynolds number irrespective of how its value was varied. He was able to change pipe size, water viscosity by temperature, water velocity but of course not density to any significant extent.

This contribution to understanding is valuable enough in its own right. In the business of wind tunnel testing we are more concerned with "external" flows (flows around the exterior of aircraft) in contrast with his "internal flow" experiments, but the reasoning and conclusions apply equally well. The states of boundary layers which form on aircraft components, that is whether they are laminar or turbulent, and their thicknesses, depend on Reynolds number.

However, he was able to add more understanding to this branch of fluid mechanics by using a flow visualisation technique. He had been introducing a dye streak as a means to show the state of the flow. Vigorous mixing of the streak indicated transition. By illuminating the glass tube by a spark he was able to distinguish the eddy-like structure of turbulent flow and also bursts of turbulence. He used a wire to artificially induce turbulence. These are techniques still widely investigated and practised today, showing him to be a remarkable pioneer. Some of his sketches are reproduced as my Figure 2. The central sketch on this figure shows his observation of bursts of turbulence.

On viewing the tube by the light of an electric spark, the mass of colour resolved itself into a mass of more or less distinct curls, showing eddies, as in Fig. 5.



Fig. 5.



In order to test this, an open coil of wire, as in Fig. 15, was placed in the tube so as to create a definite disturbance.

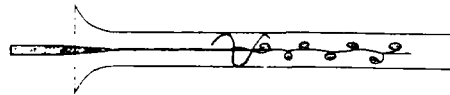


Fig. 15.

Figure 2. Reproductions of some of Reynolds' sketches of observed features in internal flow.

1.2 The Wind Tunnel

This test facility has been used for many years for two prime reasons: it provides a controlled environment for aerodynamic measurements, also it introduces economy by testing scaled-down models. The spectrum of flight speeds covered by the various products of aerospace industries is very wide, ranging from the low speeds of gliders to the high speeds of missiles, launch and re-entry vehicles. This range of speed has led to a range of tunnel designs. The use of a model tends to result in a low test Reynolds number in contrast with that of the flight vehicle. Consequently there is uncertainty over whether the incorrect value of the test Reynolds number is a source of error in the test data. The cryogenic wind tunnel, that is a wind tunnel employing a very cold test-gas, is one device which has been introduced to close the Reynolds number gap arising from difference in scale.

There are many geometries of wind tunnel which have evolved to satisfy testing requirements over the wide speed range just mentioned. However, as the test gas in a cryogenic wind tunnel must be kept very dry in order to avoid contamination by ice, and that it finds application in the aerospace field only at low speeds and transonic speeds, a narrow range of designs of cryogenic wind tunnel has resulted. Either they employ a stored compressed dry test gas which is allowed to expand, accelerate and flow past the model then away to the atmosphere, or they comprise a closed racetrack-like circuit containing the model, where the test gas is driven around by a fan. A common feature of the latter type is that the cooling of the test gas (and portions of the tunnel itself), which results directly in a raising of the Reynolds number in a way which will be described later, is by means of evaporating liquid nitrogen into the gas. This leads to nitrogen forming a large percentage of the test gas, dominating its properties. The Reynolds number advantage, which increases with reduction of temperature, is then limited by the need to avoid condensation of a nitrogen-rich gas stream. At one atmosphere pressure, N_2 condenses at about 77.4K. Minimum tunnel operating temperatures are usually somewhat higher than this.

The principal components of the closed-circuit cryogenic tunnel comprise therefore:

- the shell of the tunnel to contain the cold, often pressurised gas
- thermal insulation to minimise heat gain
- a drive system (often a fan)
- the liquid nitrogen storage and feed system
- an exhaust system to vent gas from the tunnel
- tunnel controls

- model, model mount and instrumentation
- methods for model preparation and geometry changes

These topics are covered in detail in the lectures which follow. The purpose of the following sections of this lecture is to act as a general introduction to this new application of cryogenic technology.

2. Reynolds Number Effects

The state of the boundary layers in external flows can have effects ranging from mild to profound, and not always in a predictable way. This is one very good reason for testing if possible at the correct Reynolds number. A classic example of change of behaviour with Reynolds number is the flow around a circular cylinder, illustrated on Figure 3. Somewhere within this 3-fold change in Reynolds number the boundary layer on the forward surface has changed from laminar to turbulent, affecting the pressure distribution (which is shown in the widely used dimensionless form of a pressure coefficient C_p) very strongly aft of 60° from the nose. As a direct consequence the drag coefficient C_D has also changed, in this case by about 30%. The two sets of data were taken in a small cryogenic wind tunnel at roughly the same Mach number as can be seen, which serves to raise another point of importance. Aerodynamic behaviour depends also on Mach number, the ratio of the test speed to the speed of sound in the gas. The values seen in this example are relatively low for aerospace vehicles, well below 1. In these circumstances aerodynamic behaviour is often insensitive to such changes in Mach number. However there are certain geometries of model which are sensitive to Mach number even at this low level. Further, as Mach number rises towards unity, virtually all geometries become sensitive to its change. Therefore it is very often the case that a wind tunnel must be capable of reproducing not only the correct flight value of Reynolds number but also the correct flight Mach number.

A second example of a Reynolds number effect is that of its influence on the lift of an aerofoil section, in particular on the maximum lift which can be generated. Figure 4 shows the variation of lift coefficient with the angle of attack of a section, measured at two widely different Reynolds numbers. It is seen that the maximum lift is rather sensitive to Reynolds number. The ratios of the two Reynolds numbers in this example, 20:1, roughly corresponds to the disparity in Reynolds number between large aircraft in flight, and the values which typically are attained on models of these aircraft in non-cryogenic wind tunnels.

The final example to be introduced in this lecture refers to a transport aircraft designed for cruise at a high subsonic speed where localised regions of supersonic flow exist over the wing. This is a very common situation on jet propelled aircraft. Flight and wind tunnel data are contrasted on Figure 5. The data comprises the chordwise distribution of pressure coefficient over the upper surface of

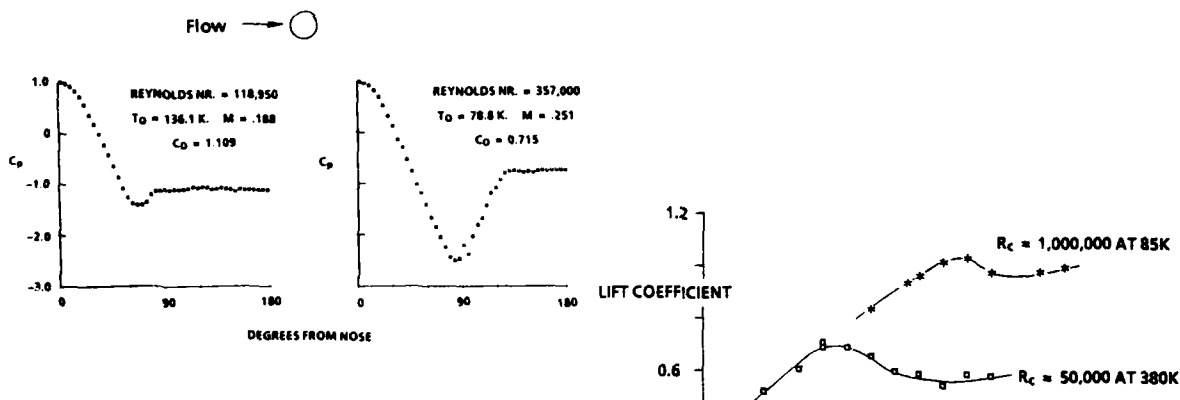


Figure 3. Effects of difference in Reynolds number on the pressure distribution around a circular cylinder.

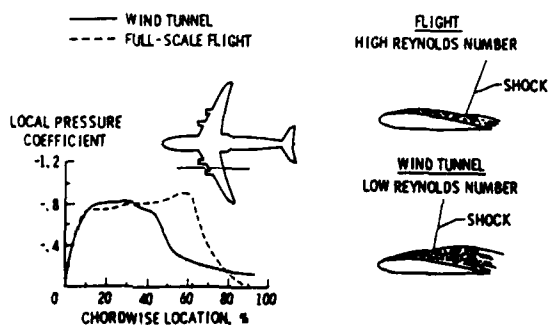


Figure 5. Effects of Reynolds number on the position of a shock.

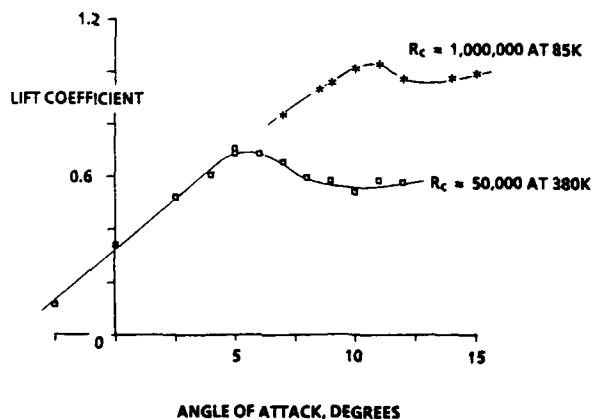


Figure 4. Effects of Reynolds number on the lift coefficient of a two-dimensional aerofoil. Measurements in a low speed cryogenic wind tunnel.

the wing along the line indicated. The Reynolds number of the test was well below the flight value, one consequence of which was that the boundary layer on the wing was disproportionately thick. This is illustrated (not to scale) on the right where the wing section is shown along with the upper surface boundary layer and a shock wave. The shock wave is a flow phenomenon through which the pressure of the air rises abruptly. The rise in pressure is shown inducing a thickening of the boundary layers. In the plot on the left hand side of this sketch the shock and its pressure rise corresponds in position with the rises in pressure coefficient (note the pressure coefficient signs): at about 50% chord in the tunnel test and 70% chord in flight. The movement of the shock and its consequences are attributed to the disparity in Reynolds number. This is an example where in the wind tunnel the flight value of Mach number was matched correctly whereas the Reynolds number was not, respectively because the economics of tunnel construction have permitted one match but not the other.

3. Dynamic Pressure

It is appropriate at this stage to introduce another feature of wind tunnel testing which does not necessarily match flight. This relates to the shape of the model. While the model designer and maker do their utmost to produce the correct shape in all significant details, there are various reasons for not being able to produce a perfectly modelled reproduction of the (proposed) flight article. One of these reasons relates to an error in shape induced by changes in the aerodynamic load on the model.

It will be seen later that it can be beneficial to raise the level of Reynolds number by employing a pressure in the tunnel substantially above that experienced by a high speed transport aircraft in cruising flight. This raises the aerodynamic load experienced by the model and, especially for high speed tests, dictates the use of near-solid wings with quite different bending and twisting characteristics from the aircraft.

Figure 6 illustrates the variation of Reynolds number R_c and dynamic pressure q through the Mach number range of interest. The figure applies to a tunnel operating at fixed values of pressure and temperature and therefore the data applies to many wind tunnels. The only input variable is fan speed, which directly affects airspeed and hence Mach number. Curves are shown for two slightly different tunnel variants, differing only in the ways in which the internal pressure is controlled. In many conventional low speed wind tunnels the internal pressure is controlled by venting the test section region. This holds constant the static pressure in the test section, P on Figure 6. In other wind tunnels including most cryogenic wind tunnels, the tunnel is vented elsewhere and the stagnation pressure P_0 is held constant. The influence of these options is seen to be significant only at higher Mach numbers.

Returning to the question of the deformation of the model it is seen from Figure 6 that although dynamic pressure varies strongly at low Mach number, roughly as M^2 , nevertheless it is rather low. In low speed tests the effect on the model of the load and load variation therefore is typically less of a problem than in high speed tests. At higher Mach numbers the dynamic pressure not only varies with the Mach number but is also high. In these circumstances the models may deform by varying amounts under the variations of dynamic pressure. Therefore if the Mach number is changed, say to determine Mach number effects, not only is the Reynolds number changing simultaneously but so might be the shape of the model. Three variables are present each having the potential to affect the aerodynamics. But, as they vary together, how each affects the aerodynamics cannot be separated, leaving the aerodynamicist in a dilemma.

An example of effects of model deformation, that is effects of variations in wing bending and twist, is illustrated on Figure 7 which shows two sets of test data for a transport model.⁽⁴⁾ The data, which is the wing upper surface pressure distribution, was taken at the same Mach number, 0.99, but with two values of Reynolds number. It is seen that with increase in Reynolds number the expected

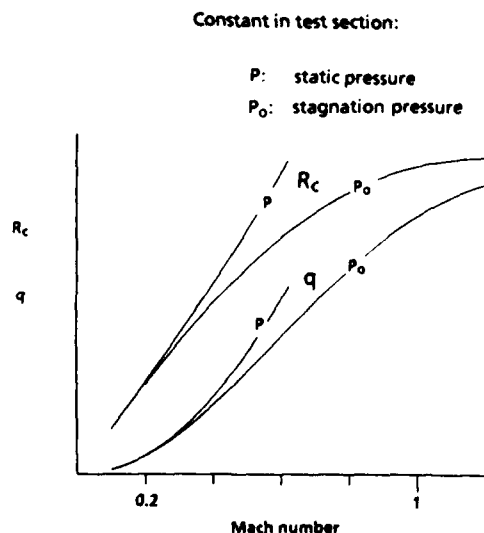


Figure 6. Variations in Reynolds number R_c and dynamic pressure q with Mach number in constant pressure tunnels.

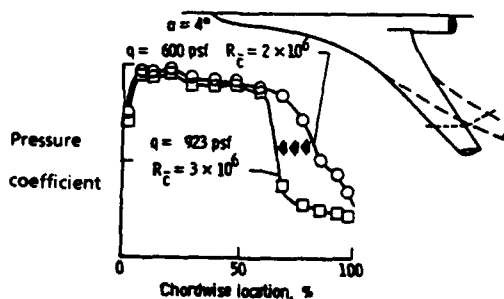


Figure 7. Example of aeroelastic problem of models in pressure tunnels.

rearward shift in the position of the recompression shock (see also Figure 5) did not occur, in fact the contrary. This was attributed to the fact that in this test the increase in Reynolds number was accompanied by a proportionate increase in dynamic pressure which, by inducing a change in wing bending and twist, introduced a contrary and stronger influence on shock position.

It is seen that it is important to be able to separate-out these effects. Normal temperature variable pressure tunnels have been built to economically raise the Reynolds number. The type of operating envelope which they provide is shown on Figure 8: a band of Reynolds number can be traversed at constant Mach number, and conversely. But the resultant aerodynamic coefficients might be affected by aeroelastic distortions arising from the changes of dynamic pressure which accompany both. Therefore there is still an uncertainty over cause and effect.

The cryogenic tunnel offers a way around the difficulty as will be seen.

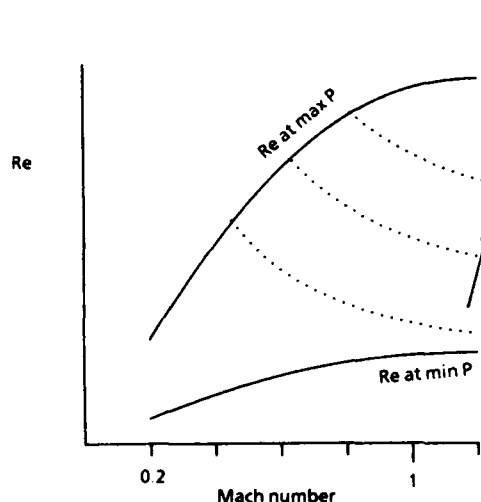


Figure 8. The operating envelope available from a variable pressure normal temperature transonic wind tunnel.

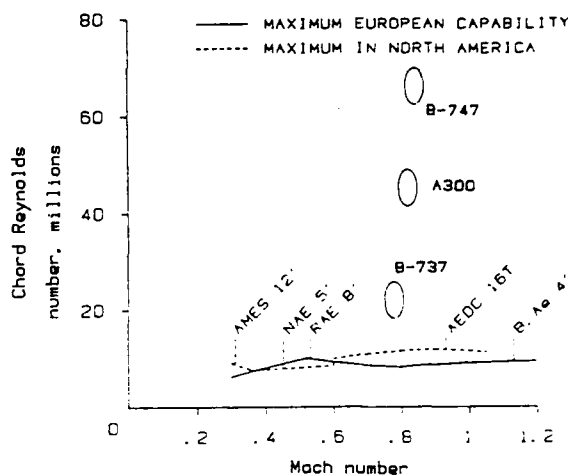


Figure 9. The disparity between the Reynolds numbers of some aircraft in cruising flight, and those attainable in the largest conventional wind tunnels.

4. The Reynolds Number Gap

Figure 9 compares the requirements of cruising flight with the highest Reynolds number capabilities of conventional wind tunnels each side of the Atlantic. A representative selection of transonic transport aircraft is shown, and it is apparent that conventional tunnel maximum capability is below flight by factors up to 5:1 in the case of larger transonic aircraft.

In principle the gap may be reduced or closed in various ways including using a larger tunnel, changing the test gas, raising its pressure or reducing its temperature, all either individually or in combination. They will be discussed briefly in turn.

Raising Reynolds number by a factor of 5 over the levels presently reached would need a tunnel 5 times as large as the largest, requiring 25 times the drive power. In light of the fact that the largest transonic tunnels absorb up to 200,000 HP the capital cost implications of raising this to 5 million HP are obvious.

Closing the gap by means of raised pressure is a more economical approach in terms of drive power because it would rise in proportion to the desired Reynolds number factor which is also the factor in pressure. The tunnel would need, therefore, around 1 million HP, a somewhat less daunting figure. However as existing tunnels frequently employ some pressurisation in order to raise Reynolds number to their present values, pressures typically around 2 atmospheres, the additional pressurisation needed to bridge the Reynolds number gap would raise the circuit pressure (strictly the stagnation pressure in the test section) to around 10 atmospheres. Opinion among users of transonic tunnels is that such a pressure would lead to an excessive dynamic pressure, therefore load and deflection of aircraft models. While there is no clearly defined upper limit on pressure, its value being at least model-configuration and support system dependent, the opinion is that modest increases in pressure are permissible in most circumstances above those used in most current wind tunnels.

Searches for alternative test gases to air have revealed some gases which are not too toxic and which would provide useful increases in Reynolds number, by factors of up to 4 when compared with air at otherwise the same conditions. However these gases are polyatomic with ratios of specific heats γ much lower than in air and it is felt that for testing at compressibility speeds their behaviour might not always be close enough to that of a diatomic gas. A viewpoint is that it is no use replacing one system which occasionally and unpredictably gives wrong answers (that is the use of air at low Reynolds number) with another which might also do the same. Mixtures of gases having $\gamma = 1.4$ give too small rewards.

The route which has been followed in the design of NTF and ETW is to combine the maximum reasonably usable pressure with

a cryogenic diatomic test gas. This combination leads to economy in construction and running costs, together with a very useful versatility arising from combinations of test variables

5. The Fundamentals of Cryogenic Wind Tunnels

5.1 Influence of temperature on Reynolds number and Dynamic Pressure

While the ideas can be applied to almost any gas, with particular advantage in low speed testing where a wider range of possibilities opens up if there is a relaxation of a constraint on $\gamma^{(5)}$, in transonic tests there is little if anything to be gained from gases other than air or nitrogen, which the following comments assume.

The basics can be introduced very simply by substituting into the Reynolds number expression

$$\text{Reynolds number } R = \frac{\rho V c}{\mu}$$

density ρ in terms of pressure P and temperature T in the ideal gas equation of state, velocity V as the product Mach number M and speed of sound, and viscosity μ by the approximation $\mu \propto T^{0.9}$. The advantage in terms of Reynolds number of cooling a gas may be conveniently written as a ratio, that is the ratio of the Reynolds number at reduced temperature T to that in the same gas at normal temperature T_1 , other factors such as wing chord c , flow Mach number and pressure remaining constant.

The resultant expression is

$$\text{Reynolds number ratio} = \left(\frac{T_1}{T} \right)^{1.4}$$

the value of the ratio depending on the choice of the higher temperature which might be typically about 320K in a continuous tunnel, and on the factors limiting the lower temperature. The lower limit is not necessarily completely defined. It depends on the test Mach number, on the equilibrium saturation boundary of the gas and therefore on the test pressure, but also on the amount of supersaturation permissible in the flow, which may prove to be size- or model-dependent. It should be mentioned that controlled levels of supersaturation have been exploited in hypersonic tunnels for years without adverse effects. During the life of the cryogenic wind tunnel the phenomenon has been the subject of research, because the rewards in terms of Reynolds number and in other respects can be quite useful. There is strong evidence that it is safe to approach the saturation boundary in the free stream ahead of the model. If this is adopted along with a Mach 1 test then the ratio takes the approximate maximum values

6.4 at 1 atmosphere stagnation pressure

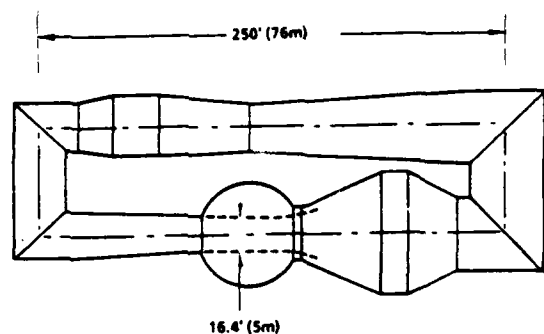
5.0 at 5 atmospheres stagnation pressure

In either case it can be seen that the factor is nicely in accord with the needs outlined in the preceding section.

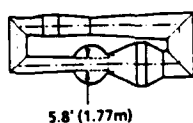
In the second example in the preceding paragraph the combination of high pressure with low temperature would result in a wind tunnel 4% of the size of an atmospheric pressure conventional tunnel which gives the same Reynolds number, surely resulting in economies in terms of capital cost.

An illustration of the impact of adopting cryogenics on the size of wind tunnels is illustrated on Figure 10. At the top is the outline of a normal temperature low speed wind tunnel designed for Mach 0.33. It would be used typically for investigations of take-off and landing configurations. For economy of size and in the drive power for the fan it is designed to operate at pressures up to 3 atmospheres. A cryogenic wind tunnel operating at the same pressure but at close to LN_2 temperature would have a test section 3ft (0.9m) across. This is regarded by many engineers as being impractically small because the model, at about 2ft. span, cannot be built to the necessary accuracy, detail and finish. Therefore a larger test section is preferred such as that sketched lower on Figure 10. The span of a model for this tunnel might be about 3½ft., say 1.1m. Once the cryogenic approach is adopted it is advantageous to use the minimum practical temperature. For this tunnel, with N_2 as the test gas, the same Reynolds number is obtained at 100K and 1.7 atmospheres pressure. The difference in sizes is striking, implying economy in tunnel construction and perhaps in model construction. Although the issue of tunnel drive power has not yet been raised, the powers quoted are representative of those required by the fans, showing an economy in this area for the cryogenic tunnel, in terms of capital and running costs. Offsetting this economy is the cost of cooling the cryogenic tunnel.

The force coefficients for a particular model at one attitude vary with the Mach and Reynolds numbers, and with dynamic pressure as we have seen. Dynamic pressure is $\frac{1}{2}\rho V^2$ where ρ is the density of the test gas and V is its speed - the equivalent of flight speed. The influence of the operating temperature of a cryogenic wind tunnel on dynamic pressure is not immediately obvious. The reduction of temperature increases density, tending to increase dynamic pressure. However the velocity, the product of Mach number



CONVENTIONAL TUNNEL. $P_0 = 3$ atmos. DRIVE POWER 14,750 H.P.



CRYOGENIC TUNNEL. $P_0 = 1.7$ atmos. $T_0 = 100$ K. DRIVE POWER 590 H.P.

Figure 10. Two wind tunnels giving the same model Reynolds number and Mach number of 0.33. The cryogenic wind tunnel represents what might be the smallest practical size of wind tunnel.

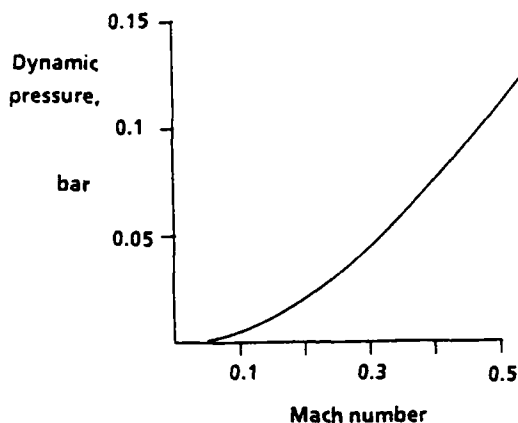
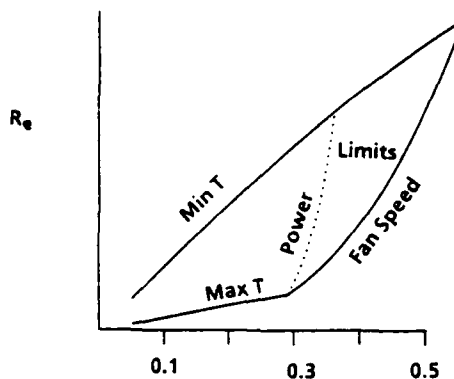


Figure 11. An operating envelope typical of a low speed atmospheric pressure cryogenic wind tunnel is shown at the top. The lower curve shows the dynamic pressure varying only with Mach number.

(which must not be allowed to vary when analysing the effect of temperature alone) and speed of sound, falls because the speed of sound falls with the temperature. In fact the effects cancel. Introducing the ideal-gas equation of state $p = P/RT$ into $\frac{1}{2}\rho V^2$ together with $V = Ma = M\sqrt{\gamma RT}$, where M is the Mach number, R is the gas constant and P is the static pressure in the test section, it is readily shown that dynamic pressure is $\gamma PM^2/2$, quite independent of temperature. The conclusion is that raising Reynolds number by means of reduced test temperature does not simultaneously affect model load

5.2 Drive Power

Particularly if the tunnel is to be driven by a fan there is interest in the influence of temperature on the required power. Fan drive power can be written

$$\text{power } p = \lambda \frac{1}{2} \rho V^3 A$$

where A = test section flow area and λ is a coefficient which varies primarily with the tunnel design and the flow Mach number.

For a given tunnel, Mach number and pressure, this simplifies to

$$p \propto \sqrt{T}$$

showing that fan power reduces as Reynolds number is increased by means of reduced temperature.

5.3 Cooling

There are two basic methods open for exploitation. One is the near-isentropic expansion of a gas from high pressure storage to the test stagnation pressure. The gas may be stored at normal temperature but is cooled in the expansion process, and then used in the tunnel. With a diatomic gas beginning at room temperature a pressure ratio of 40 is required to expand to 100K. Several wind tunnel projects have exploited this method

The alternate is to inject a cryogenic liquid (perhaps produced in plant separate from the tunnel, but stored alongside) into the test gas, using the latent heat of the coolant and in some circumstances an appreciable component of sensible heat. It is usual to use liquid nitrogen. The quantity of liquid nitrogen needed as a coolant may be calculated with reasonable precision from the approximate expression

$$\text{cooling effect of } \text{LN}_2 \approx 100 + 1.2 T_o \text{ kJ/kg}$$

where T_o is the tunnel stagnation temperature. More precise information is readily available⁽⁶⁾.

The cooling capacity is dissipated in several ways. There is a requirement to absorb fan power or, in the case of the induced flow tunnel, to cool the inducing air. For tunnels operating at 100K, in the former case the exchange rate, LN_2 flow rate to fan power, is 0.0045 kg/sec per kW., and in the case of the induced flow tunnel supplied with air at 300K the ratio of LN_2 mass flow rate to inducing air flow rate is about 0.9. There is also the need to account for the cooling of at least a proportion of the tunnel structure, the proportion depending on the thermal insulation scheme and on run time. However the exchange rate, expressed as the ratio of LN_2 mass to structure mass, in cooling from 300K to 100K is about 0.25 for steels.

Additional coolant is required to absorb heat inflow through insulation. The quantity required is strongly design and run-time dependent and it is difficult to provide very general information. However the specific example of the Langley 0.3 Meter Transonic Cryogenic Tunnel⁽⁷⁾ may be cited for guidance. In this reference the proportion of LN_2 consumption estimated as attributable to heat inflow is 1½% of the total. While the authors naturally are guarded about the general applicability of the information, it is nevertheless a useful guide to expectations for fan driven transonic tunnels. One estimate for low speed tunnels⁽⁸⁾ attributes up to 10% of the LN_2 consumption to heat leakage.

While the total requirements of a cryogenic wind tunnel for coolant and therefore cooling power depend on its design and operating cycle, studies have shown that the total energy consumption of a cryogenic wind tunnel is appreciably less than a conventional tunnel when comparisons are made on the basis of equal pressure, Mach and Reynolds numbers.

6. Operating Envelopes of Cryogenic Wind Tunnels

6.1 Constant pressure tunnels

A number of cryogenic wind tunnels are arranged to operate at essentially constant pressure, usually close to atmospheric stagnation pressure in the flow entering the test section. The two independent test variables which they then possess are speed and temperature, with the result that such a tunnel offers an envelope of test conditions typified by that sketched on the upper portion of Figure 11. This figure is drawn for a hypothetical low speed fan-driven tunnel. The Mach and Reynolds numbers are influenced by fan speed and gas temperature. The tunnel can be operated anywhere inside the envelope, shown here bounded by the maximum temperature (often close to ambient), the minimum temperature, the maximum fan speed and a less well defined minimum Mach number which, depending on circumstances, may be set by fan speed or by the onset of problems raised by measurement resolution. A constant power line is added to highlight the portion which might be clipped if fan drive power is limited.

Operation within the envelope allows independent variation of Reynolds number and Mach number, allowing the effects of the variation of each on model behaviour to be examined independently: Reynolds number can be varied at constant Mach number, and vice-versa. However, as has been explained, the dynamic pressure is a function only of Mach number in such a constant pressure tunnel. The variation of dynamic pressure is sketched below to emphasise its link with Mach number. It is apparent therefore that a Reynolds number sweep (a vertical cut across the operating envelope) should show Reynolds number effects without the data being corrupted by change of Mach number or dynamic pressure. This is an improvement over the situation arising in a constant temperature variable pressure tunnel.

The same cannot be said for the Mach number sweep, the horizontal cut across the envelope. In this case only Reynolds number is constant: dynamic pressure varies also with Mach number with the attendant uncertainty over cause and effect, as with the variable pressure normal temperature tunnel.

6.2 The cryogenic pressure tunnel

The word "pressure" is linked with "cryogenic" to infer that both pressure and temperature may be varied. The freedom to vary pressure arises from designing the tunnel to operate at elevated pressure for reasons introduced in Section 4. The rewards arising from the use of elevated pressure include increased Reynolds number and improved power economy. Three tunnel control inputs may be considered to be fan speed, circuit pressure and temperature. These may be independently adjusted and they provide the ability to separate the effects of Mach and Reynolds numbers, and dynamic pressure. The operating envelope becomes a volume, conveniently viewed relative to axes of Reynolds number, Mach number and dynamic pressure.

In order to illustrate the range of possibilities, a typical constant Mach number slice through the volume is shown on Fig. 12 for a tunnel having a 2.5 x 2.5 m. test section. The envelope shows the range of dynamic pressure and Reynolds number available for

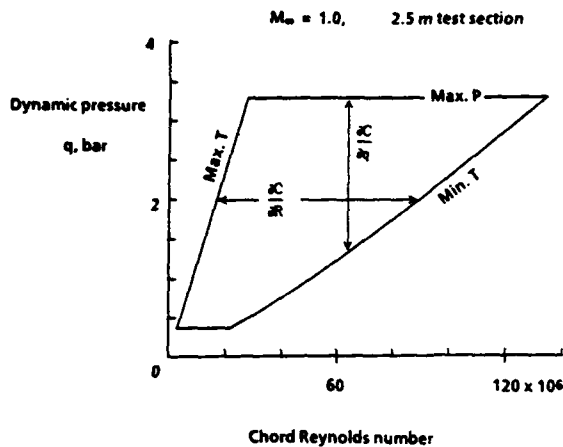


Figure 12. One slice, at constant Mach number, through the operating volume of a transonic cryogenic pressure tunnel.

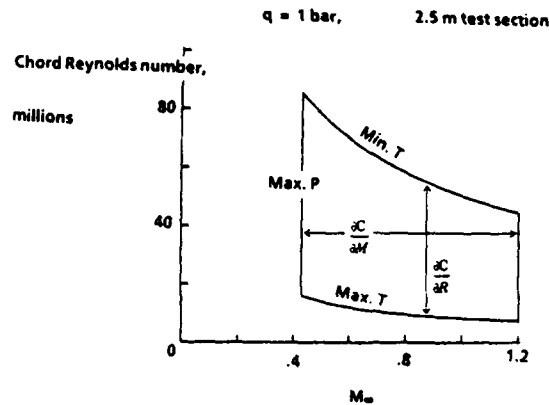


Figure 13. A constant dynamic pressure slice through the operating volume of a transonic cryogenic pressure tunnel.

sonic testing. It is bounded by the maximum temperature boundary (340 K), the minimum temperature boundary, the maximum pressure boundary (8.8 atm), and the minimum pressure boundary (1.0 atm). The partial derivatives on Figure 12 are used to show typical paths followed in determining the pure Reynolds number effects on an aerodynamic coefficient, $\partial C/\partial R$, and pure dynamic pressure effects $\partial C/\partial q$.

For the same wind tunnel a constant dynamic pressure slice through the volume is shown on Figure 13. This serves to illustrate typically the ranges available for Mach number variations giving pure Mach number effects $\partial C/\partial M$, and again $\partial C/\partial R$.

7. Real Gas Effects

The analyses of flows and the test data from wind tunnels usually assume the working fluid to behave as an ideal gas, that is a gas which obeys the equation of state for an ideal gas while having constant specific heats. In the case of flows in the cryogenic wind tunnel a profound departure from this behaviour would arise if the test gas began to condense. This is first likely to occur in localised low pressure/high Mach number regions around the model, and therefore the onset of condensation should depend on the configuration of the model as well as on the flow conditions of stagnation pressure P_0 and temperature T_0 in the free stream. Figure 14 has been

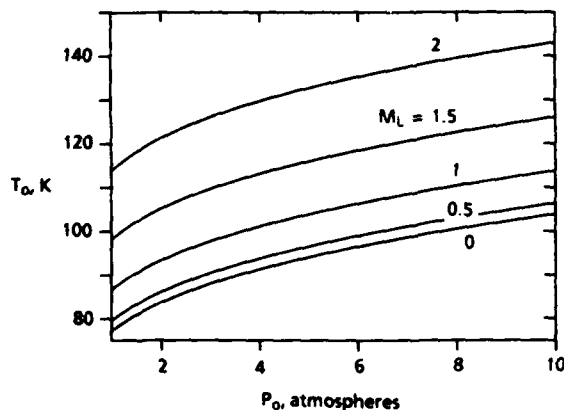


Figure 14. The combination of test section stagnation pressure P_0 and temperature T_0 where nitrogen will reach its equilibrium saturation boundary in an isentropic expansion to Mach number M_L .

computed for nitrogen and shows the relationship between the maximum local Mach number on the model M_L and the reference values of P_0 and T_0 for the flow just to reach the saturation boundary at M_L .

This chart can be used as a guide to the expected minimum operating temperature of a cryogenic nitrogen tunnel, and hence maximum attainable unit Reynolds number. However users of tunnels should note that there is evidence^(9,10) that some local supersaturation is acceptable, even to the point of reaching saturation in the free stream and therefore the guidance of Figure 14 should be considered conservative.

Other real gas effects are the departures of the working fluid in its gaseous state from that of a perfect gas: (1) thermal imperfection where, in the equation of state $PV = ZRT$, the compressibility factor Z is not unity (P = pressure, T = temperature, V = specific volume, R = gas constant), (2) caloric imperfection where the ratio of specific heats departs from the ideal gas value, 1.4 for the diatomic gas nitrogen. Variations of both are shown on Figure 15 for a pressure representative of a high Reynolds number wind tunnel, and a range of temperature down to about the minimum usable. It is seen that each varies several percent from its value at room temperature. Effects of these variations were computed by Adcock^{9,11} and were shown to be very small. He computed representative isentropic, shock and boundary layer flows and examples of the first two are included here.

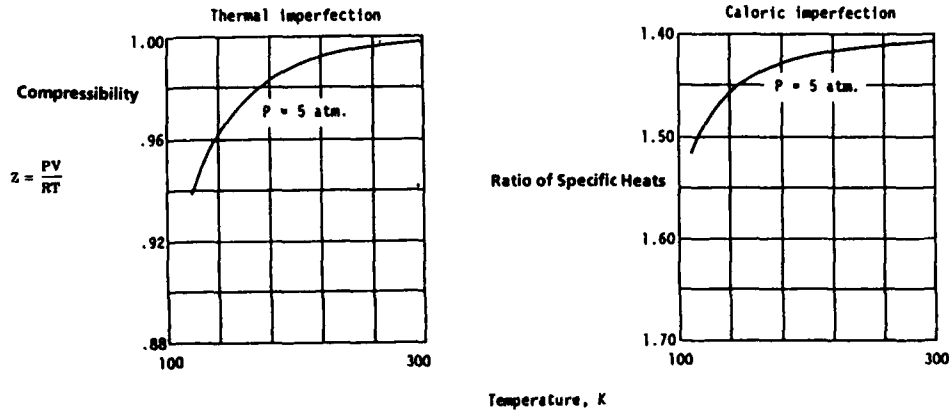


Figure 15. Variations in compressibility and ratio of specific heats with temperature for nitrogen at 5 atmospheres.

Figure 16 is concerned with the pressure ratio, static to stagnation, associated with an isentropic expansion from a reservoir to Mach 1 in nitrogen. The figure shows the ratio of the real to the ideal-gas pressure ratio as a function of test stagnation pressure and temperature. The departures from ideal-gas behaviour are small, and much smaller than would be computed using in isolation the real gas ratio of specific heats shown on Figure 15.

Similar results were obtained for flows through shocks. Figure 17 is illustrative of the computations and shows the real:ideal ratios of pressure rise across a normal shock in a nitrogen flow at Mach 1.4.

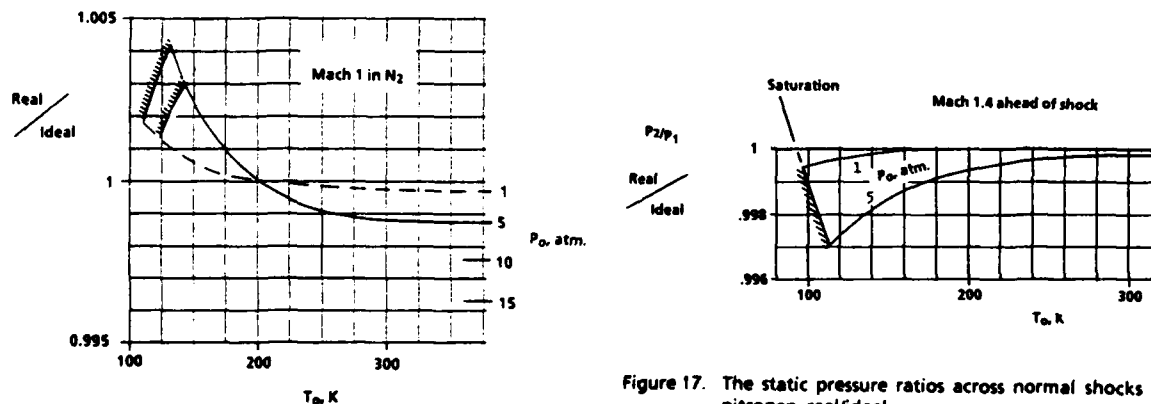


Figure 16. Real gas effects in isentropic expansions from a reservoir to Mach 1 in nitrogen. The ratio of real to ideal static to stagnation pressure ratios.

Figure 17. The static pressure ratios across normal shocks in nitrogen, real/ideal.

The conclusion from the various real gas studies are that a cryogenic wind tunnel can be operated at conditions very close to saturation without real gas effects becoming apparent, over the range of pressures acceptable in wind tunnel testing.

8. Fan/Tunnel Matching

In a given wind tunnel the matching of the fan to the tunnel may involve arranging for the fan to be at its "design" point at some representative high tunnel speed, where the efficiency of the fan would be at or near its maximum and the fan would be operating far enough clear of stall. At reduced air speed or Mach number the nature of fans and tunnels is for the operating point of the fan to move safely further away from stall. The locus of these points is the running line. This line is of broadly fixed character, but is moved

generally towards stall if the model under test has high drag, and away from stall and perhaps to a higher fan efficiency with increase in the unit Reynolds number in the tunnel circuit, but none of these effects is particularly strong.

It might be expected that this situation could change in response to marked changes in tunnel pressure or temperature. In fact this is not the case: a fan which is well matched to the tunnel at its highest Mach number will not experience any adverse aerodynamic effect from such changes. Of course the power required to drive the fan is affected, in the manner indicated in Section 5.2.

References

1. Papers on mechanical and physical subjects by Osborne Reynolds. Three volumes. Cambridge University Press, 1900-1903.
2. Gibson, A.H. Osborne Reynolds and his work in hydraulics and hydrodynamics. Longmans, 1948.
3. Reynolds, O. An experimental investigation of the circumstances which determine whether the motion of water shall be direct or sinuous, and the law of resistance in parallel channels. From Philosophical Transactions of the Royal Society, 1883.
4. Campbell, J.F. The National Transonic Facility - A Research Perspective. Paper 84-2150, AIAA 2nd Applied Aerodynamics Conference, Seattle, August 1984.
5. Goodyer, M.J. Introduction to the Principles of Cryogenic Wind Tunnels with Outlines of Potential Applications. Presented as Paper No.1 at the AGARD/VKI Lecture Series 111, May 1980.
6. Kilgore, R.A., Adcock, J.B. Specific cooling capacity of liquid nitrogen. NASA TM X-74015, Feb. 1977.
7. Lawing, P.L., Dress, D.A., Kilgore, R.A. Description of the Insulation System for the Langley 0.3 Meter Transonic Cryogenic Tunnel. NASA TM 86274, Jan. 1985.
8. Kilgore, R.A. The Cryogenic Wind Tunnel for High Reynolds Number Testing. Southampton Univ., U.K., Ph.D Thesis, Feb. 1974.
9. Adcock, Jerry B., Kilgore, Robert A. and Ray, Edward J. Cryogenic Nitrogen as a Transonic Wind Tunnel Test Gas. 13th Aerospace Sciences Meeting, Pasadena, Calif, Jan. 20-22, 1975, AIAA Paper 75-143.
10. Hall, Robert M. and Ray, Edward J. Investigation of Minimum Operating Temperatures for Cryogenic Wind Tunnels. AIAA Paper 76-89. 14th Aerospace Sciences Meeting, Wash. D.C., Jan. 1976. Also Journal of Aircraft, vol.14, no.6, June 1977.
11. Adcock, Jerry B. Real-gas Effects Associated with One-Dimensional Transonic Flow of Cryogenic Nitrogen. NASA-TN-D-8274, Dec. 1976.

THE NASA LANGLEY 0.3-METER TRANSONIC CRYOGENIC TUNNEL

by

Edward J. Ray

NASA, Langley Research Center
Hampton, VA 23665-5225
U.S.A.

SUMMARY

The Langley 0.3-Meter Transonic Cryogenic Tunnel (0.3-m TCT) was placed in operation at NASA's Langley Research Center in 1973. This facility was the world's first cryogenic pressure tunnel. The 0.3-m TCT can operate from ambient to cryogenic temperatures at absolute pressures ranging from about 1 to 6 atmospheres. Three major test section concepts have been developed and refined in this unique facility. The 0.3-m TCT has been a leader in the evolution of cryogenic pressure wind tunnel test techniques, instrumentation, control strategy and model technology.

This paper presents an overview of the evolution and 15 years of experience with the 0.3-m TCT. The historical background concentrates on the technical challenges and proof-of-concept validations during the establishment of the first cryogenic pressure wind tunnel. The various test section concepts are described. Highlights of operational experience and test results determined from these first time exploratory tests are presented. Operating costs and effective test techniques for the 0.3-m TCT are discussed. Finally, current and future plans for the facility are presented.

1. INTRODUCTION

Personnel at the NASA Langley Research Center have been investigating the application of the cryogenic concept to high Reynolds number transonic tunnels since the autumn of 1971. The initial efforts were aimed at extending the theoretical analysis and modifying a small low-speed model tunnel for cryogenic operation¹. The encouraging results obtained from these initial studies stimulated the design and construction of the Langley Pilot Transonic Cryogenic Tunnel. The initial proof-of-concept results obtained in the pilot tunnel^{2,3,4} had a profound effect on the U.S. decision to apply the cryogenic concept to the National Transonic Facility (NTF). As a result of the successful operation during these validation studies, the pilot tunnel was later reclassified as the 0.3-Meter Transonic Cryogenic Tunnel (0.3-m TCT). The original three dimensional test section was replaced with a two dimensional test section insert during the summer of 1976. About 2 years later, an extensive program was undertaken to recertify the entire tunnel circuit for testing at 6 atmospheres stagnation pressure.

After a rewarding period of about 10 years of research with the two dimensional test section, an adaptive wall test section insert was installed in the tunnel circuit. Several years of experience has been gained with this advanced test section concept. The purpose of this paper is to: (1) briefly review the reasons for the selection of the cryogenic pressure tunnel concept⁵, (2) present an overview of the development, design characteristics, and current capabilities of the 0.3-m TCT, (3) present highlights of cryogenic operational experience, and (4) indicate current and future plans for the 0.3-m TCT facility.

This paper is presented from the standpoint of a wind tunnel user and represents a broad overview based on 15 years of cryogenic wind tunnel experience. Details of many of the studies discussed are subjects of complete papers which are referenced herein as appropriate. Several of the subjects mentioned in this paper are covered in more detail in papers which will be presented later in this lecture series.

2. WHY CRYOGENIC WIND TUNNELS?

2.1 Simulation of Flight Conditions

The flow about an aerodynamic body such as a wing section of a transonic aircraft (see figure 1) is often characterized by shocks, shock boundary-layer interactions, and boundary-layer separation from the airfoil surface. The location of the recompression shock and its interaction with the boundary layer is critical to aerodynamic performance of the airfoil and the proper simulation of this complex flow is necessary for accurate stability, control, and performance predictions. To achieve "flow similarity" between a vehicle in flight and a model in the wind tunnel at speeds where compressibility effects are important, it is necessary to match both Mach number and Reynolds number. Since the development of the slotted-wall test section, it has been relatively easy to duplicate flight Mach number, the ratio of flight velocity to sound velocity in transonic wind tunnels. Unlike Mach number, however, the ability to simulate the Reynolds number parameter, the ratio of the inertia forces to the viscous forces, had not kept pace with advances in flight technology. Flight Reynolds number of modern aircraft had increased to the point where they were about five times greater than the capabilities of the existing wind tunnels. The

concern with the growing "Reynolds number gap" at subsonic and transonic speeds stimulated a renewed national and world-wide interest in the development of advanced high Reynolds number test facilities.

2.2 Methods to Increase Reynolds Number

There are several well-known ways to increase Reynolds number that have been tried or proposed for transonic tunnels. However, cooling the test gas to cryogenic temperatures (150 K or less) appeared in the early 1970's to be the best solution in terms of model, balance, and model support loads, as well as initial and operating costs. In addition, as will be shown later, having temperature as an independent test variable offered new and unique testing capabilities in addition to the achievement of full-scale Reynolds numbers.

The use of low temperatures in wind tunnels as a way of increasing the test Reynolds number is expressed as

$$R = \frac{\text{Internal forces}}{\text{Viscous forces}} = \frac{\rho v^2 l^2}{\mu v l}$$

which reduces to the familiar equation

$$R = \frac{\rho v l}{\mu} = \frac{\rho M a l}{\mu}$$

As the temperature is decreased, the density increases and the viscosity decreases. The equation shown above indicates that both of these changes result in increased Reynolds number. As temperature decreases, the speed of sound, a , decreases. For a given Mach number, this reduction in the speed of sound results in a reduced velocity, V , which, although offsetting slightly, the Reynolds number increase due to the changes in ρ and μ , provides advantages with respect to dynamic pressure, drive power, and energy consumption.

Some of the overall effects of reduced temperature on the gas properties, test conditions, and drive power are shown in figure 2. For comparison purposes, a stagnation temperature of 322 K (+120°F) for normal ambient temperature tunnels is assumed as a reference. The variations in gas properties (at a constant pressure) with temperature are shown on the left of the figure. The corresponding variation in Reynolds number, dynamic pressure, and driver power are shown on the right for conditions of constant model and tunnel size, constant pressure, and constant Mach number. An approximate temperature dependence associated with the various characteristics is shown for each curve. It can be seen from this illustration that cooling the test gas sufficiently results in an increase in the Reynolds number by more than a factor of 7 with no increase in dynamic pressure and with a large reduction in the required drive power. The inherent advantages associated with operating at cryogenic temperatures coupled with moderate increases in stagnation pressure offered an attractive approach for achieving high Reynolds number test capabilities in continuous flow wind tunnels at reasonable levels of cost and model loading.

2.3 Unique Operating Envelope

A very important additional advantage of cryogenic pressure tunnel operation is the unique ability to vary pressure and temperature independently of Mach number. This new capability provided for the first time the independent control and assessment of aeroelastic, Reynolds number, and Mach number effects on the aerodynamic parameters being measured. An example of this attractive capability is illustrated in figure 3 which shows a typical cryogenic pressure tunnel envelope for a Mach number of 0.85. This envelope indicates the range of dynamic pressure and Reynolds number available for testing at Mach 0.85 with just one model. The conditions which define the outer boundaries of these envelopes are the horizontal lines of maximum and minimum stagnation pressure and the diagonal lines of maximum and minimum stagnation temperature. Conventional pressure tunnels can operate only along or very near to the ambient temperature lines, and increases in Reynolds number can only be accomplished by increasing the stagnation pressure. This obviously results in large increases in dynamic pressure, q , and consequent increases in model loading and distortion. The addition of temperature as an independent variable expands the envelope and studies at constant dynamic pressure or at constant Reynolds number can be accomplished with just one model. For example, at a Mach number of 0.85 and a stagnation pressure of 6 atmospheres, a pure Reynolds number study can be made with Reynolds number varying from about 80 to 380 million per meter.

3. ORIGINAL 0.3-M TCT WITH OCTAGONAL TEST SECTION

The 0.3-m TCT was placed in operation at NASA's Langley Research Center as a pilot facility in 1973. During that time there was an urgent requirement to select a valid and economically feasible approach for the national high Reynolds number transonic tunnel. As a result of this urgency, the pilot tunnel was designed, constructed, and calibrated in an impressively short time period of about 8 months. At that time, this new and unproven facility was envisioned as a "short-life" (about 60 operating hours), pilot tunnel, with the primary purpose of validating the fan-driven cryogenic concept at subsonic and transonic Mach numbers.

3.1 General Description

The pilot tunnel was a continuous flow, fan-driven tunnel with a slotted octagonal test section, 34.3 cm across flats. A sketch of the tunnel is shown in figure 4. From the vantage point shown in figure 4, the fan is in the lower right hand corner of the tunnel circuit and the flow is clockwise.

The tunnel was constructed of 6061-T6 aluminum alloy and was originally encased in thermal insulation consisting of about 12.7 cm of urethane foam, covered with a fiberglass-reinforced epoxy vapor barrier (see figure 5). The fan is driven by a 2.2 MW (3000-hp) variable-frequency motor. With the three-dimensional octagonal test section installed, the Mach number of the pilot tunnel could be varied from about 0.05 to 1.2 at stagnation pressures varying from about 1.2 to 5 atmospheres. Liquid nitrogen was originally stored in 15,000 liter mobile trailers. The tunnel temperatures could be reduced to about 78 K by spraying liquid nitrogen directly into the tunnel circuit. Viewing ports 3.5 cm in diameter were provided for monitoring the test section and nitrogen injection zones.

3.2 Original Proof of Concept Testing

The initial theoretical real-gas studies made at the Langley Research Center indicated that for moderate operating pressures, flow characteristics are insignificantly affected by real-gas imperfections of nitrogen at cryogenic temperatures. However, due to the fact that the cryogenic concept represented an entirely new type of wind tunnel testing, the first noncalibration test was designed to provide experimental confirmation of the cryogenic concept. The configuration selected for these studies was a 12-percent thick, NACA 0012-64 airfoil equipped with pressure orifices. A photograph of the model installed in the three-dimensional test section is shown in figure 6. The 13.7 cm chord airfoil completely spanned the octagonal test section. The insert sketch included in figure 6 indicates that at subcritical speeds, this airfoil has a "flat-top" velocity distribution, similar to the upper surface distribution of current supercritical designs. This feature added to the appeal of the selection of this airfoil for the proof-of-concept tests.

There were several conditions which were selected to assure a fair and adequate cryogenic evaluation: (1) tests at ambient and cryogenic temperatures were to be made in the same tunnel, on the same model, at identical Mach numbers and Reynolds numbers; (2) the airfoil was to be tested with free transition to allow any possible temperature effect on boundary-layer development; (3) the symmetrical airfoil was to be tested at a lift coefficient of zero to eliminate any shape or angle-of-attack change due to dynamic-pressure differences; and (4) the test Mach number would exceed the leading edge Mach number of typical sonic transport designs. The test results obtained in this important proof-of-concept study indicated excellent agreements between the selected ambient and cryogenic cases at both subcritical and supercritical conditions.⁴

Additional experimental tests were made in support of the analytical real-gas analysis⁶ and to determine the proper procedures for setting the tunnel test conditions. For these tests, the tunnel Mach number was set according to the pressure ratio (p/p_0) as indicated by the real-gas isentropic expansion solution for nitrogen or by the ideal-gas equations in combination with the actual ratio of specific heats for the stagnation conditions under consideration.

The effect of these two procedures for setting Mach number on the two-dimensional airfoil pressure distributions were determined. Samples of the results obtained from this study are presented in figure 7 for a nominal Mach number of 0.85. A baseline pressure distribution is the high pressure, ambient temperature case (square symbols) since the thermodynamic properties for this condition ($\gamma = 1.40$) are such that use of either procedure gives the same result. For the cryogenic 1.2 atmosphere case, there is excellent agreement with the baseline distribution when the tunnel is set by the real-gas p/p_0 ratio (circular symbols) indicating the validity of the real-gas procedure. When the tunnel was set by the ideal-gas equation and the actual ratio of specific heats, 1.44 (dashed curve), the shock location occurred some 2 or 3 percent further downstream on the chord of the airfoil. Even for this case, where the specific heat ratio is very close to the ideal diatomic value of 1.4, it is obvious that this procedure for setting Mach number is incorrect. These results supported the findings of the analytical work where it was shown that the use of ideal-gas equations in combination with actual specific heat ratios at cryogenic conditions results in erroneous indications of the magnitude of real-gas effects. When this procedure for setting Mach number was applied at a high pressure, low temperature conditions (see long-short dashed curves, figure 7) where the specific heat ratio is 1.52, the recompression shock is located about 10 percent further downstream on the airfoil. (It is realized that this case represents a considerably higher Reynolds number, but the detailed studies of the 0012-64 airfoil had shown that the shock location for this particular airfoil was extremely insensitive to variations in Reynolds number within the range of these studies.)

As mentioned earlier, the wide range of operating temperatures was obtained by spraying liquid nitrogen directly into the tunnel circuit to cool the structure and to remove the heat added to the stream by the drive fan. Because of this method of cooling, the uniformity of the temperature distribution was one of the primary areas of concern at the beginning of the 0.3-m TCT studies. In order to determine the extent of the mixing process and to evaluate the temperature distributions in the circuit, a temperature survey rig was placed just upstream of the turbulence damping screens in the low velocity area of the tunnel. A photograph of the survey rig is shown in figure 8. The rig incorporated 24 thermocouples which were evenly spaced along 8 spokes, 45 degrees apart. A sketch of the temperature survey rig showing the general location of the thermocouple probes is shown in figure 9 along with a listing of some early results which were obtained at a Mach number of 0.85. The mean value of temperature T_p , the difference in the extremes in temperature, RANGE, and the standard deviation are listed for stagnation pressures from 1.20 to 5.00 atmospheres. It can be readily seen that there was a relatively uniform temperature distribution even at the extremely low cryogenic temperatures approaching free-stream saturation conditions.

Since the temperature survey station was located upstream of the turbulence damping screens and the contraction section, it was expected that a more uniform distribution would occur in the test section. Subsequent temperature measurements obtained in the test section verified this assumption, and indicated that at Mach number of 0.85 at 5 atmospheres stagnation pressure and a cryogenic temperature of about 120 K, the standard deviation was about 0.2 K. In addition, tests were made to assess the thickness of the thermal boundary layer near the tunnel walls. This preliminary assessment indicated that the thermal boundary layer is extremely thin, and that temperatures, even in the low velocity screen section of the tunnel, approach free-stream values at about 1.3 cm from the wall.

The temperature studies indicated remarkably good distributions. This evidence was particularly encouraging in view of the fact that it is not uncommon for some classes of ambient temperature wind tunnels to have temperature gradients of over 11 K across the test section.

Economy in power consumption was expected with cryogenic operations based simply on the ideal-gas $\text{Power} \propto \sqrt{T}$. (There is also an additional decrease in power required due to the increased Reynolds number noted in reference 7.) A series of verification tests were made to map the fan power as a function of Reynolds number. These tests, as shown in figure 10, included a range of pressures and temperatures at a constant Mach number of 0.85. The savings in power by operating at cryogenic temperatures is illustrated on this chart by considering the example of a constant Reynolds number of 12.5 million. The power required to produce the same Reynolds number by increasing stagnation pressure is an order of magnitude higher than the power required at the minimum cryogenic test condition. Experimental evidence substantiated that at selected test conditions, the power required was about 16 percent less than expected from the simple ideal-gas relation $\text{Power} \propto \sqrt{T}$ as a result of the sizable Reynolds number increase and real-gas effects⁸.

3.3 Development of Original Operating Techniques and Procedures

One of the most fundamental cryogenic wind tunnel techniques which was developed in the early days of operation was the pre-run purge and cool-down procedure. The pre-run purge is a process which is conducted at warm temperatures to eliminate all the moisture from the nitrogen test gas. (The pre-run purge procedure is described in detail in reference 9.) An early record of stream and tunnel wall temperature as a function of time is shown in figure 11. The particular run does not include the normal pre-run purge described in reference 9 due to the fact that the tunnel had not been opened to the atmosphere prior to this test. The tunnel was normally cooled down at a rate of about 10 K/minute or less in an attempt to avoid excessive thermal stresses in the tunnel structure. This particular cool-down was fairly typical and took about 40 minutes. It will be noticed that near the end of the cool-down, the cooling rate was reduced to enable the tunnel wall and stream temperatures to equalize. It will be noted that at one point during the cool-down there was about an 80 K "lag" between the wall and stream. An 80 K "lag" would be considered to be excessive by today's procedures. (The effects of large temperature differentials will be discussed later in this paper.) During the 52 minute test time, however, the differences between the wall and stream temperatures were maintained within 10 K. The normal run procedure was to keep the wall and stream temperatures at about the same temperatures. It should be noted, however, that there has been no evidence of any aerodynamic discrepancies due to differences in temperature between the wall and stream. In the example shown in figure 11, there were eight different test conditions established which ranged in temperatures from 86 K to 103 K at pressures between 4.3 and 5 atmospheres and Mach numbers ranging from 0.740 to 0.755. If a tunnel entry were required, the normal procedure was to warm the tunnel to ambient temperatures at a rate roughly equivalent to the cool-down rate. It was later proven in the 0.3-m TCT that the tunnel can be left cold when not running without any possible material damage even to the drive system. If a tunnel entry is not required, this procedure avoids the significant time and expense of warm-up and cool-down.

At the beginning of operations with the original tunnel configuration there were many "lessons learned." In addition to the purge and cool-down procedures just described, many techniques had to be developed in this totally new experimental environment. For example, with the original exhaust stack design, a severe fogging problem existed during periods of high humidity and low wind velocities. A very simple and effective solution to this problem was the incorporation of exhaust driver ejectors. The low pressure ejectors (which are still used today) induced ambient air at the base of the exhaust stack, which dilutes and rapidly warms the cold nitrogen gas. The resulting foggy mixture is propelled high into the air and normally dissipates rapidly and completely (see figure 12).

3.4 Reclassification to Operational Facility

In retrospect, the operation of the pilot tunnel as the first transonic cryogenic tunnel was very successful and relatively trouble-free. As a result of the successful operation during the validation studies, the pilot tunnel was reclassified by NASA (with Congressional approval) as the 0.3-m TCT. Shortly after the reclassification, an engineering team representing a variety of disciplines (electrical, structural, cryogenic, aerodynamic, and safety) was formed to inspect the facility and evaluate its long range suitability as a research facility from the standpoint of design features and structural integrity. Considering the haste of the original construction and installation and the 18 months of intensive cryogenic operation, there were surprisingly few major deficiencies. There was, however, one general class of internal structural damage which occurred in cases where "spoke-like" aluminum struts or turning vanes were rigidly attached to the tunnel pressure vessel. This class of failures which was later eliminated in most cases with a redesign will be discussed in a later lecture in this series.

3.5 Examples of Model Testing Experience

The operational experience gained with the original 0.3-m TCT included a broad variety of models and range of instrumentation. There was a concerted effort to investigate experimental techniques in the new cryogenic pressure test environment. The scope of tests, therefore, was probably as extensive as would be experienced in normal conventional wind tunnel testing. In addition to the original proof-of-concept studies, tests were conducted with the 0012-64 airfoil installed to determine the onset conditions of condensation effects. This test and other studies^{10,11} were made to determine the condensation temperature limit on "useful" cryogenic wind tunnel testing. These interesting results indicated that significant increases (about 15 percent) in Reynolds number capability can be achieved by testing at temperatures below local saturation conditions while remaining above the conditions corresponding to the onset of disturbing condensation effects. Other tests, as shown in figure 13, included a study of a first generation cryogenic strain gage balance. The three-dimensional model installed on the experimental balance was a thick highly swept delta wing with sharp leading edges. The purposes of these tests were to (1) investigate any possible effects of cryogenic conditions on the flow phenomenon characterized by a leading-edge vortex separation and reattachment, and (2) to obtain cryogenic experience with an electrically heated strain gage balance. There were some problems associated with balance zero shifts but the moment and force results indicate that flows with leading-edge vortex effects were duplicated properly at cryogenic temperatures.

Tests were conducted to determine the effects of Reynolds number on the boattail drag of two wing-body configurations¹². The boattail drag studies were undertaken in the original 0.3-m TCT due to concern over the effect of Reynolds number variations on boattail pressure drag. Flight tests which had been made with an F-106B aircraft with two research nacelles mounted under the wings. In addition to the flight tests, wind tunnel tests had been conducted with two subscale models of the flight test configuration. The results from these previous flight and tunnel tests indicated large Reynolds number effects on boattail drag, showing that the low Reynolds number tunnel data could not be extrapolated to flight conditions.

A photograph of two of the boattail models installed in the tunnel is included in figure 13. The 0.3-m TCT studies¹²⁻¹⁶ were designed to determine the exact Reynolds number effects on the boattails. With the 0.3-m TCT cryogenic-pressure capability, the existing flight and low Reynolds numbers wind tunnel test large could be completely surveyed. The 0.3-m TCT results showed essentially no change in the boattail pressure drag with Reynolds number. This trend essentially agreed with theoretical predictions¹³ and it was concluded that the difference between the flight test results and other wind tunnel results was caused by installation effects. The 0.3-m TCT investigation did, however, reveal strong local effects of Reynolds number over the region of the boattail. These strong local effects were hidden by compensating effects with a net result being no discernible effects of Reynolds number on the total boattail drag. This investigation, as with all investigations which have been made in the 0.3-m TCT, included tests designed to provide exact Reynolds number and Mach number comparisons at ambient and cryogenic temperatures. Even with the extreme sensitivity of the boattail characteristics to local scale effects, the ambient-cryogenic comparison showed excellent agreement¹⁵.

One of the advantages of the cryogenic tunnel concept is, of course, the capability of covering a large Reynolds number range while maintaining the tunnel dynamic pressure at a constant level. This capability eliminates the variations in aeroelastic effect that occur when tunnel stagnation pressure is used to generate the desired Reynolds number variation. An early exploitation of this advantage was the measurement of the base drag of the space shuttle orbiter in the three-dimensional test section of the 0.3-m TCT. In order to eliminate the sting interference effect on the base, the model was supported by slender wing tip extensions which, in a conventional pressure tunnel, might have been subjected to sizable and varying torsion effects. A photograph of the 0.0045-scale model installed in the test section is shown in figure 13. Static pressures were measured at the base of the model with individual pressure transducers. Base axial force coefficients had been determined during various tests in other wind tunnels using sting mounted models. The results from these previous sting mounted tests gave values substantially below the empirical estimates made by the contractor. The 0.3-m TCT results for the wing tip mounted model agreed almost exactly with the contractor estimates. The abnormally lower base drag values indicated for the sting mounted models was presumed to be associated with sting interference effects.

4. 0.3-M TCT FACILITY WITH TWO DIMENSIONAL TEST SECTION

The 0.3-m TCT has undergone almost continual evolution from the original pilot facility concept to its present configuration¹⁷. During the summer of 1976 the original three-dimensional test section was replaced with a 2-D test section insert. This major change took advantage of the interchangeable test section feature of the 0.3-m TCT leaving the major portion of the tunnel circuit in its original state (see figure 14). The two-fold purpose of this extensive modification was to assess the feasibility of two-dimensional testing at cryogenic temperatures and to take additional advantage of the very attractive high unit Reynolds number capability of the relatively small, economical test facility.

During this major modification, a workshop and model preparation area were constructed adjacent to the tunnel. A new control and instrumentation room was added and the data acquisition system was upgraded by connecting it to a remote control data acquisition system¹⁷.

4.1 General Description

The two-dimensional insert consisted of a new contraction section, a rectangular pressure plenum encompassing a 20 x 60 cm test section and a completely new diffuser. A photograph of the original two dimensional test section installed in the 0.3-m TCT is shown in figure 15. The photograph indicates only one nitrogen injection station located in the diffuser section of the "upper-leg." This location reflects the results of injection studies which indicated that adequate cooling and mixing could be accomplished with the upper injection station alone and an original lower injection station was eliminated.

As shown in figure 16, the two-dimensional test section provided removable model modules. In this photograph, the plenum lid and test-section ceiling have been removed and the module is in the raised position. This removable feature and duplicate module assemblies allow for the complete preparation of one model during the testing of another model. The tunnel incorporated computer-driven angle-of-attack and momentum rake systems. The momentum rake, shown in figure 17, was programmed to traverse automatically through the wake, determine the boundaries of the wake, and then step through the wake at a prescribed rate and number of steps.

4.2 Evaluation of Two-Dimensional Test Section and Test Techniques

From early 1977 until early 1979 the facility was used to evaluate the two-dimensional test section and develop airfoil testing techniques.

4.3 Recertification of Facility to 6 Atmosphere Capability

During most of 1978, an extensive program was undertaken to recertify the entire tunnel circuit for testing at 6 atmospheres stagnation pressure. This upgrading was supposedly consistent with the strength of the basic shell and would provide an additional Reynolds number capability and the ability to approximate more closely the stagnation pressures to be used in the National Transonic Facility. The tunnel was completely stripped of its original insulation, and the entire circuit visually inspected and x-rayed for any possible structural damage. (It is estimated that at this time, the tunnel had operated for about 2000 hours and had been subjected to about 600 complete pressure-temperature cycles.) In order to comply with the USA codes and requirements for testing and certification of the 6 atmosphere pressure vessel, a considerable number of the original welds were replaced with higher quality welds and certified by x-rays and other forms of non-destructive testing. In addition, a major portion of the contraction section was completely replaced. Several other sections were reinforced with additional structural members. It should be noted, however, that even after 4 years of fairly intensive cryogenic operation at pressures up to 5 atmospheres, the pressure vessel maintained structural integrity. On completion of the structural modification, the entire circuit was pressure tested to 1.5 times the 6 atmospheres operating pressure.

4.4 Replacement of Original Insulation System

During the recertification period, the original insulation was replaced with a relatively simple and inexpensive insulation concept which facilitated rapid, uncomplicated modifications and repairs. The primary insulation material is chopped untreated fiberglass loosely sewn into a mat approximately 1.0 in. (2.5 cm) thick. A photograph showing the application of the new insulation material to a portion of the tunnel is shown in figure 18. Moisture control is accomplished by the outer layer of fiberglass/elastomeric coating and an internal gaseous nitrogen purge system¹⁸. Mr. Lawing will describe this particular insulation system in more detail in a later lecture.

4.5 Airfoil Test Capability

The 0.3-m TCT with the two-dimensional test section installed was capable of operating at temperatures varying from about 80 K to about 327 K and stagnation pressures from near ambient pressure to 6.0 atmospheres. Mach number could be varied from about 0.05 to 0.95. The ability to operate at cryogenic temperatures combined with the newly acquired 6 atmosphere pressure capability provides an extremely high Reynolds number capability at relatively low model loadings. For example, to achieve an equivalent Reynolds number in an ambient-temperature pressure tunnel of the same size would require a stagnation pressure capability of about 36 atmospheres. In addition, the unique ability to vary pressure and temperature independently of Mach number provides independent control and assessment of aeroelastic, viscous, and compressibility effects on the aerodynamic parameters being measured.

Figure 19 represents a summary of the two-dimensional 0.3-m TCT Mach number and Reynolds number test capability, and the flight Reynolds number design conditions for two classes of aircraft. The general aviation design envelope, shown in the low Mach number, low Reynolds number corner of the figure, had not changed significantly over the past several decades. The transport-cargo aircraft design trend, however, had changed rapidly and dramatically. The large transport-cargo types, such as the 747 and C-5, established the upper requirement for two-dimensional design considerations. It can be noted from figure 19, that the 0.3-m TCT provided an adequate Mach number and Reynolds number capability to simulate the design flight condition for the largest class of, transport-cargo aircraft flying in the 1970's.

4.6 Pressure Instrumentation

For two-dimensional-airfoil tests, the 0.3-m TCT was equipped to measure static pressures on the airfoil surface, total pressures in the airfoil wake, and static pressures on the tunnel sidewall, floor, and ceiling. Static pressure taps were also

located throughout the tunnel circuit to provide measurements of contraction and diffuser section performance, fan pressure rise, and pressure loss across various elements of the tunnel circuit.

Because of the large changes in dynamic pressure of the facility over its operational range (a factor of about 75), the range of static pressures to be measured is large and conventional strain gage transducers are not used. Instead, commercially available high-precision capacitive-type transducers are used. A more complete description of this type of pressure instrumentation is presented in reference 19.

4.7 Boundary Layer Control System and Other Facility Improvements

In 1980 a passive sidewall boundary-layer removal system was installed in the facility. The purpose of this system was to reduce the thickness of the boundary layer in the region of the test section occupied by the model, thus reducing the possibility of sidewall boundary-layer separation at high lift coefficients or high Mach numbers. Experience had shown that this type of separation can be detrimental to the validity of the data obtained during tests of two-dimensional airfoils.

Porous plates were located on both sides of the test section (slightly upstream of the model mounting turntables) and extended the full height of the test section. For the 8 x 24 in (20 x 60 cm) test section, these plates were about 6.00 in. (15.24 cm) long and the downstream edge was located about the same distance upstream of the center of rotation of the turntable. For the 13 x 13 test section, the plates are 6.99 in. (17.75 cm) long and the downstream edge is about 10.75 in. (27.31 cm) upstream of the center of the turntable. These plates are manufactured with a sandwich-type construction. The airstream side consists of a thin plate with small electron-beam drilled holes, the interior contains a honeycomb structure, and the backside consists of a relatively thick perforated plate. A photograph of a magnified sample of a typical plate is shown in figure 20.

A duct system, shown in figure 21, was connected to the back of the porous plate assembly to provide for the removal of the boundary-layer flow. Two control valves were located in the removal lines to control the mass flow removal rate, one valve for each side of the test section. As originally installed, the flow was exhausted to the atmosphere. As a result, the test envelope was restricted since the maximum mass flow removal rate is limited by the liquid nitrogen injection rate required to maintain the test conditions in equilibrium, and the test-section pressure must be above the atmospheric exhaust pressure.

During the 1980 and early 1981 period, a two-story-building addition was constructed adjacent to the facility complex. The first floor of this addition was used to relocate the tunnel controls (figure 22) and provide space for a new on-site data acquisition system (figure 23). The second floor was used to provide space for a shop and model preparation area that could be used while the facility was running. (This two-story addition was enlarged in late 1985 to provide additional model preparation area and on-site office space for the operators and test engineers of the data acquisition specialists.)

4.8 Examples of Airfoil and Other Testing Experience

Igoe of the Langley Research Center made a study of various cooling coils being considered for large cryogenic-pressure tunnels²⁰. The unique features of the 0.3-m TCT provided the capability to assess the aerodynamic behavior of the cooling coils from very low to full-scale Reynolds numbers. A photograph of one of the cooling coil models installed in the two-dimensional test section is included in figure 24. The tube bundle models completely spanned the width of the test section. The pressure drop, flow uniformity, turbulence, and noise characteristics were measured using stagnation and static pressure measurements, thermocouples, two-component hot wire probes, and microphones. Some of the instrumentation is visible in the photograph included in figure 24. The hot wire probes consisted of crossed, platinum-coated 5 micron tungsten wire with an effective length-to-diameter ratio of about 250. (The hot wires were operated in the constant temperature mode.) It is obvious from this instrumentation inventory, that specialized measurements can be considered in cryogenic test environments. On the general subject of instrumentation, a philosophy has been adopted of keeping the various transducers at ambient temperatures if at all possible in order to avoid temperature related changes in zeros and sensitivity. With but few exceptions, if the transducer must be located inside the tunnel, it is insulated and heated to ambient temperature by thermostatically controlled electric heaters. The exceptions are such things as microphones, strain-gage balances during special evaluation tests, and obviously, hot wire probes.

An interesting finding during this study was that at low Reynolds numbers, there is virtually no difference in the turbulence characteristics of the various coil configurations. At full scale conditions, however, an elliptical coil displayed the lower level of turbulence as well as significantly lower pressure loss.

As previously mentioned, the two primary reasons for installing the two-dimensional insert were to evaluate the feasibility of two-dimensional testing at cryogenic temperatures and to take advantage of the high unit Reynolds number offered by a cryogenic-pressure tunnel. The 0.3-m TCT offered a first time experience for testing both conventional and advanced supercritical airfoils at transonic Mach numbers and flight equivalent Reynolds numbers^{21,22}. About 20 different airfoils were tested in this unique facility. These extensive studies represent one of the most systematic, two-dimensional airfoil studies conducted during recent times. (Additional remarks will be presented regarding airfoil testing in the 0.3-m TCT in a following section of this paper.)

A second generation balance was tested in the 0.3-m TCT during a cooperative program between NASA and the NRL of the Netherlands. The results obtained during this study indicated substantial improvements in balance measurements at cryogenic temperatures compared to earlier studies.

Buffet tests were conducted in the 0.3-m TCT to evaluate the use of "conventional" strain gage techniques to measure unsteady wing root bending moments at cryogenic temperatures²¹. The semispan models used in this study were on unswept RAE (NPL) 9510 "peaky" wing and a sharp leading-edge delta wing with 65 degrees leading edge sweep back. The versatility provided by the cryogenic pressure tunnel enabled the researcher, for the first time, to evaluate the Reynolds number effects on buffet at constant dynamic pressures. In addition, the unique cryogenic pressure envelope provided an opportunity to determine the effects of model aeroelastic distortion on buffet at constant Reynolds numbers. (A complete discussion of these tests is presented in reference 23.) The buffet onset conditions determined for the swept back delta wing correlated almost exactly with previously determined research indicating the breakdown of the leading-edge vortex. The "peaky" wing results indicated that in lower Reynolds number range there was a dramatic increase in angle of attack for buffet onset. At Reynolds numbers higher than about 5×10^6 , the angle of attack for buffet onset gradually decreased.

As mentioned earlier, the 0.3-m TCT with its unique capabilities was used extensively in the research of both conventional and advanced airfoils. During the early 1980's, an airfoil research program entitled Advanced Technology Airfoil Test (ATAT) Program was conducted in the 0.3-m TCT. This program was a cooperative effort between the NASA, the U.S. transport industry and the DFVLR of West Germany. A complete description of the overall approach and objectives of this joint effort is presented in reference 24. The program included tests of four correlations, NACA and NASA airfoils, an additional advanced NASA airfoil, six U.S. industry advanced airfoils and three advanced West German airfoils.

Figure 25 presents typical performance and efficiency summary results for one of the program airfoils, the Boeing 1 model²⁵. It is interesting to review in the upper left hand of this figure the effects of transition on airfoil drag at a transonic Mach number from low to flight equivalent Mach numbers. It is also interesting to note the Mach numbers and section normal-force coefficients at which drag divergence occurred for this supercritical class of airfoil. The area to the left of the curve represents the test conditions which can be achieved before encountering the transonic drag rise.

The variations in the Boeing airfoil performance with Mach number and Reynolds number are shown in the right-hand portion of figure 25. In general, these results indicate an increase in the range performance factor, Mn/d_{max} , with increasing Mach number up to conditions where the transonic drag rise results in significant reductions in performance. The dip in the performance curves, most prominent for the low Reynolds number case at a Mach number of about 0.74, is directly related to the low Reynolds number drag-creep phenomenon.

During this era of intense airfoil testing, experience was gained and exported on cryogenic testing skills and model technology. Model technology was advanced in many areas including: the effects of model material instabilities, importance of contour accuracy and pressure orifices size, the expected effects of Reynolds number variations, casting techniques, advanced bonding and pressure channeling methods, and composite structures. In addition, several very significant cost reduction fabrication techniques, such as EDM wire shaping of airfoils, were employed during this important period of cryogenic research.

As additional confidence was gained, the 0.3-m TCT program was expanded to include advanced experimental research on rather elaborate model systems. These studies included many "firsts" such as a cryogenic flutter test, a hot-film investigation, and an extremely complicated oscillating airfoil system test. Considerable success was achieved with these advanced cryogenic model systems. Pierce Lawing will expand on some of the model details in a later paper in this lecture series.

During this period of intense cryogenic wind tunnel research, some of the investigations were supported with information provided by various flow visualization techniques^{26,27}. However, flow visualization is certainly a complicated subject for cryogenic pressure testing and research on this subject should be intensified. Dr. Goodyer will present some future plans on this subject in a later lecture in the series.

4.9 Typical LN₂ Cost for a 1980 Airfoil Program

At the top of figure 26 a typical two-dimensional airfoil test program is presented. This figure also presents a qualitative assessment of average liquid costs for several types of research programs. In the typical airfoil program shown in figure 26(a), the upper boundary represents the Reynolds number capability at the 6 atmosphere, cryogenic temperature conditions. It will be noted from this illustration that the highest density of tests were in the low to moderate Reynolds number range. In the low Reynolds number range for this typical 1980 airfoil program, several tests are scheduled to determine the effects of artificial transition. An early assessment of the effects of artificial transition could have reduced the quantity of high Reynolds number tests required and, in addition may have provided guidance for fixing transition when testing in conventional low Reynolds number wind tunnels. Tests of the NACA 0012 and 0012-64 airfoils in the 0.3-m TCT has indicated that significant scale effects occurred in the Reynolds number range up to 10 million. It will also be noted that this 1980 program included several Mach number, Reynolds number "cuts" which decrease in density at the higher, more costly, Reynolds number conditions.

The three diagonal lines shown in figure 26(b) represent comparative cost rates for a low to moderate Reynolds number program (lowest rate), the typical airfoil program shown in figure 26(a), and a relatively expensive high Reynolds number program. A data point (one angle of attack at one test condition) in this illustration consisted of airfoil upper and lower surface pressure distribution, and a drag coefficient obtained from the traversing momentum rake described earlier. The vertical lines represent: (1) the time required for one data point on an airfoil in the 0.3-m TCT with the 1980 open-loop tunnel control capability, (2) the predicted time per point with computer-based tunnel controls, and (3) the predicted time per point with computer-based controls, an improved data acquisition system, and individual pressure transducers. It should be emphasized that the time required to acquire a data point during this 1980 airfoil program was extremely long compared to other types of testing such as force testing using a strain gage balance.

5. 0.3-m TCT FACILITY WITH ADAPTIVE WALL TEST SECTION

In late 1985 a two-dimensional adaptive wall test section was installed in the basic tunnel circuit (figure 27). This very major modification to the 0.3-m TCT was undertaken by NASA to evaluate the possibility of testing relatively large chord two-dimensional airfoils under nearly interference free conditions. The ability to increase the airfoil chord length while maintaining the high unit Reynolds number capability offered a dramatic increase in the airfoil testing capabilities of the 0.3-m TCT (see figure 28). The design and operational features of this new test section were based on work carried out at the University of Southampton in Southampton, England, under a NASA grant. At the same time that this test section was being installed, the basic length of the circuit was increased by about 94 in. (2.4 m). This increase in length was intended to provide space for a longer and more efficient diffuser and, at some future date, an enlarged diameter contraction section. These modifications were directed toward improvements in the flow quality of the facility. (A preliminary assessment by Igoe of NASA has indicated a significant improvement in the test section flow quality²⁴.)

5.1 General Description

The description here of the 0.3-m TCT facility with the adaptive wall test section (AWTS) installed is brief. Additional information regarding details of the 0.3-m TCT facility prior to, and after the 1985 installation of the AWTS, are available in the literature²⁴.

A photograph of the lengthened tunnel circuit with this test section installed is presented in figure 29 and a sketch is shown in figure 30. The changes which were made during this very major modification included the addition of a new contraction section (with an overall ratio 10.71), a totally new, advanced test section, a new diffuser, and circular "spool" sections to accommodate lengthening the tunnel.

The AWTS is nominally 13 in. (33 cm) square and has an effective length of 55.8 in. (1.42 m). The four walls are solid with only the floor and ceiling flexible. The complete test section is enclosed in a pressure shell which forms a 73.2 in. (1.86 m) long insert into the 0.3-m TCT tunnel circuit (see figure 31).

A system of 21 jacks supports each flexible wall as shown on the schematic diagram in figure 32. The length of the flexible walls is 71.7 in. (1.82 m) with the downstream 15.9 in. (40 cm) providing a smooth transition from the adaptive portion of the test section to the fixed diffuser. The flexible walls are made of 308 stainless steel. The wall thickness varies along the length of each wall to optimize flexibility and resistance to bending due to pressure load. The volume surrounding the entire test section is vented to the test section downstream of the model to minimize pressure loading on the flexible walls.

Individual stepper motors power each wall jack giving a slow wall movement speed of .009 in. (0.24 mm) per second. A dedicated computer controls the displacement of each jack and measures the current position of each jack with an individual Linear Variable Displacement Transducer (LVDT). Both the stepper motors and the LVDTs are mounted outside the pressure shell. The jack mechanisms are therefore isolated from the severe cryogenic environment in the test section. The jack mechanisms are connected to each jacking point on the flexible walls by a pair of push/pull rods. The associated 84 rods penetrate the pressure shell to attach to the flexible walls. Two rods per jacking point are used to minimize unwanted spanwise wall movement.

5.2 Wall Adaption Process

The wall adaption process employed in the 0.3-m TCT is the method suggested by Judd et al which has been validated by extensive tests in the University of Southampton streamlined wall test section. The method uses the measured wall pressures to determine the successive wall contours by a process of minimizing the loading on the wall³⁰. The real time calculation of the final streamlined wall contour is accomplished by a dedicated computer, and the final contour was obtained for most of the cases tested so far within a couple of interactions. It was found during testing of a highly cambered airfoil that by allowing the most upstream jack station to float rather than constraining it to assume the position calculated by the streamlining criterion, it was possible to extend the range of the tunnel streamlining capability to much higher lift coefficients. This was necessary because of the larger thickness of the plate towards the upstream anchoring of the plate to the tunnel frame. Further, this elimination of the first jack from the streamlining process also helped to relieve excessive loads on the motor.

5.3 Airfoil and Other Experiment Studies

Validation tests using two different size NACA 0012 airfoils have confirmed the successful operation of the test section. One model has a chord of 6.5 in. (16.5 cm) and the other a chord of 13 in. (33 cm). The tunnel-height to model-chord ratio for these airfoils is extremely large, i.e. 2.0 and 1.0, respectively. Even with the large model, it was possible to repeat the minimal interference conditions obtained with the small model up to transonic speeds.

Several cambered airfoils have been successfully tested to evaluate the adaptive wall testing technique with large Reynolds number effects present on the model. Of these, two CAST 10 airfoils of 9 in. (22.86 cm) and 7.09 in. (18 cm), were tested as part of co-operative agreements between DFVLR, NAE, ONERA, and NASA. One of the purposes of these agreements has been to investigate data differences due to testing environments and the application of either theoretical or experimental correction techniques, using the same model in different tunnels. The larger chord NAE CAST 10 airfoil was tested in both the NAE two-dimensional facility³¹ and in the NASA 0.3-m TCT. The smaller chord, ONERA-provided airfoil, was tested in both the ONERA T-2 and the NASA 0.3-m TCT AWTs facilities. Some of the early results from this challenging and unique airfoil study are presented in figure 33.

Figure 33 shows results that indicate the general degree of agreement in the data taken on the NAE (porous floor and ceiling) conventional, two-dimensional facility and the NASA, 0.3-m TCT AWTs facility. These particular results were taken at a Reynolds number (based on chord) of 10 million. The NAE 9.0 in. (22.86 cm) model was used on both of these tests. The dramatic difference in the tunnel height (h) to airfoil chord (c) ratios between these two tests should be emphasized here. With the same model for the NAE facility tests the h/c ratio was about 6.7. In the NASA AWTs facility the ratio was only 1.4. This certainly represents a difficult challenge for the AWTs concept considering that the normally accepted height to chord ratios for conventional two-dimensional testing is generally a ratio of 4.0 or larger. The transition was fixed identically for both of these studies. It should also be pointed out that the NAE data has been corrected for wall effects³². The NAE results³³ are shown with the dashed lines and the NASA results³⁴ are indicated by the solid curves.

In general it can be readily seen from this brief summary that the comparisons are remarkably good considering the dramatic difference in the model to tunnel ratios. A preliminary review of these results has indicated that, within the range of attached flow, the maximum differences in angle of attack $\approx \pm .05$, Mach $\approx \pm .0025$ and $C_d = .004$. These and other tests of highly cambered airfoils represent the most ambitious combinations of Mach number, Reynolds number, and lift ever experienced in an adaptive wall test section. Wall "streamlining" has been carried out with normal force coefficients up to about 1.53, angle of attack through stall, and at Mach numbers far beyond drag rise. High chord Reynolds number up to 75 million have been obtained.

In addition to the previously described airfoil tests, the 0.3-m TCT AWTs has been used to study second generation semi-span buffet wings at cryogenic temperatures. A significant amount of NTF support work has been accomplished in support of condensation and other fundamental cryogenic pressure tunnel concerns. At least two assessments have been completed to evaluate the feasibility of using the two-dimensional AWTs to reduce wall interference for three-dimensional tests. A preliminary review of this technique has indicated that this approach is highly feasible.

5.4 Development and Installation of a Residual Correction Method

The test section wall shapes in the fully adapted conditions correspond to free air streamline shapes. Therefore, the wall interference effects on model measurements in the fully adapted conditions are likely to be small. However, factors such as control at a finite number of jack locations, approximations in the wall adjustment technique, and complex flow situations at high incidences can cause departure from totally interference free conditions. The extensive testing over a number of entries of a 9 in. (22.86 cm) chord CAST 10 airfoil in the 0.3-m TCT indicated difficulties³⁵ in obtaining consistently low interference conditions with the wall adjustment method previously employed. The correction to test Mach number blockage effects varied from being negligible to as high as about 0.01. In order to quantify the corrections during the test, an on-line residual interference calculation method was developed and installed as a real-time assessment routine. The objective was to ensure that the walls are adapted to a shape having low interference on model measurements. Also, such on-line calculations help in estimating the residual corrections for hard to streamline test conditions.

The residual interference calculation method³⁰ used in the 0.3-m TCT is based on the two-variable method. The two-variable method requires the distribution of flow velocity and direction along a closed contour surrounding the model. For the adaptive wall tunnels using solid flexible plates, the shape of the closed contours is easily determined by the curved top and bottom wall, and the test section upstream and downstream ends. The measured wall pressures and displacements determine the local flow velocity and direction. Usually measurements are not available along the upstream and downstream ends and some kind of interpolation is necessary. The wall velocities along and normal to the freestream are then integrated using Cauchy's integral formula to give wall induced velocities at the model station. The method does not require knowledge of model forces and is particularly suitable when the model size is relatively large.

The on-line interference calculation method has been successful in the 0.3-m TCT for several tests. The experience gained has substantiated that the 0.3-m TCT adaptive wall test section is capable of testing large models with very low interference levels. The corrections to Mach number and angle of attack are generally less than .002 and .1 degree, respectively, even under test conditions involving large regions of supercritical flow over the airfoil.

5.5 Active Boundary Layer Control Apparatus and Strategy

Shortly after the installation of the passive boundary layer removal system in the early 80's, an effort was commenced to install an active system with a 1000 horse power compression. This system was designed to both remove and reinject flow back into the tunnel circuit. The removal and reinjection plumbing for this system is shown in figure 29.

The maximum amount of mass flow that can be removed from the test section through boundary-layer removal depends on the mode of operation. In the passive mode³⁷, the massflow removed exhausting directly to the atmosphere, the highest removal rate is about 2 percent of the test section flow at transonic Mach numbers. At lower Mach numbers, the removal capability reduces significantly. However, the use of active mode overcomes this limitation and gives much higher removal rates over the entire operating envelop of the tunnel. The highest removal rate in the active mode is about 10 percent of the test section flow at low speeds and reduces to about 4 percent at transonic Mach numbers³⁸. A summary of the total passive and active removal capabilities is shown in figure 34.

The higher removal rates available in the active mode should be employed with caution. The associated changes in the test section Mach number can be large. The boundary-layer measurements made at the model station in the empty tunnel shows that beyond about 2 percent removal, the corresponding reduction in the boundary-layer thickness is not significant. Hence, for most of the test conditions, we feel the removal rate should be kept about 2 percent.

The addition of sidewall boundary-layer removal capability makes the 0.3-m TCT a unique facility for testing airfoils. The cryogenic test conditions, adaptive walls and thin side wall boundary-layers provide almost ideal two-dimensional tunnel test conditions.

The sidewall boundary-layer removal is intended to serve as a tool to examine select data points suspected of significant contamination by sidewall boundary-layer effects. Our experience with several airfoil tests indicates that the sidewall boundary-layer effects on the mid-span pressure distributions may not be significant due to thin sidewall boundary-layers³⁷. Also, considerable care taken in the fabrication of the perforated plate helps to keep the boundary-layer growth to about the same level as over solid smooth plate. This is an important factor since significant thickening caused by certain types of commonly used porous materials might overshadow any actual improvements of the removal system when the boundary-layer is applied.

5.6 Incorporation of a New Pressure Temperature Mach Number Controller

Earlier during this year, Dr. Balakrishna developed, installed, and validated a new Pressure Temperature and Mach automatic controller for the 0.3-m TCT. A computer-generated schematic of this controller is shown as figure 35. This noteworthy task was completed in a period of less than 4 months with very small hardware expenditures. It has functioned remarkably for hundreds of hours and appears to be totally safe. The quality and efficiency of the tunnel operation has improved dramatically and there are definite improvements in certain previously experienced areas of safety concerns. These safety concerns will be addressed in a later lecture and Balakrishna will discuss the technical aspects of our controller in a later paper.

5.7 Operating Costs

The overall efficiency of the 0.3-m TCT has dramatically improved over the past 15 years. Control, instrumentation, data acquisition systems, test techniques and other characteristics have all improved. In so far as LN_2 consumption for a given amount of time there has been a significant improvement in the cost of running. It is believed that there are two major reasons for this sizable improvement: (1) The installation of the improved diffuser and (2) the improved tunnel circuit efficiency gained with the AWTS installation. It would be impossible to provide a quantitative assessment on the two improvements. However, it is conjectured that the diffuser improvement probably accounted for about 70 to 80 percent of the overall improvement with the solid walled AWTS accounting for the remaining 20 to 30 percent. As mentioned earlier, there has also been a definite reduction in the noise and turbulence levels of the 0.3-m TCT. One known fact is that the previous two-dimensional insert diffuser was seriously separated at Mach numbers higher than 0.65.

Figure 36 shows the relationship of tunnel stagnation temperature and pressure with LN_2 consumption. These results are representative of LN_2 consumption with the NAE CAST 10 airfoil installed in the AWTS at test conditions of chord Reynolds number of 18 million at a Mach number of 0.765. The consumption rate for "cooldown" is not considered in the vertical scale at the left of the plot; however, as noted on the figure, it would require about 400 US gallons to cooldown. This figure provides a quick assessment of the effects of pressure and temperature on consumption at a fixed Reynolds number and Mach. For instance, if it was necessary to achieve 18 million at Mach 0.765, would it be better to achieve the desired Reynolds number with pressure or reduced temperature? As derived from figure 36, if we selected pressure at an ambient temperature, our consumption would be about 50 gallons per minute but we would avoid the 400 gallon "cooldown." If we selected to "go cryogenic," we would cooldown with about 400 gallons and our consumption rate at 100 K would only be a modest 10 gallons per minute.

6. CURRENT AND FUTURE PLANS FOR THE 0.3-M TCT

At this time the 0.3-m TCT is temporarily not operating while making several advanced improvements to the AWTs and facility software. The AWTs updates include several new innovative "fixes" to allow larger movements in the flexible walls. These methods include new sliding slots, thinning the walls at selected positions, and improved flexible devices which support and "drive" the flex walls. If these modifications are successful, higher lifts with larger chord model can be achieved. In addition, a considerable number of floor and ceiling static pressure "taps" are being added in preparation for the validation of testing three-dimensional models in a two-dimensional AWTs. Two tests of this type are now planned for late summer 1989. Major software efforts will be made to improve both two-dimensional and three-dimensional strategies. The time required to take an AWTs data point needs to be reduced. An emphasis will be placed on "user friendly" approaches.

The 0.3-m TCT should return to operations this coming July. At that time we will proceed with the three-dimensional validations, measure noise and turbulence, support several NTF requirements, and launch a flow visualization program.

In the autumn of this year, it is planned that the facility will again be modified to include a new rapid diffuser section with honeycombing and multiple screens and a new three-dimensional model support system (see figure 37). During this downtime period, the LN₂ storage and supply system will be reworked to further reduce LN₂ usage and automate most of the LN₂ functions. The LN₂ storage tanks will be elevated to reduce cavitation in the system. The overall thrust of this project is to update our safety status by reducing the need for technicians to be in the LN₂ areas, as well as reducing LN₂ usage and operating time.

In about two years, plans are now approved to totally replace the 1950 vintage 0.3-m TCT drive and electrical systems with solid state equipment and modern technology. In addition, it is planned at that time to improve the tunnel circuit from the test section to the first "turn," install new turning vane designs and strengthen the pressure vessel.

7.0 CONCLUDING REMARKS

It is the opinion of this observer that the 0.3-m TCT "Experience" will be remembered for many years. It is doubted if there will ever again be a period when a dedicated team will design, build, and calibrate a "first time" major facility in a period of about 8 months. Many mistakes were made, but the final analysis will show that a great deal of experience and accomplishment was gained with the world's first cryogenic pressure tunnel. Our collaborative efforts with our European and Canadian partners during this endeavor has been rewarding and educational.

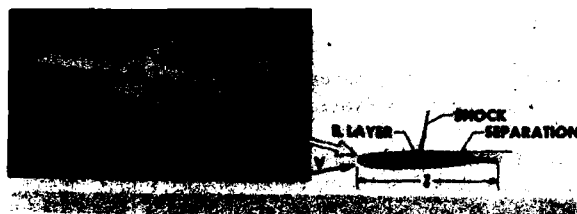
Several observations may be useful here to summarize the accomplishments of the 0.3-m TCT experience. The cryogenic pressure tunnel concept has been proven to be a viable, good way to achieve high Reynolds number results. Two-dimensional testing in cryogenic pressure tunnels is feasible and can provide flight equivalent Mach and Reynolds numbers in a relatively small tunnel. We have not experienced any experimental test technique that cannot be accomplished. Extremely complicated models and apparatus have been tested satisfactorily in the 0.3-m TCT. However, cryogenic pressure flow visualization techniques require much additional work and support. The unique cryogenic pressure tunnel operating envelope has provided a method to solve many problems. Flutter and buffet research appears to be very attractive in this environment due to the versatility of the operating envelope. Instrumentation has presented challenges but no unsolvable situations. Model and test apparatus failures have been dramatically reduced during the 15 years. Cryogenic pressure tunnel control has been dramatically improved and boundary layer control at cryogenic pressure conditions can be accomplished. Significant knowledge has been gained regarding hardware, control strategy and overall approaches for boundary layer removal systems.

8. REFERENCES

1. Goodyer, Michael J.; and Kilgore, Robert A.: **High-Reynolds-Number Cryogenic Wind Tunnel**. AIAA J., vol. 11, no. 5, May 1973, pp. 613-619.
2. Kilgore, Robert A.; Adcock, Jerry B.; and Ray, Edward J.: **Flight Simulation Characteristics of the Langley High Reynolds Number Cryogenic Transonic Tunnel**. AIAA Paper No. 74-80, Jan-Feb, 1974.
3. Kilgore, Robert A.; Adcock, Jerry B.; and Ray, Edward J.: **Simulation Of Flight Test Conditions in the Langley Pilot Transonic Cryogenic Tunnel**. NASA TN D-7811, 1974.
4. Ray, Edward J.; Kilgore, Robert A.; Adcock, Jerry B.; and Davenport, Edwin E.: **Analysis of Validation Tests of the Langley Pilot Transonic Cryogenic Tunnel**. NASA TN D-7828, 1975.
5. Margoulis, W.: **A New Method of Testing Models in Wind Tunnels**. NACA TN-52, 1921.
6. Adcock, Jerry B.: **Real-Gas Effects Associated with One-Dimensional Transonic Flow of Cryogenic Nitrogen**. NASA TN D-8274, Dec. 1976.

7. Kilgore, Robert A.: **Design Features and Operational Characteristics of the Langley 0.3-Meter Transonic Cryogenic Tunnel.** NASA TN D-8304, 1976.
8. Adcock, Jerry B.; and Ogburn, Marilyn E.: **Power Calculations for Isentropic Compressions of Cryogenic Nitrogen.** NASA TN D-8389, 1977.
9. Kilgore, Robert A.; Adcock, Jerry B.; and Ray, Edward J.: **The Cryogenic Wind Tunnel for High Reynolds Number Research.** Paper No. 1, AGARD Fluid Dynamics Panel Symposium on Wind Tunnel Design and Testing Techniques. London, England, Oct. 1975.
10. Hall, Robert M.: **Onset of Condensation Effects with a NACA 0012-64 Airfoil Tested in the Langley 0.3-Meter Transonic Cryogenic Tunnel.** NASA TP-1385, 1979. (Supersedes NASA TM 78666.)
11. Hall, Robert M.: **Onset of Condensation Effects as Detected by Total Pressure Probes in the Langley 0.3-Meter Transonic Cryogenic Tunnel.** NASA TM 80072, 1979.
12. Reubush, David E.: **The Effect of Reynolds Number on the Boattail Drag of Two Wind-Body Configurations.** AIAA Paper No. 75-1294, 1975. Also Reynolds Number Effects on Boattail Drag of Wing-Bodies, *Journal of Aircraft*, Vol. 14, No. 5, May 1977, pp. 455-459.
13. Reubush, David E.: **The Effect of Reynolds Number on Boattail Drag.** AIAA Paper No. 75-63, 1975. Also *Journal of Aircraft*, Vol. 13, no. 5, May 1976, pp. 334-337.
14. Reubush, David E.; and Putnam, Lawrence E.: **An Experimental and Analytical Investigation of the Effect on Isolated Boattail Drag of Varying Reynolds Number up to 130×10^6 .** NASA TN D-8210, 1976.
15. Reubush, David E.: **Effect of Reynolds Number on the Subsonic Boattail Drag of Several Wing-Body Configurations.** NASA TN D-8238, 1976.
16. Reubush, David E.: **Experimental Investigation to Validate Use of Cryogenic Temperatures to Achieve High Reynolds Numbers in Boattail Pressure Testing.** NASA TM X-3396, 1976.
17. Ladson, Charles L.; and Ray, Edward J.: **Evolution, Calibration, and Operational Characteristics of the Two-Dimensional Test Section of the Langley 0.3-Meter Transonic Cryogenic Tunnel.** NASA TP 2749, 1987.
18. Lawing, Pierce L.; Dress, David A.; and Kilgore, Robert A.: **Description of the Insulation System for the Langley 0.3-Meter Transonic Cryogenic Tunnel.** NASA TM 86274, January 1985.
19. **Wind Tunnel Pressure Measuring Techniques.** AGARD-AG-145-70, Dec. 1970.
20. Ray, Edward J.; Ladson, Charles L.; Adcock, Jerry B.; Lawing, Pierce L.; and Hall, Robert M.: **Review of Design and Operational Characteristics of the 0.3-Meter Transonic Cryogenic Tunnel.** NASA TM 80123.
21. Ray, Edward J.: **A Review of Reynolds Number Studies Conducted in the Langley 0.3-m Transonic Cryogenic Tunnel.** AIAA Paper 82-0941, presented at the AIAA/ASME 3rd Joint Thermophysics, Fluids, Plasma and Heat Transfer Conference, St. Louis, MO June 7-11, 1982.
22. Stanewsky E.; Demurie F.; Ray, Edward J.; and Johnson, Charles B.: **High Reynolds Number Tests of the CAST 10-2/DOA2 Transonic Airfoil at Ambient and Cryogenic Temperature Conditions.** AGARD Conference Proceedings, No. 348, September 26-29, 1983.
23. Boyden, R. P.; and Johnson, W. G., Jr.: **Preliminary Results of Buffet Tests in a Cryogenic Wind Tunnel.** NASA TM-81923, July 1981.
24. Ladson, C. L.; and Ray, E. J.: **Status of Advanced Airfoil Tests in the Langley 0.3-m Transonic Cryogenic Tunnel.** *Advanced Aerodynamics*, NASA CP-2208, Sept. 1981, pp. 37-53.
25. Johnson, W. G., Jr.; Hill, A. S.; Ray, E. J.; Rozendaal, R. A.; and Butler, T. W.: **High Reynolds Number Tests of a Boeing BAC1 Airfoil in the Langley 0.3-m Transonic Cryogenic Tunnel.** NASA TM 81922, April 1982.
26. Gartrell, Luther R.; Gooderum, Paul B.; Hunter, William W., Jr.; and Meyers, James F.: **Laser Velocimetry Techniques Applied to the Langley 0.3-Meter Transonic Cryogenic Tunnel.** NASA TM 81913, April 1981.
27. Snow, Walter L.; Burner Alpheus W.; and Good William K.: **Improvement in the Quality of Flow Visualization in the Langley 0.3-Meter Transonic Cryogenic Tunnel.** NASA TM 87730, August 1983.

28. Wolf, S. W. D.; and Goodyer, M. J.: **Self Streamlining Wind Tunnel - Low Speed Testing and Transonic Test Section Design.** NASA CR-145257, 1977.
29. Wolf, S. W. D.: **Self Streamlining Wind Tunnel - Further Low Speed Testing and Final Design Studies for the Transonic Facility.** NASA CR-158900, 1978.
30. Wolf, S. W. D.; Ray, Edward J.: **Highlights of Experience with a Flexible Walled Test Section in the NASA Langley 0.3-Meter Transonic Cryogenic Tunnel.** NASA TM 101491, September 1988.
31. Ohman, L. H.: **The NAE High Reynolds Number 15 in. x 60 in. Two-Dimensional Test Facility. Part 1. General Information.** NRC/NAE Laboratory Technical Report LTR-IIA-4, April 1970.
32. Mokry, M.; and Ohman, L. H.: **Application of Fast Fourier Transform to Two-Dimensional Wind Tunnel Wall Interference.** Journal of Aircraft, Vol. 17, No. 6, June 1980, pp. 402-208.
33. Chan, Y. Y.: **Wind Tunnel Investigation of the CAST-10-2/DOA-2 12% Supercritical Airfoil Model.** NAE Laboratory Technical Report LTF-IIA-5x5/0162, May 1986.
34. Mineck, Raymond E.: **Wall Interference Tests of a CAST 10-2/DOA 2 Airfoil in an Adaptive-Wall Test Section.** NASA TM 4015, November 1987.
35. Murthy, A. V.; and Ray, E. J.: **Experience with Some Repeat Tests on the 9" Chord CAST 10-2/DOA2 Airfoil Model in the Langley 0.3-Meter TCT Adaptive Wall Testsection.** Paper presented at the CAST10-2/DOA2 Airfoil Studies International Workshop, Langley Research Center, Hampton, Virginia, September 23-27, 1988.
36. Murthy, A. V.: **Residual Interference Assessment in Adaptive Wall Wind Tunnels.** NASA Contractor Report (to be published).
37. Murthy, A. V.; and Ray, E. J.: **Sidewall Boundary-Layer Removal Effects on Wall Adaptation in the Langley 0.3-m Transonic Cryogenic Tunnel.** AIAA Paper 89-0148, January 1989.
38. Balakrishna, S.; Kilgore, W. Allen; and Murthy, A. V.: **Performance of the Active Sidewall Boundary-layer Removal System for the Langley 0.3-Meter Transonic Cryogenic Tunnel.** NASA Contractor Report 181793, February 1989.
39. Balakrishna, S.; and Kilgore, W. Allen: **Microcomputer Based Controller for Langley 0.3-Meter Transonic Cryogenic Tunnel.** NASA CR 181808, March 1989.



- FLIGHT VELOCITY
SOUND VELOCITY = $\frac{V}{c}$ MACH NO. (M)
- INERTIA FORCES
VISCOUS FORCES = $\frac{\rho V L}{\mu}$ = REYNOLDS NO. (R)

Figure 1. - Flow similarity parameters

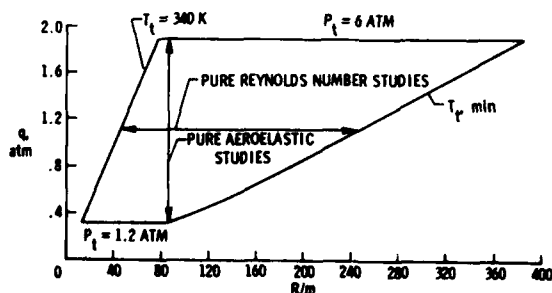
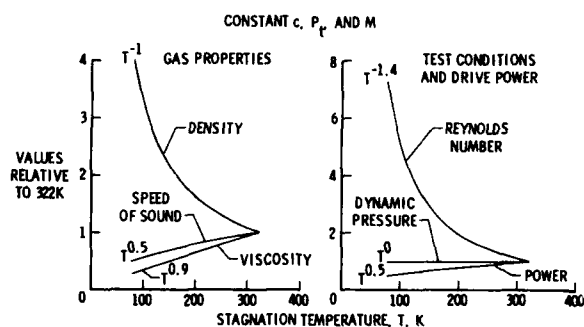
Figure 3. - A typical cryogenic pressure tunnel operating envelope, $M_{\infty} = 0.85$.

Figure 2. - The cryogenic tunnel concept.

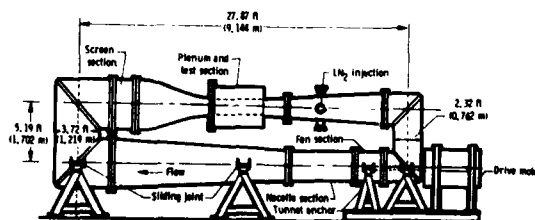


Figure 4. - Sketch of the 0.3-m TCT with three-dimensional test section installed.

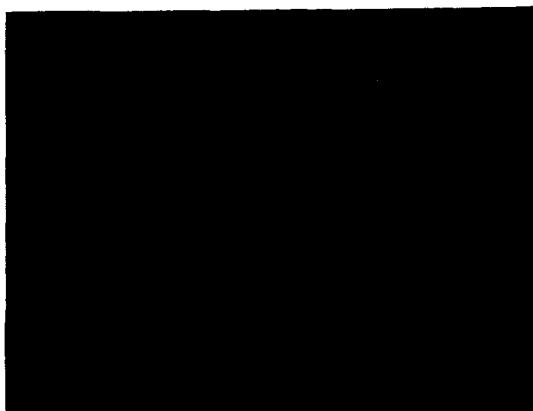


Figure 5. - Original insulation technique.

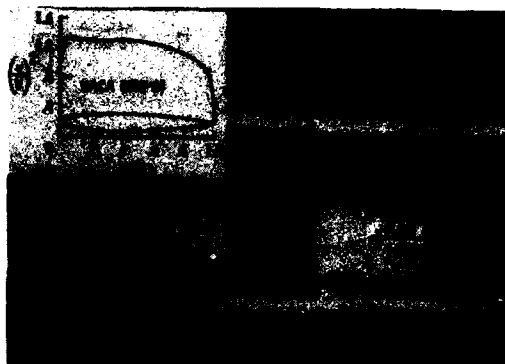


Figure 6. - Photograph of the proof-of-concept model installed in the three-dimensional test section.

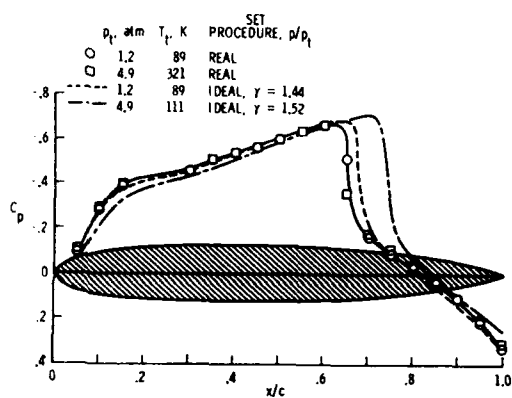


Figure 7. - Typical results obtained during proof-of-concept study.



Figure 8. - Photograph of temperature survey rig installed in the screen section of the tunnel.

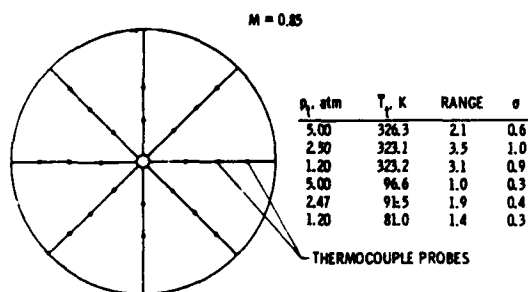


Figure 9. - Typical temperature results obtained from the temperature survey rig.

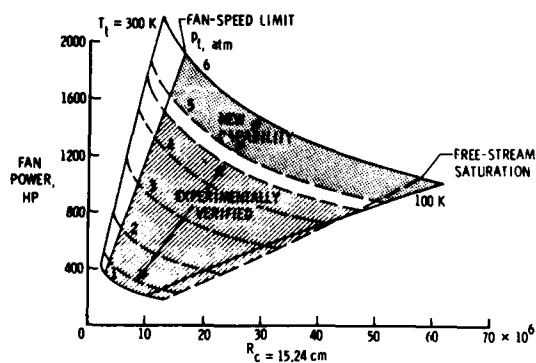


Figure 10. - Fan power - Reynolds number map for the 0.3-m TCT.

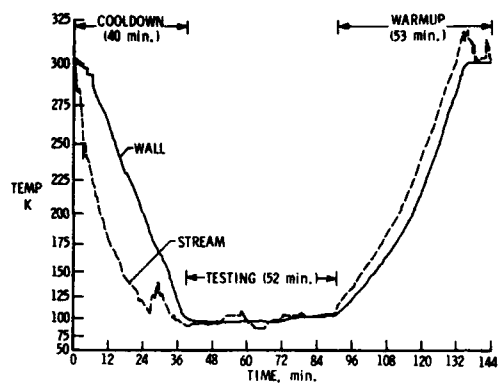


Figure 11. - Wall-stream temperature variation during typical run.



Figure 12. - Nitrogen gas exhaust plume with ejector stacks.

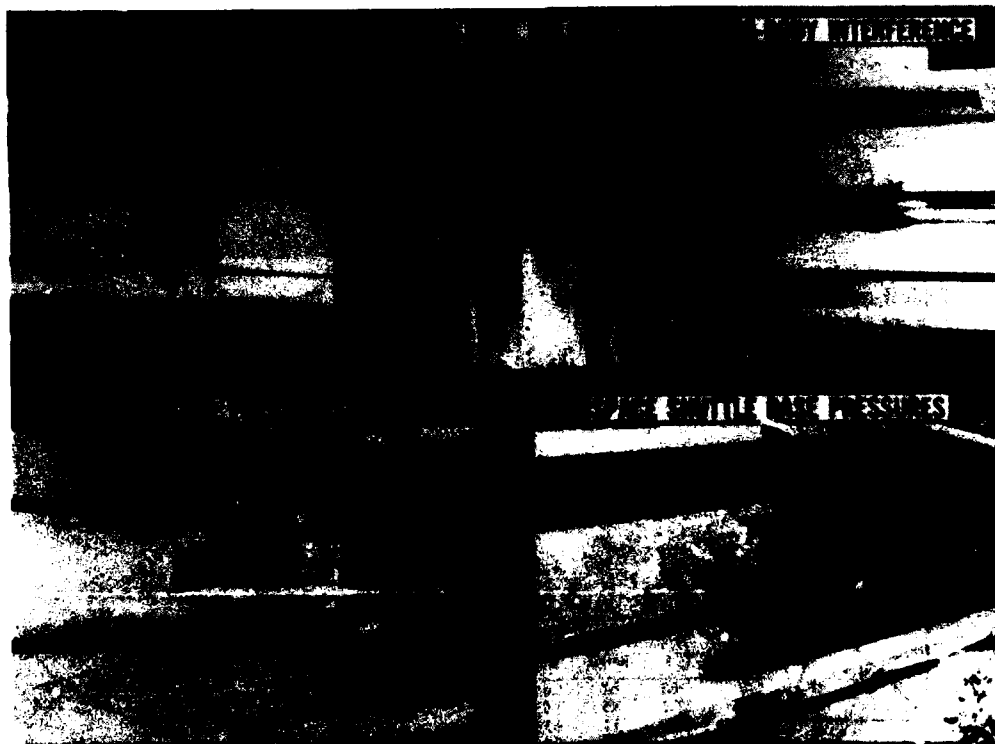


Figure 13. - 0.3-m TCT tests in the three-dimensional test section.

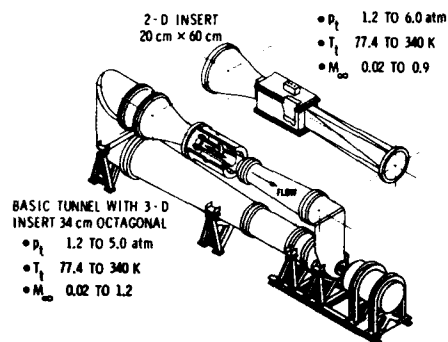


Figure 14. - Interchangeable test section feature. Three-dimensional and two-dimensional test section inserts.

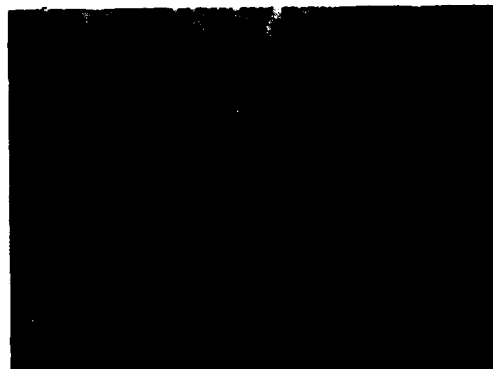


Figure 15. - Photograph of the 0.3-m TCT with the two-dimensional test section installed.

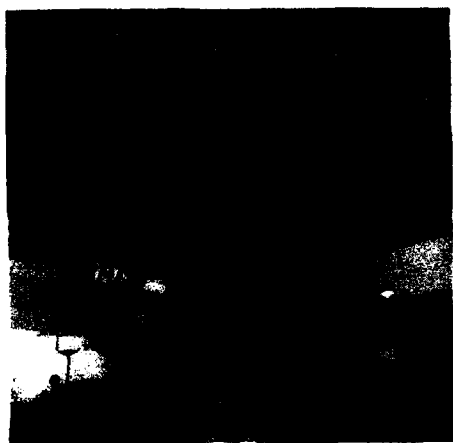


Figure 16. - Removable model module feature of the two-dimensional test section.

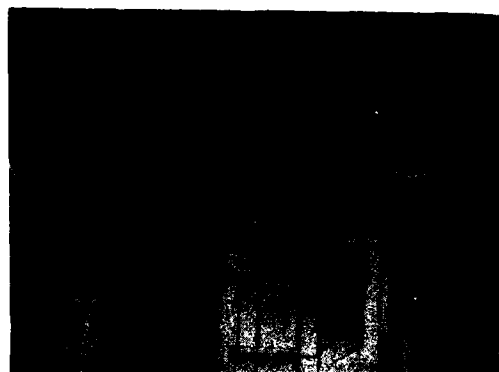


Figure 17. - Top view of the two-dimensional test section.

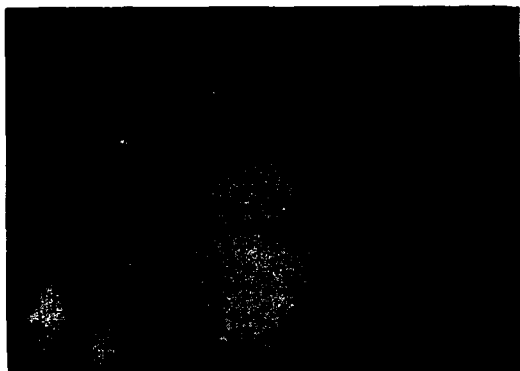


Figure 18. - Current insulation technique.

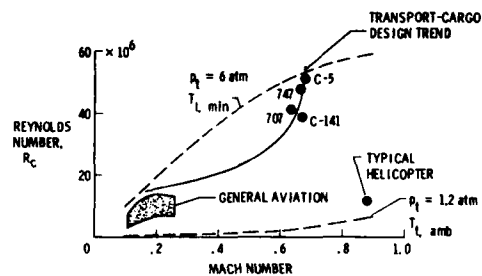


Figure 19. - Reynolds number capability of two-dimensional test section of the 0.3-m TCT.

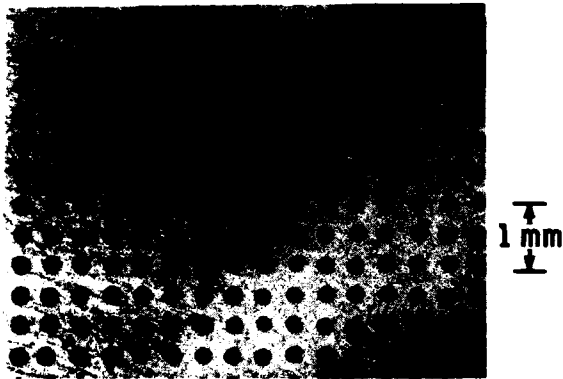


Figure 20. - Magnified photograph of porous plate used in boundary-layer removal system.

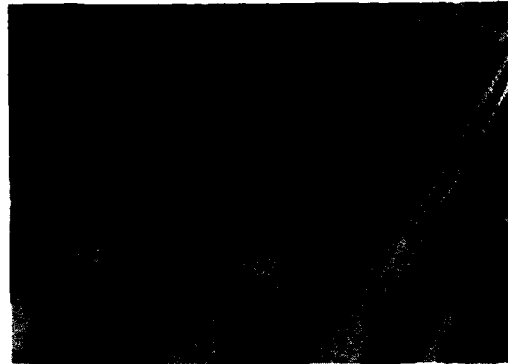


Figure 21. - Photograph of two-dimensional test section showing details of boundary-layer removal plates.



Figure 22. - Photograph of data acquisition system and tunnel control consoles.

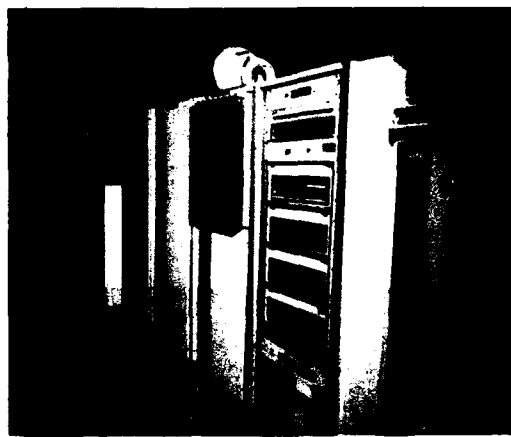


Figure 23. - Photograph of arrangement of data acquisition system in current control room.



Figure 24. - 0.3-m TCT tests in the 20 cm by 60 cm, two-dimensional test section.

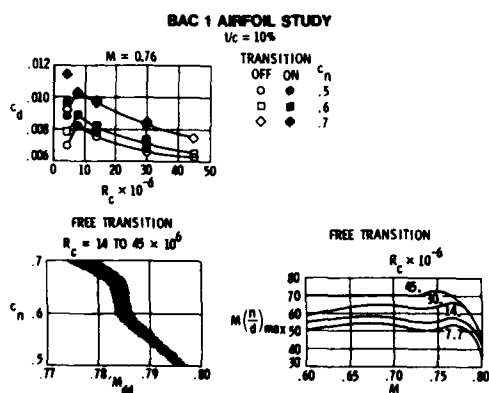


Figure 25. - Boeing 1 airfoil study. Thickness to chord ratio, $t/c = 10\%$.

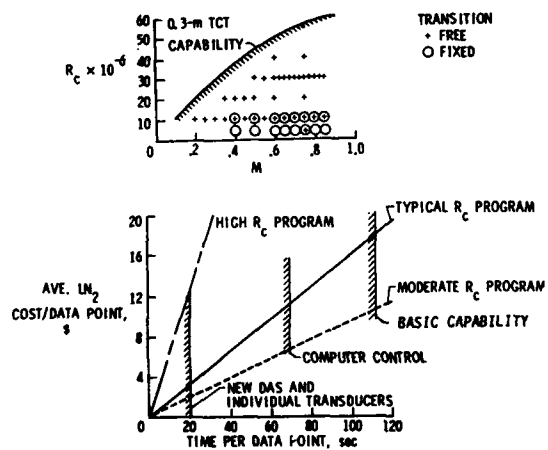


Figure 26. - Typical 1980 airfoil test program and liquid nitrogen cost trends.

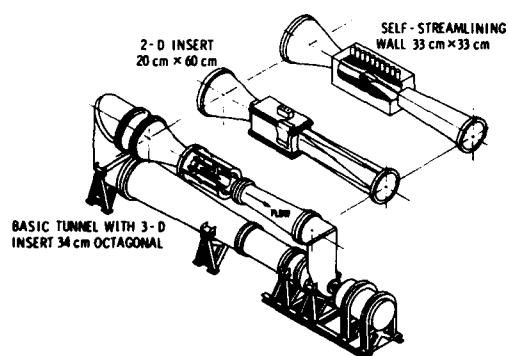


Figure 27. -Interchangeable test section feature, three-dimensional, two-dimensional, and flexible wall inserts.

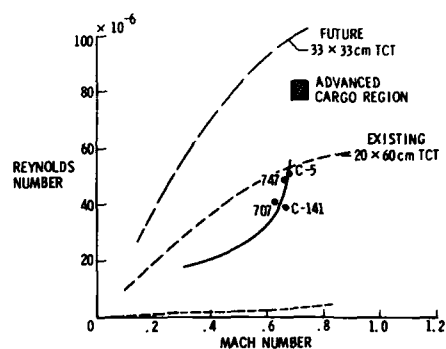


Figure 28. - Airfoil test capabilities of the 0.3-m TCT with the flexible wall insert installed.



Figure 29. -Photograph of the 0.3-m TCT with the flexible wall test section.

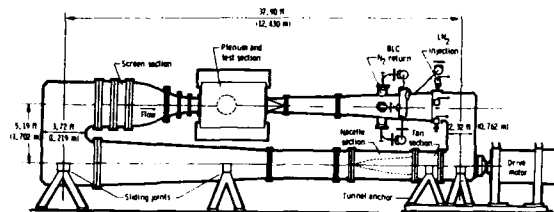


Figure 30. - Sketch of the 0.3-m TCT with the flexible wall test section installed.

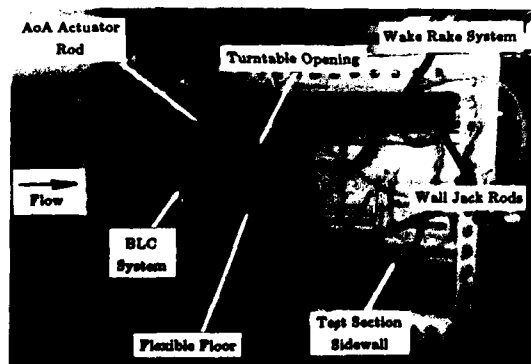


Figure 31. -View of the flexible wall AWTS with plenum wall removed.

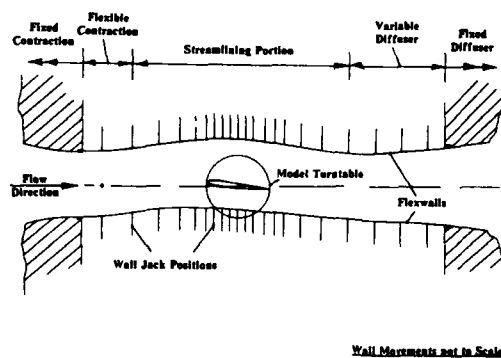


Figure 32. - Schematic diagram of the flexible walled AWTS.

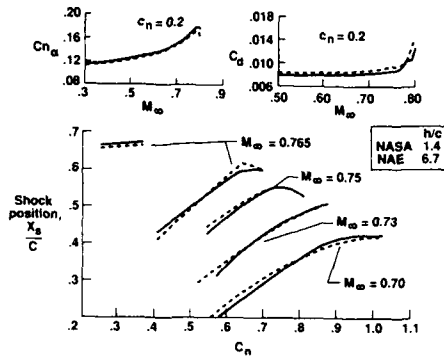


Figure 33. -Comparison of NAE and NASA CAST 10 airfoil results. NAE 9-inch (22.86 cm) airfoil tested in both the NAE two-dimensional and NASA 0.3-m TCT AWTS.

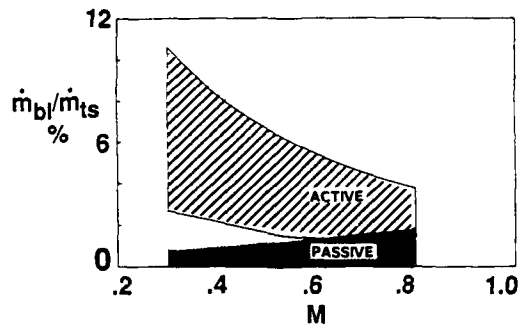


Figure 34. -0.3-m TCT sidewall boundary layer removal capability. Empty test section.

	LN PUMP AUTO	TEMP LOOP AUTO	Pt/Re LOOP AUTO	RPM/MACH LOOP AUTO
LN2 Flow	117.6, psia		68.00, Psia 20.06, Mils/Chrd	0.765, Mach 2400, RPM
LN2 Temp	117.6, psia		68.00, Psia 20.06, Mils/Chrd	0.765, Mach 4412, RPM
LN2 Pressure	77.3, %open		40.0, % open V1 0.0, % open V2	59, % Rhat
LN2 Level	B=		Pres= Ryso= AGV%= Chrd=	Mach= Nrpm=
			CHORD= .2286, m Pstat=46.16, psia Del P= 0.00, psi	

Figure 35. -Computer generated schematic of new 0.3-m TCT, P-T-M controller.

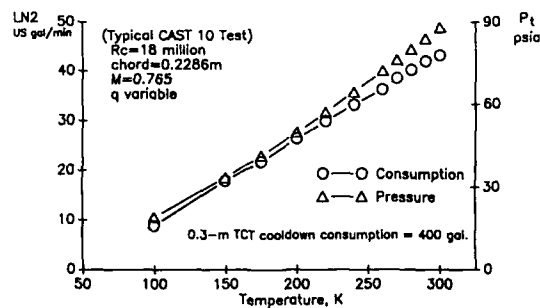


Figure 36. - Effects of temperature and pressure on LN₂ consumption in 0.3-m TCT.



Figure 37. -Schematic of 0.3-m TCT with AWTS, rapid diffuser section, and three-dimensional sting support.

THE U.S. NATIONAL TRANSONIC FACILITY, NTF

by
Walter E. Bruce, Jr. and Blair B. Gloss

NASA, Langley Research Center
Hampton, VA 23665-5225
U.S.A.

SUMMARY

The construction of the National Transonic Facility was completed in September 1982 and the start-up and checkout of tunnel systems were performed over the next two years. In August 1984, the Operational Readiness Review (ORR) was conducted and the facility was declared operational for final checkout of cryogenic instrumentation and control systems, and for the aerodynamic calibration and testing to commence. Also, the model access system for the cryogenic mode of operation would be placed into operation along with tunnel testing.

Since the ORR, a host of operating problems resulting from the cryogenic environment have been identified and solved. These range from making mechanical and electrical systems functional to eliminating temperature induced model vibration to coping with the outgassing of moisture from the thermal insulation. Additionally, a series of aerodynamic tests have demonstrated data quality and provided research data on several configurations.

This paper will review some of the more significant efforts since the ORR and summarize the NTF status concerning hardware, instrumentation and process controls systems, operating constraints imposed by the cryogenic environment, and data quality.

SYMBOLS

c	Chord
C_L	Lift coefficient
C_N	Normal force coefficient
c_p	Pressure coefficient
HP	Horsepower
LN_2	Liquid Nitrogen
M	Mach number
\bar{p}	Root mean square value of fluctuating component of static pressure
p_∞	Free stream static pressure
P_T	Total pressure
q	Dynamic pressure
R_c	Reynolds number based on chord
T	Temperature
T_T	Total temperature
U	Streamwise mean velocity
\bar{u}	Root mean square value of fluctuating component of U
W	Wall angle
x	Distance measured from wing leading edge in streamwise direction
α	Model angle of attack

INTRODUCTION

The United States' National Transonic Facility (NTF) which was constructed by NASA with a goal of meeting the national needs for high Reynolds number testing has been operational in a checkout and test mode since the facility was declared operational in August, 1984. The order of magnitude increase in Reynolds number over existing transonic wind tunnels provided by the NTF, figure 1, is the result of operating at cryogenic temperature and stagnation pressures to 8.8 atmospheres. Although the cryogenic temperatures provide significant and well documented benefits from a Reynolds number standpoint, the harsh environment provides equally significant challenges for reliable operation of large mechanical systems and instrumentation.

The approach followed since the Operational Readiness Review (ORR) of operating in a combined checkout and test mode had some obvious advantages for a facility like the NTF where there is not a significant experience base. Known problems can be solved while identifying and solving those problems that will only show up by using the tunnel in a testing mode. The end result is a fully operational facility at an earlier date. However, there are also some disadvantages. Most significant among them is that aerodynamic calibration and testing during this time period is at a much reduced level of efficiency.

Since the ORR, a host of operating problems resulting from the cryogenic environment have been identified and solved. These ranged from making mechanical and electrical systems functional to eliminating temperature induced model vibration to coping with the outgassing of moisture from the thermal insulation. Additionally, a preliminary flow calibration has been completed and a series of aerodynamic tests have demonstrated data quality and provided Reynolds number effects on several configurations. During the summer of 1988, a major effort was devoted to improving operating efficiency in order to efficiently support both research and development testing requirements.

In January 1989, a metal band surrounding the fan drive shaft broke loose which dislodged several other metal components located near the leading edge of the fan blades. These metal parts damaged all 25 fan blades beyond use. Currently, structural repairs and new blades are being made with plans to return to operational status in October 1989.

The initial start-up and checkout of the NTF system (before the ORR) are well documented^{1,2,3}. This paper will review some of the more significant efforts since this time and summarize the NTF status concerning hardware and instrumentation systems, operating constraints imposed by the cryogenic environment, data quality, and process controls.

TESTING AND CHECKOUT EXPERIENCE

The testing and checkout experience is summarized in figure 2. As stated previously, the testing that has been accomplished to date had a twofold purpose of providing aerodynamic data and exposing testing problems associated with the tunnel and instrumentation systems. Nine of the configurations tested are shown in figure 3 which collectively utilized the maximum capability of the NTF in both the air and cryogenic modes of operations over the Mach number range. The primary model used for checkout of both tunnel and instrumentation systems was the Pathfinder I which has a high aspect ratio wing with a supercritical airfoil. This model was first installed in the tunnel in December 1984.

The major areas which received attention during the checkout are listed at the bottom of figure 2 and involved model access system, process controls, moisture in the tunnel, model vibration, and tunnel/test instrumentation. All of these problems were worked simultaneously as indicated by the chart and were phased in with the testing schedule as appropriate. The tunnel was unavailable for cryogenic operation during the first half of 1987 due to a malfunction of a thrust balanced type expansion joint in the liquid nitrogen piping system.

MODEL ACCESS

Access to the model requires the movement of large components within the tunnel (figures 4, 5, and 6) over the temperature range from ambient to fully cryogenic. The details of this system are defined in references 3 and 5. The test section plenum may be isolated from the rest of the tunnel circuit by large isolation valves. The process of putting these valves in place involves unlocking and translating a large section of the contraction cone and the high speed diffuser away from the plenum; this process uses dual electrical driven actuators on each component with a seven-foot stroke which must operate in phase. Additionally, the ability to make up limit switches or components to fairly close tolerance where the components may be exposed to large temperature excursions is required. With the plenum vented to atmospheric pressure, the 9- by 12-foot plenum doors in the pressure shell are opened and the test section sidewall doors are lowered so that access housings may be inserted to encapsulate the model as shown in figures 5 and 6. The reliable movement of these large components at cryogenic temperatures has required several modifications to the basic actuation concept. These modifications have resulted from operational experience and were implemented over the past years. Final modifications to the doors in 1988 provided for successful operation.

Also during 1988, vapor lock rooms were installed at the entrance to each of the 9- by 12-foot plenum door (figure 7) to prevent frost or ice from forming on the outside surface of the access housings and on the 9- by 12-foot door around the pressure seals. The vapor lock rooms are constantly purged with dry air having a dew point of -55° F to -80° F. Figure 8 is a

view with the access housings inserted with the tunnel circuit approximately -225° F; a normal work environment is provided inside the access housings and, as can be seen in the figure, the inside walls of the access housings are also frost free.

During the checkout of the access housings, model heating procedures were being developed. In general, the most difficult part of the model to warm is the strain gage balance, and this component is currently being warmed to a temperature above the dew point of the environment during the access period. Figures 9 and 10 are for the same event and show typical temperature warm up profiles for a transport model.

PROCESS CONTROLS

The primary controls for the tunnel are electrical-hydraulic closed loop interactive systems which provide fast response for control of pressure, temperature, and Mach number (figure 11). The controls for the test section variables (tunnel walls and re-entry flaps) are also closed loop, have slower response, and are driven by electrical operated ball screw jacks. The model attitude is also controlled by closed looped systems, the pitch being a fast response electrical-hydraulic type and the roll being driven by an electrical motor system.

A description of the process controls is provided in reference 6 and will not be repeated here in any detail. In summary, however, the approach used in design of the pressure, temperature, and Mach number controls involved developing a mathematical model of the tunnel process with controls to determine circuit response characteristics in order to establish the design criteria for the control hardware and the initial control laws. This approach, as indicated in figure 12, required measurement of actual tunnel response characteristics for verification of the control laws and update of the math model. This effort was a first priority in the early tunnel operation and indicated that the control precision of design could not be obtained due to insufficient system resolution and excessive instrumentation noise. To correct this problem, the micro-processors, servo control valves, and instrumentation were upgraded. The upgraded stagnation pressure and Mach number control system were completed in the first half of 1987 and the temperature control system around the beginning of 1988. The basic Mach number control loop is shown in figure 13. The system controls the pressure ratio (test section plenum to settling chamber) for the desired test section Mach number by either varying the fan speed or the inlet guide vanes angle at the fan. Currently, the fan speed is set at a constant RPM to cover the desired Mach number range and the inlet guide vanes are automatically controlled to maintain Mach number. The response of the Mach Number system to a step input of plus and minus 0.02 ΔM is given in figure 14. As can be seen, the Mach number steady state condition is controlled within plus or minus 0.001 of set point.

The basic pressure control loop is shown in figure 15. The system controls the pressure in the settling chamber by regulating one or two 24 inch diameter vent valves. The response of the pressure system to a step input of plus and minus 4.5 psid is given in figure 16. The steady state condition is controlled to within plus or minus 0.1 psi of set point.

The temperature control loop is shown in figure 17. This system was initially based on measuring the liquid nitrogen flow rate entering the tunnel. However, minimal success was obtained in making this measurement and an alternative approach which calculates the flow rate required for set point has been recently implemented. Figure 18 gives response of system to a step input of 2° F. The steady state condition is controlled to within plus or minus 1° F of set point.

For all three of the above process control systems, the control loops have been adjusted for obtaining steady state set points to a very high accuracy level. For the pressure system, the transient response has been optimized to minimize time required to obtain set points. This effort is yet to be performed for the Mach and temperature control loops.

MOISTURE CONTAMINATION

During the early operation of the NTF at cryogenic temperatures a coating was observed on several models that had a frost like appearance. Quantifiable measurements of the extent of the coating were not available. However, it was clear that frost like crystals were forming and that reflected light was making it visible with a television system. An extensive study was undertaken to determine what the contaminating substance was and its source as well as its possible effect on the aerodynamic data.⁷ This study identified the contaminant to be water.

Further evaluation of the incoming liquid nitrogen, various tunnel purge techniques, and samples of the thermal insulation system identified the thermal insulation as the water source. The closed cell polyisocyanurate foam used for the thermal insulation has been shown to have approximately 1.5 percent water by weight. (As a reference, dry wood has approximately 6 percent water by weight). The problem, as shown in figure 19, is that at the cryogenic temperatures only a very small quantity of water is required to saturate the stream. For example, at -70° F only about 0.2 pounds of water is required to saturate all of the gas in the tunnel at atmospheric pressure while at +70° F about 200 pounds of water is required. Two questions naturally arise at this point. How to eliminate the moisture, and what is its effect on the aerodynamic data measurements? Extensive investigations have been conducted in both areas. With regard to the question of eliminating the moisture, the studies have indicated that the simplest solution appears to be drying the tunnel. The diffusion of water from the insulation in the NTF is a function of temperature as indicated in figure 20, and, as would be expected, there is a reduction in diffusion with decreasing temperature which is of course a favorable effect. Aerodynamic studies conducted with frost like coating on the model, which will be discussed later, have indicated that the resulting effects on the aerodynamic data are not measurable. Therefore, a dry air supply system has been installed in the tunnel circuit that

will always preclude atmospheric air from entering, even for maintenance. In addition, the vapor lock rooms installed at the entrance to the test section, see figure 7, also precludes atmospheric air from entering the tunnel for all operational modes of the facility. Hence, the drying process takes place in static as well as operating conditions; therefore, the insulation continues to dry over weekends and non-working shifts. This drying process has been successful and during the last cryogenic tunnel operation, there were no indications of frost on the model during testing.

MODEL VIBRATION

Significant vibration of the model/balance combination in the lateral plane has been encountered at some conditions since the initial testing of models in the NTF. After some period of operation the vibration was found to be influenced by the internal structural temperature. The vibration was more severe when the structure had been cold soaked for one day or more. The model pitch system is illustrated in figure 21 and is composed of an arc sector driven by a hydraulic cylinder. Restraint is provided by a series of bearing pads located at both the top and bottom of the sector. The loads are transmitted through the pads to the internal tunnel structure. There is also a fairing on the downstream part of the sector that is fixed to the tunnel structure and provides a cavity initially designed for instrumentation leads. The attachment of the fixed fairing to the arc sector is a slip joint which allows the sector to move independently of the fairing. The bearing pads, while providing restraint, also have clearance to allow for thermally induced movement of the bearing support.

The vibration problem has been investigated both experimentally and analytically. In the experimental investigation, the Pathfinder model was used as a test vehicle. Both it and the model support system were extensively instrumented as follows:

- a. Six component force balance and 3-axis accelerometer package in Pathfinder model.
- b. Pressure transducers in fixed fairing and test section walls.
- c. Accelerometers on fixed fairing, bearing pads, and the surrounding tunnel support structure.
- d. Strain gages and thermocouples on tunnel support structure.

The analytical investigation involved detailed calculations of the dynamic structural response and of the unsteady aerodynamic characteristics of the model support system.⁸

Experimental measurements were made of the dynamic structural response characteristics, Mach number, dynamic pressure, test temperature, and cold-soak time. The installation of vortex generators and splitter plate on the fixed fairing afterbody helped to identify it as one of the sources of dynamic excitation. Eventually, the primary factor governing the dynamic response of the model was found to be the clearance tolerance between the bearing pads and the surface of the arc sector. A procedure was evolved for setting the clearance adjustment which reduced the model dynamic response to acceptably low levels independent of temperature cycling. Some of the test results are illustrated in figure 22 by showing the dynamic yawing moment as a function of stagnation temperature for several of the test configurations of the arc sector.

Although the low level shown in the figure for the last case is completely satisfactory, the bearing pads may be sensitive to adjustment with time due to temperature cycling.

INSTRUMENTATION

For several years prior to initial operation of the NTF, an extensive research and development program was undertaken by the Instrument Research Division at Langley^{9,10,11} to develop instrumentation systems for basic measurements of forces and moments, pressures, and angle of attack that would function with both reliability and accuracy in the cryogenic environment. The results of this program were the development of strain gage balances that were not temperature controlled and heated instrument packages for pressure and angle of attack measurements. These instrument systems were developed in cryogenic chambers and verified to the extent possible in the 0.3-Meier Transonic Cryogenic Tunnel and indicated good performance and soundness of the basic concepts. Upon application of these instruments to models in the NTF, there were several system problems that had to be resolved. The most significant of these problems were the effect of leads, to support the pressure instrumentation system, on the balance axial force component and the calibration system for the electronic scanning pressure (ESP) system. Tests in the NTF cryogenic checkout chamber have indicated satisfactory direction for solving these problems.

A strong concern from the outset has been data quality. In this regard, an extensive effort has been carried out to eliminate data scatter due to electrical noise and extraneous signals.¹² Care was taken from the beginning to provide a "clean" instrumentation ground, but as is often the case, extraneous electrical signals can creep into the system. A significant effort has been ongoing over the past year to identify, locate and eliminate noise sources that were infiltrating the data system.

The results of this effort in terms of electrical noise for a six-component balance is shown in figure 23 and in terms of standard deviation in figure 24 (the data represents 50 sample average). The test cases are data taken: prior to any corrections being made (Test 14); after the implementation of power and grounding system changes (Test 17); after

completion of improvements in shielding and guarding (Test 23); and after elimination of EMI/RFI noise (Test 27). The effect of corrective measures can clearly be seen as a reduction in data scatter by a factor of 5.

Figure 25 shows, in engineering units, the 95% confidence limits for 5, 10, and 50 sample averages for the balance components prior to system modifications. Figure 26 shows the same data following completion of all modifications. In a comparison of figures 25 and 26, the extent of the improvement in performance becomes very apparent; the 95% confidence limits for five sample averaging after modifications is significantly better than that achievable with 50 sample averaging at the outset.

OPERATING CONSTRAINTS

The NTF has the general appearance and is often talked about as a typical continuous operating fan-driven wind tunnel that has the potential to mass produce data on a continuous basis. Although in principal the potential exists, it is somewhat misleading to think about a large cryogenic tunnel in this context. In reality, the operation must be viewed much as a blow-down tunnel with efforts directed toward minimizing run time and maximizing data gathering rates. The main constraints with regard to run time are liquid nitrogen logistics and costs, and model access. It was shown in the early 1970's that the application of cryogenics to wind tunnel testing provided the most cost effective approach to high Reynolds number testing. This does not mean, however, that testing at high Reynolds numbers will carry the same cost and degree of complexity as testing in the many ambient temperature and pressure tunnels around the country. This is illustrated in figure 27 where the energy cost ratio (liquid nitrogen is a form of energy) is shown as a function of Reynolds number ratio for the NTF compared to the Langley 16-Foot Transonic Tunnel. An order of magnitude increase in Reynolds number has an energy cost ratio of approximately 44. Nevertheless, in the cases where high Reynolds number is required for research or development testing, the cost is very economical, especially when compared to flight testing. However, since the NTF is more costly to operate than conventional tunnels, test programs and objectives must be carefully defined and supported by adequate precursor studies at low Reynolds numbers.

The LN₂ supply system has been sized to support an annual testing productivity capability based on typical test programs, facility operating schedule and budget. Hence, for any one day or time during a test program, the LN₂ quantity available may not satisfy that desired. The operating profile for the NTF is given in figure 28; this is based on operating 16 hours per day for five days per week.

Liquid nitrogen is supplied to the NTF by a commercial air separation plant located adjacent to the Langley property and connected to the NTF site by a pipeline. The capability of this system is shown in figure 29. The challenge is to optimize the interface of the plant, which operates continuously 24 hours per day at a 300 ton per day rate, with the intermittent operation of the NTF which can use LN₂ to a maximum rate of 30 tons per minute. This requires, of course, storage tanks to serve as a buffer. The current system has a 2100 ton storage tank at the plant and a 700-ton tank (nominal LN₂ available for use) located at the NTF with capability to transfer approximately one tank per 24-hour day. The system can sustain a use rate of 2,100 tons per week and if the tunnel has not been using nitrogen for a while, this can build up to a maximum quantity available of 4,800 tons for a week. This tends to optimize on two-week test programs using liquid nitrogen assuming all tanks are full at the start. As shown in figure 30, if operation is started on Monday morning with four equivalent NTF tankfulls available and used at a rate of 1 tank per day with 0.5 tanks being resupplied by the plant and no use over the weekend, the total supply is exhausted by the end of the second week. The options at that point are either to operate on one-half tank per day (the plant output) which is not practical or to allow 8 days for the nitrogen supply to be replenished and use the tunnel in the air mode or change models or some other capacity during this period. This use senerio can be changed, of course, by increasing the plant capacity and/or storage and transfer rate. A decision to increase the plant capacity must take into consideration long-term use rates. The most immediate benefit will be provided by an increase in storage capacity and associated transfer rates.

The most important aspect of the tunnel operation from cost considerations is the speed of changing test conditions and data acquisition. This is driven primarily by the degree and quality of automation. Figure 31 illustrates the impact of time per data point for a typical test condition of $M = 0.8$ and temperature = -250°F . The bottom illustration, figure 31, is the total cooldown and pressurization cost. The top illustration, figure 31, is the cost per data point as a function of R_c for various times per data point which includes time to change angle of attack, Mach number, temperature pressure and acquire data. When the NTF was first brought on-line manually, times averaged greater than 45 seconds per point. After the enhancement period during the summer of 1988, the time average was around 30 seconds per point with a goal to further reduce time with further refinements in the control and operating system. The liquid nitrogen cost is large compared to electricity as shown in figure 32, and hence, is the primary factor controlling operating cost.

For efficient and effective use of the NTF, special operating requirements and considerations have been established as outlined in figure 33.

DATA QUALITY

In this section the status of flow calibrations and efforts to assess data quality will be discussed. The discussion will include both steady and dynamic aspects of the flow calibration, the ability to measure Mach numbers and angle of attack, importance of wall boundary effects, and the effect of moisture contamination or "frost" on the data.

Flow Calibration

As reported previously, references 3 and 13, the NTF has been operated throughout the operating envelope as shown in the upper left of figure 34. The initial calibration looked at tunnel centerline distributions of temperature, pressure, and Mach number, and flow angularity as measured by testing the model upright and inverted. More recent efforts have looked at the details of the Mach number calibration and the effect of temperature on flow angle.

The ability to vary the test section wall angle provides the capability to maintain zero Mach number gradient through the test section, thus eliminating model buoyance effects, for all test conditions. A typical variation of wall angle with Mach number is shown in the left of figure 35. This particular case is for a warm temperature of 100° F and varies from approximately 0.2° convergence at $M = 0.2$ to 0.4° divergence at $M = 1.15$. A typical correction to Mach number is calculated from the plenum static or reference pressure is also shown. In general the quality of the steady flow appears to be excellent and sufficient adjustments are available on the test section geometry, i.e., wall angle and re-entry flap settings, to eliminate the existence of any Mach number gradients.

In order to investigate the internal structural changes due to temperature gradients in the structure and its effects on flow angle in the test section, frequent measurements of flow angle have been made during the last several test programs. The data presented in figure 36 are typical of results obtained from these measurements and the flow angularity varies up to 0.17° at cold temperatures.

NTF Dynamic Flow Quality

In 1980 while the NTF was still under construction, the plans for flow quality measurement were described extensively in reference 14. The measurements were to consist primarily of fluctuating pressure and velocity measurements. Since that time, hot-film probes and fluctuating pressure gages have been operated in the test section at the locations indicated in figure 37, and further tests are planned as also shown.

Some results of the measurements made to date in the NTF are shown in figures 38 and 39. These results have been excerpted from work by W. B. Igoe on a proposed doctoral dissertation to be submitted to George Washington University. Figure 38 shows the root-mean-square fluctuating static pressure as a function of Mach number for a unit Reynolds number of 6 million per foot. The fluctuating pressures were measured in air on the test section side wall and have been divided by free stream static pressure. Fluctuating static pressures have been measured in the free stream in a number of other large transonic wind tunnels using a 10° cone on the centerline (see reference 15 for example), and some of these results have been included for comparison in figure 38 for a Reynolds number range of 1.3 million per foot.

The results of hot-film probe measurements at low Mach number in the test section are shown in figure 39. These measurements were made in the free stream in air with the test section slots closed. Results are shown for the streamwise measurements at total pressure of 1 and 8 atm. Although there is considerable scatter at a pressure of 1 atm, the measurement levels are about 0.1 percent which was the target level for the NTF. The lateral measurements (not shown) were about twice that value. Streamwise hot-wire probe measurements made in the Langley Low Turbulence Pressure Tunnel (LTPT) at total pressure of 1 and 10 atm (reference 16) are shown for comparison.

Further measurements in the NTF are planned using fluctuating static pressure probes in the test section free stream, and hot-film probes in the test section, settling chamber, and in the vicinity of the cooling coil and screens. The measurements will be made over the full operating range of the NTF. By the time the measurements are completed, the dynamic flow quality of the NTF will have been fully documented.

Mach Number and Angle of Attack Sensitivities

Prior to looking at either Reynolds number effects or the effects of frost on data quality, it was desirable to obtain an assessment of the sensitivity of the model to the basic test parameters, Mach number and angle of attack, and some qualitative assessment of our ability to control and measure them. As stated in the introduction, the primary model used for assessing data quality was the Pathfinder I Model. This model was built early in the program for the purpose of developing model design and fabrication technology as well as providing a research model. It has an aspect ratio 10 wing with a supercritical airfoil design technology of the mid 1970's. As a result, shock movement is very sensitive to small changes around the design point in Mach number and angle of attack. This made it a good model for use in assessing our ability to measure Mach number and angle of attack in the NTF. Figures 40 to 41 illustrate the results obtained from this assessment. The figures show pressure distributions for an inboard and an outboard wing station at a Mach number around 0.82 and for transition fixed at 10 percent of chord. The data of figure 40 shows that a Mach number increment of 0.0038 results in a shock movement of about 6 percent of chord for the out board wing station. In light of the high degree of sensitivity to Mach number, a series of runs were made where all variables except Mach number were held constant and Mach number varied in very small increments of 0.0001 to 0.0006. Wing pressure distributions for these cases are shown in figure 41. The data show an orderly progression of shock movement and the well defined curves suggest that both wing pressures and Mach number are being measured with a high degree of accuracy.

The sensitivity of this model to angle of attack is illustrated in figure 42. In this case, the angle of attack increment was 0.054° with a Mach number difference of 0.0013. Again, the shock movement is about 5 to 6 percent. However, about one half of the movement can be attributed to Mach number effects. These data support the point that the highest quality

instrumentation is an absolute requirement for using the NTF to understand incremental effects of Reynolds number and compressibility. Further they support the conclusion that a high degree of accuracy is currently available in the Mach number, angle of attack, and model pressure measuring systems. The data also underscores the importance of being able to accurately assess wall boundary effects. Recent research of this subject¹⁷ has provided sophisticated techniques which utilize measured tunnel wall static pressures to calculate model induced variations of Mach number and upwash through the test section. Figure 43 shows contours, in the region of the model, of wall induced Mach number corrections. For this size model at the conditions illustrated, the corrections are relatively small $M = .001$. But as illustrated in the previous figures, corrections of this magnitude are significant if high quality data are to be obtained.

MOISTURE CONTAMINATION "FROST" EFFECTS

Having established confidence that small incremental effects of the basic test parameters, Mach number, and angle of attack could be both controlled and measured, an investigation to assess the possible effects of frost on the data was undertaken. Care was also taken to insure that comparable tests parameters were obtained where the only significant variable was that in one case frost was visible on the model and in the other case it was not visible. Wing pressure distributions from these two cases are compared in figure 44. Although care was exercised in setting the test parameters, it should be noted that the Mach number is different by 0.0004 and the angle of attack by 0.01°. These differences are in the direction, and based on previous discussion, believed to account for the small differences in shock location shown in the data of figure 44 for the outboard wing station. After accounting for the difference in shock location, there is a small difference in pressure level ahead of the shock that may be a small effect of frost. In general, the two cases are in very close agreement and provide confidence that when planned tunnel drying procedures are used and the inside of the tunnel kept closed to atmospheric air, frost on the models will not be a problem with regard to data quality.

CONCLUDING REMARKS

The National Transonic Facility has been operational in a checkout and test mode since the ORR in late 1984. During this time, there have been many challenges associated with testing in a large cryogenic wind tunnel. For the most part they centered around the effect of large temperature excursions on the mechanical movement of large components, the reliable performance of instrumentation systems, and an unexpected moisture problem with dry insulation. Most of these challenges have been met; the current effort is devoted primarily to building new fan blades and repairing structural components that were damaged in January 1989 due to a tunnel component failure.

Also, during this period, a preliminary flow calibration has been completed and a data quality evaluation conducted along with high Reynolds number aerodynamic test of several configurations. There is still a requirement for a major effort to develop and implement flow visualization and diagnostic techniques for maximum utilization of the facility. The current NASA program includes funding for these activities in Fiscal Years 1989 and 1990. However, from a basic facility standpoint and pending current ongoing repairs, we believe that the NTF is ready to efficiently support research and development testing.

REFERENCES

1. McKinney, Linwood W.: Operational Experience with the National Transonic Facility. AGARD-CP-348. Paper presented at the AGARD Fluid Dynamics Panel Symposium on Wind Tunnels and Testing Techniques, Cesme, Turkey, September 26-29, 1983.
2. Bruce, Walter E., Jr.; Fuller, Dennis E.; and Igoe, William B.: National Transonic Facility Shakedown Test Results and Calibration Plans. Paper No. 84-0584CP, AIAA 13th Aerodynamic Testing Conference, San Diego, CA, March 5-7, 1984.
3. Bruce, Walter E., Jr.: The U.S. National Transonic Facility - Parts I and II. AGARD Report No. 722, 1985. Paper presented at the AGARD FDP Special Course on Cryogenic Technology for Wind Tunnel Testing, Rhode-Saint-Genese, Belgium, April 22-26, 1985.
4. McKinney, Linwood W.: Considerations in the Selection of the Pathfinder Model Configurations, NASA CP 2122 Part II, 1980.
5. Igoe, William B.: Characteristics and Status of the U.S. National Transonic Facility, Lecture No. 17 of AGARD Lecture Series No. 111, May 1980.
6. Osborn, James A.: A Description of the National Transonic Facility Process Control System, NASA CP 2122 Part I, 1980.
7. Gloss, Blair B. and Bruce, Robert: A Solution to Water Vapor in the National Transonic Facility. AIAA Paper 89-0152, AIAA 27th Aerospace Sciences Meeting, Reno, Nevada, January 9-12, 1989.

8. Whitlow, Woodrow, Jr.; Bennett, Robert M.; and Straganac, Thomas W.: Analysis of Vibration of the National Transonic Facility Model Support System Using a 3-Dimensional Aeroelastic Code. AIAA Paper No. 89-2207, AIAA 7th Applied Aerodynamics Conference, Seattle, WA, July 31-August 2, 1989.
9. Cryogenic Wind Tunnel Models, NASA CP-2262, May 1982, pp. 215-256.
 - A. Ferris, Alice T.: Strain Gage Balances and Buffet Gages.
 - B. Kern, Frederick A.: NTF Model Pressure Measurements.
 - C. Finley, Tom D.: Angle of Attack System.
10. Kern, Frederick A.; Knight, Charles W.; and Zasimowich, Richard F.: National Transonic Facility Mach Number System. ISA Paper No. 85-0174, 1985.
11. Ferris, Alice T.: Cryogenic Strain Gage Techniques Used in Force Balance Design for the National Transonic Facility, NASA TM 87712, 1986.
12. McPhee, J. R.: Electrical Noise Reduction Techniques Contributing to Improved Data Quality at the National Transonic Facility, NASA CP 4193, November 1988.
13. Fuller, Dennis E. and Williams, M. Susan: Testing Experience with the National Transonic Facility. AIAA Paper No. 86-0748. Presented at the AIAA 14th Aerodynamic Testing Conference, West Palm Beach, FL, March 5-7, 1986.
14. Stainback, P. Calvin and Fuller, Dennis E.: Flow Quality Measurements in Transonic Wind Tunnel and Planned Calibration of the National Transonic Facility. NASA CP 2183, High Reynolds Number Research 1980, pp. 105-121, L. Wayne McKinney and Donald D. Baals, eds., December 9-11, 1980.
15. Dougherty, N. S., Jr. and Steinle, Frank W., Jr.: Transition Reynolds Number Comparisons in Several Major Transonic Tunnels. AIAA Paper No. 74-627, AIAA 8th Aerodynamics Testing Conference, Bethesda, MD, July 8-10, 1974.
16. McGhee, Robert J.; Beasley, William D.; and Foster, Jean M.: Recent Modifications and Calibration of the Langley Low Turbulence Pressure Tunnel. NASA TP 2328, July 1984.
17. Kemp, William B., Jr.: A Panel Method Procedure for Interference as Assessment in Slotted-Wall Wind Tunnels. AIAA Paper No. 88-2537, Applied Aerodynamics Conference, Williamsburg, VA, June 6-8, 1988.

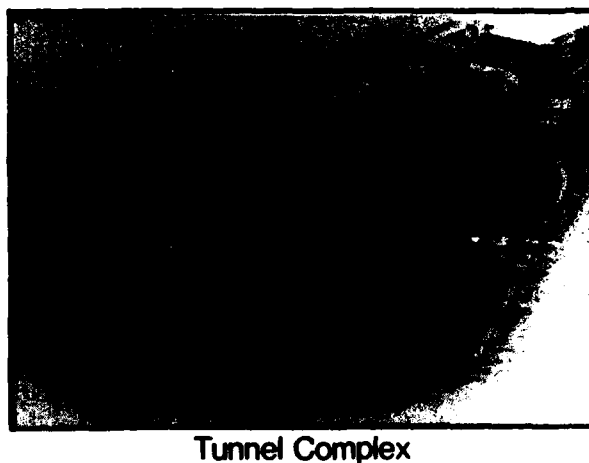
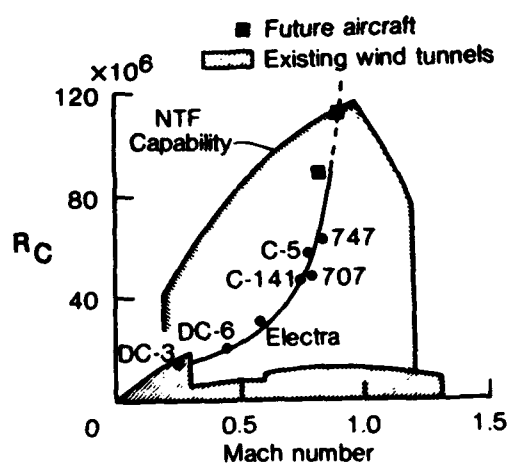


Figure 1.- National Transonic Facility

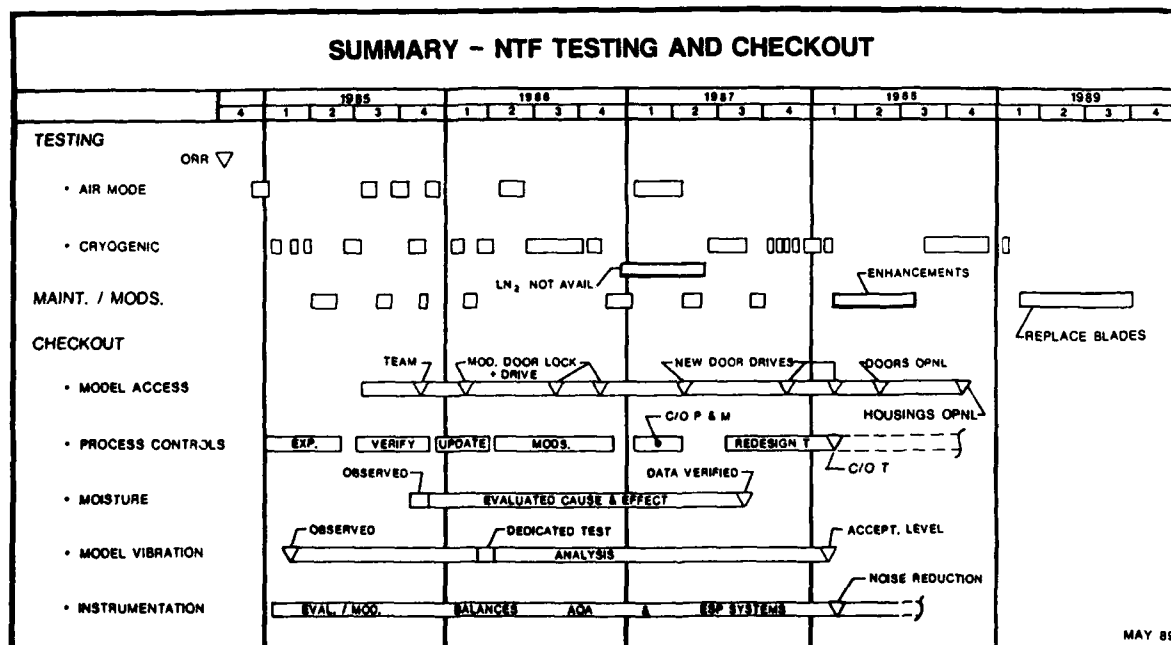


Figure 2.- NTF operations experience since the operational readiness review (ORR).

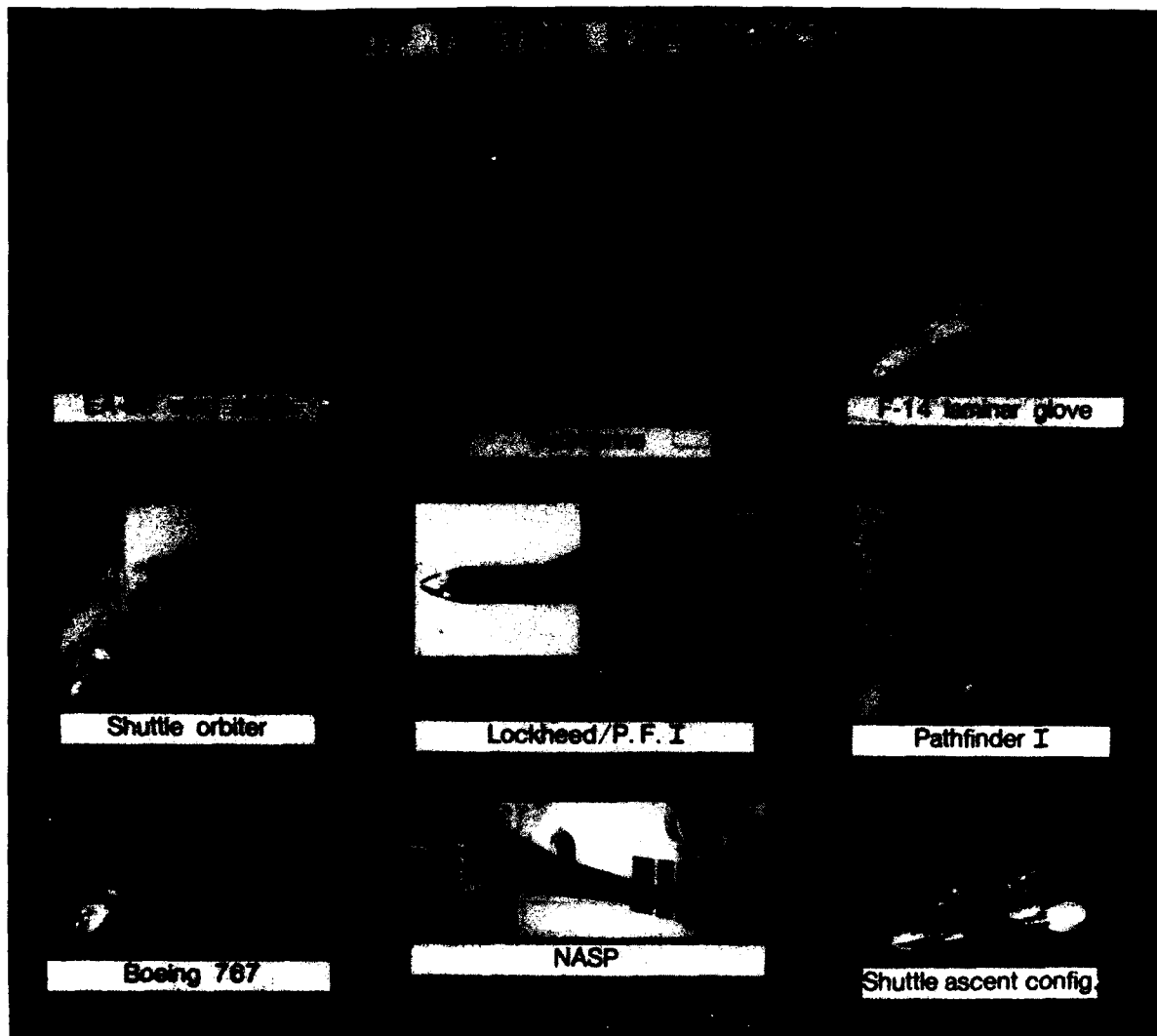


Figure 3.- Various models tested in the NTF.

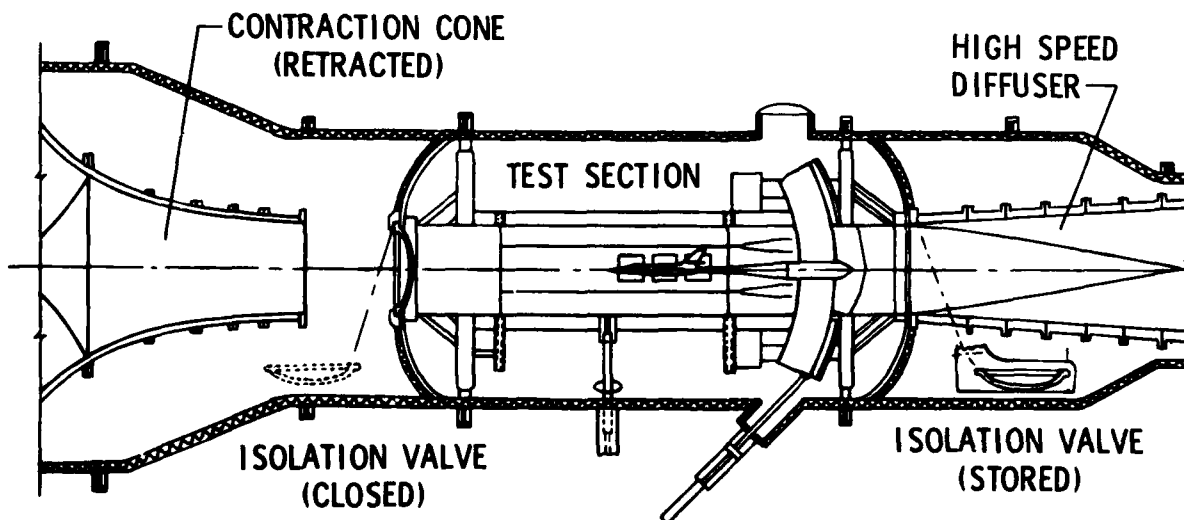


Figure 4.- NTF plenum/test section isolation system.

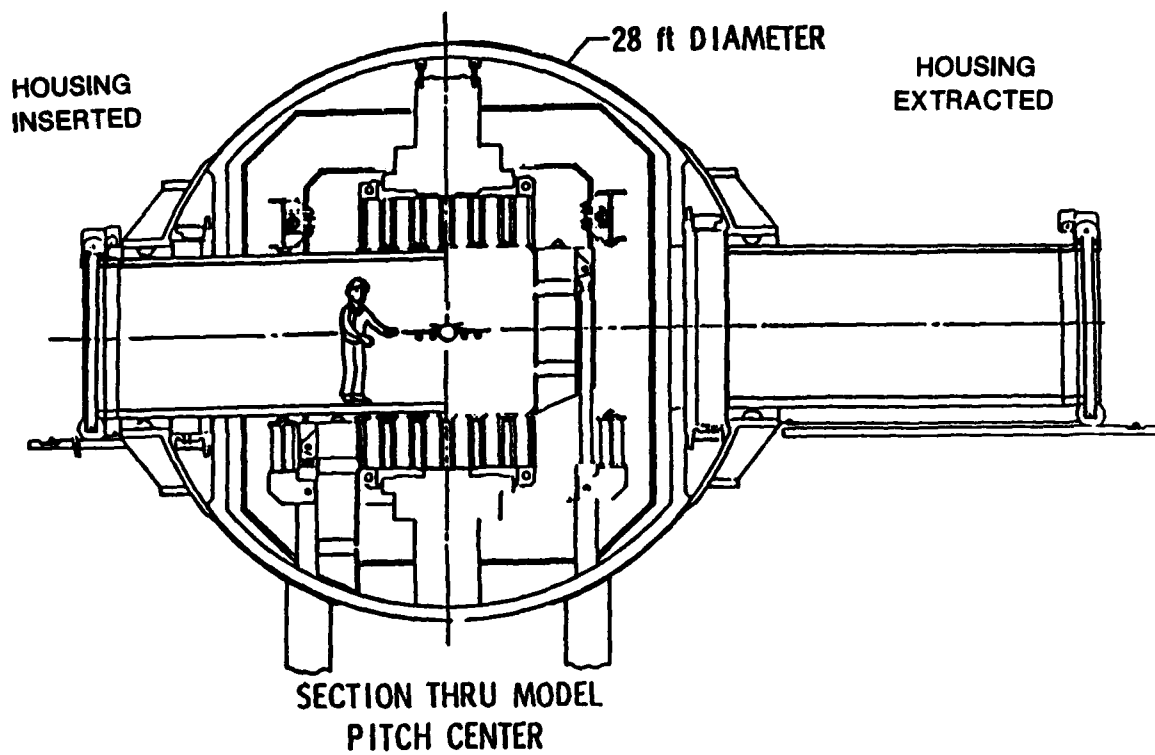


Figure 5.- NTF model access system.

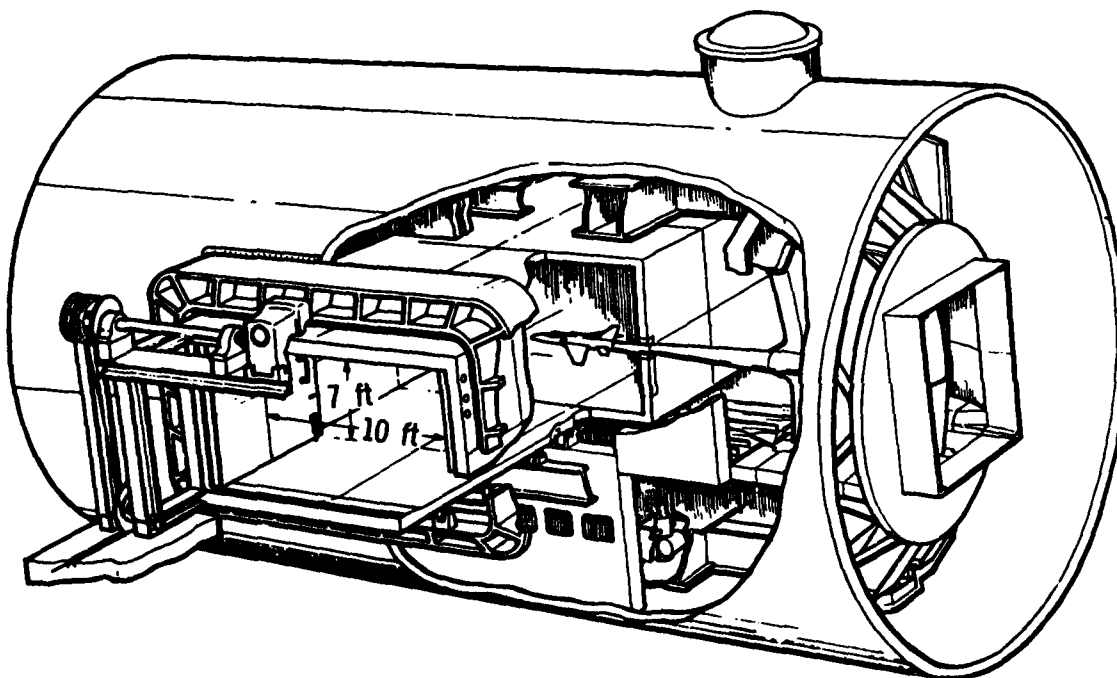


Figure 6.- NTF model access system with access housing inserted.

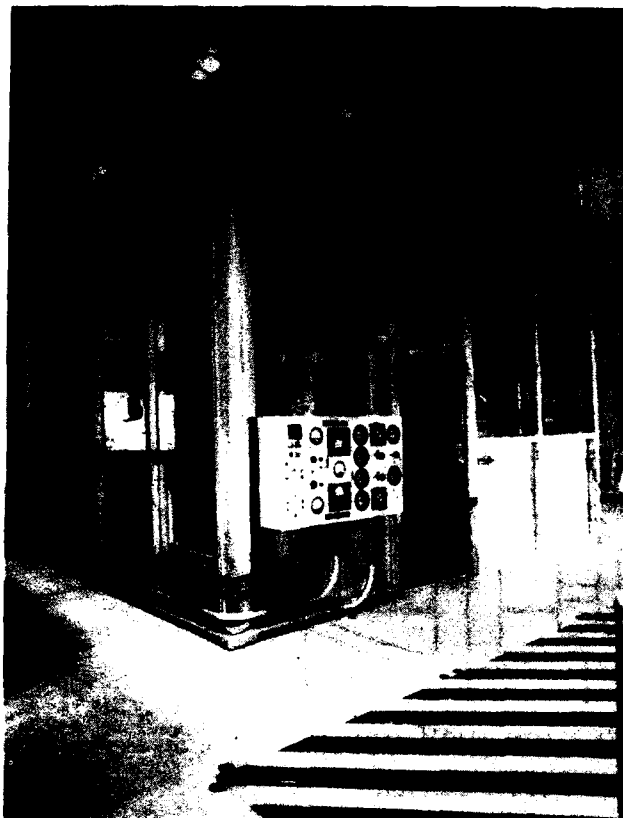


Figure 7.- Vapor lock room at entrance to test section.



Figure 8.- Model mounted in the NTF with access housings inserted.

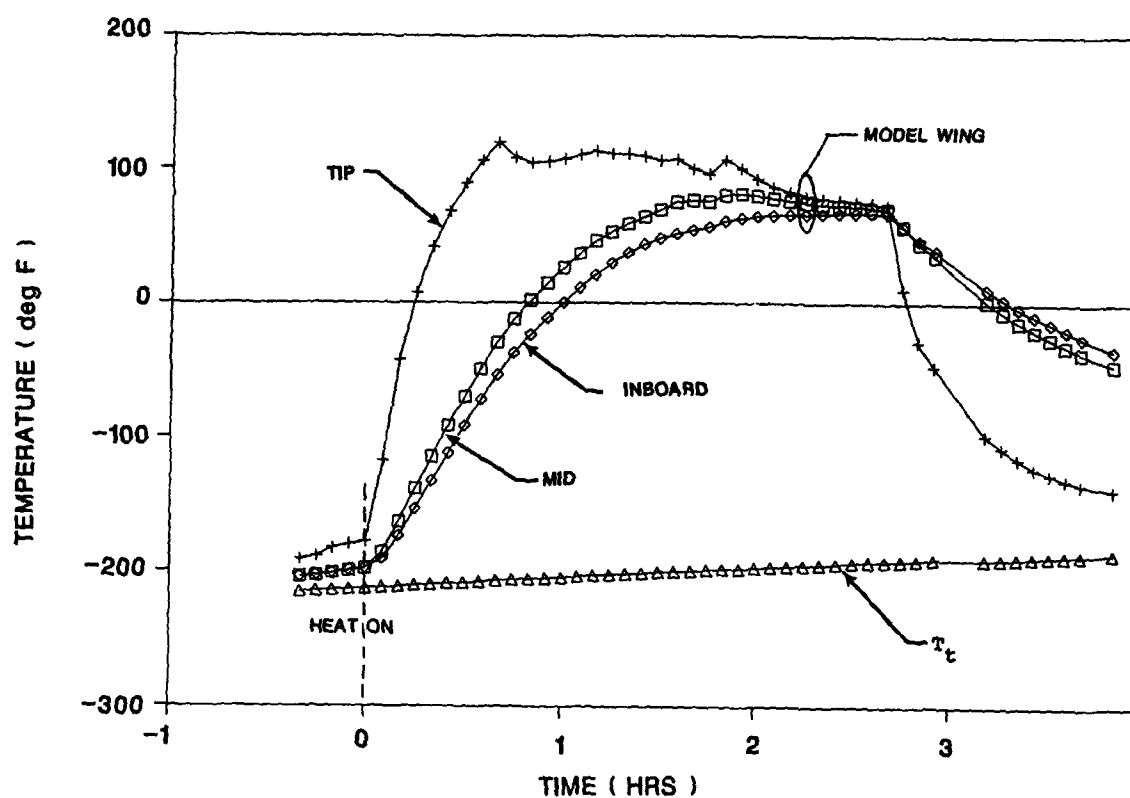


Figure 9.- Warm up of transport model using model access housings.

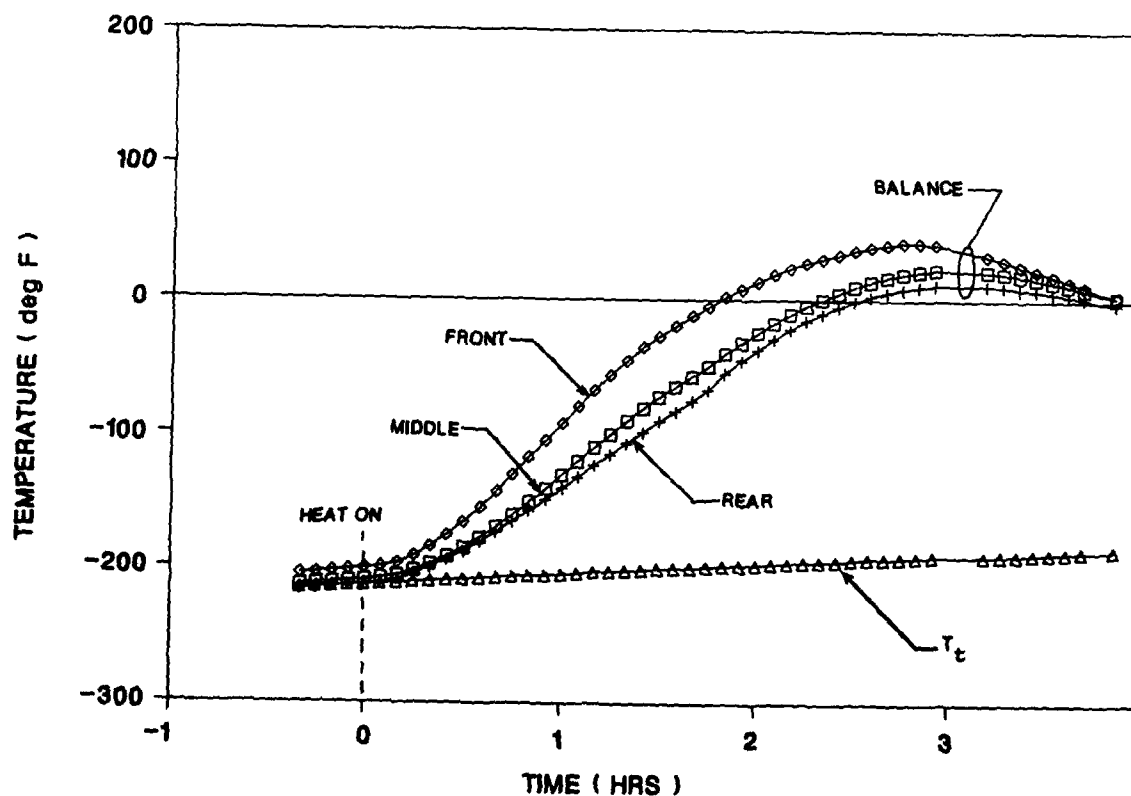


Figure 10.- Warm up of a strain gage balance using model access housing.

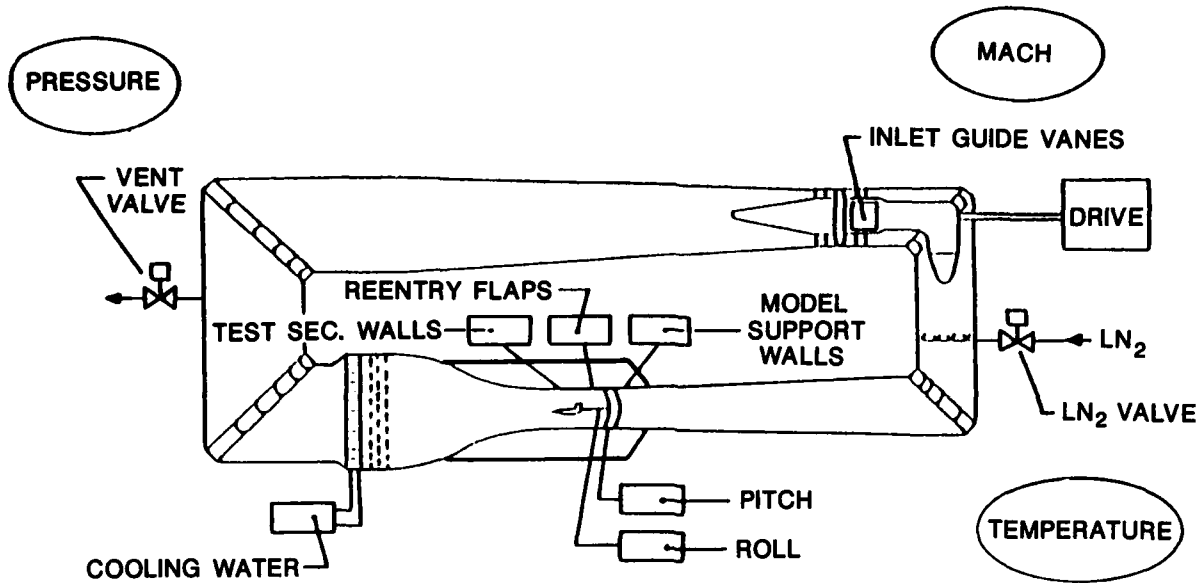


Figure 11.- NTF primary process controls.

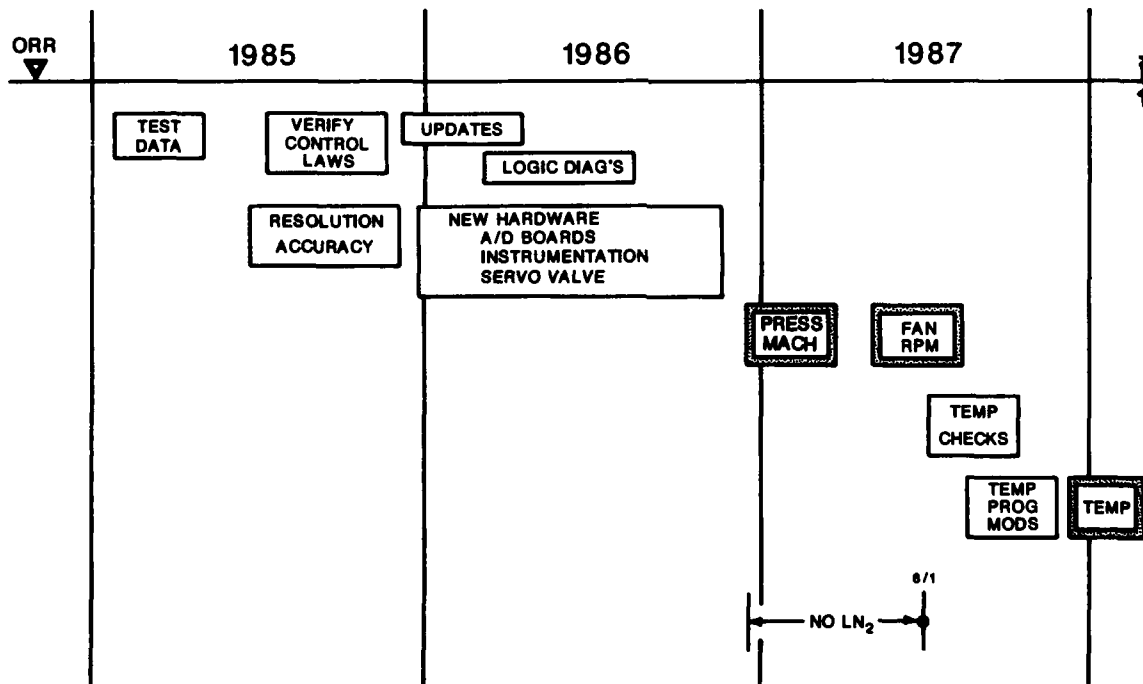


Figure 12.- Chronology of events: pressure, mach no. and temperature controls systems.

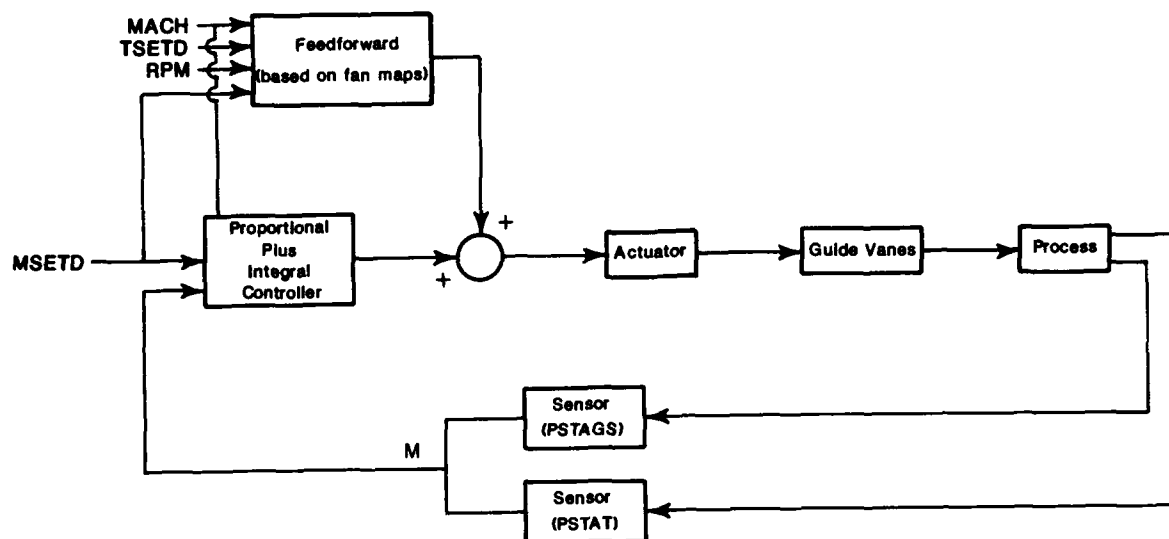


Figure 13.- Mach number control system.

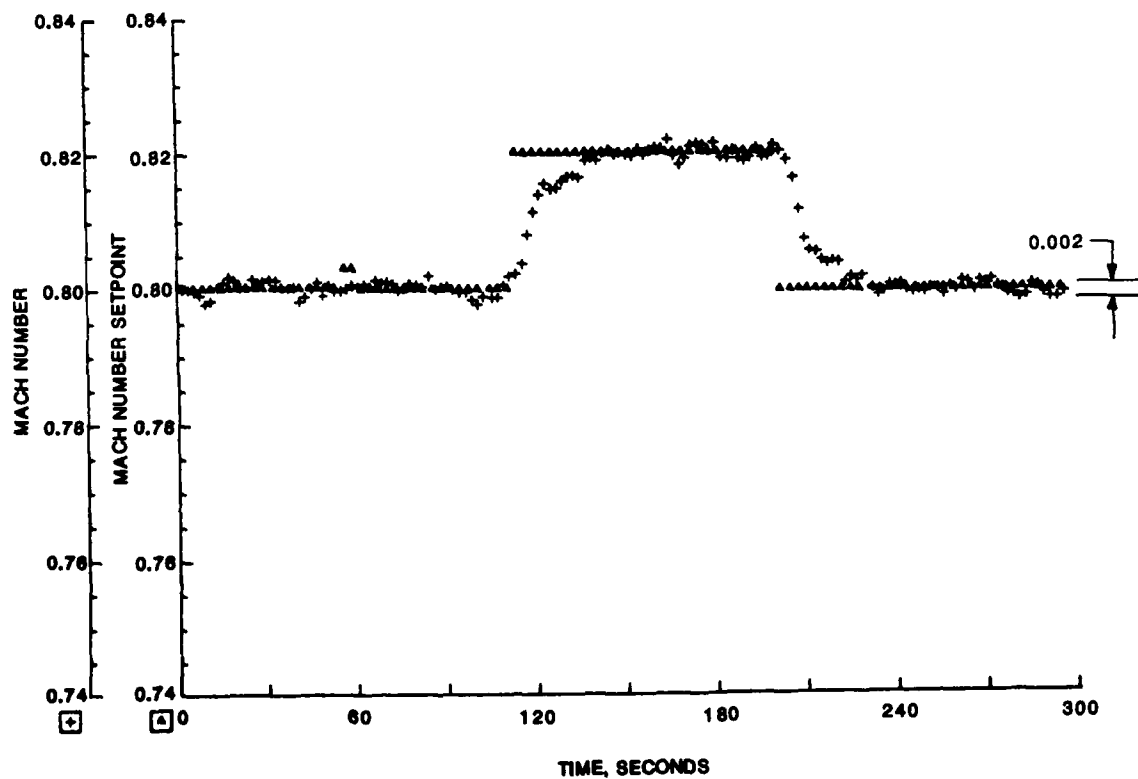


Figure 14. - Mach number response to a step input; $T_T = -175^{\circ}\text{F}$ and $P_T = 30$ psia.

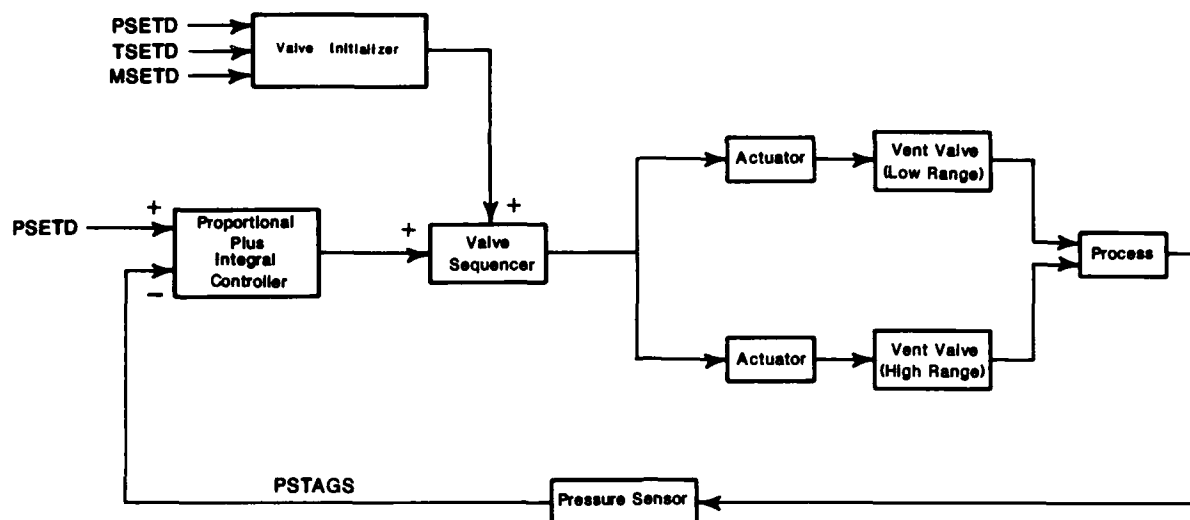
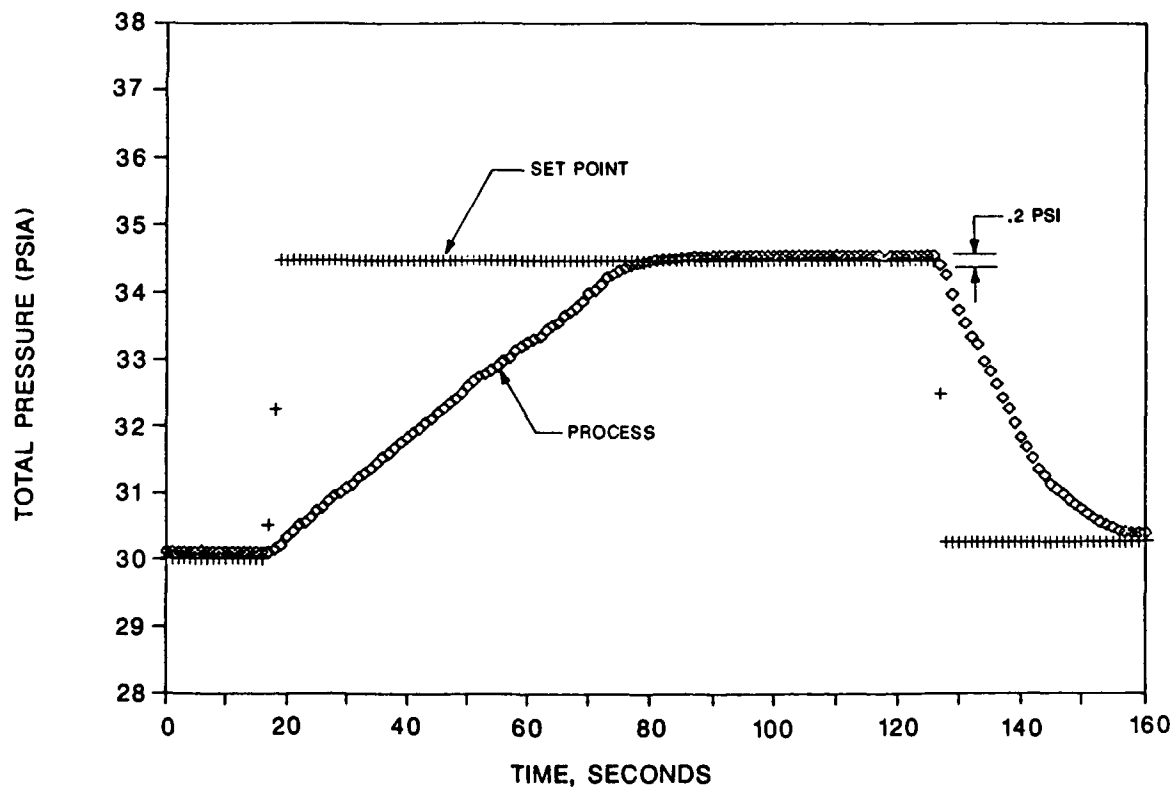


Figure 15.- Pressure control system.

Figure 16.- Pressure response to a step input; $T_m = -260^\circ\text{F}$ and $M = .8$

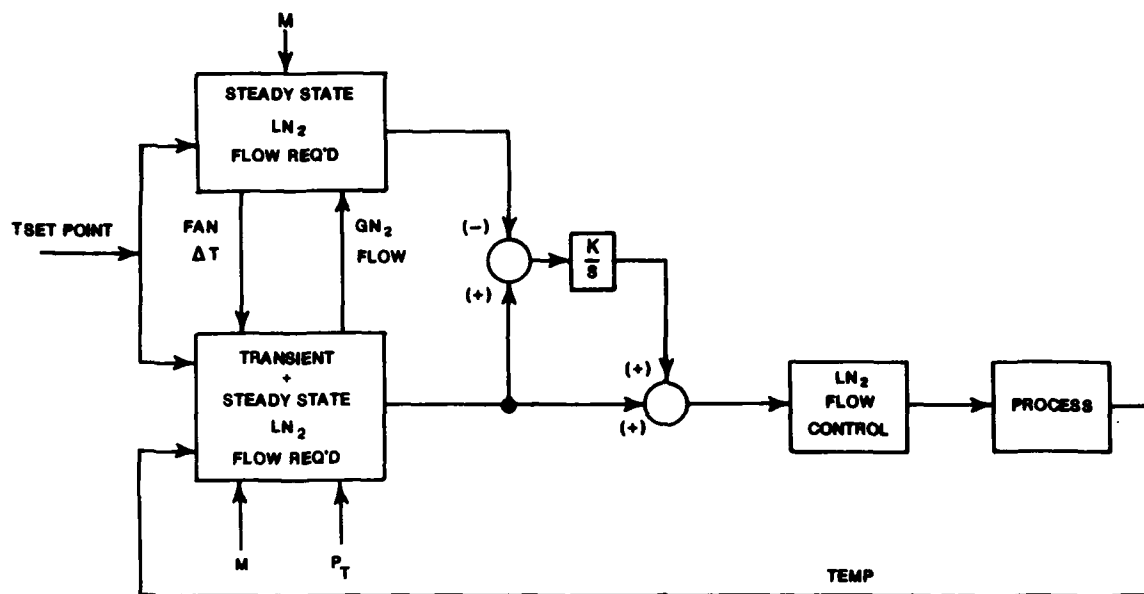
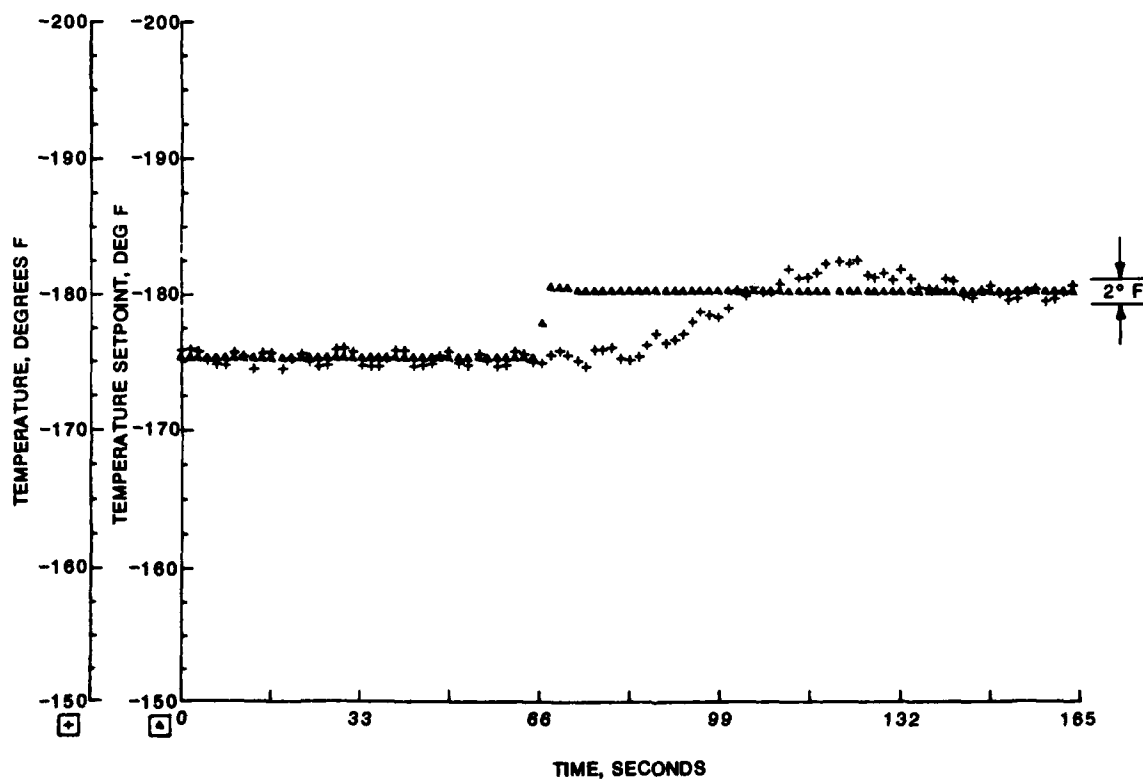


Figure 17.- Temperature control system.

Figure 18.- Temperature response to a step input; $M = 0.8$ and $P_T = 30$ psia.

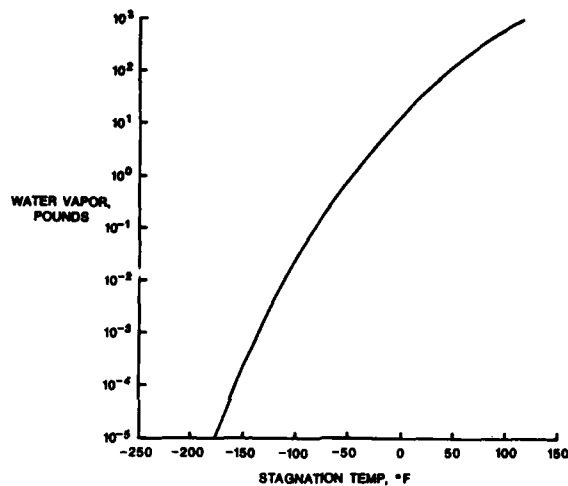


Figure 19.- Water required to saturate freestream gas at 14.7 psia tunnel pressure.

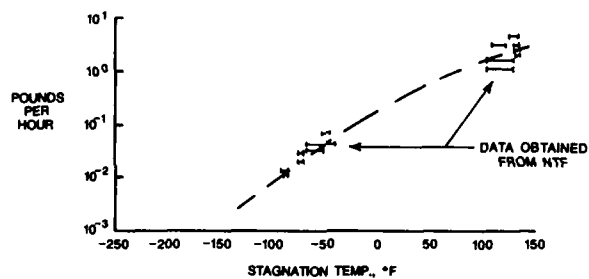


Figure 20.- Water transfer rate from insulation to freestream gas.

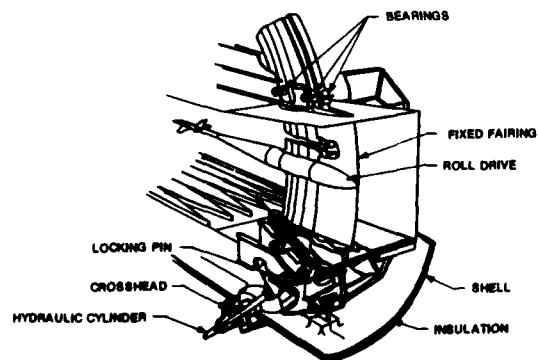


Figure 21.- NTF model support system.

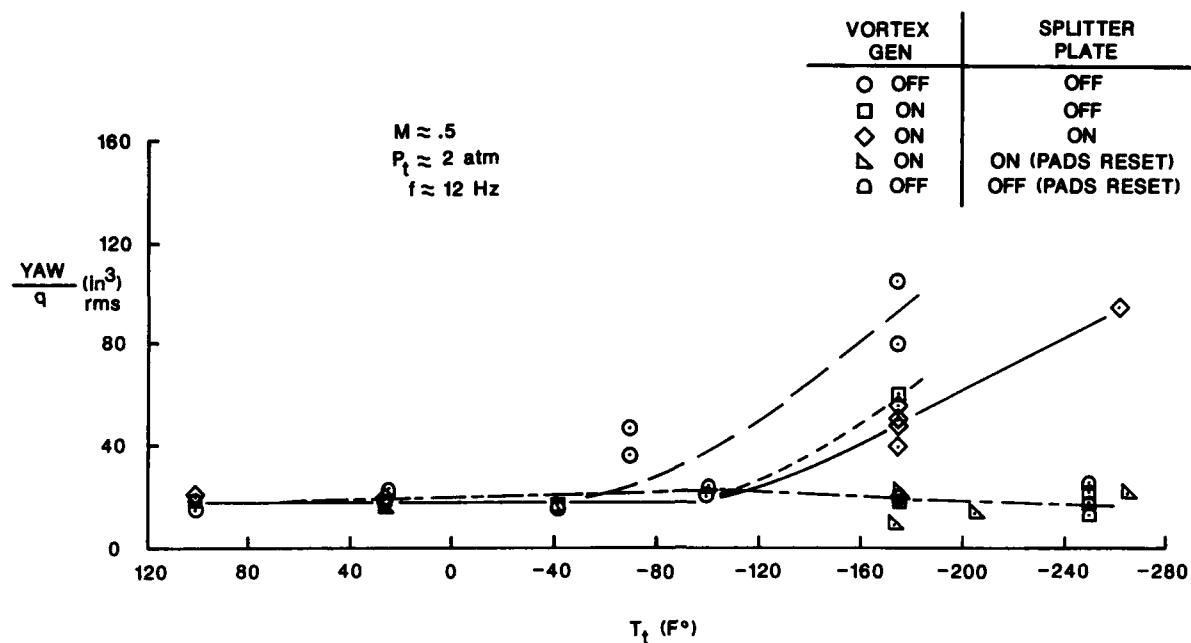


Figure 22.- Pathfinder I dynamics using the NTF 104 force balance.

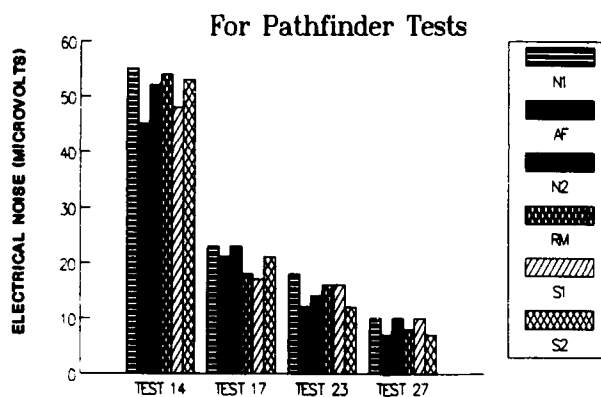


Figure 23.- Balance data scatter due to electrical noise.

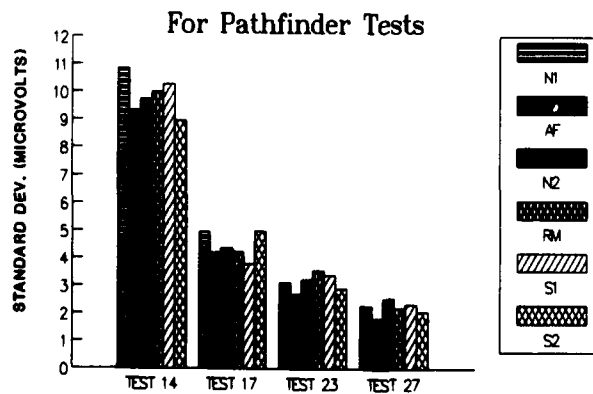


Figure 24.- Standard deviation of balance data due to electrical noise.

Test 14 Balance Forces

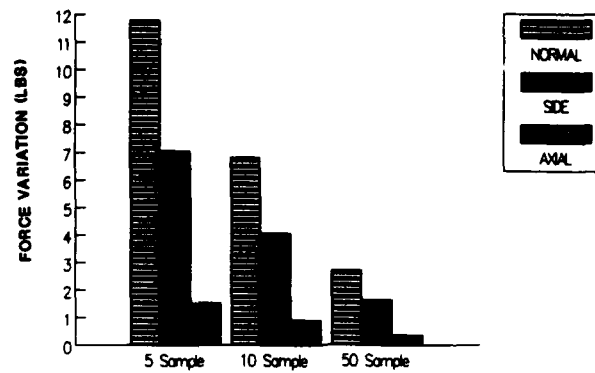


Figure 25.- Showing 95 percent confidence intervals of balance data due to electrical noise before improvements.

Test 27 Balance Forces

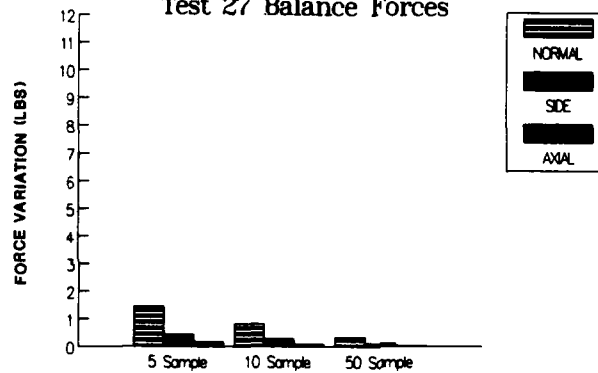


Figure 26.- Showing 95 percent confidence intervals of balance data due to electrical noise after improvements.

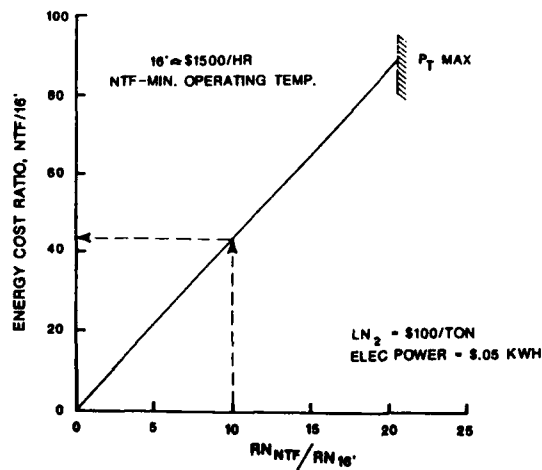


Figure 27.- Energy cost comparison between the NTF and the 16 foot transonic tunnel at NASA Langley for $M = 0.8$.

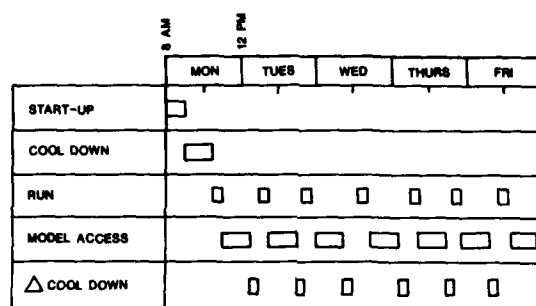
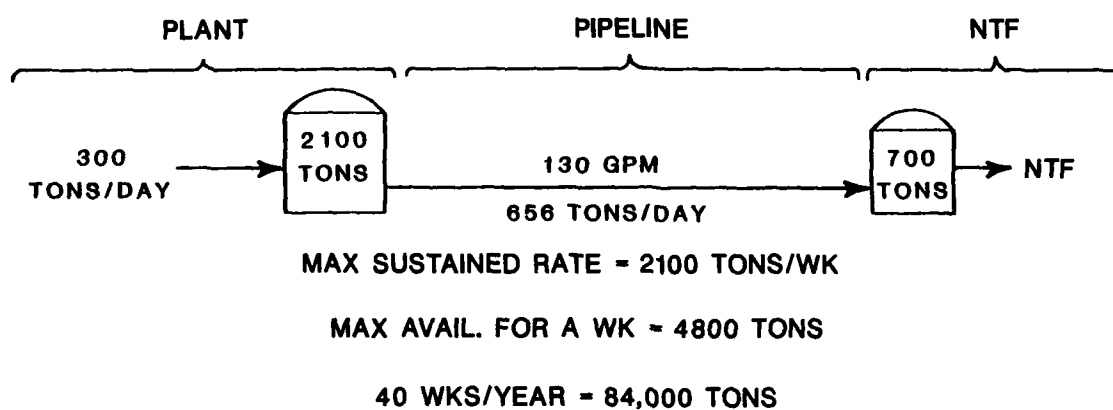
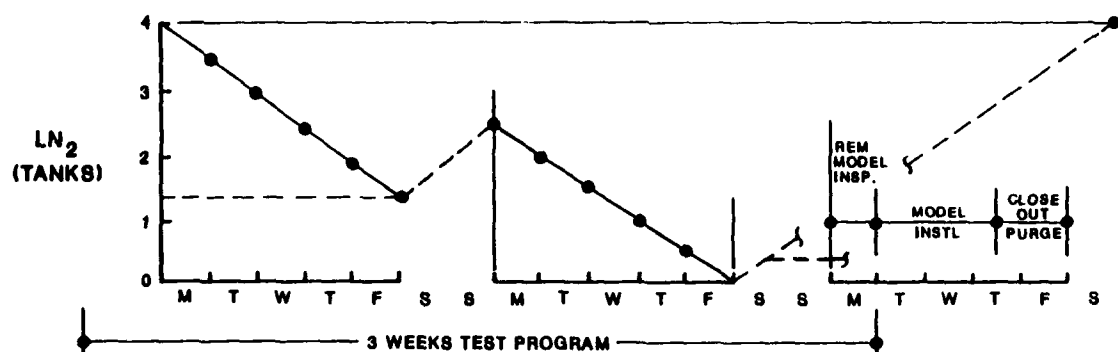


Figure 28.- Typical NTF operating profile.

Figure 29.- LN₂ supply system.

FOR TWO WEEKS OF TESTING

LN ₂ AVAILABLE (MAX.)	TONS LN ₂
BULK STORAGE = 2900 TONS	6300
PLANT OUTPUT = 3360 TONS	
COOLDOWNS	
2 LARGE ΔT's (300 TO 350°F)	945
8 SMALLER ΔT's (100°F)	
PRESSURIZATIONS - 1 PER DAY (AVG)	86
AVAILABLE FOR TESTING	5269

Figure 30.- NTF maximum cryogenic utilization based on LN₂ from plant.

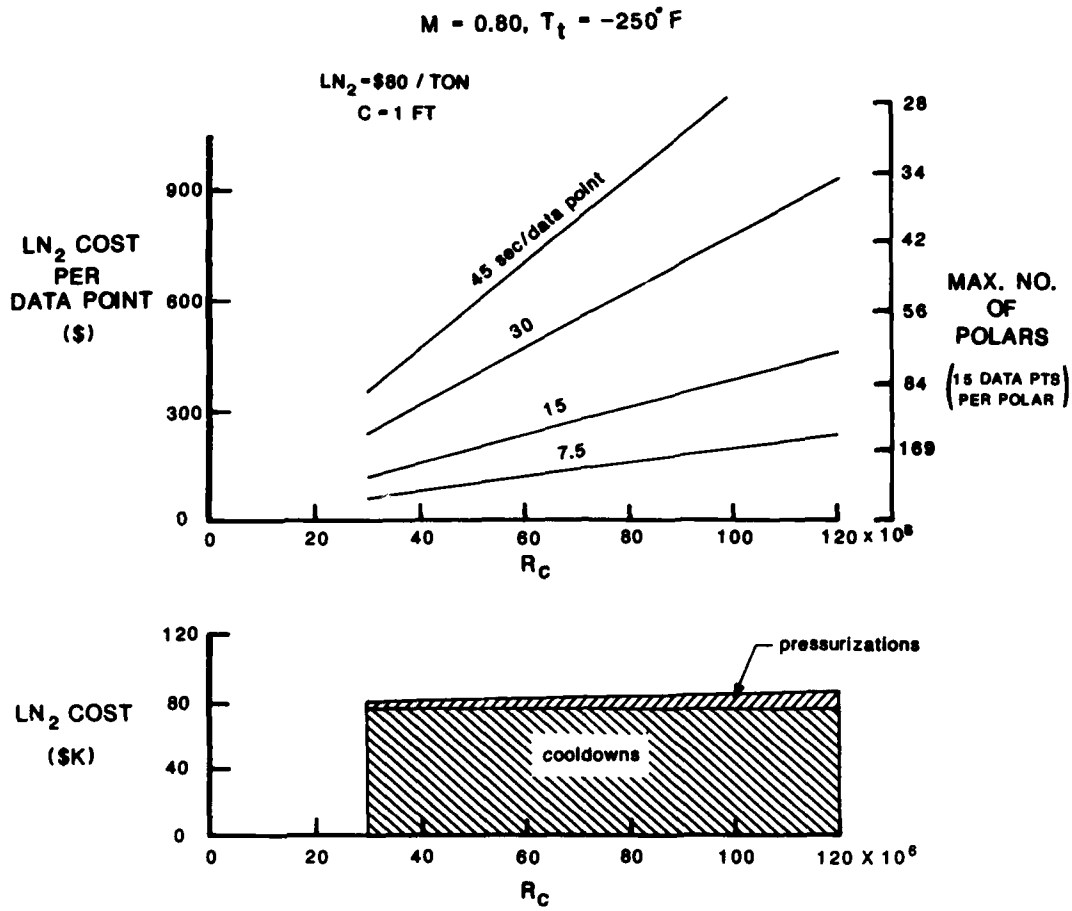


Figure 31.- NTF on-point LN₂ cost rates for various data sampling rates.

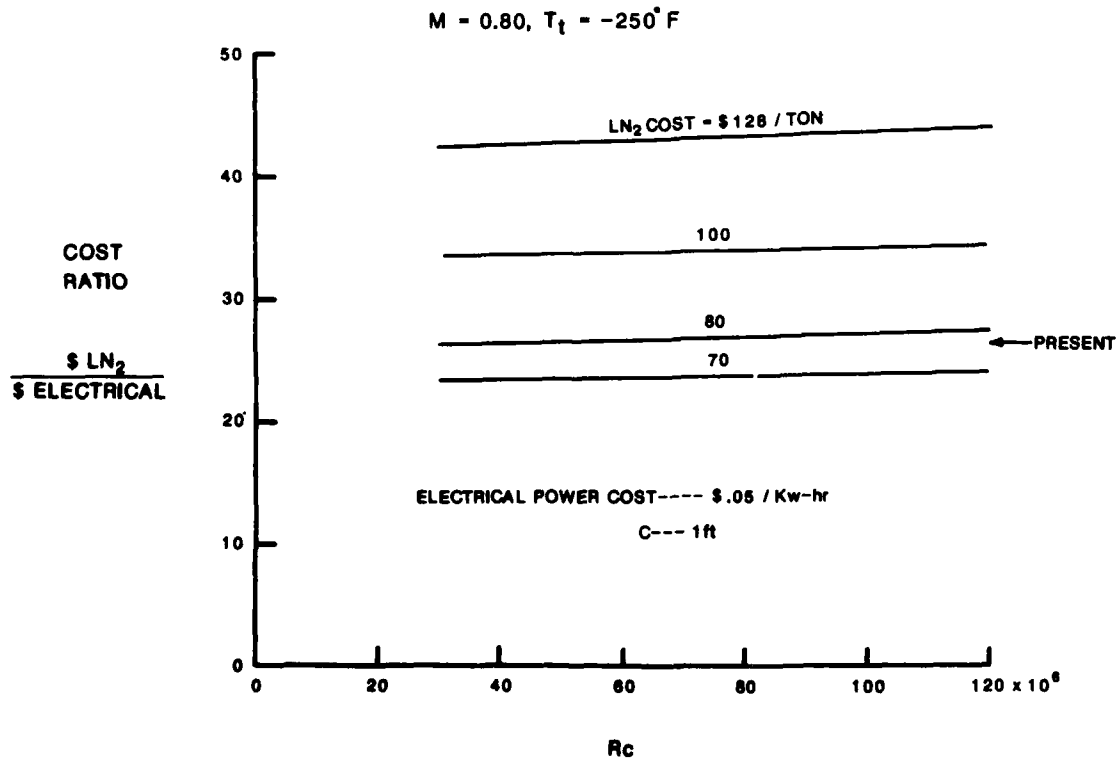


Figure 32.- Comparison of the on-point LN₂ and electrical power costs for the NTF.

- DEDICATED OPERATIONS STAFF MOTIVATED TO MINIMIZE LN2 CONSUMPTION AND MAXIMIZE DATA QUALITY
- MINIMIZATION OF OPERATING TIME CHANGING SET POINT, ETC.
- MINIMIZATION OF DATA ACQUISITION TIME
 - HARDWARE
 - SOFTWARE
 - INSTRUMENTATION
- SOPHISTICATED AUTOMATION
 - FEED FORWARD CONTROL
 - INTERACTIVE CONTROL
 - PREPROGRAMMED TEST DIRECTION
- HIGH DEGREE OF RELIABILITY
 - INSTRUMENTATION SYSTEMS
 - DATA ACQUISITION SYSTEM
- DEVELOPMENT/ADAPTATION OF SPECIAL TEST TECHNIQUE
 - FLOW DIAGNOSTICS
 - FLOW VISUALIZATION

Figure 33.- NTF operational requirements/considerations.

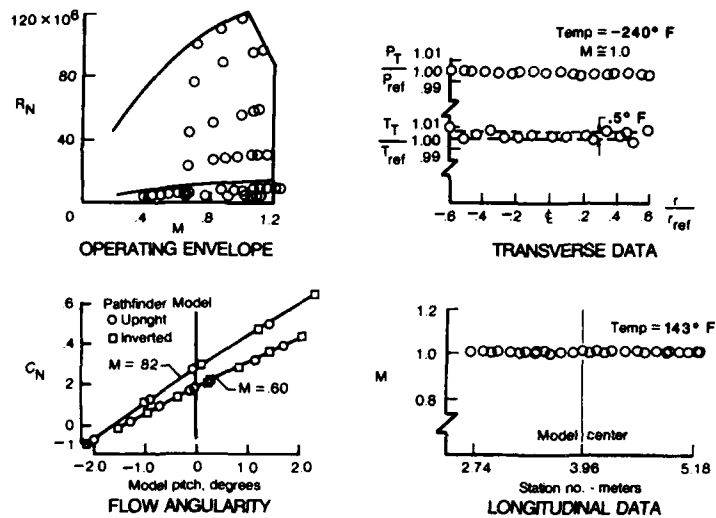


Figure 34.- Typical NTF calibration results.

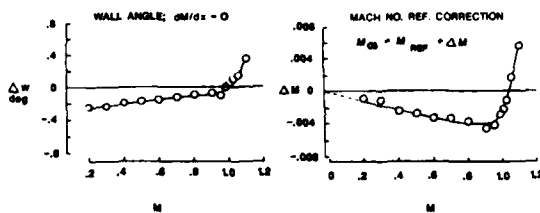
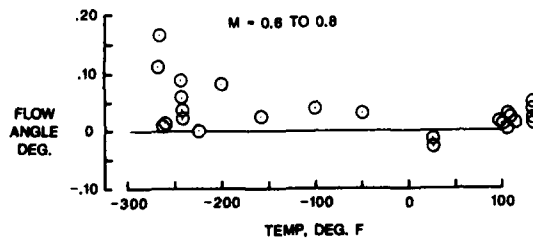
Figure 35.- NTF calibration results for $T = 100^\circ \text{F}$.

Figure 36.- Typical variation of flow angle.

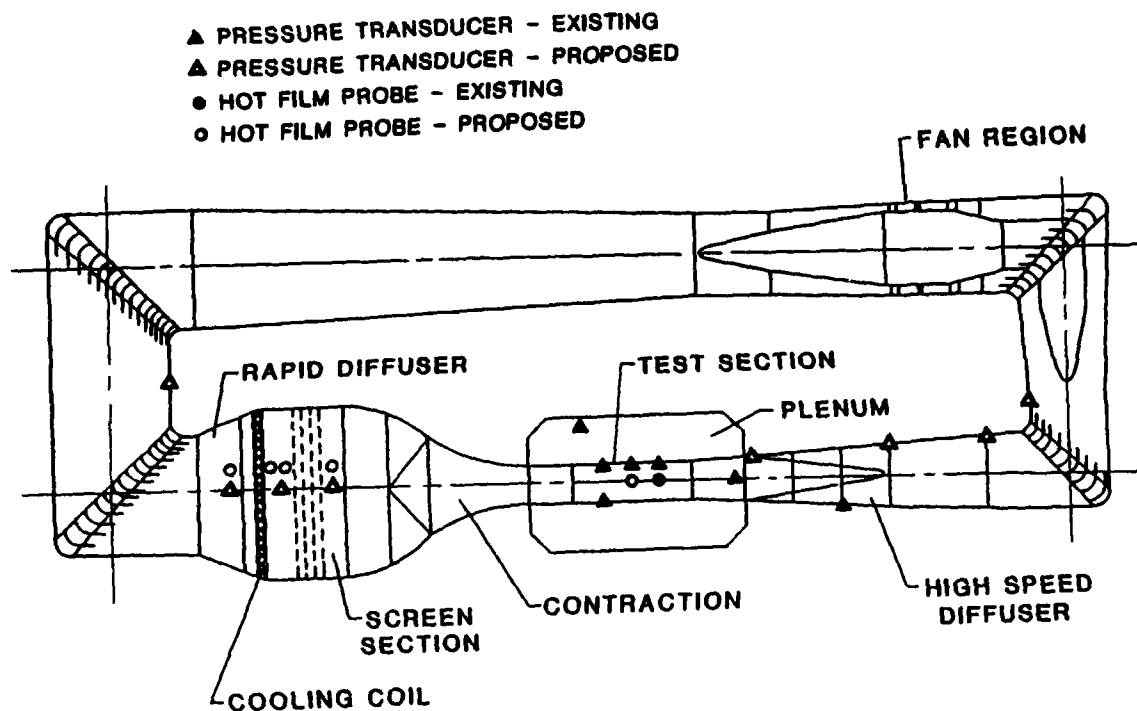


Figure 37.- Locations of dynamic flow quality measurements.

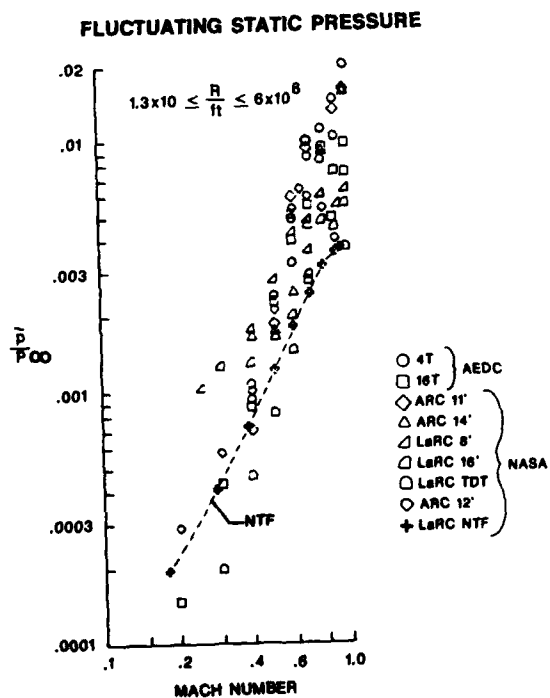


Figure 38.- Fluctuating static pressure.

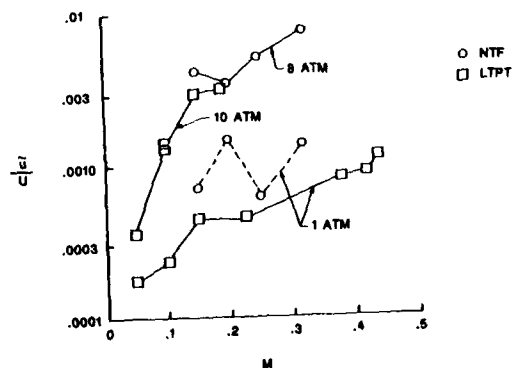


Figure 39.- Freestream turbulence.

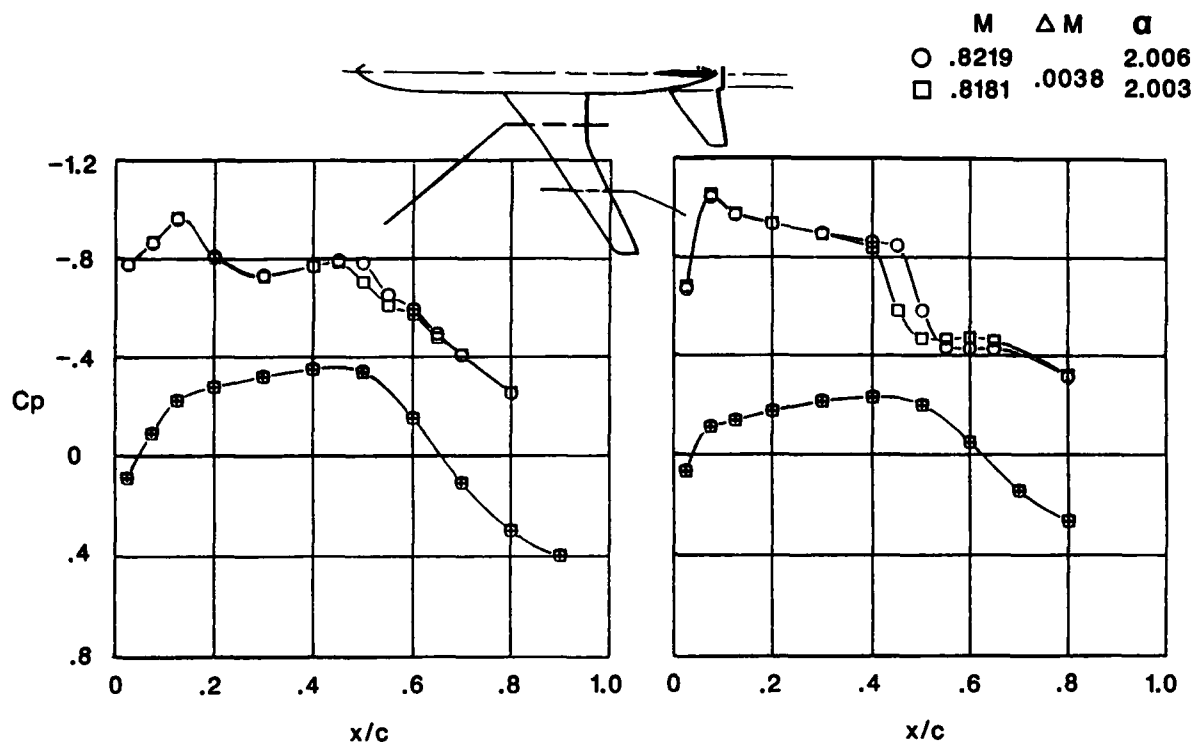


Figure 40.- Effect of mach number on pressure distribution; Pathfinder I; low RN; transition at .10c.

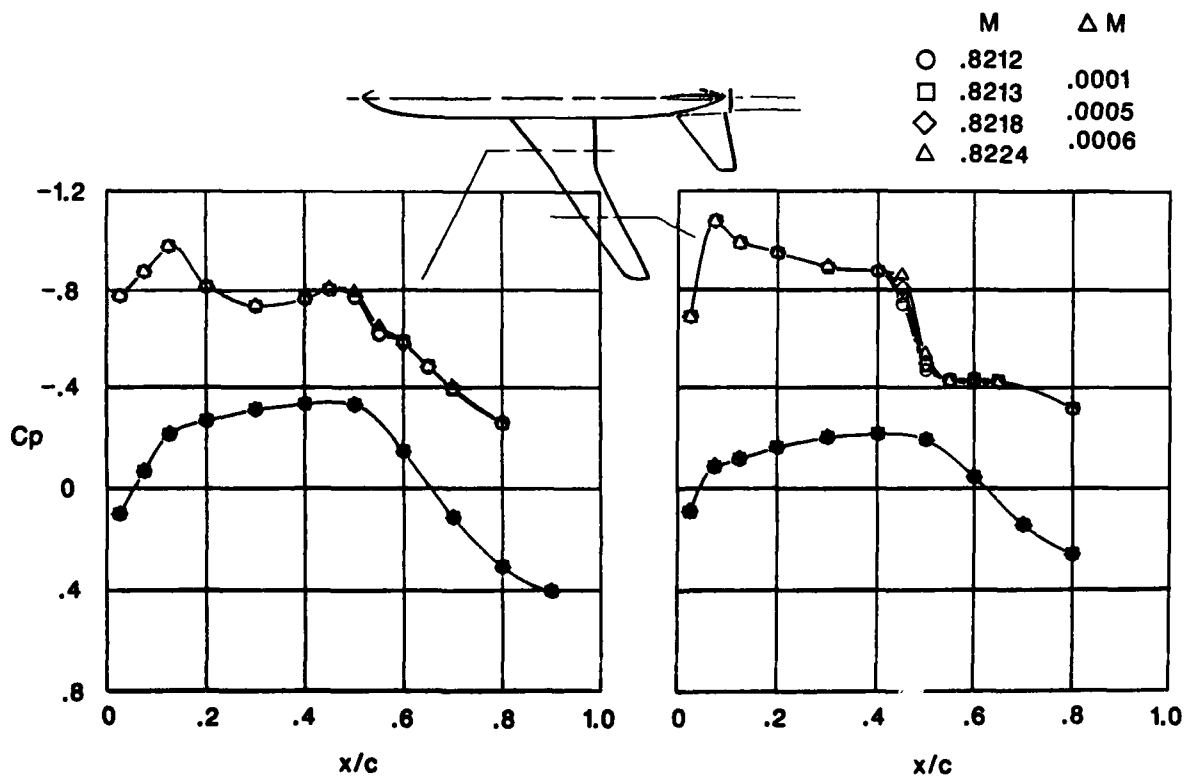


Figure 41.- Effect of mach number on pressure distribution; Pathfinder I; low RN; transition at .10c.

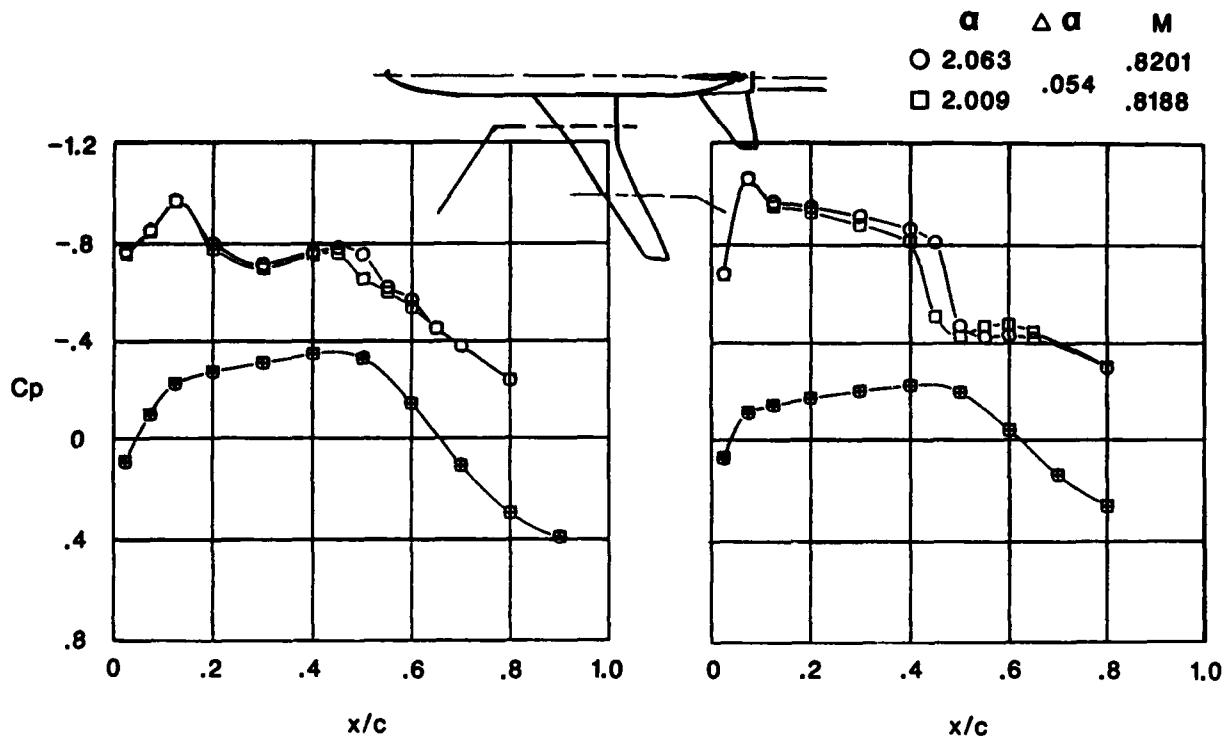


Figure 42.- Effect of angle of attack on pressure distribution; Pathfinder I; low RN; transition at .10c.

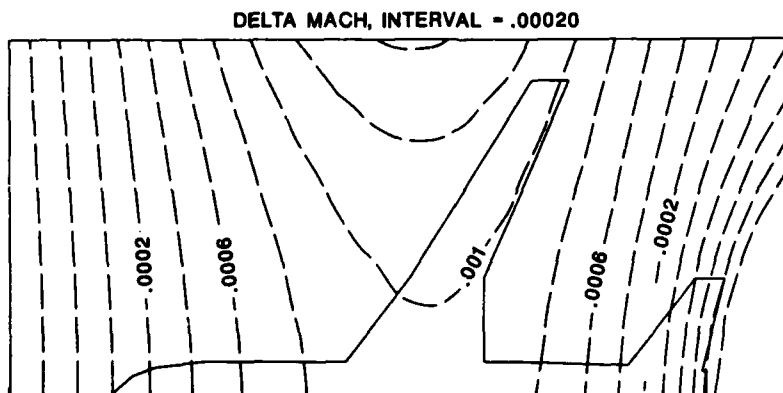


Figure 43.- Typical example of calculated wall boundary induced mach number contours.

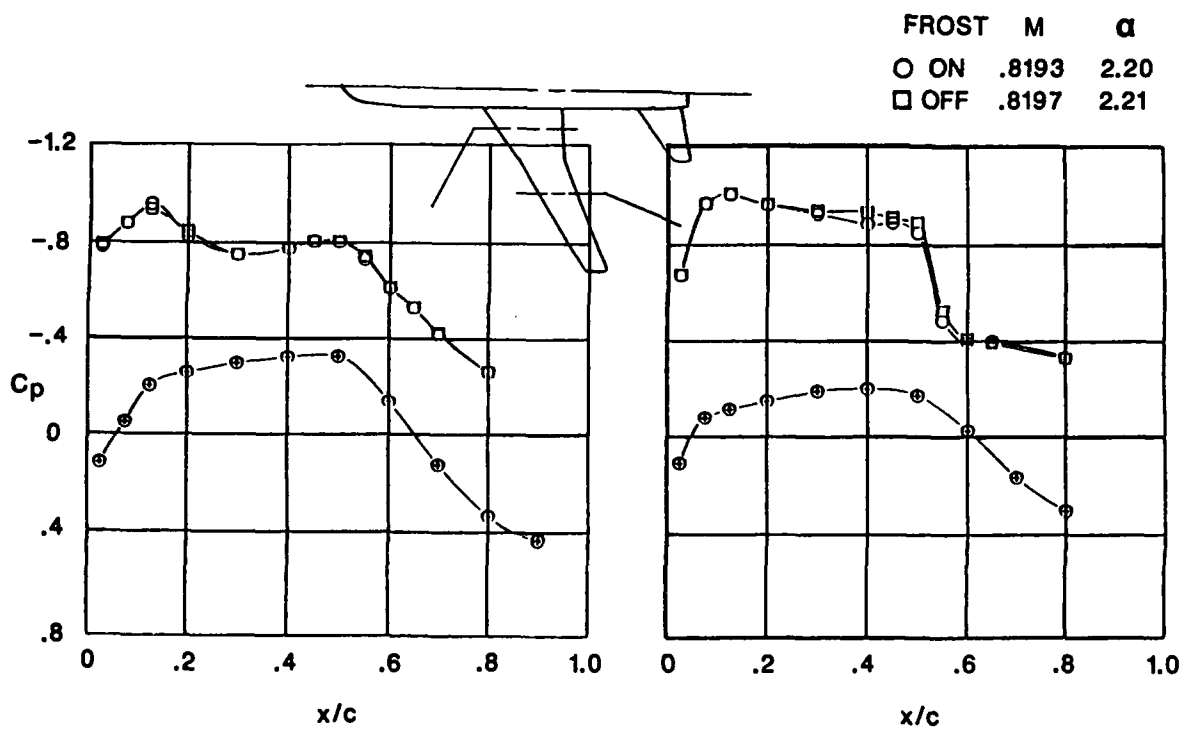


Figure 44.- Effect of frost on pressure distribution; Pathfinder I; high RN.

THE KRYO-KANAL KÖLN (KKK): DESCRIPTION OF THE TUNNEL CONVERSION
Thermal Insulation, Instrumentation, Operational Experience,
Test Results and Operating Costs
 by

F. Viehweger
 Deutsche Forschungsanstalt
 für Luft- und Raumfahrt e.V.
 5000 Köln 90
 Postfach 90 60 58
 Federal Republic of Germany

Summary

The construction of the Kryo-Kanal Köln was completed in May 1985. After check out of all systems the aerodynamic and cryogenic calibration was started one year later and completed in the third quarter of 1988.

During this time operating problems in the circuit and in the subsystems resulting from the cryogenic mode of operation were identified and solved. Some basic tests were performed to understand the physics of the desorption of moisture from the internal insulation.

The aerodynamic tests demonstrated the flow quality in the test section. This paper will give a review on the experimental experience and the test results gathered during the calibration phase.

List of Symbols

u	m/s	velocity
u_{TS}	m/s	velocity in the test section
$T_u = \frac{\sqrt{u'^2}}{u}$		turbulence factor
\dot{m}_{LN_2}	kg/s	mass flow rate of the injected LN_2
T	K	temperature
T_{TS}	K	temperature in the test section
T_G	K	gas temperature
p	N/m^2	pressure
p_{TS}	N/m^2	static pressure in the test section
p_{ges}	N/m^2	total pressure
t	s	time
K_0	-	loss coefficient of the tunnel
K_{MO}	-	loss coefficient of the test model
Re	-	Reynolds number
Ma	-	Mach number
P	W	drive power
x, y, z	m	coordinates

Introduction

The KKK is the second big cryogenic wind tunnel in operation following the NTF at the NASA Research Center in Langley [1]. Both tunnels have nearly the same test section dimensions but in contrast to the NTF the KKK can not be pressurized and the maximum Mach-Number which can be achieved is 0.38. But nevertheless the physical and the thermal problems are similar in both tunnels.

The KKK is to be seen in connection with the European project ETW. The fact, that KKK and ETW have nearly the same test cross section, turned out to be an essential advantage. In both tunnels the same models can be tested and there is additionally an overlap in the operation range. During the phases of design, construction and operation of the ETW a fruitful transfer of experience and know how can flow from the KKK into this project. A first step was made conducting functional tests on preselected insulation systems in two rigs, to prove the reliability of the systems during pressure cycles and to measure the desorption rate and the desorption gradient of moisture.

As is well known, the KKK originally was a conventional low speed tunnel, which was modified within 5 years for cryogenic operation.

From the original tunnel version only the concrete shell could be taken over, all the other components inside the circuit like the fan and the corner vanes had to be redesigned for operating at low temperature [2,3].

Like each cryogenic wind tunnel, the KKK has some unconventional features, which are necessary for cryogenic wind tunnel testing: - a closed test section including an access lock and a model conditioning room for model handling, when the tunnel is cooled down, - a liquid nitrogen injection system, - a fan driven blow-off system, - an internal insulation for protecting the concrete shell from the low temperature and last but not least a control system to control velocity, temperature and pressure in the test section in the required accuracy (fig. 1).

The materials mainly used inside the circuit are of 9% Nickel steel, stainless steel, Aluminium and laminated Plywood of beech which is installed in those critical sections where high loads have to be transferred from inside into the shell of concrete, and at the same time avoiding the induction of low temperature peaks arising in the concrete.

The modified tunnel has following data:

Test section dimensions	2.4 m x 2.4 m
Model wing span	1.5 m
Static pressure in the test section	atmospheric
Temperature range	100 K to 300 K
Max. Mach number (100 K)	0.38
Max. Reynolds number	8.9×10^6
Fan power	1 MW
Loss coefficient	0.17

The Re-Ma number capability of the tunnel is shown in fig. 2 calculated for a model loss coefficient of $K_{MO} = 0.03$ [4].

So the Reynolds number can be increased by a factor of 5.5 by decreasing the flow temperature from 300 K to a value to 100 K. The originally planned increase of the Reynolds number above this level by using higher pressures or higher velocities was not possible, because the construction of the concrete shell could not stand the resulting stresses. Already now, after the modification, the static pressure in the settling chamber is more than twice the pressure as before with the same fan power of 1 MW.

The completion of the modification of the tunnel was followed in the second half of 1985 by check out and the start up of the different cryogenic systems. In 1986 the aerodynamic and cryogenic calibration was started and completed last year.

This paper will give a review on the facility components and summarizes the testing experience with regard to cryogenic operating considerations. Also presented are the results of the aerodynamic and cryogenic calibrations.

2. Description of the Facility

An aerial view of the KKK is presented in fig. 3. The two liquid nitrogen tanks are located in the

background near corner vane two and the stack of the blow off system can be seen near the second cross leg inside the circuit. The capacity of the two tanks allows one cool down to 100 K and testing over a period of some days.

2.1 Test Section, Access Lock, and Model Conditioning Room

The test section as shown in fig. 4, is 4.5 m long and 2.4 m square with a cross-section area of 5.76 m². The top and bottom walls are parallel, the side walls are slightly divergent with provision for 4 windows. The first cryogenic window with a diameter of 500 mm has been installed and already tested under real operating conditions (fig. 5). This window has been developed by the TU of Darmstadt in the course of the German Cryogenic Technology Programme, sponsored by the Ministry of Research. It consists of two panes of glass with Schlieren quality which each have a thickness of 32 mm. During the cryogenic operation the intermediate space between the two panes must be evacuated as well as the window being heated from outside when the operation temperature is below a level of 200 K. The next three windows will be installed in July of this year. Then the test section is fully instrumented for optical measurement methods. At present the installation of the metal stripes along the four walls is being prepared. These metal stripes are equipped with small pressure holes which will allow the static pressure needed for wall correction methods to be measured during model testing.

For model handling during cryogenic operation in the KKK another access system is used than in the NTF. The access lock and the smaller model conditioning room are located below the test section (fig. 6). After a test run, the model cart is lowered from the tunnel into the lock by help of a simple lifting system consisting of cog wheels and chains. (fig. 7). The cog wheels are driven via special adapters by electrical motors which are installed outside of the lock. When the model cart reaches the right position, the lock will be separated from the tunnel by a horizontal door, which is stored in a parking room when the tunnel is running.

For model changes the interior of the closed lock can be warmed up to ambient temperature by blowing in warm gaseous nitrogen (GN₂). A heating system has been installed outside the testing hall which heats and recirculates the GN₂ to the access lock. In order to get a good heat transfer from the blown in warm GN₂ to the model, the support system, the cart and the other structural parts inside the lock, a number of smaller fans (500 mm diameter) have been installed in different sections of the lock. These fans are used in the other direction too, i.e. when the above mentioned parts have to be cooled down (fig. 8). Finally, before opening the rig door and before human entry dry air is blown in. The access time to the lock takes approximately 4 hours, because of the great masses of the model support, the cart and the lifting system. For minor changes, for example a flap angle change, the model is shifted into the model conditioning room, which then will be separated from the lock by help of two double doors, moving in a vertical direction. In this small room the warm up process can be carried out in about 30 minutes. To use the model conditioning room is considerably cheaper than the lock because the ratio of the operating costs is 1 to 10.

The subsystems of the tunnel, the lock and the model conditioning were designed for an independent cool down and warm up of all the systems.

During the first cryogenic tests there were problems regarding the tightness of the double doors between the lock and the model conditioning room and regarding the reliability of the positioners of the lifting system. The problem of the tightness of the doors, resulting from deformations of the doors in the case of temperature gradients, was solved in a short time.

In the case of the positioners - 14 of them are installed in the lifting system - no suitable commercial equipment was available. Therefore the contractor of the lock had to develop a new design for the positioners, which lasted a time of more than one year. The design of this equipment is very simple and it operates successfully during low temperatures even if there is moisture.

2.2 Model Support System

The model support system of the KKK as shown in fig. 9 will allow the sting configuration and the adaption of the model from below. In the sting configuration the support system permits a pitch range of 40 degrees with a change rate of 0.2 degrees up to 1 degree per second. The model roll range is ± 90 degrees. Sideslip angles are obtained by combinations of pitch and roll.

The drive motors and the positioners are installed in super insulated boxes, which are heated inside.

The hollows of the structural parts of the support system, such as the interior of the sword are flown through continuously by help of a number of small fans, which are installed in the model cart, to ensure that there is no temperature gradient in the different systems. For example the gas flowing through the sword will be blown out near the two bearings of the rolling system, achieving the same temperature for both.

During the first test under cryogenic conditions there were difficulties at the plugs of the cables coming from the balance and from the positioners. That means the problems were concentrated only on the transfer of the electrical signals at a low level.

Having installed these critical plugs in heated boxes in the interior of the model cart, the model support system operates as required.

We have learned from this experience, that the number of cable connections in cryogenic environment should be as small as possible.

2.3 Fan and Drive System

The fan with a diameter of 4.3 m has 12 fixed blades and 11 guide vanes (fig. 10) and is powered by a 1 MW variable speed motor. It is made of 18% Ni steel and has some properties which permit reliable operation at very low temperatures:

- It lies on an assembly of prestrained springs which permit a change of diameter due to the temperature change up to 12 mm. These bearings are heated.
- During cryogenic operation of the wind tunnel the inside of the nacelle is ventilated with warm GN_2 to keep the temperature of the bearings, couplings and shaft at approximately 300 K.
- Important supply and control systems are redundant for safety reasons during operation.

The original philosophy was to maintain a constant pressure in the heating system independent of the tunnel pressure in the fan section to ensure that no cold GN_2 would penetrate from the tunnel into the nacelle. During the check out of the fan system it was seen that the consumption of GN_2 of the heating system was too high resulting from the untightness in the labyrinths located between shaft and nacelle. Therefore the concept was changed and now the pressure in the heating system follows synchronously the pressure in the gap between the nacelle and the blower.

In contrast to the other sections of the circuit the fan house is the only system with an external insulation (fig. 11). The transition from the internal insulation of the shell to the external insulation of the fan house upstream and downstream of the fan is taken over by two rings of the above mentioned special plywood with a thickness of 50 mm and a height of 450 mm. These rings are screwed on the one hand to the fan house and on the other hand by compensators to the shell. During cool down and warm up these rings must adjust to the change of diameter of the fan house due to temperature change. Although this transition is a critical section it operates without problems. An upstream view of the installed fan can be seen in fig. 12.

2.4 Liquid Nitrogen System

The requirement of LN_2 for a steady state operation is shown in fig. 13 with the fan power as a parameter. Without taking into account the heat transfer through the insulation, the LN_2 -mass flow reaches values between 0.1 kg/s and 4.6 kg/s. For tunnel cool down and run up the requirement of LN_2 is nearly twice as high.

The LN_2 -system has been developed and optimized by experimental tests and theoretical calculations. In an early phase of the project it had been decided to locate the LN_2 -system downstream of the fan to avoid additional risks for this component. Theoretical calculations performed before had shown, that a mixing length of 80 m from the injection station to the test section would ensure an uniform temperature field at the location of the model [5, 6].

Temperature measurements during the cryogenic testing of the tunnel upstream corner 3 and in the test section have confirmed the calculations and have shown that the distribution of the cold sources in the injection section and the direction of injection was optimally selected (fig. 14). Already after a mixing path of nearly 40 m in the exit of the second diffuser the deviation of the temperature in vertical direction is smaller than 10 K. For small mass flow rates of LN_2 the injection is achieved by help of the pressurized tanks (5 bar) which is more economical than injection by pumps (fig. 15). Furthermore by this method strong throttling of the pumps in the case of low mass flow is avoided, by which the LN_2

would be warmed up by about 10 K or more.

For high mass flow rates the LN_2 is led via 2 pumps from the tanks to the control valves at a constant level of 25 bar independent of the injected mass flow. In order to ensure an accurate control of the injected mass flow rate of LN_2 by the control computer, the pressure is measured downstream of every control valve and furthermore the temperature is measured in every injection rake by help of PT 100 probes (fig. 16). So it can be controlled if there is a one-phase flow or a two phase-flow upstream of the spreading nozzles.

2.5 Blow-Off and Blow-In Systems

The tunnel pressure is controlled by a ball valve which is installed in the pipe between tunnel and stack (20 m high). Originally, this valve was pneumatically driven but because the velocity for adjusting a new position of the valve was not high enough and additionally the reproducibility of the angle of the valve was not sufficient, an electric hydraulic drive motor was then installed. This new drive enables the pressure of the tunnel to be controlled with the required velocity and accuracy (fig. 17).

To support the exhausting of the cold GN_2 an injector of ambient air is used. As can be seen in fig. 18, this injector may be driven by several fans which supply the collector from the bottom. The necessity to use an injector in this tunnel with small overpressure will be demonstrated in the next two figures. Fig. 19 and fig. 20 will show the vent plume of KKK with and without injector.

In the blow off system, a relief system and a blow in system are incorporated. The blow in system allows gaseous nitrogen or dry compressed air to be injected into the tunnel. This is the purging process as a preparation for the cool down stage of the tunnel.

2.6 Internal Insulation

The internal insulation system which has been developed especially for this tunnel, consists of nearly 3000 panels with the dimension of 1 m x 1 m which are divided into three layers with different physical characteristics. As can be seen in fig. 21, there is a small layer between the first layer, glued to the concrete shell and the panel, which will come to serious deformations during cryogenic operation. The task of the small layer, consisting of elastified polystyrole, is to avoid additional tension in the insulation [7].

Wooden covers are used as flow liners; they are connected to the shell with rods of low thermal conductivity. To protect the insulation system from non-evaporated liquid nitrogen, downstream of the injection station over a length of 20 m a special foil consisting of glass fibre and Teflon has been installed (fig. 22). This foil is located between the insulation panels and the wooden liner. Along this foil a number of thermo couples have been installed, which are connected to the control room to inform the operator of the presence of liquid nitrogen.

3. Modeling and Control of the Tunnel

For a cryogenic wind tunnel it is essential, that the tunnel can be operated in an efficient manner in order to minimize liquid nitrogen consumption and the operating costs. The control system of the KKK is constructed on a modular basis [8]. The tunnel can be operated in a hand mode or in a computer-controlled mode, respectively. In the stand-by phases a micro computer unit takes over the control which possesses a higher reliability than a normal computer. It also automatically takes over control of the tunnel if the control computer should fail. Mr. Kronen, who has developed this system will hold a detailed lecture on the same following my lecture [9].

4 Aerodynamic Calibration of the Tunnel

After completion of the KKK and check-out of all systems, the aerodynamic calibration of the tunnel under ambient conditions was started to determine the flow quality in the test section and the loss coefficients in the various tunnel sections.

The determination of the performance of the tunnel up to the maximum drive power of 1 MW has shown, that the highest velocity in the clean test section is more than 115 m/s and better than calculated (fig. 23). The loss coefficient of the circuit of 0.171 is a result of the smooth surface of the wooden cover of the insulation, the efficiency of the diffusors and the high contraction of the nozzle of more than 10:1.

Fig. 24 shows the velocity distribution in the test section in horizontal direction. The deviation of the velocity from the ideal value is equal to the required quality. Information on the turbulence level of the test gas at the location of the model in the KKK in relation to the DNW, a very modern wind tunnel with excellent flow qualities, is given in the next figure (fig. 25).

For velocities lower than 75 m/s the turbulence level in longitudinal direction is about 0.065 %; it increases up to 0.11 % when the tunnel is running at 100 m/s.

The mentioned data for the velocity distribution and the turbulence level in the test section of the KKK are in accordance with the requirements for a modern wind tunnel.

5. Cryogenic Calibration of the Tunnel

The first cool down was started half a year after the completion of the modification and served to check the reliability of the cryogenic components and to reveal possible malfunctions. The temperature set point of this test was 180 K.

Before injecting liquid nitrogen the circuit was purged very carefully, at first with dry compressed air with a dew point of -60 degrees and finally with gaseous nitrogen to reduce the humidity and the O_2 concentration inside the tunnel (fig. 26).

By blowing in 10 t of compressed air over a time of 3 hours in steps of 250 kg the dew point of the test gas could be reduced by 12 degrees. After this 15 t of gaseous nitrogen were blown in with the result that the final dew point was -18 degrees and the O_2 concentration was below a level of 2 %. At each step where 250 kg were blown in the pressure in the tunnel increased by 50 mbar. This pressure was maintained over a period of 2 min while the tunnel was running at a speed of 5 m/s in the test section. The pressure was then decreased and the next step initiated.

The pressure increase during purging ensures that all dead volumes and hollows below the liner are also purged. To accelerate this process the liner is equipped with many holes.

The complete purging procedure covers a period of 7 hours.

The mechanism of this process can not be described in detail in this short lecture. The fact is, that the humidity inside the circuit where the test gas initially has a capacity of nearly 54 kg of water (for a humidity of 80%), can be reduced to 5 kg for a volume of the tunnel of 4300 m³. During this time the desorption of water from the insulation into the circuit is about 1.5 kg and from the wooden liner less than 20 kg. During the following cool down of the tunnel this desorption process is blocked by frost. The only remarkable deficit found during this first cryogenic test were cold spots, which appeared near the junction points of the concrete shell at the beginning on the end of the second diffuser after an operation time of about 20 hours (fig. 27). These cold spots were a result of leaks between the concrete and the rubber compensator installed there.

After elimination of these deficits, the tunnel was cooled down to the specified set point of 100 K, with a constant temperature gradient of 10 K/h. Up to this point, the consumption of LN_2 was 90 t (fig. 28). When the lowest temperature was reached, downstream of the injection station on the bottom wall, liquid nitrogen was registered by sensors installed on the upper side of the above mentioned foil. The reason for this was a too small velocity of the test gas in this tunnel section in relation to the injected mass flow of LN_2 .

During this cool down, the performance of the fan and the distribution of the temperature in various tunnel sections, especially in the test section, were measured.

Fig. 29 shows a typical scenario of a cryogenic wind tunnel which enables the achievement of a spectrum of Reynolds numbers by a combination of temperature and velocity.

One of the most important test results - shown in fig. 30 - is the vertical temperature distribution in the test section for different velocities. For small velocities, there is an undesired gradient of nearly 10 K as a result of the dominating free convection in the tunnel sections with big dimension, especially in the settling chamber upstream of the contraction. By increasing the velocity to more than 15 m/s this effect disappears and the deviation of the temperature is smaller than ± 0.5 K. During model testing these critical low velocities will not be used.

Temperature measurements in the configuration sting balance and model have shown that there exists a high temperature gradient over the balance of more than 16 K during the unsteady phase, when the tunnel is

being cooled down (fig. 31). The time of delay of the temperatures along the balance is nearly one hour. It can be seen in this figure that the heat transfer from the model to the balance is carried out in a shorter time than from the sting to the balance. The reason for this effect is the higher ratio of surface to included mass of the model compared to that of the sting. The big gradient automatically has consequences on the accuracy of the measuring results. To achieve accurate wind tunnel test results it is necessary that the gradient over the balance is smaller than 5 K. To achieve this it is necessary to control and to manipulate the heat transfer at the adapters of the balance to the model and to the sting. A first step in this direction was carried out by some basic research with the following strategy:

- to throttle the heat transfer at the model adapter during cool down
- to accelerate the heat transfer at the sting adapter during warm up.

The throttling during cool down is done by heating the model adapter and on the other hand the acceleration of heat transfer during warm up process by heating the sting adapter.

Fig. 32 shows the test arrangement and the result of these first investigations. The balance dummy, the sting and the fuselage are equipped with a number of thermocouples, furthermore the sting adapter and the model adapter are fitted with heating foils.

The tests were performed in the model conditioning room of the tunnel. During all tests performed, the temperature was lowered to a level of 100 K within 30 min.

As can be seen in this diagram in the case of unheated adapters the temperature in the front section of the balance follows quickest the temperature of the gas in the model conditioning room.

The second curve is the result of the test with heated model adapter. The heating process was started immediately after the cool down procedure. After a testing time of 30 min (100 K test gas temperature), the temperature on both ends of the balance was indeed at the same level, but in the middle of the balance the deviation of the temperature was higher than 30 K. This result was not satisfactory.

The third curve was achieved after installing a radiation shield around the balance dummy. By help of this equipment there is almost a constant temperature along the balance. That means by help of heating the model adapter and of the installation of a radiation shield during cool down, the required uniform temperature along the balance will be achieved.

These tests will be continued.

6. Operation Costs

It is well known that the operation costs of a cryogenic wind tunnel are higher than the operation costs of a conventional tunnel operating with the same fan power. But on the other hand it is well known too that it is remarkably cheaper to achieve a definite Reynolds number in a cryogenic wind tunnel than in a conventional tunnel. The drive power can be described by the formular

$$P \sim p_{TS} \cdot Ma^3 \cdot l^2 \cdot T^{1/2}$$

When decreasing the temperature from $T_0 = 300$ K to $T_1 = 100$ K, the fan power is reduced for $Ma = \text{const}$ to

$$P_1 = P_0 \cdot \left(\frac{T_1}{T_0} \right)^{1/2} = P_0 \cdot 0.577$$

while the Reynolds number at the same time is increasing to

$$Re_1 = Re_0 \cdot \left(\frac{T_0}{T_1} \right)^{25/18} = Re_0 \cdot 4.59$$

Additional costs in relation to a conventional wind tunnel are

- costs for cool down
- cost to maintain the low temperature.

In fig. 34 the consumption on LN_2 required to achieve the low temperatures in the KKK is shown.

Approximately 90 t of LN_2 are required to cool down to 100 K.

It can be seen furthermore that the daily consumption of LN_2 to maintain the tunnel at a level of 100 K

is about 24 t. This means that after a period of 4 days, the injected mass of LN_2 is the same as for one cool down procedure to this temperature level.

The concrete shell of KKK has a surface of nearly 2500 m^2 and the internal insulation a thickness of 320 mm with a heat transfer coefficient of only 0.028. For cryogenic tunnels with a smaller thickness of the insulation the consumption of LN_2 during the stand-by phases will therefore be proportionally higher.

Parallel to these experiments the mass flow rate per second and the consumption of LN_2 for different cool down gradients to the set point of 100 K, starting at 295 K were calculated.

In fig. 35 the results of these calculations can be seen for the three temperature gradients of 10 K/h, 20 K/h and 50 K/h. The diagram shows the mass flow of LN_2 per second during the cool down and stand-by phases. The KKK is cooled down with a gradient of 10 K/h and the results of these calculations agree with the results of the test.

In order to operate a cryogenic wind tunnel economically and efficiently it is necessary to have detailed information about the consumption of LN_2 during the different operating phases. In fig. 35 it is shown that the consumption of LN_2 is remarkably lower for higher cool down rates than for smaller rates. However, it can also be seen that the highest cool down rate is coupled with the highest consumption of LN_2 during the stand-by phase. The reason for this effect is the marked unsteady temperature condition in the liner and in the insulation at the end of the quick cool down phase.

7. Planned Testing Programme

Several testing programmes are now in preparation.

- AGARD calibration model (fig. 36). Maximum Re-number: 17 mill.
- Airbus model
- TST model
- 2-D model, maximum Re-number: 35 mill.

For the AGARD calibration model a special instrumentation box installed in the nose of the model has been developed. The measurements of the forces and the moments will be conducted with a cryogenic balance, developed by the TU Darmstadt in cooperation with MBB/Bremen.

8. Conclusion

The aerodynamic calibration under ambient and cryogenic conditions is completed. The tunnel operates without problems in the specified temperature range. The temperature of the test gas in the modified tunnel ranges from 300 K to 100 K. The maximum Reynolds number achieved at the lower temperature is 8.9×10^6 . Even at the lowest temperature in the tunnel, the deviation of the temperature in the test section is smaller than $\pm 0.5 \text{ K}$.

References:

- [1] W. E. Bruce Testing and Check out Experiences in the National Transonic Facility since
B. B. Gloss becoming operational
L. W. McKinney Second Cryogenic Review Meeting
DLR Köln-Porz, June 28th - 30th 1988
- [2] G. Viehweger Kryogenisierung des Niedergeschwindigkeits-Windkanals Köln-Porz
- Spezifikationsphase -
WKT 11/80, DLR, Köln-Porz 1980
- [3] G. Viehweger The Cryogenic Wind Tunnel Cologne
AGARD-CP-348, Paper 4, Sept. 1983
- [4] G. Viehweger Windkanäle höherer Reynoldszahlen am Beispiel des Kryo-Kanals Köln (KKK)
DGLR-Jahrestagung, Okt. 1984

- [5] R. Schräwer Konzeptstudie zum Stickstoff-Einspritzsystem des Kryo-Kanals Köln
Messer Griesheim, Frankfurt, 1980

- [6] D. Distelrath Experimentelle Untersuchungen zum Stickstoffeinspritzsystem des Kryo-Kanals Köln
DLR - IB - 157 - 80C30, DLR, Köln-Porz, 1980

- [7] B. Palancz Unsteady Thermal Stress Analysis of Cryogenic Foam Insulation Element
B. Schäfer DLR-FB 81 - 17, 1981

- [8] R. Kronen Das Control System des 0.3 TCT (Langley) und des KKK
DLR - IB - 39114 - 87B05, 1987

- [9] R. Kronen Automatic Control of KKK Requirements, Sensors, Actuators and Control Performance
Results
VKI, Brüssel, June 1989

- [10] G. Viehweger Erste Versuche im Tieftemperaturbereich mit dem KKK
R. Rebstock
W. Becker DLR - IB - 39114 - 87A17, 1987

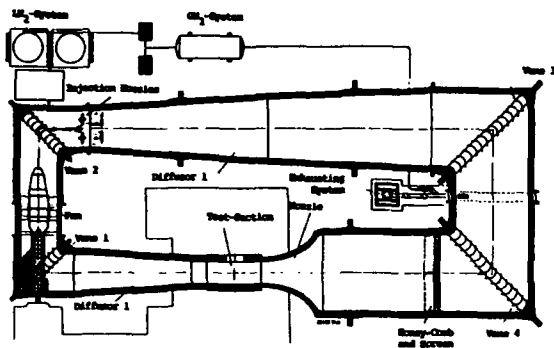


Fig. 1: Plan view of KKK tunnel circuit showing components and arrangements.

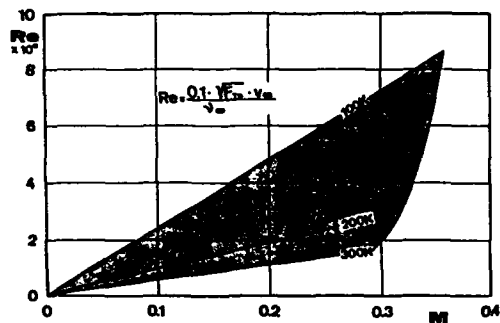


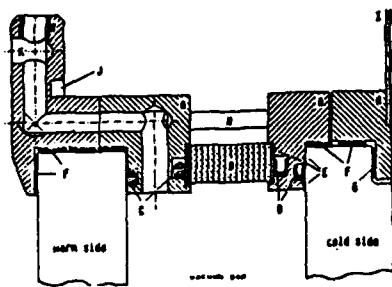
Fig. 2: The Reynolds-Mach number capability of KKK



Fig. 3: Photograph of the KKK facility



Fig. 4: View of the test section looking downstream



- A: stainless steel frame
- B: central insulation ring
- C: NBR-O-ring vacuum seals
- D: spring-loaded PTFE-rings
- E: location of Indium gaskets
- F: Teflon gaskets
- G: Graphite counterlayer
- I: Aluminium cold plate

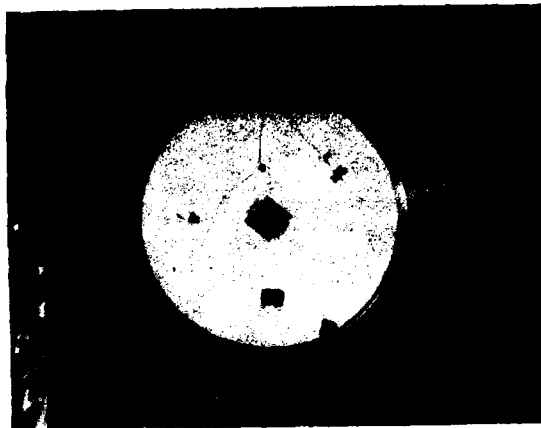


Fig. 5: Cryogenic measurement window

- a) Construction
- b) Installation in the test section

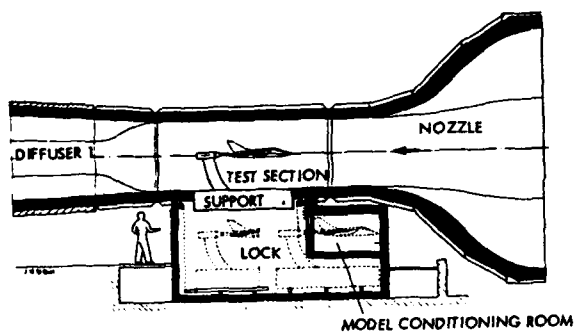
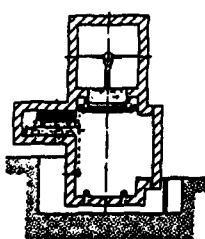
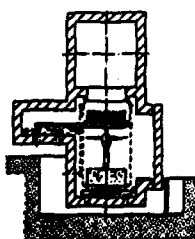


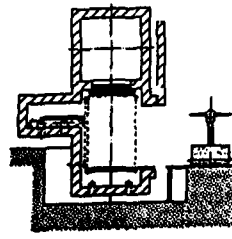
Fig. 6: Test section including access lock and model conditioning room



MODEL CART IN TESTING POSITION



HORIZONTAL DOOR ON THE LIFT



TUNNEL SEPARATED FROM THE LOCK
MODEL CART OUTSIDE THE LOCK

Fig. 7: Model cart and horizontal door in different operating phases

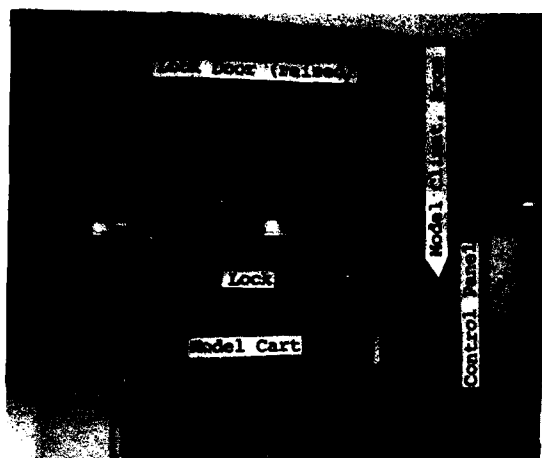


Fig. 8: Access lock and model conditioning room installed. Shown in the opened condition

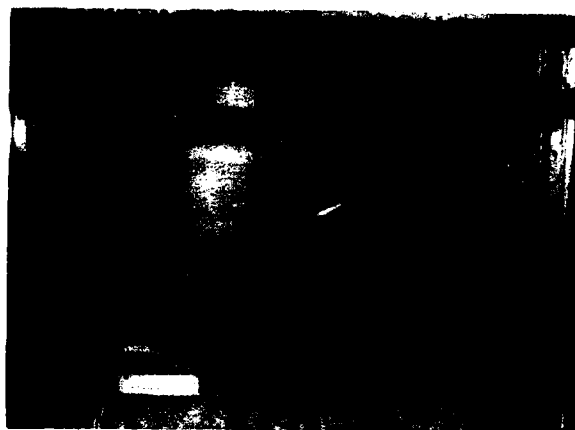


Fig. 9: Model support for pitch and roll

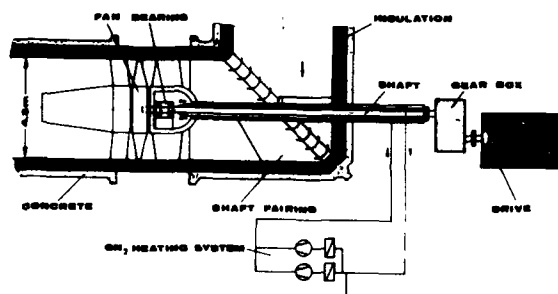


Fig. 10: Schematic view of fan heating system

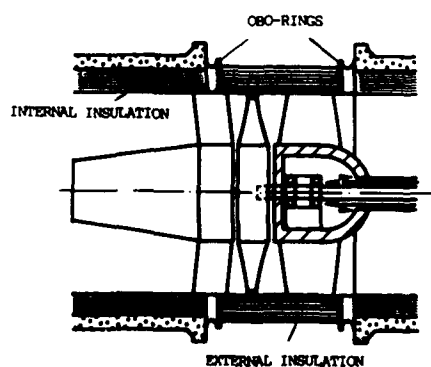


Fig. 11: Transition from external insulation in the fan section

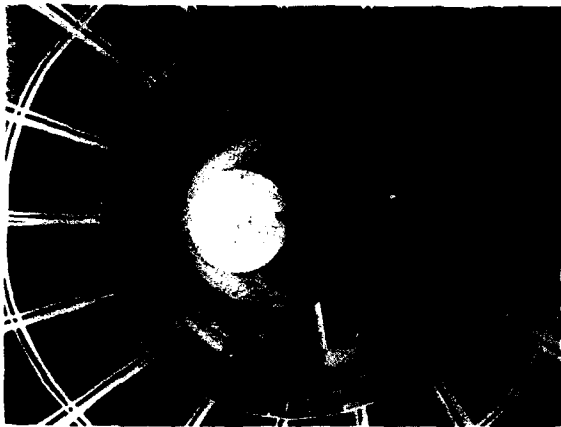


Fig. 12: View of the fan

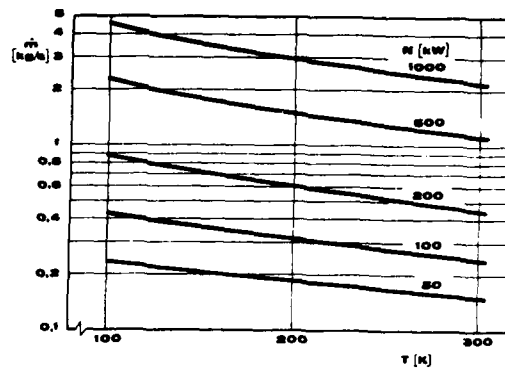


Fig. 13: Consumption of liquid nitrogen in dependence on fan power and test gas temperature

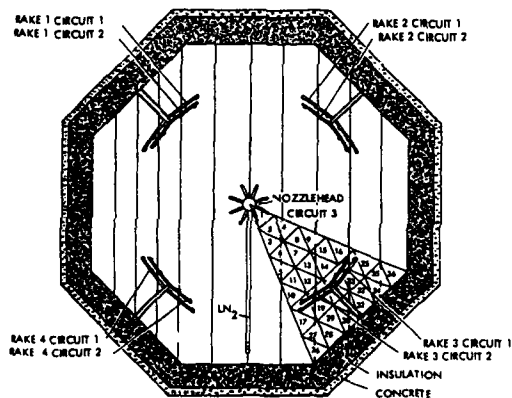


Fig. 14: Arrangement of the rakes with theoretical selected location of the nozzles

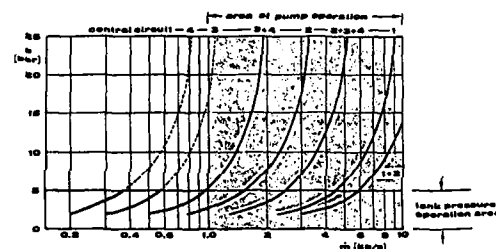


Fig. 15: Mass flow of liquid nitrogen system

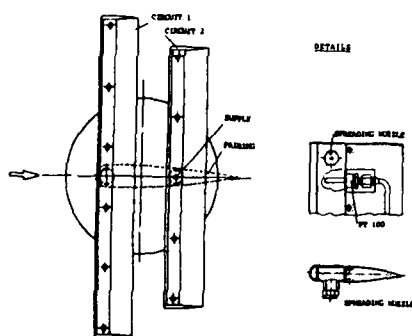


Fig. 16: Rakes with installed nozzles and PT 100 probes

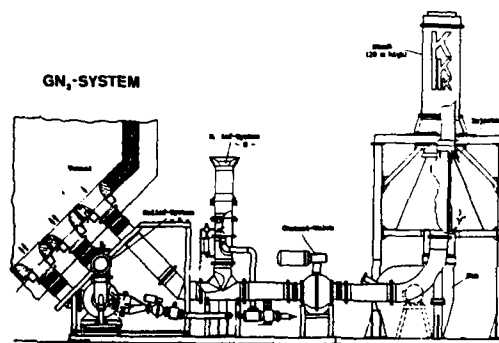


Fig. 17: The blow off system with control valve, injector and stack

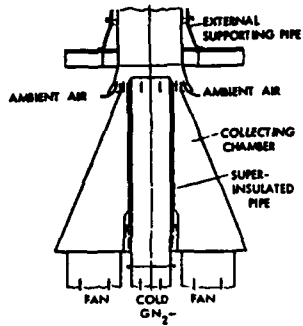


Fig. 18: The fan driven injector of the blow off system



Fig. 19: View of the KKK vent plume taken during check out $\dot{m}_G = 10 \text{ kg/s}$, $T_G = 100 \text{ K}$
 $T_A = 278 \text{ K}$

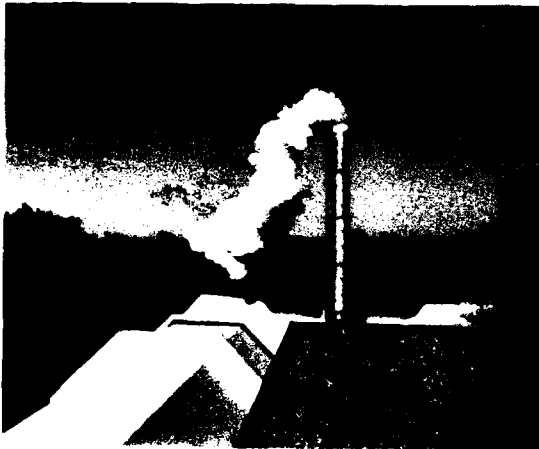


Fig. 20: View of KKK vent plume injector not in operation $\dot{m}_G = 10 \text{ kg/s}$, $T_G = 100 \text{ K}$

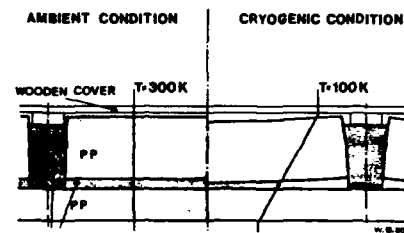


Fig. 21: Schematic view of an insulation panel for ambient and for cryogenic temperature conditions



Fig. 22: Installation of the foil downstream the injection station

1.) Calculation

Section	K_1
Test section	0,02606
Diffusor 1	0,06308
Corner vane 1	0,02421
Fan section	0,00166
Corner vane 2	0,01915
Diffusor 2	0,01051
Corner vane 3	0,00134
2. Cross leg	0,00005
Corner vane 4	0,00134
Settling chamber	0,00016
Honey comb, Screens	0,0235
Contraction	0,00284
K_0	0,17390

2. Measurement

$$K_0 = 0,171$$

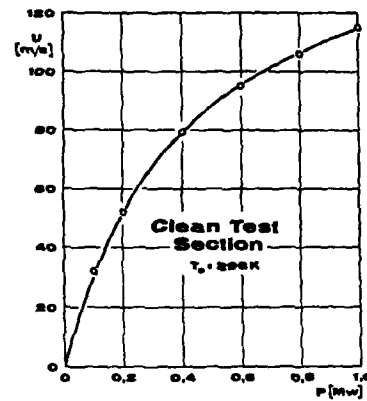


Fig. 23: Loss coefficient and performance of the tunnel

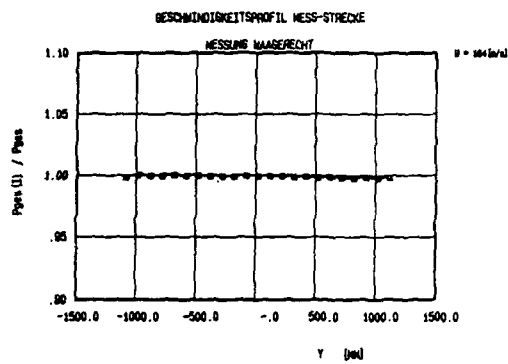


Fig. 24: Horizontal velocity distribution in the test section

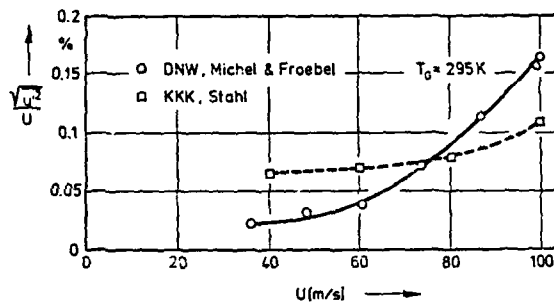


Fig. 25: Turbulence in the test section comparison between KKK and DNW

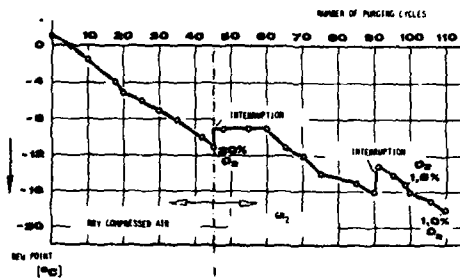


Fig. 26: Change of the dew point of the test gas during the purging cycle



Fig. 27: Cold spots near the junction points of the shell in the section of diffusor 2

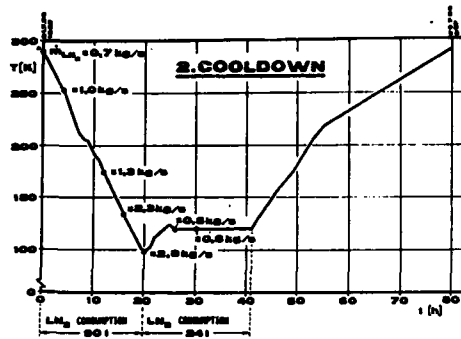


Fig. 28: Temperature diagram of the
2. cool down

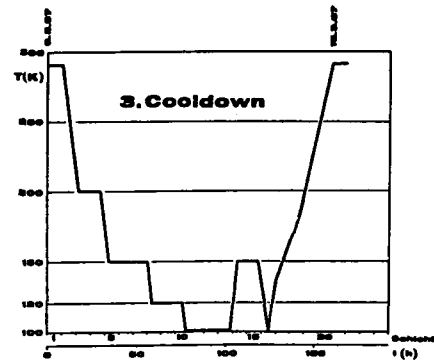


Fig. 29: Temperature diagram of the 3. cool down

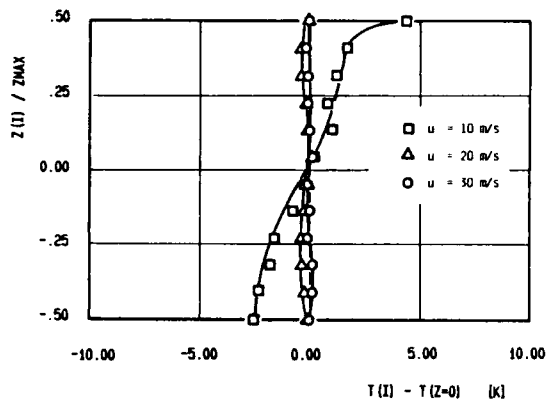


Fig. 30: Vertical temperature distribution in the
test section in dependence from the
velocity. $T_G = 120$ K

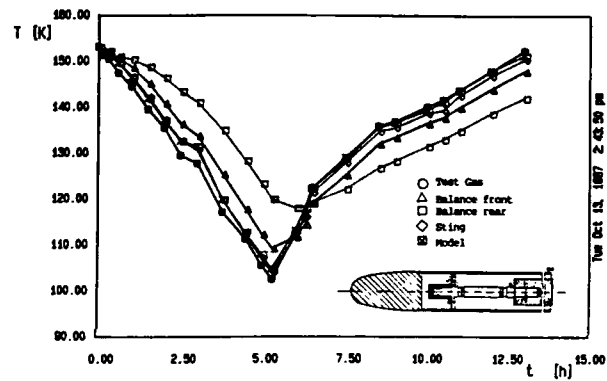


Fig. 31: Temperature distribution in the configu-
ration sting, balance, model

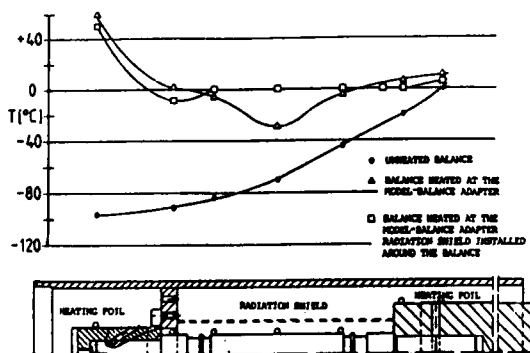


Fig. 32: Temperature distribution over the
balance-dummy for heated and
unheated conditions

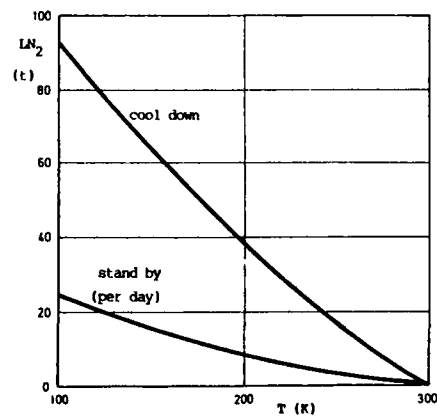


Fig. 33: Consumption of LN_2 during the cool down
and stand-by phases

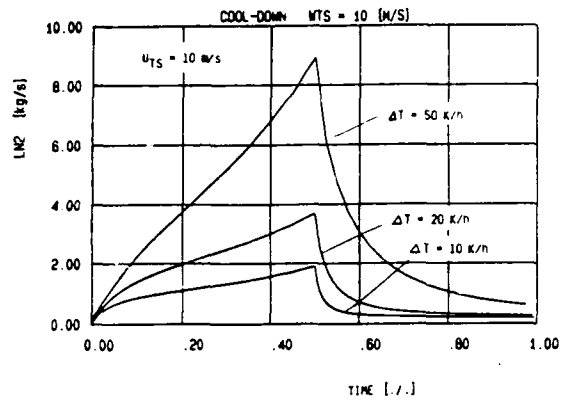


Fig. 34: Mass flow of LN_2 per second during the cool-down and stand-by phases for different cool down gradients. Start condition: $T = 295 \text{ K}$ Set point: $T = 100 \text{ K}$

ΔT [K/h]	Consumption LN_2 [t]		
	Cool down	Stand by	
50	65	58	123
20	78	36	114
10	84	24	108

Fig. 35: Consumption of LN_2 in the cool-down and stand-by phases for different cool-down gradients. Start condition: $T = 295 \text{ K}$ Set point: $T = 100 \text{ K}$



Fig. 36: AGARD-model in the lock below the test section during preparation

AUTOMATIC CONTROL OF KKK Requirements, Sensors, Actuators, and Control Performance Results

by

R.Kronen
Deutsche Forschungsanstalt
für Luft- und Raumfahrt e.V.
5000 Köln 90
Postfach 90 60 58
Federal Republic of Germany

Summary

After the modification of the low speed wind tunnel at the DLR Research Center at Cologne to a cryogenic wind tunnel a new control system was necessary. For lay out of the control system and for studying the tunnel behaviour some mathematical models were developed. The models and the controller were tested by computer simulations. Furthermore the control system was tested with the real tunnel for the run-up, testing, run-down phases.

List of Symbols

A_T	m^2	tunnel surface
A_{TS}	m^2	cross section area of the test section
A_{ME}	m^2	surface of the metal parts
V	m^2	geometrical factor of the tunnel
u_{TS}	m/s	velocity in the test section
n_F	min^{-1}	revolution per minute
\dot{m}_{LN_2}	kg/s	mass flow rate of the injected LN_2
\dot{m}_{GN}^-	kg/s	mass flow rate of the exhausted GN_2
$\dot{m}_{GN_2}^+$	kg/s	mass flow rate of the injected GN_2
m_G	kg	total gas mass in the tunnel
T_{TS}	K	temperature in the test section
T_G	K	gas temperature
T_G^*	K	temperature of the injected GN_2
T_{ME}	K	temperature of the metal parts
T_W	K	temperature of the wooden cover
T_I	K	temperature in the insulation
T_S	K	temperature of the injected LN_2
ρ_{TS}	kg/m^3	density in the test section
p_{TS}	N/m^2	static pressure in the test section
Δp_F	N/m^2	pressure increase by the fan
t	s	time
τ	s	time delay
i_{LN_2}	kJ/kg	enthalpy of the injected LN_2
c_{PG}	$kJ/kg \cdot K$	specific heat capacity of the test gas
α_K	$W/m^2 \cdot K$	heat transfer coefficient through the insulation
α_K	$W/m^2 \cdot K$	heat transfer coefficient between the metal parts
η_F	-	efficiency of the fan

K_T	-	loss coefficient of the tunnel
K_{MO}	-	loss coefficient of the test model
Re	-	Reynolds number
M	-	Mach number

1. Introduction

After the modification of the low speed wind tunnel at the DLR Research Center at Cologne to a cryogenic wind tunnel (fig. 1) with a closed test section, there were new requirements necessary to the control system of the tunnel [1].

In a conventional subsonic wind tunnel with an open test section only the velocity u_{TS} has to be controlled.

Now after the modification, two additional fluid dynamics parameters have to be controlled, the static pressure P_{TS} and the temperature T_G . To control the velocity in the KKK a conventional RPM-controlled DC-engine is used. The LN_2 -system allows the compensation of the dissipation heat as well as of the variation of temperature. Static pressure control is performed by the GN_2 -system which alternatively allows warm gaseous nitrogen to be blown in, or to be blown out of the tunnel [2, 3].

Every action of these three systems has not only an effect on one parameter as described above, but also an undesired influence on the other two variables. This strong coupling makes it hard to control the tunnel by hand. Therefore an automatic system is recommended for a safe and economical operation of the KKK, to minimize liquid nitrogen consumption and the operating costs. An automatic control system has furthermore to yield accurate and reproducible test conditions.

2. Operating Phases

During the operation of the KKK six different operating phases can be distinguished (fig. 2):

- Cool-Down
- Stand-By
- Run-Up
- Testing
- Run-Down
- Warm-Up

Before starting the cool-down phase, some preparations must be carried out. To prevent freezing of moisture in the tunnel the enclosed ambient air with ambient humidity is exchanged to dry compressed air. After this, the new dry air in the tunnel is changed to the gaseous nitrogen, to decrease the oxygen concentration below 2 %.

Cool-Down

During cool-down the temperature is decreased by injecting liquid nitrogen. At this phase the maximum gradient is 10 K/h to limit thermal stress in the internal insulation and in the structure. So a 20 h cool-down is necessary to decrease the temperature from ambient to the lowest test temperature of 100 K. During this cool-down phase the fan is driven at a low speed to prevent vertical temperature gradients in the tunnel which are not allowed for the fan itself and to enable sufficient heat transfer from the gas to the enclosed parts.

The static pressure in the test section must be constant and equal to the atmospheric pressure. Thus the unnecessary test gas must be blown off by the GN_2 -system.

Stand-By

For a new configuration of the test model or during a break between two tests the tunnel is maintained at a constant temperature. This phase is called stand-by phase. During stand-by phase the tunnel runs at low speed, and the LN_2 -system must compensate only for the fan power and for the heat loss through the insulation.

Run-Up

During this phase the velocity is increased by a given trajectory up to the test Mach number. At this run-up phase the GN_2 -system must blow in gaseous nitrogen to hold the static pressure at a constant level in the test section.

Testing

During the testing phase all tunnel states must be held at the required set point with a sufficient accuracy. All control loops are active. The controller has to compensate too the variation of the loss coefficient of the tunnel due to changing model angle of attack.

Run-Down

After testing, the velocity must be decreased to the slow stand-by velocity. Since there is no active break for the fan-drive available the falling off of velocity depends on friction loss in the tunnel. The unnecessary gas mass must be blown off by the GN_2 system.

Warm-Up

If a break between two test series is longer than four days it is more economical to warm-up the tunnel than to maintain it at low temperature. The warm-up can be done actively or passively depending on time and cost.

2.1 Required Accuracy for Different Operating Phases

For every operating phase the limits and tolerances for all tunnel states were defined. But some restrictions are always valid independent of the operating phase (table 1), [4].

The old concrete shell of the tunnel was not designed as a pressure shell, so there is a stringent restriction for the difference of the maximum static pressure and the outside pressure which may never be above 100 mbar.

At cold test condition the velocity in the test section may not be lower than approximately 10 m/s over a longer period, so as to prevent thermal stress damages and deformations at the fan-house due to temperature gradient in the tunnel [5].

3. Modeling of the Tunnel

For some investigations it was necessary to be able to describe the process in the wind tunnel. Therefore several mathematical models were developed [6, 7]:

- single segment model
- inverse single segment model
- linearized model
- multiple segment model.

The single segment model is a further development of the dynamic model, which already has been used for the design of the injection and exhaust systems. The inverse single segment model is included in the modular controller. The linearized model was used for the layout of the control system and the multiple segment model was used for the testing of the single segment model.

3.1 The Single Segment Model

In the single segment model the variables of state are considered to be concentrated in one discrete point. In this simplification it is assumed that the internal compensation process is fast with respect to a change of the tunnel variables u_{TS} , P_{TS} and T_G with time. (An example for the internal compensation process is the temperature distribution along the tunnel axis). The non linear and cross coupled behaviour of the KKK can be described with the help of the equations of equilibrium which show the relation between one variable of state and the other variables of state and the input variables.

The variables of state for the KKK model are:

- test section gas temperature T_G
- concentrated metal part temperature T_{ME}

- velocity in the test section u_{TS}
- static pressure in the test section p_{TS}
- total mass of the gas in the tunnel m_G

As input variables influencing the process in the wind tunnel are used:

- injected LN_2 mass flow rate \dot{m}_{LN_2}
- exhausted GN_2 mass flow rate $\dot{m}_{GN_2}^-$
- injected GN_2 mass flow rate $\dot{m}_{GN_2}^+$
- fan revolutions per minute n_F

Each control input affects all the tunnel variables and the thermofluid dynamical interaction occurs both in the space of the tunnel and in time. The equations of the mathematical model for the processes in the wind tunnel are derived from the equations of equilibrium. These equations are the heat equilibrium derived from the first law of thermodynamics, the mass equilibrium and the momentum equilibrium equation. This model is completed with the time-delay model, the wall insulation model and the fan model. Most of the equations are differential equations.

Equilibrium of Heat

$$\begin{aligned} \frac{dT_G}{dt} \cdot m_G \cdot c_v = & - \dot{m}_{LN_2} \cdot (i_{LN_2} + T_G \cdot c_v - T_S \cdot c_{pG}) \\ & + \dot{m}_{GN_2}^+ \cdot (T_G^* \cdot c_{pG} - T_G \cdot c_v) \\ & - \dot{m}_{GN_2}^- \cdot T_G \cdot (c_{pG} - c_v) \\ & + \alpha_K \cdot A_T \cdot (T_W - T_G) + \alpha_{KM} \cdot A_{ME} \cdot (T_{ME} - T_G) \\ & + (K_T + K_{MO}) \cdot \rho_{TS} \cdot u_{TS}^3 \cdot A_{TS} / 2 \eta \end{aligned} \quad (1)$$

This means that the change of enthalpy of the gas contained in the tunnel must be equal to the sum of the heat transfer through the insulation, heat of dissipation and the change of enthalpy between the gas and the injected GN_2 , minus the enthalpy due to evaporation and minus the enthalpy due to the overheating of the injected LN_2 . The sum has also to be reduced by the amount of heat transport between the different metal parts (e.g. fan, corner vanes) and the tunnel gas, and by the enthalpy of the gas being blown off.

Equilibrium of Momentum

$$\frac{du_{TS}}{dt} = \left[\Delta p_F - 1/2 \cdot (K_T + K_{MO}) \cdot \rho_{TS} \cdot u_{TS}^2 \right] / V \cdot \rho_{TS}$$

The variation of the momentum of the gas equals the pressure increase by the fan minus the pressure loss in the tunnel and at the model.

Equilibrium of Mass

$$\frac{dm_G}{dt} = \dot{m}_{LN_2} - \dot{m}_{GN_2}^- + \dot{m}_{GN_2}^+$$

The variation of the mass of the enclosed gas is equal to the sum of the injected LN_2 and GN_2 mass, reduced by the sucked GN_2 mass.

In addition to the above mentioned equations there are some sub-models in the mathematical procedure:

- fan model: the relationship between speed of rotation n_F and p_F is described
- wall-model: the temperature in the wooden cover T_W and in the insulation ΔT_I is calculated.

- test-model drag model: with the angle of attack the loss coefficient K_{MO} is calculated.
- time-delay model: the transport time delay for an injected LN_2 -particle up to the test section is determined.

3.2 The Inverse Single Segment Model

One module of controller is the inverse single segment model. This model calculates the necessary actuator trajectories for a given set of state variables trajectories.

For this model the same equations as in the single segment model are used. But in contrast to the single segment model the input variables are the tunnel states, and the outputs are the actuator movements.

3.3 The Linearized Model

For the layout of the control system the single segment model was linearized for 5 different operating points (fig. 3). The common description in the time domain is chosen for the mathematical description.

$$\dot{x} = A \cdot x(t) + B_0 \cdot u(t) + B_1 \cdot u(t - \tau) + D \cdot d(t)$$

It is $x(t)$ vector of state
 $u(t)$ input vector
 $u(t - \tau)$ time delayed input vector
 $d(t)$ disturbance parameter
 (influence of the test model)

The system's own dynamical behaviour is described by the system matrix A. The influence of the input parameters on the parameters of state is described by the matrix B (B_1 for the time delayed dependence and B_0 for the other dependences). D describes the influence of the angle of attack on the vector of state x.

There are great differences between the single elements of the matrix at the different working points, as the calculations have shown. This indicates the non-linearity of the system. The details are described in Ref. [8].

3.4 The Multiple Segment Model

To be able to describe the temperature distribution along the tunnel axis the Multiple-Segment-Model was developed. For this model the equilibrium of heat equation was modified, and the gas-mass of the tunnel was divided into segments. The number of segments can be chosen freely, because the segments of the mathematical model are independent of the segments of the KKK. Each segment passes the whole tunnel circuit with a velocity not identical with a real local flow velocity.

For each segment the equilibrium of heat is calculated whereas the injection of LN_2 is taken into account only for the segment located in the injection section. The segment located in the test section is representing the temperature in the test section. Because there is no heat exchange between the discrete segments the heat is distributed only by heat transfer between the segments and the components of the tunnel. Test calculations were carried out with the single and multiple segment model. They have shown that the simplification of the single segment model is a good approximation. Furthermore the simulation with the single segment and the linearized model for some operation points has shown that the dynamic behaviour of the tunnel is described with a sufficient accuracy by the linearized model at any given working point.

4. Actuators and Sensors

LN_2 System

The location of the LN_2 system is chosen as far away as possible from the test section to achieve good evaporation and good mixing between the injected liquid nitrogen and the tunnel gas.

The LN_2 system supplies a mass flow from 0.1 kg/s to 10 kg/s. This range is divided in four independent groups of valves. The valves are pneumatically driven. The computer must choose the right group of valves for a calculated mass flow. For a mass rate above 5 kg/s two pumps supply the necessary pressure. Since the mass rate depends on the pressure in the LN_2 system, the pressure is measured and considered in the computer calculation.

GN₂ System

The location of the GN₂ system is between the third and fourth turning vanes, because the lowest velocity in the tunnel is there. Consequently the least influence of blow in or blow off GN₂ on the gas stream is found here. The range of mass flow of the blow in system is from 0 kg/s to 4 kg/s. This range is realized with one ball valve. The electric-hydraulic actuator is controlled by an analog signal of the control computer ranging from 0 V to 10 V.

The valve for blow off is also electric-hydraulically driven. The valve allows a mass rate from 0 kg up to 10 kg/s. The electrical level is in the same range as above mentioned.

Fan Engine

The fan is driven by a conventional DC-engine. The control computer output 0 V to 10 V corresponds to a speed of rotation from 0 rpm to 500 rpm. The speed of rotation is held constant by the fan-engine itself, independent of the required fan power.

Sensors

For the closed loop control all tunnel states must be measured (fig. 4). In the test section three pressures can be measured [9]:

- Static pressure (difference)
- Static pressure (absolute)
- Dynamic pressure

The static pressure is measured as the difference between the static pressure in the test section and the ambient pressure outside of the tunnel. This pressure difference is necessary for the controller, but for calculation of the density of the tunnel gas it is also necessary to know the absolute value of static pressure. The high voltage output of the pressure transducer can be used directly for the computer without further amplification.

For the temperature measurement four platin resistor sensors are used. The sensors are connected to transmitters with a high level output. The computer calculates an average temperature for use in the control algorithm.

5. Controller

The controller of the KKK is a modular type (fig. 5). This has some advantages. Thus it is possible to carry out the initial operation step by step. In the minimal configuration adequate operation is possible, and in the extended version an economical and comfortable operation is feasible.

5.1 Minimal Configuration

In the minimal configuration only the control algorithm is computed. The control algorithm is designed as a robust type, this means the controller is not sensitive to differences between the mathematical model, which was the base for the design, and the real tunnel behaviour [10].

For the realization in a computer system the controller is a discrete type with a variable cycle computation time. The controller consists of three control loops. For all control loops there is a gain adaption available. Between the temperature and the pressure loop there is a coupling in the controller itself. The gain adaption for the pressure loop is divided for the case of blow in and blow off gaseous nitrogen.

The gain level of coupling depends on the tunnel variables:

<u>control loop</u>	<u>tunnel variables</u>
temperature	u_{TS}, T_G
pressure (blow off)	u_{TS}, T_G
pressure (blow in)	T_G
velocity	T_G

The cycle time of computation depends on the velocity in the test section. For three control loops the following controller types are used:

<u>control loop</u>	<u>controller type</u>
temperature	P I D
pressure	P I D
velocity	P I

In addition the controller is completed with a feed back of the calculated control actions.

5.2 Expanded Configuration

In the expanded configuration the inverse single segment model is added. The inverse single segment model calculates the necessary instantaneous actuator movements for a given set of set-point trajectories. If there is no difference between the real tunnel behaviour and the inverse single segment model the tunnel variables are always equal to the required set points.

But there is always a difference between the model and the real tunnel, and so the control module must adapt the tunnel dynamic to the model dynamic.

5.3 Comfortable Configuration

It is planned to calculate trajectories for set-point changes in order to minimize liquid nitrogen consumption or save time during the different operating phases.

The trajectories can be calculated under consideration of the limits and restrictions of the actuators and the tunnel variables [11].

6. Results

During the first closed loop tests for velocity and pressure only the part of the controller being responsible for controlling the velocity has worked as required. In contrast to this system the pressure loop did not work sufficient. The reason for this were deficits in the drive of the GN_2 valves. Originally the valves were pneumatically driven but the velocity for adjusting a new position of the valve was not high enough and additionally the reproduction of the angle were not as exact as required.

As a result the mass flow of GN_2 and therefore the pressure in the tunnel could not be controlled with the needed accuracy. Therefore the drives of the GN_2 valves have been changed to electric-hydraulically actuators. After exchange of the actuators the response of the two GN_2 valves on the setpoints given by the controller were reproducibly and exactly. In the closed loop tests the pressure loop has shown an excellent functionality. The pressure and the velocity controller were tested for the run-up, testing, and the run-down phases. It was possible to improve the closed loop results by varying the controller the gains. These tests were performed at ambient temperatures. In fig. 6 one result of the test is shown. In the upper part of fig. 6 the true velocity is shown and in the lower part of fig. 6 the static pressure response is shown. The results are in the order of the required accuracies during the operating phases.

It is planned for the next time to check the velocity and the pressure controller at cryogenic temperatures. If they will work with the same success the temperature controller will be optimized.

Conclusion

After the modification of the low speed wind tunnel at the DLR Research Center at Cologne to a cryogenic wind tunnel some new mathematical models were developed to study the new behaviour and to lay out a new automatical control system.

The control system has been tested and it yields accurate and reproducible test conditions. Thus a safe and economical operation under cryogenic conditions is possible.

Literature

- [1] Viehweger, G. Kryogenisierung des Niedergeschwindigkeits-Windkanals
Köln-Porz
- Spezifikationsphase -
WKT 11/80

- [2] Distelrath, D. Die Stickstoffanlage des KKK
Teil 1: Das LN_2 -System
IB - 39151 - 83A13, 1983
WKT 24/83

- [3] Distelrath, D. Das GN_2 -System
In Vorbereitung

- [4] Viehweger, G. Anforderungen an das Steuer- und Regelsystem des KKK
Kronen, R. in den verschiedenen Operationsphasen
Spezifikation März 1981

- [5] Viehweger, G. The Kryo-Kanal Köln, KKK, Description of the Tunnel
Conversion. Thermal Insulation, Instrumentation,
Operational Experience and Test Results. Operating
Costs.
Brüssel, Juni 1989

- [6] Palancz, B. Analysis of the Performance of a Liquid Nitrogen Cooled,
Closed Circuit, Cryogenic Nitrogen WindTunnel and
its Application to the DLR's 3m-Tunnel in Cologne
Part two: Dynamical Performance Study, WKT 9/80

- [7] Palancz, B. Mathematische Modellierung, simulation und Regelung
eines kryogenen Windkanals
Teil 1: Mathematisches Modell und Simulation des
dynamischen Verhaltens
IB - 29100 - A03, März 1982

- [8] Kronen, R. Die Regelungssysteme der beiden Kryo-Windkanäle
0,3 m TCT (NASA Langley) und KKK (DLR Köln)
IB - 39114 - 88A22, August 1988

- [9] Kronen, R. Software und Hardwaresystem für den Betrieb des KKK
Teil 1: Anforderungen und Gesamtkonzept für die
Steuerung und Regelung
WKT 27/85

- [10] Steinhauser, R. Reglerentwurf für einen Tieftemperatur-Windkanal mittels
Gütevektroptimierung
DLR FB-85-37, 1985

- [11] Kraft, D. Optimalsteuerungen
DLR FB-23/86, 1986

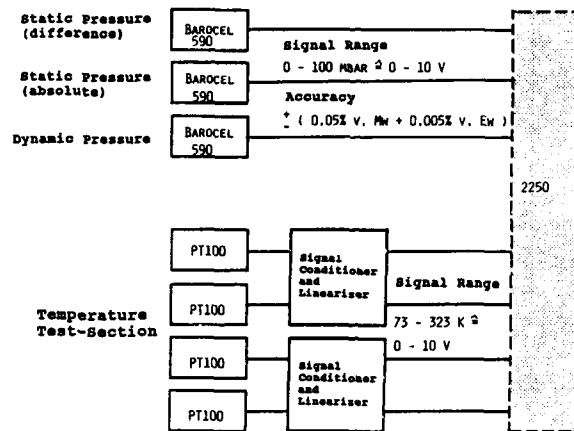


Fig. 4: Data Acquisition for the Control System

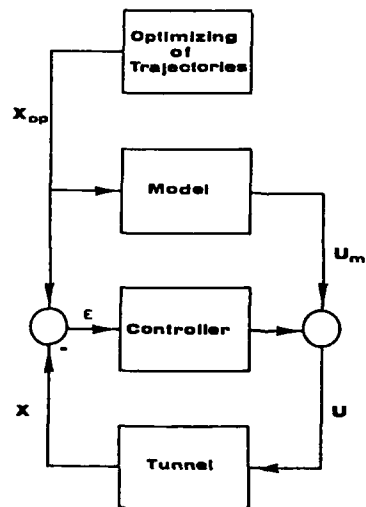


Fig. 5: Control System of KKK

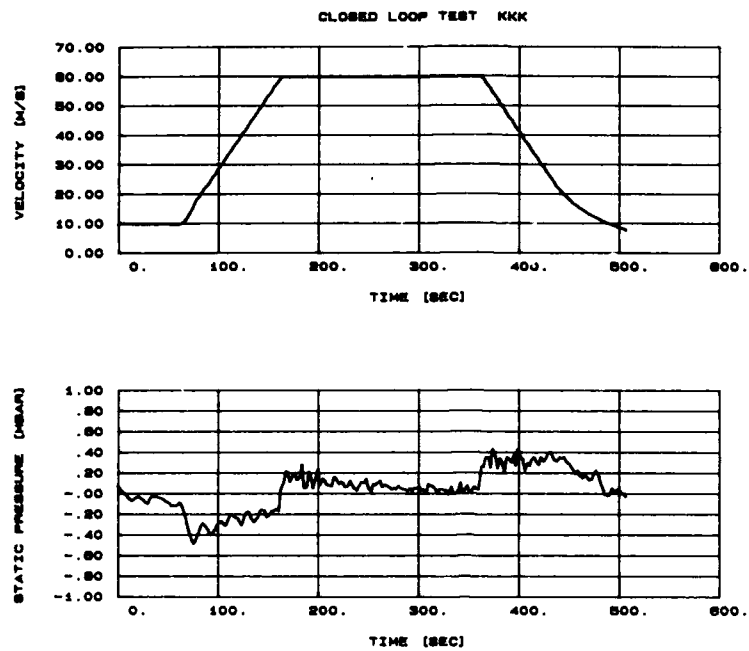


Fig. 6: Closed Loop Test Results

	p [mBar]	T_g [K]	u_{rs} [m/s]
Stand-By	$\begin{smallmatrix} + \\ - \end{smallmatrix} 2$	$\begin{smallmatrix} + \\ - \end{smallmatrix} 5$	const. rpm
Cool-Down	$\begin{smallmatrix} + \\ - \end{smallmatrix} 2$	decrease	const. rpm
Run-Up	$\begin{smallmatrix} + \\ - \end{smallmatrix} 2$	$\begin{smallmatrix} + \\ - \end{smallmatrix} 2.5$	increase
Testing	$\begin{smallmatrix} + \\ - \end{smallmatrix} 0.1$	$\begin{smallmatrix} + \\ - \end{smallmatrix} 0.5$ K	$\begin{smallmatrix} + \\ - \end{smallmatrix} 0.1$
Run-Down	$\begin{smallmatrix} + \\ - \end{smallmatrix} 2$	$\begin{smallmatrix} + \\ - \end{smallmatrix} 2.5$ K	decrease

Table 1: Required Accuracy for Different Operating Phases

THE EUROPEAN TRANSONIC WINDTUNNEL (ETW)

by

Xavier Bouis
ETW GmbH
Köln
Federal Republic of Germany

Summary: The construction phase of the European Transonic Windtunnel started recently at Cologne, West-Germany. Ambitious goals in aerodynamic quality and cost-effectiveness are reflected in the design philosophy. The main features of the future facility are presented.

INTRODUCTION

The construction phase of the European Transonic Wind Tunnel officially started in 1988 after the signature of a Memorandum of Understanding by the four participating nations (France, West-Germany, Great Britain, Netherlands) and the establishment of a new company, ETW GmbH in charge of building and later operating the facility. Since that date most of the important calls for tenders have been issued and three major contracts have already been awarded to design and build the most critical mechanical work packages.

ETW has been presented several times in the past, (1), (2), (3) especially at the last session of the Von Karman Institute on the same subject, in 1985. These presentations were generally based on the "preliminary design" of 1981. During the last three years, following a review of the main specifications by the aeronautical community of the four participating nations, many concepts proposed in the "preliminary design" were changed, reflecting more closely the needs of the future operators and users and the state of the art in continuously progressing wind-tunnel testing techniques.

This paper has a double objective: It highlights the key aspects of the design philosophy i.e. aerodynamic quality and future cost-effectiveness, and it provides an updated description of the wind-tunnel. It also gives the opportunity to answer numerous questions raised in the functional design phase by specialists and non-specialists in wind-tunnel technology.

1 MAIN SPECIFICATIONS

A joint analysis, under the auspices of AGARD showed in the early seventies that a need existed on both sides of the Atlantic for a large transonic wind-tunnel able to simulate flight Reynolds numbers or at least to provide Reynolds numbers (*) around 40 million in transonic conditions. Several original concepts were proposed to meet this ambitious specification. U.S. and European teams concluded in favour of the cryogenic concept. (4,5) In the USA the National Transonic Facility (NTF) was studied and built by the NASA from 1975 to 1982 (6) and now starts operating for the American aerospace industry whilst in Europe a project group was created in 1978 to prepare a joint undertaking. Various reasons delayed the project until 1986 when it restarted on a new basis.

But ten years later, although tremendous progress have been made in Computational Fluid Dynamics and in conventional wind-tunnel testing, the situation is not fundamentally different: The complexity of practical situations met by the aircraft manufacturers in high-Reynolds transonic flows is such that it is very likely that for several decades high-Reynolds wind-tunnels will still be used together with conventional tunnels to (I) confirm and refine theoretical predictions at the basic design stage of an aircraft, (II) explore advanced configurations (III) provide data to numerical models.

Then, setting the target Reynolds number at 40 million for Mach 0.9 and a range of Reynolds number variation at constant pressure more or less determines the main specifications of the facility:

- At a given Mach number, taking viscosity as roughly proportional to temperature, Re is nearly proportional to
 $(\text{Dimensions}) (\text{Pressure}) (\text{Temperature})^{-1/2}$
- Likewise, the power required to drive the fluid is nearly proportional to
 $(\text{Dimensions})^2 (\text{Pressure}) (\text{Temperature})^{1/2}$
- No need to run a very sophisticated optimisation process to conclude that for a given target Reynolds number, the cheapest facility has the minimal temperature (but not too low to avoid gas condensation) the maximal pressure (but not too high for model strength and deformations) and the consequential dimensions.
Remarks: (I) Taking into account the high costs associated with the generation of cryogenic conditions seriously moderates this simplistic thinking process but does not change the final conclusions. (II) A cryogenic facility also offers the possibility to change independently the Reynolds number and the dynamic pressure of the flow.

 (*) For non specialists let us recall that the Reynolds number is the ratio between "inertia + pressure forces" and "viscous forces". It is expressed as $(\text{density}) (\text{length}) (\text{velocity}) / (\text{viscosity})$.

Following above considerations the main specifications of ETW are:

Mach number	0.15 to 1.3
Reynolds number	up to 50 million
Pressure	up to 4.5 bars
Temperature	90 to 313 K
Dimensions of the test section	2.4 x 2 m ²

Figure 1 compares the Mach-Reynolds envelope with that of European conventional wind-tunnels.

In addition to these aerodynamic specifications, two other targets are given to ETW, both concerning productivity:

ETW shall cover the needs of the European research and industry in transonic high Reynolds number testing. These needs are presently considered as equivalent to 5000 "polars" per year *).

ETW shall generate enough income by running tests for industry and research establishments to be self-supporting.

This is already reflected in the type of organisation running the project: ETW GmbH has a few features resulting from its international organisation structure but operates under the statutes of a private company with limited liability under German law.

Above requirements gave a very challenging task to the team of engineers in charge of developing the functional specifications. As requested by the program of this VKI short-course, the following pages concentrate only on two aspects which are of remarkable importance for the aerodynamicists and the future users:

- ° Provide the necessary aerodynamic quality
- ° Optimize the cost-effectiveness of future operations.

Some information about other major aspects like operational safety or development of the testing techniques may however be found here and there in the paper.

2 AERODYNAMIC QUALITY GOALS

Important preliminary remark: Numerous conditions must be achieved to obtain high quality test data. They concern the mechanical and aerodynamic design of the facility, the quality and repeatability of the models, the accuracy of the measurement devices, especially the force balances and the angle of attack sensors (read for instance (7)), the quality of the testing methods (see (8,9) on development of testing techniques for ETW) and the qualification of the testing teams. This paper only addresses the first aspect, in other words the establishment of proper flow conditions. Of course, ETW GmbH is or will soon be active on all other conditions!

2.1 Mach Number Distribution, Flow Angularity

2.1.1 subsonic conditions

Let us first recall that ETW will have initially a slotted test section (6 slots on top and bottom walls, 4 on each side wall, maximal opening 12 %). The mechanical design will incorporate a capability to retrofit easily at a later date a set of top and bottom adaptive walls. The shape of the contraction has been optimized and tested on the DLR (ex-DFVLR) test-rig (scale 1/8.8) in 1981. Figure 2 shows this test-rig. Figure 3 indicates that the local angularity of the flow will not exceed 0.1° in the volume occupied by the model under test.

Two means will be available to reduce the Mach number gradient along the test section: the top and bottom walls will be adjustable (hinged upstream) to take care of the boundary layer growth and the variable plenum reentry geometry will allow some additional tuning when the tunnel is operated in open slots configuration.

*) In the wind-tunnel operators jargon, a "polar" is a set of data measured in a few seconds or tens of seconds with all test parameters except one being kept constant.

As in conventional high quality wind-tunnels, the requirements for an excellent repeatability of the wall geometry under varying Mach number, pressure, temperature conditions are extremely strong. They correspond to local Mach number deviations of 0.001 around Mach 0.9 in solid wall configuration, which means 0.1 mm for each wall in a 2 x 2.4 m² test section. They also correspond to changes in flow angularity well below 0.01°. It is required that such conditions will be met 2.5 minutes after a 40 K temperature change. Under pressure loads some more (repeatable) distortion is allowed.

At such a level of accuracy, the changes in boundary layer growth in function of the temperature differences between the flow and the test section walls can also modify the Mach number distribution. Specifications on the wall thickness and appropriate operating rules will take care of this effect. Above requirements are consistent with the nearly standard goals of high quality tests in present good conventional tunnels i.e. drag measurement repeatability within 1 "drag-count" (error on CD \leq 0.0001) for typical cruise conditions around Mach 0.8. Of course, besides obvious instrumentation and model problems, the quickly changing temperature conditions do not make life easy for the mechanical designers and the future operators...

2.1.2. supersonic conditions

Mach numbers above unity will be basically generated by a flexible nozzle, visible on Fig. 4. As the whole of the system will be surrounded by varying temperature conditions, the specified accuracy will be difficult to meet. It corresponds to 0.008 in Mach number deviation on the test section centerline and means tolerances of 0.5 mm on the positioning of the flexible walls, including thermal distortion. Achieving good results on this nozzle will considerably encourage ETW to proceed towards the above mentioned retrofitting of adaptive walls for which higher repeatability goals seem to be necessary. The contours of this nozzle are based on theoretical calculations made by Sverdrup and presently being checked by DLR (Fig. 5).

Two supersonic nozzle blocks were built for the pilot tunnel PETW (scale 1/8.8). This facility is shown on Fig. 6. A Mach 1.35 block was tested in 1988. This test revealed an important default of the region just downstream of the test section. The flow chokes between the strut simulating the model support system and the plenum reentry flaps (Fig. 7). 2.D calculations (Fig. 8) led to a better shaping of this area, recently tested successfully in PETW (Fig. 9).

2.2 Noise, Turbulence, Flow Unsteadiness, Model Vibrations

2.2.1 turbulence

Few experimental data are available to quantify the tolerable noise and turbulence levels for very high Reynolds numbers. The example on Fig. 10, extracted from ref. 10 seems to indicate that serious doubt may appear at least for laminar flow testing if turbulence levels exceed 0.15 % at Re = 10 million and 0.05 % at Re = 40 million. At ETW, considerable attention is given to upstream generated turbulence in order to approach the 0.05 % level. The low speed diffuser downstream of the fourth corner, although equipped with a screen, is not very favourable but a honeycomb and three screens properly designed and aligned, followed by a factor 12 contraction (Fig. 11) should produce the expected result. The configuration of PETW does not allow to check the validity of this semi-empirical prediction.

Turbulence generated by temperature distortion and fluctuation is also a problem in a facility cooled by liquid nitrogen injection, as shown by simple fluid dynamics considerations. For this reason the nitrogen injection rake is located as upstream as practical and the distribution of the nozzles should reduce temperature gradients to ± 5 K at the compressor entry plane and below ± 0.25 K in the settling chamber. Experience of NTF and ONERA T2 indicate that liquid nitrogen vapourization and mixing is less difficult than expected in a high speed facility.

2.2.2 noise

ETW specifications are based on AGARD AR 644. As the proposed ideal result is not achievable with a conventional wall configuration, the target is presently to reduce the pressure fluctuations (Cp r.m.s) below 0.4 % for the usual slotted walls case and "as low as possible", towards 0.2 % for the solid walls configuration and the future adaptive walls case.

Such levels are unusual in conventional wind-tunnels. A combination of efforts is necessary to meet these goals: the compressor noise will not exceed 131 dB at the compressor exit, a second throat will be active for Mach numbers between $M=0.6$ and $M=1$ and the test section will get an optimal shape in the downstream region, based on experience gained recently at PETW after a first set of half successful tests (Fig. 12), followed by 2-D calculations and confirmed by excellent results obtained by NLR in a similar situation.

2.2.3 flow unsteadiness

In the lower frequency range (say between 0.2 Hz and a few Hz, below what is usually designated as "turbulence" small fluctuations of the flow may disturb the tests in two ways: one can be corrected, the other not. Small, slow changes of the flow parameters (Mach, pressure, temperature) can be measured accurately, filtered synchronously with model data and then only need to complete the test campaign with a few additional polars to interpolate the results in the most critical areas. Of course it does not make life easier for wind-tunnel operators but finally this is more a question of time and energy cost than a question of quality. Unfortunately, in a typical ventilated walls configuration with a big plenum chamber such as ETW, Mach number and total pressure fluctuations generate significant exchanges of gas between the plenum and the rest of the circuit. These exchanges may create distorted Mach number distributions or local flow angularity. Experiments made in the past by the author and his colleagues at ONERA allowed to determine which static pressure stability was compatible with present goals in test data accuracy. Based on these figures, the specifications of the control system of ETW are fairly strong as regards stability, with compressor rotational speed within ± 0.3 r.p.m., blow-off aerodynamic area within 0.00015 m' (i.e. <0.04 % of maximum opening) and liquid nitrogen mass-flow within 0.25 %.

2.2.4 model vibrations

It is well known that the high stiffness of a good model support system (including the balance) and its extremely low damping allows the models to be severely excited by any aerodynamic or mechanical source exciting its vibration modes.

Unfortunately, little can be done to reduce these disturbances which in some circumstances are even stronger in cryogenic conditions. The flow turbulence will be minimal, the specifications for various parts of the circuit should prevent generation of resonances or large vibrations in the most critical frequency ranges and fairly strong goals are given to the compressor manufacturer in terms of rotor unbalance, including provisions in the design for a possible future retrofit of magnetic bearings.

2.3 Flow Purity

2.3.1 dust

Any operator in large transonic facilities now knows how small quantities of dust can be critical for certain kinds of tests, especially if a substantial amount of laminar flow is aimed at. A simple calculation shows that in a typical 15-minutes run, any particle carried by the flow of a size between a few microns and a few tenths of millimeter is likely to hit one or several times the model at a bullet speed. Remembering that the surface finish of the models has to be locally below 0.4 microns and that the skin of these models is not necessarily built with the hardest materials, it is easy to conclude that all precautions will be taken at ETW to prevent dust generation in the tunnel, dust introduction during maintenance periods and, because perfection is not achievable, relatively easy cleaning. The internal insulation system and its "liner" obviously complicate the situation compared with conventional (metallic) wind-tunnels. The specifications for minimal oil leakage through the seals of the compressor (solid particles in the cold!) also consider this particular aspect. This argument has been used in the discussion on magnetic bearings.

2.3.2 humidity and other pollutants

Very tiny quantities of humidity or CO_2 (or other gas, liquid or solid at ETW cryogenic temperatures) could create various problems on the models. The most obvious problem, i.e. erosion, is not very different from above mentioned dust effects and may even combine with them.

Another one is H_2O or CO_2 icing on the models, affecting first turbulent transonic areas. Information given by ONERA-T2 operators on provoked CO_2 icing and hints from first NASA-NTF tests supported some theoretical analysis made by ETW team.

The conclusion is quite simple: It is easy to lower the concentration of CO₂ and other gases in a way which makes them totally harmless for the tests, but reducing humidity at such a level that the dew-point temperature is never reached during the cool-down of the facility seems nearly impossible. Conventional insulation materials (Polyurethane foam covered with plastic layers) outgas very small but still disturbing quantities of moisture, access to the tunnel without precautions brings substantial amounts of water vapour and even good quality dry air and liquid nitrogen are not totally moisture free. Combining a specially designed insulation system, convenient purging sequences and a sophisticated model access system will allow to reach this dew-point line around or better below 200 K. At this temperature, the water concentration is about 1.3 part per million (ppm). As it is known that icing effects are hardly noticeable with 10 to 30 times higher concentrations, ETW team considers that icing will not be detectable and may even not exist at all on the models.

3 TOWARDS AN OPTIMIZED COST-EFFECTIVENESS

3.1 General

As already mentioned the productivity objectives are set at "5000 polars/year". With typically 15 to 30 tests per year, 186 days of active test operations and an expected average of 10 polars per run, it means that ETW will perform 2 to 5 runs per day, including model changes and temperature changes. This is fairly usual in large conventional facilities but represents a serious challenge with the relative heaviness inherent to cryogenic operations. In addition, as already said, the quality of test data must be absolutely outstanding (flow and measurement techniques) to get full benefit from the high Reynolds conditions: ETW will not directly compete with conventional facilities but provide services which cannot be found elsewhere in Europe. In other words would the flow quality not be obtained or would the measurement quality be significantly lower than that of today's good conventional tunnels ETW GmbH would loose most of its expected clients. But assuming that quality and productivity goals, like number of polars, will be achieved the cost of the future results must still be kept within reasonable limits ... For a few major technical/commercial decisions the cost of the tests may be of secondary importance but for many other studies on large aircraft projects which will constitute most of the workload, these costs are far more critical!

The following paragraphs illustrate a few aspects (not all!) of the design philosophy followed by ETW team in order to optimize cost-effectiveness without relaxing on quality goals: Increase time available for the tests, make the best use of testing time, reduce operating costs.

3.2 Time Available For Effective Testing

Various activities occur in such a facility which stop or delay ongoing test campaigns independently of the efforts made by the testing teams: maintenance, failures, cool-down/warmup times, dry-air/nitrogen purging times, non-integrated safety procedures, adverse weather conditions etc...

- ° scheduled maintenance will not be fundamentally different from that of conventional facilities with two exceptions: (I) in spite of all efforts made to use simple, easy to maintain, standard solutions, the amount of equipment to maintain will inevitably be larger than in most of the existing wind-tunnels with obvious consequences on costs and time. However, it is planned that after a few years of operations maintenance and inspection periods will not exceed a total of 6 weeks per year. (II) the use of a nitrogen atmosphere increases the duration of routine internal inspections which can only be done after a dry air purging of the tunnel. Providing a large mass flow of dry air has been identified as the easiest and cheapest mean to cope with this difficulty (alternatives would have been protective suits or the use of oxygen enriched mixtures).
- ° down-time subsequent to failures could be much longer than for conventional facilities if they affect components in the cryogenic environment (warm-up time, very long if the compressor cannot be run etc...) Therefore, from the basic architecture to the detail design all efforts are being made to reduce the number and complexity of components "in the cold" and to provide judicious redundancy in order not to be stopped for one full day by a minor failure.
- ° cool-down/warm-up times are explicitly mentioned in the specifications. A ± 200 K change will be done in less than 3 hours. This is enabled by the use of an internal insulation system and a clever design of the heaviest structural components which otherwise could suffer thermal fatigue.

- ° dry air/nitrogen purging times depend on the mass flow of the appropriate utilities but also on the quality of the insulation system (as far as practical moisture free and/or easy to dry) and on the arrangement and operating procedures of dry air locks protecting each access to the tunnel. Efforts have been made in these three directions.
- ° Excepting very low temperatures, where liquid oxygen can appear, the cold conditions are not extremely dangerous (it means not instantaneously dangerous: ETW team members visited for several minutes a 150 K room used for medical treatment in an hospital!) but uncontrolled nitrogen emissions may locally create an asphyxiation hazard. The overall layout of the building takes this risk factor into consideration, clearly separating nitrogen areas and nitrogen circuits from normal working areas. Although some additional precautions will appear necessary during the detailed safety reviews, it is not expected that they will severely impact on the operating time.
- ° Meteorological studies have shown that 16 % of the time ETW could be forbidden to run because either the cold nitrogen blow-off plume would sink and create problems (fog, ice) at ground level or climb and still be visible above 150 m and then disturb air traffic on the neighbouring Cologne airport. These pessimistic predictions will be checked and provisions are already made to incorporate in the blow-off a warming system which would reduce the range of adverse weather conditions.

3.3 Optimal Use of Testing Time

When one considers the overall time spent in any wind-tunnel to get a "polar" it appears that most of it is devoted to model preparation, model configuration changes and checking, various trouble-shooting, wind-tunnel start/stop procedures etc... With cold conditions, these operations could be far longer! Since the early days of the project it has been recognized that the use of the more than 40 years old "cart concept" could considerably alleviate the difficulties. In 1988 the so-called carts lost their wheels, being replaced by new units, transported by an overhead "gantry crane" (fig. 13). Each unit comprises the test model, the sting support system, an upper wall for the test section, a pressure door closing the wind-tunnel shell and an instrumentation cabin containing the data acquisition system associated to this test. The advantages of such an architecture are developed hereafter:

- ° Parallel thorough preparation. Experience shows that the better a test is prepared, the more efficient is the test campaign. Adequate "cart-rigging bays" (CRB) and "variable temperature check-out rooms" (VTCR) provide ideal conditions for a thorough preparation, including full instrumentation and data systems checking under cold conditions and simulated loads. Of course, during this possibly long preparation, the tunnel is available for a test campaign with an other "cart" (fig. 14, 15, 16, 17).
- ° Fast access to the models. Fully applying the "cart concept" it has been decided not to go to the models but to bring the models to adequate rooms for configuration changes. This takes only 15 minutes, reduces to very few pieces the number of active mechanical components "in the cold" and allows to keep the tunnel at its original temperature conditions, full of dry nitrogen. If necessary it is even possible to interleave the runs of two test campaigns ... The test model is transferred with the "cart" to one of three variable temperature rooms. Some precautions are taken to limit the heat exchanges when the cart is transported (through a dry air hall) from the tunnel to this room and to protect the model from possible thermal shock and icing. There, two possibilities are offered for model rigging, either a "glove-box" type system to handle cold models in perfectly dry conditions (fig. 18) or a warm-up system bringing quickly part or the whole model above the local dew-point temperature for a more conventional model rigging. With such a sophisticated equipment, the duration of model configuration changes could ideally, in the future, be only slightly higher than in large conventional facilities, say half an hour more. But significant progress still needs to be made to take full benefit of these means, either on the response of force balances to fast temperature changes and/or on model design to allow extensive configuration changes in cold conditions.

- ° Interactive testing. Without really innovating in this area, ETW will implement the best methods developed by its supporting establishments to process test data in "real-time", allowing clients and test engineers to make appropriate decisions possibly during the runs or a few minutes after.
- ° Short running time. In a cryogenic facility the runs need to be very short and very efficient for an even stronger reason than time saving, i.e. the cost of liquid nitrogen used to compensate the heat input of the compressor (typically 600 US \$ per minute). This subject is addressed below. However, efforts are also made to reduce any unnecessary extra time or notice period to start or stop the runs.

3.4 Energy Costs

Coming back to the thinking process leading to the "ETW main specifications" it should be recalled that the lower the temperature the more energy consuming is the generation of the cold (direct application of the Carnot theorem in basic thermodynamics). In an ideal wind-tunnel running continuously the total power at a given Mach number would therefore be nearly proportional to:

$$(\text{Dimensions})^2 (\text{Pressure}) (\text{Temperature})^{-1/2}$$

with the cooling process included in the energy balance. This is less optimistic than the formula given at the beginning of the paper but unfortunately still far lower than the real trend in energy demand, including non ideal efficiency of the process. Example: At full power, 50 MW, ETW may need for instance to be cooled by a permanent flow of, say, 200 kg/s of LN2. If this LN2 is produced by a very economical continuous process, it needs "only" 2 Mega Joule/kg. It means that ETW dissipates 50 MW in the drive motor of the compressor and the equivalent of 200 kg/s x 2.10⁶ Joule/kg = 400 MegaWatts "hidden" in the energy which contributed to produce the cooling fluid! This total of 450 MW happens to be the power that would need a tunnel like ONERA-S1 (ø 8 m test section) if it could be pressurized at 4.5 bar ... also giving flight Reynolds numbers but presumably at a much higher cost! Therefore, questioning nearly all aspects of the specifications ETW engineers asked themselves in 1986, as many others had done before, whether liquid nitrogen cooling is a cost-effective process because it consumes at any temperature a negative enthalpy built in expensive conditions, below 77 K. Various associations of ideal and non-ideal thermal machines were simulated with a simple computer program, including compressors, turbines and counter-flow heat exchanges. For the small pressure ratio of a transonic wind-tunnel (and the corresponding small temperature rise) all continuous machines were either too powerful and expensive (hundreds of megawatts in associations dominated by compressor + turbine cycles) or too heavy and voluminous (little energy savings but considerable expenses to change the temperature in associations dominated by nearly ideal heat exchanges) to be practically considered. Storing or recycling cold nitrogen emitted during a run (or just the cold of it) also appeared uneconomical.

The viable alternatives would be like NASA-NTF to incorporate a water cooler for ambient temperature runs and even to think of exotic cooling fluids for moderately cold conditions. For the relatively low share of testing that ETW will perform at ambient temperature (see fig. 19) the increased pressure losses, the circuit volume extension (for the cooler itself and the additional downstream anti-turbulence devices) and a few other arguments like potential humidity problems and additional capital cost led to a negative conclusion, primarily based on economic aspects.

Remembering that a transonic wind-tunnel is essentially a very intermittent type of machine it is finally not surprising to conclude in favour of a cooling process based on stored enthalpy which is produced by a continuous process in today's best thinkable conditions. After all, liquid nitrogen is much cheaper than mineral water! The same does not apply to the driving system: extrapolating the ONERA-T2 situation with a huge nitrogen or air storage is tempting but does not resist careful examination for a 4.8 m² test section and the most optimistic run durations (*).

It leaves ETW team with the need to optimize the total energy balance (compressor/drive costs + liquid nitrogen costs) including cool-down/warm-up, runs and heat losses.

(*) N.B. Although the ETW runs are expected to be very short for a so-called "continuous" facility, it was preferred not to go further i.e. not to move towards a "blow-down" type concept: with runs as short as two or three minutes, a different optimisation process would take place but the above mentioned 1 drag-count accuracy would be more difficult to reach ... In addition producing 5000 polars/year would not be that easy with such a facility.

3.4.1 cool-down and warm-up, heat losses

Although thermal fatigue calculations are made on the basis of 100 cool-down/warmup cycles per year, the energy balance optimization is based on 50 cycles only (200 K each). Some figures are given hereafter based on a LN₂ cost of 170 DM/ton and an average cooling capacity between 100 K and 300 K of 320 kJ/kg. In such conditions, 1 ton of stainless steel in the tunnel would "cost" 3000 DM/year, 1 ton of aluminium 4800 DM/year.

Savings in operating costs have been looked for in three ways:

(a) insulating part of the shell internals with or without heating, (b) using alternative, non-metallic materials to reduce thermal inertia (c) designing in a way which optimizes the thermal masses.

(a) is very attractive if the facility can be run in a typical "blow-down" mode. But as soon as the thermal cycles last 48 hours (or more) this solution becomes clearly uneconomical. For much shorter times, the thermal inertia of the most critical aerodynamic/measurement components has been compared with typical run durations: The risk of never being in stabilized or at least "known" conditions appears so great that the "cold internals" situation is finally preferred, to achieve above mentioned stringent flow quality goals. For about 600 tons of "cold internals" it will cost around 1.7 million DM/year.

(b) is also very attractive and quite possible. Unfortunately the cost estimates received for several massive elements which could be built in composite materials (turning vanes etc...) are totally demotivating...

(c) is the subject of a permanent effort, is already considered in the very compact general layout of the circuit and will be further developed in the detail design phase. It often conflicts with stiffness requirements but less or not at all with thermal stability (response time) and thermal fatigue requirements.

Heat losses depend on insulation type and thickness. Of course, above criteria on thermal inertia are also applicable to the insulation itself, together with other less evident operating aspects applicable to "non-tight" insulation systems. However, already mentioned dryness requirements and obvious mechanical criteria are overruling. It leaves only some flexibility on the thickness of the material. This thickness has been selected in order to reduce the total heat losses to 60 W/m² for a tunnel at 100 K and 300 K outside temperature. This figure includes all losses due to penetrations, attachments of internals etc... For a typical year, with 120 days "in the cold" at an average temperature of 150 K it needs 5000 tons of LN₂. Altogether, the optimum is relatively "flat" and more practical considerations on acceptable temperatures for an easy pressure shell certification helped to make the decision.

3.4.2 energy spent during a wind-tunnel run

Of course, "energy" means the sum of electrical energy input in the compressor-drive unit and the energy necessary to produce the LN₂ consumed during a run. This energy is the integral of power versus time. Therefore, parallel efforts are being made to reduce both. Essential contributions to these factors are:

- wind-tunnel pressure losses
- compressor efficiency
- start/stop durations
- set point changes durations
- duration of a "polar"

Let us discuss their influence on energy balance (or costs) and how an optimum can be found.

- ° Wind-tunnel pressure losses depend on the overall layout of the circuit and on how some details of the internals are designed.

A compact circuit has been chosen as a result of an overall optimization process (Fig. 20). Its losses are rather high especially in the low speed parts but this is compensated by a low mass of internals and a short "response time".

The LN₂ injection is located upstream of the compressor, which gives a marginal power benefit (ref. 11). The associated limitation of the lowest attainable temperature does not influence the transonic range. The nitrogen blow-off is located between corners 3 and 4 which is not ideal in terms of power. It would better be installed as a plenum suction device or somewhere between the test section and the LN₂ injection station. But, as developed further, the extreme difficulty of controlling accurately enough the pressure makes it very risky to install the blow-off in one of the most fluctuating areas of the facility. In addition, for the lowest pressure range, additional equipment would be necessary for the exhaust of a subatmospheric pressure gas.

Coming to local details each part of the circuit has been subject to some level of pressure loss optimization but for 75 % of the losses, especially between corner 4 and corner 1 the flow quality is the overruling design criteria...

- Compressor efficiency was one of the criteria for the selection of a compressor manufacturer. With the two-stage concept selected on the basis of noise considerations and maximal achievable pressure ratio, the blade path efficiency will reach 92 % with a weighted efficiency across the interesting operating range of 86 %.
- Start-stop durations mostly depend on the acceleration of the compressor and on the means to pressurize the tunnel. Acceleration from zero to full speed in less than 100 seconds is relatively easy with the variable frequency drive-motor. Going much faster appears unnecessary. Tunnel pressurization will be achieved in vaporizing LN₂ whilst the blow-off is kept closed during the starting phase. At very low Mach number it is a lengthy process but for the normal (transonic) range of the facility a typical 1 bar increase at 200 K is achieved in 1 to 2 minutes at Mach 0.9 to 0.6. As gaseous nitrogen would in any case be taken from the LN₂ storage tank and then vaporized, the process of vaporizing it with the main compressor is not more expensive. The question was raised of installing pressure gates, like NASA NTF to keep part of the tunnel under pressure during model changes. First, the concept and safety of model access is quite different at ETW, second, the investment in such a complex and heavy system working in the cold cannot be economically justified with regards to the 1500 tons of LN₂ that it could contribute to save annually.
- The set point changes are the changes from one set of stabilized tunnel parameters (Mach, Temperature, Pressure) to another set. Their duration obviously depends on the magnitude of the change. Besides conventional or necessary systems like the compressors, the LN₂ injection, the blow-off etc... the second throat will help considerably to achieve the fast control goals. Its effect is clear in choked conditions. It is also expected to be very efficient in unchoked conditions with the capability to compensate almost instantaneously the test section losses changes by actuating fast "trim-flaps" located immediately down-stream, on the centerbody of the second throat. Studies of expected test sequences showed that the set-point changes could however represent from one third to two thirds of the annual LN₂ and electrical energy consumption, and this, with an already very efficient control system. For this reason a computerized dynamic model of ETW aerodynamic circuit was built by the ETW team in a very simple form in 1986 and subsequently improved by incorporating the plenum chamber behaviour in 1988. Control algorithms are applied to the model. They follow the principles of those working successfully at ONERA-T2 wind-tunnel. They could well be used with little modifications for the real ETW. This allowed to quantify the effects of the various control subsystems on the overall response time and stability. The result of this exercise in a set of specifications for these subsystems (compressor speed change rate of 10 rpm/s, LN₂ mass flow change of 20 kg/s, blow-off aerodynamic area change 0.04 m²/s, trim-flaps movements 30 degrees/s etc...). Sensitivity studies show that around these levels there is no use for a significant improvement of one of the system if the others are not simultaneously improved. They also show that significant degradation of the response would occur if one of the main systems did not meet its requirements. We see on Fig. 21, 22 a few examples of set-point changes.
- Polar duration is the visible part of the iceberg. It is planned to perform continuous pitch polars and pitch/pause polars. The use of fast pressure scanners is foreseen for pressure measurements. The speed of the sting support system varies from 0 to 4 degrees/second. However, for high accuracy polars the limiting factor is likely to be the stability of the flow itself (Mach number stability and/or plenum "breathing" effects). Under such conditions, pitch rates as low as 0.2 to 0.5 degree/second may be necessary. As the detailed behaviour of the model + plenum + trim-flaps system is not easy to predict, assumptions have been made, hopefully conservative, based on experience of conventional facilities giving average polar durations (including return polar) of 0.7 to 5 minutes. Why "hopefully conservative"? Because conventional wind-tunnels, if they have no "trim-flaps" system, rely for their stability on a "comfortable" inertia in pressure and temperature. It will be quite different at ETW with an active cooling system (LN₂) strongly coupled with pressure control. For this reason the specifications of the LN₂/blow-off systems are very strong in terms of stability and fine tuning. Would they not be met, the polars would need to be multiplied and the results even more interpolated, leading to substantial increases in LN₂ consumption and possibly lower test quality.

- ° Just to illustrate above discussion, Fig. 21, 22 also give examples of typical runs. The share of the set-point changes is clearly visible, close to 50 % of the run duration. It helps for instance to understand why ETW has a small circuit with relatively high losses rather than a much bigger circuit with 10 or 20 % lower losses:
a 1 %-volume increase incurs about a 0.5 % increase in running time and is far from permitting the same pressure loss savings ...

3.4.3 towards an optimum

Although a wind-tunnel like ETW is less complex, less integrated than an aircraft, the scope of possibilities is such and the subsystems so inter-acting that nobody can state that the optimum has been reached. But sensitivity studies around the achieved result may show that a reasonable, workable situation has been obtained which cannot be improved without drastic changes of several key features.

This is presently the situation at ETW.

3.4.4 energy and LN₂ for auxiliary systems

Rather late in the functional design phase, it appeared that electricity and LN₂ consumption by auxiliary systems were significantly increasing their share of the total energy balance. This includes the cool-down/warm-up sequences of the temperature conditioning rooms but also the dry air consumption to keep a dry atmosphere around the tunnel and miscellaneous items like the sealing gas (LN₂/air) in the labyrinths around the compressor shaft ...

For each of these systems the concept itself is directed towards a minimal energetic consumption. When particular refinements are proposed by the manufacturers, they are evaluated on an economical basis and accepted if the pay-back occurs before 10 years of nominal use.

Under such conditions, about 14000 Mwh and a total of about 10000 tons of LN₂/GN₂ and dry air are still expected to be needed annually by these auxiliary systems.

3.4.5 electricity and LN₂ prices

- ° Electricity tariffs are rather high in the area of Cologne and ETW, like all large transonic/supersonic facilities cannot be seen as a nice customer by the electricity supplier (peaky demand, irregular consumption). However, reasonable conditions are expected from the local company which would lead to a total bill of 4 to 5 million DM/year for the following conditions:

Main compressor drive: Maximum power 50 MW, consumption 5000 MWh
Site auxiliaries: Power around 10 MW, consumption 14000 MWh

- ° Getting the best conditions for liquid nitrogen is a major issue for ETW: estimates of the future LN₂ consumption for a fully booked ETW exceed 70.000 tons/year. This single budget item might represent more than 30 % of the operating costs. Studies have been made to determine which supply solution is the cheapest. Although the subject is very complex and strongly dependent on the future trends of the liquid gas market some indications may be given here: Producing one ton of LN₂ requires today about 0.6 MWh. One MWh costs today in Cologne area about 130 DM for a middle size industrial consumer including discount for night tariff.

Excluding energy costs, it has been estimated that operation, maintenance and amortizing of an ETW dedicated plant could cost up to 6.5 million DM/year.

In the first years of operation, ETW will use about 30.000 tons/year or less. The LN₂ cost would therefore be 295 DM per ton or more. Later, with 70.000 tons/year, the cost would fall under 170 DM/ton.

As LN₂ can be produced below 100 DM/ton from areas where electricity is cheaper (night tariffs, nuclear energy in France and Belgium) and trucked to ETW at a total price around 160 DM/ton it is likely that ETW will start in 1993 with LN₂ delivered by trucks. Depending on the workload a dedicated air separation plant will presumably be installed later on an already reserved area (Fig. 23).

However, operational advantages, LN₂ purity requirements and possibilities of selling LN₂ surplus, Argon and noble gases might lead to an earlier decision to build this plant.

3.5 Other Costs

Besides energy costs, two major budget items deserve a special attention in the design phases: personnel and maintenance. They are expected to represent together nearly 40 % of the operating costs.

3.5.1 personnel

Efforts are being made in automatic and remotely controlled systems in order to reduce manual operation and routine work to a very minimum. Modern design features should compensate for the relative complexity of cryogenic systems. Hence the staff will be similar in size to that of a conventional wind-tunnel but slightly higher qualified. In addition, and although a very good cooperation exists with the neighbouring DLR the stand-alone position of ETW GmbH must be taken into account: Besides a possibly higher proportion of administrative staff, a number of engineers in very specialised areas will be needed who will not be shared with other facilities, as it happens in bigger establishments. However, the small size and flexible structure of the company should help to create an excellent working spirit and good communications and lead to an overall excellent effectiveness. Therefore it is planned to start with about 50 persons and to increase slowly to 90 as the workload increases.

3.5.2 maintenance

Unfortunately it is not possible to win everywhere. The sophistication of ETW, partly reflected in the construction costs tends to generate cost increases and complexity in the future maintenance programme. ETW project team is aware of that risk and tries in any circumstance to select concepts which alleviate the future burden of the maintenance teams. Among others, let us mention "minimal number of active components in the cold", "clever design rather than easy design + active control", "easy access for maintenance", "in-built redundancy on critical items", "enough redundancy to wait until the next maintenance period", "QA procedures including criticality rating and corresponding equipment checking", "monitoring system with some expert system features", "standard components especially for electronic devices, computers and software", "ad-hoc policy on long delivery spare-parts", etc...

But as a whole, inspite of these efforts, it is likely that the maintenance budget will be somewhat higher than that of a simpler, 3 times less expensive conventional facility of similar dimensions ...

3.6 Costs and Durations, Summary

Following above technical explanations on operating costs, let us now look at the whole picture: Figure 24 shows the relative importance of various operations in time and in cost as presently estimated by ETW engineers. For these estimates it is assumed that the facility is fully booked with 3 model-carts active, producing 5000 polars/year in 15 (or more) rather complex test campaigns and is occupied 9 to 10 hours per day with some temperature conditioning and GN, purging out of normal working hours. It is also assumed that present functional specifications will be fully achieved in the construction phase.

The main lesson from this figure is that energy and LN₂ expenses represent about 40 % of the bill whilst test preparations and model configuration changes take 55 % of the operating time.

These are the reasons for putting much emphasis on energy/LN₂ expenses and on model handling ... They are the next critical subjects after safety and aerodynamic quality!

The next priority item is "tunnel preparation" (start-stop, temperature conditioning, drying/purging). However, if above higher priority goals make it necessary to slightly relax on this "tunnel preparation", solutions could possibly be found by running a larger share of these activities out of working hours under automatic control. And last but not least, maintenance takes a substantial share of the annual costs, partly due to the external expenses but also due to the time spent.

Let us now conclude this chapter on productivity:

As a whole, if these statistics differ significantly from what is usually experienced in conventional facilities, they are not out of proportion. It means that an adapted design can compensate for the relative heaviness of cryogenic operations.

4 CONCLUSION

Quality is essential, cost-effectiveness is also necessary! This could be a simple formula to illustrate ETW specifications. This paper tried to present both aspects with similar emphasis. Unfortunately if some very interesting developments like the dynamic model could only be briefly summarized, a number of other areas had to be totally omitted. Let us quote a few of them: on quality, the provisions for future adaptive walls, the efforts on balances and balance calibration techniques, the flow-diagnostic methods, etc..., on cost-effectiveness the concepts and layout of the temperature conditioning rooms, the hall and the dry air lock, a number of details of the LN₂ systems and the compressor-drive unit, etc...

But what about the future?

Three big contracts (shell + insulation, compressor + drive, high speed internals and cart handling) have been awarded, others will follow soon. Above concepts and functional specifications need now to be implemented. This will be the task of the contractors, ETW and their Industrial Architect keeping the client's role, taking care of the interface hook-up and making sure that above mentioned objectives will be achieved. Much effort has still to be made before the facility not only looks like the model shown on Fig. 25 but also provides its clients with the expected levels of quality and productivity.

REFERENCES:

- (1) Hartzuiker, J.P., The European Transonic Wind-Tunnel ETW: A Cryogenic Solution. Aeronautical Journal, Nov. 1984.
- (2) Tizard, J.A. and Hartzuiker, J.P., The European Transonic Wind-Tunnel Project ETW, AGARD R 722, July 1985.
- (3) Bouis, X., La Grande Soufflerie Européenne, La Recherche, No. 203, Oct. 1988.
- (4) The Need For a Large Transonic Wind-Tunnel in Europe, Second Report of the Large Wind-Tunnels Working Group AGARD-AR-70, 1974.
- (5) Christophe, J., Projet de Soufflerie Transonique Européenne, 14e AAAF meeting, Nov. 1977 and Aéronautique et Astronautique No. 72, 1978-5.
- (6) McKinney, L.W., and al. The Characteristics of the Planned National Transonic Facility AIAA 9th Aero Testing Conf. A76-38626 June 1976.
- (7) Ewald, B., Krenz, G., The Accuracy Problem of Airplane Development Force Testing in Cryogenic Wind-Tunnels. AIAA Aerodynamic Testing Conference 86-0776, March 1986.
- (8) Bazin, M., Instrumentation for Cryogenic Wind-Tunnels, VKI Short-Course, June 1989.
- (9) Schimanski, D., Status of the Development Programme for Instrumentation and Test Techniques of the European Transonic Wind-Tunnel - ETW, to be issued at the 13th ICIASF, Göttingen Sept. 1989.
- (10) AGARD.CP-348. Owen, K., + al., No. 12. Feb. 1984.
- (11) Adcock, B., Effect of LN₂ Injection Station Location on the Drive Fan Power and LN₂ Requirements of a Cryogenic Wind-Tunnel. NASA TM-X-74036, June 1977

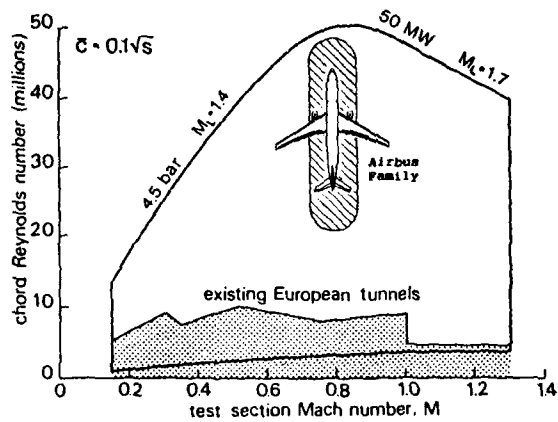


Fig. 1 - Mach-Reynolds envelope of ETW

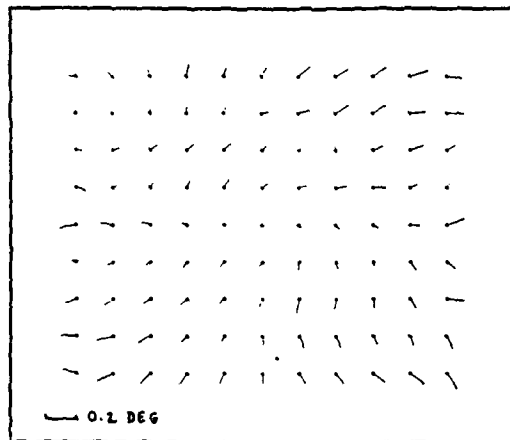


Fig. 3 - Typical flow angularity distribution in test section

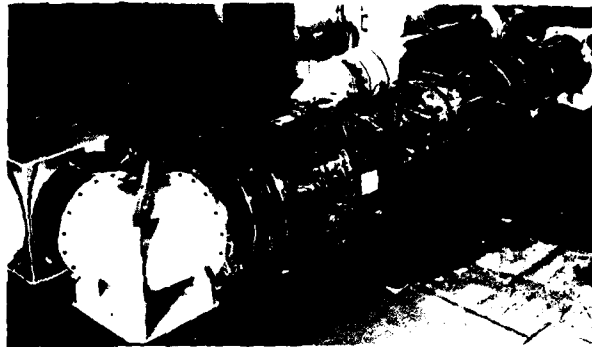


Fig. 2 - DLR ETW test rig

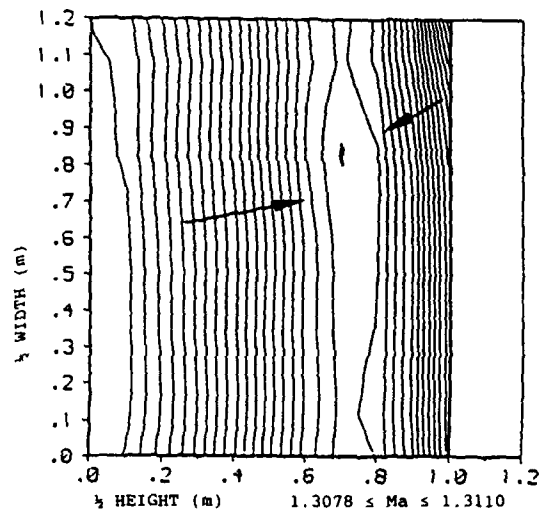


Fig. 5 - Test section inlet M distribution at M = 1.3

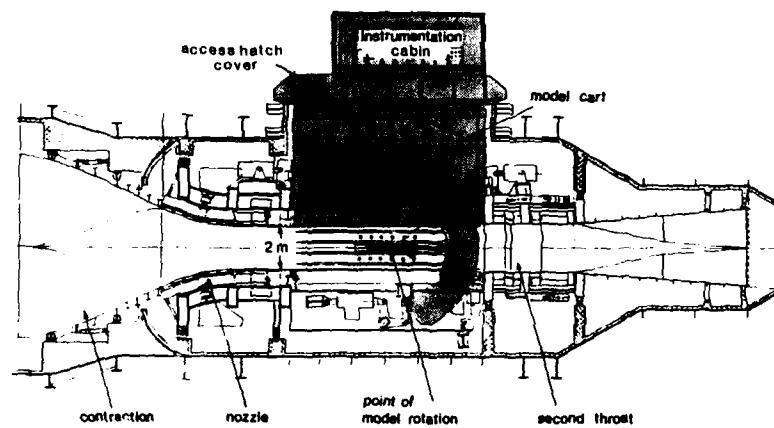


Fig. 4 - High speed leg internal components

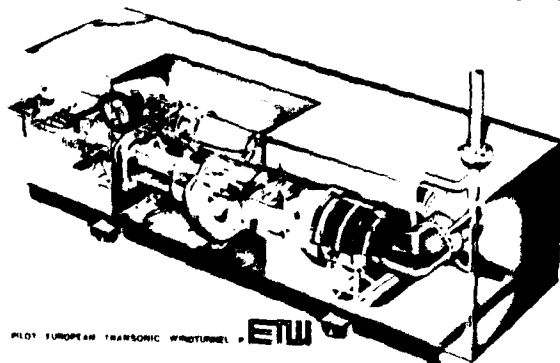


Fig. 6 - Artist's impression of PETW

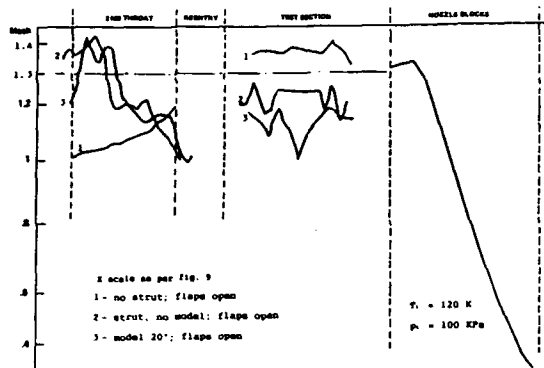


Fig. 7 - Longitudinal supersonic flow distribution in original PETW

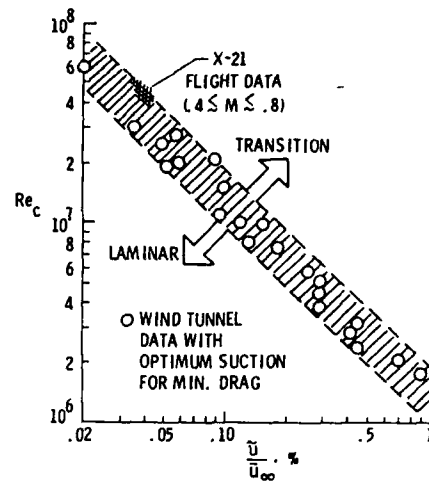


Fig. 10 - Influence of turbulence in a high Reynolds number test

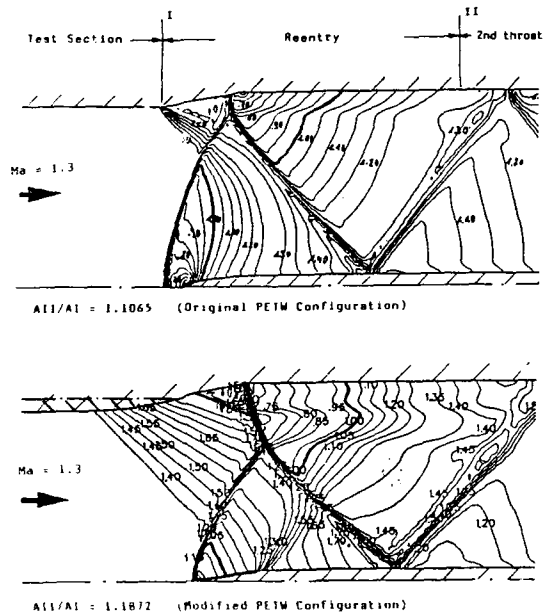


Fig. 8 - Two dimensional flow field calculations for PETW

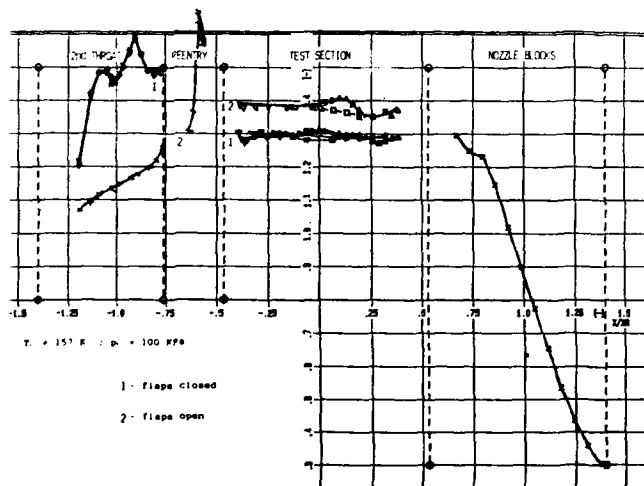


Fig. 9 - Longitudinal supersonic flow distribution in modified PETW

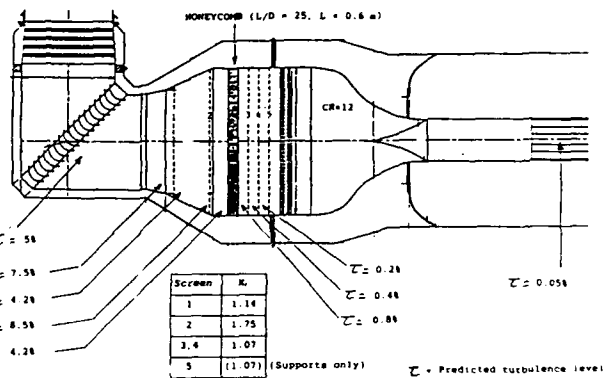


Fig. 11 - Flow conditioning devices in ETW

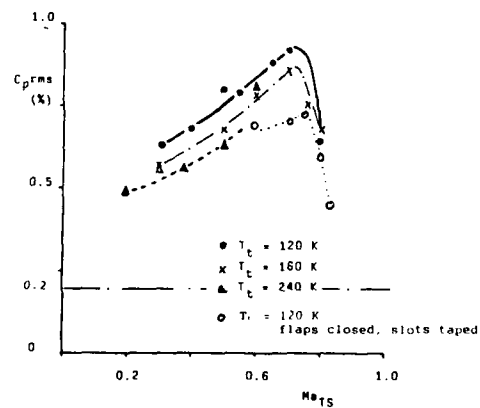


Fig. 12 - PETW noise measurements

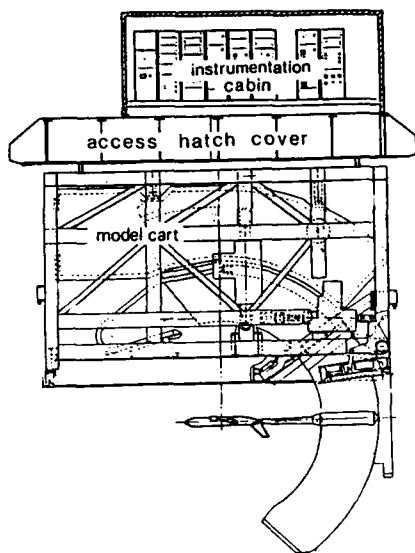


Fig. 13 - Model cart

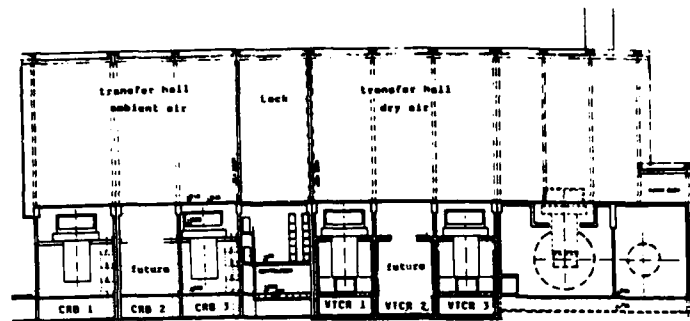


Fig. 16 - ETW building section through transfer hall

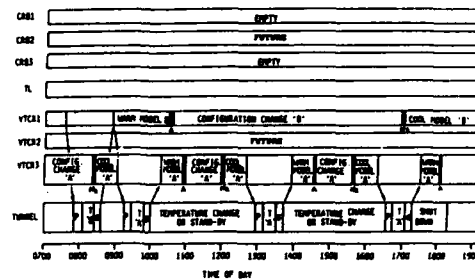


Fig. 17 - ETW possible operating sequence

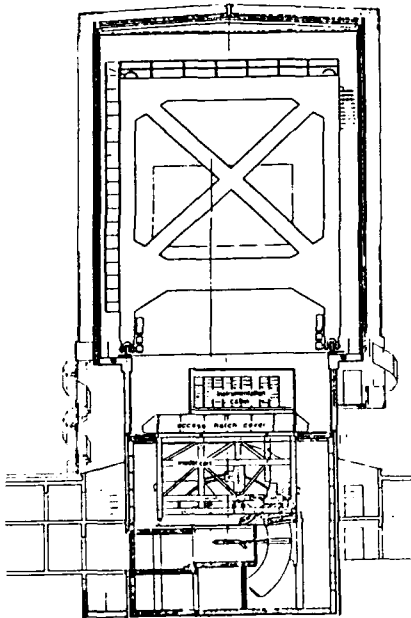


Fig. 14 - Model cart and transporter (elevation)

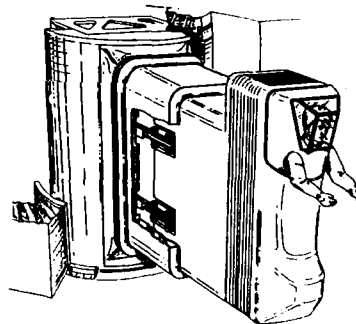


Fig. 18 - Glove box unit for cold model handling

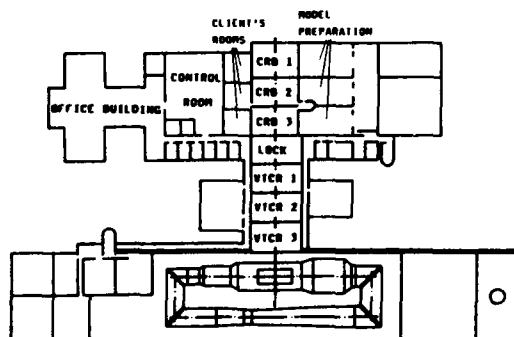


Fig. 15 - ETW building layout (plan view)

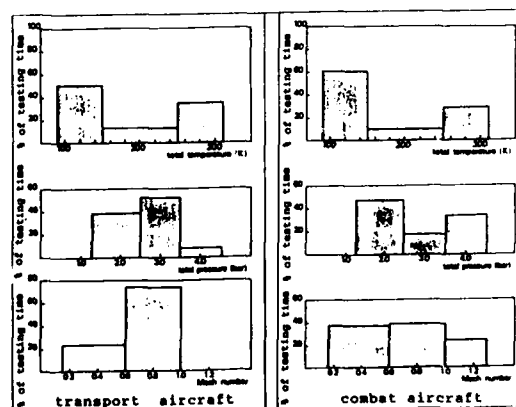


Fig. 19 - Forecast of distribution of testing time

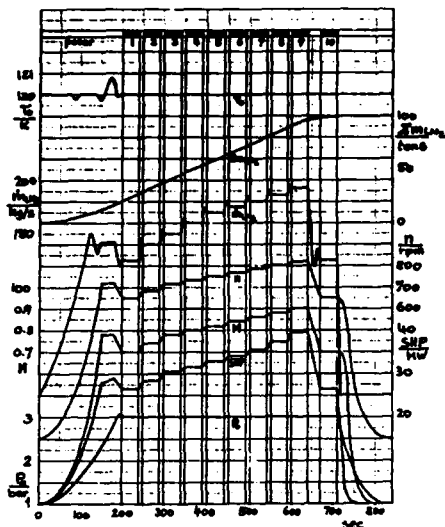


Fig. 21 - Set point changes for a constant temperature run

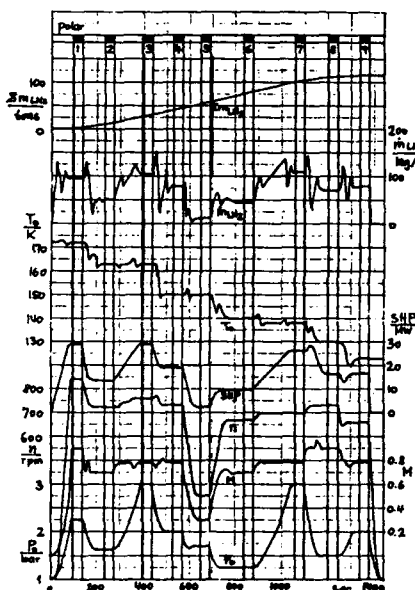


Fig. 22 - Set point changes for a variable temperature run

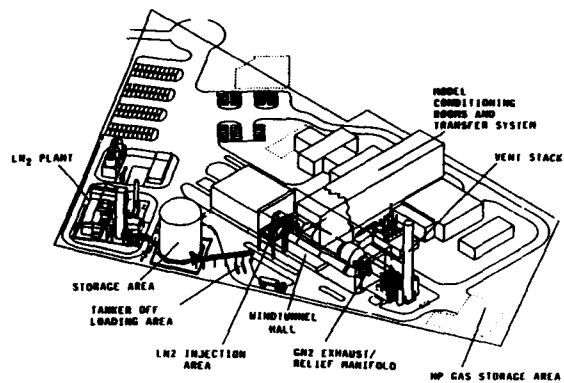


Fig. 23 - Nitrogen supply layout

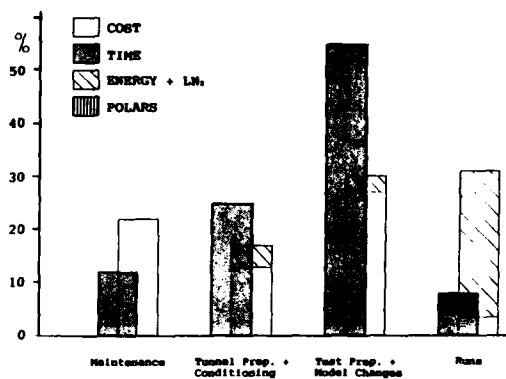


Fig. 24 - Forecast of operational times and costs

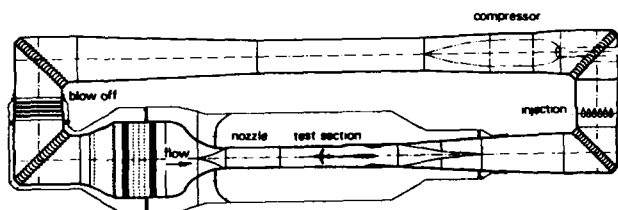
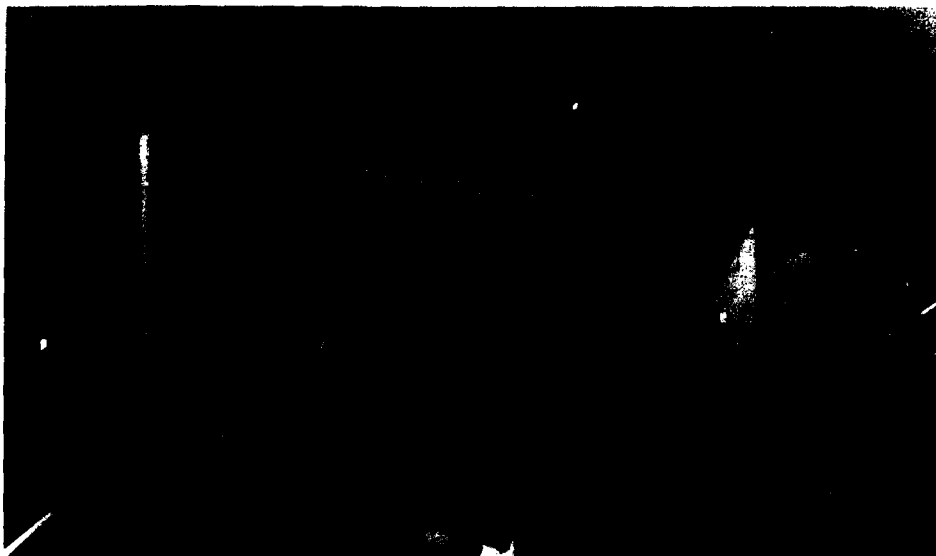


Fig. 20 - ETW aerodynamic circuit

Fig. 25 - ETW model
(scale 1/100)



THE CRYOGENIC INDUCTION TUNNEL T2 AT TOULOUSE

Jean-Pierre ARCHAMBAUD

ONERA / CERT
 Département d'Aérodynamique
 2, avenue Edouard Belin
 31055 TOULOUSE CEDEX (FRANCE)

ABSTRACT

This paper presents the activity of the ONERA-CERT in the aerodynamic cryogenic experimental branch. Firstly, it describes the T2 induction wind tunnel, acting in cryogenic conditions since 1981, and indicates the flow characteristics. Then the paper develops the hollow model conception and its cooling during the run and underlines the importance of the wall temperature measurements. The presence of ice particles in the flow, tripping the transition on the model, is discussed; an efficient solution is given, providing fairly good results on a laminar profile at high Reynolds number. Finally the paper shows cryogenic test results on a three-dimensional model.

NOMENCLATURESymbols

c model chord
 M freestream Mach number
 p pressure
 q mass flow
 RMS root mean square
 S_e exhaust area
 T temperature
 φ swept angle

Subscripts

j drive air
 LN2 liquid nitrogen
 t stagnation variable
 TS test section variable
 w wall

Superscript

\sim RMS value
 \wedge dynamic pressure

1 - INTRODUCTION

The T2 transonic wind tunnel has been in operation since 1975 at the Centre d'Etudes et de Recherches de TOULOUSE.

This facility was initially a 1:10 scale model of a large wind tunnel proposed by ONERA in the framework of the European L.E.H.R.T. (Large European High Reynolds Tunnel) project.

This induction driven wind tunnel operated by runs of about 1 up to 2 minutes and its closed circuit could be pressurized up to 5 bars.

In 1978, the T2 test section was equipped with a first set of top and bottom flexible walls; in 1980, the walls were improved to be self-streamlined during a run by a two-dimensional adaptation code and a three-dimensional code was added to minimize wall interference around three-dimensional models in 1983.

In 1981, ONERA decided to modify the T2 wind tunnel for cryogenic operation in order to increase the test Reynolds number. The circuit has been inside insulated and has been fitted with a liquid nitrogen injection system. Main features of the T2 cryogenic facility are described in the first part of this paper.

Since then, many various cryogenic tests have been performed. Several typical problems were met and solved, such as the model cooling, the drawback of residual moisture in the flow, which are discussed in this presentation.

Some test results achieved in cryogenic conditions at high Reynolds number on a two-dimensional profile and on a body/wing half-model are shown in the last part of the paper.

2 - THE T2 WIND TUNNEL2.1. Description of the facility

The figure 1 is a schematic sketch of the T2 wind tunnel and its ancillary equipment.

The fluid of the closed circuit is driven by induction in the first corner. This air induction consists of seven hollow turning vanes which are supplied with high pressure dry air (80 bars) [1], [2]. This air exists through the trailing edge of the turning vanes at $M_j = 1.6$ (fig. 2).

The flow is cooled down by a liquid nitrogen injection located immediately downstream of the first corner. There are 32 injectors of different sizes, distributed on two circles around the tunnel interior

(fig. 2) and supplied by a 2 m³ run tank pressurized at approximately 15 bars. Each injector has a solenoid valve for on-off control. This gives accurate digital regulation of the liquid nitrogen flow rate ([3], [4]). The high velocity flow provides a good vaporization and mixing of the liquid nitrogen droplets.

The 1.8 x 1.8 m² stilling chamber, equipped with a dust filter, a honeycomb and several screens, supplies the test section through a 22:1 contraction ratio convergent.

The T2 test section (fig. 2 ; [8]) is 1.32 m long, 0.39 m high and 0.37 m wide. Sidewalls are solid, parallel and insulated inside by a 5 mm thick wood sheet. Flexible top and bottom walls are composed of 1.3 mm thick steel sheet (INVAR) and are not insulated. Each flexible wall is moved by 16 hydraulic jacks controlled by stepper motors (0.2 mm unit step). The movement is transmitted to metallic stiffeners welded to the wall ; slots bored into the stiffeners create an efficient thermal barrier. Consequently, all the mechanical displacement system is kept at about ambient temperature while flexible walls are rapidly cooled down. The two- and three-dimensional adaptation codes are iterative procedures using wall pressure data [8]. They request respectively 4 to 6 iterations (4 s/iteration) and 3 iterations (10 s/iteration).

The exhaust of the injected flow rate is made just upstream of the injector corner.

Schematically, the internal insulation of the T2 circuit includes [5] :

- In the low velocity parts, i.e. the return leg and the stilling chamber, 10 mm thick layer of polyurethane locally reinforced by kevlar fabric. This material is covered with kevlar to improve the surface finish downstream of the LN₂ injection.

- In the high velocity part, 5 mm thick layer of agglomerated cork of Norcoat type on the air induction corner and the collector ; wood layer on the test section sidewalls (5 mm thick) and on the LN₂ injection region (10 mm thick).

For a dual purpose of measurement and safety, about a hundred of thermocouples are distributed in the entire circuit and give permanently the temperature of the flow, of the internal wall and of the metallic structure ; this structure is built with mild steel and can become fragile at low temperature.

2.2. Development of a cryogenic run

The regulation system carried out for cryogenic operation at T2 ([3]) has benefited from many improvements since 1982.

The three flow parameters (M , P_t , T_t) are controlled by an HP 1000 minicomputer which regulates the drive air flow rate q , the liquid nitrogen flow rate q_{LN_2} and the exhaust area S_e ; this computer uses simple models of the wind tunnel with the temperature control separated from the pressure control. A fourth parameter, the cross section of the sonic throat, allows to adjust the test Mach number. A second computer handles control of the measurement and exploration system, data acquisition and wall adaptation.

At the beginning, bulky two-dimensional models were precooled in an ancillary precooling box and the organization of the run was built around this essential phase ([7]). Now, the hollow model concept leads to another run structure which is explained below, with an example at $M = 0.725$, $T_t = 120$ K, $P_t = 3$ bars (fig. 3).

The first phase consists in cooling down the model at reduced flow conditions ($M = 0.25$, $P_t = 1.1$ bar). An overabundant liquid nitrogen flow rate begins to cool the flow more rapidly before entering the closed loop regulation of the measured stagnation temperature. When the model temperature, which decreases more slowly than the stagnation temperature, reaches the nominal value fixed for the test ($T_t \leq \text{nominal value} \leq T_t + 15$ K), the first phase ends.

The second phase consists in simultaneously increasing the Mach number and stagnation pressure up to the nominal values while holding the flow temperature roughly constant. At the beginning of this phase, the regulation valves close on the exhaust circuit and the drive air flow increases linearly. Then the regulation stabilizes the stagnation pressure and the Mach number on the nominal values.

During the third phase, the pressure and the temperature regulations held the test parameters at the desired values for the time required by the aerodynamic measurements (T_t stabilized to within about ± 0.5 K). The iterative wall streamlining is carried out during the first part of this last phase ; then, valid aerodynamic data acquisition is made : model pressure distribution, wake probing, ...

The operating chart of the T2 wind tunnel is presented in figure 4. Two constant stagnation temperature envelopes ($T_t = 290$ K and 120 K) are drawn, bounded by the capabilities of T2 in terms of Mach number and pressure. In fact, the envelope which has been now covered by the tests is the cross-hatched area which exceeds a Reynolds number of $20 \cdot 10^6$ ($c = 150$ mm).

2.3. Cryogenic operating performance

Among the first tests conducted after conversion of the wind tunnel, a series of runs at various temperature levels made it possible to determine the performance characteristics in cryogenic operating mode, i.e. the influence of the temperature on the drive effect of the drive air jets and on the liquid nitrogen flow rate required to obtain a given stagnation temperature.

For tests at Mach number $M = 0.8$ in the test section and at stagnation pressure $P_t = 1.8$ bar, the variations in the ratios of the drive air flow rate q , and the injected liquid nitrogen flow rate q_{LN_2} to mass flow rate in the test section q_{ts} , during the final stabilized phase of the test are shown in the

figures 5 and 6 respectively.

It is observed that the ratio q_i/q_{ts} decreases as the operating temperature decreases, which confirms the increase in the induction efficiency predicted by the injector theory, as the temperature ratio between the drive fluid and driven fluid T_{ij}/T_{its} increases. The black spot on the figure 5, corresponding to ambient temperature, represents the induction efficiency before conversion of the circuit : the slight decrease in performance recorded is explained by a moderate increase in the pressure loss of the circuit due to the presence of the internal thermal insulation.

The ratio of the liquid nitrogen flow rate to the test section flow rate is obviously zero at room temperature. It increases practically linearly as the operating temperature decreases. At level $T_i = 120$ K, the liquid nitrogen flow rate represents approximately 8 percent of the flow rate in the test section. The dashed line curve in the figure 6 represents the ratio of a liquid nitrogen flow rate, computed to cool only the drive air flow rate of the test at nominal temperature, to the test section flow rate. The difference between the experimental curve and the computed curve gives the order of magnitude of the thermal losses of the circuit : from zero at room temperature, they increase as the temperature decreases and represent approximately 15 percent of the total liquid nitrogen flow rate for $T_i = 120$ K, which confirms the efficiency of the internal insulation.

It should also be noted that at low operating temperatures, the drive air and liquid nitrogen flow rates are of the same order of magnitude (8 to 10 % of q_{ts}), i.e. approximately 10 Kg/s for a flow rate in the test section $q_{ts} = 100$ kg/s ($M = 0.8$, $P_t = 2$ bars, $T_i = 120$ K).

2.4. Quality of the flow

This paper presents only a few results about the flow quality. The references [7] and [9] gather more information on this subject.

The pressure fluctuation level shown in figure 7 is quasi constant versus Mach number ($\frac{\bar{p}}{P} \approx 2.8 \cdot 10^{-3}$), for various test conditions of pressure and temperature. This level seems to correspond to the turbulent boundary layer noise at the walls.

Mass flow fluctuations have been measured with a hot film probe, in the test section. The RMS value of this variable (fig. 8) is roughly constant versus Mach number and the mean value of about 1 % is fairly low.

Stagnation temperature fluctuations have been measured in the stilling chamber by means of a cold wire 9 microns in diameter, in the range 0-50 Hz. The figure 9 shows the variation of thermal turbulence level versus stagnation temperature, at $M = 0.83$. This ratio increases from $0.12 \cdot 10^{-3}$ up to $1.25 \cdot 10^{-3}$ when the test temperature varies from 300 K to 100 K. This increase is due to the decrease in the stagnation temperature T_t and also to the increase in the RMS value \bar{T} from 0.03 K at ambient temperature up to 0.14 K at $T_t = 100$ K. It appears important not to neglect this increase in temperature fluctuation level when interpreting the test results, especially for cases of free transition on the model.

In order to measure the temperature uniformity in a section of the stilling chamber, 25 thermocouple probes were mounted on a grid with a square mesh of 0.3×0.3 m² (fig. 10). The temperature distribution is practically uniform within a 1 K on the 1.2×1.2 m² measurement area, excluding larger differences of about 2 K mainly measured in the corners of the grid.

The transverse temperature distribution in the test section presents a warmer flow zone of about 50 mm wide near each sidewall and a good uniformity in the remaining center part. The maximum difference located on sidewall increases when the test temperature decreases from $T_t = 290$ K to $T_t = 150$ K and is approximately constant and equal to 12 K below $T_t = 150$ K.

3 - MODELS

The main problem relative to the model is to satisfy as well as possible the thermal equilibrium condition during cryogenic tests [10]. To achieve this condition, two procedures are used at T2 tunnel.

3.1. First model design and run procedure

In parallel with the wind tunnel transformations, ONERA has worked on cryogenic model design. In the first stage, it appeared that a conventional metallic model constituted with thick electron beam welded pieces was a reasonable solution [6]. Two profiles of this type were built in Marval 18 maragin steel and tested in T2 : a 150 mm chord CAST 7 airfoil and a 180 mm chord CAST 10 airfoil.

The run time was too short to be able to cool down the model to the thermal equilibrium during the test. So, an ancillary precooling system has been added near a test section sidedoor : it was a small closed circuit containing a cold gaseous nitrogen flow cooling down the airfoil to the prescribed temperature, in 10 to 20 minutes. After this initial phase, the run is started at low Mach number ($M = 0.3$) and low pressure ($P_t = 1.1$ bar) and then the flow temperature decreases and is stabilized around the test value. At that time, the cold model is introduced into the test section and locked in place. After that, pressure and Mach number increase to the test values and the data acquisition begins when all the parameters are stabilized.

This operating procedure has been used successfully with three models : the CAST 7 and CAST 10

airfoils already mentioned and a small three-dimensional model. With this cooling procedure, the access to the test section is much reduced around the concerned sidedoor. On the other hand, an extension of this operation to various three-dimensional models leads to very complex precooling box design.

3.2. New procedure with low thermal inertia models

After some years of cryogenic operation, a simple new idea was explored to reach the thermal equilibrium. A model having a low thermal inertia can be cooled down directly by the flow, in the test section. Such a model consists of a thin skin (3 mm), locally reinforced. The soldering of the different parts is a little more difficult and it is possible to screw them together. Internal thermocouples allow to control the cooling and to verify the temperature uniformity. The first model of this conception was a laminar swept airfoil ($c = 177 \text{ mm}$, $\varphi = 25^\circ$), composed of four electron beam welded parts of 3 mm thick. The upper and lower surfaces were coupled by small cylinders.

The run procedure relative to this model design is already described in the Chapter 2.2. However, let us give more details upon the first phase. At the beginning of the run, a cylinder is introduced just upstream of the leading edge (fig. 19) in order to generate a turbulent flow on the entire model and so to reduce the cooling duration. We can also decrease this phase by the effect of a temperature undershoot. This cooling phase lasts 25 s up to 50 s (fig. 3). When the model temperature reaches a prescribed value (the flow temperature is already stabilized), the cylinder is put out of the test section and the second phase begins.

The figure 11 shows some low thermal inertia models tested in cryogenic condition at T2 : a swept wing made in two parts fastened with screws and columns ; this model, called AS100 and manufactured by AEROSPATIALE, is airtight and presents a good surface finish near the joinline. The main interest of that technique is to avoid model deformation due to the welding and also to check all the instrumentation before to close the model. There is also an Axxx half model manufactured by ONERA LILLE [11] ; the fuselage and the wing are hollow ; this model is weighed by a wall balance. Finally, an axisymmetrical body (C5) and fuselages are built with the same technique. All these models fit well the moderate pressure range ($P_t \leq 3 \text{ bars}$) and they are light and easy to instrument.

3.3. Importance of the thermocouples

Low thermal inertia models are equipped with several thermocouples (20 up to 46) which are distributed on the internal surface and glued. The first function of these thermocouples is to qualify the wall temperature of the model. The second function is to supervise the cooldown of the model ; if the thermal equilibrium is reached at the end of the cooling phase, there are risks of frost coating of the model inducing perturbations on the measurements. Now, the cooldown at low conditions ($M \approx 0.3$, $P_t \approx 1.1 \text{ bar}$; Chapter 2.2) is stopped when the model temperature is slightly greater than the flow temperature ($T_w = T_t + 15 \text{ K}$). Then, when the test parameters are stabilized at the end of the second phase, the model temperature continues to decrease and is equal to about $T_t + 10 \text{ K}$. During the wall adaptation, this temperature decreases up to $T_t + 1$ to 3 K and the following data acquisition occurs at approximately thermal equilibrium of the model which is free of frost.

A third and important function of the thermocouples is to indicate the transition of the model boundary layer if it occurs on a skin part of constant thickness. In the case of a thermal imbalance model which is described above, the temperature in the material is always decreasing. Turbulent boundary layer mixes very much the fluid than laminar boundary layer and produces locally greater fluxes, cooling more rapidly the model. So, the thermocouples located near turbulent boundary layer measure lower temperature than those influenced by laminar boundary layer.

The temperature jump of about a few degrees is sufficient to determine approximately the transition location just before the data acquisition, as shown in figure 12, if thermocouples are little spaced. In this case, the Mach number distributions confirm clearly the transition positions (shock-laminar boundary layer interaction on the upper side, transitional bubble on the lower side). If there is some doubt about this result, the different speeds of decrease in thermocouple temperatures all along the wall adaptation iterations constitute a useful help. The figure 13 presents clearly two different temperature levels corresponding to laminar flow on the upper side (until $x/c = 65 \%$) and turbulent flow on the lower side of the model, the Mach number levels being close. It is important to note that the real thermal equilibrium should invert the temperature levels, the recovery factor of turbulent boundary layer being the greatest one.

4 - MOISTURE CONTAMINATION

4.1. Problem of moisture in the tunnel

Moisture problem concerns most of the cryogenic tunnels. At T2, an obvious proof is the frost coating of the model when it becomes colder than the flow, at the end of a cryogenic run (tests at $T_t < 200 \text{ K}$). This moisture can have two different aspects : frost and icicles.

Frost coating is visible on models when the wall temperature is lower than the flow one. In this case, the model appearance is clearly changed and tends to be white when the frost coating thickness grows

(fig. 14). We can reasonably think that this frost introduces aerodynamic behaviour and measurement perturbation : effect of roughness, distortion of balance measurements, blockage of pressure holes ... Fortunately it seems that the problem of the frost can be easily removed. First, a flow temperature under-shoot in order to cool down more rapidly the flow and the model increases the risk to produce frost coating condition and is now rejected. In addition, to be sure that this condition cannot occur, we stop the cooldown of the model when its temperature is 15 K higher than the flow temperature (see Chapter 3.3.). This safety rule allows to keep the model always warmer than the flow (about 2 or 3 K during the data acquisition). We verified that a safety gap of 15 K was not damaging for accurate results. These cautions are efficient to suppress the frost formation.

Presence of icicles into the flow is a more complex problem. During a run, below the dew point temperature, we can see through a window more or less dense white fog, according to the instantaneous conditions. A laser beam exhibits more clearly this possible fog and can measure its density evolution during the run. Icicles induce two consequences : they can produce an erosion of the model and degrade its surface finish ; such a result occurred at T2 at the time of certain model tests, when the tunnel was equipped with a bad dryer. Secondly, icicles hit the model at random and create locally a roughness which can produce the transition of the laminar boundary layer. This phenomenon is pointed out by visualization with frost that makes a thicker coating on the turbulent zones at the end of the run (Chapter 4.6). The photograph (fig. 14) shows some transitional cones created by upstream icicles.

In this case, there is a risk to probe the wake downstream of a turbulent cone. In another hand, two or three cones on the upper side are sufficient to perturb also the lift coefficient computed with pressure distribution. The figure 15 shows the drag (C_D) and lift (C_L) coefficients versus Reynolds number corresponding to the laminar wing previously photographed. We note the large increase in drag coefficient and the decrease in lift coefficient for Reynolds number higher than $8 \cdot 10^6$ ($C = 188$ mm) for that we always observe turbulent cones.

4.2. Sources of moisture

Several sources can provide moisture to the tunnel flow (fig. 16) : drive dry air and liquid nitrogen supplied by tanks, internal insulation material, inlet pipes and exhaust area if they communicate with room environment during non-working periods.

The figure 17 presents a part of the water equilibrium diagram, drawn versus temperature, at $P_t = 1$ bar. At constant water mass in the gas and decreasing temperature, the first icicles appear when the flow temperature becomes lower than the corresponding dew point. So large Reynolds number range without ice requires a very low dew point. Unfortunately, to shift the dew point from 200 K to 190 K for instance it is necessary to change moisture rate from 1.2 mg/m^3 to 0.24 mg/m^3 , in other words to divide it by 5 in a range of fine purity (industrial LN2 purity = 0.4 mg/m^3). Two small cross-hatched zones indicate the fairly good moisture levels of the drive dry air ($T_{dp} = 197$ K) and the LN2 ($T_{dp} = 195$ K) measured just before to be injected. On the contrary, the flow dew point due to the insulation desorption takes place in a higher range (210 K - 240 K), according to the state of purge (Chapter 4.4.) of the wind tunnel.

4.3. Run development

At the beginning of the cooling phase of the run (fig. 18, $T_t > 220$ K), water vapor carried by the flow is partly removed by exhaust while insulation material desorption supplies the circuit with new water vapor. When the temperature crosses the dew point ($T_{dp} \approx 220$ K), a part of the water vapor is changed into small icicles which constitute a more or less dense fog. The laser beam is brightly shining and indicates a peak of icicle density (fig 18). It is the run period ($220 \text{ K} \geq T_t \geq 190 \text{ K}$) inducing the maximum risk of formation of local ice roughness near the model leading edge. Below $T_t = 190$ K, ice fog becomes finer, sometimes invisible. It seems that, at low temperature, a new equilibrium between the filter retention of icicles, the exhaust rate and the probably more reduced wall desorption takes place.

In the case of the figure 18 ($T_t = 92.5$ K), we find a similar peak of icicle CO2 density at about 135 K and the model can be covered by a very thin CO2 frost. The central peak corresponds to the oxygen and nitrogen condensation below 93 K. When the flow is reheated, the same phenomena occur at $T_t = 135$ K and 190 K.

The figure 15 shows results obtained with the laminar wing AS100 in the conditions $P_t = 1.7$ bar, $M = 0.74$, $C = 0.187$ m. For $T_t \geq 225$ K, $R_e \leq 6 \cdot 10^6$ (T_t , test stagnation temperature), the drag and lift coefficients vary correctly versus Reynolds number. For $225 \text{ K} \geq T_t \geq 190$ K, we obtain by chance some correct tests corresponding to a few transition cones ($6 \cdot 10^6 \leq R_e \leq 7.5 \cdot 10^6$) ; but these cones perturb partly the lift coefficient (integration of pressure coefficients). For $T_t < 190$ K, all the tests are wrong (4 up to 8 transition cones, see fig.14) : drag increases while lift decreases.

4.4. Improvements to minimise icicles effects

Two kinds of improvements can be performed :

- Firstly, we can try to reduce moisture in the tunnel for cryogenic tests. The choice of a better insulation material containing less water or isolating it from the flow by a vapor barrier is a par-

tial solution which is not discussed here ; anyway, the expected advantage is limited by moisture of the drive air ($T_{dp} \approx 197$ K).

- A more direct improvement is to purge all the circuit. Each morning, before the first run, we purge the LN2 run tank and its inlet pipes by high pressure LN2 stream. Then, one or two runs are realized at ambient temperature in order to purge all the wind tunnel, mainly to carry out a partial desorption in the best conditions of high velocity and warm temperature. This operation is more easily performed in an induction drive tunnel like T2 than in a fan drive one. Then, the circuit must stay all the day closed. After this purge procedure, the first cryogenic run has a dew point of about 230 K and the last one, in the evening, reaches 215 K. This procedure is usually valid after a short opening of the test section. On the contrary, after one day opening, purge needs one or two days.

- It should also be interesting to condense the moisture by a cold device located in the wind tunnel which will concentrate frost before to remove it regularly. We intend to develop this technique.

- We achieved another concept of improvement which consists in protecting the leading edge of the model where icicles are hitting it ; this protection is realized by a mechanical system during the critical phases, i.e. when ice fog is running in the tunnel. This system and its efficiency are presented in the next chapter.

4.5. Leading edge protection and results

The figure 19 shows a schematic sketch of the protection system. A cylinder of triangular cross section is pushed into the test section by a jack, at the start of the run ; thereby, the cylinder is parallel to the model leading edge, at about 1 cm upstream of it. Model and cylinder are fixed to a turntable and turn together when the angle of attack varies. The flow is strongly turbulent just downstream of the cylinder and it cools down more efficiently all the model. In another hand, the cylinder is hit by some icicles and it deviates other ones from the model vicinity. During this cooling phase characterized by low velocity and low pressure, the protection is mainly efficient around the dew point. During the second phase of establishing and stabilizing the test Mach number and pressure, the protection by the cylinder is still necessary ; this transitional period is favourable to an increase in the icicles number carried by the flow, maybe due to a momentary bad filter operation. Many tests demonstrate this fact.

When all the test parameters are stabilized, the cylinder is automatically pulled out from the test section and the wall adaptation phase begins. At the end of the data acquisition phase, the cylinder is pushed again into the flow and then the run is stopped and the temperature increases.

This device and this procedure have been used to complete the series of tests with the laminar wing AS100. The stagnation temperature range is $125 \text{ K} \leq T_t \leq 240 \text{ K}$ ($7.5 \cdot 10^6 \leq R_e \leq 19 \cdot 10^6$). Very few tests are perturbed by icicles. We can observe in the figure 15 that this protection allows to shift the laminar operation of this wing from $7.5 \cdot 10^6$ up to $14 \cdot 10^6$ Reynolds number ($P_t = 2$ bars). From $14 \cdot 10^6$ to $19 \cdot 10^6$, transition goes forward naturally as explained by MIGNOSI [10] and the cylinder acts still well.

After this promising series of tests, the principle of the leading edge protection has been successfully applied to a laminar fuselage. The cylinder was replaced by a sort of racket which has been efficient to protect the model from the icicles damages.

4.6. Frost visualization

At ambient temperature, a visualization with acenaphtene shows that the sublimation is more intense over turbulent zones than over laminar ones. In cryogenic condition, a similar phenomenon occurs for the water condensation which is more active over turbulent region. The photograph (Fig. 14-a) shows a visualization realized with favourable frost formation conditions at $T_t = 200 \text{ K}$ ($R_e = 7 \cdot 10^6$). We can see a turbulent white cone creates by a bad pressure hole geometry located near the leading edge. Around this cone, the laminar zone, covered by a thinner frost coating, seems to be grey. At the back of the profile, a transversal straight line indicates a short transition produced by the shock-laminar boundary layer interaction. The photograph (Fig. 14-b) shows a frost visualisation carried out at $T_t = 140 \text{ K}$ ($R_e = 11 \cdot 10^6$) with some turbulent cones due to local icicles tripping transition near the leading edge.

Usually, frost visualization appears slightly during the test when the model and the flow are at the same temperature. When the run is stopped ($T_{model} > T_t$), condensation is intense, especially if the model is not protected by the cylinder during this phase, and the visualization becomes more contrasted.

This visualization technique can supply interesting information. It has to be better studied and developed.

5 - CRYOGENIC TEST RESULTS

5.1. 2D test results

CAST 10 airfoil has been tested in several wind tunnels in a cooperation framework between DFVLR (TWB) - NASA Langley (TCT) and ONERA/CERT (T2 [14]). The figure 20 presents T2 results for free and fixed

transition and for two Reynolds numbers ($R_c = 4 \cdot 10^6$ and $21 \cdot 10^6$). Free transition polar at low Reynolds number shows a large drag reduction. At high Reynolds number ($R_c = 21 \cdot 10^6$, $T_t = 120$ K) the two polars are very close. Variation of the fixed transition polar underlines a simple Reynolds effect. On the other hand, free transition goes upstream when Reynolds number increases because this airfoil is very sensitive, and the configuration trends to a fixed transition condition.

5.2. 3D test results

This chapter points out the difficulty to separate Reynolds effect and temperature effect in unsteady phenomena. Twelve pressure transducers are located as shown in figure 21, in a Δ wing/body half model ; measurements performed at a rate of 2500 pts/s at different temperature levels are plotted below. There is a strong correlation between signals measured on the same chord ; on the other hand, the Reynolds number effect is very small and is only underlined by a slight downstream shift of the shock location near the D31 transducer [11].

When the temperature decreases, aerodynamic frequencies decrease as $\sqrt{T_t}$ while mechanical frequencies are constant. We can make two remarks.

Firstly, the real parameter to analyse correctly Reynolds effect on aerodynamic variables is the reduced frequency called Strouhal number $S = \frac{f l}{U_\infty}$ (f , frequency ; l , characteristic dimension ; U_∞ infinite flow velocity $\sim \sqrt{T_t}$) which appears in non-dimensional instationary aerodynamic equations. The figure 22 shows that the maximum energy of the pressure spectra occurs at almost constant Strouhal number when the temperature decreases ; this result was already observed in 2D tests [13].

Secondly, if the Reynolds effect carried out by temperature variation allows to keep constant the model deformations, this technique introduces a temperature effect which cannot be separated when the temperature decreases, the aerodynamic characteristic frequency gets closer to the mechanical one and excites more actively the first model vibration mode in our case.

5 - CONCLUSION

T2 transonic wind tunnel has been converted for cryogenic operation in 1981. It benefited from an efficient internal insulation and an accurate regulation control system as well as performing auto-adaptive walls (2D/pseudo-3D strategies).

Constraints due to the short run duration, the required data quality and the extension of the tunnel capabilities led us to develop new concepts such as low thermal inertia models, powerful instrumentation, model protection device and technique to avoid moisture effects.

The association of research and industrial activities allowed to analyse various subjects in an extended Reynolds number range : model coefficients, transition, laminar flow, buffeting.

In the next future, a three-dimensional laser anemometer system will be used to get more information in ambient and cryogenic environment.

REFERENCES

- [1] CARRIERE P. "The injector driven tunnel". AGARD LS 1972 - AGARD Report R-600-72
- [2] QUEMARD C., MIGNOSI A. "Definition of a high flow quality injector driven tunnel : the pressurized transonic wind tunnel T2 at ONERA/CERT". 18th Israël Annual Conference (1976)
- [3] BLANCHARD A., DOR J.B., MIGNOSI A., BREIL J.F. "Recherches sur une soufflerie cryogénique fonctionnant par induction". La Recherche Aéronautique 1981-2 (French and English Editions)
- [4] MIGNOSI A., FAULMANN D., SERAUDIE A. "La soufflerie transsonique à induction T2 : fonctionnement à température ambiante et adaptation cryogénique". La Recherche Aéronautique 1981-3 (French and English Editions)
- [5] FRANCOIS G. "Thermal behaviour and insulation of a cryogenic wind tunnel". ETW Meeting, AMSTERDAM (September 1982)
- [6] PACI P. "Practical problems of design and manufacture of two-dimensional model and the device for its cooling and introduction into the T2 pressurized cryogenic intermittent tunnel". ETW Meeting, AMSTERDAM (Septembre 1982)
- [7] DOR J.B. "The T2 cryogenic induction tunnel in TOULOUSE". AGARD FDP Special Course "Cryogenic Technology for Wind Tunnel Testing". VKI (22-26 avril 1985)
- [8] ARCHAMBAUD J.P., MIGNOSI A. "Two-dimensional and three-dimensional adaptation at the T2 transonic wind tunnel of ONERA/CERT". AIAA 15th Aerodynamic Testing Conference, SAN DIEGO, CA (May 1988)
- [9] BLANCHARD A., DOR J.B., SERAUDIE A., BREIL J.F. "Flow quality in the T2 cryogenic wind tunnel : problems and solutions". 2nd Cryogenic Technology Review Meeting
- [10] MIGNOSI A. "Fundamental considerations for testing in cryogenic wind tunnels". AGARD FDP Special Course "Advances in Cryogenic Wind Tunnel Testing" VKI (5-9 June 1989)

- [11] ARCHAMBAUD J.P., BLANCHARD A., DOR J.B., PAYRY M.J. "Procès-verbal d'essais de tremblement sur Axxx dans la soufflerie T2 (2ème campagne)". Procès-verbal d'essais OA N° 3423 AYD (DERAT N° 13/5017.13) Mars 1988
- [12] ARCHAMBAUD J.P., SERAUDIE A., PAYRY M.J. "Etude expérimentale de la laminarité sur l'aile AS409 du nombre de Reynolds maximum possible ($R_e \approx 7,3 \cdot 10^6$ - $C = 0,187$ m) dans la soufflerie T2". R.T.S. N° 32/5006.12 (Mars 1989)
- [13] DOR J.B., MIGNOSI A., SERAUDIE A., BENOIT B. - "Wind tunnel studies of natural shock wave-separation instabilities for transonic airfoil tests". - IUTAM Symposium, Göttingen, 24-25 May 1988.
- [14] SERAUDIE A., BLANCHARD A., BREIL J.F. - "Rapport d'essais du profil CAST 10 en transition déclenchée, effectués dans la soufflerie transsonique cryogénique T2 en présence de parois auto-adaptables" - Rapport Technique ONERA/CERT-DERAT n° 6/5019 DN, août 1988.

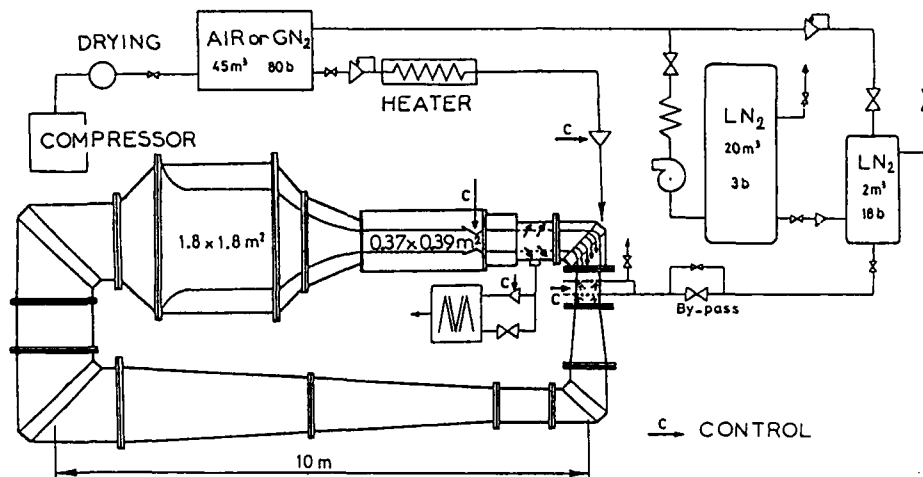


FIG. 1 : Schematic diagram of the wind-tunnel T2.

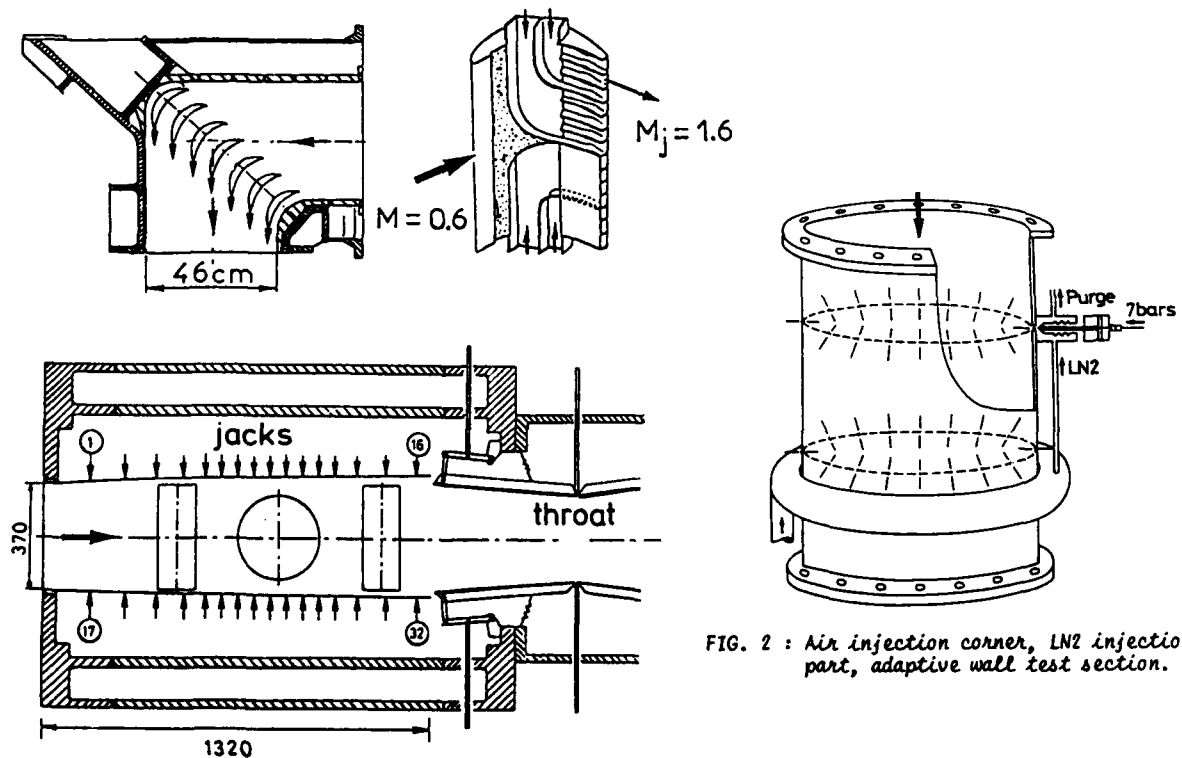


FIG. 2 : Air injection corner, LN2 injection part, adaptive wall test section.

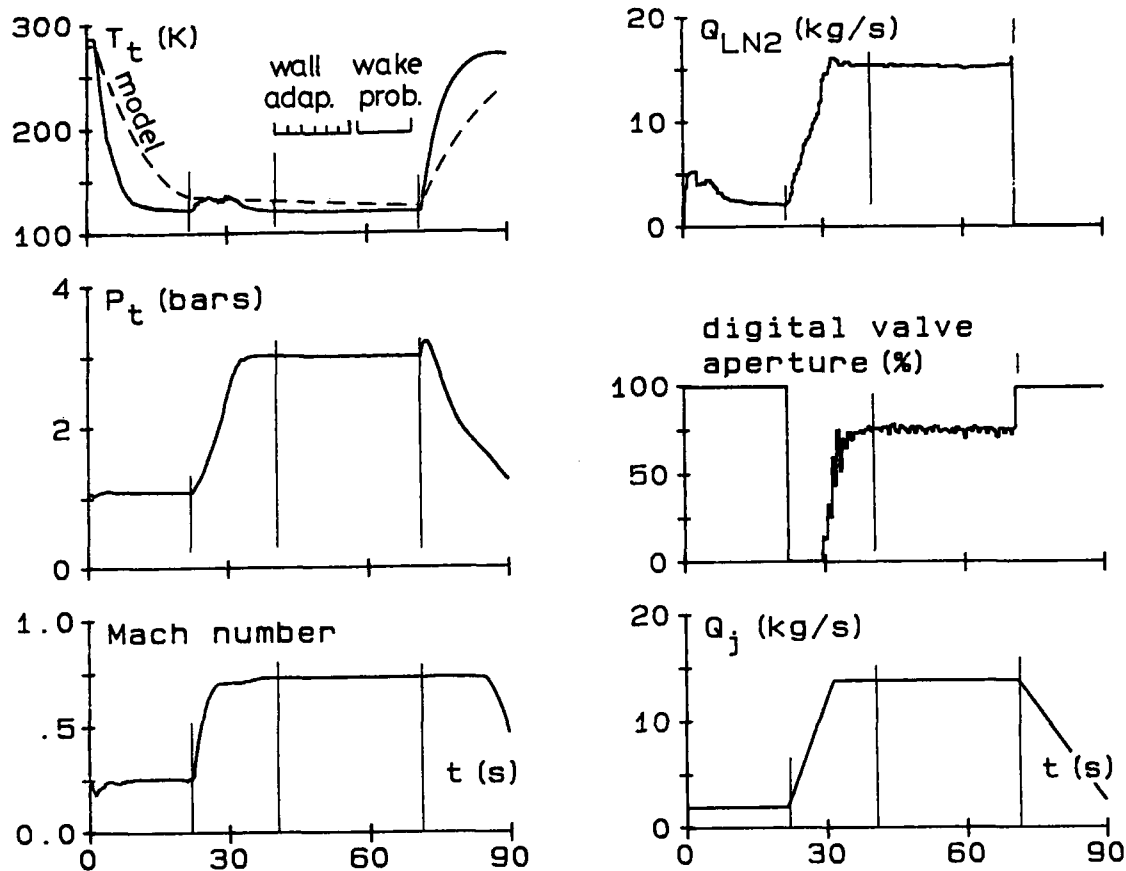


FIG. 3 : Typical Cryogenic Run. $M = 0.75$, $P_t = 3$ bars, $T_t = 120$ K.

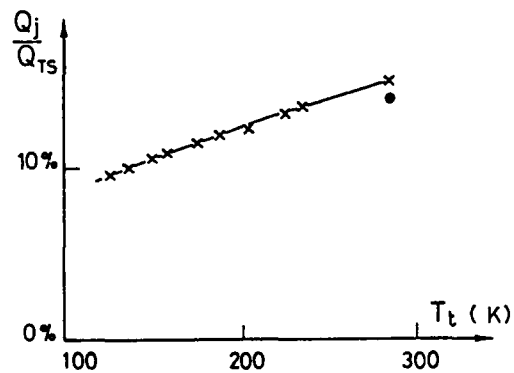
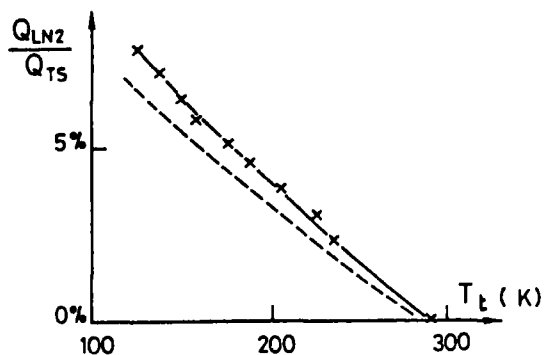


FIG. 5 : Induction efficiency variation with flow temperature.



→ FIG. 6 : Liquid nitrogen consumption.

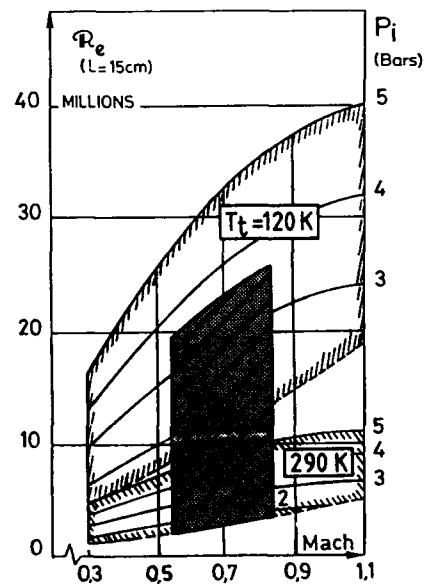


FIG. 4 : T2 operating envelope.

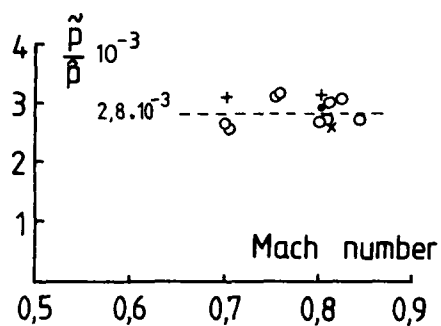


FIG. 7 : Pressure fluctuation level at T2

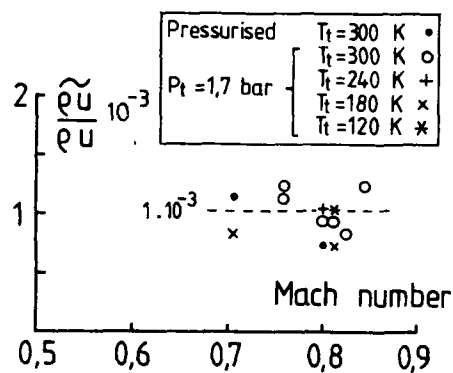


FIG. 8 : Mass flow fluctuation level at T2.

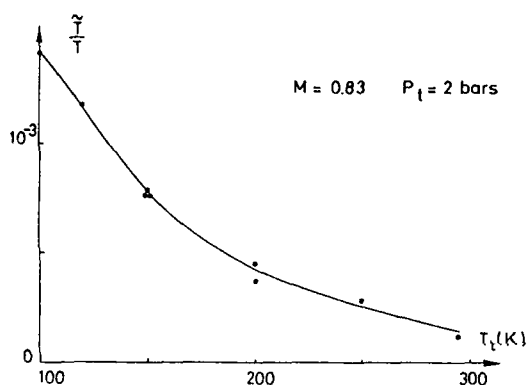


FIG. 9 : Temperature fluctuation level at T2.

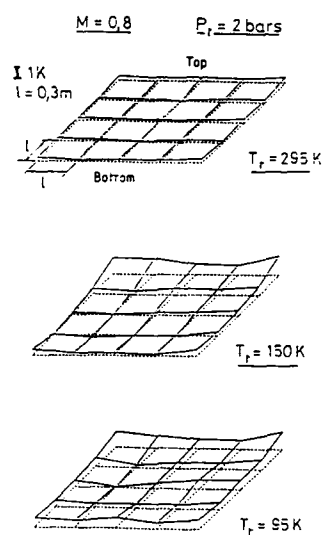


FIG. 10 : Thermal gradient in the T2 stilling-chamber.

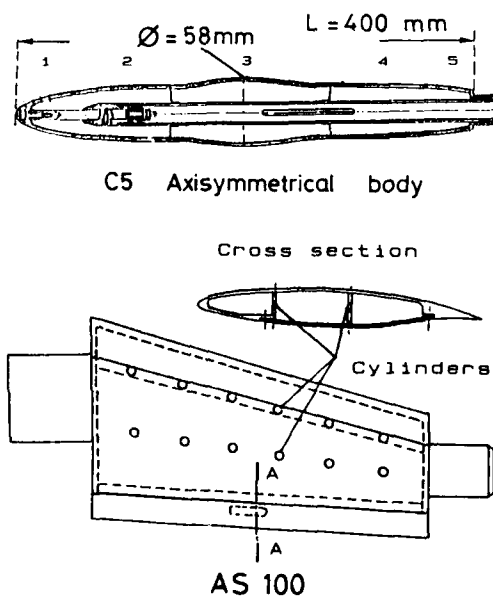


FIG. 11 : Low thermal inertia models.

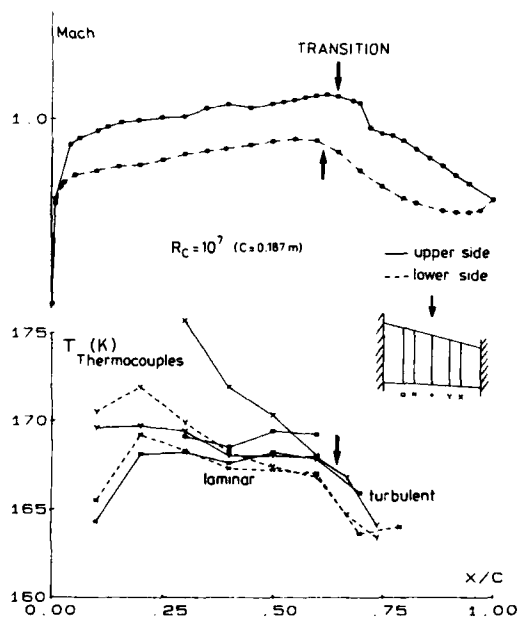


FIG. 12 : Correlation between thermocouple measurements and transition location.

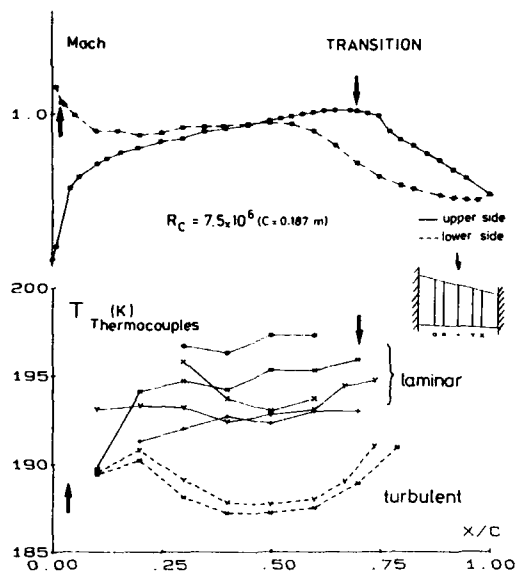
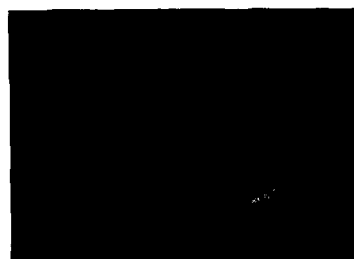


FIG. 13 : Correlation between thermocouple measurements and transition location.



a)
 $T_t \approx 200$ K
 $R_c = 7 \cdot 10^6$



b)
 $T_t \approx 140$ K
 $R_c = 11 \cdot 10^6$

FIG. 14 : Frost visualizations on laminar wing.

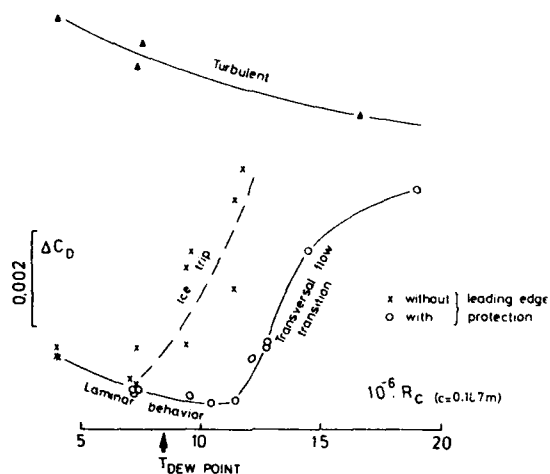


FIG. 15 : Drag and lift coefficients-AS 100 - Efficiency of the leading-edge protection.

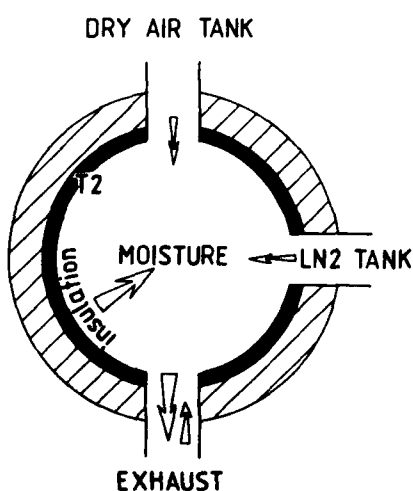
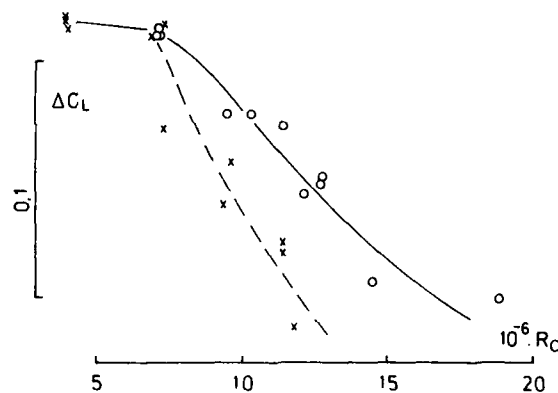


FIG. 16 : Sources of moisture.

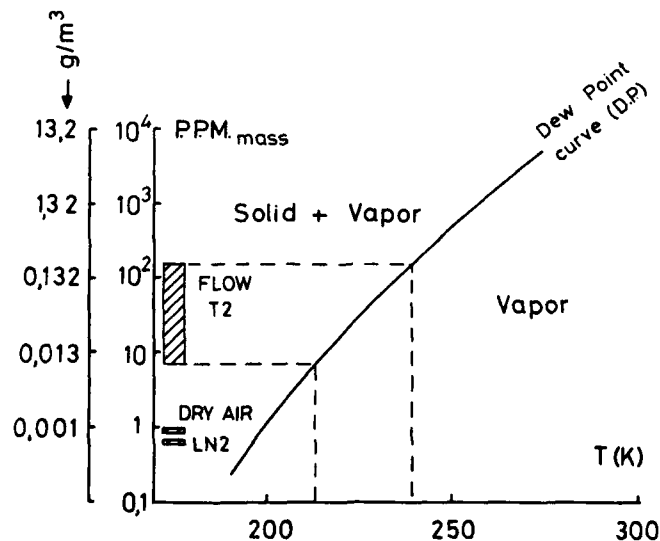


FIG. 17 : Water equilibrium diagram in air.

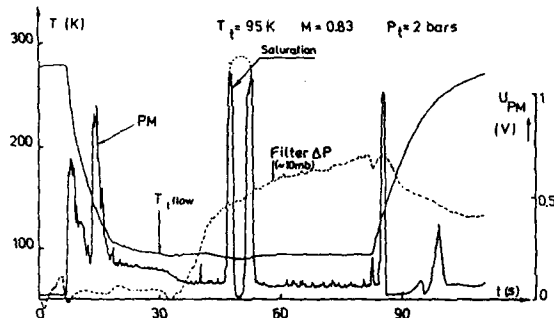


FIG. 18 : Particle detection during a run at very low temperature ($T_f = 95$ K).

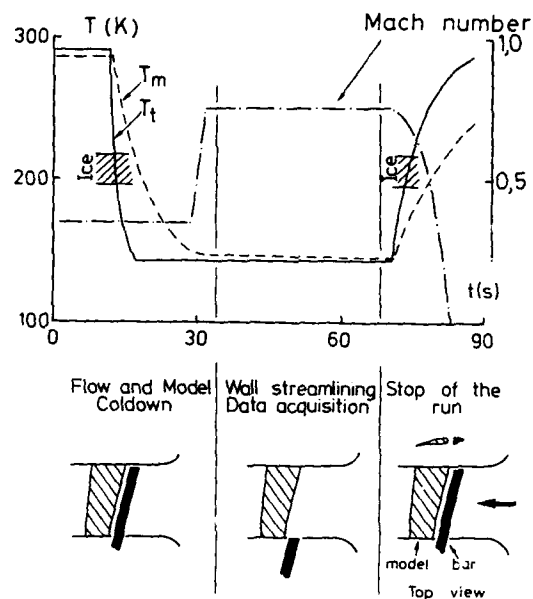


FIG. 19 : Typical run with leading edge protection system.

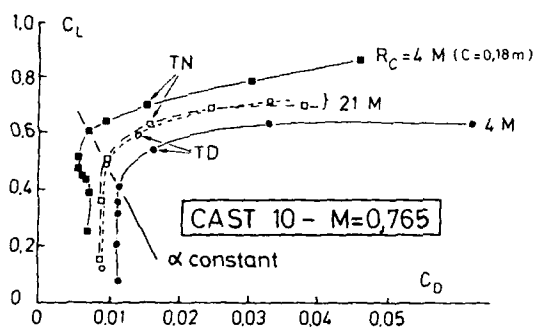


FIG. 20 : Results on CAST 10 model.

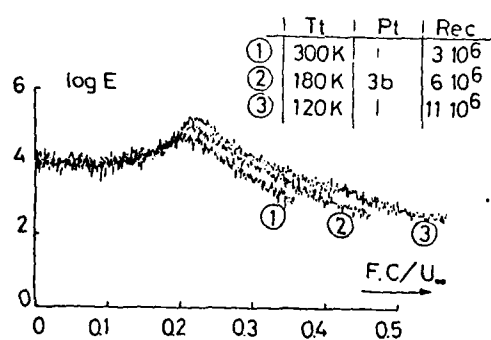
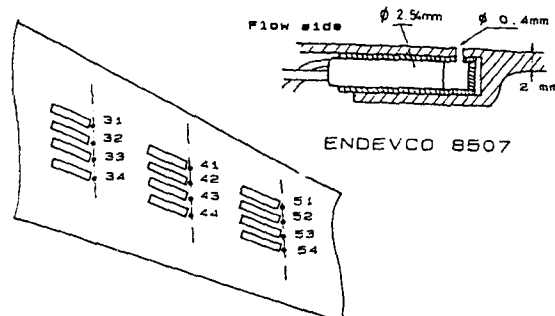


FIG. 22 : Temperature effect on pressure spectra (Axxx model).

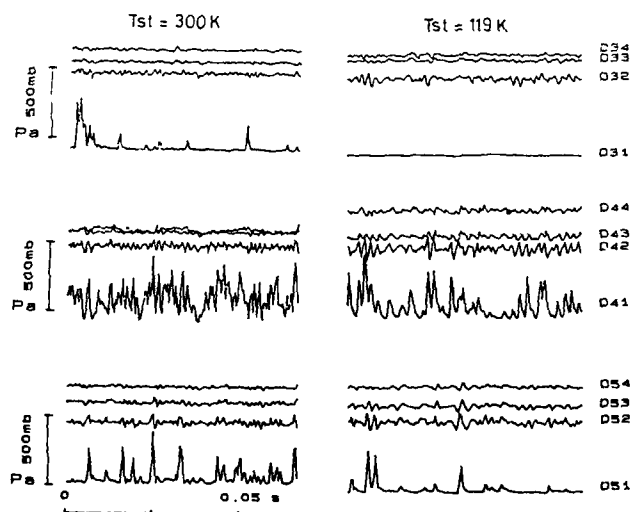


FIG. 21 : Pressure transducers (Axxx model).

THE CRYOGENIC LUDWIG TUBE TUNNEL AT GÖTTINGEN

G. Hefer

Deutsche Forschungsanstalt für Luft- und Raumfahrt e.V.
 Institut für Experimentelle Strömungsmechanik
 Bunsenstr. 10
 D-3400 Göttingen
 F. R. Germany

SUMMARY

At the Research Center Göttingen of the DLR a cryogenic Ludwig tube wind tunnel for transonic operation has been constructed. The tunnel, having an effective run time of 1 second, a test section of $0.4 \times 0.35 \text{ m}^2$, and a maximum stagnation pressure of 10 bars, is to be operated with nitrogen at temperatures between ambient and 120 K, achieving a Reynolds number of $70 \cdot 10^6$ based on a model chord of 0.15 m.

This lecture gives a brief review of the Ludwig tube concept, the main design features of the tunnel, and the status of the project and presents the first results of the calibration.

NOMENCLATURE

c	Chord of two-dimensional airfoil	Subscripts	
L	Length of the charge tube		
Ma	Mach number	c	Charge conditions
p	Pressure	t	Stagnation conditions
Re	Reynolds number	ts	Test section
S	Cross-sectional area of the test section	f	Flow conditions in the charge tube
t	Time		
T	Temperature		
x	Linear dimension		
v	Velocity		

1. THE CRYOGENIC LUDWIG TUBE CONCEPT

Basically, a Ludwig tube wind tunnel [1] is a blow down tunnel with a very long storage vessel. Therefore, the discharge process is not a continuous one but takes place in batches with constant flow parameters for each batch. The gasdynamic process is sketched in Fig. 1. The high pressure tube is separated from the low pressure dump tank by a quick opening valve. When the valve is opened, an expansion wave, whose initial spread is given by the opening time of the valve, moves upstream into the tube and accelerates the gas to a Mach number Ma_1 , determined by the area ratio of the sonic throat of the valve and the tube, A^*/A_{tube} . The flow parameters behind the wave (region (1) in Fig. 1) are constant as long as viscosity effects can be neglected. The measuring time is determined by the time it takes the wave to travel to the end of the tube and back to the test section. The stagnation conditions (denoted by the subscript t_1) are different from the charge conditions (denoted by c). Fig. 2 shows the ratios p_{t_1}/p_c , T_{t_1}/T_c , the Mach number in the tube, Ma_1 , and the length ΔL of the gas column passing through the test section as functions of the Mach number in the test section, Ma_{ts} , for a nozzle contraction ratio A_{tube}/A_{ts} of 3.6 which applies to the tunnel to be described below.

The advantages of a Ludwig tube wind tunnel are

- simplicity of the system,
- low capital cost,
- high flow quality, provided the running time is not too long,
- high discharge efficiency since the stagnation pressure is higher than the pressure of the gas remaining in the tube.

For cryogenic use, additional advantages are

- no temperature distortions due to LN_2 -injection,
- lower stagnation temperature than charge temperature,
- extended measuring time as the expansion wave moves with the reduced speed of sound.

The operating costs are determined by the consumed nitrogen; they can be kept low compared to continuous tunnels.

Concerns about the Ludwig tube tunnel are dealing mainly with the short run time and the impairment of the flow quality due to the boundary layer growth associated with a long run time (long tube) or a small tube to test section area ratio which causes variations of the flow parameters in time and space and increases the turbulence level.

In the present design, this has been obviated by choosing a relatively high contraction ratio and installing a boundary layer bleed system at the nozzle inlet.

2. DESIGN FEATURES

2.1 SPECIFICATIONS

The basic requirement for the design of the tunnel was to obtain a Reynolds number of at least $50 \cdot 10^6$ on an airfoil model at transonic speed. For reasons of manufacturing accuracy we have considered a chord of 150 mm necessary with the intention of increasing it to 200 mm when an adaptive wall test section is available. The minimum aspect ratio of an airfoil model being 2 [2], the test section width has been determined to be 400 mm. As the majority of investigations is expected to be carried out on wall mounted models, a relatively high maximum stagnation pressure of 10 bars has been chosen, yielding a Reynolds number of about $70 \cdot 10^6$ at a stagnation temperature of 120 K. In Fig. 3 the Ma, Re-diagram is given for reference lengths of 200 mm, 150 mm and $0.1\sqrt{S} = 37.4$ mm.

Considering flow quality, there is a relationship between run time (i.e. tube length), tube diameter and contraction ratio of the nozzle which determines the discharge Mach number and with it the boundary layer growth in the tube. In the present case, the basic requirement was a run time of 1 second at cryogenic temperatures resulting in a charge tube length of about 130 m. To keep the maximum discharge Mach number sufficiently low, the contraction ratio has been chosen to be 3.6, yielding a boundary layer displacement thickness of less than 6% of the radius at moderate stagnation pressures and ambient temperature. At cryogenic temperatures and high pressures the displacement thickness is less than 4% of the tube radius.

2.2 GENERAL DESCRIPTION

A sketch of the general tunnel arrangement is given in Fig. 4. There are two main shut-off devices, separating the test section from the tube and the dump tank. The main starting device is located downstream of the test section and includes the sonic throat for Mach number control (see 2.3.3). The gate valve upstream of the nozzle separates two charging and temperature conditioning loops: Tube and test section (i.e. model) temperature can be adjusted independently offering the possibility of preconditioning the model to the correct temperature. In addition, the gate valve prevents air from entering the tube when the test section is opened or removed.

Upstream of the gate valve and downstream of the starting device, there are two thrust stands taking the reaction forces. The contraction due to cooling between the stands will be compensated by a bellows upstream of the rear stand; for the same reason the dump tank is seated on sliding supports and the charge tube on rolls.

The entire wind tunnel has been manufactured of stainless steel, German standard X 10 CrNiTi 189 (equivalent to Z6 CNT 18-11 (France), 321 S12 (UK), AISI 321 (USA)), except the nozzle and the part connecting the test section and the quick opening valve which has been made of cast steel.

The external insulation of the tube consists of an inner layer of mineral wool and an outer layer of polystyrene covered by a vapor barrier and a sheeting. The total thickness is 200 mm. Every twelve meters, the tube is supported by rings of plywood without any metal connection between the shell and the external support ensuring a uniform temperature along the tube. A nitrogen purge system maintains the entire insulation at a low overpressure to preclude entry of air or moisture.

2.3 DESCRIPTION OF ESSENTIAL COMPONENTS

2.3.1 NOZZLE WITH GAS FEEDING AND BOUNDARY LAYER BLEED SYSTEM

Since in a Ludwig tube tunnel the gas is accelerated from the state of rest, the initial turbulence level is very low. However, during the measuring period, the boundary layer growing along the charge tube affects both the stagnation conditions and the turbulence level. The first effect can be compensated by a continuous re-adjustment of the control valve. In general, the turbulence level in the test section could be reduced by increasing the contraction ratio (i.e. the tube diameter) or by insertion of a conical diffusor and a settling chamber with screens [3]. These approaches are costly and, in the case of the settling chamber, detrimental to the performance of the tunnel since the starting time would increase reducing the run time. In the present case, a boundary layer bleed system has been designed which is located at the entrance of the nozzle (Fig. 5). A sliding cylinder, moving from the annular space surrounding the nozzle in upstream direction and thereby covering the openings left by the gate and the feeding ring, opens an annular gap which allows the boundary layer to enter the low pressure annulus. The bleed mass flow rate can be controlled by adjusting the gap width according to the boundary layer displacement thickness.

The fixed contour nozzle is made of austenitic cast steel. The cross section changes from a circle at the lip of the bleeding system to a rectangle of 400 mm by 350 mm at the exit. The design of the bleed system entails a very gradual contraction at the nozzle entrance, thus preventing boundary layer separation in front of the lip.

2.3.2 TEST SECTION

A sectional view of the test section is schematically given in Fig. 6. A circular pressure vessel comprises the test section proper which has solid side walls and slotted top and bottom walls with an opening ratio, based on top and bottom wall area, of 3%. The length of the test section is 2 m, the cross section 0.4×0.35 m. The side walls have turn tables to mount a two-dimensional model. Each wall has three openings for the installation of movable probes. Wall pressure distributions can be taken along the centerline of each wall of the nozzle and the test section. - The pressure equalization between the test section and the surrounding space during the starting process is accomplished by slots in the rear part of the test section. The volume of this space has been reduced by wood, indicated by the dotted area in Fig. 6.

In view of the projected adaptive wall test section the present design has been kept simple as it will mainly be used for the verification of the tunnel concept, calibration, and comparative measurements to verify the performance and flow quality of the tunnel.

2.3.3 DIFFUSOR AND MAIN STARTING DEVICE

The crucial components of a Ludwig tube wind tunnel are the quick-opening valve which starts the flow and the sonic-throat diffusor which controls the Mach number in the test section. Both functions have been combined in the fast-acting control valve sketched in Fig. 7.

The valve consists of an enlarged tube with a centerbody which contains two hydraulic actuators used to operate the control cone and the sleeve valve. The control cone can reproducibly be located with an accuracy of 0.01 mm in order to adjust the test section Mach number. - The sliding cylinder at the rear of the valve starts the flow by moving downstream. The opening time can be adjusted to be less than 0.1 sec.

The centerbody is insulated on the inside; the temperature will be controlled by electrical heating.

3. FIRST TESTS

A main concern about the successful operation of a cryogenic Ludwig tube refers to the temperature distribution in the tube. For a run with constant flow conditions, the gas temperature in the first third of the tube has to be at constant temperature in the horizontal and vertical direction. It turns out that the latter condition is the more severe one to achieve. To avoid any stratification, a uniform wall temperature along the circumference of the tube has to be achieved by an appropriate cool down procedure. During cooling down, a fan circulates the nitrogen through the charge tube back to an

LN_2 -injection device. The minimum velocity in the charge tube for an even heat transfer rate around the tube circumference has been determined by temperature measurements inside and on the wall of the tube. The results have been summarized in Fig. 8. The figure shows temperature differences with respect to a fictitious initial point along a vertical diameter of the tube and along the centerline of the tube.

At a low velocity (0.6 m/s) a temperature distribution with cold gas at the bottom of the wall develops. When the LN_2 flow is throttled, the distribution takes on a more uniform shape. A good cooling down of the tube up to half of the length ($x = 63$ m) is accomplished by a velocity of 1.2 m/sec. From these tests the performance of the blower has been determined.

The flow in the test section has been investigated at ambient temperature by taking pressure distributions along the walls, Pitot pressures at the model location and velocities at the same location by a laser-Doppler anemometer [4]. Fig. 9 shows Mach number distributions along the nozzle and test section for various control valve positions taken from the mean value of the wall static pressure over the last third of the run time.

The time dependence of the velocity, Pitot pressure and Mach number is given in the following diagrams. Fig. 10 shows the velocity at the model position for two different Mach numbers for about 1.5 run periods, measured by an LDA. For the lower Mach number, the starting process is characterized by a velocity peak, caused by compression waves emanating from the widening nozzle as it is passed by the main expansion wave. At the higher Mach number this effect can not be seen because the opening time of the valve is longer. The velocity during the second period ($t > 1.0$ s) is, at the lower Mach number, slightly smaller because of the lower stagnation temperature. At the high Mach number, the dump tank is filled up to a higher pressure causing the control valve to become subcritical and the velocity to be reduced.

The characteristic behaviour of the flow at the beginning and the end of the test period can also be seen in Fig. 11, where the Pitot pressure is plotted versus the time. The Pitot pressure is constant within the measuring accuracy during 80% of the run time. Fig. 12 shows the Mach number versus the time derived from wall static pressures at model position. Because of the long tubes and small taps the response time is so long that details of the flow establishment cannot be seen. The Mach number constancy during the run time is better than $\Delta Ma = 0.002$ without any correcting movement of the control valve.

4. STATUS OF THE PROJECT

The construction of the wind tunnel was planned to be done in two phases: In the first phase all parts have been built that are necessary to operate the tunnel at ambient temperature and to perform the cool down tests described above. The second phase comprises the installation of the blower for the cool down circuit, the boundary layer bleed system and an adaptive wall test section. The first phase has been completed in 1988, the second one will be finished in the fall of 1989 except for the test section which we hope to get finished in 1990.

First model tests will be performed in 1989 on an LV2 airfoil. A two-dimensional CAST-10 model is under construction and will be tested early in 1990.

REFERENCES

- [1] Ludwig, H.: Der Rohrwindkanal. Z. f. Flugwiss. 3 (1955), p.206-216.
- [2] Ganzer, U.; Stanewsky, E.; Ziemann, J.: Sidewall Effects on Airfoil Tests. AIAA Journal 22 (1984), p.297-299.
- [3] Ludwig, H.; Grauer-Carstensen, H.; Lorenz-Meyer, W.: The Ludwig Tube. A Proposal for a High Reynolds Number Transonic Windtunnel. AGARD CP 174, p.3-1 to 3-7.
- [4] Bielert, F.: Stationäre Druck-, Temperatur- und LDA-Geschwindigkeitsmessungen im Kryo-Rohrwindkanal zur Überprüfung von Theorien des Rohrwindkanalprinzips. Diplomarbeit, Universität Göttingen, 1989.

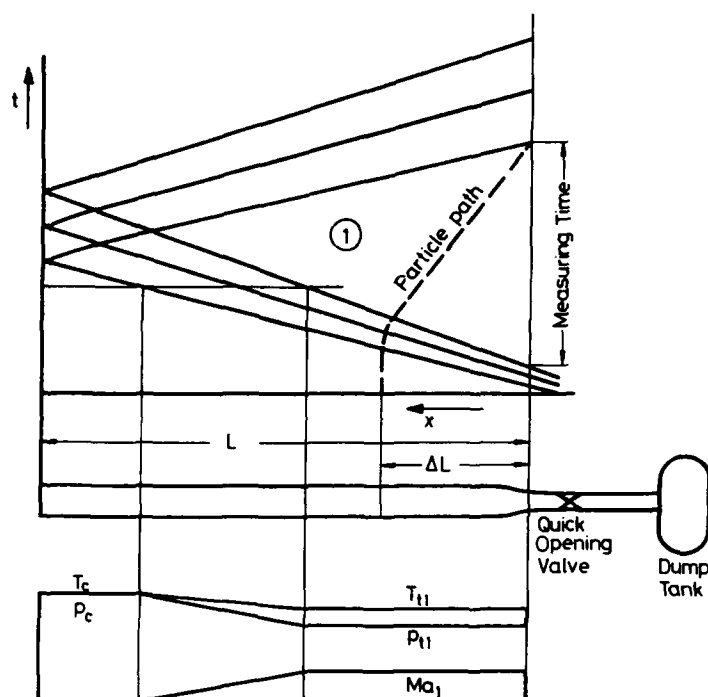


Fig. 1: x,t -Diagram of a Ludwieg tube wind tunnel.

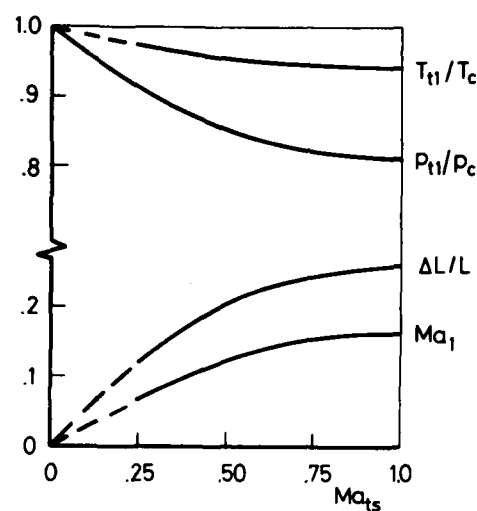


Fig. 2: Characteristic flow parameters as functions of the test section Mach number.

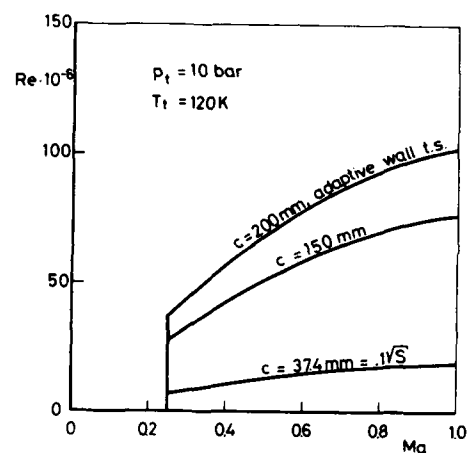


Fig. 3: Re, Ma -diagram.

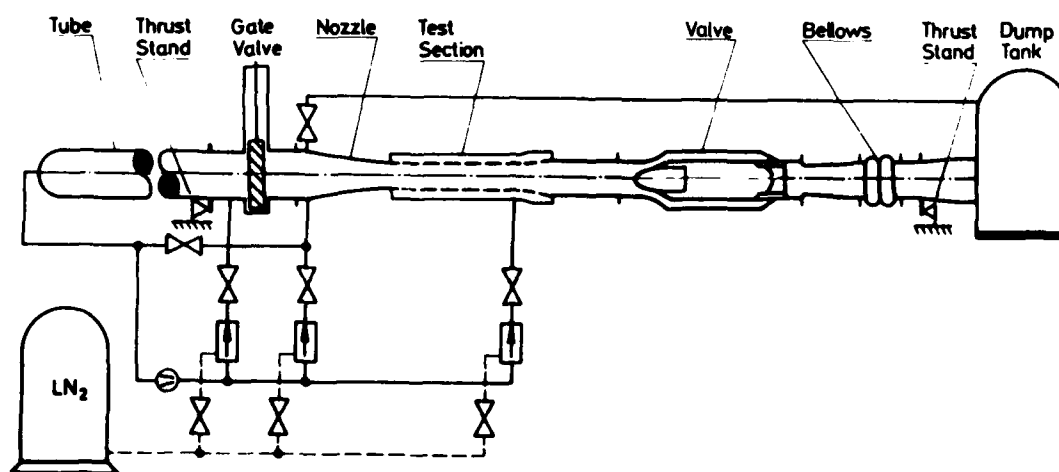


Fig. 4: Cryogenic transonic Ludwieg tube, general arrangement.

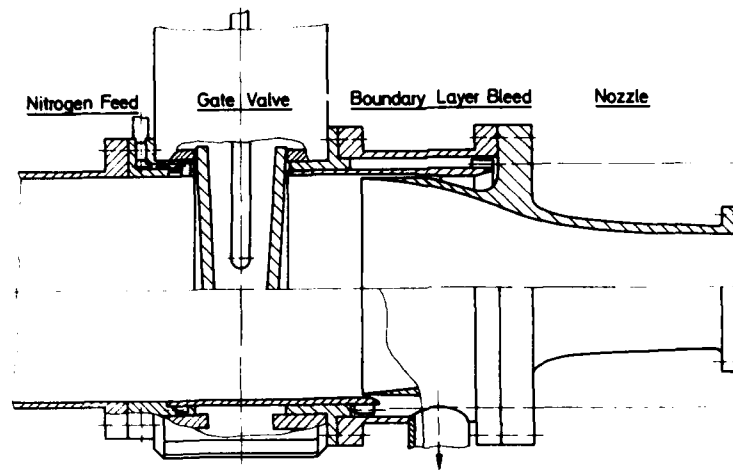


Fig. 5: Nitrogen feed and boundary layer bleed system.

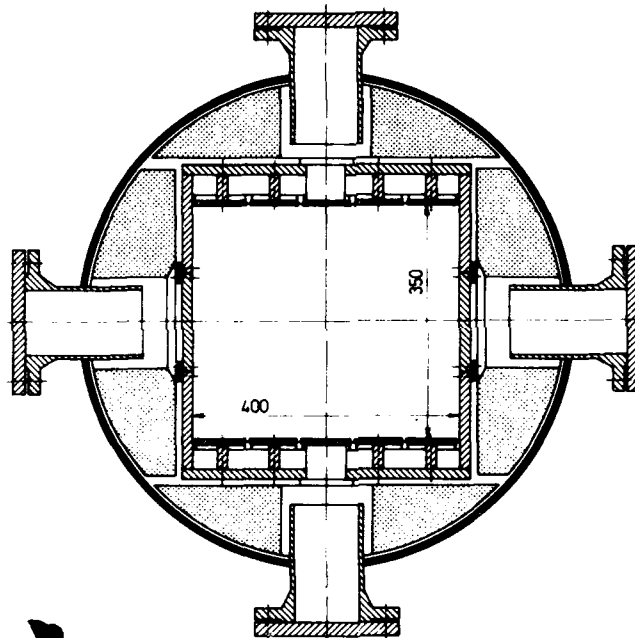


Fig. 6: Sectional view of the test section.

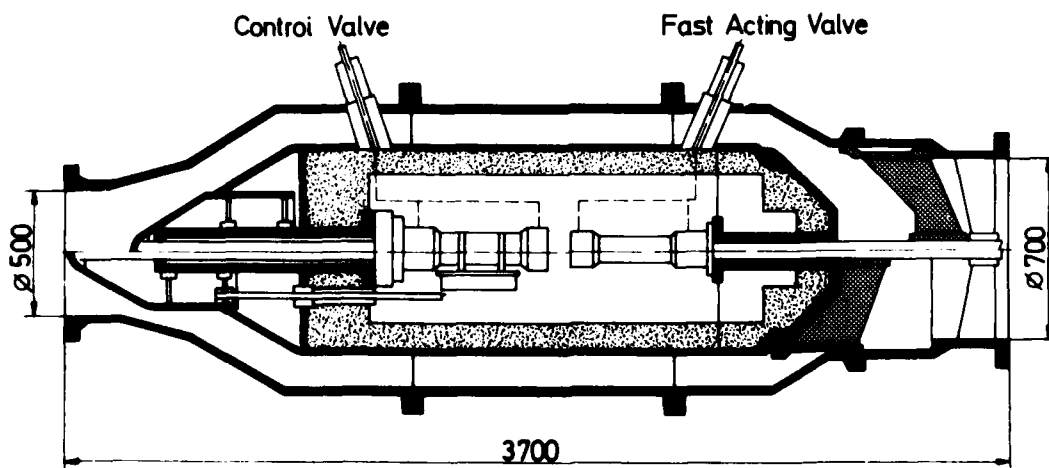


Fig. 7: Control valve and fast acting valve.

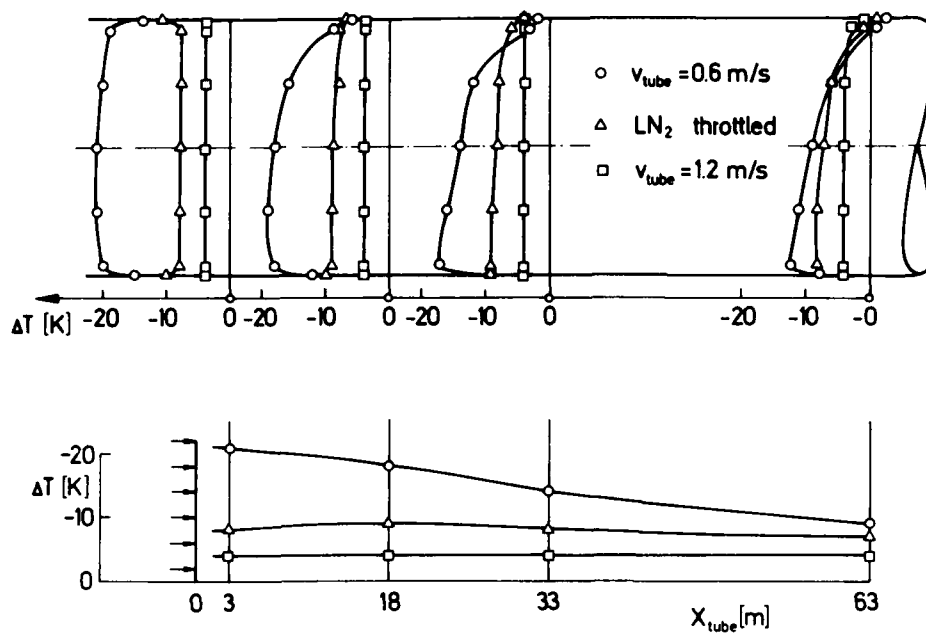


Fig. 8: Temperature distributions in the tube during cooling down.

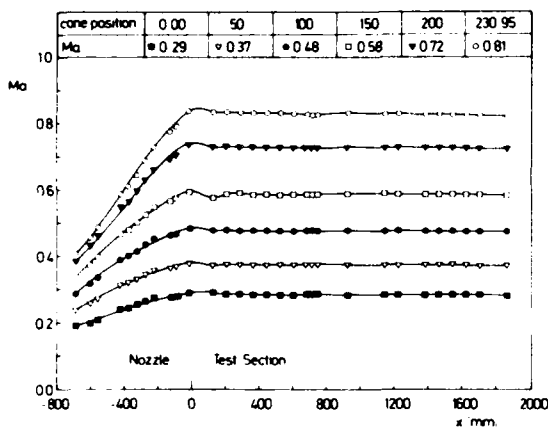


Fig. 9: Mach number distributions in nozzle and test section.

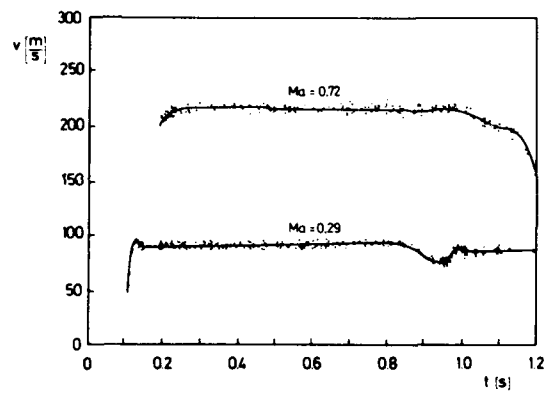


Fig. 10: Velocity in the test section during run time.

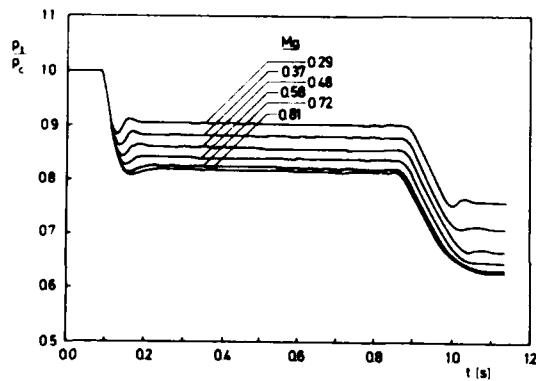


Fig. 11: Pitot pressure in the test section during run time.

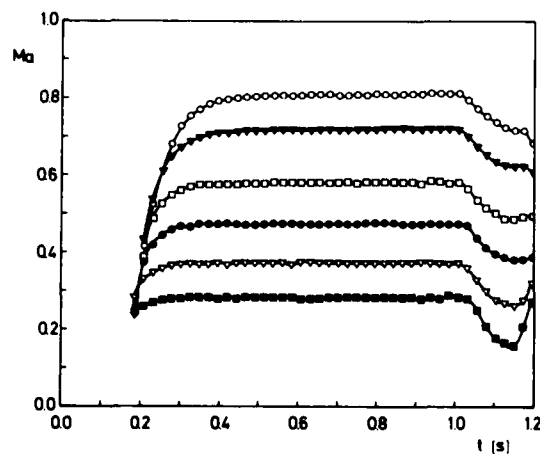


Fig. 12: Mach number from wall static pressures at model position during run time.

Other Cryogenic Wind Tunnel Projects

Robert A. Kilgore
NASA Langley Research Center
Hampton, VA 23665-5225
U.S.A.

SUMMARY

The first cryogenic tunnel was built in 1972. Since then, many cryogenic wind-tunnel projects have been started at aeronautical research centers around the world. This lecture describes some of the more significant of these projects not covered by other lecturers at this Special Course.

Described in this lecture are cryogenic wind-tunnel projects in five countries: **China** (Chinese Aeronautical Research and Development Center); **England** (College of Aeronautics at Cranfield, and Royal Aerospace Establishment - Bedford); **Japan** (National Aerospace Laboratory, University of Tsukuba, and National Defense Academy); **United States** (Douglas Aircraft Co., University of Illinois at Urbana-Champaign, and NASA Langley); and **U.S.S.R.** (Central Aero-Hydraulics Institute [TsAGI], Institute of Theoretical and Applied Mechanics [ITAM], and Physical-Mechanical Institute at Kharkov [PMI-K]).

1. INTRODUCTION

So far in this lecture series, we have heard about some of the cryogenic wind-tunnel projects in the member countries of AGARD. In the opening lecture, Dr. Goodyer described the Low-Speed Cryogenic Tunnel at Southampton. Mr. Ray told us about the Langley 0.3-m Transonic Cryogenic Tunnel (0.3-m TCT) which has been in operation since 1973. The 0.3-m TCT has the distinction of being the first transonic cryogenic tunnel. Mr. Bruce told us about the U.S. National Transonic Facility (NTF). The NTF is, by any standard, the most significant transonic cryogenic tunnel project thus far completed. From Germany, Dr. Viehweger reported on the DLR Kryo Kanal Koeln (KKK). The KKK is the largest and most significant low-speed cryogenic tunnel project completed. Mr. Bouis has reported on the European Transonic Tunnel (ETW), the most ambitious cryogenic tunnel project now underway. From France, Mr. Archambaud reported on the cryogenic induction tunnel T2 at ONERA-CERT in Toulouse. Also from Germany, Dr. Hefer reported on the DLR Cryogenic Ludwig Tube Tunnel at Göttingen.

The lectures of this AGARD-FDP/VKI Special Course, taken together, show a high level of cryogenic tunnel activity within the AGARD community. It should come as no surprise to learn there are several other cryogenic tunnel projects, either completed or planned, in both AGARD and non-AGARD countries. It is my purpose in this lecture to describe briefly some of these projects.

I do not try to describe all of the cryogenic tunnel projects not otherwise covered in this series of lectures. Rather, I have selected projects to exemplify the wide variety of cryogenic tunnel projects which have arisen since we built the first cryogenic wind tunnel 17 years ago.

I give much of the information about the various tunnel projects in tables. Unless otherwise indicated, the value of Reynolds number is per metre. I have tried to make sure the information contained in this lecture is accurate. However, the reader should contact directly the people involved with each of the projects for more detailed information, particularly about the status of on going projects.

2. CHINA

Starting in 1975, researchers at the Chinese Aerodynamic Research and Development Center (CARD C), Mianyang, Sichuan, China, have studied various schemes for high Reynolds number transonic wind tunnels. Their studies have included the cryogenic nitrogen tunnel. They have concluded that the continuous flow cryogenic nitrogen tunnel is especially attractive for meeting their high Reynolds number transonic testing requirements. However, the initial cost of such a tunnel is high. Therefore, they have studied alternative intermittent cryogenic wind-tunnel schemes as a way to get high Reynolds numbers at less cost. Reference 1 reports the results of their studies.

The intermittent cryogenic tunnel scheme proposed by CARD C would use precooled high pressure air. The air is further cooled by throttling before passing through the wind tunnel test section into a storage tank. As noted in Reference 1, using an existing high pressure air storage system considerably reduces the capital cost of the proposed cryogenic tunnel. Table 1 gives the major characteristics of the proposed CARD C 2.4 x 2.4 m high Reynolds number cryogenic transonic wind tunnel.

The CARD C intermittent cryogenic wind tunnel will consist of an existing high pressure air supply, the various parts of the wind tunnel, and a system for collecting the cold air which has passed through the test section. Figure 1 shows a schematic diagram of the proposed tunnel.

TABLE 1. - Proposed Cryogenic Transonic Tunnel at CARD C (China)

Type	intermittent
Material of construction	?
Insulation	?
Cooling	throttling
Test gas	air
Test section size (h,w,l)	2.4 x 2.4 x ? m
Mach range	0.5 - 1.6
Contraction ratio	?
Stagnation pressure	up to 1013 kPa
Stagnation temperature	sat. to ambient
Running time	?
Max. Reynolds number/m	167 million

There are five axial-flow compressors in the existing high pressure air supply system, each capable of compressing 130 m³ per minute to 22.3 MPa (220 atm). The high pressure storage tanks are made of 09Mn2VR low temperature steel and have a total volume of about 1290 m³. The initial filling time for the storage tanks is about 5 hours. During normal operation, where the pressure in the storage tanks is not reduced below 15.2 MPa (150 atm), filling time is about 2 hours. The precooling system not only cools the compressed air but also reduces the water content to less than 0.2 gram per kg of air. They alternately use two heat exchangers; one operating while the other is defrosting.

There will be constant temperature equipment to compensate for the temperature reduction in the air expanding adiabatically in the high pressure container. In all, the tunnel will use 636 x 10³ kg of FL5 aluminum alloy in the constant temperature equipment. As explained in Reference 1, the large pressure regulating valve and the constant pressure throttling valve will be very important elements in the tunnel control system.

There will be a shock wave stabilizer in the last part of the wind tunnel diffuser. It will control the position of the shock wave to hold the test section Mach number constant. During a test, the air pressure in the collecting container will increase continuously. The shock wave of the wave stabilizer will continuously move forward. However, the wave stabilizer will fix the shock wave at the downstream end of the throat to keep the test Mach number constant.

The air container collects the low temperature air after it has passed through the test section. They use a portion of the air to cool the pre-cooling system. They recompress the remainder of the air and store it in the storage tanks. A typical volume envisioned for the air collecting container will be about 2.7 to 3.6×10^4 m³. Under conditions where they exhaust the low temperature air directly to the atmosphere, they will provide a way to increase the temperature of the air to avoid problems with fogging.

3. ENGLAND

3.1 College of Aeronautics, Cranfield

Schultz and his coworkers at Oxford University proposed and built an isentropic light piston tunnel (ILPT). The purpose of the ILPT was to measure heat transfer rate on gas turbine blades in a short duration, hot, low-Reynolds-number flow.² Figure 2 shows a schematic of the ILPT.

In this tunnel concept, compressed air drives a light piston into a charge tube, compressing and heating the gas in the tube almost isentropically. The piston acts as a barrier between the compressed air expanding into the charge tube and the gas it is compressing. Compression continues until the gas in the charge tube reaches the desired pressure and temperature. A fast-acting valve (or diaphragm) at the end of the charge tube then opens to allow the hot test gas to pass through the test section. By properly designing the tunnel, the volumetric flow of compressed air from the reservoir into the charge tube exactly matches the flow of gas from the charge tube through the test section. By matching the flows in this way, it is possible to maintain constant test conditions.

At the College of Aeronautics, Cranfield Institute of Technology, Bedford, Stollery and Murthy suggested the Oxford type of light piston tunnel could operate in reverse. This arrangement would generate intermittent low-temperature, high-Reynolds-number flows.³ Figure 2 shows the simplest form for the cryogenic isentropic light piston tunnel (CILPT) in which high pressure gas in the charge tube vents to the atmosphere. Opening the vent valve causes the pressure and temperature in the charge tube to expand isentropically. The vent valve is closed when the pressure and temperature reach the values required for the test. The valve separating the test section from the charge tube is then opened. Following a predetermined delay of a few milliseconds, the piston is set in motion by opening the valve between the charge tube and the medium pressure reservoir. This pushes the cold gas in the charge tube out through the test section. Again, matching the incoming and outgoing volumetric flows keeps the test conditions constant. Figure 3 shows the idealized pressure and temperature time history for both the ILPT and the cryogenic version of the ILPT.

Stollery and his coworkers built a pilot intermittent cryogenic wind tunnel based on this light piston concept. Using nitrogen as the test gas, they achieved both the low stagnation temperature and the required matching of volumetric flows. Reference 6 gives an analysis of the CILPT, the design details of the pilot CILPT, and experimental results from the tunnel. Table 2 lists the

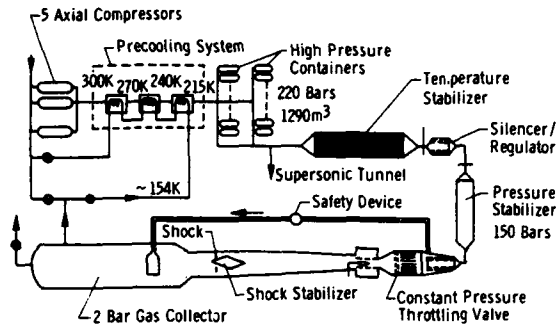


Fig. 1 Proposed 2.4 x 2.4 m Cryogenic Transonic Tunnel at CARD. [Ref. 1]

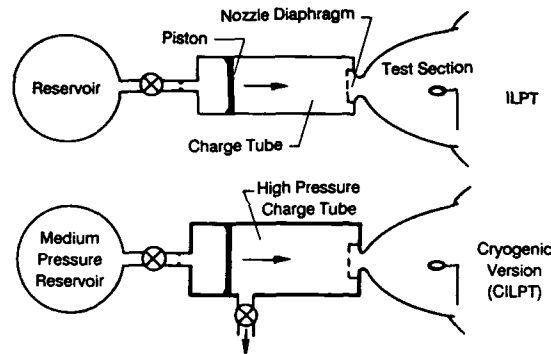


Fig. 2 Cryogenic ILPT compared with standard ILPT. [Ref. 3]

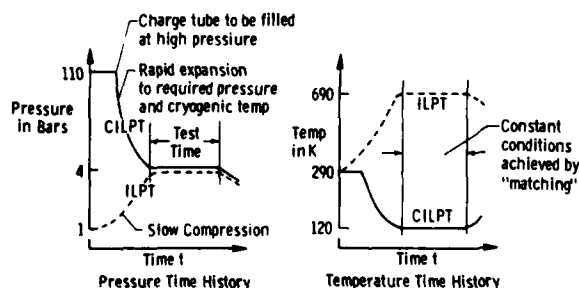


Fig. 3 Pressure and temperature time histories for cryogenic and standard version. [Ref. 4]

TABLE 2. - Pilot Cryogenic Isentropic Light Piston Tunnel at Cranfield (England)

Type	isentropic expansion, light piston
Material of construction	stainless steel
Insulation	none
Cooling	isentropic expansion
Test gas	nitrogen
Charge tube pressure	up to 3549 kPa
Test section size (h,w,l)	2.86 x 2.86 x 15 cm
Mach range	transonic
Contraction ratio	6:1
Stagnation pressure	100 kPa
Stagnation temperature	down to 110 K
Running time	0.3 s
Max. Reynolds number/m	42 million

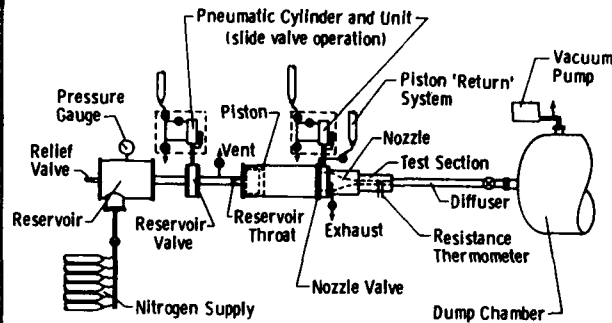


Fig. 4 General arrangement of Pilot CILPT at Cranfield. [Ref. 6]

major characteristics of the pilot CILPT at Cranfield. Figure 4 shows the general arrangement of the pilot CILPT.

Stollery and his coworkers have made preliminary studies of much larger versions of the CILPT.⁵ For example, when they assume the original specifications for the cryogenic version of the European Transonic Windtunnel, that is, $p_1 = 440$ kPa (4.4 bars), $T_1 = 120$ K, 1.95×1.65 m test section and $R_e = 40$ million at $M = 0.9$, the total test mass required for 10 seconds running time is 53,000 kg. The corresponding charge tube volume is 4060 m³ which would require, for example, a 4 m diameter cylinder over 300 m long.

To achieve the required temperature during the expansion process, the ideal pressure ratio through which the gas expand is 25:1. Thus, part of the charge tube must be built to accommodate pressures of 11 MPa (110 bars). In fact, departure from the ideal, caused by heat transfer from the walls of the charge tube to the gas, requires expansion of the gas through a considerably larger ratio. To achieve a stagnation temperature of 120 K from an initial temperature of 300 K, requires an expansion ratio of about 35:1.⁵

If we used the CILPT concept to achieve the maximum design Reynolds number of 120 million of the 2.5×2.5 m U.S. NTF at the design maximum stagnation pressure of 880 kPa (8.8 bars), the test mass would be 194,000 kg stored in a 7400 m³ charge tube at 22 MPa (220 bars). As noted in Reference 5, CILPT versions of the ETW or the NTF would be very large facilities but would have the virtue of being simple. Reference 5 also notes that concerns remain over the quality of the flow in such facilities and possible variations in the stagnation temperature during the run because of heat transfer from the charge tube to the gas.

Stollery and his coworkers also studied a more modest use of the CILPT. An example given in Reference 5 assumed an arbitrary structural limit of 600 kPa (6 bars) and a 0.6×0.6 m test section designed for $M = 0.9$. The charge tube volume required for a 1 second run would be a modest 47 m³, that is, a 2 m diameter cylinder 15 m long. Such a facility could achieve a Reynolds number of 19 million compared with 5.2 million for a straight blowdown tunnel operating at $p_1 = 600$ kPa (6 bars) and $T_1 = 300$ K.

3.2 Royal Aerospace Establishment - Bedford

Law and his colleagues at the Royal Aerospace Establishment (RAE), Bedford have built a closed circuit Cryogenic Test Duct. The Test Duct is part of the United Kingdom support for the European Transonic Windtunnel (ETW) program.⁷ The Test Duct is an inexpensive and convenient way to provide cryogenic gas flow for testing wind tunnel balances and model components. The maximum gas velocity through the 0.3 m square test section is 25 m/s, falling with temperature. By controlling the rate of injection of LN₂ in the circuit, the gas temperature can rapidly be reduced and controlled at any level between ambient and 90 K.

Law fitted the Test Duct with external insulation for the early experiments. The external insulation consists of a plywood shroud containing vermiculite in a 10 cm gap between the plywood and the aluminum Duct. He provided a dry nitrogen purge in the insulation space for dryness and to reduce the chance of oxygen enrichment. In a successful effort to increase the rate at which they can change temperature, Law lined about 75 percent of the inner surface of the Duct with a 3 mm thick layer of either cork or FEP insulation. Table 3 gives the major characteristics of the Cryogenic Test Duct at RAE-Bedford.

They use a simple calibration device to load small wind tunnel balances mounted in the test section. They have observed the behavior of a 3-component balance under transient temperature conditions. In addition, the test section of the Duct has transparent sides which allow direct visual observation during tests. Reference 7 gives details of

TABLE 3. - Cryogenic Test Duct at RAE-Bedford (England)

Type	closed circuit, centrifugal fan
Material of construction	aluminum
Insulation	external and internal
Cooling	liquid nitrogen
Test gas	nitrogen
Test section size (h,w,l)	0.3 x 0.3 x 1.5 m
Speed range	up to 25 m/s
Contraction ratio	1:1
Stagnation pressure	atmospheric
Stagnation temperature	90 K - ambient
Running time	typically 1 hour
Max. Reynolds number/m	11.4 million
Drive motor	9 kW
Fan speed	up to 2500 rpm
LN ₂ tank volume	1.28 m

the design and performance characteristics of the RAE Cryogenic Test Duct Facility and some of the test results on the NLR 771 strain gage balance.

4. JAPAN

There are many good wind tunnels in Japan. Some of the best are at the National Aerospace Laboratory (NAL) in Chofu, Tokyo. The tunnels at NAL include the 2 m x 2 m Transonic Wind Tunnel and the 5.5 m x 6.0 m Low-speed Wind Tunnel. These are the largest transonic and subsonic tunnels in Japan. However, these tunnels cannot achieve the test Reynolds number needed to develop modern aircraft.

To overcome the problem of low Reynolds number, three groups in Japan have developed and are now using cryogenic wind tunnels. In 1982 and again in 1987, I visited Japan to see firsthand their cryogenic tunnels and meet the people involved with their development. It is apparent to me that Japan have more than a passing interest in the development and use of cryogenic wind tunnels. I have been able to maintain close technical contact with my friends in Japan who have very kindly provided me with up-to-date information on the cryogenic tunnel projects described in this section.

Two new transonic cryogenic tunnels have been proposed to meet the high Reynolds number testing needs in Japan. The first would have a 0.6 x 0.6 m test section and serve as a pilot tunnel for a much larger tunnel. The larger tunnel would have a 3 x 3 m test section. It would operate at Mach numbers from 0.2 to 1.2 at pressures up to 9 bars.

A recent review article in Cryogenics describes the four cryogenic wind tunnels in Japan.⁸ Emphasis in the review article in Cryogenics is on the cryogenic engineering aspects of their design and operation. In this section I briefly describes the cryogenic tunnel activities in Japan with emphasis on the mechanical, aerodynamic, and operational aspects. I also describes two new cryogenic tunnels proposed to meet the transonic high Reynolds number testing needs of Japan.

4.1 Existing Cryogenic Wind Tunnels

Ishikawajima-Harima Heavy Industries Co., Ltd. (IHI) has been the general contractor for the four cryogenic wind tunnels built in Japan. Sub-contractors did much of the detailed work on the tunnels. However, in Japan the custom is to refer only to the general contractor who assumes full responsibility for the success or failure of the project.

4.1.1 National Aerospace Laboratory (NAL)

In 1982 IHI designed and built the 0.1 x 0.1 m Transonic Cryogenic Tunnel for NAL.^{9,10} Sawada and his colleagues at NAL have used this relatively small tunnel to gain operational experience. They also use this tunnel to support design studies for much larger transonic cryogenic tunnels proposed for Japan.

Figure 5 is a sketch of the 0.1 x 0.1 m Transonic Cryogenic Tunnel at NAL. Liquid nitrogen is injected into the tunnel through pipes in the cross-leg at the right. Gaseous nitrogen exhausts from the tunnel from the opposite cross-leg. The plenum moves on a trolley to give access to the perforated-wall test section.

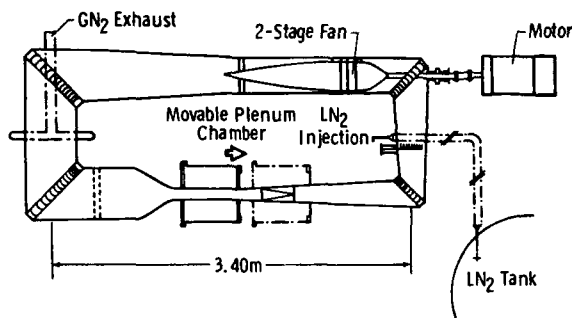


Fig. 5 Sketch of Transonic Tunnel at NAL.

Sawada and his colleagues at NAL have made a wide variety of operational tests in the 0.1 x 0.1 m tunnel. They used the original manual control systems for the typical purging, cooldown, running, and warm-up operations. In 1985 they installed automatic controls for nitrogen injection and exhaust and fan speed. Under manual control, changing from one test condition to another took from 5 to 10 minutes. The same changes in test conditions now take only about 1 minute under fully automatic control. Table 4 gives some of the design and performance details for the 0.1 x 0.1 m Transonic Cryogenic Tunnel. Note the relatively high contraction ratio of 18:1.

The 0.1 x 0.1 m tunnel is now under completely automatic control through a small NEC computer.¹¹ The operators make excellent use of computer graphics (in color) to display tunnel conditions during a run. They store the test conditions on a hard disk and can quickly plot them (again, in color) for study after the run. The NAL 0.1 x 0.1 m tunnel usually runs 2 days each week. The runs can last for several hours with each run using about 1000 litres of liquid nitrogen.

In October of 1987, I was at NAL for 1 week and took part in the running of their cryogenic tunnel and magnetic suspension and balance system. Both systems run remarkably smoothly, showing good use of automatic controls. The 0.1 x 0.1 m tunnel has logged over 560 hours of operation since first running in 1983.

The 0.1 x 0.1 m tunnel has good visual access to the test section through windows in the plenum. They keep the

TABLE 4. - Transonic Cryogenic Tunnel at NAL (Japan)

Type	closed circuit, fan
Material of construction	A5052 Al-alloy
Insulation	external, purged
Cooling	liquid nitrogen
Test gas	nitrogen
Test section size (h,w,l)	0.1 x 0.1 x 0.3 m
Mach range	up to 1.02
Contraction ratio	18:1
Stagnation pressure	up to 2 bars
Stagnation temperature	90 K - ambient
Running time	more than 2 hrs
Max. Reynolds number/m	130 million
Drive motor	55 kW
Fan speed	600 - 5700 rpm
LN ₂ tank volume	2.17 m ³

1985. Researchers completed the initial tunnel calibration in 1985.¹⁴ Researchers at the Academy use this tunnel for basic fluid mechanics studies.

Figure 7 is a sketch of the closed circuit tunnel. Table 7 gives the major characteristics of the cryogenic tunnel at NDA. The sketch is a side view showing the centrifugal compressor at the right. The plenum mounts on a trolley which moves to the right to allow access to the test section. The test section has two 30-cm diameter optical observation windows to allow for flow visualization.

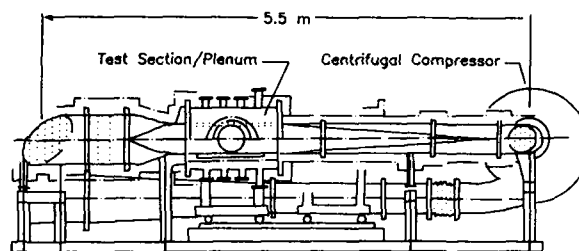


Fig. 7 NDA High Reynolds Number Flow Facility.

4.2 Notional Cryogenic Wind Tunnels

There are many possible combinations of size and pressure for a transonic cryogenic tunnel to meet the high Reynolds number testing needs of Japan. Sawada of NAL has suggested one possible scenario for meeting this need.

Based on his experience with the 0.1 x 0.1 m tunnel, Sawada has suggested two new transonic cryogenic tunnels for Japan. The smaller tunnel would have a 0.6 x 0.6 m test section. This tunnel would obviously be useful in its own right for aerodynamic testing. However, its main purpose would be as a pilot for a second transonic cryogenic tunnel having a 3.0 x 3.0 m test section.

NAL has not officially endorsed Sawada's suggested cryogenic tunnels. However, his suggestion represents a reasoned approach to providing Japan with a world class high Reynolds number transonic tunnel. Tables 8 and 9 give some of the design characteristics of the cryogenic tunnels suggested by Sawada.

Sawada envisions operating pressures up to 9 bars for the 3 m tunnel. The main purpose of the high pressure is to give high Reynolds numbers at Mach numbers below about 0.8. This will provide a unique high Reynolds number testing capability for take-off and landing studies. Sawada would size the drive motor and nitrogen systems of the 3 m tunnel to operate with reduced total pressures above $M_\infty = 0.8$. Even at reduced pressure, the large test section would allow testing at nearly the same Reynolds number as the NTF at Mach numbers up to 1.2.

TABLE 7. - High Reynolds Number Flow Facility NDA (Japan)

Type	closed circuit, centrifugal compressor
Material of construction	SUS 304 and SCS 13 stainless
Insulation	external
Cooling	liquid nitrogen
Test gas	nitrogen
Test section size (h,w,l)	0.30 x 0.06 x 0.72 m
Speed range	up to 157 m/s
Mach range	up to 0.83
Contraction ratio	14:1
Stagnation pressure	up to 1.77 bars
Stagnation temperature	108 K - ambient
Running time	up to 100 min.
Max. Reynolds number/m	93 million
Drive motor	75 kW
LN ₂ tank volume	4.9 m ³

TABLE 8. - 0.6 m Transonic Cryogenic Tunnel under study at NAL (Japan)

Type	closed circuit, fan
Cooling	liquid nitrogen
Test gas	nitrogen
Test section size (h,w,l)	0.6 x 0.6 x 1.8 m
Mach range	0.2 - 1.2
Contraction ratio	14:1
Stagnation pressure	1.2 - 5 bars
Stagnation temperature	90 - 300 K
Running time	45 min
Max. Reynolds number/m	340 million
Drive motor	5 MW

TABLE 9. - 3.0 m Transonic Cryogenic Tunnel under study at NAL (Japan)

Type	closed circuit, fan
Cooling	liquid nitrogen
Test gas	nitrogen
Test section size (h,w,l)	3.0 x 3.0 x 6.0 m
Mach range	0.2 - 1.2
Contraction ratio	14:1
Stagnation pressure	1.2 - 9 bars
Stagnation temperature	90 - 300 K
Running time	60 min.
Max. Reynolds number/m	540 million
Drive motor	90 MW

Reference 15 gives details of the cryogenic tunnels suggested by Sawada. Reference 8 also describes the specific role the 3 m tunnel might play in Japanese aerodynamics.

5. SWEDEN

Nelander and his colleagues at Aktiebolaget Rollab in Sweden proposed an innovative cryogenic tunnel concept.¹⁶ Figure 8 shows the principal components of a cryogenic wind tunnel based on this new concept.

The main idea behind the concept is the use of a turbine, fed from high-pressure air storage, to drive the fan in a tunnel with a return circuit. The temperature rise in the tunnel due to the fan is balanced by dumping the outlet air from the turbine into the tunnel circuit. This air, of course, has been cooled in the process of expanding through the turbine. The same amount of air dumped into the tunnel from the turbine is dumped from the tunnel through a heat exchanger to the atmosphere or to a vacuum tank, depending on the desired tunnel operating pressure. As shown in Figure 8, the air from the high-pressure storage passes through the heat exchanger and is thus cooled before it passes

through the turbine. As an example of this concept, Nelander has considered a transonic tunnel having the characteristics given in Table 10.

The compressed air storage envisioned for such a tunnel would contain 36×10^3 kg of air at 12 MPa. The power demand on the compressor plant would be about 6 MW.

Details of the operating principal of this new approach to cryogenic tunnels as well as a discussion of the thermodynamic process are given in References 16 and 17.

Also contained in Reference 16 is an economic study comparing this quasi-continuous tunnel to both continuous and blowdown tunnels cooled with liquid nitrogen. Some of the results of the economic study are shown in Figure 9. As shown, the quasi-continuous tunnel offers significant savings in operating costs relative to the other concepts.

As noted in Reference 16, this entirely new quasi continuous cryo-genic tunnel concept combines the advantage of low power demand and operational flexibility of a blowdown tunnel with the high efficiency and long testing times of a continuous-flow tunnel. Therefore, this new type of cryogenic tunnel should, for a number of uses, provide an attractive alternative to either blowdown or continuous fan-drive for a high Reynolds number transonic tunnel. No objections to the theory have been found and all of the practical problems seem to be solvable.

6. UNITED STATES

6.1 Douglas Aircraft Company

The Douglas Aircraft Company, Long Beach, California, modified two blowdown transonic tunnels for cryogenic operation. The first had a 1-ft test section and the second had a 4-ft test section. Reference 18 gives a description of some of the modifications to the tunnels required for cryogenic operation.

Douglas demonstrated the world's first blowdown cryogenic wind tunnel when their 1-ft tunnel first ran at cryogenic temperatures on May 20, 1977. The success of the 1-ft tunnel led to approval of a program to modify the Douglas 4-ft tunnel for cryogenic operation.

They used the 1-ft tunnel for a series of tests to determine the effect of nonadiabatic model wall conditions on supercritical airfoil characteristics. They found serious effects with only small deviations from adiabatic conditions at test conditions critical to the transonic transport designer.¹⁹

Figure 10 shows a sketch of the Douglas 4-ft Cryogenic Wind Tunnel (4-CWT). Table 11 gives the basic specifications for the 4-CWT. They modified the 4-CWT and successfully ran it at cryogenic temperatures in 1980-81.

The 4-CWT was capable of Reynolds numbers greater than 200 million per metre (60 million per foot). However, Douglas dropped the project, primarily because of the high cost of providing a system for model thermal conditioning to the strict tolerances required.

6.2 University of Illinois at Urbana-Champaign (UIUC)

Clausing and coworkers in the Department of Mechanical and Industrial Engineering at UIUC have built a special-purpose low-speed fan-driven cryogenic tunnel. They have used this tunnel to study forced, natural, and combined convective heat transfer at very large values of both Reynolds number and Grashof number.

The need to predict accurately combined convective losses from large, high temperature bodies prompted the building of the cryogenic tunnel at UIUC. Typical of such bodies is the receiver for a solar "power tower" where both the Grashof and Reynolds numbers are large. Clausing and his coworkers proposed to use a cryogenic heat transfer tunnel as an economical way to get the large Grashof and Reynolds numbers with an appropriate and near constant Prandtl number.²⁰

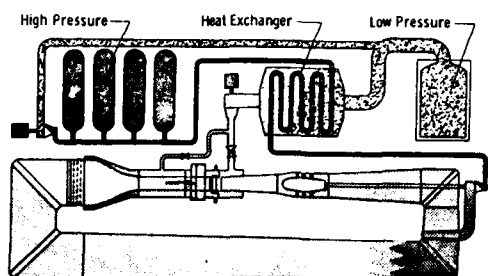


Fig. 8 High Reynolds number transonic wind tunnel based on a new cryogenic cycle. [Ref. 23]

TABLE 10. - Transonic Cryogenic Tunnel studied at Rollab (Sweden)

Type	closed circuit, intermittent
Material of construction	?
Insulation	?
Cooling	pre-cooled air expanded through turbine
Test gas	air
Test section size (h,w,l)	2.0 x 2.0 x ? m
Mach range	up to 1.4
Contraction ratio	?
Stagnation pressure	50-250 kPa
Stagnation temperature	140 - 280 K
Running time	at least 30 s
Frequency of runs	8 times per day
Max. Reynolds number/m	105 million

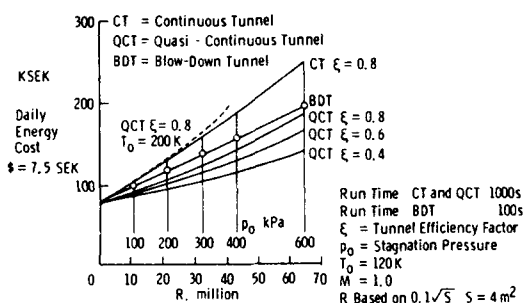


Fig. 9 Cost comparison between three cryogenic wind tunnel concepts. [Ref. 23]

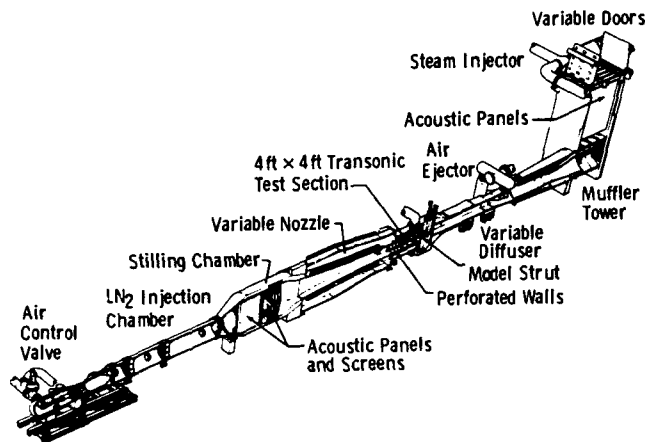


Fig. 10 Sketch of Douglas 4-ft. Cryogenic Wind Tunnel (4-CWT). [Ref. 25]

TABLE 11. - 4-ft Cryogenic Wind Tunnel (4-CWT) at Douglas (USA)

Type	blowdown
Material of construction	mostly mild steel; stainless injection chamber
Insulation	internal
Cooling	liquid nitrogen
Test gas	air + nitrogen
Test section size (h,w,l)	1.2 x 1.2 x 3.7 m
Mach range	0.5 - 1.2
Contraction ratio	7.8:1
Stagnation pressure	170 - 480 kPa
Stagnation temperature	100 K - ambient
Running time	45 s at R/m = 135 million; 30 s at R/m = 200 million
Max. Reynolds number/m	200 million
LN ₂ tank volume	151 m ³

Figure 11 shows the variations of Grashof number and Reynolds number with temperature. As shown in Figure 11, the use of cryogenic temperatures is a good way to get higher Reynolds numbers but an even better way of getting higher Grashof numbers.

Also, the cryogenic environment virtually eliminates the influence of radiative heat transfer. Radiative heat transfer often causes large errors in natural convection data taken in conventional facilities.²¹ Clausing and his colleagues have extensively reported both the theory and advantages of the cryogenic heat transfer tunnel^{21,22} and I will not repeat them here. Table 12 gives the basic specifications for the UIUC cryogenic heat transfer tunnel.

Figure 12 shows a sketch of the UIUC Cryogenic Facility. They cool the tunnel by passing liquid nitrogen through a heat exchanger/vaporizer located just downstream of two 0.5 m diameter cast aluminum fans. They vent the resultant gaseous nitrogen from the heat exchanger/vaporizer into the tunnel circuit. In this way, they avoid any problems that

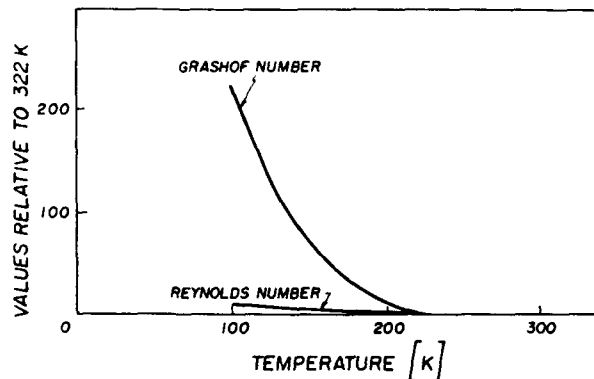


Fig. 11 Effect of temperature on Grashof and Reynolds number. [Ref. 27]

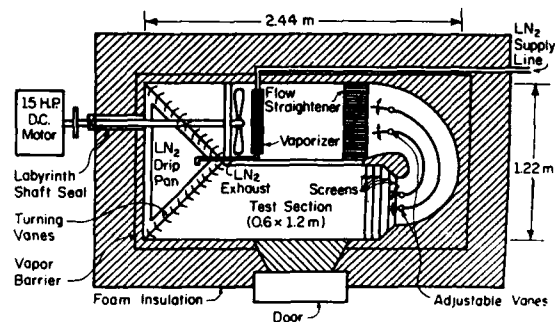


Fig. 12 Cross-sectional view of UIUC Cryogenic Facility. [Ref. 27]

might arise from incomplete evaporation of liquid nitrogen using direct injection. During operation they keep a slight overpressure in the tunnel to keep out room air. Reference 23 gives a complete description of the UIUC Cryogenic Facility.

The UIUC Cryogenic Facility has been an extremely successful use of the cryogenic tunnel concept. Since first operated on August 17, 1978, they have used it for a variety of forced, natural, and combined convective heat transfer research.^{24,25} The receiver for "Solar One" is a right-circular cylinder about 7 metres in diameter and about 13 metres high. The ability to make such measurements in a relatively small cryogenic wind tunnel is a dramatic demonstration of the usefulness of the simulation laws. It also demonstrates the ingenuity of researchers who take advantage of emerging technology to solve long-standing problems.

6.3 NASA Langley

The first demonstration of the cryogenic wind tunnel concept came with the building and operation of an atmospheric low-speed tunnel at NASA Langley in January 1972.²⁴ The Langley low-speed cryogenic tunnel started its life as an abandoned 1/24-scale model of the Langley V/STOL tunnel. It was therefore typical of modern low speed-wind tunnels in its aerodynamic design. It needed only minor changes for cryogenic operation. The first true cryogenic

operation, that is, stagnation temperature less than about 172K (-150°F), was on January 31, 1972. At 12:05 pm we reached a temperature of 133 K (-220°F).

The 1/24-scale model of the V/STOL tunnel no longer exists as a cryogenic tunnel. We have reconverted it to an ambient temperature tunnel. However, I will briefly describe it for several reasons. First, this low-speed tunnel was typical in both layout and operating principle to the majority of cryogenic tunnels built or proposed. Secondly, it is a tunnel of considerable historical significance. It proved the validity of the cryogenic wind tunnel concept and served as the test bed for the development of operational procedures and testing techniques. Finally, I describe the low-speed tunnel to show that not all cryogenic wind tunnels must be expensive and complex. Figure 13 shows a sketch of this historic tunnel. Table 13 gives the basic specifications and operational characteristics for the Langley low-speed cryogenic tunnel.

We cooled the low-speed tunnel and removed the heat of compression added by the fan by spraying liquid nitrogen directly into the tunnel circuit. We used simple spray nozzles in either of the two locations shown in Figure 13. The rate of cooling was fairly rapid. For example, we could stabilize a temperature of 116 K within 10 minutes of the start of cooling from room temperature. During the early part of 1972, we operated the tunnel at temperatures from 333 K to 80 K. Approximately 40 hours of tunnel operation was at cryogenic temperatures, that is, below 172 K.

At a reference station in the test section, we could hold the test temperature to within about ± 1 K by automatic on-off control of one or more of the injection nozzles. We could hold much closer temperature control using a simple wire-grid electric heater built into the low-speed end of the tunnel. By injecting a slight excess of liquid nitrogen, we could establish temperature equilibrium by manually adjusting the heat input from the heater. Using this technique, we could hold test temperature to within about ± 0.2 K.

Since we already had the basic tunnel circuit, the low-speed tunnel project was a very low-budget research effort. The cost of materials used to modify and insulate the tunnel was less than \$2000 (1971-1972). Materials of construction included wood, plywood, plexiglass, mild and stainless steels, aluminum, brass, copper, and fiberglass reinforced plastic. The fan blades were made of laminated wood.

We made simple viewing ports to let us see key areas of the tunnel circuit. These included the test section, spray zones, corner vanes, screen section, and contraction section. We made the viewing ports from either 3 or 4 layers of plexiglass separated by air gaps. Thermal insulation for the rest of the tunnel circuit was a 7.6 to 10.2 cm layer of expanded polystyrene applied to the outside of the tunnel and covered with a 0.0127 cm polyethylene vapor barrier.

We spent a lot of time measuring the temperature distribution around the tunnel circuit. In the early days of the project, one of our main concerns was finding an efficient yet simple way to cool the tunnel and still have temperature uniformity, in both time and space, in the test section.

Once we worked out adequate operating procedures, we used the low-speed cryogenic tunnel to verify, as far as possible, the validity and practicality of the cryogenic tunnel concept.²⁷

We made two simple "proof-of-concept" tests in the low-speed cryogenic tunnel. The first used a flat plate with a laminar boundary layer. It showed that the true aerodynamic effects of Reynolds number increases are indeed provided when temperatures are reduced to the cryogenic range. The second used a sharp leading edge delta wing model. It showed we could use ordinary strain-gage balance techniques to measure forces and moments at cryogenic temperatures.

TABLE 12. - Cryogenic Heat Transfer Tunnel at UIUC (USA)

Type	closed circuit, fan
Material of construction	mostly aluminum
Insulation	external, urethane
Cooling	LN heat exchanger with GN injection
Test gas	nitrogen, air for $T > 290$ K
Test section size (h,w,l)	1.22 x 0.60 x 1.0 m
Speed range	0 - 8 m/s
Contraction ratio	1:1
Stagnation pressure	atmospheric
Stagnation temperature	80 - 300 K
Running time	several minutes
Max. Reynolds number/m	4 million
Drive motor	11.2 kW
Fan speed	0 - 1750 rpm
LN ₂ tank volume	1 m ³

TABLE 13. - The Low-Speed Cryogenic Tunnel at NASA - Langley (USA)

Type	closed circuit, fan
Material of construction	mostly plywood and plastic
Insulation	external
Cooling	liquid nitrogen
Test gas	nitrogen
Test section size (h,w,l)	17.8 x 27.9 x 63.5 cm
Speed range	up to 50 m/s
Mach range	up to 0.14
Contraction ratio	9:1
Stagnation pressure	atmospheric
Stagnation temperature	80 - 333 K
Running time	typically 1 hour
Max. Reynolds number/m	20 million
Drive motor	7.4 kW
Fan speed	up to 3500 rpm
LN ₂ tank volume	1.14 m ³

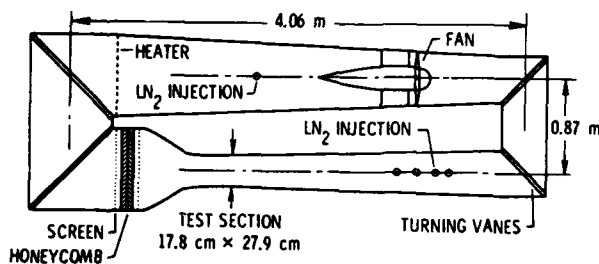


Fig. 13 Sketch of Langley Low-Speed Cryogenic Wind Tunnel. [Ref. 34]

In addition to the two proof-of-concept tests, we made other studies in the low-speed cryogenic tunnel. These were related mainly to developing acceptable cooling techniques and operating procedures." Table 14 outlines the main conclusions, both aerodynamic and operational, drawn from the experiments as well as the day-to-day operation of the low-speed tunnel.

7. U.S.S.R.

At the last Special Course on Cryogenic Tunnels in 1985, I asked those present if they knew of any cryogenic wind tunnels in the U.S.S.R. Not a word either then or later. However, I had some hints of work going on in the U.S.S.R. related to cryogenic tunnels.

In August of 1988, one of my colleagues, Dr. Stephen Wolf, attended a symposium on experimental techniques in Novosibirsk, U.S.S.R. Dr. Wolf met researchers working on cryogenic tunnels, adaptive wall test sections, and magnetic suspension and balance systems. His trip provided a gold mine of information which he kindly passed on to me to include in this lecture. In this section, I give some of the characteristics of the existing and planned cryogenic tunnels in the U.S.S.R.

7.1 Existing Cryogenic Wind Tunnels

7.1.1 Central Aero-Hydrodynamics Institute (TsAGI), Zhukovsky, near Moscow

Researchers at TsAGI have built a transonic cryogenic transonic tunnel driven by induction. Table 15 gives some of the design and performance details for the KAT Cryogenic Induction Tunnel.

7.1.2 Institute of Theoretical and Applied Mechanics (ITAM), Novosibirsk, Siberia

Table 16 gives some of the design and performance details of the MT-324K Pilot Cryogenic Tunnel at ITAM. This pilot cryogenic tunnel is a 1/5 scale version of the low-speed tunnel T-324 which has a 1 metre test section.

**TABLE 15. - Cryogenic Induction Tunnel
KAT at TsAGI (U.S.S.R.)**

Type	closed circuit, induction driven with cooled air
Material of construction	12Kh18N10T steel (austenite steel)
Insulation	external
Cooling	liquid nitrogen
Test gas	nitrogen rich air
Test section size (h,w,l)	0.2 x 0.2 x 0.74 m (perforated walls)
Mach range	0.1 - 1.15
Contraction ratio	7.5:1
Stagnation pressure	1 - 6.5 bars
Stagnation temperature	100 - 300 K
Running time	1.5 hr cool down 1.5 hr testing
Max. Reynolds number/m	200 million
LN ₂ tank volume	8 m ³

**TABLE 16. - Pilot Cryogenic Tunnel
MT-324K at ITAM (U.S.S.R.)**

Type	closed circuit, fan driven
Material of construction	wood
Insulation	external
Cooling	liquid nitrogen
Test gas	nitrogen
Test section size (h,w,l)	0.2 x 0.2 x 0.8 m (solid walls)
Mach range	up to 0.2
Contraction ratio	17:1
Stagnation pressure	atmospheric
Stagnation temperature	80 - 300 K
Running time	typically several hours
Max. Reynolds number/m	N/A
LN ₂ tank volume	0.5 m ³
Drive motor	? MW

**TABLE 14. - Major results from the Low-Speed
Cryogenic Tunnel at NASA - Langley (USA)**

Aerodynamic

- * Boundary-layer development with Reynolds number identical for ambient and cryogenic conditions
- * Drive-power and fan-speed decrease as predicted

Operational

- * Cooling with liquid nitrogen is practical
 - Rapid cooldown
 - Automatic temperature control
 - Gas stream is clear, dry, and frost free
- * Use of conventional strain-gage balances is practical
- * Trouble-free operation of drive motor and fan

7.1.3 Physical-Mechanical Institute (PMI-K), Kharkov, Ukraine

Table 17 gives some of the design and performance details of the Low Speed High Reynolds Number Tunnel at PMI-K. The purpose of this tunnel is to study the processes of cryogenic condensation of some gas mixture components on various cryogenic surfaces. The gas mixture components include N₂, O₂, H₂, CO₂, K₂, X₂, and H₂O.

7.2 Proposed Cryogenic Tunnels

There are two transonic cryogenic tunnels proposed for the U.S.S.R. The first is to be built at Novosibirsk. The ground breaking for this tunnel was scheduled to begin in the autumn of 1988. Table 18 gives the characteristics of this tunnel, to be known as T-312K.

We know even less detail about the proposed U.S.S.R. equivalent to the U.S. NTF. The dimensions are similar to the U.S. NTF. The U.S.S.R. NTF is likely to be built alongside other industrial type tunnels at TsAGI Zhukovsky near Moscow. The design phase of this tunnel was nearly complete in July of 1988.

TABLE 17. - Low Speed High Reynolds Number Tunnel at PMI-K (U.S.S.R.)

Type	closed circuit, fan driven
Material of construction	stainless steel
Insulation	external
Cooling	liquid or gaseous nitrogen
Test gas	mixture of gases, (see text)
Test section size	0.22 (circular) (open jet)
Mach range	up to 0.05
Contraction ratio	4:1
Stagnation pressure	1 - 10 bars
Stagnation temperature	130 - 300 K
Running time	unknown
Max. Reynolds number/m	1 million
LN ₂ tank volume	unknown
Drive motor	1 kW

TABLE 18. - Transonic Cryogenic Tunnel T-312K at ITAM (U.S.S.R.)

Type	closed circuit, drive unknown
Material of construction	unknown
Insulation	unknown
Cooling	liquid nitrogen
Test gas	
Test section size (h,w,l)	0.6 x 0.6 x ? m
Mach range	transonic
Contraction ratio	unknown
Stagnation pressure	1 - 10 bars
Stagnation temperature	80 - 320 K
Running time	unknown
Max. Reynolds number/m	up to about 350 million
LN ₂ tank volume	unknown
Drive motor	unknown

8. CONCLUDING REMARKS

Following the development of the cryogenic wind tunnel at the NASA Langley Research Center in 1972, a large number of cryogenic wind-tunnel projects have been undertaken at various research establishments around the world. The purpose of this lecture has been to describe briefly some of the more significant cryogenic wind-tunnel projects not covered by other lecturers at this Special Course.

9. REFERENCES

1. Pan Ruikang: A Cryogenic High-Reynolds Number Transonic Wind Tunnel With Pre-Cooled and Restricted Flow. *Acta Aerodynamica Sinica*, No. 2, 1984, pp. 87-92.
2. Schultz, D.L.; Jones, T.V.; Oldfield, M.L.G.; and Daniels, L.C.: A New Transient Cascade Facility for the Measurement of Heat Transfer Rates. *Oxford Univ. Eng. Lab. Report 1207/77*, 1977.
3. Stollery, J.L.; and Stalker, R.J.: The development and use of Free Piston Wind Tunnels. *Proceedings of the 14th International Symposium on Shock Tubes and Waves, Sydney, 1983*, pp. 41-50.
4. Mohan, S.R.; and Stollery, J.L.: A Study of the Temperature Achievable by Expansion of High Pressure Gas. *Aeronautical Journal*, vol. 84, Aug. 1980, pp. 253-255.
5. Stollery, J.L.; and Murthy, A.V.: An Intermittent High- Reynolds-Number Wind Tunnel. *Aeronautical Quarterly*, vol. 28, Nov. 1977, pp. 259-264.
6. Mohan, S.R.: Cryogenic Wind Tunnels High Reynolds Number Testing. Ph.D. Thesis. College of Aeronautics, Cranfield Institute of Technology, U.K., June 1983.
7. Law, R.D.: Early Experiments In Using the Cryogenic Test Facility at RAE Bedford, England. Paper 8, ETW Cryogenic Technology Review Meeting, NLR-Amsterdam, 1982.
8. Dress, D. A.; and Kilgore, R. A.: Cryogenic Wind Tunnel Research: A Global Perspective. *Cryogenics*, vol 28, January 1988, pp. 10-21.
9. Takashima, K.; Sawada, H.; Aoki, T.; and Kayaba, S.: Trial Manufacture of NAL 0.1m x 0.1m Transonic Cryogenic Wind Tunnel. *NAL TR-910*, 1986, 58 pp.

10. Sawada, H.: NAL TCWT Status - Cryogenic Operation. NAL News, 1984-3, No. 299, pp. 2-4.
11. Sawada, H.: Automatic Operation of the NAL Cryogenic Wind Tunnel. NAL News, 1986-1, No. 321, pp. 2-4.
12. Sawada, H.: Heated External Balance for Cryogenic Wind Tunnel. NAL News, 1987-1, No. 333, pp. 2-3.
13. Adachi, T. et al.: Force and Vortex Shedding On A Circular Cylinder From Subcritical Up To Transcritical Reynolds Numbers. Bull JSME (1985)
14. Yamaguchi, Y.; Kuribayashi, N.; and Kaba, H.: Characteristics for Ambient Conditions of NDA Cryo-tunnel and an Attempt on its Automatic Cryogenic Operation. Proceedings of the 1988th Annual Meeting of JSASS, April 5-6, 1988, pp. 73-74.
15. Sawada, H.: Cryogenic Wind Tunnels. Journal of JSASS, June 1987, pp. 285-293.
16. Nelander, Curt: Quasi-Continuous Transonic Wind Tunnel for Cryogenic Operation. Rollab Memorandum RM 096, 1983.
17. Nelander, Curt A.: Ett Unik Drivsystem för Vindtunnlar. FFA Memo 126, 1984.
18. Cadwell, J.D.: Progress Report on the Douglas Aircraft Company Four-Foot Cryogenic Wind Tunnel. Paper 18, AGARD LS 111, 1980. pp. 7
19. Lynch, F.T.; et al: Nonadiabatic Model Wall Effects on Transonic Airfoil Performance in a Cryogenic Wind Tunnel. Paper 14, AGARD CP-348, 1983.
20. Clausing, A.M.; Clark, G.L.; and Mueller, M.H.: The Cryogenic Heat Transfer Tunnel - A New Tool for Convective Research. Presented at the Winter Annual Meeting, ASME, San Francisco, Calif., 1978. pp. 73-78.
21. Clausing, A.M.: Experimental Studies of Forced, Natural and Combined Convective Heat Transfer at Cryogenic Temperatures. Paper 24, 1st Int. Symp. on Cryogenic Wind Tunnels, Southampton, U.K., 1979.
22. Clausing, A.M.: Advantages of a Cryogenic Environment for Experimental Investigations of Convective Heat Transfer. Int. J. of Heat and Mass Transfer, vol. 25, no. 8, 1982, pp. 1255-1257.
23. Mueller, M.H.; et al: Description of UIUC Cryogenic Wind Tunnel Including Pressure Distributions, Turbulence Measurements and Heat Transfer Data. Univ. of Ill. Tech. Rept. ME-TN-79-9180-1, 1979. 82 pp.
24. Clausing, A.M.; Wagner, K.C.; and Skarda, R.J.: An Experimental Investigation of Combined Convection from a Vertical Cylinder in Cross-flow. ASME J. of Heat Transfer, vol. 106, no. 3, 1984, pp. 558-562.
25. Clausing, A.M.: Natural Convection Correlations for Vertical Surfaces, Including Influences of Variable Properties. ASME J. of Heat Transfer, vol. 105, no. 1, 1983, pp. 138-143.
26. Goodyer, M.J.; and Kilgore, R.A.: The High Reynolds Number Cryogenic Wind Tunnel. AIAA Paper 72-995, 1972. Also, AIAA Journal, vol. 11, no. 5, 1973, pp. 613-619.
27. Kilgore, Robert A.; et al: The Cryogenic Wind Tunnel for High Reynolds Number Testing. NASA-TN-D-7762, 1974, 96 pp.

10. ACKNOWLEDGMENTS

I am grateful to NASA for permission to give this lecture and to my colleagues at the Langley Research center for helping prepare it. I am indebted to the following people for providing information and material for this lecture: Prof. Han and Mr. Pan of the Chinese Aeronautical Research and Development Center (CARDIC), Mr. Takashima and Dr. Sawada of the Japanese National Aerospace Laboratory (NAL), Prof. Adachi of the University of Tsukuba, Professor Yamaguchi of the Japanese National Defense Academy (NDA), Prof. Stollery of the College of Aeronautics at Cranfield, Mr. Law of the Royal Aircraft Establishment - Bedford, Mr. Fancher of the Douglas Company, and Professor Clausing of the University of Illinois at Urbana-Champaign (UIUC). I am especially indebted to my colleague, Dr. Wolf, for providing information about the cryogenic tunnel activities in the U.S.S.R. I also thank Dr. Y. Y. Wu for providing the translation into English of Mr. Pan's Research Note.

CRYOGENIC ENGINEERING AND MATERIALS

by

D. A. Wigley.

Director, Cryogenic, Marine and Materials Consultants
17 Bassett Wood Drive, Bassett
Southampton, SO2 3PT, England

SUMMARY

This paper summarises the effects of cryogenic temperatures on the mechanical and physical properties of materials. Heat capacity and thermal conductivity are considered in the context of conservation of liquid nitrogen, thermal stability of the gas stream and the response time for changes in operating temperature. Particular attention is given to the effects of differential expansion and failure due to thermal fatigue. Factors affecting safety are discussed, including hazards created due to the inadvertent production of liquid oxygen and the physiological effects of exposure to liquid and gaseous nitrogen, such as cold burns and asphyxiation. The preference for using f.c.c metals at low temperatures is explained in terms of their superior toughness and the limitations on the use of ferritic steels is also considered. Non-metallic materials are discussed, mainly in the context of their LOX compatibility and their use in the form of foams and fibres as insulants, seals and fibre-reinforced composites.

1. INTRODUCTION

The industrial production and handling of cryogenic fluids such as liquid nitrogen, oxygen, hydrogen and helium, as well as liquefied natural and petroleum gases is now based on mature technologies developed and refined over many decades. The needs of a cryogenic wind tunnel using large quantities of liquid nitrogen do not differ significantly from those of, for example, a large chemical plant or food freezing factory and thus much of this technology is directly transferable. It is, however, important to recognise that the majority of those involved in running or using a cryogenic wind tunnel are unlikely to have had previous experience of cryogenic fluids. It is therefore particularly important to ensure that the accumulated experience on the safe handling of cryogenic fluids is also passed on to these new users. Much of this experience has now been gathered together in manuals and texts such as references 1, 2 & 3. This information should be digested and understood not only by those with managerial responsibility for safety, but also by those directly involved, and as far as is practical, by those indirectly involved in the use of cryogenic fluids. Unjustified alarm created in the minds of those in receipt of a suitable training program can usually be allayed by a full and frank examination of the facts. Justifiable alarm is better exposed before an accident, when remedial action can be taken, than after a tragedy. Finally, the old adage "familiarity breeds contempt" is unfortunately true and even experienced personnel can get careless. Cryogenic fluids such as liquid nitrogen deserve a healthy respect, but when handled with care, their use can open up new areas of technology such as the cryogenic wind tunnel. In view of the importance of using the correct procedures in the design, construction and operation of cryogenic tunnels, those sections of this paper that have a direct bearing on safety will be highlighted by the use of bold print.

Those involved in the design and construction of cryogenic wind tunnels and the models that are to be tested in them need a more thorough understanding of the properties of cryogenic fluids and materials and techniques of construction. In the previous AGARD lecture series No. 111 on Cryogenic Wind Tunnels, (Ref. 4), the author gave two lectures on the Physical and Mechanical Properties of Materials and Dr. R. G. Scurlock gave three lectures on Cryogenic Engineering. These lectures set out basic principles for the safe handling of cryogenic liquids and the construction of cryogenic equipment and, five years later, these principles are equally valid. In this lecture we will try and distill the essence from the material contained in these five lectures and update it in the light of the progress made since the first lecture course. For a more thorough understanding of the subject the reader is, however, encouraged to consult the original papers, particularly as much numerical data on the physical and mechanical properties of materials was collated in the tables therein (Refs. 5 & 6). Further valuable information is also contained in Toblers excellent report on "Materials for Cryogenic Wind Tunnel Testing" (Ref. 7)

Before considering these factors in detail, it is worth taking a brief overview of a typical large installation. Firstly, let us consider the storage and transfer of the large quantities of liquid nitrogen needed to run a tunnel. In principle, this is virtually identical to the situation which exists in, for example, a large food freezing plant. The storage vessels, pumps, valves and control equipment, all serve the same purposes and there are, therefore, sound reasons for considering them as a commercial package once the relevant design specification has been established. Thus, for example, it should not matter whether 9% nickel steel, 304 stainless or 5083 aluminium is chosen for the construction of the LIN storage vessel as long as it is carried out by a technically competent organisation. In many respects the design and construction of the transfer line should also be a relatively simple commercial consideration once local constraints and requirements have been identified.

Secondly, in the design and construction of the tunnel itself it is necessary to bear in mind the extra constraints that cryogenic operation will introduce. For example:

- thin, light structures cool down more rapidly and evaporate less cryogenic fluid than do heavy sections, thus, if fast thermal response is required it is essential to minimise the thermal mass of the structure.
- insulation is necessary to cut down the heat inleak to the working space and hence the effective refrigeration power used. This insulation can be applied either internally or externally and the implications of this decision are manifested in considerations of the smooth profile of the inner liner in the first case and in the toughness of the pressure shell at cryogenic temperatures in the second.

- all materials contract to a greater or lesser extent when they are cooled and one of the essential aspects of the successful design of cryogenic equipment lies in avoiding the problems created by differential contraction caused by temperature gradients or the juxtaposition of dissimilar materials.
- some materials embrittle at low temperatures and it is of critical importance to select materials with strengths and toughnesses adequate for their intended duty. The failure of even a non-structural component could possibly cause damage further down the tunnel, or lead to the premature end of a test run.
- all materials used must be compatible with their working environment both internally and externally. Design must ensure the prevention of accidental condensation of liquid oxygen, particularly in the presence of hydrocarbon based polymers which are LOX incompatible.

Thirdly, it is important that designers and operators are aware of the differences that a low temperature environment will induce in a tunnel and its associated equipment as compared to conventional operation at ambient temperatures. Thus, certain aspects of the model suspension and force measuring systems will have to be reconsidered in the light of their cryogenic operating environment, for example:

- the materials used to construct the sting assembly have to be very strong and stiff. In many alloys high strengths are associated with low toughnesses and as the strengths of all metals increase at low temperatures, it is essential to ensure that their toughness does not fall to unacceptably low levels: current state of the art technology seems to favour the various grades of maraging steel and the precipitation hardened and high-nitrogen forms of stainless steel for sting construction.
- if the force balance systems are to operate at ambient temperature in a cryogenic tunnel, heaters must be used to warm the appropriate regions. Low conductivity materials have to be used to provide the necessary heat breaks between warm and cold regions, while high conductivity inserts can even out unwanted temperature gradients.
- alternatively, if the whole system is to operate at low temperature it has to be possible to calibrate out the variations in the gauge constants brought about by changes in the electrical resistivity of the metallic films or wires and adequate moisture proofing is essential.
- provision should be made for the removal of the model assembly from the test section without the need to warm up the whole tunnel. Furthermore, a cold model assembly should be allowed to warm up in an atmosphere of dry nitrogen if problems caused by moisture condensation and frost build up are to be avoided.

At this stage it is worth emphasising that care needs to be exercised in the use of data taken from compilations and reference manuals because some properties are more "structure sensitive" than others. For example, the electrical and thermal conductivities, strength, ductility and toughness of materials are properties that are highly dependent on the microstructural and chemical condition of the material. In contrast, the specific heat, thermal expansion and elastic moduli are relatively unaffected by the presence of structural defects. Thus, although it is possible to apply the data taken from the literature for the structure-insensitive group of properties, it would be unwise, and even dangerous, to use uncritically the values given for the defect sensitive properties. These should be used for guidance only and if at all possible, they should be backed up by data obtained experimentally on material obtained from the suppliers of the batch of material to be used: in the absence of such experimental verification, generous safety margins should be applied to the literature data.

2. THERMAL AND OTHER PHYSICAL PROPERTIES OF MATERIALS

2.1 Heat Capacity and Specific Heat

Information on the heat capacity or specific heat of materials used in the construction of cryogenic equipment is necessary in order to calculate the energy that has to be supplied for cool-down to the operating temperature. Structures with the highest heat capacities require the largest amount of cooling and this has to be supplied by the latent heat of the evaporating liquid or by the sensible heat of the cold gas. For structures which have to undergo frequent cooling and warming cycles, it is important to minimise the total heat capacity, or thermal mass, to achieve both low liquid boil-off rates during cool-down and also short cooling times: for equipment that rarely warms up once it is cooled, low heat capacities are not so important. A further, and highly relevant, example of the effect of thermal mass may be illustrated by comparing the operating experience of the NASA 0.3-m TCT with that of the tunnel at the University of Tsukuba, Japan. In the NASA tunnel virtually no problems were experienced in controlling the temperature of the working gas by varying the liquid nitrogen injection rate, while the Japanese group found the maintenance of steady temperatures much more difficult. The clue to this difference is to be found in the designs of the tunnel liner and insulation system. The NASA tunnel is insulated on the outside of the 6061-T6 aluminium alloy pressure shell and thus a large thermal mass of metal is cooled down to the working temperature. The thermal inertia of this large mass evens out fluctuations in the gas temperature that would otherwise be created by variations in the liquid nitrogen injection rate. In the Tsukuba tunnel the insulation is inside the mild steel pressure shell and the inner wall is thin and has a low thermal mass. It is thus unable to absorb much heat without its temperature rising and the liquid nitrogen injection control system has to work much harder to achieve temperature stability. On the other hand, deliberate changes in the operating temperature are achieved more rapidly in the Japanese tunnel.

For heat balance calculations it is, in fact, the enthalpy, $H = \int C_p dT$, which is of most direct use and in Reference 8 tabulated values of the enthalpy relative to absolute zero are given together with the specific heat at constant pressure, C_p , for a range of metals and non-metals. The specific heats of all materials drop off at low temperatures eventually to become zero at 0 K, and the very low values found at hydrogen and helium temperatures can cause large temperature differences to be set up by a small heat-influx. At liquid nitrogen temperatures and above these effects are not so severe.

Although large amounts of cold work may cause a slight decrease in heat capacity, for practical purposes specific heats are largely unaffected by the normal range of conditions found in metals. The

specific heats of pure crystalline solids over the complete temperature range is given by the Debye theory and knowledge of the characteristic temperature, Θ_D , allows calculation of the specific heat at the required temperature. (Ref. 9). Specific heats of alloys at room temperature are given approximately by the Kopp-Newman rule of mixtures in which the specific heat of a metallic solution is given by the sum of the products of specific heat and molar fraction for each constituent element. Although the rule gets less applicable at low temperatures, in the absence of alternative data it gives an acceptable first approximation. Furthermore, it is worth noting that the lattice structure has a strong influence on specific heats as illustrated by the observation that the measured specific heat of f.c.c. austenitic stainless steels are closer to those calculated for gamma iron than those measured on the b.c.c. alpha iron. The specific heats of non-crystalline and amorphous materials cannot be described by the Debye theory and there is, therefore, no satisfactory alternative to measured values for materials such as glass and amorphous ceramics, as well as all polymers, elastomers, composites and adhesives. When considered on a unit mass basis most of these materials have high heat capacities compared to metals, but this discrepancy is reduced if they are considered on a unit volume basis.

2.2 Thermal Conductivity

Conduction of heat in solids takes place through the vibration of their lattice atoms, and in the case of metals, by the movement of their conduction electrons. Any mechanism which makes these processes more difficult lowers the thermal conductivity of the material and hence high conductivities are found in pure, strain free, large grain or single crystal metals and non-metals, while low conductivities are associated with impure, stressed, amorphous or microcrystalline structures. As it is difficult, if not impossible, to recognise these different conditions by looking at the surface of a material, and as the physical and mechanical history of the sample is rarely well documented, great uncertainties can arise in using thermal conductivity data from the literature. However, in many cases, conductivities at one extreme or the other are required - for example, very low conductivities where heat breaks are required to reduce heat influx, or very high conductivities to minimise thermal gradients. In general, good conductors are materials of high purity and in an annealed state, while bad conductors are either alloys with many components and complex microstructures, or non-metals with amorphous or microcrystalline structures. Still lower conductivities may be obtained by increasing the number of interfaces crossed by the heat flux. For example, stacks of stainless steel discs may be used for compressively loaded, thermally-insulating supports, while the combination of many fine glass filaments with a thermo-setting plastic matrix (G.R.P) gives a material with the highest known ratio of tensile or compressive strength to thermal conductivity. The use of G.R.P. supports to separate the inner and outer skins of modern vessels for storing cryogenic liquids is, in a large measure, responsible for the low boil-off rates currently achieved.

It should, however, be noted that although the amorphous or microcrystalline structures of most non-metals make them very efficient thermal insulators, it also makes them very brittle, especially in the bulk form and they can be excessively prone to thermal shock if cooled rapidly. Furthermore, variations in their density, structure and processing history can change their thermal conductivities by about an order of magnitude as well as causing considerable anisotropy, so care has to be taken in extracting suitable values from the literature.

2.3 Thermal Expansion

This is probably the most important of the physical properties because the stresses set up in components by differential thermal expansion can very easily cause severe distortion or, at the worst, failure. The total linear contraction of a number of representative materials is shown as a function of temperature in Fig. 1. It can be seen from the figure that the total linear contraction at 77 K varies from about 0.05% for Invar and Pyrex glass to over 2% for some thermosetting resins, and it is not surprising, therefore, that problems can arise when materials are used together without adequate forethought. Problems can, in practice, usually be resolved into two basic categories.

i) those in which only one type of material is involved and where differential contraction is a result of temperature gradients,

ii) those in which the same temperature gradient is applied across two or more materials of different expansion coefficient.

Considering first the case of dissimilar materials, a common mercury in glass thermometer uses the large differences in expansion coefficients between the two components, but no stresses are set up as the mercury is free to move inside the glass tube (Fig. 2a). In contrast, a bi-metallic strip consists of two metals firmly fixed together, and when the temperature decreases the free end moves towards the side containing the metal with the higher expansion coefficient (Fig. 2b). If the end were not free to move the metal with the higher expansion coefficient would be put into tension and the other metal into compression (Fig. 2c). An idea of the forces that can be set up by contraction in dissimilar metals can be obtained by considering the hypothetical arrangement illustrated in Fig. 2(d), in which co-axial copper and steel pipes joined at both ends are cooled to 80 K. The total linear contraction of copper is 302×10^{-6} , while that of a 0.2% carbon steel is 192×10^{-6} , a difference of 110×10^{-6} or just over 0.1%. Thus the differential strain is slightly larger than that considered to give the 0.1% proof stress, which in copper at 80 K is about 88 MPa. If the joint between the two metals were a soft lead-tin solder it would have to yield and flow in order to accommodate this degree of mismatch. (Data from Ref. 10)

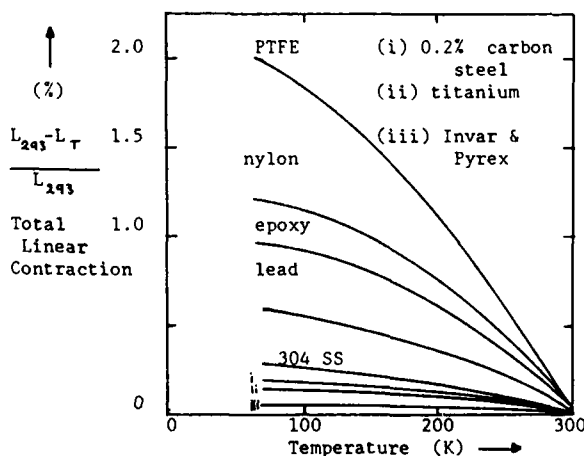


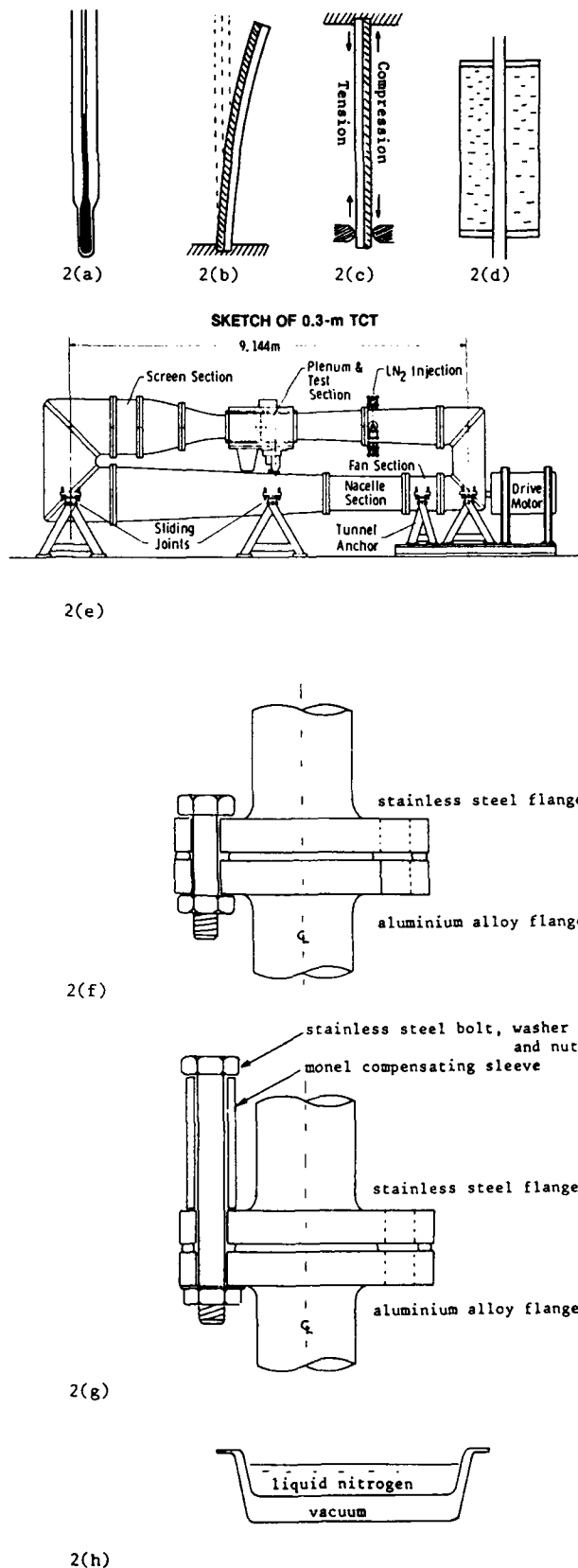
Figure 1. Total Linear Contraction of Selected Materials

An even more relevant example is illustrated in Fig. 2(e) which shows a section of an externally-insulated, closed-circuit cryogenic tunnel. When cold the wall of the tunnel contracts relative to its warm mountings and, as one end is effectively clamped by the fan shaft bearing, the other end must be able to move to prevent thermally-induced stressing on cooldown. In the NASA LaRC 0.3-m TCT this is accomplished by supporting the wall on a stainless steel supports which slide on re-inforced PTFE pads. Differential contraction between the inner and outer walls is a common design problem in transfer lines for cryogenic fluids and some form of expansion joint has to be built into the system. It was noted earlier that the total linear contraction of Invar from 300 to 77 K was very much smaller than other alloys, about 1/6th of that of austenitic stainless steels and 1/8th of that of aluminium alloys. Thus a transfer line with the inner wall made from Invar would need only 1/6th or 1/8th as many expansion joints as it would if made from stainless steel or aluminium alloy respectively and the savings thus achieved are sometimes more than enough to offset the higher material and fabrication costs associated with Invar.

A further example of mismatched materials is illustrated in Fig. 2(f) by a flanged joint between aluminium alloy and stainless steel pipes. Aluminium alloys contract more than stainless steels and if an aluminium alloy bolt were used its loading would be increased as it contracted more rapidly than the stainless steel flange. It is possible that the bolt might in fact fail on cooling; if not it would yield and stretch so that on warming to room temperature it would now be too long to compress the gasket adequately and a room temperature leak would be created. The use of a stainless steel bolt would also cause problems because on cooling it would contract less rapidly than the aluminium flange and so be unable to keep the same compressive stress on the gasket - the likely outcome being a low temperature leak which would then seal itself up when the joint were rewarmed to ambient temperature. This type of low temperature leak will be recognised by those with cryogenic experience as a source of considerable frustration!

One elegant solution to this problem is shown in Fig. 2(g). A long stainless steel bolt passes through the centre of a Monel compensating sleeve as well as through the two flanges, the length of the Monel sleeve being calculated to compensate exactly for the lower contraction in the bolt. The total linear contractions at 80 K relative to 293K are 391×10^{-5} for aluminium, 236 for Monel and 285 for type 304 stainless respectively, hence the difference between the stainless bolt and the aluminium flange is 106×10^{-5} and that between stainless and Monel is 49×10^{-5} . If the aluminium flange were 10 mm thick a Monel sleeve $10 \times 106/49$, i.e. 21.6 mm long would be needed for exact compensation. The same principle may be used for joints between 9% nickel steel and aluminium flanges by using an Invar (Nilo 36) sleeve to compensate for the contraction in the 9% Ni steel bolt.

Returning to the case where temperature differences can cause problems even when the material is the same, Fig. 2(h) shows schematically a situation in which co-axial, thermally-insulated vessels are joined at their extremities. If the vessels were made of mild steel the total linear contraction of the inner shell at 80 K would have been 192×10^{-5} relative to the outer shell which remained at ambient temperature.



Figures 2(a) to (h) Examples of Differential Thermal Contraction caused by Dissimilar Materials or Temperature Gradients.

This strain was too large to be accommodated by the mild steel which was not only below its ductile-brittle transition, but in all probability embrittled by the welding used in its fabrication.

The whole question of fits and clearances at low temperatures has to be kept very much in mind. Most of us are familiar with the practice of heating a gear wheel before placing it onto a shaft so that it will shrink to a tight fit on cooling. Some will also be aware that the same operation is sometimes carried out by cooling the shaft with liquid nitrogen prior to fitting the gear so that the required fit is obtained when the shaft expands on rewarming to room temperature. These examples should be remembered when constructing models, balances or other fittings where there are close fits and small clearances. On cooling these clearances could either decrease and cause a seizure, or increase and lead to looseness and possible leakage. This can also manifest itself in changes in the clamping force applied to models which could decrease on cooling and allow the model to vibrate loose, or increase and possibly cause damage. Reference to Fig. 1. will remind us that these problems are likely to be particularly severe where non-metallic materials are involved as their total linear contractions are so large.

Finally it is worth reiterating the comment made earlier about thermal shock. We have now seen that most non-metals have low thermal conductivities and high expansion coefficients, and we will find later that many of them also become embrittled at low temperatures. We thus have a combination of the three factors that lead to thermal shock and they are particularly severe if the materials are present in thick sections and/or cool-down rates are high. Nevertheless, brittle materials can be used safely at low temperatures if enough care is taken. For example liquid hydrogen bubble chambers have plate glass windows for viewing ports which are cooled at a rate of a few degrees K per day to prevent thermal shock. In the case of viewing ports for cryogenic wind tunnels, it is probably much better to follow the practice adopted in the prototype NASA tunnel of adopting quadruple glazing purged with dry nitrogen. This not only minimizes thermal shock but it cuts down the heat loss and prevents condensation on the outer skin. When purging a multi-layer system it is important to ensure that the purge gas is fed in from the warm side and exhausted at the cold face, as flow in the opposite direction is liable to cause condensation on the outer layers as they are cooled by the cold gas being fed from the inside.

3. PROPERTIES OF CRYOGENIC FLUIDS

The production of tonnage quantities of liquid oxygen and nitrogen by the fractional distillation of liquid air is a commercial process that has been developed continuously over almost 100 years. The availability of liquid nitrogen in tonnage quantities initially came as a bye-product of the requirement for large quantities of liquid oxygen for use in steel making, rocket fuels and other applications. Liquid nitrogen is readily available and relatively inexpensive and it was this combination that triggered the initial development of the prototype cryogenic wind tunnels in the early 1970's. Modern large tunnels such as the NTF consume so much nitrogen that a dedicated air separation plant is needed for their supply, the liquid oxygen now being the saleable bye-product. Although the designer or operator of a cryogenic wind tunnel does not need to know the details of the commercial liquefaction process, some understanding of the basic thermodynamic mechanism of the separation of liquid air into its major constituents is desirable as incorrect design or operation of equipment that uses liquid nitrogen can cause the inadvertent production of liquid oxygen and create a potentially serious fire hazard. Basic aspects of Cryogenic Engineering are described in references 11 and 13.

3.1 Liquid Air, Oxygen and Nitrogen

The basic properties of liquid air and its constituents are set out in Table 1 and discussed in the next two sections.

Table 1 Properties of Liquid Nitrogen, Air, Argon and Oxygen (Refs. 1 and 11)

Property	Nitrogen	Air	Argon	Oxygen
Molecular Weight	28	28.8	40	32
Critical Pressure (atm.)	33.5	38.7	48.3	50.1
Critical Temperature (K)	126	132	151	154
Normal Boiling Point (K)	77.4	Bubble 78.8, Dew 81.8	87.3	90.2
Freezing Point (K)	63.2	-	84	54.8
Liquid Density at Normal Boiling Point (kg/m ³)	808	876	1402	1138
Specific Gravity of Gas at 288 K and 1 atm.	0.97	1	1.38	1.10
Vol. Gas @ 288K & 1 atm. /unit vol. liquid @ B.P.	683	730	823	843
Latent Heat of Vaporisation (kJ/kg)	199	205	161	213
Specific Heat of Liquid Cp. (J/kg.K)	2.038	1.967	1.138	1.699
Liquid Viscosity (microPascal.sec)	158	163	256	189
Paramagnetism	none	oxygen / 5	none	strong
Colour	colourless	light blue	colourless	blue
Oxidizing Power	none	moderate	none	very strong

3.1.1 Binary phase diagram for oxygen-nitrogen mixtures

The binary phase diagram between pure oxygen, B.P. 90.2° K, and pure nitrogen, B.P. 77.3° K, is shown in Fig. 3. The composition of gaseous air is taken as 21% oxygen, 79% nitrogen, the minor constituents such as argon being ignored for the sake of simplicity. For air the dew point temperature, where droplets of liquid start to condense from the saturated vapour, is 81.8° K. The bubble point temperature, where bubbles of gas start to form in the saturated liquid, is 78.8° K. The horizontal tie-line drawn at 81.8° K connects the composition of the vapour, 21% oxygen-79% nitrogen, with that of the liquid with which it is in equilibrium, 50% oxygen-50% nitrogen, thus illustrating that the liquid is enriched with oxygen. In commercial air separation this enrichment is exploited by re-evaporating the liquefied air and allowing the nitrogen-enriched gas to rise up the column while the liquid descends and becomes progressively richer in oxygen as more and more nitrogen evaporates.

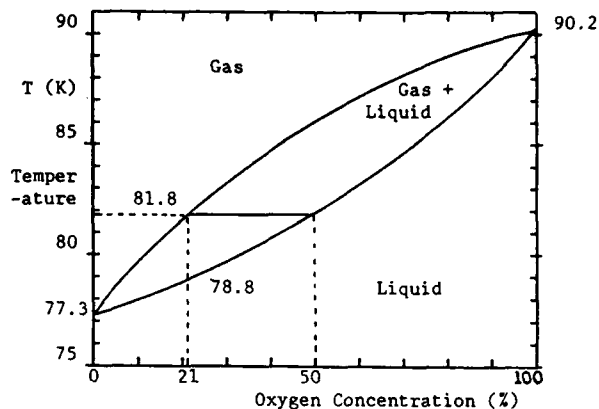


Figure 3. Nitrogen / Oxygen Phase Diagram

3.1.2 Inadvertent Liquid Oxygen (LOX) formation.

It is, however, the inadvertent formation of oxygen-enriched liquid that is of much greater significance to the operator of a cryogenic wind tunnel. If air comes in contact with a surface cooled to temperatures below 81.8° K, it will condense and form a liquid enriched in oxygen. Subsequent evaporation of the nitrogen will further enrich the liquid until the remaining liquid is virtually pure oxygen. This can constitute an extremely serious fire hazard if there are combustible materials present. All hydrocarbon-based solids, liquids and gasses are LOX incompatible and the greatest care should be taken to avoid their presence in an oxygen-enriched atmosphere. If the cold surface is visible and covered with frost, its temperature is too high to condense liquid oxygen. If it looks wet and free of frost it is probably because the condensing liquid air has washed any frost away.

Despite its low temperature, liquid oxygen is an extremely efficient oxidizing agent and many materials, including some metals, will burn violently if ignited in its presence as the heat released during combustion is about an order of magnitude greater than the latent heat needed to vaporise the liquid to gas. Particularly reactive metals such as titanium and magnesium are a hazard even in the bulk form, while ferritic and austenitic steels, aluminium and zinc will burn fiercely when in the finely divided form of dust or fibres. All hydrocarbons, including ordinary clothing, human hair and tissue as well as many of the plastic foams and fibres used in insulation systems are LOX incompatible materials. Further details of the LOX compatibility of plastics materials are given in Table 10 of Ref. 5. There are two ways in which such materials may be used safely. The first is to apply an impervious vapour barrier to the outside of the insulation to prevent air ingress. This has the additional benefit of excluding water vapour which might otherwise lead to ice formation and degradation of the insulation material. The second is to ensure that the material is continuously purged with a dry, inert gas such as nitrogen. In practice these two techniques are best combined by gas purging the space inside the vapour barrier. A further point to note is that, although the appropriate measures may have originally been taken to prevent LOX condensation, subsequent servicing or modification may result in the incomplete re-establishment of an effective vapour barrier. In other cases, especially where the operatives have changed, potential hazards have arisen when LOX-incompatible materials have been substituted for the original, correctly-specified material. A further potential hazard can arise where control valves are hydraulically actuated if the inevitable fluid leakage from old installations is allowed to contaminate the insulation system or, as often happens, is allowed to saturate the flooring material. The combination of these saturated materials and oxygen-enriched air drifting down from an improperly insulated nitrogen-cooled surface would be a serious combustion hazard should they be inadvertently ignited. (Ref. 12).

3.2 Physiological Effects of Nitrogen and Other Safety Considerations

3.2.1 Cold Burns

Despite the apparent contradiction in terminology, the physiological effect of the exposure of human flesh to cryogenic temperatures is similar to that of a thermal burn. The affected tissue dies. In a controlled form this effect is utilized in cryosurgery to destroy unwanted growths and cancers. Even more unpleasant effects are caused if moist, bare flesh is held in contact with a very cold surface, for example an uninsulated pipe carrying liquid nitrogen. The moisture on the skin is frozen hard to the surface and it may be impossible to release the skin without tearing or cutting off the frozen layer. Non-absorbent clothing should be worn when handling cryogenic liquids and care taken to ensure that any spilled liquid cannot be trapped inside shoes. Gloves should be dry, non-absorbent and loose-fitting so that they could be removed rapidly if liquid got inside. Should a cold burn occur, flowing cold water should be used to thaw the affected area.

3.3.2 Oxygen Deficiency, Anoxia or Asphyxiation

It is only necessary for the oxygen content of breathing air to fall a few percent below its normal value of about 20% for bodily functions, both mental and physical, to be adversely affected, hence the use of oxygen breathing sets for climbing mountains and high altitude flight. Reduction of the oxygen level towards about 14% causes anoxaemia which is characterised by an increase in pulse rate, laboured breathing and difficulty in concentration. At oxygen levels between 14 and 10% the victim is still conscious but muscular effort causes rapid fatigue and mental processes such as co-ordination and judgement

deteriorate. When the oxygen concentration falls below 10% there is a severe risk of asphyxiation and possibly permanent brain damage. By the time the victim realises that something is wrong it may be too late for him to save himself as his muscles will be unable to function and allow his escape. If the oxygen level falls below 6% death is virtually inevitable - apparently painless, but nonetheless permanent! It is, in fact, surprisingly easy to achieve such low oxygen concentrations. Inhaling just a few breaths, or even one deep breath of pure nitrogen, or any other inert gas, can flush the oxygen out of the lungs and the loss of muscle function can prevent them refilling even if the victim is removed from the inert atmosphere. Some form of rapid resuscitation would be necessary to restore oxygen to the lungs and allow possible recovery. A typical scenario for such an accident is where someone opens and inspection hatch in a nitrogen-purged vessel, puts his head inside to "take a quick look" for something only to collapse within a few seconds because his lungs have become filled with nitrogen. Little or no warning is given by the body of this form of anoxia, unlike the gradual loss of breathable air that takes place in a sealed volume when the oxygen is not replaced.

There are two important areas in which the effects of anoxia can be avoided. Firstly, it is necessary to be able to detect the presence and extent of regions of low oxygen concentration. Oxygen monitors have replaced the traditional canary for this purpose and used correctly they are invaluable. Care is, however, needed in their location. If, for example, they are placed too high up they will not register a dangerous loss of oxygen at working head height. Placed directly over a nitrogen vent or on the floor below an outlet they will trigger prematurely. Such false alarms are likely to lead to distrust or complacency that could prevent operatives from reacting to a truly dangerous situation. Pits and ducts are particularly hazardous as cold gasses tend to sink and accumulate at low levels. When using liquid nitrogen it is essential to maintain a flow of fresh air, often simply by opening the appropriate doors and windows, to prevent the build up of an inert gas.

The second area involves the provision of the appropriate equipment for dealing with an emergency. Particularly important is an advance evaluation of the likely mode and extent of a possible spillage and the measures that should be taken to minimize its effect. For example, evacuation routes should be marked and kept clear. Breathing equipment should be kept handy and personnel properly trained in its use so that they could reach safety and/or effect rescue even in the event of a large spillage and severe nitrogen build-up. Alternatively, the availability of a breathing set could allow someone to remain safely in the affected area to permit rapid remedial action that could prevent a small incident from becoming a major accident. Thus, although automatic shut-down of pumps and closure of valves should be designed into a liquid handling system wherever possible, the ability to close back-up valves manually could also be an advantage in some situations.

STORAGE AND TRANSFER OF LIQUID NITROGEN

4.1 Heat-Transfer into Cryogenic Liquids

Energy has to be expended in liquefying cryogenic fluids such as nitrogen and heat influxes need to be reduced as far as possible in order to minimise the rate at which it re-evaporates. It is important to realise that even after a cryogenic fluid has absorbed enough heat to overcome the latent heat of vaporisation, additional thermal energy is needed to warm up the gas. Furthermore, the amount of "sensible heat", as it is called, required to warm evaporated nitrogen gas to room temperature is approximately equivalent to the latent heat. In good cryogenic design practice this sensible heat is used to cool radiation shields, entry pipes and other sources of heat-inleaks and thus reduce the net heat flux that is absorbed by the latent heat.

4.1.1 Insulation Systems

A schematic liquid nitrogen storage vessel is shown in Fig. 4. and there are three mechanisms by which heat reaches the cryogenic fluid: conduction, radiation and convection. Consider first conduction. This comes mainly from heat flowing along the load-bearing supports and connecting pipes and it is minimised by using thin sections of materials with low thermal conductivities such as glass reinforced plastics and cold-worked stainless steels, etc. Many non-metallic materials used for thermal insulation at low temperatures are in the form of finely divided powders, fibres, films or foams and their low conductivities arise not only from the inherent low conductivity of the material, but even more so, from the poor thermal contact between adjacent particles or layers. Further improvements can be achieved in powdered or fiber insulation systems by removing the gas from between the layers and so cutting down convection losses. In the case of insulating foams, it is important to appreciate the role played by the gas or vapour trapped in the cells. If the blowing gas has high melting or boiling points it may be possible to solidify this gas at low temperatures, reduce convection within the cells and thus improve its insulation value. However, if the cells are not completely closed, gas or vapour may permeate from the warm to the cold faces. Not only will this lower the efficiency of the insulation but permeation of water vapour will break down the cell structure by cyclic freeze-thaw action. As noted earlier, an even more serious problem can be caused by the permeation of air through imperfect foam insulation surrounding liquid nitrogen cooled surfaces as this can lead to preferential condensation of liquid oxygen and the creation of a potential combustion hazard. The solution to both of these problems is to provide a efficient vapour barrier on the warm side of the foam to prevent the ingress of gas or vapour, and this also helps to minimise ageing problems. Closed cell foams are widely used for the thermal insulation of liquid nitrogen and other cryogenic systems. They are relatively cheap, efficient and easy to apply, some being foamed in situ. Other types of foam, particularly the extruded type of polystyrene slabstock, have good load bearing characteristics - in general the strongest foams have the highest densities and the highest conductivities.

Radiation, particularly the infra-red component, is reduced by the use of heat-shields, which are either actively cooled by contact with the evaporated, cold gas or act passively by increasing the number of radiating layers between ambient and cryogenic temperatures. Absorption of radiation at the liquid surface is sometimes reduced by a layer of floating spheres called Kroffels which reduce the area of liquid that "sees" higher temperature radiation. In the most effective systems of all, the super-insulants, thin metallic films intercept the infra-red radiation and chemical getters are used to soak up any residual gas.

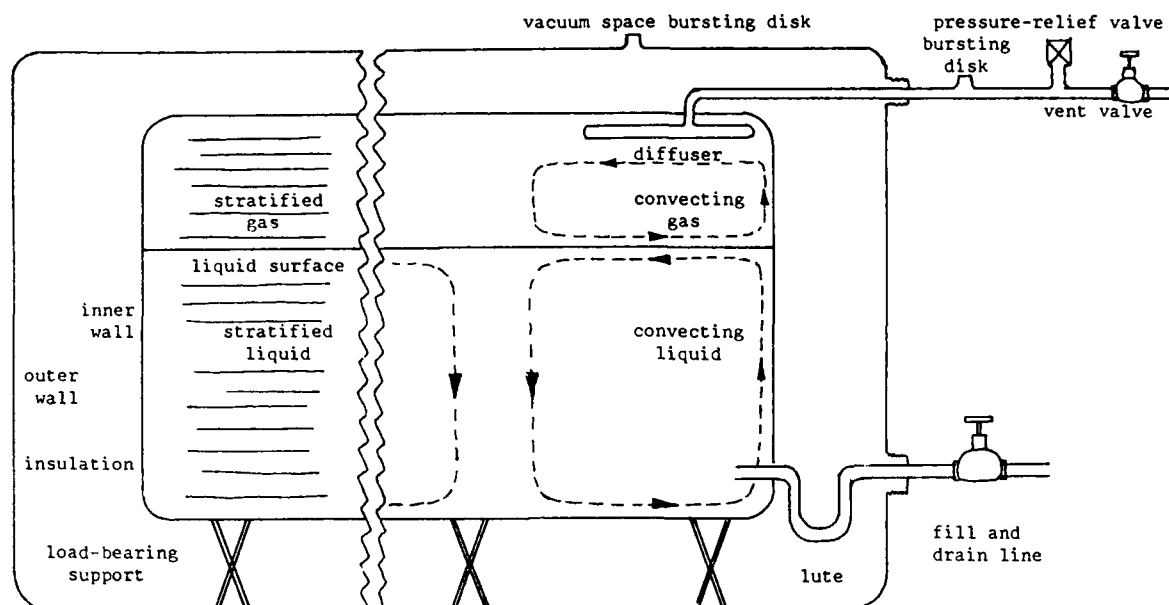


Figure 4 Schematic Representation of Aspects of Liquid Nitrogen Storage

4.2 Storage of Liquid Nitrogen

Storage vessels for cryogenic liquids such as nitrogen are not designed to be full of liquid and about 10% of the total volume, called the ullage space, is left above the liquid surface. This space also allows liquid to separate out and settle as the vessel is filled and in a typical transfer, once the vessel is about 90% full, liquid appears in the gas stream venting from the vessel indicating transfer is effectively complete. Even with an efficient insulation system, there is always a net influx of heat reaching the cryogenic fluid in its storage vessel and this evaporates gas which collects in the ullage space. If the heat influx is minimal, stable stratified layers build up in both liquid and gas with density gradients that tend to oppose any natural convection, as inferred on the left hand side of Fig. 4. For larger heat influxes the gas and liquid in contact with the wall are warmed causing them to rise and set up separate Convection systems in both the liquid and the gas. Consider first the gas. The walls are hotter than the gas and so absorb some of its sensible heat, thus becoming cooled. Correct design should enable all of the incoming heat flux reaching the unwetted wall to be absorbed by the cold gas so that there is no heat flow down to the wetted walls where it would have to be absorbed by the latent heat of the liquid. The warming gas rises by convection in the boundary layer adjacent to the walls and falls again in the centre to flow outwards across the liquid surface sweeping with it the cold evaporating gas, so completing the convection cycle, as indicated in the right hand side of Figure 4.

4.2.1 Storage Instabilities

Similar convection cycles exist in the liquid, with upward flow in the boundary layer at the walls and then across the surface where it absorbs heat from the counter-flow of gas and evaporates from the surface of the superheated liquid. This surface evaporation, or boil-off as it is often called, has an irregular nature and takes place in cells whose locations move over the surface. If, however, the liquid is left undisturbed for long periods, the boil-off rate decreases and a stable layer of highly superheated liquid develops on the surface. When subsequently disturbed, this superheated layer evaporates suddenly, leading to a rapid increase in the boil-off rate and a rise in pressure. In smaller-sized storage vessels the temperature of this superheated layer can sometimes rise by up to 40 K before explosive boil-off takes place. Condensation of liquid oxygen or argon in the surface layer can take place if air can leak into the vessel and, as these liquids are both hotter and denser than liquid nitrogen, rapid boil-off occurs if the surface layer is disturbed. It is, in fact, considered good practice to stir liquid nitrogen slowly to prevent the build-up of unstable stratified layers.

4.2.2 Provision of Relief Valves and Bursting Disks.

In Table 1 it was noted that if 1 litre of liquid nitrogen was evaporated and warmed to room temperature and 1 atmosphere pressure it would create approximately 680 litres of gas. If such evaporation were to take place in a enclosed volume the resultant pressure would thus increase to over 600 atmospheres should the structure be strong enough to withstand such a pressure. In practice no storage vessels, transfer lines or other components would be stressed to this level and they would therefore rupture, possibly explosively. To prevent such a hazard, enclosures that could possibly become over-pressurised have to be fitted with relief valves and bursting disks set to trigger and vent the gas safely. It should be noted that the capacity of these items needs to be adequate to cope with the maximum gas flow rate and that the bursting disk should be fitted between the enclosure and the relief valve. Vacuum spaces between the inner liquid container and the external shell must be fitted with bursting disks as a guard against sudden failure of the inner container and consequent ingress of liquid into the insulation. One spectacular rupture of a cryogenic pressure vessel not fitted with a relief valve occurred in Apollo 13 on its way to the moon when an electric heater was accidentally left on in the titanium alloy liquid helium

storage vessel. Other more common causes include the blockage of liquid hydrogen and helium storage vessels by the condensation and solidification of air and the plugging of liquid nitrogen vents and lines by condensed and frozen water vapour. The lute shown in Fig. 4 fitted in the fill and drain line between the inner vessel and the valve helps to prevent localised evaporation of liquid from the warm pipe and the possibility of blockage due to the build-up of impurities such as dissolved water vapour and carbon dioxide.

4.3 Transfer of Liquid Nitrogen

4.3.1 Removal of Liquid from the Storage Vessel

There are three principle methods used to remove liquid from the storage vessel (1) self pressurization of the inner vessel, (2) external gas pressurization and (3) pump transfer.

The liquid flow rates obtainable with self pressurization are relatively low and this technique is most frequently used for smaller sized vessels and laboratory scale applications. Some of the liquid is removed from the storage vessel and passed through an external vapourising coil where it evaporates, expands and causes the pressure to increase. This warm gas is fed back into the storage vessel through the diffuser which, together with stratification in the gas prevents the warm gas flowing directly into contact with the liquid and recondensing.

External pressurization can utilise either the same gas as that liquefied in the storage vessel, or a separate, often non-condensable, gas. Considerably higher transfer rates can be achieved by external pressurization together with rapid response times. In the Douglas Aircraft Company 4ft blowdown cryogenic tunnel, liquid nitrogen from a 9000 gallon capacity run tank was pressurised to 300 psia using compressed air stored in separate tanks. Transfer rates of 1440 litres/second (300 gallons/second) of liquid were achieved giving a maximum run time of the order of 30 seconds.

Both the 0.3-m TCT and NTF at NASA Langley used pumps to transfer their liquid nitrogen, 3 pumps being run in parallel when the maximum flow rates of about 450 kg/sec (5.5×10^3 litres/sec) are needed by the NTF. It should be noted that a Net Positive Suction Head (NPSH) must be maintained at the pump inlet if cavitation is to be avoided. Furthermore as the evaporation rate during liquid transfer is low to maintain the pressure in the ullage space above atmospheric, nitrogen gas has to be returned to the ullage space to prevent possible collapse of the inner vessel.

4.3.2 Transfer Lines

As noted earlier structures with low thermal mass cool more rapidly and evaporate less cryogenic liquid than those with larger thermal masses and this is one factor that has to be taken into consideration in deciding whether to insulate transfer lines or to leave them bare. When liquid oxygen or pressurised liquid nitrogen is passed through an uninsulated pipe, frost builds up on the outside and tends to insulate it by preventing convective cooling by the air. If, however the nitrogen is subcooled, condensation of liquid air tends to wash away the frost and heat losses are higher. Nevertheless short lengths of bare pipe are often used to transfer liquid nitrogen from delivery tankers to small storage vessels as they are cheaper and less cumbersome than insulated lines. For longer runs and permanent installations transfer lines are, however invariably insulated. An evacuated double walled construction, with or without powder or superinsulation, is usually favoured for the larger and longer lines and, as noted earlier some form of expansion joint has to be provided to prevent the build up of tensile stresses on the inner pipe during cool-down. Flexible foams, with suitable vapour barriers to prevent LOX condensation are frequently used for shorter, smaller runs.

4.3.3 Liquid Transfer

In a perfectly insulated, pre-cooled pipe cryogenic fluid would be transferred as a single phase liquid, but in most practical cases some degree of two phase flow is usually present. This can take many forms depending on whether the pipe is horizontal or vertical, the mass flow rate, pressure drop across the line and heat inleaks to the line. In general, stratified flow with the liquid at the bottom of a horizontal pipe and vapour above it occurs at low flow rates, but at higher flow rates, shear between gas and liquid sets up waves or plugs which can completely fill the pipe with liquid. Under some circumstances annular flow occurs and this can be beneficial if it can be arranged in such away that the gas is on the outside completely surrounding a central core of liquid, as in this case heat inleaks from the pipe walls will be absorbed by the sensible heat of the gas not the latent heat of the liquid.

During initial cooldown the first liquid introduced into a warm pipe evaporates on contact with the warm sides. This gas then flows ahead of the advancing liquid front precooling the walls as it progresses towards the outlet, a process that can often take a surprisingly long time. Increasing the liquid delivery pressure can be an expensive way of speeding up the process as less of the sensible heat of the gas is used in precooling the pipe. Furthermore, as the evaporated gas occupies a much greater volume than the liquid, gas velocities can be very high and frequently the flow is choked at the exit during practically the entire cooldown and leaves at sonic velocity. If, however, the flow resistance in the pipe is large it may be impossible to make the liquid front advance more than partially along the pipe such that liquid never emerges from the other end and a zero delivery condition is obtained. The usual solution to such a problem is to modify the line by installing a sufficient number of intermediate venting points to allow the liquid front to be advanced progressively by venting from these intermediate points until liquid emerges and then moving on sequentially to the next vent point. Unpredictable two phase flow through the liquid nitrogen injectors of a cryogenic wind tunnel can also create problems with its temperature control, particularly if the condition does not occur evenly with all injection positions. One design that overcomes this problem is to feed all injectors from a circular "ring-main" of liquid as this prevents vapour building at any particular location.

Control of nitrogen flow through the injectors is achieved using servo-controlled valves, digital valves being used in the 0.3-m TCT but the more conventional gate and globe valves being preferred for the NTF. Rapid and accurate control of the liquid flow is obtained when the system is cold, but care should be taken during cool-down to prevent rapid opening or closing of valves that allow liquid to enter warm areas. The sudden build-up of pressure from the vaporising liquid could lead to pressure surges and even flow reversal, with the risk of damage to pumps and other equipment in the line. Even emergency vent or stop valves should be arranged so as to operate over a few seconds rather than slamming shut.

5. STRENGTH AND TOUGHNESS OF METALS AT LOW TEMPERATURES

One of the principal design requirements of any piece of equipment is that it should have adequate stiffness, strength and toughness to withstand safely any load or stress that may be applied to it. Operation at low temperatures effectively increases the requirement for adequate toughness at the operating temperature, as virtually all materials are both stiffer and stronger at low temperatures than at ambient. A load-bearing structure must, therefore, be able to cope with not only the static and dynamic stresses which can be predicted for normal operation, but also the thermal shocks it may be subjected to on cool down, the thermal stresses induced by differential expansion during warming and cooling cycles, as well as the accidental overstresses or impact loads that it may receive in the presence of the scratches and dents it is liable to suffer during service.

Most materials are designed to operate within their elastic limits and typical stress and deflection formulae require the use of appropriate values for the elastic constants such as the Youngs, Shear and Bulk moduli and Poissons ratio. Fortunately, the elastic constants are relatively insensitive to structure variations such as changes in grain size, the degree of cold working, heat treatment and small compositional variations etc., while decreasing the temperature in general increases Youngs modulus by about 10% between 300 K and 80 K. Accuracies greater than about 1% are rarely required in the calculations normally used to avoid buckling failure (elastic instability) or excessive elastic deformation (jamming) and thus values taken from the literature can be used with a reasonably high degree of confidence. The design problems created at ordinary temperatures by the relatively low moduli of aluminium alloys when compared to either austenitic or ferritic steels are also encountered at low temperatures where stiffness is important, for example, where shell bending is a significant design limitation, as in a column subjected to a lateral air flow loading. In such cases, the higher moduli offered by, for example, the austenitic stainless or 9% nickel steels would allow either stiffer structures for the same section or thinner sections for the same stiffness.

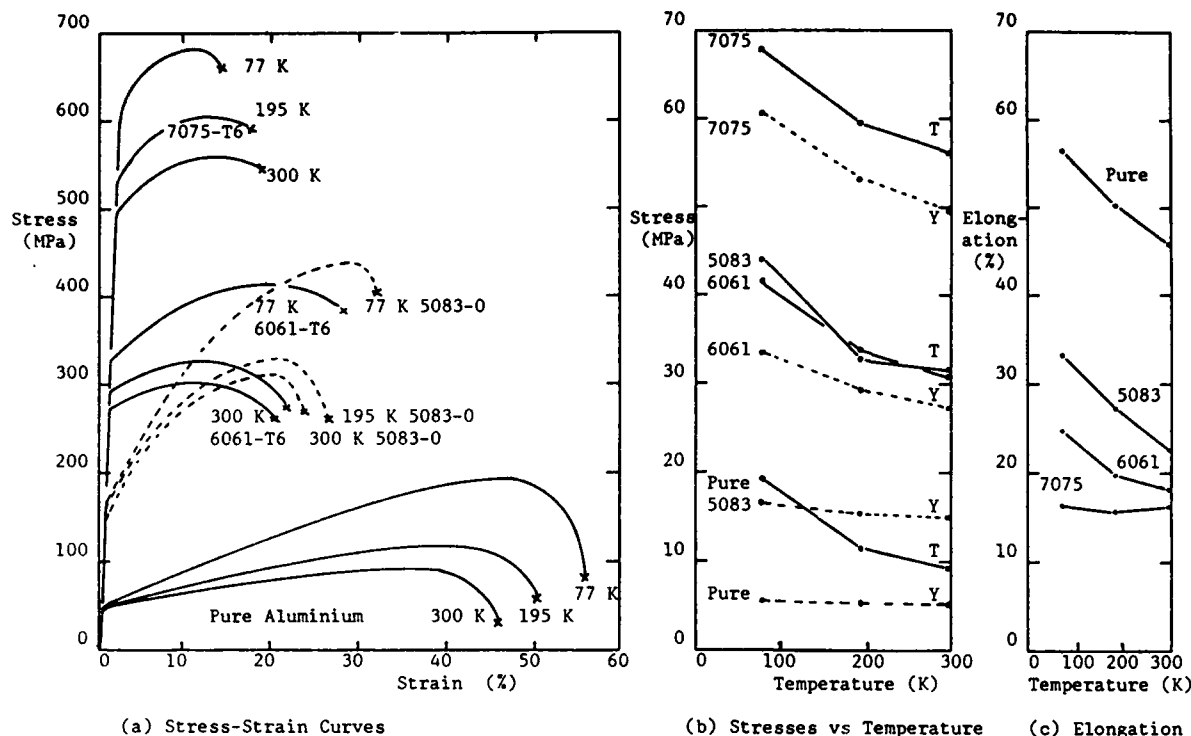
Yield and plastic deformation in metals are processes strongly influenced by their structure and condition to such an extent that accurate predictions are difficult and experimentally determined data invaluable. General classification of their properties is best started by considering their crystal structures, most metals and alloys having face-centred-cubic, body-centred-cubic or hexagonal-close-packed lattices. Of these the face-centred-cubic metals are greatly to be preferred for low temperature use as almost without exception their strengths, ductility and toughness all improve as the temperature falls, thus making them ideal for cryogenic applications. F.c.c. copper-, nickel-, and aluminium-based alloys, together with Invar and the austenitic stainless steels are, in fact, the metals most widely used for the construction of equipment operating below about 150 K. Of the hexagonal-close-packed metals only magnesium and titanium are used in significant quantities below room temperature, the high specific strengths offered by titanium alloys being particularly attractive for certain specialised applications in the aerospace industry.

It is the body-centred-cubic group of metals that offer the greatest challenge but which constitute the greatest risk as they almost all undergo a transition from ductile to brittle behaviour at some temperature, usually below ambient. Furthermore, small changes in their chemical composition, grain size, the degree of plastic constraint brought about by a notch or flaw, and even the rate at which a load is applied, can all have a marked effect on the delicate interrelationship between strength, toughness and the temperature at which the ductile-to-brittle transformation occurs. As, however, the economically irreplaceable ferritic steels have b.c.c. structures, their use at low temperatures cannot be precluded and it is necessary to define the temperature and stress limits to which a certain grade, thickness and condition of steel may be safely used. These limitations are traditionally laid down by codes of practice issued by independent bodies such as the American Society of Mechanical Engineers, government agencies such as the British Standards Institution, local or national insurance agencies or even state regulatory authorities, and there are very few load bearing structures which can be built without conforming to one or more such codes. There is also, however, an increasing and very welcome tendency towards backing up these codes by a scientifically rigorous failure analysis based on the concepts of fracture mechanics - a study of the resistance offered by a material to the continued propagation of a crack nucleating in the vicinity of a sharp crack. Such analyses are also applicable to high strength alloys with f.c.c. and h.c.p. structures, as well as to the rate at which cracks propagate during fatigue and so constitute a powerful analytical technique which the aerospace industry in general was quick to develop and exploit.

The mechanical properties of materials at low temperatures are considered in detail in References 5, 7, 14 and 15, while data is presented in References 16 to 19.

5.1 Face-Centred-Cubic Metals and Alloys

Although some copper and nickel based alloys are used for particular applications in cryogenic wind tunnels, the quantities involved are small and they are best considered in the next lecture in the context of their use in model construction. It is only aluminium alloys and the austenitic iron-based alloys that are likely to be used in significant quantities.



Figures 5(a), (b) and (c). The Mechanical Properties of Aluminium and its Alloys at Low Temperatures.

5.1.1 Aluminium Alloys

It is instructive to start by considering the properties of pure aluminium because it shows very clearly the basic characteristics of f.c.c. metals which make them so useful at low temperatures. In Fig 5(a) a series of engineering stress-strain curves are shown for aluminium and some of its alloys tested at and below 300 K. The following features should be noted from the curves for pure aluminium.

- i) Yield is a gradual process and the yield stress is only a weak function of temperature.
- ii) The strain hardening rate (slope of the stress-strain curve after yield), the ultimate tensile stress (maximum point in the curve) and the total plastic elongation all increase as the temperature falls. Thus the metal becomes both stronger and more ductile at low temperatures essentially because it is able to accommodate a greater degree of strain hardening before the onset of necking (plastic instability).
- iii) The large drop off in measured stress between the onset of necking and final failure is indicative of a large reduction in area and hence a very ductile type of fracture at all temperatures.

In Figs 5(b) and (c) the data is cross-plotted to show more clearly the temperature dependence of the yield and tensile strengths and the elongation. It is the combination of increase in ductility and tensile strength, together with the relative temperature-insensitivity of the yield stress that is the definitive characteristic of face-centred-cubic metals and alloys which makes them so eminently suitable for use at low temperatures. It is brought about by their ability to slip and deform to prevent the build-up of high stress concentrations at the tips of cracks and flaws.

Pure aluminium has high electrical and thermal conductivities and it has replaced copper in many instances where these characteristics are required. Its alloys are widely used where moderately high strengths combined with high toughness and low density are necessary, such as in road and rail transporters for liquid gases, as well as in static liquid storage tanks. Aluminium alloys may conveniently be divided into two groups according to the basic metallurgical strengthening mechanism involved: (1) the solution-hardened alloys, which are very ductile but only moderately strong in the annealed state (although their strengths can be improved by cold working), and (2) the precipitation-hardenable types, which can be heat treated to give considerably higher strengths.

Of the solution-hardened types, those containing manganese as the main alloying addition (3000 series) have only moderate strengths, but they are very ductile and hence easily formed. Type 3003 is used for tubes, bends, junctions, plate fin heat exchangers, tube plates and trays, as well as in distillation columns and many other applications. Their role in heat exchangers arises largely because they can be dip-brazed in molten salt baths using aluminium-silicon eutectic alloys. They can also be extruded and cut with roller cutters, characteristics which are advantageous for volume production. They can be cold-worked for higher strengths, but, as they are so often used in the welded or brazed condition where these advantages would be lost, it is more usual to use one of the higher-strength alloys where necessary.

The aluminium-magnesium alloys (5000 series) have higher strengths than the 3000 series and they are widely used for the construction of land-based storage tanks, road and rail transporters and for the primary containment of liquid natural gas in LNG ships. A series of stress-strain curves from tests at

300, 195 and 77 K on a 5083 alloy is also shown in Fig 5(a). It can be seen that the yield strengths are higher than those of pure aluminium but still relatively independent of temperature. The strain hardening rate is also higher and becomes still more so at lower temperatures so that both tensile strength and elongation improve at low temperatures and thus the alloy is ideal for low temperature use. Type 5083 alloy is, in fact, the largest-tonnage alloy in cryogenic service largely due to its combination of moderately high strength with excellent weldability. Gas-metal-arc and tungsten-metal-arc systems have been used to weld plates up to 175 mm thick; even in the as-welded condition its full strength is retained thus giving it an advantage over the higher strength 2000 and 7000 heat-treatable alloys if post-weld heat treatment is not possible. Additional strength can be achieved in the 5000 series alloys by cold-rolling but the consequent loss of ductility is not always acceptable. Most of the internal structure of the NTF is fabricated in 5000 series alloys. The contraction, test section, high speed diffuser and upstream nacelle are made from welded 5083, as in the non-cryogenic operating mode the temperatures of these parts does not exceed 66 C (150 F). This is the maximum temperature at which 5083 can be operated continuously in a highly stressed state while avoiding the possibility of grain-boundary stress corrosion. Due to the increase in temperature of the gas stream created by the power of the fan, which can be as much as 14 C (25 F) at the high power ambient temperature operating condition, those sections between it and the cooling coil, the downstream nacelle, shrouds and rapid diffuser, are made of type 5454. This alloy can be used safely at the higher temperatures but, as its yield stress is about 50% of that of 5083, thicker sections are necessary.

Aluminium-magnesium-silicon alloys (6000 series) have the lowest strengths of the heat-treatable types and, in general, they are the only ones used outside the aerospace industry. Type 6061 in the T6 condition is stronger than the 3003 and 5083 alloys but its strength in the as-welded condition drops below that of the solution hardened alloys. It is generally available in the forms of pipe, pipe fittings, extruded tubing and other shapes. Stress-strain curves for 6061-T6 are also shown in Fig 5 (a) and it can be seen that their shapes differ from those of pure aluminium and the solution hardened 5083. The yield stresses of 6061-T6 are higher and more temperature dependent and the strain hardening rates are lower. The tensile strengths do not greatly exceed the yield strengths and elongations are smaller at all temperatures than for 5083. Nevertheless, the mechanical properties of 6061-T6 make it suitable for cryogenic applications and it was used for construction of the pressure shell and internals of the NASA LaRC 0.3-m TCT.

The aluminium-copper alloys (2000 series) have higher strengths than the Al-Mg-Si types but their toughness, especially their notch toughness, begins to fall seriously at low temperature and they are not widely used. Moreover, they are often considered to be less easy to weld reliably. Nevertheless, welded type 2014-T6 was employed in the construction of the liquid-oxygen and liquid-nitrogen fuel tanks for the Saturn V Rocket where its high strength/weight ratio proved advantageous.

The final series of stress strain curves in Figure 5 (a) is for one of the very high strength aluminium-zinc-magnesium heat-treatable alloys, 7075-T6. As may be seen, very high yield strengths are attainable at and below room temperature. However, it is also apparent that the ductility, which is already rather low at room temperature, falls even further at low temperatures. If the samples were notched and/or loading rates higher, the picture would appear even blacker as these very high strength alloys have low notch-toughness and are thus rarely used below room temperature. They do, however, provide a convenient example of how a very high strength alloy, even with an f.c.c. structure, can have such a low fracture toughness as to make it necessary to use fracture mechanics analyses for safe design. Even though the alloy does not fail by cleavage, slip is so inhibited by the metallurgical process used to create its high strength that it is no longer able to deform easily and reduce stress concentrations at the tips of cracks and flaws.

5.1.2 Austenitic Stainless Steels

This is one of the most important class of materials used in the construction of equipment for operation at low temperatures. The face-centred-cubic gamma phase of iron is normally only stable at high temperatures, but the addition of alloying elements such as nickel, manganese, carbon and nitrogen suppresses the gamma-alpha transformation and enables the austenitic gamma phase to be retained to room temperature and below. The gamma structure is, however, only metastable and under certain conditions of stressing and/or cooling a partial transformation to martensite can take place in some of the less highly alloyed steels such as type 304. Two martensite phases are formed having h.c.p. and b.c.c. structures respectively, and it is the b.c.c. form which leads to an increase in strength but loss of toughness in the transformed state. Furthermore, b.c.c. martensite is ferromagnetic and its presence is a severe disadvantage in applications where magnetic fields are present. Finally, to make matters even worse, the transformation is accompanied by a volume expansion which can spoil the fit of accurately machined components such as shafts and flanges.

In general, the most stable steels are those with the highest nickel contents such as the 25-Cr, 20-Ni type 310 wrought alloy and the analogous casting alloys CK20 and Kromarc-55. One disadvantage of 310 is its rather low yield strength of about 200 MPa at room temperature, but if some loss of ductility can be tolerated this may, however, be raised to about 500 MPa by cold working without either a significant drop in toughness or transformation to martensite. Because of its high nickel content type 310 is more expensive than other 300 series stainless steels and it is somewhat more difficult to obtain in a wide range of product forms than the more popular alloys. In most other 300 series austenitic stainless steels some degree of martensitic transformation may be induced by stressing or thermal cycling. The ferromagnetic nature of b.c.c. martensite allows its existence to be established very simply by the use of a small pocket magnet, while a somewhat more sophisticated, and hence expensive, variation on this theme uses a calibrated spring balance to measure the force required to remove a magnet from the surface of the sample.

In a series of experiments carried out by the International Nickel Company, the magnetic permeability of a series of austenitic stainless steels was measured before and after cold rolling at 300K and 77 K. It was found that type 310 showed no transformation while type 301 was strongly affected by both treatments. The samples of 316, 321 and 347 showed an increasing tendency to transform during cold rolling

but were relatively unaffected by thermal cycling. Type 304, one of the most widely available of all the austenitic stainless steels, has the greatest variability in its behaviour because small decreases in the carbon and nitrogen contents can be very harmful as both elements are strong austenite stabilisers. It is therefore worth noting that the recently developed 'Hi-proof' grades of 304, 316 and 347 which contain 0.2% nitrogen to increase their yield strengths by about 70 MPa, will also be very much more resistant to martensite transformation than the normal grades. In contrast the low carbon grades of 304 used to prevent weld decay will be least resistant to martensitic transformation! When the nitrogen bearing grades 304N, 316N and 347N become more readily available in the product forms required, they will offer probably the best combination of properties available for low temperature applications from any austenitic stainless steel and their use should be encouraged. Regrettably, they are, at present, difficult to obtain in small quantities and in forms other than sheet and plate.

A further point worth noting from the results of the International Nickel Company experiments concerns the effect of thermal cycling. If the ferromagnetic nature of a partially martensitic 300 series steel is not a drawback for a particular application which demands good dimensional stability, it is possible to ensure that transformation is complete before final machining. This may be achieved by cycling repeatedly between 300 K and 77 K, if necessary taking measurements after each few cycles, until no further significant dimensional changes occur. Further consideration of dimensional instability, particularly in the context of wind tunnel models, will be given in the next lecture.

Type 304 is the most readily available of the austenitic stainless steels and the low carbon welding grade 304L was used for the outer pressure shell of the NTF. Under normal operating conditions the outer shell is unlikely to be cooled more than a few tens of degrees below room temperature, due possibly to localised degradation of the insulation. Furthermore, should some malfunction lead to the build up of liquid nitrogen inside the shell, the inherent toughness of the austenitic structure ought to ensure that no embrittlement problems would be encountered.

5.2 Body-Centred-Cubic Metals and Alloys

As a general rule metals with b.c.c. crystal structures undergo a ductile-brittle transition which occurs at some temperature which may be above or below room temperature. There are a few exceptions, but for practical purposes the potentially brittle nature of b.c.c. metals at low temperatures puts a severe limitation on their use. However, they cannot be disregarded as they include the whole range of carbon, low-alloy and nickel steels which are economically irreplaceable for the construction of equipment operating at moderately low temperatures. The basic philosophy behind their successful application lies in ensuring that they have adequate toughness at their minimum operating temperature for them to withstand not only their design stresses but also accidental impact and other overloads without failing in a brittle and catastrophic manner.

5.2.1 The Ductile-Brittle Transformation in Ferritic Steels

One manifestation of the ductile-brittle transformation in low-alloy ferritic steels can be observed in the sharp decrease in the tensile elongation that occurs at the transition temperature. A much more realistic indication of the seriousness of the problem is, however, obtained from the tough-brittle transformation measured by the decrease in the impact energy absorbed in Charpy V notch tests carried out over the transition temperature range. For a plain carbon steel the toughness transition takes place at or above room temperature, whereas the ductility transition occurs at some 220 °C lower. About half of this drop can be accounted for by the very much higher strain rates involved in an impact test, as ferritic steels are highly strain rate sensitive. Thus in practice ferritic steels should not be subjected to sharp blows or impact loading when they are below their toughness transition. The remainder of the decrease is due to the presence of the stress concentration at the notch root, an indication of the importance of avoiding sharp corners and minimising stress concentrations. Small variations in the depth or sharpness of the notch also account for much of the scatter in the impact energies measured over the transition range. In general most metallurgical and other factors which strengthen the material, e.g. cold work, increased alloy additions, precipitation hardening, etc., also lower its toughness. The only exception to this rule is the action of grain refinement as this increases both the strength and the toughness. Indeed grain refinement is one of the most important methods of obtaining toughness in ferritic steels at low temperatures, and this is achieved in part by increasing the manganese concentration relative to that of carbon, high Mn/C ratios giving finer grained structures. The degree to which the steel is deoxidised, or killed, by the addition of silicon and aluminium is also important, fully-killed steels being tougher, but more expensive, than semi-killed steels. Niobium and vanadium are also added to high grade steels to produce additional grain refinement, while careful control of the aluminium, nitrogen and vanadium concentrations can lead not only to enhanced grain refinement but also to precipitation hardening by their resultant nitrides and carbides.

It is, however, the nickel alloy steels that are most widely used at and below 220K. In Britain 2.25, 3.5, and 9% Ni steels are readily available and these grades adequately span most required temperature ranges. 2.25% Ni steel is used down to 210 K, particularly for equipment handling liquid propane at 230 K, while 3.5% Ni steel down to 170 K and is commonly specified for tanks, pipes, and other applications involving liquid ethylene, ethane, acetylene and carbon dioxide. It is, in fact, also often employed for higher-temperature applications because the additional safety margins given by its higher toughness compensate for its marginally higher cost compared to 2.25% Ni steel. A 5% Ni steel is also used quite widely in Europe at temperatures down to 150 K, particularly in the fabrication of welded vessels for the handling and storage of liquid ethylene. The use of 9% nickel steel in thicknesses up to 50 mm and at temperatures down to 77 K without post-weld heat-treatment has been allowed since 1962 under ASME code case 1308. This steel is available in both (1) the quenched and tempered, and (2) the double normalised and tempered conditions, (1) having a marginally higher yield stress and lower ductility at room temperature: it is unusual in that post-weld heat treatment actually lowers its toughness and this treatment is therefore not recommended. It is the only ferritic steel permitted for use at liquid-nitrogen temperatures and it is economically competitive for the construction of large storage tanks for liquid nitrogen, oxygen, argon and methane. Its high proof-stress/tensile-stress ratio gives it a distinct advantage if design on the basis of proof-stress such as BS 5500 is permissible, but even when designing to tensile-stress codes

it is still a very economical material. It is readily welded, but fillers with the same composition as the parent metal must not be used as such welds lack adequate toughness. Austenitic 25% Cr-20% Ni consumables give tough welds with expansion coefficients that match those of the parent metal, but whose strengths are lower, whereas the higher-strength Inconel types have mismatching expansion coefficients and this can cause high contraction stresses to be set up during thermal cycling. Thus neither type of electrode is ideal and furthermore their high cost detracts somewhat from the favourable economics offered by the parent metal. It should be noted that 9% Ni steel, like other high-tensile steels, is particularly prone to hydrogen embrittlement and thus precautions have to be taken to prevent hydrogen pick-up during welding or in service. A special high quality version of 9% Ni steel was used for the fan shaft of the NTF. The possibility of using the standard alloy for the pressure shell must also have been considered seriously as it would have been a cost-effective alternative to the 304L stainless steel eventually chosen, the relative availabilities of the quantities and product forms required probably being one of the deciding factors.

5.2.2 Cryogenic Wind Tunnels with Ferritic Steel Pressure Shells

It should be noted that there are in fact a number of cryogenic wind tunnels in operation in which the pressure shell is made of mild steel and similar low alloy steels with tough-brittle transitions near room temperature. These may be divided into two categories, the first being blow-down tunnels or recirculating tunnels with short duty cycles. In these cases the tunnels are lined with a relatively thin layer of some form of durable insulation that can be given a clean aerodynamic profile. The thermal characteristics of the tunnel are analysed to establish that the thermal diffusivity of the insulation is low enough to prevent the walls from cooling significantly during the cold period of the tunnel duty cycle. The second type of tunnel is typified by the tunnel at Tsukuba University, Japan. Here the internal insulation is much thicker and the tunnel operates continuously. Thermocouples are used to sense the temperature of the insulation layer adjacent to the inner surface of the pressure shell and heater tapes are available to provide local heating should it be necessary to ensure that the wall temperature does not fall below its tough-brittle transition.

5.3 Fracture Toughness and Crack Propagation

In most materials the presence of a notch or flaw has an embrittling effect due to the stress concentrating effect at the tip. Modern theories of Linear Elastic and General Yielding Fracture Mechanics (LEFM) and (GYFM) can relate the fracture strength and critical flaw size to the Fracture Toughness of the material, K_{IC} . In a simplified form the basic relationship is:

$$\sigma_F = K_{IC} / [\pi a + 0.5 (K_{IC} / \sigma_y)^2]^{1/2}$$

where σ_F is the fracture stress, K_{IC} the fracture toughness, σ_y is the yield stress and a is the critical crack length. Note particularly the term $(K_{IC} / \sigma_y)^2$, as it gives an indication of the amount of plastic deformation that takes place in the material ahead of the advancing crack. If σ_y is small, (K_{IC} / σ_y) is large and there is a large plastic zone ahead of the crack tip. Relatively large amounts of energy are absorbed in tearing through this zone and crack propagation is therefore made more difficult. In contrast, if σ_y is large, (K_{IC} / σ_y) is relatively small, the plastic zone size is also small and little energy is absorbed by shear deformation. Furthermore, we have already seen that the yield stresses of many alloys increase quite rapidly as the temperature falls. Thus to maintain the same relationship between fracture strength and critical crack size the fracture toughness would have to increase in proportion to the yield stress. This does not happen in many high strength alloys and as a result the critical crack size decreases and they become increasingly notch brittle. Unfortunately the fracture toughness of a material is not only highly dependent on its physical and mechanical condition but also on its thickness and even sample width. Nevertheless the application of the concepts of fracture mechanics have provided a better understanding of fracture behaviour in high strength alloys and a firmer basis for design to prevent low energy absorbent fracture.

It is convenient to divide materials into the value of the ratio of the tensile modulus to the yield strength, E/σ_y . If E/σ_y is less than 150 the material has such a high strength that critical flaw sizes are low and load-bearing structures must be designed using fracture toughness analyses. If E/σ_y is greater than 150 the material is low strength and only those bcc metals such as ferritic steels that fail by cleavage lack toughness. Medium strength materials falling between these limits at room temperature can become effectively high strength materials at low temperatures because of the rise in their yield stresses. Fracture mechanics analyses are carried out for many of the high strength materials used in various cryogenic wind tunnel applications including the support stings, balances, models and other components that are highly stressed at cryogenic temperatures. Fracture toughness is considered further in the next lecture and selected values for K_{IC} at 300 and 77K are given in its Appendix for many of the alloys likely to be of use for these applications.

5.4 Time-Dependent Failure

As has been shown, the fracture stress of a material is strongly influenced by the presence of cracks and flaws. There are three principle mechanisms by which such cracks may form or intensify during service: (1) fatigue, (2) corrosion (especially stress corrosion and corrosion-fatigue), and (3) hydrogen embrittlement. None of these is a specifically low-temperature phenomenon, indeed the fatigue lives of many metals increase considerably at low temperatures, while the rates at which most corrosion reactions take place drop rapidly as the temperature falls - rather they increase the probability of unstable failure under service conditions which would normally be considered satisfactory. Their effect is the result of one or more of the following factors: (a) they lower the toughness of the material, (b) they provide a mechanism whereby a crack sharpens and increases the degree of stress concentration, or (c) they allow a sub critical crack to grow at stresses below the gross yield stress until it reaches the critical length required for unstable propagation.

5.4.1 Fatigue and Thermal Fatigue

Fatigue failure occurs in materials subjected to cyclic or fluctuating stresses which may or may not be superimposed on static applied stresses. Failure under such loading conditions can take place at stresses which are very much lower than the tensile or yield stresses even in materials which are normally

considered to be tough and ductile. Fatigue must therefore be considered as a possible mode of failure in any piece of low-temperature equipment subjected to cyclic loading or vibration (for example, pumps, motors and turbines), or to periodic changes in pressure (transfer lines, storage vessels, and other process plant). The severity of the problem may be indicated by the estimate that about half the failures encountered in general engineering practice are caused by fatigue. Fatigue tests carried out at low temperatures have shown that fatigue lives of most metals rise considerably as the temperature falls. It has already been demonstrated that the tensile stresses of most metals increase as the temperature is lowered and it has been found that there is a strong correlation between fatigue strength and tensile strength; indeed, experiments have shown that in some metals the ratio of the endurance limit at 10^5 cycles to the tensile stress is virtually independent of testing temperature.

Thermal fatigue is of particular relevance to cryogenic plant, such failures having occurred in regenerators after a large number of temperature reversals, and in heat exchangers and other components after a relatively small number of warming and cooling cycles caused by plant shut-down. The basic cause of this type of fatigue is the high stresses and strains that can be set up during thermal cycling if temperature gradients are non-linear or if free expansion and contraction are restricted by external constraints. In this type of low-cycle, high-strain fatigue, small amounts of plastic deformation take place during each loading cycle and cumulatively lead to failure. Such failures were in fact encountered in the early operation of NASA LaRC 0.3-m TCT where "spoke-like" aluminium struts were rigidly attached to the tunnel pressure vessel and to central "hub-like" structures. Subsequent redesign using PTFE cushioned "T" slots at the central hub attachment points allowed free thermal expansion of the spokes and elimination of the stresses that caused thermal fatigue.

Pre-existing flaws, notches, cracks, badly radiused corners and other surface defects have a strong influence on fatigue lives, causing them to drop sharply at all temperatures even in materials which are not normally considered to be notch sensitive. This is usually a result of the increase in stress intensity brought about by the sharp fatigue cracks and it is particularly severe in high-strength aluminium alloys, titanium, and stainless steels which are known to be notch sensitive. As noted earlier, it is possible to apply the concepts of fracture toughness to crack growth under cyclic applied stresses and many data compilations (e.g. Ref. 18) show the relationship between crack growth rate da/dN as a function of stress intensity factor range ΔK . Predicted component lives are then obtained by calculating how many cycles are required to increase the flaw size from its initial to the critical value. In general, fatigue crack growth rates decrease at low temperatures for most metals normally used for the construction of cryogenic equipment. In contrast they increase for ferritic steels at temperatures below the ductile-brittle transition.

Corrosion fatigue can be a problem with some low temperature equipment particularly if it is frequently cycled between low and ambient temperatures. In the presence of even mildly corrosive environments large reductions in the endurance limits can occur even though the amount of metal corroded is negligible. Some aluminium alloys are especially prone to corrosion-fatigue, ordinary moist air causing some deterioration, while salt-laden atmospheres are particularly harmful. Premature failure has been known to occur in air separation plants located by the sea or near chemical plants and if such conditions are liable to be encountered it is necessary to apply a protective coating to the metal or to specify a material such as stainless steel, which is less susceptible to this type of failure.

5.4.2 Corrosion and Embrittlement

These are two mechanisms by which failure can occur without warning long after the initial application of the stress and they can cause failure at low temperatures even though the actual corrosion or embrittlement is more likely to have taken place at or above room temperature. Stress-corrosion resulting from internal residual stresses is liable to occur in brass, aluminium, magnesium, titanium, and steel as well as some non-metals. It is usually prevented by annealing at a temperature high enough to remove the residual stresses without weakening the material. Hydrogen embrittlement is a particular problem in high-strength steels such as 9% Ni steel. The hydrogen is usually absorbed during pickling and plating processes or during welding, and, although the hydrogen can sometimes be removed from steels by baking at 350 C, it is better to prevent its initial pick-up where possible.

6. STRENGTH AND TOUGHNESS OF NON-METALS AT LOW TEMPERATURES

Non-metallic materials have much more complex structures than metals and the amorphous and microcrystalline structures typically found in glasses and ceramics almost invariably make them brittle because they are unable to accommodate the plastic deformation needed to relieve the high stress concentrations which build up around small flaws. They are thus much stronger in compression than in tension but are rarely used in the bulk form even under compressive loadings because their poor thermal conductivities and consequent liability to thermal shock make them liable to shatter. However, in the finely divided form of fibres, powders, films, foams and expanded granules they are widely used for thermal and electrical insulation at low temperatures.

6.1 Ceramics and Glasses

Glasses and ceramics have amorphous structures and they are unable to deform plastically and relieve stress concentrations caused by microcracks in their surfaces. They fail in tension at relatively low stresses at all temperatures and their use in bulk form at low temperatures is limited. Glass Dewar flasks are, however, still used for storing small quantities of cryogenic fluids and large plate glass windows are employed as viewing ports in cryogenic bubble chambers. Careful thermal annealing to remove surface cracks and residual stresses is essential for these applications, while thick sections have to be cooled extremely slowly to avoid failure due to differential contraction or thermal shock. Ceramics and glasses are stronger in compression than in tension because the microcracks are propagated by tensile stresses and residual compressive stresses are often induced in the surfaces of glass plates to toughen them. In a similar manner concrete structures, which are also brittle in tension, can operate satisfactorily at low temperatures if kept in compression and large liquid-natural-gas storage tanks have been constructed in which the concrete is maintained in compression by steel reinforcing rods placed in

tension around the warmer outside of the tank. The liquid nitrogen storage tanks for the University of Tsukuba cryogenic wind tunnel are also made of concrete lined internally to minimise the evaporation rate and keep the tension rods in the warm part of the concrete. For applications such as the floors of loading bays for road tankers transporting cryogenic liquids, it has been found that high-alumina cements such as Ciment Fondué are much more resistant to shattering by thermal shock than is ordinary Portland cement.

6.2 Thermoplastics and Thermosets

Polymeric materials can be divided basically into two structural categories: the thermoplastics and the thermosets. The long chain molecular structures of thermo-plastics give them mechanical properties which are strongly dependent on the temperature and rate at which they are stressed. Furthermore, an increase in their intermolecular forces over a temperature range known as the glass transition, which may be above or below ambient, means that most thermoplastics undergo a reversible transition to a glass-brittle state in which they are unable to deform plastically. As their glass transition temperatures are all above 150 K there are no thermoplastics which exhibit any really significant degree of ductility below this temperature.

Thermosetting polymers have a network structure which renders them brittle and they are thus rarely used in the unfilled state. However, when combined with suitable fillers their toughness is greatly improved and phenolic-impregnated cloths and papers (such as Tufnol and Paxolin) are particularly useful for the fabrication of load-bearing, electrically-insulating fitments. The inclusion of powdered glass or ceramic powders reduces the brittleness of un-filled resins while the incorporation of glass or carbon fibres and cloths in epoxy resin matrices gives the high performance composites to be considered in section 6.4.

Materials selection becomes even more complicated if these materials are needed in applications where liquid oxygen (LOX) is present, as virtually all hydrocarbon-based polymers are incompatible with LOX and burn violently in its presence. The polysulphides, silicones and fluorosilicones are more LOX compatible, but it is only the fluorocarbons that are completely satisfactory in this respect.

6.2.1 Thermoplastics of Particular Interest for Cryogenic Wind Tunnels

Applications of major interest for wind tunnel models will be considered in the next lecture. Here we will consider thermoplastics in their roles as seals and adhesives. Correctly designed fittings are important if leak-tight joints are to be made at low temperatures. As long as no dynamic stresses are involved, satisfactory seals can be obtained from elastomers, even when they are below their glass transition. In order to achieve this aim, very large compressive strains are imposed at room temperature so that the elastomer is able to exert sufficient force to offset the decrease in load caused by the contraction which takes place as it goes through its glass transition. The most satisfactory results are obtained using confined compression designs in which a follower on one flange squeezes the O-ring into the bottom of a matching groove in the face of the other flange, as well as into the clearance space between groove and follower. The O rings are typically compressed by about 80% of their original diameter and are thus not re-useable.

The fluorocarbon family of polymers, polytetrafluoroethylene (PTFE, TFE, Teflon), the fluorinated ethylene/propylene copolymers (FEP), and polychlorotrifluoroethylene (PCTFE, Kel-F), are the only materials which retain any measurable ductility (approx. 1%) down to 4 K. This is a result of their unique molecular structure in which crystallites are formed having a tight spiral formation of fluorine and chlorine groups which are unable to pack closely together, thus preventing the material from having a strong glass transition. Although these materials are not elastomers, their ability to undergo enough plastic deformation to form a satisfactory seal makes them invaluable for use at temperatures down to 4K. They do, however, suffer from a tendency to cold flow under continuous load, and seals are thus liable to leak unless the load can be increased to compensate for the cold flow. Filled-PTFE compositions have been developed to overcome this problem, glass-fibre being most commonly used for O-rings and gaskets, while graphite, bronze and other powders are also used for bearing applications. Glass fibre improves the tensile and compressive properties of the materials, while the PTFE gives it sufficient ductility to accommodate plastically the strains developed. Furthermore, the thermal contraction of the composite is reduced from the high value characteristic of unfilled PTFE, so that the expansion of the composite is more compatible with that of metals, thus making joint design easier. The confined compression designs of flanges are also to be preferred for use with fluorocarbon seals because they minimise the deleterious effects of cold flow.

In the NASA LaRC 0.3-m TCT many large and small diameter seals are made using "Gortex". This is a low-density form of PTFE created by a proprietary process that involves stretching the material to about 10 times its original length without reducing its diameter. The material has been found to be particularly suitable for the demountable seals on the plenum cover of the 2D test section. Although "Gortex" is not intended for re-use, it has been found that it is not necessary to replace the gaskets each time the cover is opened. An alternative approach is to use spring- or pressure-assisted seals. In spring-assisted seals a metal backbone spring provides the sealing force and helps to compensate for dimensional changes during cool-down, while the PTFE coating forms the actual seal with the mating surface. A "U" shape cross section seal with a type 302 stainless steel spring and PTFE coating was chosen for the NTF, the "U" shape section allowing the use of gas pressure to improve sealing efficiency. It was also found that the surface finish of the mating surface was important, a 0.8 μm (32 μin) RMS finish being acceptable, and that treatment of these surfaces with FEP or TFE tapes or lubricants improved sealing efficiency.

There are many applications in which metal-metal, metal-plastics or plastic-plastics adhesive joints are advantageous. For example, brackets, clips and other attachments can be bonded to pressure vessels without creating the stress raisers that would otherwise be caused by welding or other conventional techniques, while corrosion-free joints between dissimilar metals can be obtained if their surfaces are kept apart by an electrically non-conducting adhesive. At room temperature, adhesives are usually able to deform sufficiently for any stress concentrations to be relieved, but at low temperatures their moduli increase considerably and make this much less likely. Contraction and other stresses have to be minimized

and the key to the successful development of structural adhesives lies in the use of fillers that match the expansion coefficients of the adhesives as closely as possible to those of the substrate and the adherent. They also redistribute thermal stresses throughout the adhesive instead of concentrating them at the adhesive-substrate interface. Even so, the thermal conductivities of most adhesives are low, and temperature differentials between them and metal substrates can cause failure from thermal shock if the glue line is not kept as thin as possible. One way of achieving this is to use a 'structure' or 'carrier' between adherent and substrate. This is usually a thin layer of glass fibre mat which allows the adhesive to penetrate and wet the filaments, thus forming an even bond as well as reducing the differential contraction between adhesive and adherent. It also has the further advantage of reducing creep at ambient temperature in adhesives such as the polyurethane pastes, which in other respects are among the most successful adhesives for low-temperature applications. Other types include the epoxy-nylons, nitrile modified phenolics, epoxy-phenolics, and fluorocarbon-epoxy-polyamides.

6.3 High-Performance Composites

High performance composites are formed by the incorporation of glass, carbon or Kevlar fibres in matrices of thermosetting polymers such as epoxy resins. For most aerospace applications their attraction lies in their high specific strengths and stiffness, and these characteristics improve at low temperatures but not, perhaps, so markedly as those of metals. One major interest in glass-reinforced plastics for low temperature applications comes, as noted earlier, from their very high strength/thermal conductivity ratios which make them ideal for use as load-bearing, thermally-insulating supports.

As the reinforcing fibres are stronger and stiffer than the matrix, they support the greater part of the applied load and the strength of the composite is determined by the length, orientation, and concentration of the fibres. 50-60 per cent of fibres by volume are typical maximum concentrations unless filament-winding techniques are used. Tensile strengths of 270-420 MPa are typical of room-temperature values and these increase gradually to about 480-700 MPa at 77 K. Their moduli are less temperature dependent, increasing by about 10-20 per cent on cooling from 300 K to 20 K, while their toughness, as measured by impact or notched tensile tests, shows little significant variation over this temperature range. These are quite high strengths by most standards, and when the low density of glass-fibre-reinforced plastics (GRP) is taken into consideration, it can be seen that their specific strengths are extremely high.

Tensile tests carried out on specimens laminated from a single thickness of woven cloth show a change from a high initial modulus to a lower secondary modulus at a load equivalent to about 13-15 per cent of their ultimate load-carrying capacities. If the specimens are examined at this stage they can be seen to be full of microcracks and the material is now porous and unable to retain vapour or liquids. The root of this difficulty lies in the failure of the bond at the fibre-matrix interface in those fibres that have a large stress component resolved perpendicular to the fibres. The strength of this bond is about 12-15 per cent of the composite strength parallel to the fibres. Hence the material has become porous long before it has developed its full potential strength and its electrical properties are also degraded. Fatigue failure also develops by fibre/matrix debonding and resin cracking at stresses lower than those in comparable static tests. Where fatigue loading is expected, design stresses are usually taken as about one-tenth of the composite failure stress.

Glass fibre reinforced composites also have other drawbacks. Static fatigue, which is a characteristic failure mode in bulk glass and unreinforced thermo-plastics, can also occur in GRPs if moisture is able to penetrate the fibre matrix interface, although this failure mechanism does not operate if the composite is maintained at low temperatures. A more serious difficulty lies in the highly anisotropic nature of their mechanical properties, reinforcement being much more efficient in a direction parallel to the fibres than perpendicular to them. Cross-plying the lamination allows two-dimensional reinforcement, but strengths and moduli are reduced compared to those attainable parallel to the fibres. If the orientation of successive plies is varied from layer to layer, this anisotropy can be reduced and more homogeneous properties obtained. This type of laminated structure was utilized in the construction of the NTF fan blades. Two different types of woven E glass cloth pre-impregnated with an epoxy resin were laid up at predetermined orientations and oven cured to consolidate the laminate and fully cure the resin. Other fibreglass structures used in the NTF include pultrusion sections used to fix the foamed glass insulation between the inner aluminium liner and outer stainless steel pressure shell. Further applications of high performance composites will be considered in the next lecture.

7. MATERIAL PROCUREMENT AND QUALITY CONTROL

It should be noted that the construction of cryogenic equipment is subject to the same economic constraints as any other large technical project, in that the total cost of each stage or component needs to be considered when alternative materials are being considered. Thus, to the cost of the basic material needs to be added the cost of the appropriate forming, joining and fabrication processes, inspection and quality control, possible rework and final finishing. It is almost invariably a false economy to purchase material for demanding technical applications at 'rock-bottom' prices as the resultant 'savings' frequently lead to subsequent costly problems, or even rejection of the component. The additional costs incurred in ensuring that a project starts off with top quality material are a worthwhile premium to pay for avoiding the problems likely to arise from the use of poor quality material. It is recommended that the ultimate use of component, and possibly the intended fabrication route should be made known to the materials suppliers when quotations are being sought so that they are aware of the problems that might arise if target specifications are not met. Furthermore, it has often been found that 'misunderstandings' are kept to a minimum if the project engineer makes contact with a technical representative of the suppliers to make him aware of the project requirements, rather than just leaving the purchasing department to progress the order.

8. CONCLUSIONS

In this lecture the author has tried to bring out the philosophy that cryogenic engineering is a mature technology that has much to offer the field of aerodynamic testing through use of the cryogenic wind tunnel. It is, however, important that those without a thorough grounding in cryogenic engineering should make an effort to benefit from accumulated experience on the correct way to handle cryogenic fluids and the best materials to use in the construction of equipment for operation at cryogenic temperatures. To this end, particular emphasis has been laid in this lecture on those aspects of cryogenic engineering that have a direct bearing on safety, in the belief that if potential problems can be understood, it is less likely that actual problems will be encountered. Used with care cryogenic fluids such as liquid nitrogen can bring significant scientific and technical advantages. Misused, the cost could be injury, or even death, of those directly or indirectly involved.

9. REFERENCES

1. Webster, T. J. (Ed) "Cryogenics Safety Manual- A Guide to Good Practice", British Cryogenics Council, Mechanical Engineering Publications Ltd, London (1982)
2. Zabetakis, M.G., Safety with Cryogenic Fluids (1967)
3. Webster, T. J. "Latest Developments in Cryogenic Safety", NASA CR 166087, (1983).
4. "Cryogenic Wind Tunnels". AGARD LS 111. (1980).
5. Wigley, D. A.: "Properties of Materials: The Physical Properties of Metals and Non-Metals", AGARD LS 111, pp 4-1 to 4-10, (1980).
6. Wigley, D. A.: "Properties of Materials: The Effect of Temperature on the Strength and Toughness of Materials". AGARD LS 111, pp 6-1 to 6-24, (1980).
7. Tobler, R. L.: "Materials for Cryogenic Wind Tunnel Testing", NBSIR 79-1624, NBS Boulder, Colorado. (1980).
8. NBS Monograph 21, "Specific Heats and Enthalpies of Technical Solids at Low Temperatures." (1960).
9. Gopal, E.S.R.: "Specific Heats at Low Temperatures". Plenum Press, New York, (1966)
10. Monograph 29 Thermal expansion of technical solids at low temperatures (1961).
11. Barron, R. B.: "Cryogenic Systems", McGraw-Hill, New York, (1966).
12. Webster, T. J.: "A Report on Possible Safety Hazards Associated with the Operation of the 0.3-m Transonic Cryogenic Tunnel at the NASA LaRC", NASA-CR-166026, (1982).
13. Haselden, G.G. (Ed) "Cryogenic Fundamentals", Academic Press, London (1971).
14. Wigley, D.A., Mechanical Properties of Materials at Low Temperatures (1971)
15. Reed, R. P.; and Clark, A. F.: "Materials at Low Temperatures". American Society for Metals, (1983).
16. NBS Monograph 13, "Mechanical Properties of Structural Materials at Low Temperatures". (1961).
17. Monograph 63 Tensile and impact properties of selected materials from 20K to 300K (1963).
18. LNG Materials and Fluids Users Manual (1977 & supplements), Users Manual of property data in graphical form available from NBS, Boulder.
19. Handbook on Materials for Superconducting Machinery, Metals and Ceramics Information Centre, Battelle, Columbus, Ohio (1977)

10. ACKNOWLEDGEMENTS

The author would like to acknowledge the help recieved in the preparation and checking of the manuscript, particularly from Dr. R. A. Kilgore, Dr. C. P. Young Jr. and Mr G. C. Firth of NASA Langley, and Miss C. A. Wigley for her typing.

INSTRUMENTATION FOR CRYOGENIC WIND TUNNELS

Maurice BAZIN
Office National d'Etudes et de Recherches Aéronautiques
29, Avenue de la Division Leclerc
92320 Châtillon, France

INTRODUCTION

The use of cryogenic wind tunnels to simulate high Reynolds numbers near those occurring in subsonic and transonic flight appears today to be the best technical and economic tradeoff.

The quality of the measurements made in these new facilities must at least be equal to that obtained in the present large industrial wind tunnels. This raises problems of sensors in this hostile environment where the usual difficulties related to pressurization are compounded by temperature effects.

At these high Reynolds numbers, the skin flows are highly susceptible, in particular to thermal phenomena. As for the model, it is subjected to deformations which are higher when the flow is pressurized and when it is submitted to thermal effects even if cryogeny makes possible to increase Reynolds number without increasing the efforts. This means that it is necessary to adapt the design of the models and the instrumentation as well as to provide for the changes of configuration and repair work in an environment hostile to human life.

As concerns the essential measurements - forces, pressures, temperatures, accelerations - made with model in situ instruments, the possibility of using existing sensors and the feasibility of specially designed sensors were the subject of extensive work associated from the outset with the projects for large cryogenic wind tunnels.

This was the case for the ETW European Transonic Wind Tunnel and the results obtained since 1982 [1] demonstrated that these technologies are accessible but that the efforts must be continued, in particular for the balances.

Since 1985, the activities on the problems related to the quality of the future tests were reduced for the benefit of studies also concerning the instrumentation, the equipment and work on the models, but which could have a direct impact on the design of the wind tunnel, which was then in the final design phase (Fig. 1).

For the test section, this concerns the optical processes used to visualize and identify the flow (transition, external flow field) and measure the model attitudes and deformations.

For the areas used for preparation of the models and calibration of the instrumentation, this concerns the calibration facilities for the balances and the possibilities of working on the model.

For the models, the feasibility of the tests simulating the motors was verified and reactor simulators adapted to a cryogenic environment were designed.

All these activities often led the Europeans to develop original solutions. The T2 wind tunnel for ONERA, the KKK wind tunnel for the DLR, the PETW wind tunnel and European cryogenic facilities of the research institutes (RAE test duct) and of the manufacturers are used to develop and qualify these new methods and apparatus.

All this work is decided and followed by ETW assisted by working group WG1, whose members represent the four countries that are "shareholders" in the future wind tunnel. The group has a mission of consultation, incentive, coordination and search for competences in each country. It handles the liaisons which are necessary with the national programs.

As the project advances, the cryogenic technology program is becoming more and more directly applied to ETW and is necessarily being taken over increasingly by the engineers of ETW GmbH. The nature and volume of the work are changing and the direct participation of the research institutes in the four countries is gradually giving way to industrial subcontracting, piloted to a varying degree by the research organizations.

BALANCES

The importance of balances for ETW leads to a review of the current situation in Europe through a few examples.

The probatory balance of ONERA [2], with a diameter of 24 mm, subjected to extended temperature variations from 100 to 300 K and longitudinal gradient of up to 20 K under load in a cryogenic chamber confirmed, during real testing in T2, its insensitivity to temperature effects and the possibility of using a single calibration matrix over the full range of use (Fig. 2).

The favorable scale of this balance, approximately 1:2 with respect to the balances required for the ETW, and its qualification in a wind tunnel with short gust (approximately 60 s) do not allow any final conclusions to be drawn. Comparative testing was however conducted at the same Reynolds number under voluntarily severe conditions with rapid set of the model temperature to those of the flow: balance and model cooled first and cryogenic gust or at ambient temperature and same gusts with balance and model initially "hot" (Fig. 3).

A preliminary feasibility study of a sting balance designed for weighing a combat aircraft in ETW was also made at the request of the French government agencies. This study, which appears perfectible, shows that for a diameter of 66 mm used to simulate internal flows and individual capacities of D 11920, S 28460, L 143260, R 3270, P 4935, Y 2950 (in N and N.m) obtained for the forces with limiting to 20 hbars under gauges and 90 hbars for moments in the structure, the thermomechanical effects related to the capacity in D of the balance correspond to only 4 times those computed for the balance with a diameter of 24 mm under the same gradient hypotheses (8 K longitudinally). This result is therefore encouraging, considering the larger size of the balance.

The development work on cryogenic balances undertaken by Darmstadt University resulted in two balances designed for the KKK wind tunnel [3].

Preliminary testing on a symmetrical design of the central balance part confirmed the linear, symmetrical response of the axial strain gauges versus the average temperature of the upper and lower beams, allowing compensation of longitudinal gradient effects (Fig. 4). The qualification testing on balance 609 confirms this result under the action of a gradient simulated by local heating (Fig. 5).

The capacities of these balances for KKK are respectively:

	609	612
D	1400 N	900 N
S	1700	400
L	4000	3000
R	400 N.m	200 N.m
P	500	240
Y	400	70

Balance 771 built by NLR [4] has a traditional design but somewhat special equipment, with additional transverse gauges for each bridge to minimize the variation in sensitivity. A large number of temperature sensors are used to correct for gradient effects after very complete calibration.

After preliminary testing using the cryogenic facility of the RAE in Bedford, in particular to identify the large effect of a sheath simulating installation on a metal fuselage, this balance was tested in April 1986 in the TCT wind tunnel of NASA with a very rigid delta-wing model (Fig. 6).

A rather particular procedure was used during these tests:

- runs with the balance at stabilized temperature (after a long wait) with use of the zeros measured without wind at the same temperature,
- runs at variable wind tunnel temperatures without measurement of the loads but with measurement of the temperature distributions in the balance.

In the first case, reproducibility is good or even excellent according as the convection sheath is absent or installed, thermal equilibrium being longer to achieve with the sheath. The accuracy obtained in D is however far too low to be able to measure the drag count of a civil aircraft (Fig. 7).

The temperature distributions (Fig. 8) show a systematic delay in the center of the balance with respect to the ends connected to the model and the sting. The model incidence has a substantial influence on this phenomenon.

Several computations were made of the thermal fields in a model and its balance [5, 6]. The correlations attempted with experimental results in the RAE facility at Bedford allowed the computation model to be improved by a better definition of the transfer coefficients on the model, and the magnitude of the convection effects between model and balance to be identified (Fig. 9).

One of the applications of this work will be to minimize the number of temperature sensors required on the cryogenic balances. The tests conducted at RAE [7] also show that it is possible to achieve good measurement, by applying corrections based on temperature measurements in a real balance.

ETW issued a call for bids for a preliminary feasibility study of two sting balances, one for a civil transport aircraft model and the other for a combat aircraft.

In addition to the general specifications concerning the environment before and during the test, security (taking into account dynamic loads), the qualities desired for the instruments, etc., the specified dimensions and capacities are as follows:

	Transport	Combat
Cross section	dia. 100 mm	□ 66×62
Length	500 mm	450 mm
Capacities under combined loads:		
D	1 500 N	5 000 N
S	2 500	15 000
L	20 000	50 000
R	750 N.m	1 500 N.m
P	1 200	2 000
Y	150	1 500

BALANCE CALIBRATION RIGS

The calibration apparatus and methods directly contribute to the accuracy of the balances. They must be capable of verifying that the balance is insensitive to thermal effects or of determining and checking the correction methods. The result is a large number of loading cases, combining loads and thermal conditions, which prompted the effort to automate the system as much as possible.

The desired accuracy of 1×10^{-4} and reproducibility of 0.5×10^{-4} required complete identification of the magnitude, position and direction of the loads applied with respect to the balance references.

The installation of a thermal cooling chamber around the balance must not create spurious forces. Furthermore, it is necessary to insure protection of the balance in case of accidental overload.

A conventional solution consists of realigning the three-axis reference system of the balance from the signals supplied by inclinometers [8]. In this case, air generators are suggested for application of the loads (Fig. 10).

The other solution proposed [9], called the inverse solution, consists of applying the loads at the non-weighing end of the balance and measuring the loads applied via a reference balance to which is attached the weighing part of the balance to be calibrated (Fig. 11).

In either case, it is obviously the quality of the technological details which will allow the required accuracy to be achieved for the facility.

IN SITU INSTRUMENTATION

This document does not review the sensors installed on models whose suitability for use was demonstrated [1], in most cases subject to suitable calibration procedures and, in certain cases, the use of stabilized temperature chambers. These techniques are currently used in T2, for instance [10].

Southampton University recently suggested [11] an interesting alternative for part of the measurement system, consisting of placing in the model an electronic acquisition system with an amplifier, a multiplexer and a 16-bit converter, with data output by optical fiber (Fig. 12). This device is insensitive to temperature of 300 to 77 K and the accuracy of 0.05 percent obtained with a prototype including 8 channels (4 pressure channels and 4 temperature channels) could be improved to 0.02 percent according to the authors. The obvious interest of such a system is relative to the wiring problems raised for the acquisition of a large number of pressures and/or temperatures. In effect, the transmission of low-level analog signals between the low temperature test section and the acquisition system at ambient temperature raises many problems of passage through the stings, and line loss, contact, thermocouple, electric or magnetic field effects.

OPTICAL METHODS

It was necessary to define the optical procedures to be used in ETW sufficiently early in order to determine the impact on the test section structure and the possibility of installing the equipment in the plenum. Discussions between the awardees of the feasibility studies was necessary to insure the compatibilities between the various systems proposed (e.g. MATRA for the shadowscope and CERT for deformation measurement).

FLOW VISUALIZATION AROUND THE MODELS

In order to prepare the engineering work of MATRA OPTIQUE, C. Véret (ONERA Physics Department) identified and analyzed the various optical processes used in the wind tunnels and itemized the optical rigs installed in ONERA wind tunnels [12].

These processes are based on variations of the local refraction index, associated with variations in density of the gas subjected to changes of pressure and temperature:

$$n - 1 = k \times p \text{ (Gladstone-Dale law)}$$

$$\text{for air } p = 3.48 \text{ p/T and } k = 2.27 \times 10^{-7} \text{ m}^3 \text{g}^{-1}.$$

A light ray crossing such an optically heterogeneous flow is deviated and it is possible to visualize these deviations as variations in light level or color:

- Interferometry (Fig. 13) shows the deviations of the optical path with respect to a homogeneous reference medium. The Mach-Zehnder interferometer requires considerable precautions in making the optical parts and is very sensitive to vibrations. The holographic interferometer, born with lasers, allows an interferogram to be created between the fringe system obtained during the test and the reference fringe system obtained without wind. Any optical defects disappear in the difference between the two states and the apparatus is therefore easy to build, but it is also sensitive to vibrations.

- The schlieren apparatus converts the variations in deviation of the light rays into variations in light level or color on a flat screen. The knife edge (Fig. 14) placed in the focus of the receiving lens masks half the image of the emitting lamp filament and causes a difference in light level if the beam is deviated perpendicular to the knife edge. A grid of colored strips can replace the knife edge and cause changes of color on the screen when the filament image moves on the grid.

In practice, the spherical aberrations of lenses L1 and L2 make it necessary to use mirror collimators for a large field of view, but the limit aperture condition leads to bulky apparatus. In practice, a large number of optical arrangements can be found, with single crossing or return, the latter having the advantage of being easy to transport and adjust but with a risk of image doubling (Fig. 15).

- The shadowscope gives variations in light level which are proportional to the second derivatives of the index gradient. It is a primitive process (Fig. 16) which supplies only a projected, deformed image instead of a conformal image like a schlieren apparatus. Various optical setups are also possible, the widest useful field of view being obtained with parallel beams.

The installation studies of a field observation facility in ETW [13] rapidly led to the following conclusions:

- 1) All the optical components must be placed inside the plenum to limit the effects of temperature differences.
- 2) To reduce the risk of fracture of the optical parts due to the temperature variations, it is necessary to break up the field to reduce the size of the components and use silica instead of glass.
- 3) The high values of p planned in ETW (high pressure, low temperature) are suited to the sensitivity of optical methods. The following values were taken into account:
 - density : 1.4 to 17 kg/m³
 - jumps in density : less than 5.2 kg/m³
 - density gradient : 1.4 kg/m⁴.

The above considerations, the advantages and drawbacks of the various processes, dimensions, requirement for splitting the field, sensitivity, led to proposing a parallel field shadowscope insensitive to polarization of the ambient light, affected little by the quality of the components and the effects caused by temperature gradients in the optical parts.

Transmission would be by laser diodes or halogen lamps and reception by CCD matrices.

The number of windows in the test section would be limited by placing the transmitter and receiver on the same side of the test section, requiring the use of reflecting screens on the opposite side. The three rows of seven windows located between the slots and the structural elements of the wall allow an observation of 2.7 m × 1.3 m, but the masking is up to 40 percent (Fig. 17).

It was suggested to provide only one pair of shadowscopes per row:

- with fixed transmitters and receivers and three sets of two mobile mirrors to explore the field (Fig. 18), or
- with mobile transmitter/receiver systems (Fig. 19), the first solution leading to a larger bulk inside the enclosure but being less costly and facilitating work.

As the optical instruments are located in a pressurized, insulating chamber, it is necessary to have a high quality entrance/exit window.

The experiments conducted by Darmstadt University [14] show the feasibility of such windows (Fig. 20).

The windows of the test section wall are much simpler to make because of the low temperature differences between test section and plenum. However, only silica can be used because of the temperature variations.

The compatibility of such a system with a laser tomography facility, a laser velocimeter (2 D) and RADAC was examined.

Many mechanical, electrical and electronic problems must be solved to reproduce the entire field visualized by parts. They are not discussed herein. The amount of the development work required to obtain an observation field which is however highly masked by the wall was the major reason which led ETW to postpone this equipment. However, this study allowed the possibility of retrofit to be considered. The future test sections with adaptable walls could also simplify the problem of lateral optical accesses for the test section.

THERMOVISION

The use of a thermovision camera to remotely detect the position of boundary layer transition on a model allowed a considerable improvement in the efficiency of the current wind tunnels by comparison with conventional methods. Developed since 1976 in the ONERA research wind tunnels and in use for several years in industrial wind tunnel [15], this transition visualization method was even used during flight testing at low ambient temperature after preliminary qualification tests in T2.

The reversibility and reliability, with respect to acenaphthene sublimation for instance, are the major qualities of this process whose development was made possible by the progress registered in detector sensitivity. The main constraint resulted from the thermal conductivity of the model which attenuates the surface temperature variation related to the variation of the transfer coefficient at transition. It is necessary to use a special insulating coating or to artificially create a transient phenomenon to overcome this difficulty.

The low thickness of the boundary layer at high Reynolds numbers requires a nonintrusive method to detect transition. Thermovision appears to be the only suitable method in spite of the even higher detector sensitivity required by the low operating temperatures and weak radiation.

A detector with a higher wavelength must be used to identify the small temperature differences at 100 K. Planck's and Wien's laws show that emittance is a maximum for $\lambda \text{ mT} = 2898$, i.e., $\lambda \text{ m} = 30 \mu\text{m}$ at $T = 100 \text{ K}$ instead of $10 \mu\text{m}$ at 300K at a maximum contrast achieved for $24 \mu\text{m}$ instead of $8 \mu\text{m}$ (Fig. 21).

The difference in adiabatic wall temperatures between a laminar flow and a turbulent flow is given versus Mach number and temperature in figure 22. This difference corresponds to a perfectly insulating model and it appears that a small instantaneous heating of the model with respect to the flow (for instance by thermal flash) will be necessary for low Mach numbers.

The main difficulty resides in the choice of the detector, which must have a sensitivity at least equal to 0.3 K at 100 K. The HgCdTe detector, widely used at 300 K, must be replaced by a doped silicon photoconductive detector whose main drawback is to require substantial cooling between 4 and 20 K, obtained with helium.

The feasibility study conducted by MBB [16] concludes in favour of an SiSb mosaic but does not definitively exclude the use of an HgCdTe photoconductive detector sensitive down to 20 μm associated with a processing system to improve the signal-to-noise ratio (Fig. 22). Liquid nitrogen could be used to condition this sensor. The apparatus proposed by MBB (Fig. 23) would allow observation of a $1.5\text{ m} \times 1.5\text{ m}$ surface from a distance of 1 m. It would include a scanning system and an autofocus type device allowing correct visualization for all the possible attitudes of the models in the test section. The optical access window in the test section with a diameter of 90 mm would be made of KRS5 (thallium broiodide), well suited to the wavelength.

Among the potential sensors (Fig. 21), SiAs and SiGa, produced in the USA, are available in 32×32 and 64×64 matrices. SiGa is produced in France by the LIR for the ISO satellite as 32×32 and 64×64 matrices. The Physics Department of ONERA is to study this detector for ETW using a specially adapted cryogenic chamber. The modification of the pixel scanning time according to the temperature and correction of the detector homogeneity defects are parameters to be considered.

ETW is planning to install a camera on the model cart and is studying the camera and the associated acquisition and restitution system.

MODEL ATTITUDE MEASUREMENTS

Accurate determination (0.01 degrees) of the model incidence is essential to define the drag when the balance is connected to the model and a change of reference frame is necessary, involving projection of the lift loads.

In current wind tunnels, the inclinometers installed in the model only just achieve this accuracy subject to many precautions: frequent calibration, in particular check of the zero setting, use of temperature-controlled chambers, unsteady behavior domain precluded.

As concerns accelerometers using gravity, they are only suitable when the plane of symmetry of the aircraft is vertical and therefore for a model installed right side up or upside down. They cannot be used for testing a complete model on its side or half models on floor mounting.

For the sideslip and roll angles, and for the incidence when inclinometers cannot be used, all that are available are the readings of the position sensors associated with the motor drives of the supports allowing modification of the attitudes and it is necessary to take into account -by prior calibration- the deformations of the supports under the effect of the aerodynamic loads measured by the balance. In the case of sting setups, the deformations related to the aerodynamic loads directly affecting the stings are generally neglected so that the accuracy obtained on the incidence is below that required.

The use of adapted temperature-controlled chambers means that the situation will probably not be worse in a cryogenic wind tunnel, but the resulting bulk for the model and the additional signal transmission difficulties will add to the problem [17].

Optical methods are likely to be an attractive alternative. Several systems have already been tested in existing wind tunnels, for instance in the USA (Boeing system) and the RAE (5 m). Several feasibility studies were studied for ETW to analyze the possible solutions.

- The Boeing type solution [18] is described as holographic interferometry used to measure incidence variations. The passive reflector located on the model (Fig. 24) is a cubic wedge on whose surface is attached an amplitude hologram. The property of a cubic wedge is that the reflected ray always remains parallel to the incident ray.

An incident beam on the hologram produces two separate beams inside the cubic wedge and, after reflection, the two beams are again diffracted by the hologram. Two parallel beams can be considered at the exit: one produced by the zero order of the second beam and the other by the first order of the hologram of the first beam. In this direction, an interference depending on the phase difference between the two beams can be observed through a lens. When the reflector is rotated, this phase difference is modified. The phase of the incident beam is modulated to increase the detection sensitivity.

The computations conducted by BERTIN on this principle did not however reproduce the sensitivity and linearity announced in the literature available on the system.

A moiré effect obtained with the reflector described above does however give a very satisfactory agreement between computation and published results (Fig. 25):

An incident beam on the hologram creates images in the Talbot planes parallel to the bars and at a distance p^2/λ - p bar spacing and λ wavelength - and related to the diffractions through the periodic structure.

If the dimensions of the cubic wedge are such that one of the images is superimposed on the exit hologram after reflection on the cube, moiré fringes can be observed at the exit of the reflector. Their intensity depends on the shift between the Talbot image and the second bars and therefore on the angle of incidence between the beam and the reflector.

The computations were made with the detector located in the focal plane of the collimator or placed in the conjugate plane of the entrance surface of the reflector and for different steps or positions of the hologram and different dimensions of the cubic wedge. The incident beam is angularly modulated.

Reception is carried out with a fringe counting system. A reference signal can be measured on a reference surface of the wind tunnel (Fig. 26).

- The system proposed by COMPLERE [19] and tested in the NASA Ame 9x7 ft wind tunnel is based on the translation of a light ray by refractions through a body with parallel faces with change of index (Fig. 27). An active detector is placed in the model behind a mask and a small lens and allows a resolution of 2.5 μm , confirmed by encouraging results at Ames.

The transmission system in the ETW will probably use a 10 mW HeNe laser or a laser diode to produce the incident beam which could be moved from one window to another if necessary -for instance to measure the sideslip- by a mobile mirror aimed at the target (Fig. 28).

Photodiode detectors with two or four quadrants can be used in the model inside a temperature-controlled and pressurized chamber. A reference detector would be located in line with the transmitter to align the system. COMPLERE proposes a very complete system for supervision and control of the model attitudes.

However, in spite of the highly encouraging results discussed, it is to be feared that the index variations in the flow around the model and particular through the shocks in transonic state will disturb the optical path and affect accuracy.

The possible deviations through a shock [20] can reach values high than the 0.01 degree accuracy sought for the incidence if the angle of attack of the beam is small with respect to the shock line (Fig. 29). The conclusion is however that subject to certain precautions relative to the position of the detectors and possibly to making corrections after estimating the integral of the deviations through the field, these methods remain promising. ETW is therefore planning to install an optical device to measure attitudes.

DEFORMATION MEASUREMENTS

The model, whose geometry generally represents the deformed aircraft for the reference flight case, is also subjected to deformations under the effect of aerodynamic loading. It is therefore necessary to identify the real form tested to separate the deformation effects from effects such as Reynolds number effects.

The RADAC system [21] was developed at ONERA by CERT to equip the large industrial wind tunnels. After satisfactory laboratory testing and calibration, the prototype will very soon be tried out in the F1 wind tunnel pressurized at 4 bars.

The principle of RADAC is stereoscopic acquisition from at least two cameras with 3 D restoration of the positions of targets (light sources) placed on the model (Fig. 30).

For each light source, each RADAC camera provides a pair of coordinates obtained on two orthogonal linear CCD detectors through spherocylindrical lenses. These detectors allow high resolution (2048 pixels) and a high read rate (2 ms for read of the bars and generation of the pair of coordinates).

An associated signal processing system performs the distortion corrections and a barycenter computation on the light spot, which allows a resolution better than 1/16 pixel to be obtained, i.e., for the cameras already produced, 0.1 mm at 3 m with a field of 4 m.

The active targets are point sources of light: LED, laser or the end of an optical fiber. The wide single-lobe LEDs (120 degrees) can provide a high power of 100 mW with a small size, compatible with installation in a model.

The sources are controlled to give a fixed light level for each bar and allow automatic identification of each source if necessary. The system (Fig. 32) is capable of controlling 64 independent sources in 300 μs .

The restoration accuracy requires high relative stability of the two cameras. They are generally placed in a temperature-controlled and pressurized chamber and mounted on a position-slaved suspension. A reference calibration structure allows accurate calibration on site.

For ETW, the CERT and the associated manufacturer planned to place the two cameras and the connecting beam acting as base in the same insulated and pressurized chamber. ETW has decided on the principle of installation of a RADAC system.

CONCLUSION

The possibilities of adapting existing instrumentation for use in the ETW cryogenic wind tunnel were investigated in a previous document [1]. These efforts must be continued, especially for balances, but recent work was devoted to systems with a direct impact on the design of the wind tunnel test section. This is the case in particular for all the optical methods whose use in ETW for flow visualization (external flow-field and transition detection), accurate model attitude measurements and deformation measurements will contribute to the quality of the tests.

REFERENCES

- [0] D. Schimanski, ETW: Cryogenic Technology Programme. 2nd Cryogenic Technology Review Meeting ETW, Koln 28-30/6/1988.
- [1] M. Bazin, ONERA: Instrumentation for cryogenic wind-tunnels. VKI 22-26/4/1985.
- [2] M. Dubois, ONERA: Feasibility study on strain gauge balances for cryogenic wind-tunnel at ONERA. TP ONERA n° 1982-87.
- [3] B. Ewald, E. Graewe, University of Darmstadt, MBB: Cryogenic balance development. 2nd Cryogenic Technology Review Meeting ETW, Koln 28-30/6/1988.
- [4] J. Baljeu: Development of a multi-component internal strain gauge balance for model tests in a cryogenic wind-tunnel. NLR TR 88157 U.

- [5] W.B. Bald, University of York: Force balance errors due to temperature changes in ETW. 2nd Cryogenic Technology Review Meeting ETW, Koln 28-30/6/1988.
- [6] M. Unger, MBB Munchen: Results of temperature distribution calculations with PATRAN and P/THERMAL. 2nd Cryogenic Technology Review Meeting ETW, Koln 28-30/6/1988.
- [7] R.D. Law, RAE Bedford: Measurement of temperature gradients and assessment of balance performance using the RAE cryogenic test duct. 2nd Cryogenic Technology Review Meeting ETW, Koln 28-30/6/1988.
- [8] R. Porter, ARA Bedford: A proposed automatic calibration facility for cryogenic balances. 2nd Cryogenic Technology Review Meeting ETW, Koln 28-30/6/1988.
- [9] B. Ewald, P. Giesecke, E. Graewe, TM DARMSTADT, SCHENCK, MBB: Automatic calibration machine for internal cryogenic balances. 2nd Cryogenic Technology Review Meeting ETW, Koln 28-30/6/1988.
- [10] A. Mignosi, J.P. Archambaud, S. Prudhomme, M. Plazanet, M.J. Payry, ONERA-CERT: T2 ability concerning model design and instrumentation in short run processing. 2nd Cryogenic Technology Review Meeting ETW, Koln 28-30/6/1988.
- [11] R.G. Scurlock, R. Webb, University of Southampton: Development of cryogenic instrumentation for ETW model. 2nd Cryogenic Technology Review Meeting ETW, Koln 28-30/6/1988.
- [12] C. V  ret, ONERA: Contribution    l'  tude de faisabilit   de syst  mes d'observation pour la soufflerie ETW. RF 11/3409 PY.
- [13] F. Pointeau, MATRA: Feasibility study of the flow field observation system for the ETW. August 1987 (Confidential ETW).
- [14] H.G. Konig, B. Ewald, DARMSTADT: A measurement window for a cryogenic wind-tunnel. 2nd Cryogenic Technology Review Meeting ETW, Koln 28-30/6/1988.
- [15] A.M. Bouchardy, G. Durand, G. Gauffre, ONERA: Processing of infrared thermal images for aerodynamic research. TP 1983-32.
- [16] B. Schulze, G. Lange, S. Craubner, MBB: An infrared camera system for detection of boundary layer. 2nd Cryogenic Technology Review Meeting ETW, Koln 28-30/6/1988.
- [17] Berdrow, E. Graewe, MBB: Feasibility study for an ETW model attitude measurement system. November 1987 (Confidential ETW).
- [18] G. Rivet, M. Lequire, BERTIN: Model attitude measurement system. 2nd Cryogenic Technology Review Meeting ETW, Koln 28-30/6/1988.
- [19] F.K. Owen, G.M. Orngard, T.K. Mc Devitt, T.A. Ambur, COMPLERE Inc: A dynamic optical model attitude measurement system. 2nd Cryogenic Technology Review Meeting ETW, Koln 28-30/6/1988.
- [20] J.E. GREEN, ARA: Comments on effects of refraction by density gradients in tunnel flow using optical measurement of model attitude. 2nd Cryogenic Technology Review Meeting ETW, Koln 28-30/6/1988.
- [21] B. Lamiscare, C. Lempereur, J.C. Paquet, ONERA-CERT, INTERSPACE: Feasibility study of RADAC st  reo optoelectronic model deformation measurement system for ETW. 2nd Cryogenic Technology Review Meeting ETW, Koln 28-30/6/1988.

			INVESTIGATED CONCEPT	COMPANY
WP 30	<u>OPTICAL SYSTEMS</u>			
30.6	FLOW FIELD OBSERVATION	a	Shadowgraph	HATRA / ONERA
30.7	SURFACE FLOW VISUALIZATION	b	Thermography	HBB
		c	Hot Film Technique	DFVLR
30.8	MODEL ATTITUDE MEASUREMENT	a	Paints, Tufts, etc.	Dr. Goodyer
		b	Boeing System	Bertin
30.9	MODEL DEFORMATION		Complere System	Complere
			Triangulation Method	ONERA-CERT
WP 31	<u>BALANCE CALIBRATION</u>	a	Excentric Load Inverse Machine	TH Darmstadt/Schenck/HBB
		b	5 m tunnel RAE	ARA
WP 34	<u>ENGINE SIMULATION</u>	a	Overall Concept + Calibration	NLR/HBB
		b	TPS	Technofan
WP 36	<u>EQUIPMENT FOR OFFICES, LAB'S, etc.</u>	a	Protective Suits	DRAGER
		b	Manipulators	HBB
		c	Glove Box System	Taylor Hitec
WP 67	<u>RESEARCH AND DEVELOPMENT</u>			
676	MODEL CONSTRUCTION	a	Model Attitude Instrumentation	HBB
		b	Transport Aircraft Sting	ONERA-INFL
		c	Combat Aircraft Sting	BAC
ETW			ACCEPTED PROPOSALS	completed: classification: number:

			CONCLUSIONS
WP 30	<u>OPTICAL SYSTEMS</u>		
30.6	FLOW FIELD OBSERVATION	a	Provisions for retrofit of shadowgraph. Study on Laser sheet
30.7	SURFACE FLOW VISUALIZATION	b	Installation of one thermography unit
		c	No priority for urgent investigations on hot film techniques
30.8	MODEL ATTITUDE MEASUREMENT	a	No priority for urgent investigations on paints, tufts, etc.
		b	Installation of one optical concept
30.9	MODEL DEFORMATION		Installation of one deformation measurement unit for transport aircraft
WP 31	<u>BALANCE CALIBRATION</u>	a	Installation of one automatic calibration machine
		b	
WP 34	<u>ENGINE SIMULATION</u>	a	No priority for urgent investigations
		b	
WP 36	<u>EQUIPMENT FOR OFFICES, LAB'S, etc.</u>	a	Protective suits
		b	Manipulators
		c	Glove Box System
			Further investigation of glove box system
WP 67	<u>RESEARCH AND DEVELOPMENT</u>		
676	MODEL CONSTRUCTION	a	Attitude Instrumentation
		b	Transport Aircraft Sting
		c	Combat Aircraft Sting
			No priority for urgent investigations
ETW			SUMMARY OF CONCLUSIONS
			completed: classification: number:

Fig. 1. Cryogenic technology program: a) research; b) conclusions.

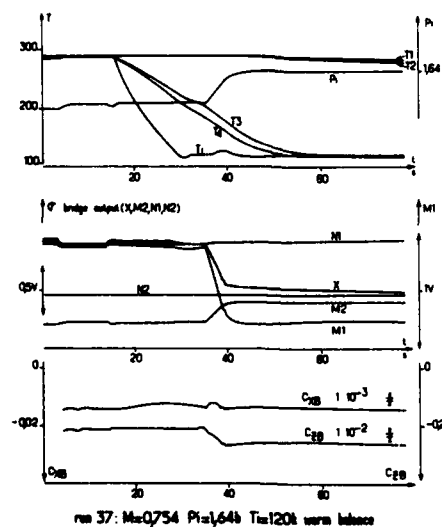
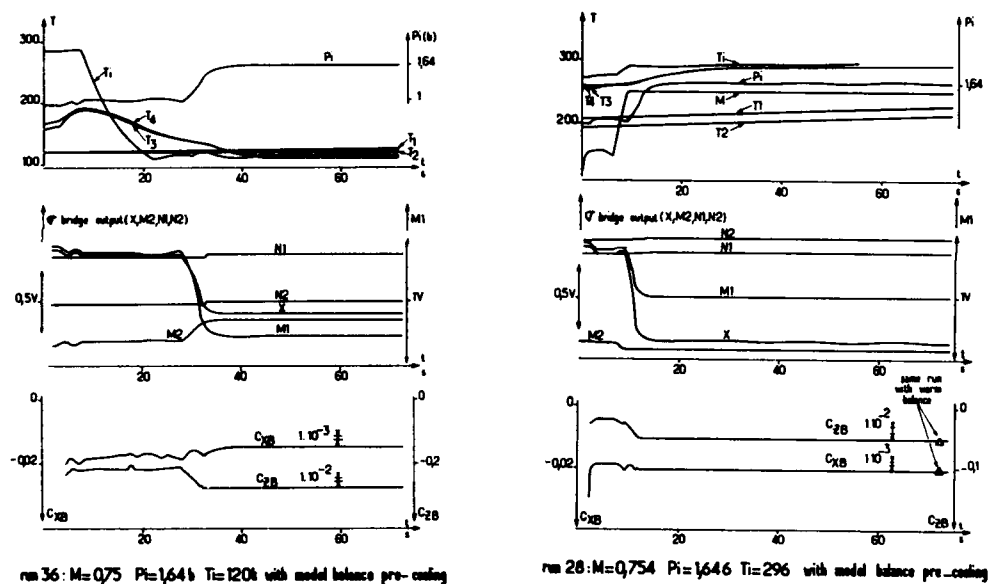
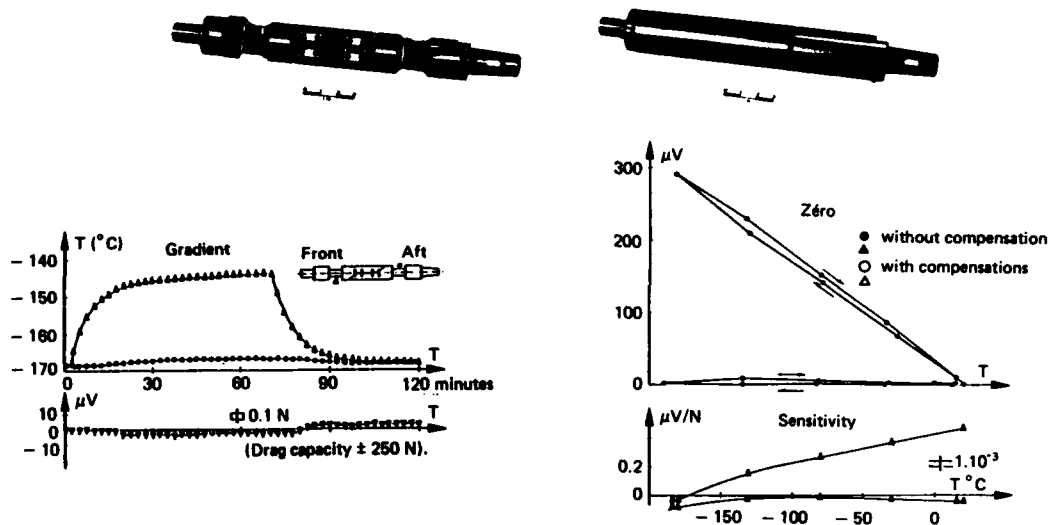
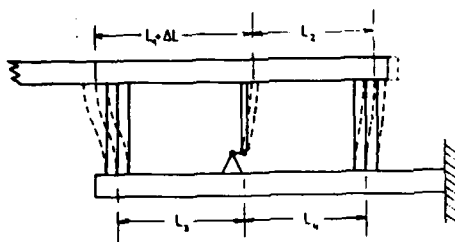
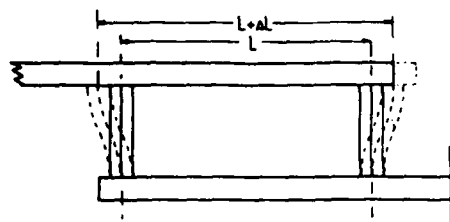


Fig. 3. ONERA balance : test results in T2.



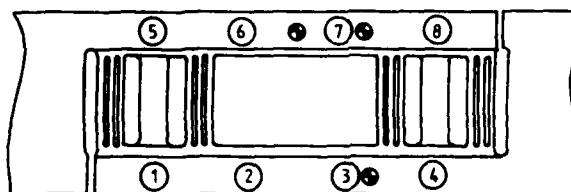
Axial Force System Distorted by Temperature Gradient



Distorted Axial Force System

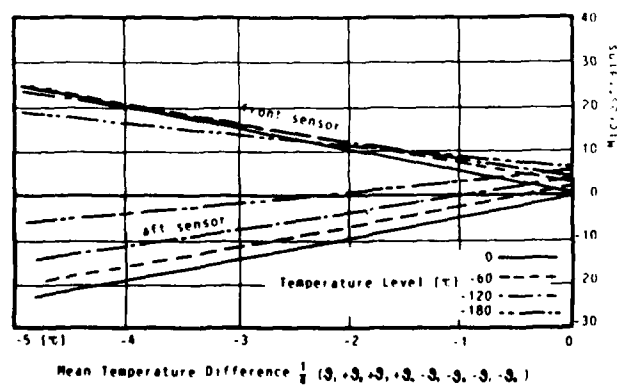


Axial Force System



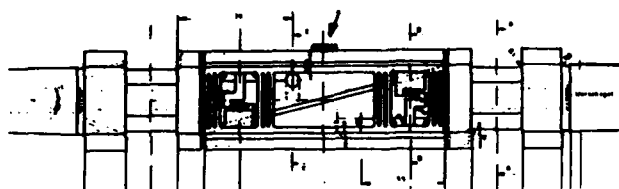
- : Position of Temperature Sensors
 ● : Position of Heating Elements

Temperature Gradient Test Arrangement

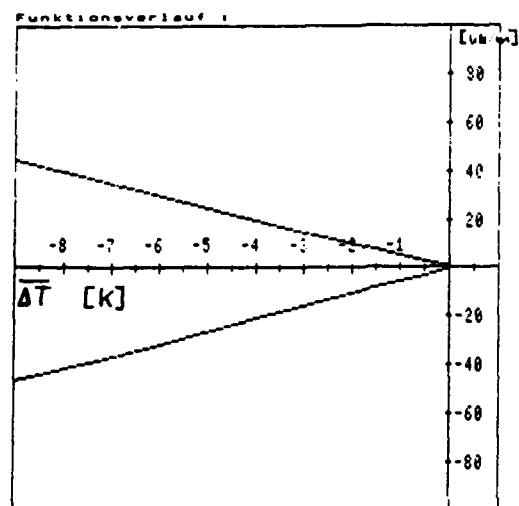


Signals due to Temperature Gradients

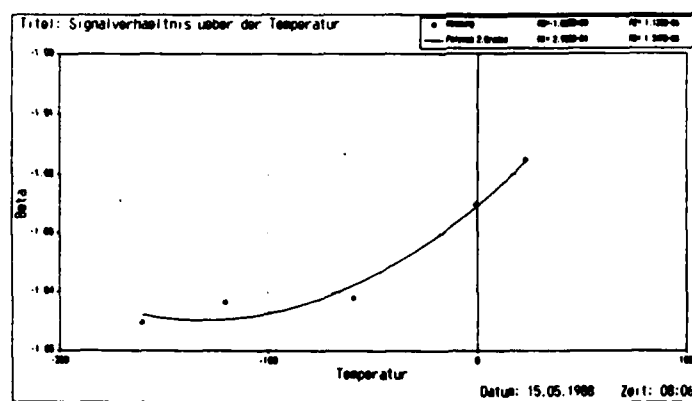
Fig. 4. Darmstadt University balance: a) design; b) tests on the central part.



Temperature Gradient Test
Arrangement W 609



Balance W 609, Signals due to
Temperature Gradients



Balance W 609, Ratio of Signals

Fig. 5. W 609 balance.

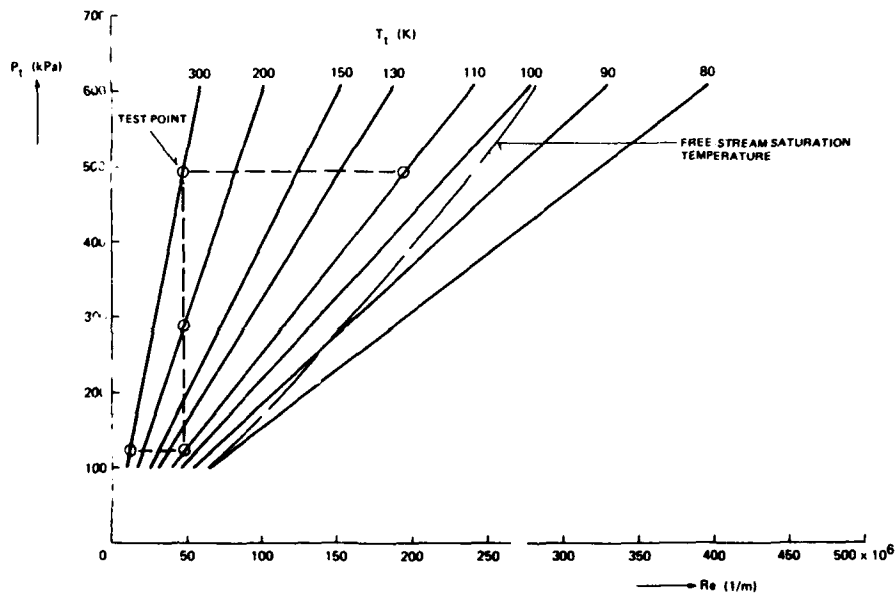
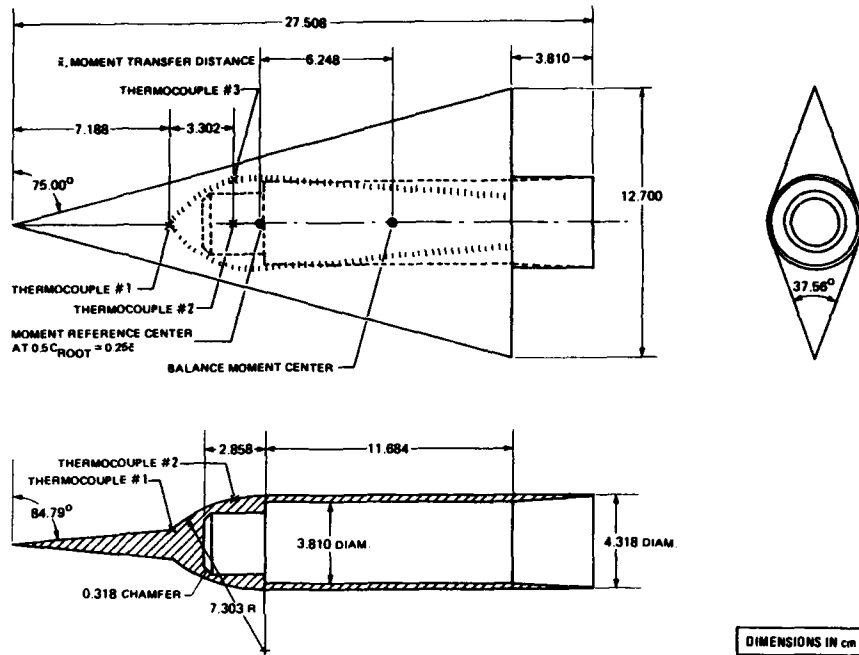


Fig. 6. Testing of NLR 771 balance in TCT.

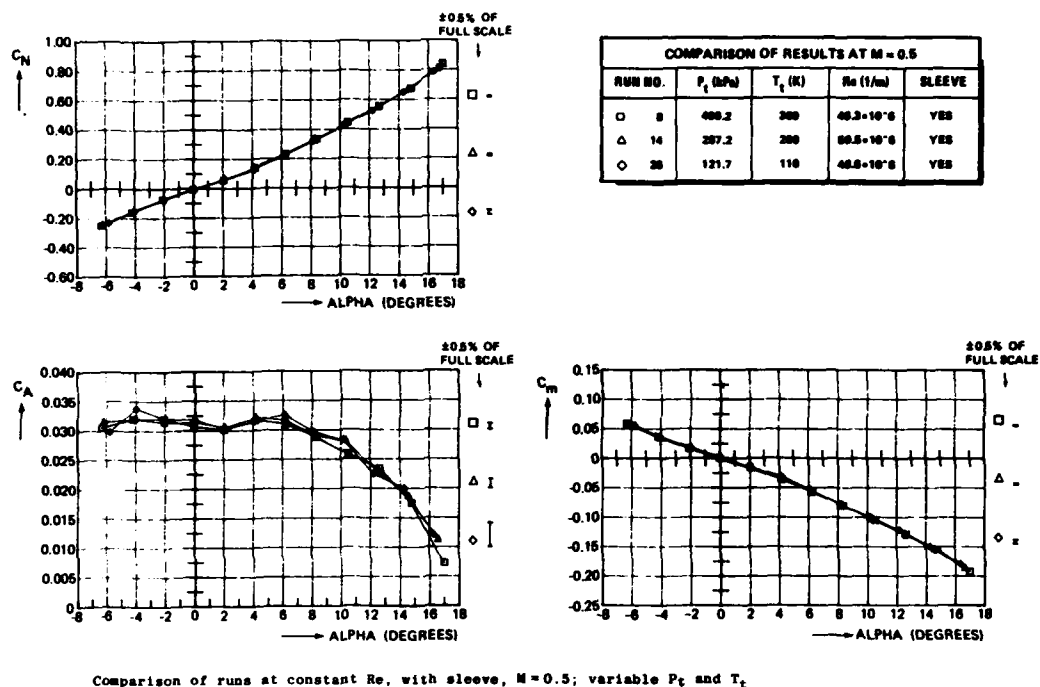


Fig. 7. Comparative testing with NLR balance.

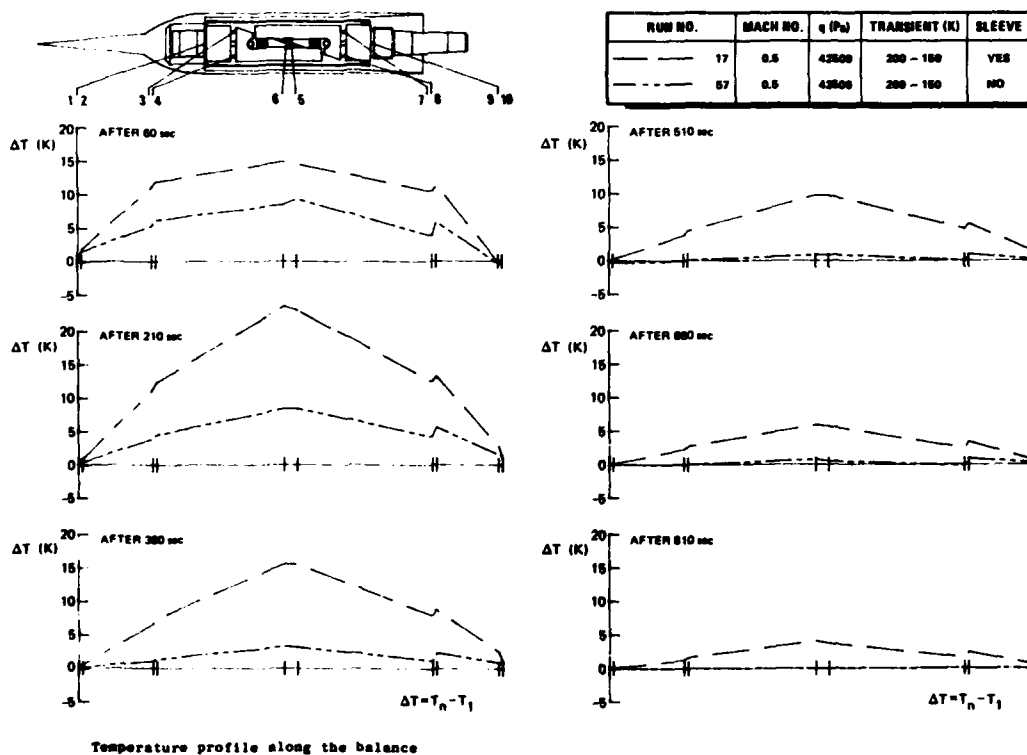
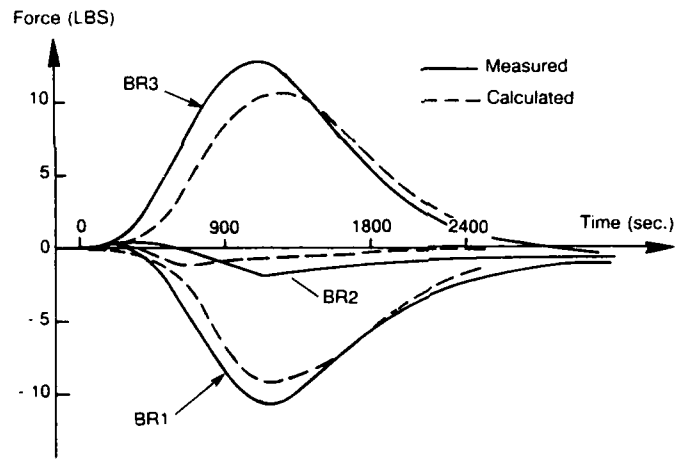
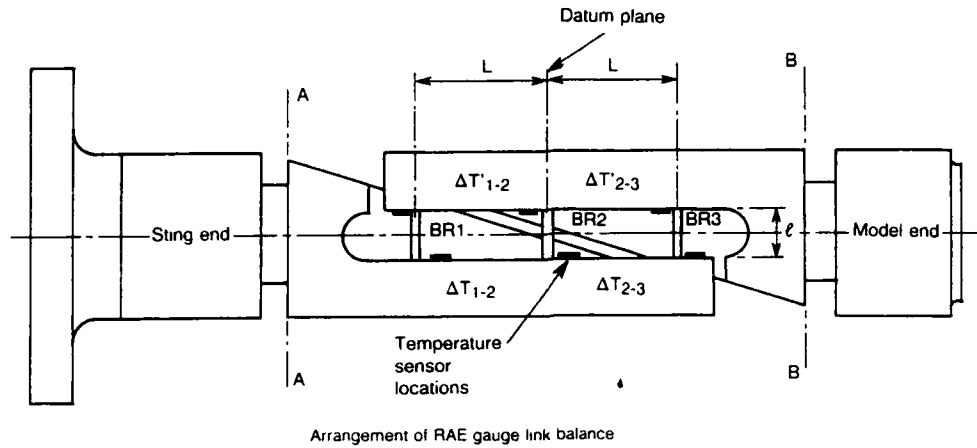
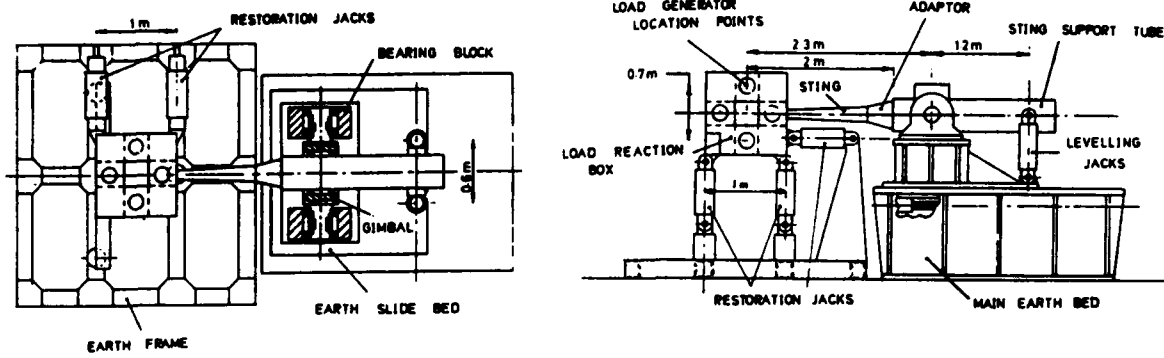


Fig. 8. Temperature distributions with NLR balance.

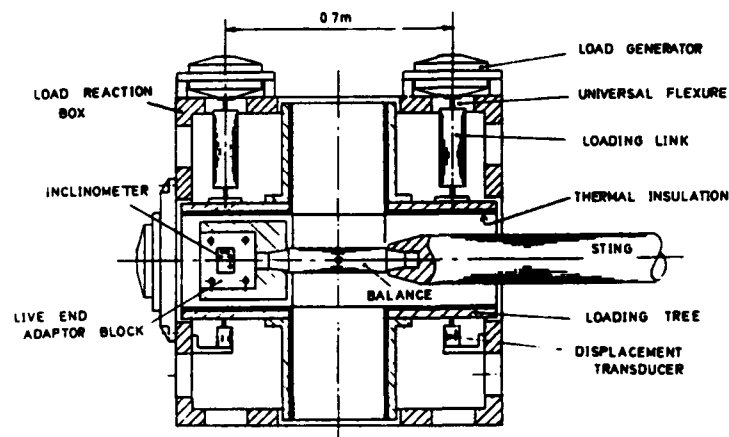


Comparison between measured and calculated thermal force changes in RAE gauge link balance

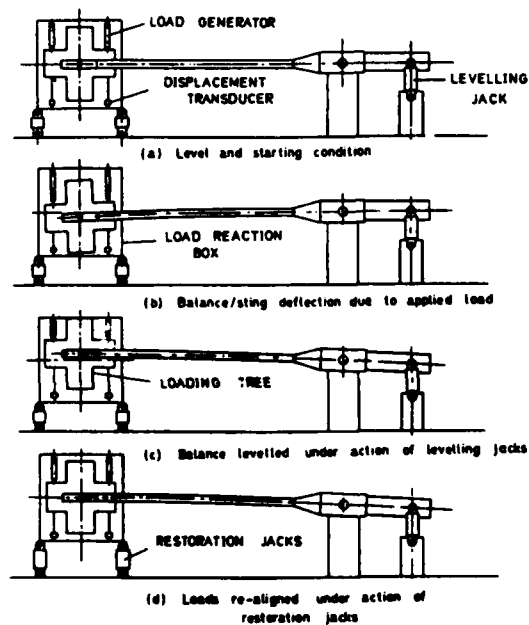
Fig. 9. Temperature distribution in a balance: comparison between computation and experimental results at RAE.



Main Elements of Calibration Machine.

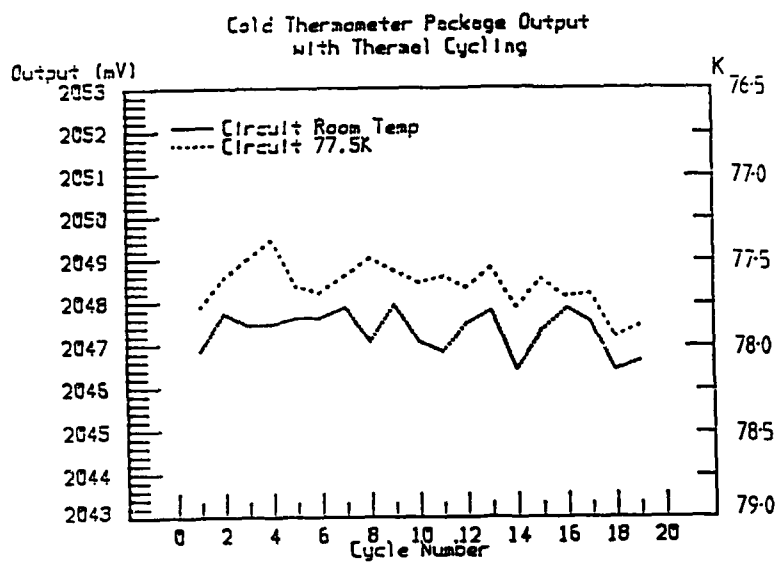


Loading Tree Assembly.

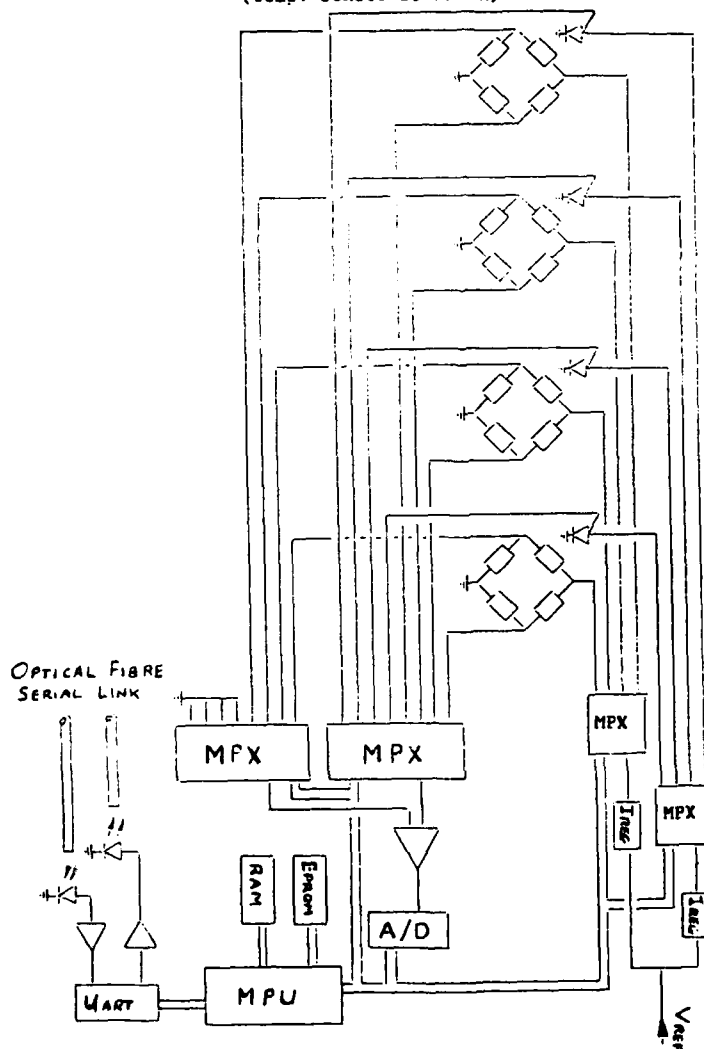


Principle of Levelling & Restoration Actions

Fig. 10. Cryogenic balance calibration facility: ARA design.

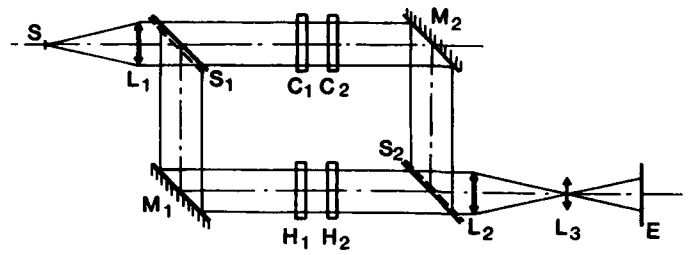


Cold thermometer package output with thermal cycling
between 77.5 and 300 K with the thermometer
package at 300 K and 77.5 K
(temp. sensor at 77.5K)

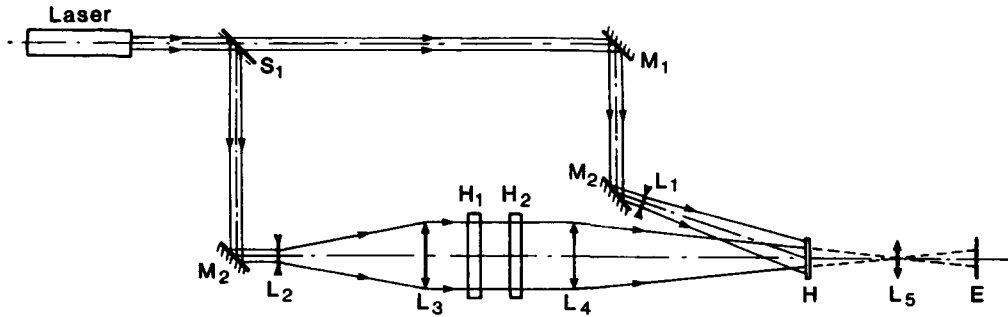


Cold Data Logger with 8 channels, 4 pressure,
4 temperature

Fig. 12. Principle of in situ instrumentation.

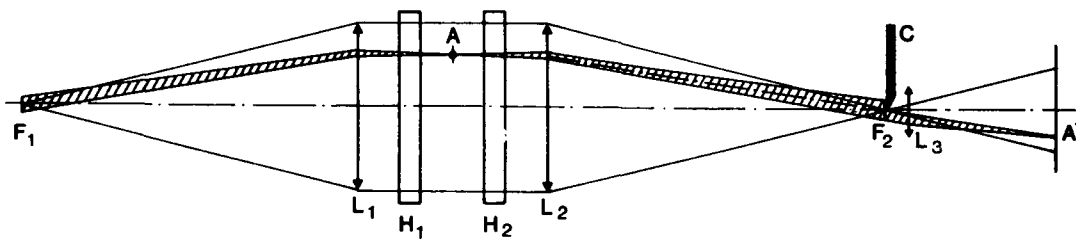


Mach-Zehnder interferometer.



Holographic interferometer.

Fig. 13. Interferometers.



strioscope.

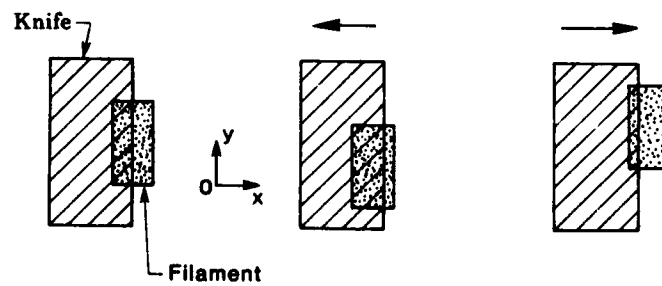


Fig. 14. Schlieren apparatus : principle.

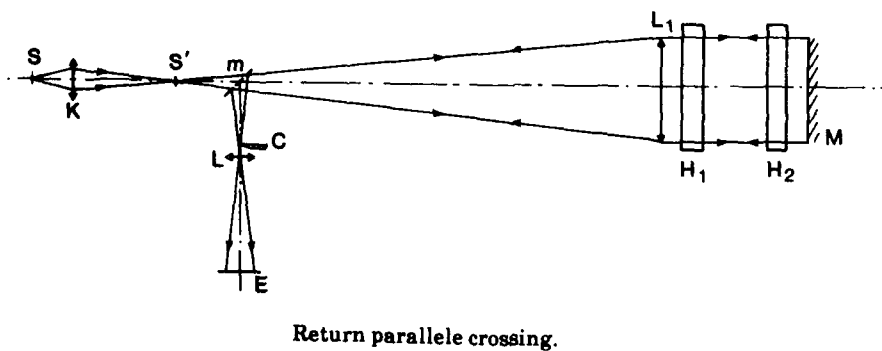
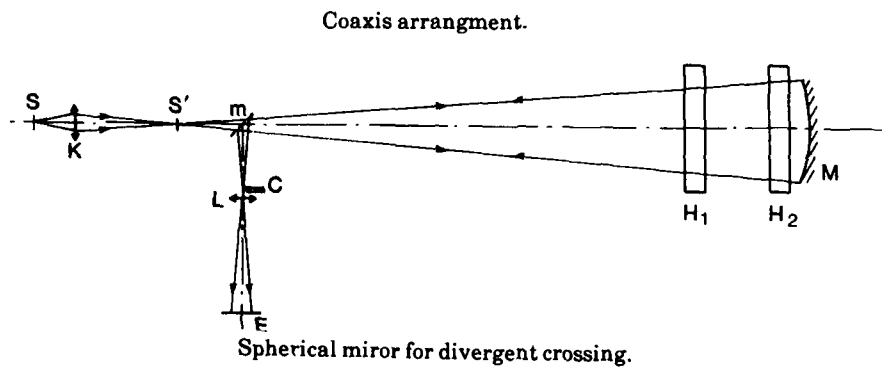
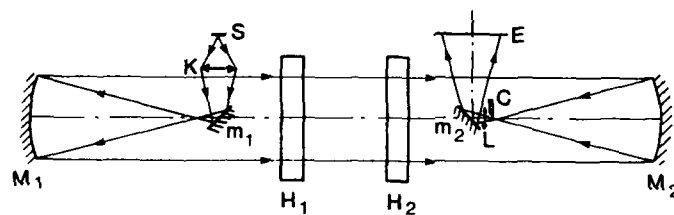
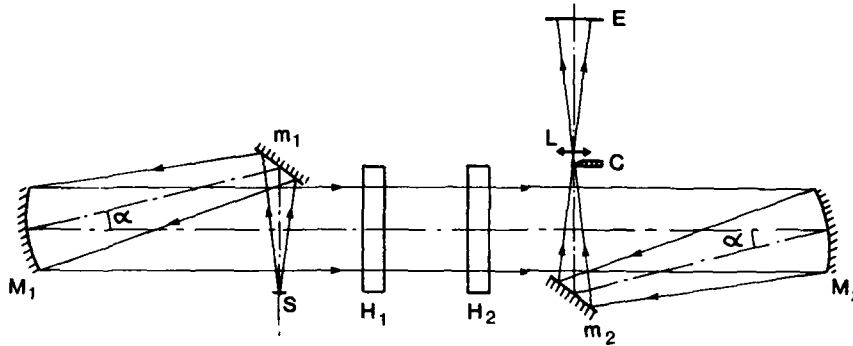
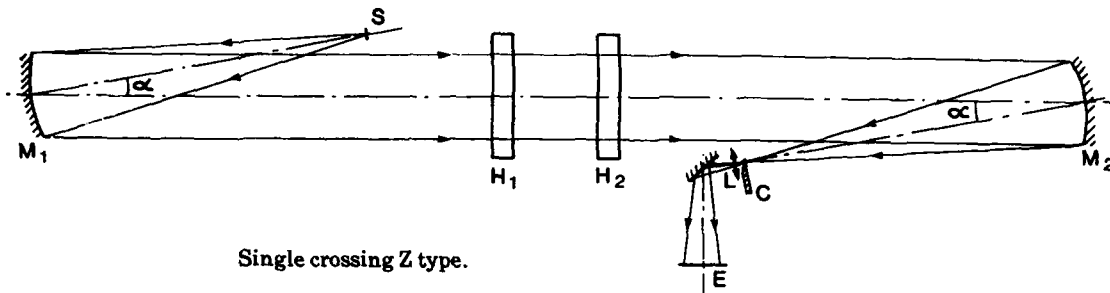
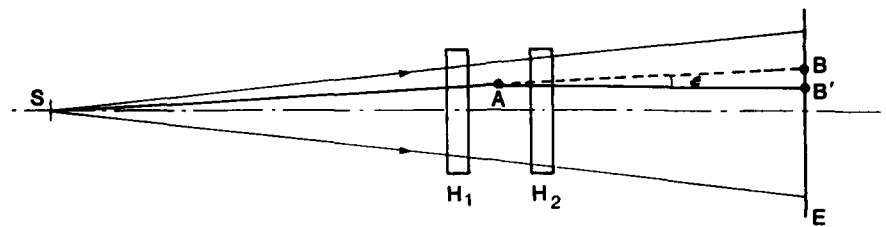
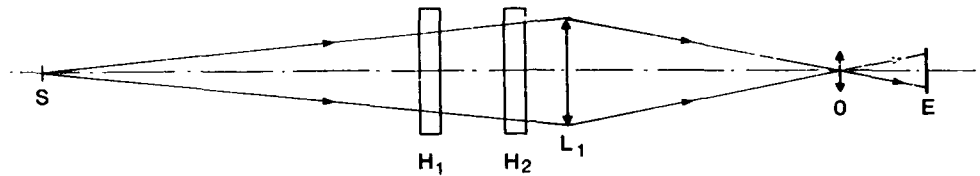


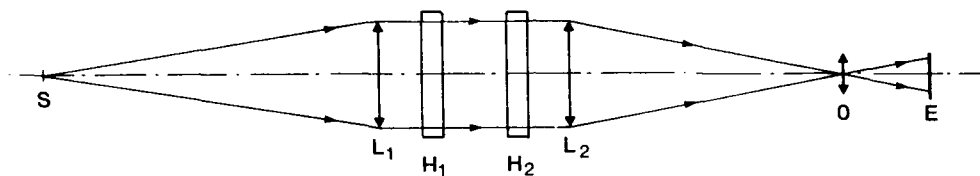
Fig. 15. Schlieren apparatus : optical diagrams.



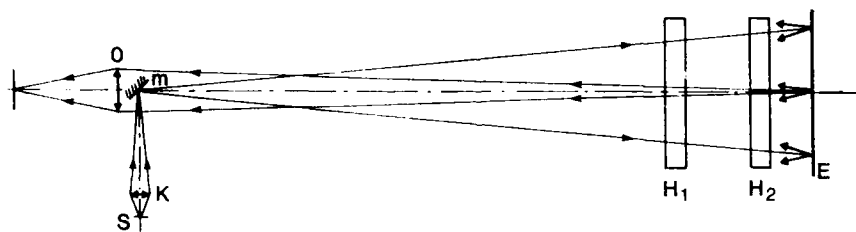
Shadowscope principle.



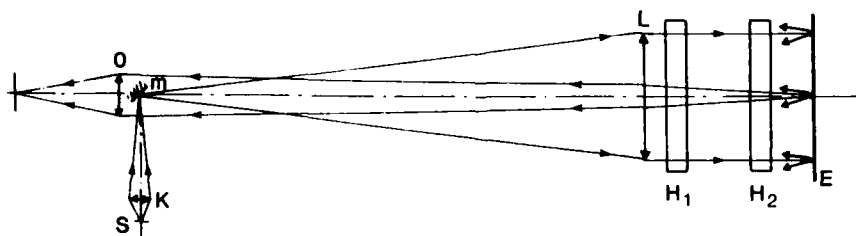
Divergent crossing.



Single parallele crossing.



Divergent return crossing



Parallele return crossing

Fig. 16. Shadowscopes.

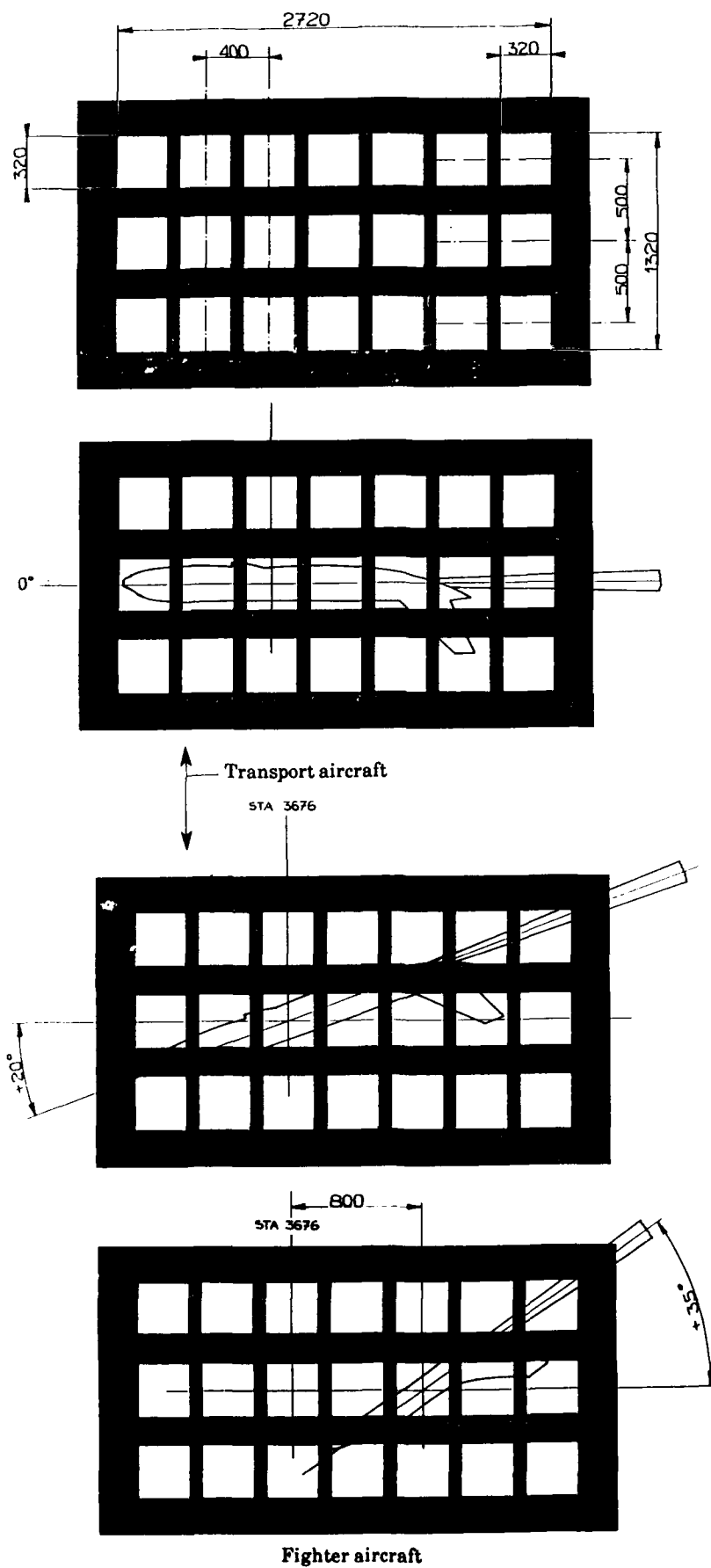


Fig. 17. Optical accesses in ETW for shadowscope observation.

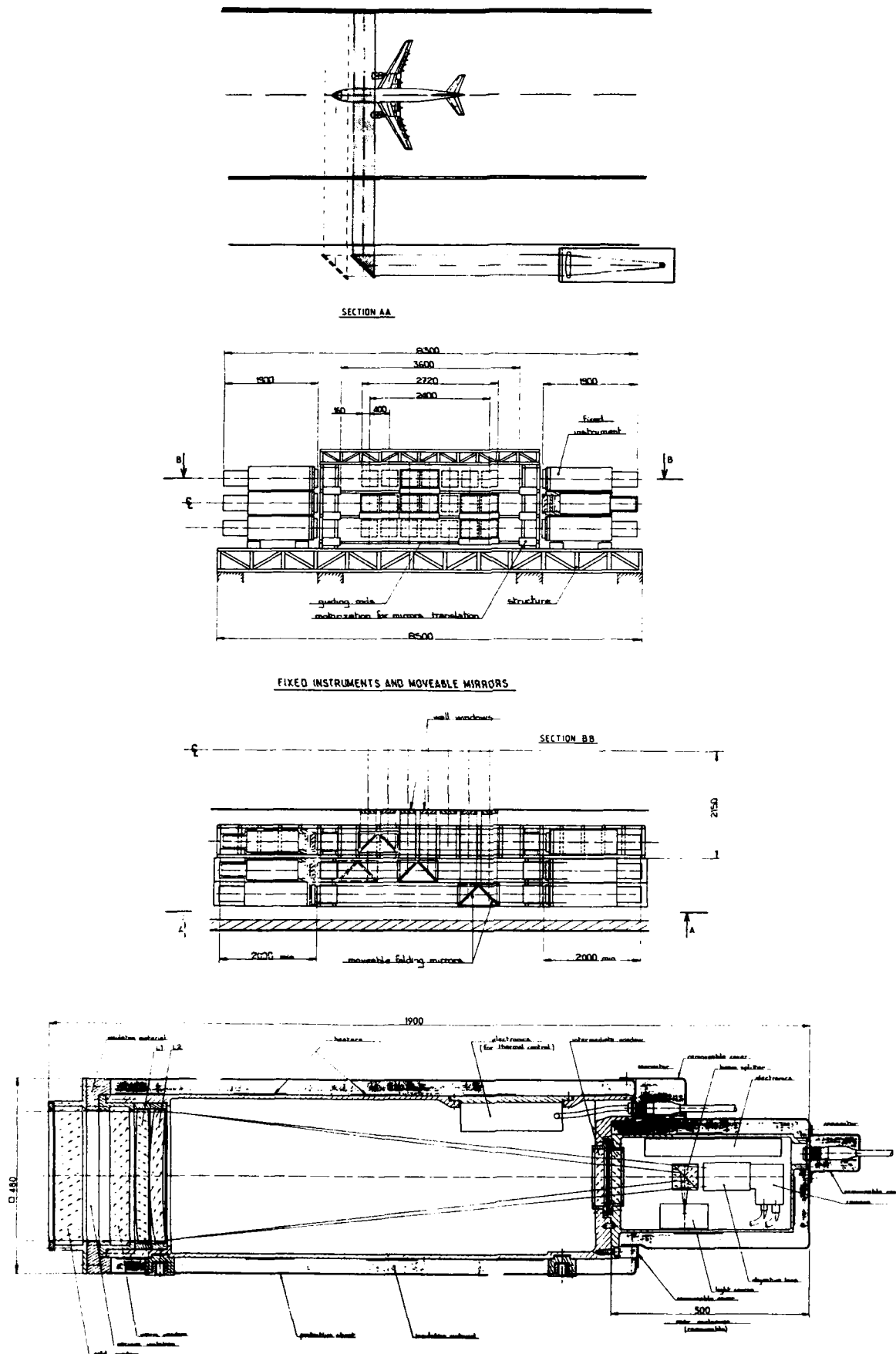


Fig. 18. Shadowscope with moving mirrors.

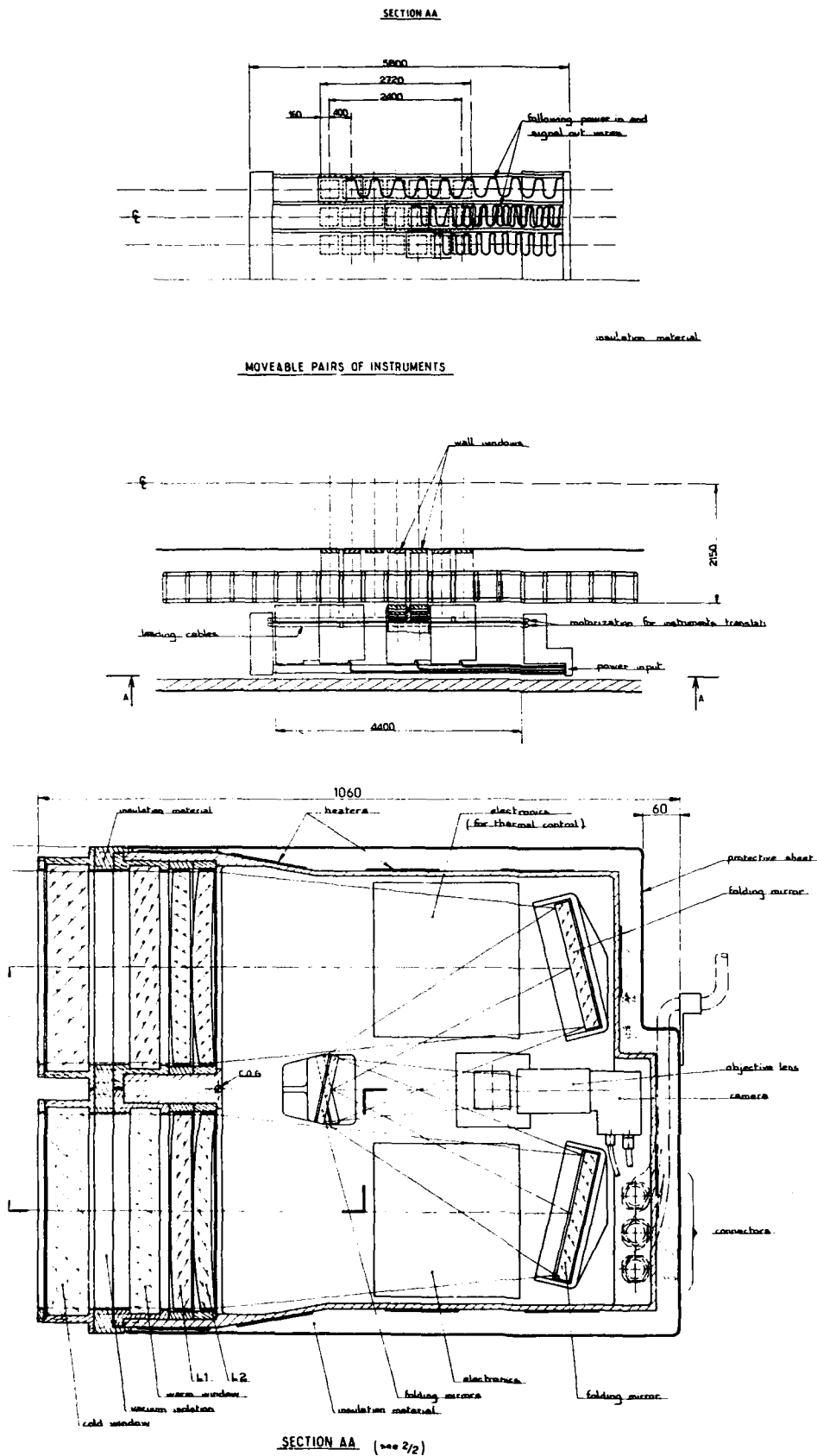
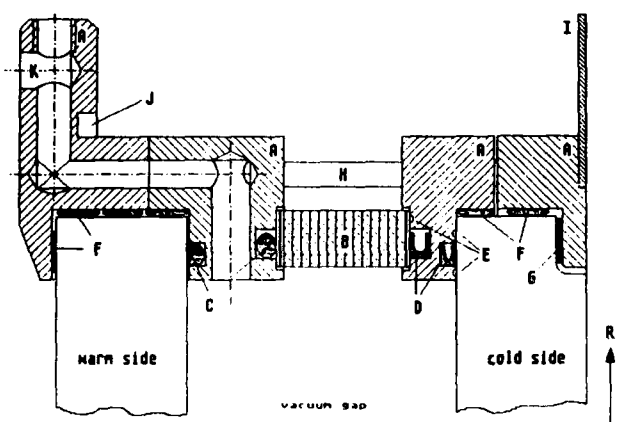


Fig. 19. Shadowscope with mobile transmitter/receiver.



Some details of the realized measurement window:

- A: stainless steel frame
- B: central isolation ring
- C: NBR-O-ring vacuum seals
- D: spring-loaded PTFE-rings
- E: location of Indium gaskets
- F: Teflon gaskets
- G: Graphite counterlayer
- I: Aluminium cold plate

Darmstadt window

ETW FLOW VISUALIZATION
WALL WINDOW

Scale 1:2

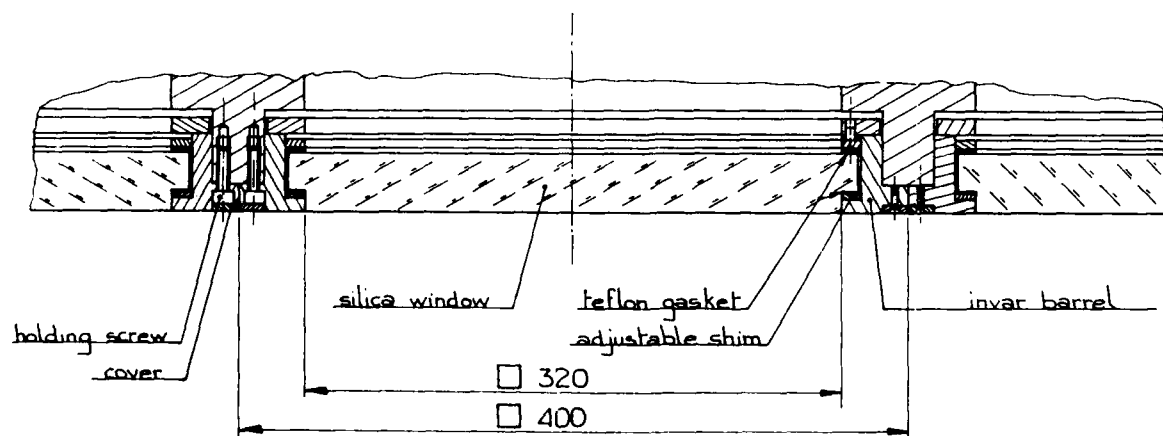
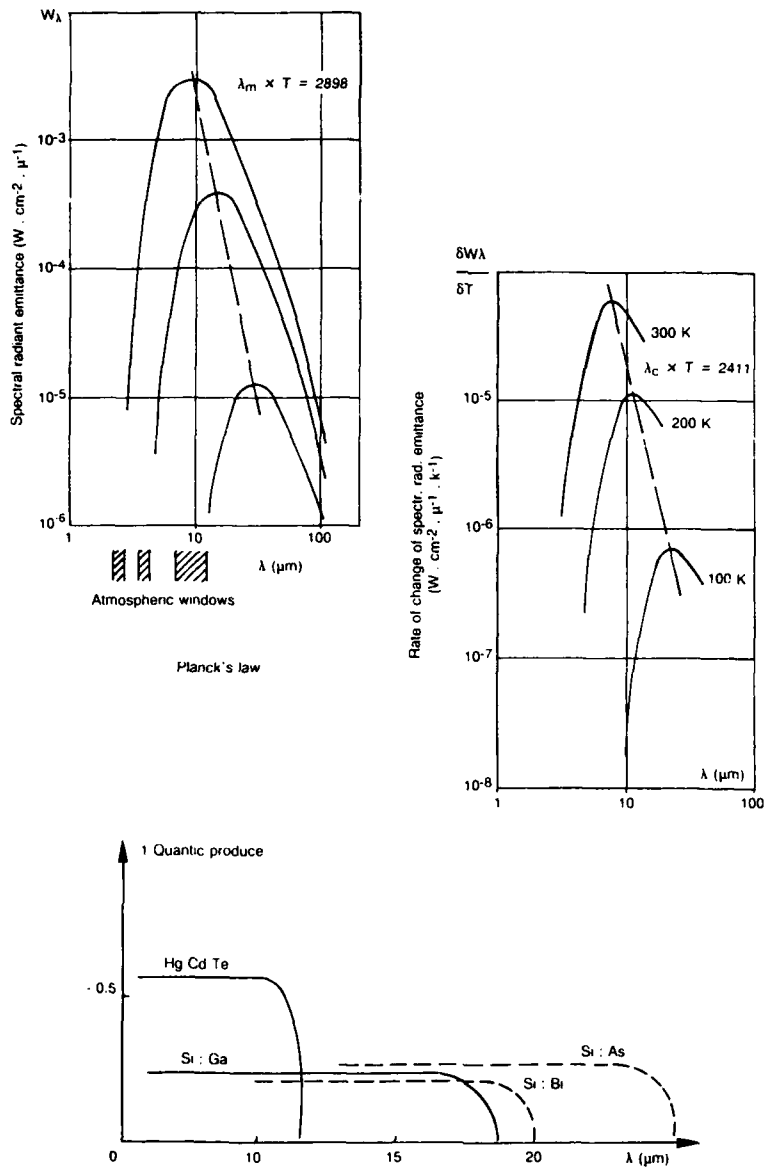


Fig. 20. Windows.



SOLUTION	CONFIG.	SENSOR MATERIAL	OPERATING TEMPERATURE	REMARKS
1	1 Element	Hg Cd Te	77 K (LN ₂)	<ul style="list-style-type: none"> very fast scanning large electrical bandwidth low SNR low thermal resolution
2	1 Matrix Array (64 x 4)	Si : Ga	20 K (LHe)	<ul style="list-style-type: none"> has to be developed expensive no off the shelf reasonably priced arrays/mosaics available
3	1 Line Array (1 x 128)	Hg Cd Te	77 K (LN ₂)	<ul style="list-style-type: none"> no off the shelf arrays/mosaics available for $\lambda_{CO} > 20 \mu m$ very expensive nonuniform detectors complex signal processing
4	1 Matrix Array (62 x 58)	Si Sb	8 K (LHe)	<ul style="list-style-type: none"> reasonably priced off the shelf mosaics are available good performance and uniformity BLIP-operation preferred solution
5	4 Matrix Arrays (62 x 58 each)	Si Sb	8 K (LHe)	<ul style="list-style-type: none"> see solution 4 but complex focal plane due to detector leads arrangement

Fig. 21. Planck's laws and sensitivity of infrared detectors.

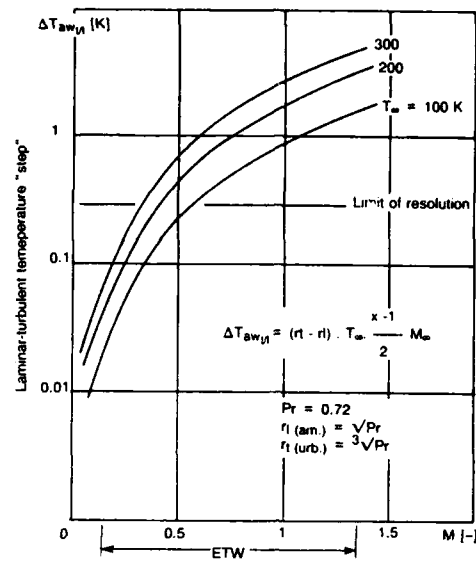


Fig. 22. Wall temperature differences at transition.

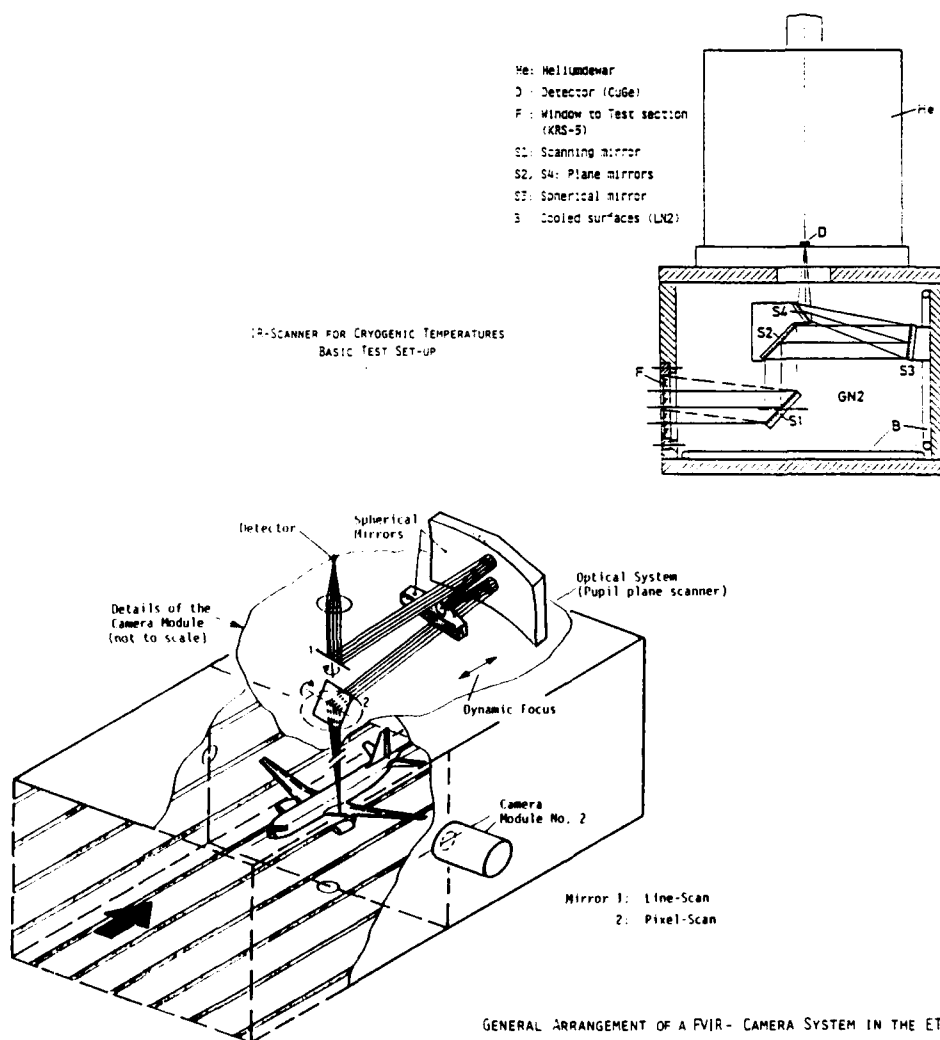


Fig. 23. Thermovision system.

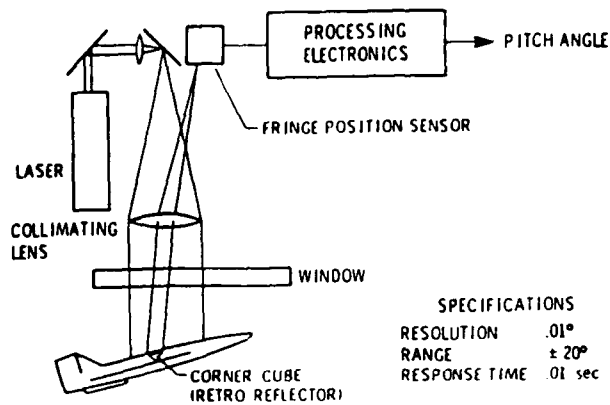
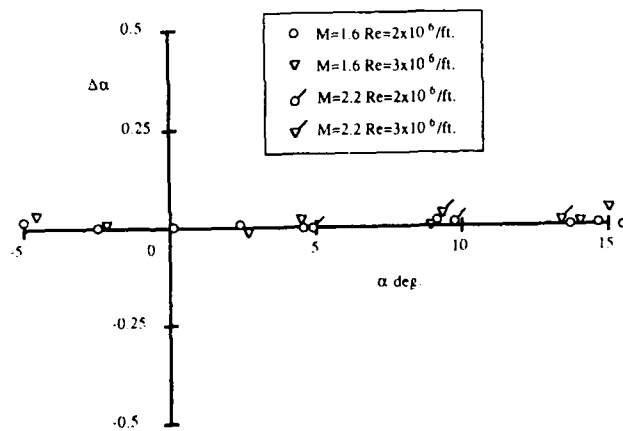
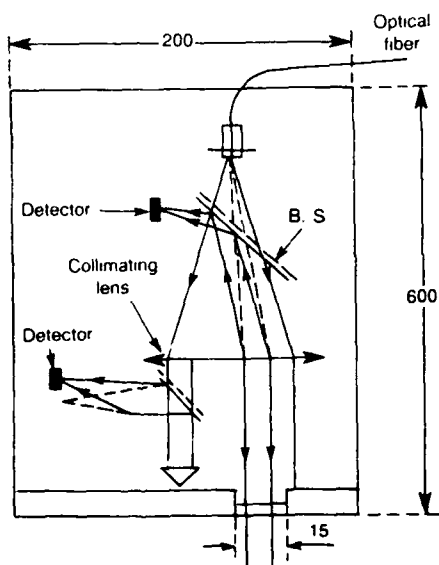
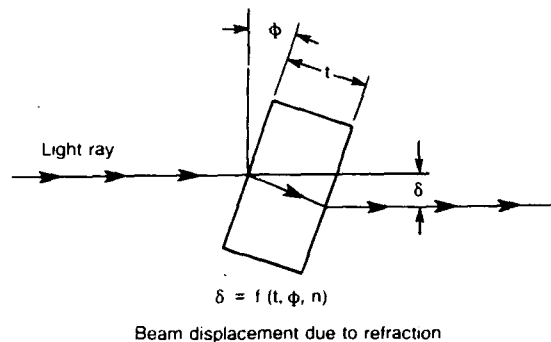


Fig. 26. Attitude detector: installation in the test section.



Comparison of In-situ Optical and Mechanical Angle of Attack Measurements in Ames 9- x 7- Ft. Supersonic Wind Tunnel.

Fig. 27. Refraction attitude detector.

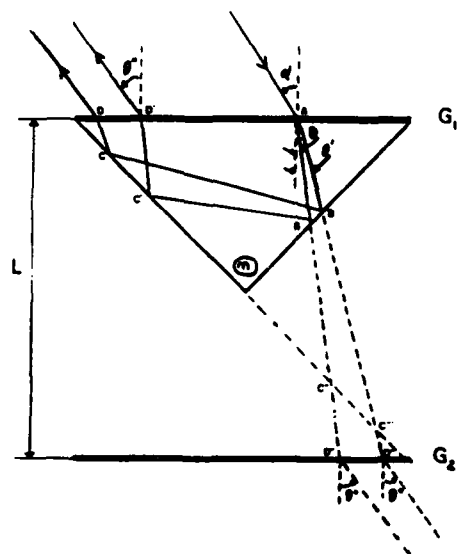
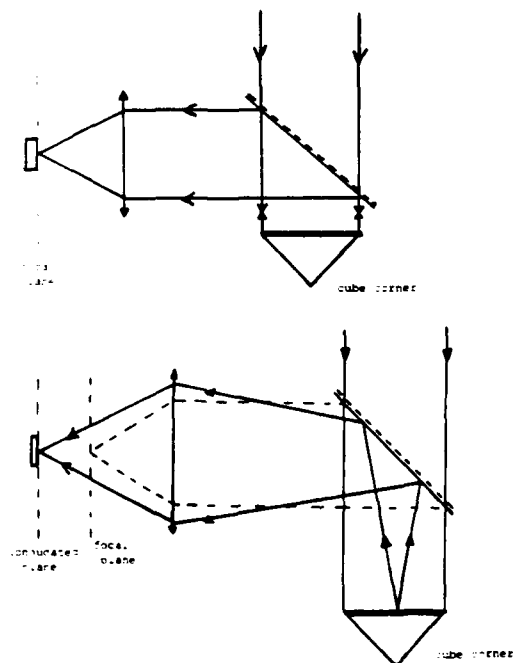


Fig. 24. Cubic wedge attitude detector: holographic interferometry.



	: Diffraction	: Pitch	: R	: Computed fringe	: Measured fringe
: Round	: angle(degree):P (m)	: (mm)	: angle (degree)	: angle (degree)	
: 15950	: 0.5	: 72.5	: 11.4	: 0.546	: 0.55
: 15951	: 0.5	: 72.5	: 11.4	: 0.546	: 0.55
: 15952	: 1	: 36.25	: 11.4	: 0.273	: 0.275
: 15953	: 2	: 18.13	: 11.4	: 0.136	: 0.138
: 15956	: 1	: 36.25	: 11.4	: 0.273	: 0.275
: 15959	: 2	: 18.13	: 11.4	: 0.136	: 0.138
: 15960	: 1	: 36.25	: 9.6	: 0.324	: 0.335
: 15961	: 2	: 18.13	: 9.6	: 0.162	: 0.164

Fig. 25. Cubic wedge attitude detector: moiré effect.

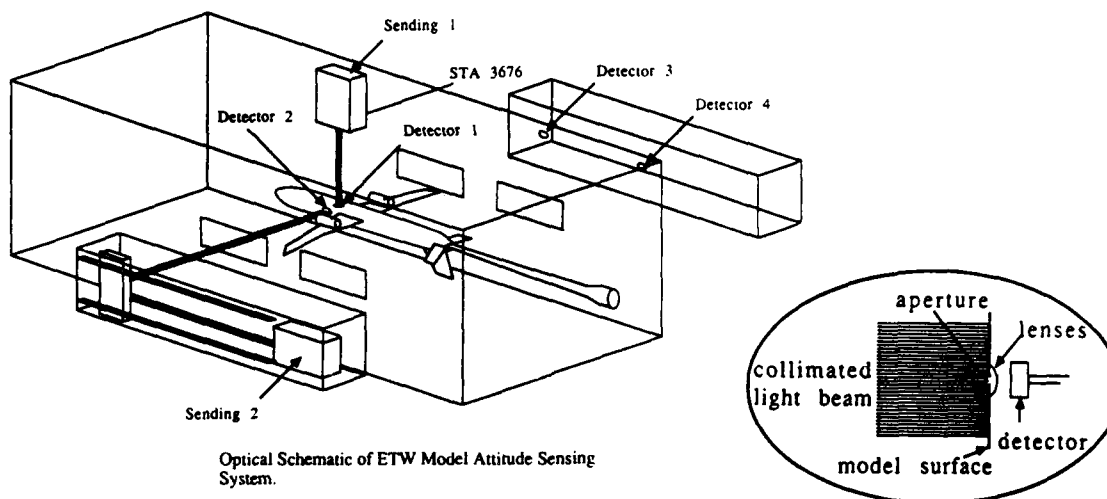
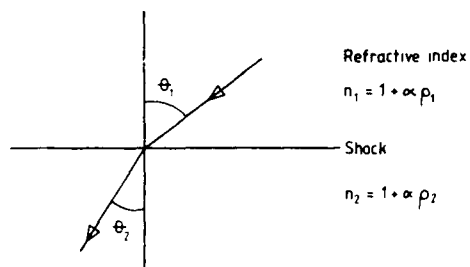


Fig. 28. Installation of an attitude detection system in ETW.



Snell's Law

$$\frac{\sin \theta_1}{\sin \theta_2} = \frac{n_1}{n_2}$$

$$= 1 + \alpha (\rho_1 - \rho_2)$$

when $1 \gg \alpha \rho$

For shock of strength 2 & $\rho_1 = 2.444 \text{ kg/m}^3$

$$\frac{\sin \theta_2}{\sin \theta_1} = 0.999421$$

REFRACTION OF LIGHT BEAM THROUGH
A SHOCK WAVE

θ_1°	θ_2°	$\Delta\theta^\circ$
90	88.05	1.95
75	74.88	0.12
60	59.94	0.06
45	44.97	0.03
30	29.98	0.02
15	14.99	0.01

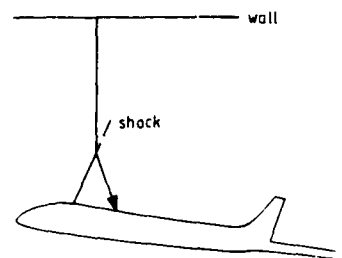
ANGULAR DEFLECTION OF LIGHT BEAM
THROUGH SHOCK WAVE FOR CASE CONSIDERED
($\sin \theta_2 / \sin \theta_1 = 0.999421$)ILLUSTRATION OF POSSIBLE REFRACTION
OF LIGHT BEAM THROUGH SHOCKFor $\sin \theta_2 / \sin \theta_1 = 0.999421$ and
beam intersecting shock at 5° ($\theta_1 = 85^\circ$),
beam deflection $\Delta\theta = 0.37^\circ$

Fig. 29. Defects in the accuracy of optical systems in wind tunnels.

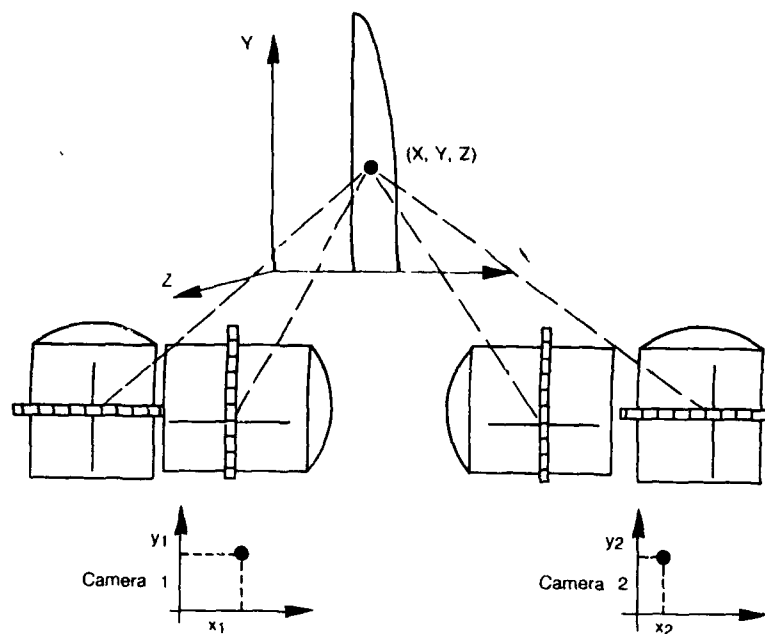


Fig. 30 - RADAC system.

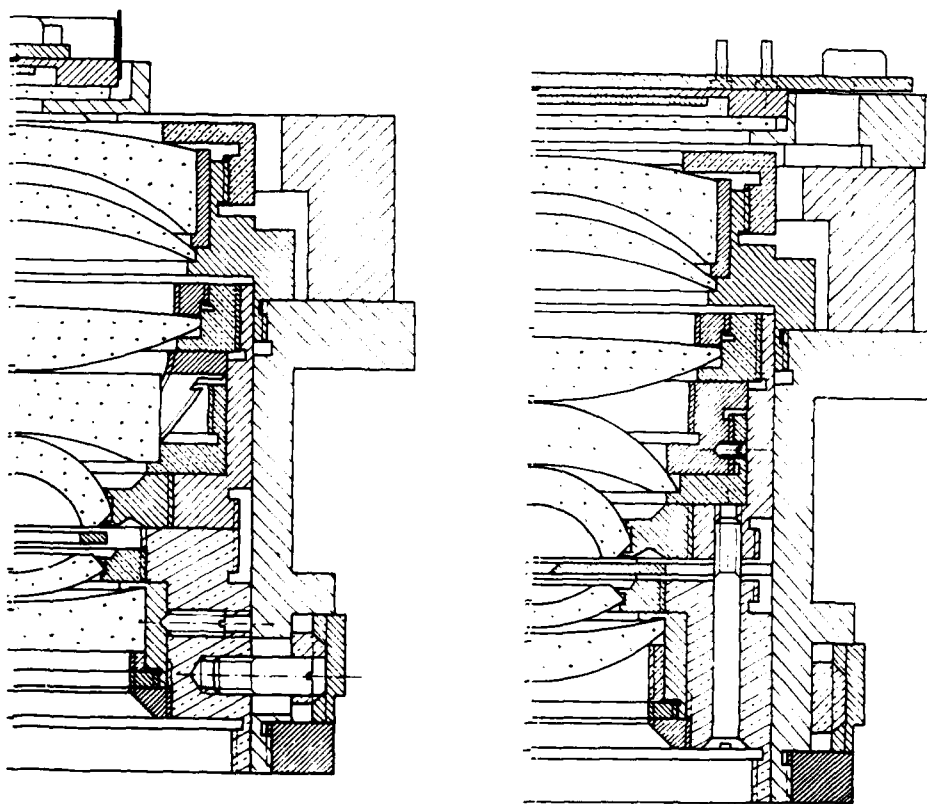


Fig. 31 - RADAC camera.

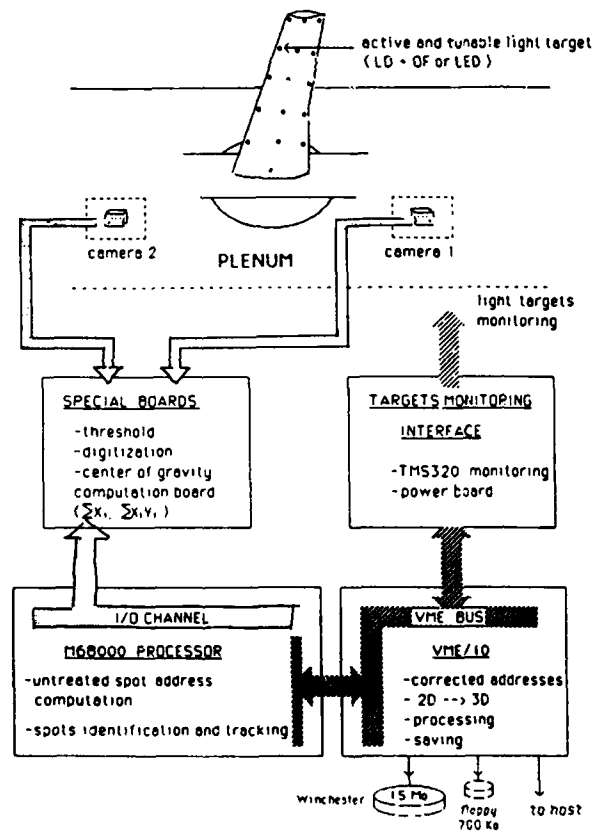


Fig. 32. Project for installation of RADAC in ETW.

FUNDAMENTAL CONSIDERATIONS IN TESTING IN CRYOGENIC WIND TUNNELS

André MIGNOSI

Office National d'Etudes et de Recherches Aéronautiques
Centre d'Etudes et de Recherches de Toulouse
Département d'Aérodynamique
2 avenue E. Belin - 31055 TOULOUSE Cedex (FRANCE)

ABSTRACT

The cryogenic technology for wind tunnel testing is strongly connected with the aerodynamic requirements. This paper concerns a number of aerodynamic problems mainly related to cryogenic testing. The first part describes the various factors involved to achieve the best similarity possible between an aircraft in flight and the model in the wind tunnel. The second part covers the analysis of these factors : effect of a non adiabatic wall, boundary layer transition, two-dimensional and three-dimensional tests, effects of the Reynolds number. In this paper, it is attempted to alternate theoretical considerations with practical examples in order to illustrate the importance of "experimental/theoretical" correlations.

MAIN NOTATIONS

c, C	chord, heat capacity	M	Mach number
C_D, C_L	drag, lift coefficients	u, v, w	velocity
C_f	skin friction coefficient	ρ	density
δ	boundary layer thickness	p	pressure
$\delta_1 = \int_0^{\delta} \left(1 - \frac{\rho u}{\rho_e u_e}\right) dy$	displacement thickness	μ	gas viscosity
$\delta_{11} = \int_0^{\delta} \left(1 - \frac{u}{u_e}\right) dy$	incompressible displacement thickness	$\gamma = C_p/C_v$	ratio of specific heats
$\theta = \int_0^{\delta} \frac{\rho u}{\rho_e u_e} \left(1 - \frac{u}{u_e}\right) dy$	momentum thickness	$q = \frac{1}{2} \rho u^2$	dynamic pressure
$\theta_1 = \int_0^{\delta} \frac{u}{u_e} \left(1 - \frac{u}{u_e}\right) dy$	incompressible momentum thickness	T	temperature
$Tu = \frac{\sqrt{u'^2}}{u}$	turbulence intensity	$R_x = \frac{\rho u x}{\mu}$	Reynolds number related to x
$H = \delta_1/\theta$	shape factor	α	angle of attack
$H_1 = \delta_{11}/\theta_1$	incompressible shape factor	ϕ	thermal flux
$\bar{K} = g/g_0$ or $\frac{g}{g_{aw}}$	ratio to a reference case or to adiabatic wall conditions	g	any variable quantity

$\gamma_{\text{effective}} = [\partial(\log p)/\partial(\log p)]_s$ partial derivative at constant entropy

Subscripts

cr	critical	w	wall
t	total pressure or temperature value	AW	adiabatic wall
T	transition	R/m	Reynolds per meter
∞	value at infinity		

1 - INTRODUCTION

The development and the use of cryogenic wind tunnels today represent a considerable progress in the area of aerodynamic testing. Cryogenic wind tunnels, in which the Reynolds number can be as high as that in flight, offer the unique advantage of an independent variation of the dynamic pressure $q = \frac{1}{2} \rho V^2$ and of the Reynolds number $R_c = \frac{\rho u c}{\mu}$ by varying the gas temperature and pressure. It is thus possible to dissociate a number of parameters heretofore coupled, such as deformation of the model and viscous effects as shown in Part 5.2.

This new wind tunnel technique available to scientists and manufacturers provides aerodynamic data in a broad domain of Reynolds numbers, allowing a better analysis of aerodynamic phenomena which can improve the prediction and the optimization of aircraft performances (figure 1). However, a number of difficulties related to cryogenics and often to aerodynamics in general must not be underestimated and it is necessary to preserve a critical attitude. Testing in a wind tunnel always involves a complex set of elements : model, support, instrumentation, "wind tunnel system", computation, data processing, etc, which must be consistent and of the best quality possible.

In this paper, we will attempt to demonstrate that the two main parameters of similarity, i.e. the Mach number and the Reynolds number, are not sufficient. A number of other parameters must be taken into account (figure 2) such as wall and sting interferences, model deformations, flow qualities in the wind tunnel, thermal fluxes on the model resulting from a disequilibrium, surface roughness, etc. Another advantage of cryogenic wind tunnels is to allow aerodynamic research to be carried out for a wide variation of Reynolds numbers.

Beside the experiments, the theoretical field has achieved important progresses in numerical methods as well as in complex viscous flow modelling. Experiments can often be checked by theoretical codes (figure 1) to confirm the coherence of the data but, conversely, the experimental data can be used to re-adjust the theoretical models or to take into account a number of parameters which were initially ignored at the start of theoretical analysis.

2 - PROBLEMS RELATED TO CRYOGENIC TESTING

When it is attempted to achieve the best possible similarity between an aircraft in flight and a model in a cryogenic wind tunnel, it is important to take into account a number of parameters, as shown in the figure 2. In addition to conventional variables such as Reynolds number and Mach number, it appears important to analyse the real gas effect and the low temperatures limitations. A number of other parameters will be studied below, mainly the non adiabatic wall effect, the transition effect and the effect of the Reynolds number.

2.1. Real gas effect

An objection which arises immediately concerns the large variations in the ratio γ of specific heats as a function of temperature for nitrogen. This objection as well as many others were practically eliminated thanks to the important works conducted at NASA by LANGLEY [3] and a few works conducted by the DFVLR, the NLR, the RAE and ONERA. In this paper, we will retain only the following essential points. If the real gas effects are studied for an isentropic flow using the best possible formulations (nitrogen characteristics given by JACOBSEN or the state equation given by BEATTIE-BRIDGEMAN), it is observed that the isentropic expansion coefficient $\gamma_{\text{effective}} = (\partial \log p / \partial \log p)_s$ remains very close to 1.4 for a wide range of pressures and temperatures : $p_t < 6$ bars and $T > T$ (saturation).

It is observed that these differences can be considered as negligible. Similar computations performed for the PRANDTL-MEYER expansion and for a normal shock demonstrated the same small differences.

The studies also show that the gas used can be nitrogen or air. In both cases, the real gas effects are negligible providing they are compared with an ideal gas preserving a constant γ of 1.4.

Many tests, conducted in T.C.T., T2, etc, show excellent correlation according as the same Reynolds number is obtained by increasing the pressure or decreasing the temperature (figure 3).

2.2. Minimum operating temperature limit

The minimum temperature limit seems to be related to the appearance of the liquid phase in the test section. The liquid phase appears probably upstream of the model by heterogeneous condensation, small particles present in the flow (dust, ice, ...) which can initiate the creation and the growth of droplets without any delay phenomenon.

3 - EFFECTS OF A NON ADIABATIC MODEL WALL

3.1. Initial approach in the case of a laminar boundary layer on a flat plate

Analyzing the development of a laminar boundary layer of very small initial thickness located in a flow with a constant Mach number of $M = 1.2$ computed by a finite volume method makes it possible to observe the following phenomena when the wall temperature is varied (figure 4) :

- The variation in the displacement thickness δ_1 is parabolic as a function of the abscissa (as appears in the initial equations for $\varphi = 0$). In addition, this thickness increases when the wall is heated.

- The variation in the momentum thickness θ is identical to that of δ_1 as a function of the abscissa but is not particularly sensitive to the wall temperature.

- There is a decrease in the local skin friction coefficient C_f and a low sensitivity of this coefficient as a function of T_w/T_{Aw} . This result is also given by the relation $C_f/2 = d\theta/dx$.

The wall temperature effect is illustrated in the figure 5 where the variation in the integral values of the boundary layer, δ_1 , δ_{11} , θ , θ_1 and the friction coefficient C_f as well as the form parameters H and H_1 are plotted for a fixed abscissa. In this figure, the various values are related to the adiabatic values noted AW for $R_x = 2$ and 10 million, giving approximately the same result for the reduced parameter $\bar{X} = g/g_{Aw}$. For a hot wall, a substantial increase in H and δ_1 is observed, a more moderate increase in δ_{11} and θ_1 whereas H_1 varies only by 1 percent. On the other hand, θ and C_f decrease very slightly, by approximately 0.5 percent. The wall temperature effect can be compared with the Reynolds number effect for an adiabatic wall (figure 6). According to the boundary layer equations, all variables δ_1 , δ_{11} , θ , θ_1 , C_f vary as $1/\sqrt{R_x}$, which means that H and H_1 remain constant. There is also an enormous variation in the integral and friction values, divided by $\sqrt{2} = 1.41$, when the Reynolds number is multiplied by 2.

3.2. Case of a turbulent boundary layer on a flat plate

A computation case corresponding to $M = 1.2$, $T_t = 120$ K, $p_t = 2$ bars is illustrated in the figure 7 where the variation of δ_1 , θ , C_f is plotted versus the abscissa for three wall temperatures.

The finite volume method applied uses a mixing length concept developed at the DERAT (the programs used were developed by B. AUPOIX). A much more linear variation in δ_1 and θ versus the abscissa is noticed immediately as well as the relatively low decrease in the friction coefficient, with a value substantially above that of the laminar case. When the wall is heated, all the parameters are affected : δ_1 increases, θ and C_f decrease.

The wall temperature effect on the boundary layer parameters is illustrated in the figure 8. As for the laminar case, all the values are related to two adiabatic values : $R_x = 20$ and 100 million, giving approximately the same result. For a hot wall, a considerable increase in H and δ_1 is observed whereas θ and C_f decrease by approximately 3.5 percent. However, the incompressible shape factor H_1 remains practically constant.

The wall temperature effect can be compared with the Reynolds number effect for an adiabatic wall (figure 9). In this case, it can be noted that the decrease in the shape factors H and H_1 of the boundary layer is very small, approximately 1 percent, when the Reynolds number is doubled, with a decrease of approximately 10 percent in the other values.

In conclusion, as for the laminar case, a hot wall thickens the boundary layer displacement thickness δ_1 . As the friction of the boundary layer is decreased, it tends to separate earlier in the areas of the profile where the velocity gradient is negative. Several differences in sensitivity between a laminar and a turbulent boundary layer are also noted, both as a function of T_w/T_{Aw} and of the Reynolds number.

3.3. Effect of non adiabatic wall on the streamwise transition

As it will be seen in the section on transition, small disturbances develop in the laminar boundary layer and become amplified until turbulence occurs. Wall heating leads to an earlier transition. Experiments as well as linearized stability theory give clear information about the great sensitivity of the wall temperature on the transition location in the case of a constant Mach number distribution. The figure 10, from reference [7], illustrates this effect on a 10° cone in flight and in wind tunnel.

A conventional criterion consists of stating that the transition corresponds to a disturbance amplified by a factor of $e^9 \approx 8\,000$ for flight test where the turbulence intensity is small Ref. [10]. In figure 10, the authors also plotted the theoretical curve for $M_\infty = 0.85$. It can be concluded that the transition location is very sensitive to wall temperature at constant Mach number since an increase of one percent in the wall temperature is equivalent to a decrease of 4 to 7 percent in the transition Reynolds number (Ref. [5], [7]).

3.4. Experimental examples of non adiabatic wall effects

The first example, drawn from the theoretical study conducted at NASA by LANGLEY (Ref. [6]), concerns the stabilization time of models subjected to rapid variation in the total temperature of the flow, from 165 to 115 K (dynamic range provided by the NTF wind tunnel : $\Delta T = 50$ K). Two important points were revealed by this study. For the case considered in the figure 11, a precision of 8 percent on the temperature appears to be sufficient so as not to result in an error above ± 0.0001 on the drag coefficient C_D .

In addition, the time required to reach equilibrium may be very long. A good solution consists of using hollow models.

A second example, given in figure 12, was made at room temperature in the T2 wind tunnel with the CAST 10 profile with a free transition, in a case where the transition location could be observed (ref. [22]). This location is identified by a disturbance which occurs in distribution of the Mach number, both on the lower surface where oil visualizations showed a practically fixed separation bubble and on the upper surface where a free transition occurred in an area where the Mach number was roughly equal to 1. Visualizations as well as the temperature variation of the model and the computation demonstrated the correlation between the location given by the bump in the Mach number distribution and the transition.

In the figure 13, the variation of the transition abscissa, identified by the start and end of the bump, is plotted as a function of the average profile temperature. The large variation of this transition abscissa versus the T_w/T_{AW} ratio can be observed.

The same figure also shows the variations in lift and drag. Drag, in this particular case, is relatively insensitive to the temperature ratio.

The movement of the transition was compared with the Reynolds number effect in this specific case. A formula of the type $R_T/R_{TA} = (T_w/T_{AW})^{-4}$ appears to give a good approximation of the phenomenon.

4 - PROBLEMS RELATED TO TRANSITION OF THE BOUNDARY LAYER

4.1. First two-dimensional approach to free transition on a flat plate

In order to gain a good understanding of the role played by transition on the drag of a flat plate ($C_D = (4 \theta_{Te})/c$), the figure 14 shows the variation of C_D versus the Reynolds number for two possible configurations (Ref. [11, 12]). The first configuration consists of setting the transition at a given percentage. A decrease in the drag with the Reynolds number is then observed since, as it was seen in section 3, the increase in the Reynolds number decreases the friction and therefore the momentum thickness.

However, if the location of the transition, assumed sudden, varies preserving a constant transition Reynolds number R_{XT} (as it will be seen below, R_{XT} is related to the turbulence level), the following phenomena are observed :

- If $R_c < R_{XT}$, the entire boundary layer is laminar and the variation is along the low 100 % laminar curve.
- If $R_c > R_{XT}$, there is first an increase in the drag, due to rapid progression of the transition towards the leading edge, which overrides the gain achieved on each boundary layer taken separately. It is only when the transition reaches $x/c = 20$ percent of the chord that the increase stops and a decrease tending asymptotically to the 100 % turbulent curve is observed. It can also be seen that the maximum drag takes place for a Reynolds number R_c between 10 and 40 million when the transition Reynolds number is close to the conventional value of 3 to 5 million.

The figure 14 also presents the difficulties to simulate the flow at $R_c = 20$ million with a free transition at $R_{XT} = 5 \cdot 10^6$ in a wind tunnel giving $R_c = 6$ million.

If the transition location is fixed at $x/c = 25$ %, corresponding to 20 million, the drag will be too high. If the transition is kept free, the drag will be too low, corresponding to a long laminar distance up to 80 % of chord. The only solution is to fix the transition at $x/c = 47$ % but, in a real case of airfoil, this location will be very sensitive to the test conditions : Mach number, angle of attack, Reynolds number, and to the calculation method used to define the transition location and the drag.

4.2. Two-dimensional criterion developed at DERAT

In order to gain a good understanding of the transition process (Ref. [8 to 10]), it is necessary to analyse the fundamental aspects relative to a boundary layer for a two-dimensional flow on an airfoil.

The boundary layer, initially laminar and stable, has the property of amplifying the disturbances above a certain critical abscissa x_{cr} . The disturbance waves, called "Tollmien-Schlichting waves", progressively increase in amplitude for a well-defined frequency domain and degenerate into turbulence after a complex, non linear transient phase called transition. A theoretical approach of this phenomenon is made by the linear stability theory. This method leads to results approaching those of the experiments in good wind tunnels when an amplification rate A/A_0 in the neighborhood of $e^8 = e^8 \approx 3\,000$ is reached for the most unstable frequency (figure 15).

Different parameters can act on the transition location like the chord Reynolds number, the surface roughness, the freestream fluctuations ($Tu = \frac{\sqrt{u'^2}}{u}$, $\bar{P}' = \frac{\sqrt{p'^2}}{q}$, $\bar{T}' = \frac{\sqrt{T'^2}}{T}$) and the wall curvature.

A new rapid method using the computed laminar boundary layer parameters was developed by D. ARNAL [20]. It predicts the amplification factors versus x even for compressible flows (for example, see figure 15).

In this code, the model is supposed to have a smooth surface at the thermal equilibrium and is used with the experimental Mach number distribution as input.

The value of the maximum amplification factor $n = \log A/A_0$ at the beginning of transition is supposed to be a function of the turbulence level $n_t = -8.43 - 2.4 \ln(Tu)$ as MACK suggested [10].

In figure 15, a transition near 45 % of chord is observed experimentally by oil visualizations and from the Mach number distribution at the upper side.

The computation restitutes correctly this location when the turbulence level Tu is 0.001 corresponding to $n = 8.15$. An hypothesis of incompressible flow at the same Reynolds number will give a bad pessimistic result. On the lower surface, the laminar boundary layer separates at 60 % and the transition takes place in a fixed separated bubble. This figure also explains, at the bottom, the Mach number bump phenomenon. This phenomenon is related to the abscissa variation of the displacement thickness δ_1 , changing the slope of the flow seen by the inviscid fluid over the upper surface.

4.3. Leading edge transition

This two-dimensional method can also be used to define the transition on an attachment line for a swept wing where the flow is locally two-dimensional. From the linear theory, the transition occurs when $Re > 250$, but another phenomenon can decrease this value : the leading edge contamination.

If the disturbances become large, as in the case for the wing root which is in contact with the turbulent boundary layer of the fuselage, transition can occur for $Re > 120$ at the leading edge. In this case, spots of turbulence can propagate along the attachment line in a non linear mode [5, 9] inducing a turbulent boundary layer along the entire wing.

4.4. Influence of the surface roughness in two-dimensional flow

The influence of the model surface roughness is capital for the transition phenomenon, all the more because cryogenic wind tunnels achieve high unit Reynolds numbers decreasing the boundary layer thickness.

A few essential points are summarized below :

- If the roughness has the shape of a sphere with a diameter k , it is considered that the transition occurs suddenly on it when $R_k = U_k k / \nu$ reaches 500 to 600 (U_k : velocity in the laminar boundary layer at height k).

- If the roughness is an overthickness with height k , perpendicular to the flow (cylindrical wire, strip of carborundum, etc), the main parameter appears to be k/δ_1 . The diagram of the figure 16 illustrates the tripping limit in the case of a flat plate. In the leading edge area of a profile, δ_1 is often in the neighborhood of 0.01 to 0.02 mm and the value of k is roughly equal to it.

- The case of a distributed roughness of the grain of sand type can be studied for a wind tunnel where the turbulence level reaches 1 %. Then it appears that a distributed roughness where $U_k k / \nu$ reaches 100 to 120 alters the transition location. Applied to cryogenics for $P_t = 2$ b, $T_t = 120$ K, $M = 1.2$ corresponding to $R/\mu = 110 \cdot 10^6$, the critical roughness height is 1 μ m.

- The case of holes was also studied and concerns particularly the risk of tripping by pressure taps. It seems that tripping occurs if $d/\delta_1 > 20$, where d is the diameter of the hole.

4.5. Transition due to crossflow instability for three-dimensional flows

When transition was not tripped on the leading edge of a wing, another transition mode can exist due to the crossflow instability of the boundary layer velocity profile (figure 17).

An empirical criterion is often used stating that transition occurs when $Re_{\delta_2} = \frac{-1}{\nu} \int_0^{\delta_2} W dy$ (W : transverse velocity) reaches a value (between 50 and 150) which is a function of the longitudinal profile form parameter /REF. 23/. An illustration of the crossflow instability is presented in figure 18 and 19.

A study has been carried out in T2 wind tunnel on a AS100 model, designed by ONERA and AEROSPATIALE to study a transonic laminar wing [74]. The shape of this model, with a leading edge swept angle of 15°, was optimized near the sidewalls in order to simulate the real three-dimensional flow around the wing.

The Mach number distribution on the upper surface is presented here for a negative angle of attack $\alpha = -2.3^\circ$ giving, at $M = 0.74$, a strong negative pressure gradient favorable to the crossflow instability. In this case, the Mach number distribution is quite Reynolds insensitive.

A boundary layer calculation was made using the experimental Mach number distribution with the hypothesis of an infinite swept wing at $\phi = 12^\circ$. The transverse Reynolds number $Re_{\delta_2}(x/c)$ is drawn with a dash line in figure 19 for different chord Reynolds numbers. In this case, where the transverse Reynolds number increases versus x , the transition will occur when the critical value $Re_{\delta_2}(H_1)$ is reached. So it appears that the transition moves forward when the Reynolds exceeds $9.5 \cdot 10^6$.

The experimental results presented in figure 18 are in good agreement with this theoretical analysis.

The location of the transition can be estimated from the drag measurements. This drag was measured in two cases with a fixed transition at $x/c = 7\%$ and in the free case where the transition is at 70% for $R_c < 10^{10}$. A simple interpolation can estimate how the drag varies with the Reynolds number if the transition was fixed at different locations. In this case, the boundary layer is always turbulent at the lower surface thanks to a strong peak in the Mach number distribution near the leading edge.

Thus we can estimate the transition location versus the Reynolds number and plot the results on the curve presented at the bottom. The location of the transition can also be obtained by the thermocouples as presented by cross-hatched domain, in good agreement with the previous determination.

5 - EFFECTS OF THE REYNOLDS NUMBER

5.1. - A two-dimensional case : CAST 10 airfoil (collaboration between DLR-NASA LANGLEY-ONERA)

In this paragraph, Reynolds number effects are analyzed in some cases extracted from test data, performed at T.C.T. and T2 with adaptive walls.

Figure 20 shows a distribution of pressure coefficients measured at T2 for $R_c = 20 \cdot 10^6$ at $M = 0.766$ and $\alpha = 0.25^\circ$ with a free transition. This case is particularly sensitive to the flow conditions.

Different computations were made at ONERA, DLR, NASA, etc [21, 22]. The results presented in figure 20 came from a ONERA NAVIER-STOKES code using initially the experimental values $M = 0.765$ and $\alpha = 0.25^\circ$. First the lower side Mach number distribution is well reproduced ; on the other hand, the upper side is poorly reproduced. The agreement can be improved by reducing the infinite Mach number of the calculation down to 0.75 and reducing slightly the angle of attack to $\alpha = 0^\circ$. This difference can be explained by the sidewall boundary layers interference. The displacement thickness of the sidewall boundary layers are modified under the pressure gradient induced by the airfoil, so three-dimensional interference effects occur reducing the upper surface Mach number seen by the airfoil. Only a part of this effect is taken into account by the adaptive walls ; the residual error is however the largest at the upper surface.

In figure 21, the Reynolds number effect is presented on the lift and drag measured at T.C.T. and T2 for the same experimental Mach number $M = 0.76$ and angle of attack $\alpha = 0.25^\circ$. Two experimental cases are studied : free or fixed transition at $x/c = 7\%$.

When the transition is fixed, the lift increases quite linearly with the Reynolds number and the points are in good continuation with free transition data for $R_c > 20 \cdot 10^6$. The agreement between T.C.T. and T2 is fairly good. On the drag, the level seems higher at T.C.T. than the one obtained at T2, but the slope is the same giving a reduction of the drag with the Reynolds number in good correlation with the computation results.

The free transition case is more complex. At low Reynolds numbers, the boundary layer is laminar from the leading edge to about 50% of chord on upper and lower sides, the lift is high and the drag very low.

When the Reynolds number increases, T.C.T. data show less laminar flow than T2. For Reynolds number higher than 10^7 at T2, the drag increases and the lift decreases joining the fixed transition curve at $R_c \approx 2 \cdot 10^7$. A comparison between the measured drag and the predictable values is plotted at the bottom of figure 21. Unfortunately even the T2 results seem pessimistic.

The analysis of these results as well as another study on the laminar wing AS100 have permitted to understand that the transition was fixed near the leading edge by ice crystals when the temperature of the flow was lower than the dew point of the water vapor in the wind tunnel as presented by ARCHAMBAUD [17].

We have supposed that ice crystals appear on the model during the starting phase of the run especially when the pressure and Mach number are increased. A protection system of the leading edge was then designed and tested. This system enables to avoid spurious transition at the leading edge and has been used up to $R_c = 14 \cdot 10^6$.

5.2. A three-dimensional case : A3ux half-model at T2 wind tunnel

In order to study the Reynolds number effect on a wing, a cryogenic transport type half-model has been designed and manufactured by the ONERA Center in LILLE [19].

This model (figure 22) has enabled us to check one of the major point of the cryogenic testing, the opportunity to simulate pure Reynolds effects by varying the stagnation temperature.

The control of the wing displacement was performed with two optic fibers located at the wing tip and observed with a video camera. An interesting result of the wing tip displacement is presented in figure 22 for two temperature levels. The very small differences due to temperature changes can be explained by the increase of few percents in the elasticity modulus of the maragin steel Marval 18 constituting the wing, added to the aerodynamic changes as function of the Reynolds number.

The Reynolds number effect on pressure coefficients for two wing sections, 1 and 6, is presented in figure 23, giving an increase in the lift coefficient as seen for a two-dimensional flow.

At the bottom of this figure, this Reynolds effect is compared to the deformation effect produced by the elasticity of the model, if the total pressure is changed. In this case, the displacement of the wing tip seems proportional to the pressure and the wing is twisted. A pure deformation effect is presented for $P_t = 1.7$ and 3 bars with two temperature levels giving the same Reynolds number of $3 \cdot 10^3$. The section 6 near the tip gives a large deviation reducing the lift when the pressure increases ; this corresponds to a reduction of the local angle of attack induced by the load on a swept wing of about 1° . In this case, the deformation effect seems to be of the same magnitude than the Reynolds effect.

6 - CONCLUSION

In conclusion, we will try to draw a lesson from the past to think over the progresses realized and to present some recommendations for the future.

First, the beginners should be warned that the respect of the Reynolds number is not the marvellous parameter guaranteeing the validity of the results. Wind tunnel technology is complex and more than ever it is necessary to preserve a critical attitude to think up new devices and to consider the wind tunnel only as a tool. However, like any tool, it has its limits which must be well mastered. One of the objectives is to take into account, by a good instrumentation and also with theoretical approaches, all the parameters which can influence the results.

Progresses have been performed in the field of model design and instrumentation ; for instance, the concept of low thermal inertia for models has been successfully used. The effects of moisture in wind tunnels is better understood. In T2 wind tunnel, a dew point of the water vapor under 220 K, the use of a protecting system of the model during the starting process and the fact to keep the model temperature always over the equilibrium level, seem enough to avoid transition fixing. Furthermore the icing of the model can be controlled and gives the opportunity to perform surface flow visualizations.

To be efficient, the cryogenic wind tunnel must also offer maximum flexibility in spite of the complexity of the tests which can be conducted in it. It is by the conjunction of many efforts in these areas that cryogenic wind tunnel testing will occupy an increasingly large place in future test facilities.

REFERENCES

- [1] R.A. KILGOORE "Model design and instrumentation experiments with continuous flow cryogenic tunnels". AGARD LS-111 (1980)
- [2] M.J. GOODYER "The principles and applications of cryogenic wind tunnels". AGARD LS-111 (1980)
- [3] R.M. HALL "Real gas effects". AGARD LS-111 (1980)
- [4] R. MICHEL "The development of a cryogenic wind tunnel driven by induction : flow control and instrumentation studies in a pilot facility at ONERA". AGARD LS-111 (1980)
- [5] F.T. LYNCH, D.R. PATEL "Some important new instrumentation needs and testing requirements for testing in a cryogenic wind tunnel such as NTF". AIAA 12 Aerod. Testing Conf., WILLIAMSBURG, VA (Mars 1982)
- [6] C.B. JOHNSON "Study of non adiabatic boundary layer stabilization time in a cryogenic tunnel for typical wing and fuselage models". J. of Aircraft, Vol. 18, N° 11, p. 9-13 (Novembre 1981)
- [7] D.F. FISHER, N.S. DOUGHERTY Jr. "In-flight transition measurement on a 10° cone at Mach numbers from 0.5 to 2.0". NASA TP 1571 (1982)
- [8] L. LEES "The stability of laminar boundary layer in a compressible fluid". NACA Rpt. 876 (1947)
- [9] D. ARNAL, M. HABIBALLAH, E. COUSTOLS "Théorie de l'instabilité laminaire et critères de transition en écoulement bi et tridimensionnel". La Recherche Aéronautique 1984-2 (1984)
- [10] L.M. MACK "Boundary layer linear stability theory". AGARD R-709
- [11] R. MICHEL "Couches limites - Frottement et transferts de chaleur". Cours ENSAE
- [12] J. COUSTEIX "Couches limites laminaires" - "Couches limites turbulentes". Cours ENSAE
- [13] A. BLANCHARD, A. MIGNOSI "Problèmes liés à l'instrumentation et à la conception d'essais cryogéniques". ETW Meeting, AMSTERDAM (15-17 septembre 1982)
- [14] J.L. GOBERT, A. MIGNOSI "Etudes réalisées sur la soufflerie cryogénique à induction T2". ETW Meeting, AMSTERDAM (15-17 septembre 1982)
- [15] J.B. DOR "The cryogenic induction tunnel T2 at TOULOUSE". LS VKI (22-26 avril 1985)
- [16] STANEWSKY et al "High Reynolds number tests of the CAST 10-2/DOA2 transonic airfoil". AGARD CP-348 (26-29 septembre 1983)
- [17] J.P. ARCHAMBAUD "The cryogenic induction tunnel T2 at TOULOUSE". LS VKI (May 5-9 1989)
- [18] A. BLANCHARD, J.B. DOR, A. SERAUDIE, J.F. BREIL "Flow qualities in the T2 cryogenic wind tunnel. Problems and solutions". 2nd Cryogenic Technology Review Meeting - DFVLR Köln/Porz (28-30 June 1988)
- [19] A. MIGNOSI, J.P. ARCHAMBAUD, S. PRUDHOMME, M. PLAZANET, M.J. PAYRY "T2 ability concerning model design and instrumentation in short run processing". 2nd Cryogenic Technology Review Meeting - DFVLR Köln/Porz (28-30 June 1988)
- [20] D. ARNAL "Transition prediction in transonic flow" IUTAM Symp. Transsonicum III - DFVLR Göttingen (May 24-27, 1988)

- [21] R. IMBERT "Exploitation des essais cryogéniques du profil CAST 10 en transition déclenchée". R.T.S. N° 66/1685 AY
- [22] CAST 10-2/DOA2 Airfoil Workshop - NASA LANGLEY (September 23-27, 1988)
- [23] A. MIGNOSI "Fundamental reflections on cryogenic testing". LS VKI (22-26 avril 1985)
- [24] J.P. ARCHAMBAUD, A. SERAUDIE, M.J. PAYRY "Etude expérimentale de la laminarité sur l'aile AS409 au nombre de Reynolds maximum possible ($R_e \approx 7.3 \cdot 10^6$, $c = 0.187$ m) dans la soufflerie T2". R.T. N° 32/5006.12 (Mars 1989)

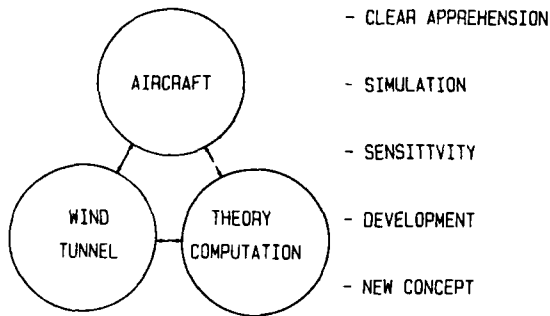


FIG. 1 : General scheme on wind-tunnel part.

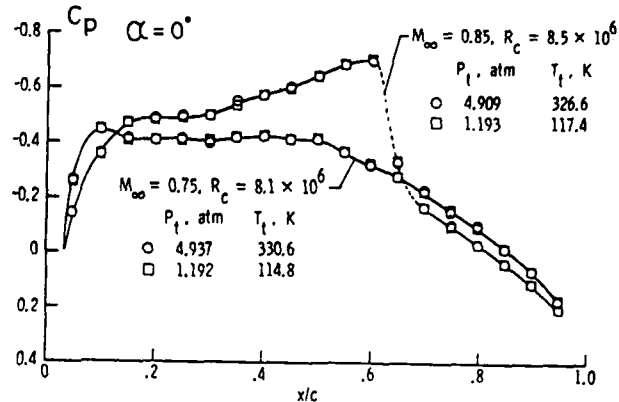


FIG. 3 : Two-dimensional symmetrical airfoil : pressure distribution at ambient and cryogenic conditions. T.C.T. NASA Langley.

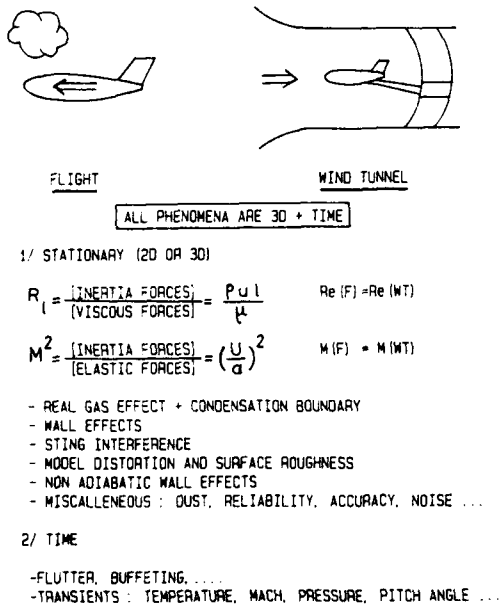
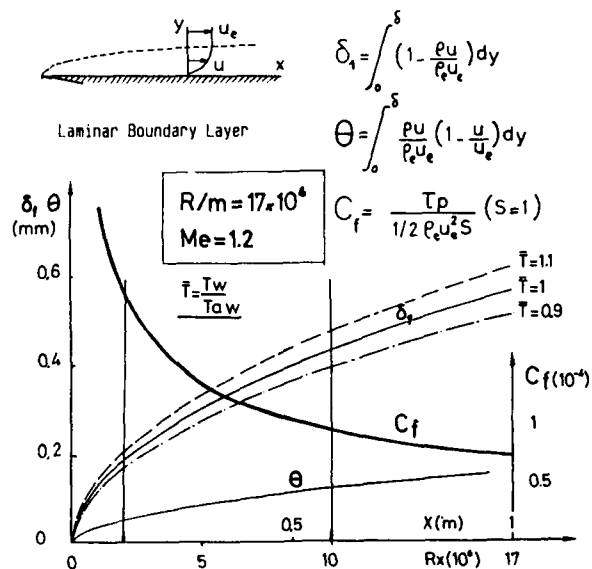


FIG. 2 : Problems involved in cryogenic testing.

FIG. 4 : Laminar boundary layer development on a flat plate at $M = 1.2$; $R/m = 17 \cdot 10^6$.

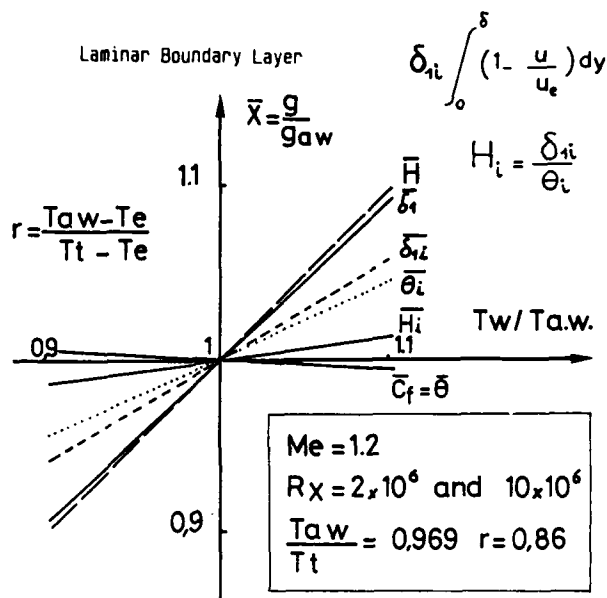


FIG. 5 : Wall temperature effects on a laminar boundary layer at $M = 1.2$.

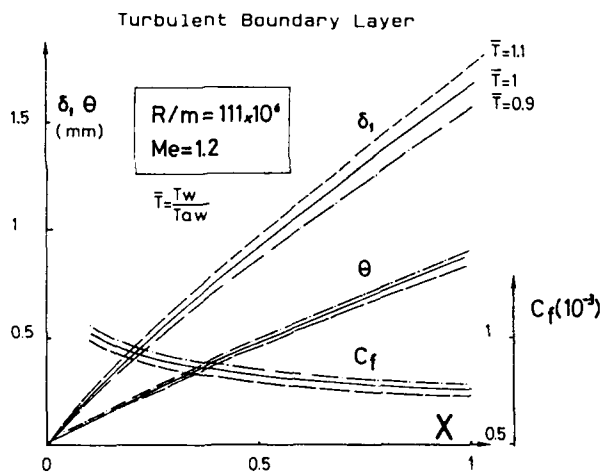


FIG. 7 : Turbulent boundary layer development on a flat plate at $M = 1.2$, $R/m = 111 \times 10^6$.

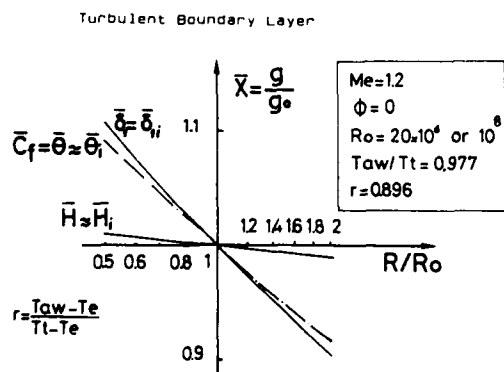


Fig. 9 : Reynolds number effects on a turbulent boundary layer at $M = 1.2$ with an adiabatic walls.

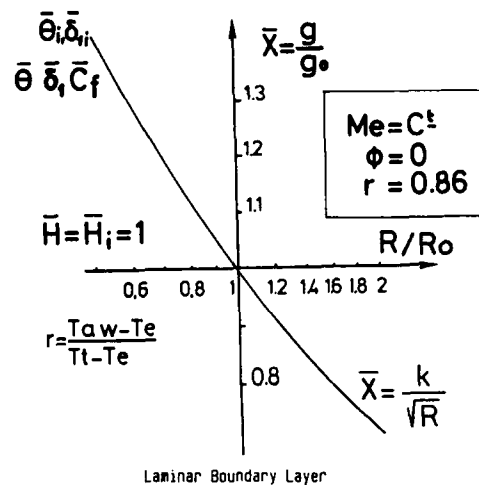


FIG. 6 : Reynolds number effects on a laminar boundary layer with an adiabatic wall.

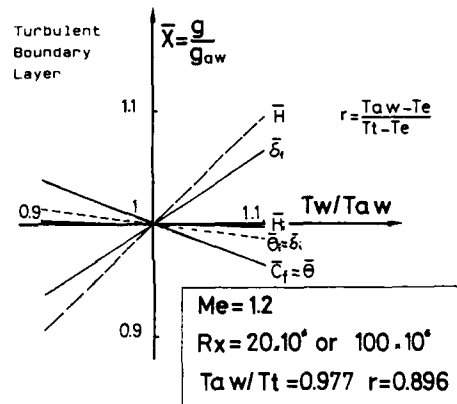


FIG. 8 : Wall temperature effects on a turbulent boundary layer at $M = 1.2$.

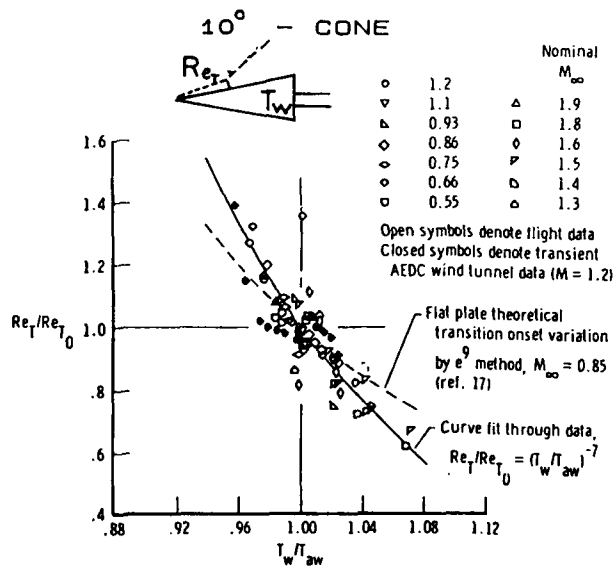


FIG. 10 : Wall temperature effects on the transition Reynolds number on a 10° cone : experimental and theoretical results.

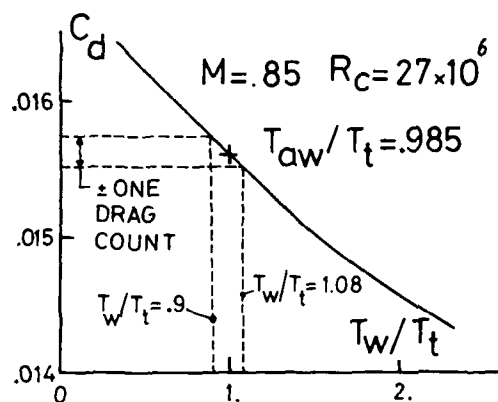


FIG. 11 : Estimated section drag coefficient of a NACA 12-64 Airfoil as function of T_w/T_t : $P_t = 2$ bars, $T_t = 116$ K from C.B. JOHNSON.

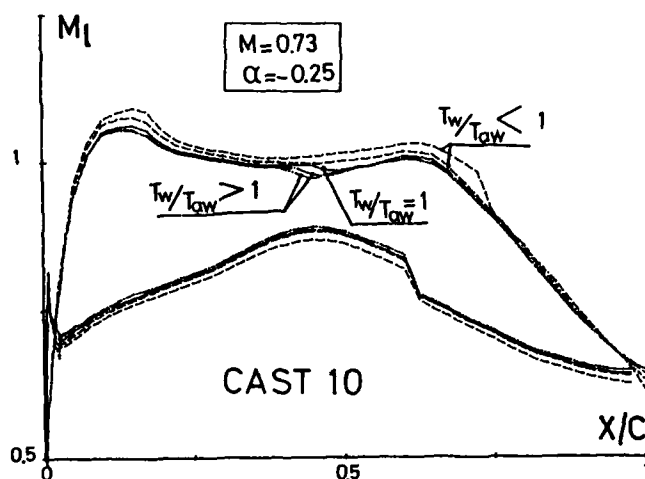


FIG. 12 : Experimental wall temperature effects on a CAST 10 airfoil with a free transition : Mach number distribution from T2 wind-tunnel.

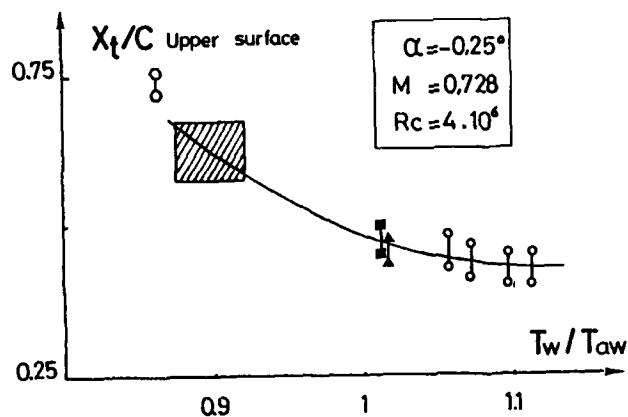


FIG. 13 : Wall temperature effects on the CAST 10 airfoil at T2 : transition location, C_e and C_d .

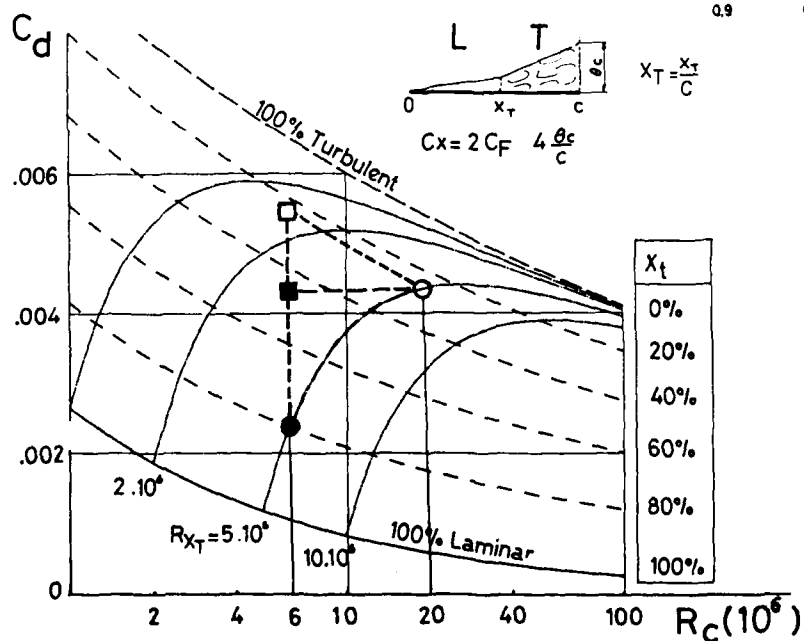
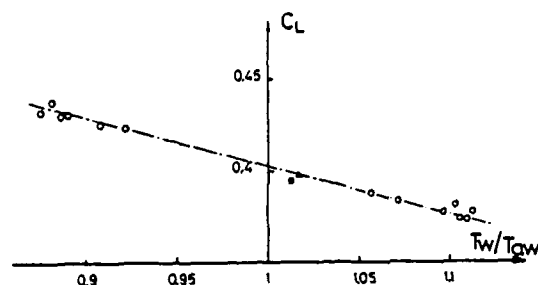
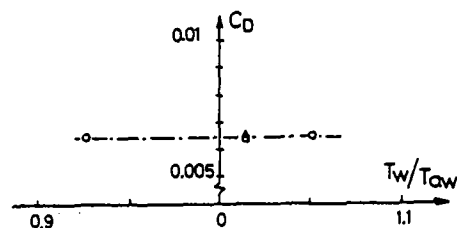


FIG. 14 : Basic Reynolds number effects on a flat plate with a fixed and free transition. Difficulties to simulate high Reynolds numbers.

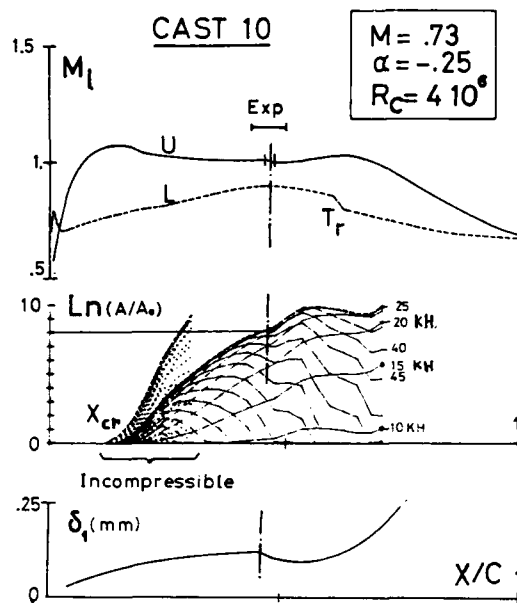


FIG. 15 : Streamwise transition on a CAST 10 Airfoil : experimental and theoretical correlations.

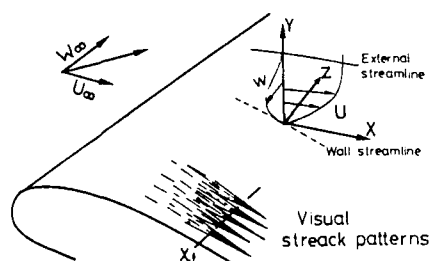


FIG. 17 : Cross-flow instability : streak patterns.

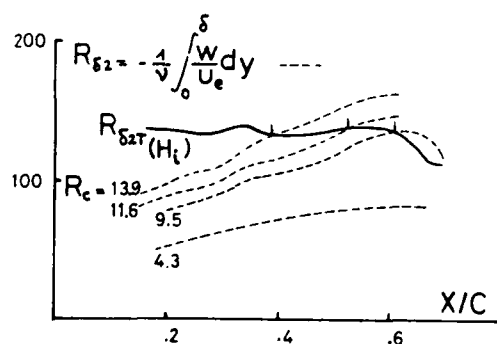


FIG. 19 : Application of the cross-flow transition criteria to AS 100 experimental results.

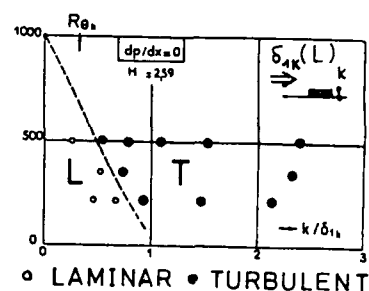


FIG. 16 : Effects of a two-dimensional wall roughness : critical size fixing the transition.

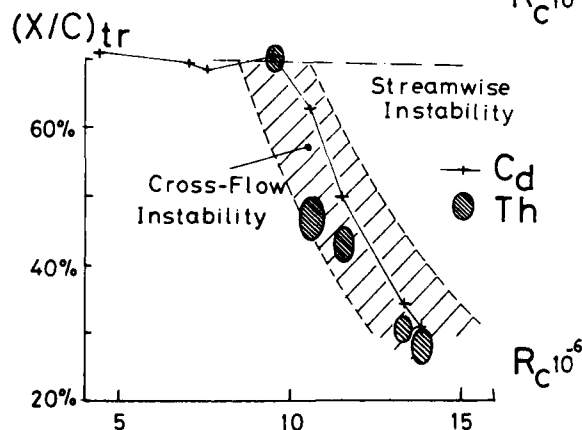
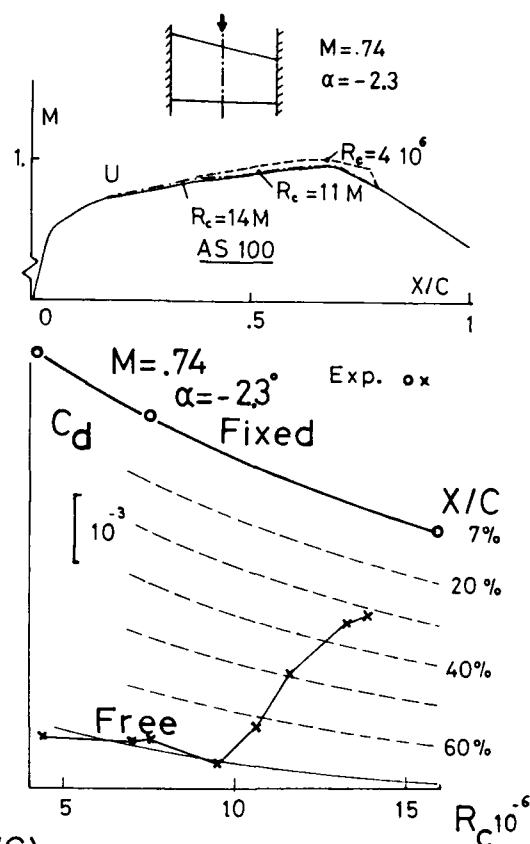


FIG. 18 : Experimental results with a cross-flow transition on a AS 100 model : $P_t = 1.7$ to 2 bars; $T_t = T_{amb}$ to 125 K.

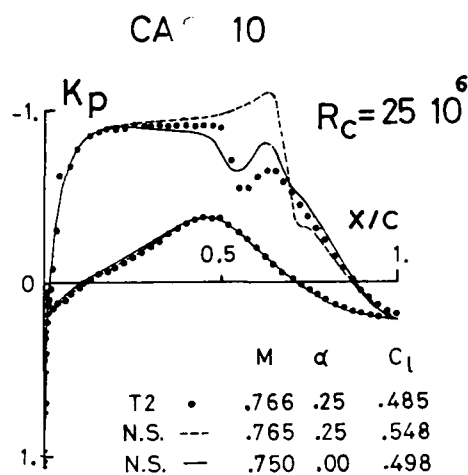


FIG. 20 : Pressure coefficient distribution on a CAST 10 airfoil at T2 : experimental and theoretical correlations at $R_c = 25 \cdot 10^6$.

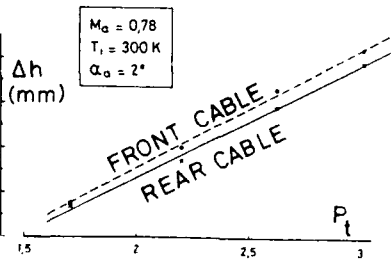
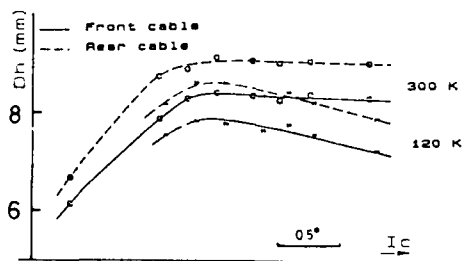
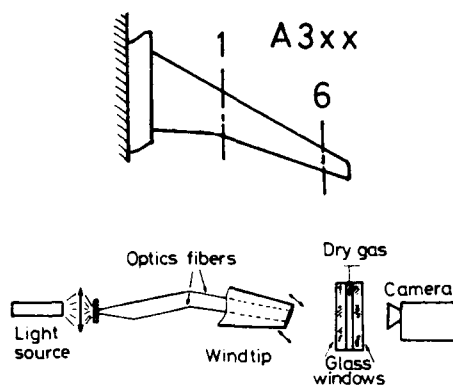


FIG. 22 : A3xx half model : wing tip displacement measured with an optic fiber system.

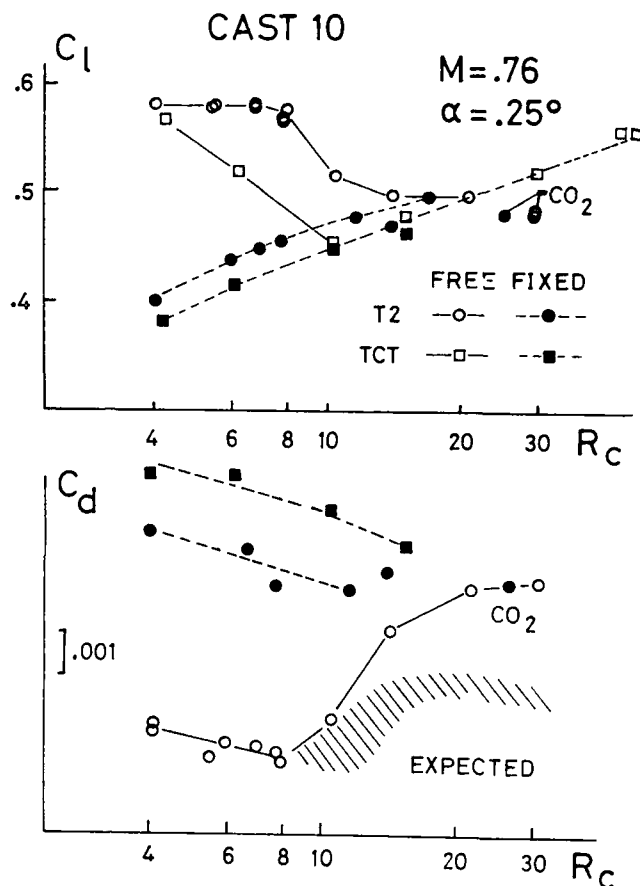


FIG. 21 : Reynolds number effects on the lift and drag coefficients : CAST 10 experimental results at T.C.T. and T2.

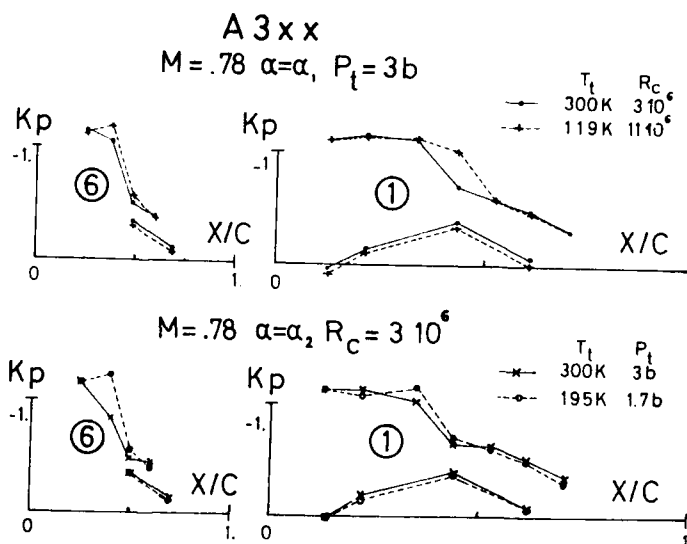


FIG. 23 : Comparison on pressure coefficients between Reynolds number and deformation effects.

TEST TECHNIQUES FOR CRYOGENIC WIND TUNNELS

by

Pierce L. Lawing

NASA, Langley Research Center
Hampton, VA 23665-5225
U.S.A.

SUMMARY

This paper brings together some of the testing techniques developed for transonic cryogenic tunnels. It emphasizes techniques which required special development, or were unique because of the opportunities offered by cryogenic operation. The first part of the paper is used to discuss measuring the static aerodynamic coefficients normally used to determine component efficiency. The first topic is testing of two dimensional airfoils at transonic Mach numbers and flight values of Reynolds number. Three dimensional tests of complete configurations and sidewall mounted wings are also described. Since flight Reynolds numbers are of interest, free transition must be allowed. A discussion is given of wind tunnel and model construction effects on transition location.

The second part of the paper deals with time dependent phenomena, fluid mechanics, and measurement techniques. The time dependent, or unsteady, aerodynamic test techniques described include testing for flutter, buffet, and oscillating airfoil characteristics. In describing non-intrusive laser techniques, discussions are given regarding optical access, seeding, forward scatter lasers, two-spot lasers, and laser holography. Methods of detecting transition and separation will be reported and a new type of skin friction balance is described. There are 29 references to assist in obtaining further information.

1. INTRODUCTION

The advantages of the cryogenic concept for wind tunnel testing are, by now, well documented and understood, references 1-3. However, the development of cryogenic testing tools is an ongoing process. Also, in order to properly take advantage of all of the research opportunities offered by cryogenic operation of a wind tunnel, it is necessary to develop some new techniques unique to cryogenic operation. In addition, the fact that the cryogenic facility can produce realistic flight boundary layers requires a quantum improvement in model construction techniques, involving surface finish, fidelity of model contours, and dimensional stability. A similar effort is required in instrumentation technique, particularly instrumentation techniques for transition detection and the study of unsteady aerodynamics.

This paper relies heavily on the effort to develop the necessary testing techniques in the Langley 0.3-m Transonic Cryogenic Tunnel, or 0.3-m TCT, and will summarize techniques used which either had special development required by the cryogenic environment, or are unique because of the opportunities offered by cryogenic operation. The citations are too numerous for a detailed description of each one, but fortunately, many of them have previous documentation, and these are referenced. An effort was made to include at least a mention of each item in order to make this presentation as current as possible. There are about 20 techniques listed and the author has been directly involved in the majority of these experimental efforts. Several of the techniques for which there is little or no information elsewhere are discussed in some detail.

2. AIRFOIL TESTING

Two-dimensional airfoil testing is a standard test technique used to examine the characteristics of an airfoil section in more detail than would be possible in a full aircraft configuration. One problem peculiar to this type of testing is error introduced by the penetration of the model through the thick, tunnel-side-wall, boundary layer. Since this boundary layer does not have as much momentum as the external stream, it will separate much easier than the free stream flow. At low lift conditions, separation may not occur. As the lift increases, the side wall boundary layer will separate. At high lift, this separated region becomes large enough to influence measurements at the center of the airfoil, thus spoiling the data. This problem can occur at even low lift conditions when there is a transonic shock present. Other errors are introduced by the presence of the floor and ceiling of the test section. One serious error is caused by the blockage of the model, especially at transonic conditions. This is commonly alleviated by slots in the walls, or in the current 0.3-m TCT test section, by adaptive walls. Methods of dealing with these error sources are described in the next sections.

2.1 Airfoil Test With Sidewall Boundary Layer Removal

Figure 1 shows pressure surveys through the wake of a 12 percent thick supercritical airfoil at three spanwise stations. Results are shown with and without "bleed". The term here refers to the removal of the tunnel sidewall boundary layer just ahead of the model to remove some of the low energy boundary layer fluid. This action has the effect of increasing the boundary layer's resistance to separation. In addition, the sidewall boundary layer interference is reduced because of the

reduction in the displacement thickness, as indicated by the values of the parameter $2\delta^*/b$, shown on figure 1. The case presented is for a high value of lift coefficient and at a transonic flow condition. The Gaussian shaped part of the curve is due to the viscous drag losses and the ragged ramp portion is due to the shock losses. The use of boundary layer removal smoothes the wake distributions, especially the shock loss part of the curve, as well as making the shape of the curves more uniform in the spanwise direction. For additional details and more information see references 4 and 5.

Mass flow may be removed from the boundary layer either by passive bleed to the atmosphere or by a compressor. The compressor, shown schematically in figure 2, must operate over a wide range of pressure and temperature (ambient to near liquid nitrogen). The mass removed from the sidewalls of the test section is reinjected. During compressor validation tests, reference 6, with sidewall boundary layer removal and reinjection, tunnel flow conditions could easily be maintained over a wide range of Mach numbers and Reynolds numbers. The successful integration of the compressor with the normal tunnel operation was not only a significant engineering achievement in its own right, but the use of the compressor greatly enhances the tunnel's research capabilities. An important aspect for two dimensional airfoil research, is the capability to treat the test section sidewall boundary layers to reduce sidewall interference. Recent improvements to the compressor/tunnel control system are given in reference 7.

2.2 Adaptive Wall Test Section

To reduce or eliminate wall interference we need to use **adaptive wall test sections**. Although we include adaptive walls under advanced techniques, British researchers first used them 50 years ago, reference 8. Modern digital controls and powerful computers have made the application of adaptive wall technology an easier process. Adaptive walls address the problem of wall interference at its source, the test section walls. We can use analytical techniques to correct any wall induced errors left after wall streamlining. For the 0.3-m TCT we have chosen an adaptive wall test section with solid but flexible top and bottom walls. We have had success with both 2-D and 3-D models through the transonic speed range. We and other researchers have demonstrated the practicality of adaptive wall test sections for transonic testing.

3. NEW TECHNIQUE FOR AIRFOIL PRESSURE MODELS

Building models for the new class of cryogenic tunnels requires advanced new technologies. In order to isolate the sought after Reynolds number effects from surface roughness induced effects, it is necessary to have very good surface finish (6 to 8 microinches at the leading edge). Special materials are utilized to provide the necessary fracture toughness at cryogenic temperatures. Exceptionally good dimensional stability is required during temperature cycling to maintain the accuracy demanded of transonic models. These requirements, together with the required high strength, make the task of building the necessary models difficult, leading to lost research time and increased model costs.

In the early years of 2-D testing in the 0.3-m TCT, the difficult fabrication task led to a rejection rate of more than 50% of the models attempted, and several parallel efforts to find new methods of building the necessary models were initiated. Improved application of the more or less conventional model building activities was one such effort, and it is documented in reference 9. Other efforts include adhesively bonded cover plates reference 10, steel pressure tubes cast in a fiberglass airfoil, and the bonded plates method described below.

The technique pictured in figure 3 is a promising new solution being researched to alleviate the model construction problem for pressure instrumented models. Here, the pressure channels are cut or etched into the opposing faces of a metal "sandwich"; the sandwich is closed and brazed together in a vacuum oven resulting in a model "blank" with high strength and low "plumbing" costs. This model has been built, successfully tested, and the data reported in reference 11. Sample test results are shown in figure 4. Part (a) of figure 4 is for the model at an angle of attack of 2 degrees, corresponding to a lift coefficient of 0.31. Part (b) is the data of part (a) with the data for -2 degrees, lift coefficient of -0.31, superimposed. Figure 4 presents pressure coefficient data from the model described above, at transonic conditions and a moderate lift coefficient. This data shows the presence of a shock wave on the upper surface between 30 and 38 percent chord. The circular symbols are the upper surface pressure taps and the square symbols are for the lower surface. Since this is a symmetrical airfoil, the pressure signatures at positive and negative angle of attack should match with the upper and lower symbols changing places. As may be observed from part b, the pressures are very nearly the same. This demonstrates good top and bottom symmetry of model construction and good testing technique. For information on present research for more advanced models including electrical discharge wire cut of airfoil contours, thin airfoils, etched pressure channels and curved bond planes, see references 12 and 13.

4. 3-D AIRFOIL TESTING

4.1 Thin Wing Testing

During our airfoil testing program in the 0.3-m TCT, we were never successful in building a pressure instrumented airfoil any thinner than 10% of chord. Since many of our military aircraft operate with wings much thinner than this, the lack of thin airfoil capability was a serious deficiency. In the course of the model construction research described above it became evident that thin airfoils were now possible. A model of the X29 fighter canard was built; the thickness was 5%. The model was tested primarily to verify the model construction technique, but also the test provided the opportunity to take unique

aerodynamic data and to exercise the solid adaptive wall test section, reference 14, for 3-D testing. The airfoil was tested over nearly the full range of conditions available with the adaptive wall test section. This included both ambient and cryogenic operation at pressures up to 6 bars at Mach numbers up to 1.07. For testing this semi-span 3-D model, the method of Rebstock, reference 15, was used to adapt the solid test section walls for minimum interference.

Aerodynamic data was taken for the airfoil (surface pressures and wake survey) at Mach numbers from 0.3 to 1.07. The tests covered angles of attack from -4° to $+15^\circ$. At most Mach numbers a 10 to 1 range of Reynolds number was covered and flight values of Reynolds number were easily obtained. Figure 5 shows an example of the airfoil data at an angle of attack of 8° , a Mach number of 0.9, and a Reynolds number based on mean aerodynamic chord of 32 million.

4.2 Mapping of Three Dimensional Wakes by Pitot Surveys

Figure 6 illustrates a technique of creating a topology of the momentum loss in the wake of a body, in this case a cylinder. Wake surveys with a vertical rake of pitot tubes are a conventional method of determining the momentum loss, and thus the drag of a body. These data were obtained by an updated version of this method where the survey rake is driven through the wake by a computer controlled actuator, and there are six tubes, in a spanwise row, which allow determination of the spanwise variation in the wake. Not only does conducting such a survey provide additional data, but doing so in a cryogenic environment is an engineering achievement. This particular sample illustrates the classic Gaussian shaped curve for those tubes near the tunnel centerline, and shows deviations from this shape at stations close to the wall. This is due to the interaction between the wall boundary layer and the cylinder. Reference 16 includes additional data.

4.3 Evaluation of a Cryogenic Strain-gage Balance

Although the 0.3-m TCT has been equipped with a special test section for two dimensional airfoil testing in recent years, it is possible to do small scale three dimensional testing as shown in figure 7. Here an airfoil shape is used to support a sting and a conventional 3-D model arrangement to allow force balance testing. The strain-gage balance is shown between the model and the 2-D support. The balance was tested at cryogenic temperatures with and without electrical resistance heaters, achieving good results in both cases. Further details are contained in reference 17.

5. UNSTEADY AERODYNAMICS

5.1 Flutter Model Testing

A flutter test has been conducted in the 0.3-m Transonic Cryogenic Tunnel to explore problems, develop testing techniques, and determine the potential of a cryogenic tunnel to advance the state of the art in flutter testing. A simple "text book" rectangular planform wing model supported by a beam flexure was used for the test. Model and support were machined from a single piece of 18 Nickel grade 200 maraging steel (trade name Vascomax 200). This material is characterized by its good dimensional stability with temperature change and its high fracture toughness at cryogenic temperatures. Although no "hard" flutter points were included in the test, the model oscillations were large enough to be easily visible on a video monitor at conditions near flutter onset. Figure 8 presents a comparison of analytical and experimental flutter results in terms of the flutter dynamic pressure as a function of Mach number. It is presented here only to illustrate flutter data taken at cryogenic temperatures, and was taken from reference 18. Further details including the effect of Reynolds number on transonic flutter are also contained in this reference.

5.2 Buffet Testing Technique

Buffet testing has been conducted in the 0.3-m TCT using semi-span models mounted on one turntable. Instrumentation included a root bending gage to indicate buffet onset. Models included both delta and straight wing planforms. The ability to hold Mach number and Reynolds number constant while varying the velocity demonstrated the strong dependence of buffet onset on the reduced frequency, figure 9. This segment of the research is documented in reference 19. This research is ongoing and recent tests have used carbon composite models to increase the resonant frequency of the model.

5.3 Oscillating Airfoil Testing

Figure 10 is a photograph of the 14 percent supercritical airfoil model mounted in a test section module of the 0.3-m TCT. The model is being viewed from the trailing edge. The drive bellows that transmitted the torque to oscillate the model from an external actuator is visible attached to the left wall of the module. The model was oscillated at frequencies as low as 4 cycles per second, and as high as 60 cycles per second. Amplitudes were as low as $\pm 1/4$ degree and as high as ± 1.0 degrees. Tests were conducted at cryogenic temperatures and well into the transonic speed range. Fluctuating pressure data was measured by 43 pressure transducers mounted in the interior of the model. This data will be helpful in the understanding of unsteady aerodynamic processes including flutter, buffet, and rapid changes in pitch over a range of Reynolds numbers including values representative of flight.

6. NON-INTRUSIVE FLOW MEASUREMENTS

The term non-intrusive implies optical access through the wind tunnel wall, usually a window. For cryogenic facilities

operating at high pressures and cryogenic temperatures, such windows pose major problems. For instance, in the 0.3-m TCT, a quartz window shrinks much slower with decreasing temperature than the aluminum structure. At room temperature, the quartz piece must fit loosely, and provide room for the aluminum to shrink around the quartz as the temperature is lowered to cryogenic operation conditions. At the same time, the window and frame must support the pressure drop at room temperatures.

A window at cryogenic temperatures exposed to room temperature air and its attendant humidity must be kept clear of fog and/or frost. One method of maintaining a clear window is to position a thin piece of glass about 10% of the window diameter away from the quartz and purge the resulting gap with dry, heated, Nitrogen gas. Since this is a transonic tunnel with a plenum chamber, there must be a window in the test section wall as well. Thus an optical beam must traverse a thin, unloaded, piece of glass with a small thermal gradient, the purge gas region, the heavily loaded, up to 6 atmospheres, pressure shell window, the nitrogen in the plenum, the lightly loaded, essentially isothermal, test section window, the tunnel wall boundary layer, and finally the test flow. In the case of some techniques, such as a shadowgraph, the process is repeated in reverse on the other side of the test section. In the case of backscatter laser measurements, the low intensity signals must travel back through the same set of conditions.

There are several additional difficulties to recognize in the application of optical techniques to the 0.3-m TCT: Since all of the structural parts must contract with decreasing temperature, and it is not possible to insure isothermal structures, provision must be made for referencing measurements in space to the model locations. For example, this required a special alignment laser for laser velocimeter measurements, reference 20. Other sources of error that must be considered are deflection of structural parts due to differential pressures or model support loads and effects such as lensing of the windows under distortion from pressure or thermal loading. Most of these difficulties are inherent in a facility designed to provide aerodynamic coefficients at flight conditions as opposed to a facility designed for pure fluid mechanics studies or for validation of analytical methods.

6.1 Optical Methods

Various flow diagnostic and visualization techniques have been tried in the 0.3-m TCT both to enhance the research utility of the tunnel and to explore the problems and opportunities offered by cryogenic testing. The use of the Laser Transit Anemometer to survey velocity distributions in flow fields and boundary layers is described elsewhere in this paper and in reference 16. Other methods reference 21-25, include laser holographic interferometry, schlieren, shadowgraph, image quality studies, and moire deflectometry measurements. All have been successful to some extent. One major problem that was encountered was a swamping of the flow features by an optical disturbance that strengthened as the tunnel temperature was lowered. This problem was isolated and identified as thermal inhomogeneities external to the test section, primarily due to convective currents in the plenum chamber. The optical degradation becomes more severe with decreasing temperature and increasing pressure, and exhibits a $(p/T)^2$ dependence. Figure 11 shows a comparison of optical quality before and after isolation of the optical beam from the plenum. This problem is discussed in detail in reference 25.

6.2 Seeding a Cryogenic Tunnel

Several of the more promising laser diagnostic techniques require the flow to be seeded with reflective particles a few microns in diameter. At this time there is no clearly satisfactory method of seeding a cryogenic tunnel. Measurements have been made using "natural" seeding generated by running the tunnel cold enough to preserve condensed nitrogen droplets, or by pulsing the liquid nitrogen control to generate a temporary cloud of liquid nitrogen droplets. A chance oil leak past the fan shaft seal provided very satisfactory data rates when the flow was cold enough to promote condensation of the oil into droplets. However, these schemes have serious drawbacks in that the errors introduced by testing in condensed flow are not defined and no correction method exists, the flow conditions are not known during injection pulsing, and at the extreme cold necessary for high Reynolds number operation, it is suspected that the oil freezes into solid particles and is responsible for eroding the model leading edges. Seeding has also been accomplished by bleeding service air into the tunnel and reducing the temperature to form condensed water, or ice, depending on the temperature. Once again, the larger condensates are expected of causing model erosion at the lower temperatures. To offset the fan heat, the tunnel must be continually injected with liquid nitrogen and the resulting gas vented. Thus the facility continually purges itself, and seeding material must be constantly replenished. Also, since the material is continually vented, it must be environmentally acceptable.

High Reynolds number testing requires good model surface finish, particularly on the leading edges, and small pressure orifices. Great care must be exercised to preserve the finish and keep the orifices unblocked even before the model is installed into the tunnel; introduction of solid particles is advisable only if they do not aggregate and form clumps that have sufficient ballistic coefficient to impact the model, and if they cannot accumulate in the model orifices or other sensitive mechanisms such as actuators. Liquid particles must not form ice clumps at low temperatures and must evaporate at room temperatures to allow cleanup. Thus far the only solid particles that have been tried are kaolin powders. The liquids are water and lubricating oil. Both the kaolin and the oil required extensive cleaning of the tunnel after use and are considered unsuitable materials.

6.3 Two-spot Laser Boundary Layer Survey

The two-spot laser, or more properly the Laser Transit Anemometer, LTA, focuses two laser beams into spots 9 microns in diameter with a spot-to-spot separation of about 20 spot diameters. When the spots are aligned with the flow in a wind tunnel, that is with one spot upstream of the other, any reflective particle in the flow that happens to pass through the

upstream spot will reflect back a pulse of light. As the particle passes through the second spot it will reflect back a second pulse of light. Since the distance between the spots is known, a measurement of the time between the two pulses yields velocity. This process may be greatly enhanced by seeding the flow with appropriate particles. The data in figure 12 was generated by such a process where the LTA was used to survey the flow field of a cylinder along the line indicated in the "scan location" inset. This data is unique in that it was taken in a cryogenic environment and is one of the first successful attempts at measuring points in the boundary with this type of device. The two decreasing velocity points nearest the cylinder surface are in the boundary layer. Further details are available in reference 16.

7. FLOW QUALITY

7.1 Measurement of Fluctuating Pressures in the Settling Chamber

Fluctuating pressures were measured on the settling chamber sidewall using a commercially available pressure transducer. Figure 13a presents the RMS fluctuating pressure normalized by local mean static pressure as a function of test section Reynolds number for a range of test section Mach numbers. These data cover a large portion of the tunnel operating envelope at a temperature of 140K. Figure 13b presents the spectra of the pressure fluctuations versus the normalized frequency, nondimensionalized by the revolutions of the fan, n , and the number of fan blades, N . The correlation of the data for fundamental frequency and approximately the first eight harmonics clearly indicates that the peaks in the fluctuation pressures are from the fan blade passage. Additional information is available in reference 26.

7.2 Measurements of Free Stream Turbulence by 3-wire Hot Wire Probe

The heat transfer characteristics of a three-wire hot-wire probe operated with a constant temperature anemometer were investigated in the subsonic compressible flow regime. The sensitivity coefficients, with respect to velocity, density and total temperature, were measured and the results were used to calculate the velocity, density, and total temperature fluctuations in the test section of the Langley 0.3-m TCT. The test section velocity and total temperature fluctuations are shown in figure 14. In the past mass flow fluctuations, referred to as velocity fluctuations, were often used to determine the disturbance levels in transonic wind tunnels. When the mass flow fluctuations for the 0.3-m TCT were calculated from the correlation coefficient of density and velocity, and the density and velocity fluctuations (see fig. 14a) from the 3 wire probe data the results were approximately an order of magnitude lower than the results shown. One should be aware of the difference between disturbance level determined from mass flow fluctuations and the 3 wire probe method. The method for the calibration and data reduction of a three wire probe is described in reference 27. By using the three wire probe technique, velocity, density and total temperature fluctuations can be measured without any further assumptions other than those usually made for hot wire anemometry in flows with small perturbations.

7.3 Measurement of Flow Dynamics in the Settling Chamber

There is theoretical and experimental evidence which indicates that a sudden or step increase or decrease in the rate of liquid nitrogen injection into the circuit of a cryogenic wind tunnel can cause a temperature front (or step) in the flow for several tunnel circuit times. Since these fronts can have an effect on the control of the tunnel as well as the time required to establish steady flow conditions in the test section of a cryogenic wind tunnel, tests were conducted in the settling chamber in the Langley 0.3-m TCT using high response instrumentation to measure the possible existence of these temperature fronts. Three different techniques were used to suddenly change the rate of liquid nitrogen injection into the tunnel and the results from these three types of tests showed that temperature fronts do not appear to be present. Figure 15 illustrates the "manual step" decrease in total temperature with no indication of temperature fronts for a circuit time of 0.89 seconds. See reference 26 for further details.

8. FLUID MECHANICS

8.1 Skin Friction Measurements

A skin friction balance has been developed by the University of Tennessee Space Institute, with the cooperation and support of the Experimental Techniques Branch, NASA Langley, for test on the test section sidewall of the 0.3-m TCT. The balance uses a belt supported by two flexures to measure shear force. Figure 16 is a section drawing of the device indicating the location of the flexures and the belt. The entire device is mounted with the belt flush with the surface of interest, in this case the test section side wall. Figure 17 is a plot of skin friction coefficient measured on the test section wall of the 0.3-m TCT and shown as a function of momentum thickness Reynolds number. Data was obtained at temperatures from ambient down to 100 K. The weak change with Reynolds number exhibited, rather than the classic power law decay, is thought to be due roughness due to joints between tunnel sections upstream of the measuring station. cursory comparison with a Moody pipe flow chart indicates an equivalent sand roughness height of 0.005 inches is sufficient to cause this type of Reynolds number trend. An interesting potential of this balance occurs with the substitution of a fiber optic pickup for the usual strain gages, which removes the barriers to miniaturization of the balance to a size where it can be installed into an airfoil model. These figures and further details may be found in reference 28.

8.2 Testing of Controlled Nonadiabatic Airfoils

The coupling of transonic flow and heat transfer has potential benefits both in boundary layer control and to enhance our understanding of fluid mechanics. The case of the model cooler than the flow is of particular interest, but the experiment is difficult in a conventional tunnel due to the formation of frost and ice. In the 0.3-m TCT cryogenic tunnel however, the working fluid is dry nitrogen and there is no water vapor to condense on the model. Testing is conducted by operating the tunnel above the temperature of liquid nitrogen and, by forcing liquid nitrogen through the model using the tubes shown in figure 18, it is possible to maintain the model surface at a much lower temperature. The model is constructed of beryllium-copper, which has a very high thermal conductivity, to aid in maintaining nearly uniform surface temperatures in the presence of heat transfer to the test gas. The model was equipped with sufficient surface pressure orifices to determine chord-wise pressure distributions. The integrated distributions were used together with the wake rake to calculate lift, drag, and pitching moment. These were determined for wall to total temperature ratios of adiabatic, slightly less than adiabatic, and as low as approximately 0.5.

9. TRANSITION DETECTION.

9.1 Transition Detection With Specialized Hot Films

An investigation to determine the location of boundary-layer transition was carried out using a similar cooled model to the one described above. The photograph in figure 19 shows the model mounted in the 0.3-m TCT with the chordwise rows of hot-film gages mounted on the upper surface. The model is a 9 inch chord, 12 percent supercritical 2-D airfoil and was instrumented with 48 hot-films. The extremely thin hot-films were applied to the surface of the model by the Douglas Aircraft Company (DAC), using a newly developed method, as part of a NASA/DAC cooperative program to develop a specialized system for detecting boundary-layer transition in cryogenic wind tunnels. The tests, conducted in the Langley 0.3-m TCT, were done both at an adiabatic wall condition and at a non-adiabatic wall condition with liquid nitrogen circulation through the model to cool the surface below the adiabatic recovery temperature. The surface cooling was done to determine the effect of wall temperature on the location of boundary-layer transition at wall to total temperature ratios as low as 0.47. The test results indicated, that with the proper electronic data acquisition equipment, an "on-line" location of boundary-layer transition could be obtained both at ambient and cryogenic conditions. The on-line signal from the hot-films clearly indicated either a laminar, transitional or turbulent boundary layer. Preliminary results indicated that model cooling actually decreased the transition Reynolds number due to the apparent dominance of surface roughness on transition at this condition.

9.2 Transition Location by Fluctuating Pressure Measurements

Figure 20 shows the outline of a 14 percent thick airfoil recently tested in the 0.3-m TCT. This two-dimensional model was largely hollow and contained 43 transducers capable of measuring fluctuating pressures. The three traces shown above the airfoil are typical of the output data from these transducers. The trace at the left is near the nose of the model, has a low length Reynolds number, and exhibits a low amplitude fluctuating pressure trace typical of laminar flow. The center trace is from a transducer measuring pressures further back on the airfoil and produces a trace typical of transitional flow with a higher fluctuating amplitude as background and with superimposed turbulent precursor bursts of much higher amplitude. The trace at the right is well into fully developed turbulent flow characterized by high amplitude, high frequency fluctuations in pressure. High amplitude fluctuations in the turbulent regime are perhaps expected for pressure measurements, as opposed to the decreased amplitudes recorded by the heat transfer devices, since the thickening boundary does little to attenuate pressure waves, but generally lowers heat transfer rates. Reference 29 presents data that indicates this same trend.

10. SUMMATION

Sophisticated test techniques have been developed to take advantage of the many research opportunities offered by the 0.3-m Transonic Cryogenic Tunnel. Although this review has not been exhaustive, sufficient material has been presented to show that test techniques used in the 0.3-m TCT are on par with the most advanced transonic facilities and that cryogenic operation poses no insurmountable handicaps.

11. REFERENCES

1. Tuttle, Marie H.; Kilgore, Robert A.; and McGuire, Peggy D.: **Cryogenic Wind Tunnels - A Selected, Annotated Bibliography.** NASA TM-86346, April 1985.
2. Kilgore, R. A.; and Dress, D. A.: **The Application of Cryogenics to High Reynolds Number Testing in Wind Tunnels. Part 1: Evolution, Theory, and Advantages.** *Cryogenics*, Vol. 24, August 1984, pp. 395-402.
3. Kilgore, R. A.; and Dress, D. A.: **The Application of Cryogenics to High Reynolds Number Testing in Wind Tunnels. Part 2: Development and Application of the Cryogenic Wind Tunnel Concept.** *Cryogenics*, Vol. 24, September 1984, pp. 484-493.

4. Johnson, C. B.; Murthy, A. V.; Ray, E. J.; Lawing, P. L.; and Thibodeaux, J. J.: **Effect of Upstream Sidewall Boundary Layer Removal on an Airfoil Test.** NASA CP 2319, 1983.
5. Murthy, A. V.; Johnson, C. B.; Ray, E. J. and Stanewsky, E.: **Investigation of Sidewall Boundary Layer Removal Effects on Two Different Chord Airfoil Models in the Langley 0.3-Meter Transonic Cryogenic Tunnel.** AIAA Paper No. 84-0598, 1984.
6. Johnson, C. B.; Murthy, A. V.; and Ray, E. J.: **A Description of the Active and Passive Sidewall-Boundary-Layer-Removal Systems of the 0.3-Meter Transonic Cryogenic Tunnel.** NASA TM-87764.
7. Balakrishna, S.; Kilgore, Allen W.; and Murthy, A. V.: **Performance of the Active Sidewall Boundary-Layer Removal System for the Langley 0.3-Meter Transonic Cryogenic Tunnel.** Vigyan Research Associates, Inc.; Hampton, VA 23665-1325. NASA CR 181793, Feb. 1989.
8. Wolf, S.W.D.; and Ray, E.J.: **Highlights of Experience with Flexible Walled Test Section in the NASA Langley 0.3-meter Transonic Cryogenic Tunnel.** AIAA Paper 88-2036, May 1988.
9. Young, C. P.; Bradshaw, J. F.; Rush, H. F., Jr.; Wallace, J. W.; and Watkins, V. E., Jr.: **Cryogenic Wind Tunnel Model Technology Development Activities at the NASA Langley Research Center.** Paper No. AIAA 84-0586, 1984.
10. Johnson, William G., Jr.; Hill, Acquilla S.; and Eichmann, Otto: **High Reynolds Number Tests of a NASA SC(3)-0712(B) Airfoil in the Langley 0.3-Meter Transonic Cryogenic Tunnel.** NASA TM-86371, June, 1985.
11. Mineck, Raymond E.; and Lawing, Pierce L.: **High Reynolds Number Tests of the NASA SC(2)-0012 Airfoil in the Langley 0.3-Meter Transonic Cryogenic Tunnel.** NASA TM-89102, July 1987.
12. Lawing, P. L.: **The Construction of Airfoil Pressure Models by the Bonded Plate Method: Achievements, Current Research, Technology Development and Potential Applications.** NASA TM 87613, September, 1985.
13. Wigley, D. A.: **Technology For Pressure-Instrumented Thin Airfoil Models.** NASA CR 3891, Contract NAS1-17571, May 1985. (Phase I SBIR)
14. Wolf, S.W.D.; and Ray, E.J.: **Highlights of Experience with Flexible Walled Test Section in the NASA Langley 0.3-meter Transonic Cryogenic Tunnel.** AIAA Paper 88-2036, May 1988.
15. Rebstock, R.; and Lee, E.E., Jr.: **Capabilities of Wind Tunnels with Two Adaptive Walls to Minimize Boundary Interference in 3-D Model Testing.** Paper given at the *Transonic Symposium*, NASA Langley, April 19-21, 1988, 26 pp. NASA CP 3020-Vol. 1, Part 2.
16. Honaker, William C., and Lawing, Pierce L.: **Measurements In The Flow Field Of A Cylinder With A Laser Transit Anemometer And A Drag Rake In The Langley 0.3-m Transonic Cryogenic Tunnel.** NASA TM-86399, April 1985.
17. Boyden, R. P.; Johnson, W. G., Jr.; and Ferris, A. T.: **Aerodynamic Force Measurements With a Strain-Gage Balance in a Cryogenic Wind Tunnel.** NASA TP-2251, December 1983.
18. Cole, Stanley R.: **Exploratory Flutter Test In A Cryogenic Wind Tunnel.** NASA TM-86380, February 1985.
19. Boyden, R. P., and Johnson, W. G., Jr.: **Results of Buffet Tests in a Cryogenic Wind Tunnel.** NASA TM-84520, Sept. 1982.
20. Gartrell, L. R.; Gooderum, P. B.; Hunter, W. H. Jr.; and Meyers, J. F.: **Laser Velocimetry Technique Applied to the Langley 0.3-Meter Transonic Cryogenic Tunnel.** NASA TM-81913, April, 1981.
21. Snow, W. L.; Burner, A. W.; and Goad, W. K.: **"Seeing" Through Flows in Langley's 0.3-Meter Transonic Cryogenic Tunnel.** NASA CP-2243, pp. 133-147, March 25-26, 1982.
22. Rhodes, D. B., and Jones, S. B.: **Flow Visualization in the Langley 0.3-Meter Transonic Cryogenic Tunnel and Preliminary Plans for the National Transonic Facility.** NASA CP-2243, pp. 117-132, March 25-26, 1982.
23. Burner, A. W., and Goad, W. K.: **Flow Visualization in a Cryogenic Wind Tunnel Using Holography.** NASA TM-84556, November 1982.

24. Snow, W. L., and Burner, A. W., and Goad, W. K.: **Image Degradation in Langley 0.3-m Transonic Cryogenic Tunnel.** NASA TM-84550, November, 1982.
25. Snow, W. L.; Burner, A. W.; and Goad, W. K.: **Improvement in the Quality of Flow Visualization at the Langley 0.3-m Transonic Cryogenic Tunnel.** NASA TM-87730.
26. Johnson, C. B.; and Stainback, P. C.: **A Study of Dynamic Measurements Made in the Settling Chamber of the Langley 0.3-Meter Transonic Cryogenic Tunnel.** Paper 84-0596, Presented at the AIAA 13th Aerodynamics Testing Conference, San Diego, California, March 5-7, 1984.
27. Stainback, P. C.; Johnson, C. B.; and Basnett, C. B.: **Preliminary Measurements of Velocity, Density and Total Temperature Fluctuations in Compressible Subsonic Flow.** Paper 83-0384 presented at the AIAA 21st Aerospace Sciences Meeting, Reno, Nevada, January 10-14, 1983.
28. Vakili, A. D., and Wu, J. M.: **Direct Measurement of Skin Friction With A New Instrument.** International Symposium on Fluid Control and Measurement, Volume 2, pp 875-880. Tokyo, Japan, 1985.
29. Harvey, W. D., and Bobbitt, P. J.: **Some Anomalies Between Wind Tunnel and Flight Transition Results.** AIAA Paper No. 81-1225 presented at the AIAA 14th Fluid and PlasmaDynamics Conference, June 23-25, 1981, Palo Alto, CA.

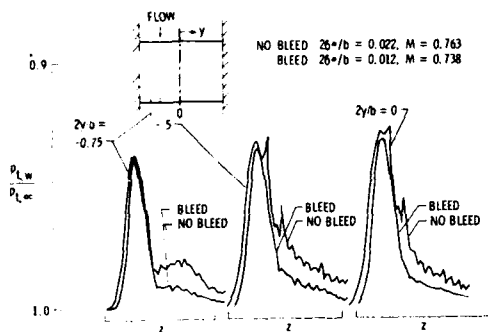


Figure 1.- Pitot surveys at three spanwise stations in an airfoil wake with and without sidewall boundary layer bleed, $M = 0.76$, $R_c = 6 \times 10^6$, $\alpha = 2^\circ$, $c_n = 0.88$.

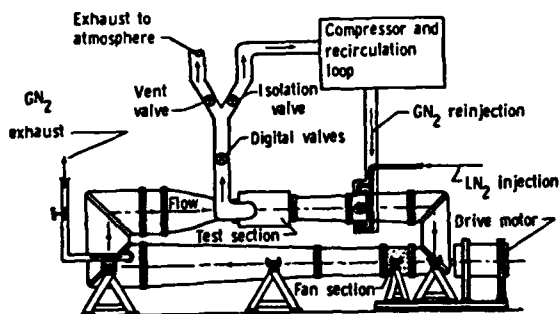


Figure 2.- Cryogenic compressor linked to the 0.3-m Transonic Cryogenic Tunnel.



Figure 3.- Pressure channels cut into opposing halves prior to brazing together to form a bonded plate model.

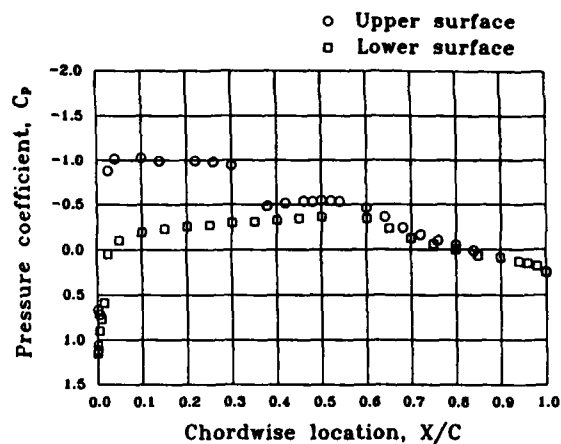


Figure 4a.- Pressure distributions on a 12% symmetrical supercritical airfoil; positive angle of attack, lift coefficient of 0.31.

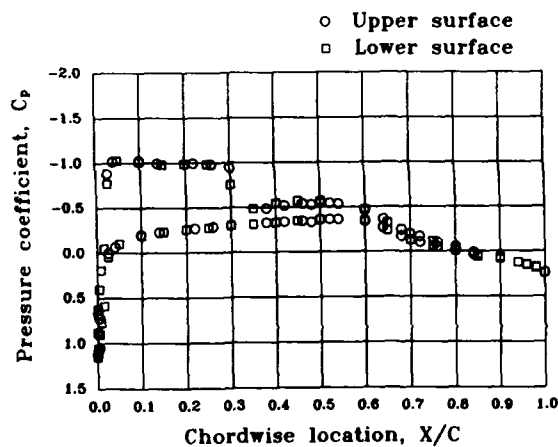


Figure 4b.- 12% symmetrical supercritical airfoil; negative angle of attack, lift coefficient of -0.31 superimposed on data of figure 4a.

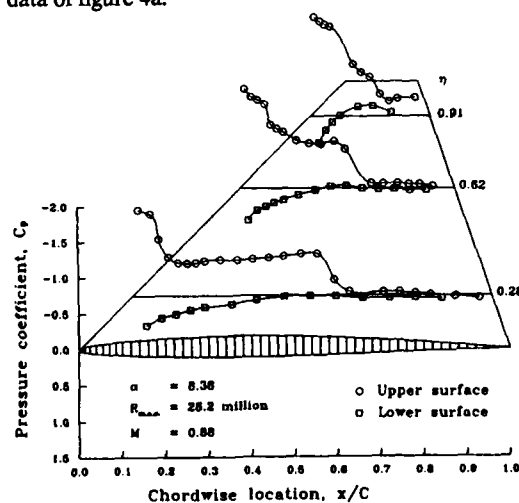


Figure 5.- Pressure distributions on the X29 canard.

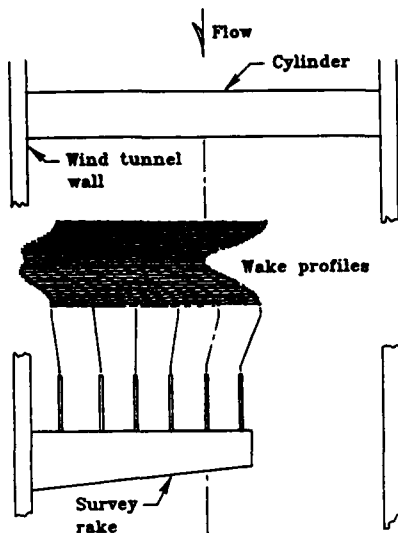


Figure 6.- Three dimensional wake topology for a transverse circular cylinder.



Figure 7.- Three dimensional model and support used in balance evaluation tests.

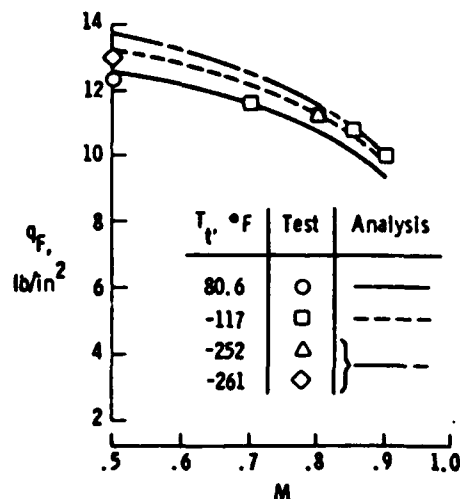


Figure 8.- Experimental and calculated flutter results.

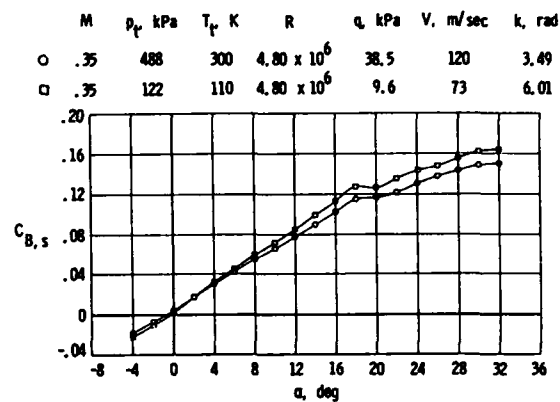


Figure 9a.- Steady and dynamic load characteristics for a sidewall mounted delta wing. Steady wing-root bending moment coefficient.

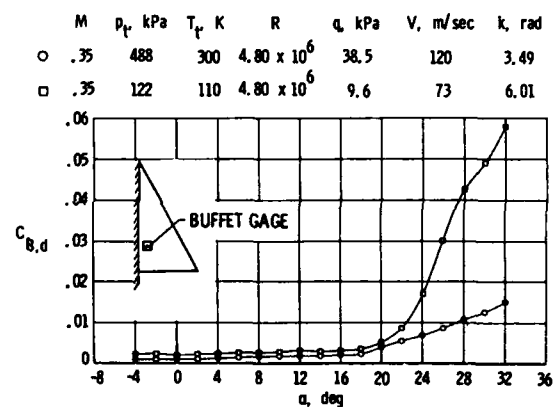


Figure 9b.- Dynamic wing-root bending moment coefficient for two values of the reduced frequency parameter.



Figure 10.- Oscillating airfoil model shown mounted in 0.3-m TCT test section.

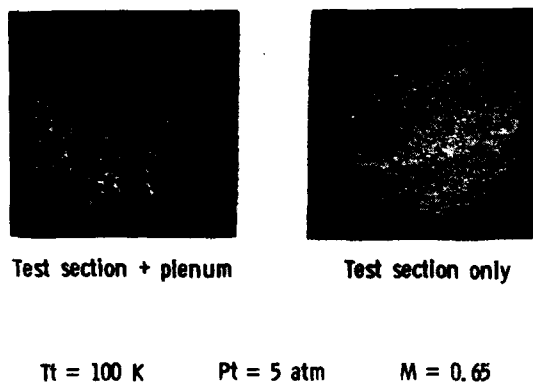


Figure 11.- Optical path through the plenum and test section before and after isolation of the beam from plenum disturbances.

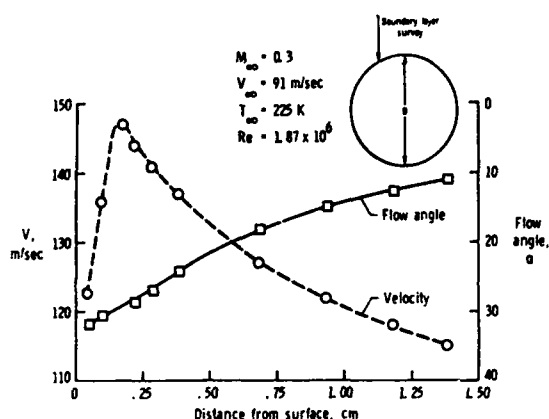


Figure 12.- Velocity and flow angle as a function of vertical distance from the surface along the indicated scan line.

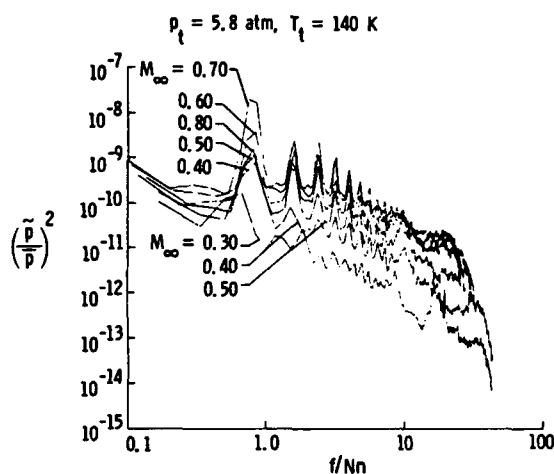


Figure 13b.- The spectra of pressure fluctuations in the settling chamber for a dimensionless frequency and a pressure of 5.8 atm.

3 wire probe, $M_\infty = 0.2$ to 0.7 , $T_t = 280 \text{ K}$, $p_t = 1.2$ to 3.3 atm

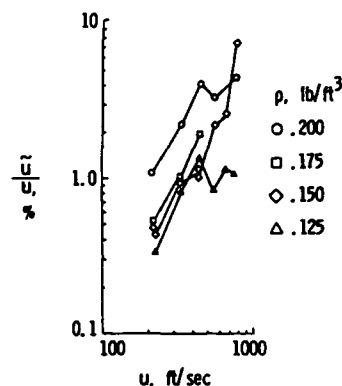


Figure 14a.- Fluctuating quantities measured in the test section at a total temperature of 280 K. Normalized velocity fluctuations as a function of free stream velocity for a range of densities.

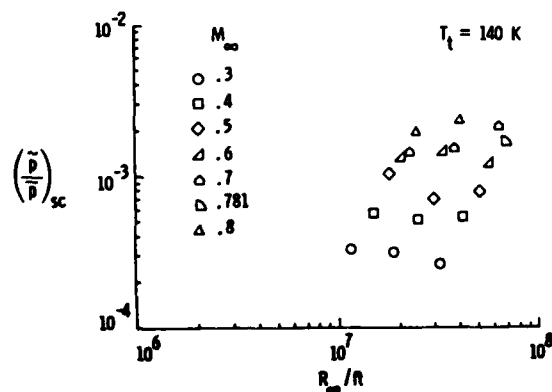


Figure 13a.- Fluctuating pressure data from the settling chamber at cryogenic conditions of 140 K. Pressure fluctuations in the settling chamber.

3 wire probe, $M_\infty = 0.2$ to 0.7 , $T_t = 280 \text{ K}$, $p_t = 1.2$ to 3.3 atm

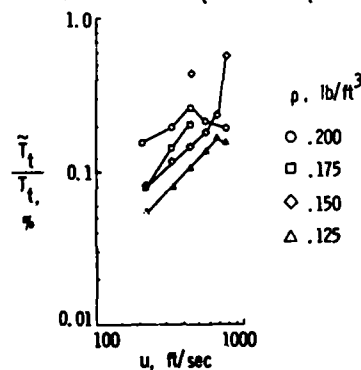


Figure 14b.- Normalized total temperature fluctuations as a function of free stream velocity for a range of densities.

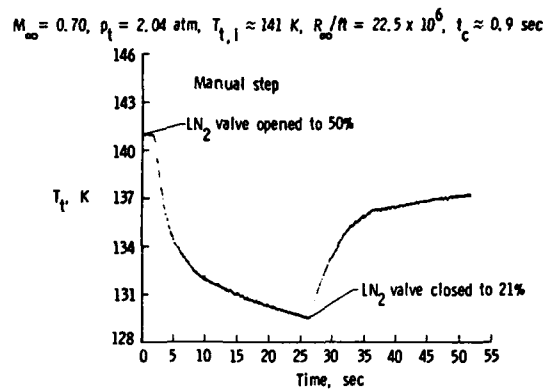


Figure 15.- Settling chamber total temperature as a function of time after a sudden input of liquid nitrogen.

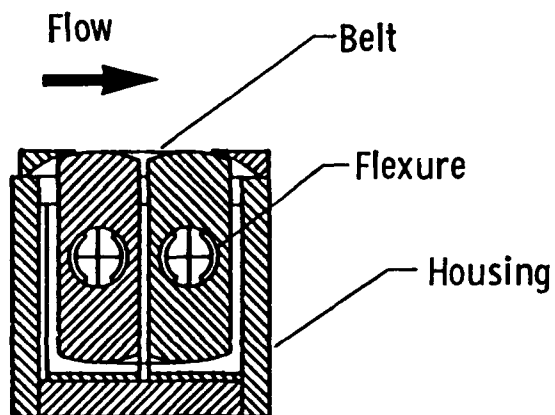


Figure 16.- Cross section of skin friction balance.

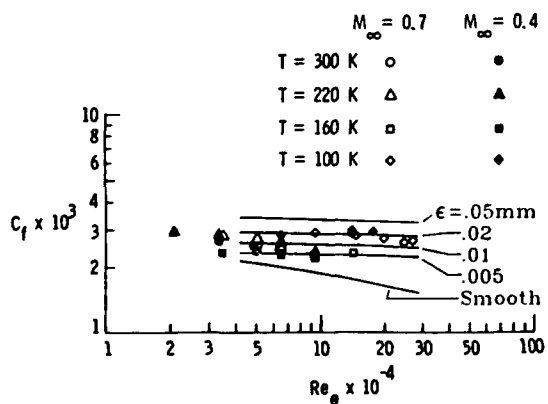


Figure 17.- Measured skin friction coefficient as a function of wall Reynolds number based on momentum thickness.



Figure 18.- Liquid nitrogen cooled airfoil model.

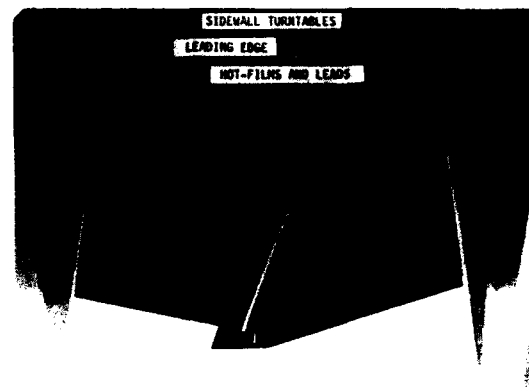


Figure 19.- Airfoil model instrumented with hot film gages shown mounted in 0.3-m TCT test section.

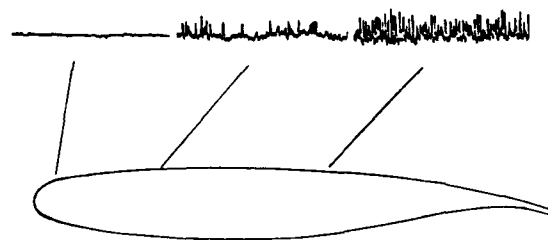


Figure 20.- 14% supercritical airfoil outline and sample fluctuating pressure traces.

FLOW VISUALIZATION IN THE CRYOGENIC WIND TUNNEL

M.J. Goodyer
Department of Aeronautics and Astronautics
The University
Southampton SO9 5NH, England

Summary

A range of flow visualization methods for possible application to model testing in the large cryogenic wind tunnel is described. Desirable features are outlined, including the flow details which should be revealed by the various methods. The risks of model and tunnel contamination are discussed, also the coverage of the model surface to be expected, the advance planning and complexity of model design and tunnel equipment required by the visualization method, and the prospects of generating multiple flow images during one tunnel run. The methods to be outlined are at an early stage of development but in all cases there is some cryogenic experience to support their consideration for use in the cryogenic environment. None is well established for use at the highest Reynolds number conditions attainable in the cryogenic pressure tunnel.

1. Introduction

The techniques fall fairly naturally into two categories: for surface flows and whole field flows. An ideal would be to provide the user with a single method for each category which will show these details in repeated tests giving complete surface/flowfield coverage over the whole operating envelope of the tunnel, with the method itself not influencing the flow. This is a challenging requirement at normal temperature and is likely to be more so over the bands of temperatures and pressures available in the cryogenic wind tunnel. As the methods available for use at normal temperatures are varied and well understood, this lecture concentrates on the issue of low temperature testing, recognising the special constraint of limited access to the model area.

The lecture is confined to the class of flow visualization methods where an image may be viewed and recorded, and excludes other methods of determining flow details from which images might be constructed, such as by the use of probes, thin films, surface force gauges and the like and also laser measuring devices which, although often appearing in references on flow visualization, do not in fact directly provide any visual information. Because our foremost interest is in the cryogenic wind tunnel, the lecture is also confined to descriptions of those visualization methods on which there is some cryogenic temperature experience. It is known that other methods are under active development.

The choice of method will be influenced by the circumstances of the test. There are two broadly different sets of circumstances in which aid from a flow visualization method could be requested. Either the need for some flow visualization is recognised well in advance of the design of the test in which case there should be a wider choice of visualization methods, or, and perhaps more likely, flow visualization is required at short notice as a diagnostic tool in which case the range of options may well be narrow. It will become apparent that the technology is very immature, requiring much more work and experience at both the development and application levels, and therefore the information in the lecture is more of a pointer towards possibilities than a guide to good practice. In these circumstances it is inevitable that the lecture will also have something of the flavour of a research report.

2. Requirements

(i) Aerodynamic

An important requirement of a surface flow visualization method is to reveal details of the boundary layer flow direction. In doing so it is likely that the method will also reveal the existence and location of separations. The user would value information on transition particularly where this is not itself influenced by the visualization method. For higher speed testing an indication of the position of the shock is an additional requirement, together with evidence of any associated separation. The visualization of whole-field flows is also expected to reveal flow direction, separations including vortices, and shocks. Non-intrusive methods are highly desirable, perhaps in all branches of aerodynamic testing but certainly at transonic speeds.

It can be seen that the ability to survey a broad area of the model is important simply because the flow is not known in advance. It would seem that a minimum requirement is for the flow visualization method to reveal details along a line, but with a preference for multiple lines, in the limit tending to area or volume coverage.

Most of the immediately more promising methods for surface flows involve the use of materials in the liquid or solid phases on or close to the surface of the model. An implication is that the boundary layer flow might be influenced by the presence of the material to the extent that the character of the boundary layer, and through this the entire flow around the model, is changed sufficiently to invalidate the test information. This is a risk which must be recognised and accepted. Normally there will be other sources of information, such as force balance data, to warn of the event. Two forms of surface contamination are possible. One is temporary,

such as might be the case with the use of a liquid as a marker to reveal flow direction, the liquid subsequently evaporating. The other form of contamination is more permanent, such as caused by the deposition of a non-volatile liquid or a solid. The persistence of such a liquid in low speed flow, and more generally a solid at any test condition, at least could prove a nuisance. Some non-intrusive optical methods for whole flowfields exploit a seeding of the flow, natural or contrived. The usefulness arises from the fact that the seeding is relatively widely dispersed through the field and, with the aid of suitable illumination, the flow can be visualized in a large volume around the model. However the question could be asked as to whether, with seeding, the method is really non-intrusive?

Contamination of the tunnel is likely to occur simultaneously if there is any contamination of the model by an aid to visualization. The aerodynamically significant forms of tunnel contamination could take the form of a gradually increasing level of seeding of the stream by liquid or solid particles, or deposits of the flow visualization medium on the tunnel's structure. Particles of either phase carried in the airstream will in time affect the surface finish of models by erosion, particularly rapidly in high speed tests. Settling chamber screens may be the tunnel components showing the most aerodynamic sensitivity to the formation of deposits, solid or liquid. Deposits can be expected to affect the pressure drop across the screen, with consequences in terms of tunnel speed/power, and screen loading. Heavier deposits may induce flow non-uniformity through uneven blockage of the screens, or modify the turbulence levels through changes in the characteristics of the screens and a shift in the operating point of the fan. Methods must be absolutely avoided which would result in a gradual accumulation of deposits which fail to disappear naturally when the tunnel is returned to room temperature.

(ii) Operational

A general operating requirement will be provision for the recording of images for post-test analysis. The environment of the large tunnel will dictate that this equipment, along with any other which may be required by the visualization method, be remotely operated. Further, time and the cost of tunnel operation will impose the need for a high level of reliability in the equipment.

Tunnel economics will also dictate that means are provided for the removal and recreation of surface flow patterns, repetitively on a particular model though different combinations of model attitude and tunnel flow condition.

Methods must be available for use over the entire, or a usefully broad portion, of the operating range of the tunnel, that is the methods must cover the types of test gas and the ranges of speed, pressure and of course temperature experienced in the tunnel circuit.

Optical access at appropriate wavelengths will be required similar in extent to that available in conventional tunnels, for viewing from appropriate angles by video or film cameras and to allow the illumination of the model. The contamination issues already raised are particularly important in respect of the windows and other optical components. Contamination can occur through erosion and the deposition of the flow visualization medium. Contamination of windows or model by deposits, if not avoided by the design of the visualization method, often can be removed by evaporation or sublimation at appropriate but sometimes quite low values of tunnel temperature, by the choice of a suitable visualization medium. A form of contamination affecting some optical methods is caused by refractive index variations along the light path outside the test section.

3. Surface Flow Visualization Methods for the Cryogenic Tunnel

This lecture describes five methods on which there is some experience and which might satisfy at least some requirements. The methods have all been demonstrated in cryogenic wind tunnels. They are:

- Tufts
- Liquid film with tracer
- Condensing or freezing gases
- The China Clay method
- Frost deposit.

All offer the prospect of showing some detail of surface flow at cryogenic temperatures and, by sensible design, most should not permanently contaminate the model or tunnel with deposits.

The first four of these techniques happen to have been developed in a small low speed cryogenic wind tunnel built for flow visualization experiments at Southampton University in 1976/77. As it is not described elsewhere in the lecture series, a few words on its features would be appropriate. It has a working section 10cm square in cross section and operates only at atmospheric pressure, at low Mach numbers and temperatures from about 80K to 380K. Its outline is shown on Figure 1, together with its control systems which are mostly closed-loop, and the data logging system. The tunnel is cooled with liquid nitrogen and the circuit pressure is held near atmospheric by a vent to atmosphere. For the developments reported here the tunnel was filled with nitrogen gas. The liquid nitrogen storage capacity permits, for example, one cooldown of the tunnel followed by 30 to 45 minutes of operation in the cryogenic temperature range at test section Mach numbers ranging from a minimum of about 0.05, to a maximum of about 0.4 depending on temperature. The high level of automation gives the user the freedom to concentrate on the experiment. There is a quadruple-glazed window for illuminating and viewing the model.

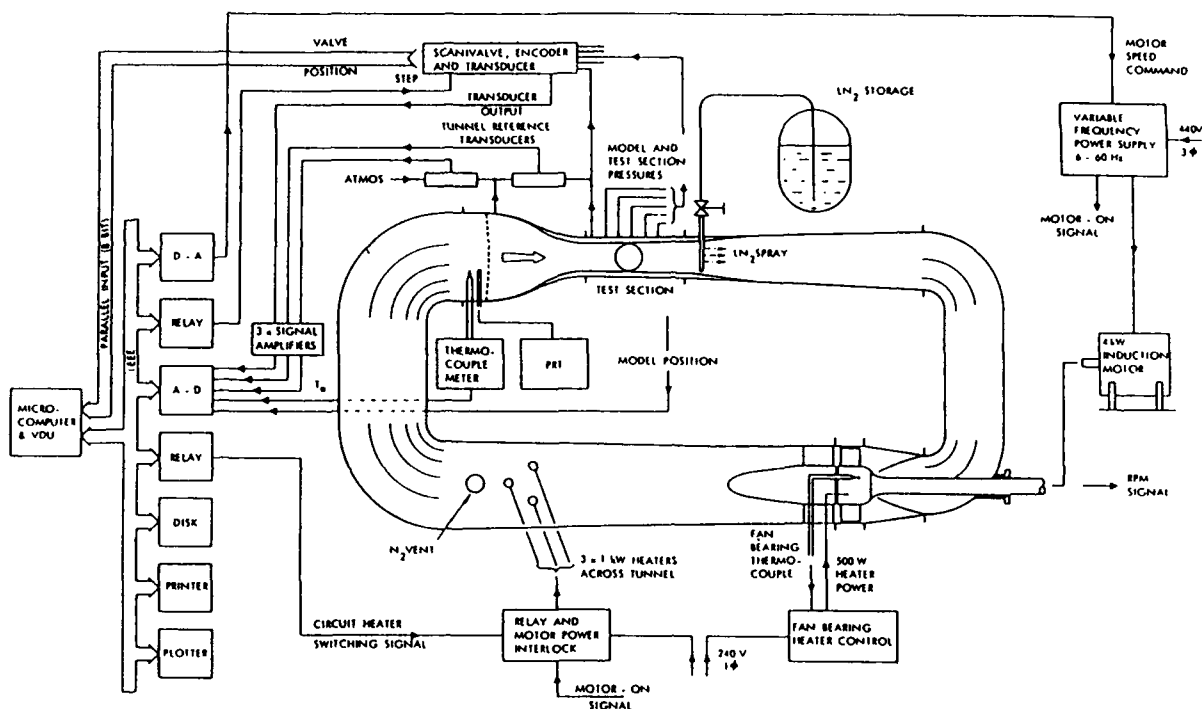


Figure 1. 0.1m Cryogenic wind tunnel and systems

The operating envelope is shown on Figure 2. The portion of the envelope used during the experiments is approximately bounded by vertical constant Mach number lines at Mach 0.07 and 0.2, and the constant temperature lines of 80K and 300K. The variations of Reynolds number which occurred during these tests do not have any particular significance in the flow visualization context: for example no determined attempt has yet been made to locate boundary layer transition. Further details of the construction and performance of the tunnel are available.^{1,2}

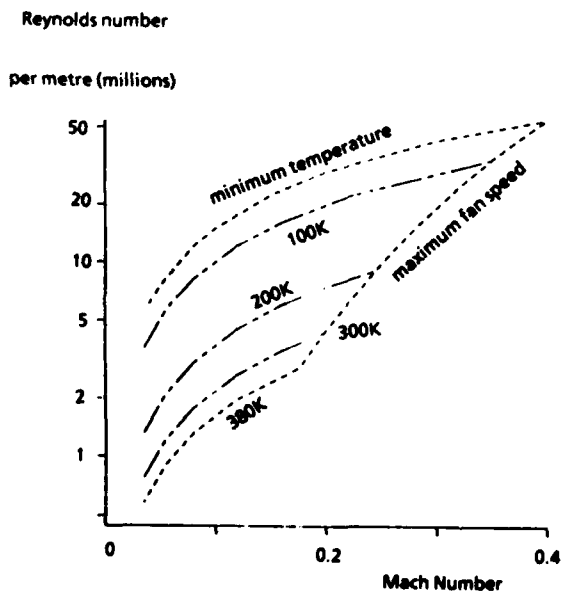


Figure 2. Operating envelope of 0.1m cryogenic wind tunnel

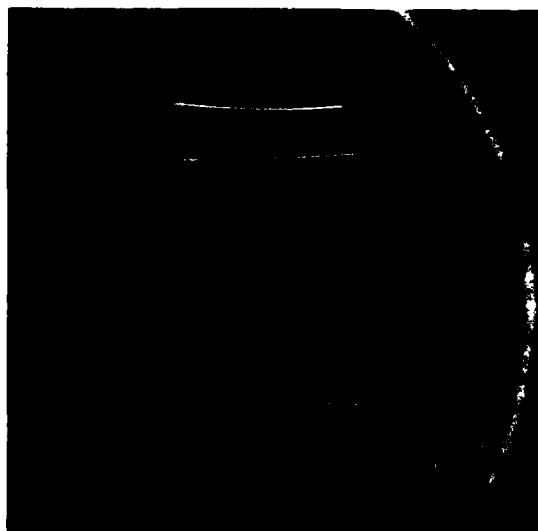


Figure 3. Fluorescent monofilaments bonded to a stainless steel plate. U.V. illumination. Wind is left to right, at 105K

3.1 Tufts

The method has been explored^{3,4} in this cryogenic tunnel and is under investigation for use in NTF. The Southampton tests covered the woven tuft materials wool, wool/nylon mix, acrylic and nylon, with additional tests using monofilament fluorescent fishing lines. The fluorescent lines had diameters of 0.2 and 0.04mm.

The attachment material was 5-minute epoxy onto unpolished brass, unpolished aluminium alloy, or polished stainless steel. No operational problems were experienced although some woven samples showed signs of erosion of the free end of the tuft in the longer term when induced into a vigorous coning motion under a vortex.

Against suitably contrasting backgrounds all were readily visible and easy to photograph from outside the test section. In these tests the model (usually a slender delta wing) was painted a light colour while the tufts (except the fishing line) had bright contrasting colours in daylight. There may not always be the freedom to change the background colour of models although contrasting tuft colours should be easy to find. Normal lighting and photographic techniques have been used. These, plus T.V. recording methods, can be expected to satisfy the requirements of larger tunnels. Fluorescent tufts under UV lighting contrast well against an otherwise unlit model and can be recorded on conventional photographic material. In the small tunnel used for these tests a 75 watt UV lamp provided adequate illumination for viewing by eye and for photography. Figure 3 is such a photograph taken at the test conditions Mach 0.15 and stream temperature 105K. Four fluorescent monofilaments of the larger diameter (0.2mm) were attached to an aluminium flat plate mounted at zero incidence. 0.04mm tufts are visible under conventional illumination on Figure 8.

The total wind-on time for each tuft was measured in hours but the wind-on experience with any one sample in the temperature range below 150K was only 30 to 45 minutes. Minimum stream temperatures were 80 to 82K in all cases, and the maximum Mach number about 0.2, but Mach 0.25 was reached at 100K with the 0.04mm monofilament with no adverse effect.

Tufts may be expected to show surface flow direction and the existence of flow separation, possibly shock position when accompanied by separation, but not transition. While it is inconceivable that practical sized tufts and their attachments can be used without disturbing the state of a laminar boundary layer, Crowder⁵ claims that mini-tufts do not produce a significant disturbance to the flow aft of transition. Tufts also offer easy recording, repeated tests, area coverage may be acceptable aft of transition and elsewhere if the user is prepared to accept a measure of flow disturbance, and tufts are usable over the whole temperature range of interest in the cryogenic wind tunnel. Their method of attachment allows them to be installed on any model without special preparation and at relatively short notice, for surface flow diagnostic purposes.

Some open questions remain concerning durability of a tuft and its attachment at the higher speeds and pressures existing in tunnels such as NTF and ETW. Durability can be explored relatively economically in smaller pilot tunnels which reproduce conditions very similar to their larger counterparts.

The difference in scale between the test section in which this investigation has been carried out [0(0.1m)] and that of a full scale Reynolds number tunnel [0(2.5m)] most probably will dictate the use of different photographic methods. In choosing the UV illumination the guidance of Crowder may be followed. He recommends⁶

- i) **Filters.** An exciter filter is used over the illumination source to pass the UV light and block visible light, and a barrier filter over the camera lens to pass the visible fluorescence and block the reflected UV.
- ii) **Flash lamps.** Photography at distances of about 3m require flash lamp powers of 1 to 4kJ. Commercial pulsed xenon flash lamps can be adapted, which provide a flash duration of about 5 milliseconds.
- iii) **The windows in the test section passing the UV light to the model area must not themselves act as UV filters.**

Conventional photography may prove to be the only feasible method of recording images. Protected and remotely operated cameras must be provided, with the means to retrieve (and perhaps replace) exposed film.

In summary, it appears that the use of tufts is a feasible method for surface flow visualization in the cryogenic wind tunnel. Although relatively crude and simple, the method promises to provide a variety of surface flow information at low cost and with a minimum of advance planning. The planning which is required applies to the tunnel itself rather than to the model.

3.2 Liquid Film with Tracer

The original notion was to transport a pigment to the surface of a model, the pigment being in suspension in a suitable carrier liquid which subsequently evaporated leaving pigment patterns of the surface flow.

The method has a similar potential to tufts in terms of coverage of model, recordability, the requirements of recording equipment and information derivable from an image. Two series of tests have been carried out using liquid propane as the carrier, the first in the Southampton tunnel^{3,7} using as tracer either a powdered conventional paint pigment or a fluorescent powder, the second at Douglas^{8,9} using a dissolved dye as tracer, perhaps fluorescent. Information on experiences with the latter is not available. A test scheduled for about May 1980⁸ is believed to have taken place but the 1982 reference⁹ surprisingly makes no mention.

Propane as a carrier liquid is quite versatile and is probably usable at almost all values of pressure and temperature reached in cryogenic tunnels. The need to dispense the liquid reasonably uniformly via galleries in the model to a set of orifices, or to a porous surface, requires the liquid to be pressurised perhaps to several atmospheres above the maximum of the tunnel. This is sufficient to keep the propane in the liquid phase while flowing inside the model, at any temperature from room temperature on downwards to around 85K and there seems to be no reason to propose the use of different liquids depending on tunnel conditions. At atmospheric pressure its melting and boiling points are respectively 85°K and 231°K. These figures, together with the fact that it is non-toxic and readily available, make propane an almost ideal substance. The viscosity of propane near its melting point is estimated to be about 1.8×10^{-3} kg/m sec. Water at 20°C has a viscosity of 1.005×10^{-3} kg/m sec.

The arrangement of the propane system and test section used in the Southampton tests is shown schematically on Figure 4. Propane is stored in bottles A and B and the powder placed in the mixing chamber C. These three components and their nearby valves and pipes remain at room temperature. The powder is driven into suspension in liquid propane by a magnetic stirrer and, with the model and wind tunnel stabilised at the desired cryogenic test conditions, the mixture at a nominal 10 atmospheres pressure allowed to pass through a cooling loop exposed in the test section and from there via pressure reducing valve V to galleries in the model. At the low temperature prevailing in the propane in the galleries it remains liquid.

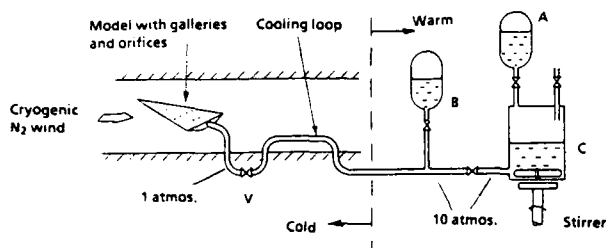


Figure 4. Propane/pigment surface flow visualization equipment



Figure 5. Flow patterns formed by propane/pigment suspension on upper surface of delta wing. Suspension is dispensed from internal galleries

The suspension emerges on the surface of the model and once in the gaseous nitrogen environment of the wind tunnel the liquid propane quickly evaporates because of the near zero partial vapour pressure of propane. In evaporating, the liquid moves with the flow and leaves deposits of pigment on the surface showing the flow pattern. When left on the model the pigment showed no tendency to blow away although it seemed to be possible to remove it by passing clear propane to the model from bottle B to wash off the pigment. This is an important feature because the ability to remove the flow pattern allows different flows to be studied during one tunnel run.

Pigment deposits have been made using this method at tunnel temperatures down to 85K. Figure 5 is a photograph of a pattern, produced at about this temperature, on the upper surface of a sting-mounted slender delta wing. The leading edge sweepback is 70° and the incidence 15°. The surface patterns induced by the vortices are readily apparent on the port half of the wing. The patterns are unclear on the starboard half because frost has begun to form: the model was removed too soon from the wind tunnel.

While there is no doubt that this method will provide surface flow information in a cryogenic wind tunnel, there are several issues to be raised relevant to its application in full-scale Reynolds number cryogenic wind tunnels. If the suspension is to be delivered through internal galleries, the need for surface flow visualization must be anticipated ahead of model design and construction. Orifices which can pass the pigment without blocking may prove too obtrusive. There is the untried option of spraying a model with a similar suspension, which might prove satisfactory at low speeds. It is unlikely that dispensation of this mixture through orifices ahead of transition would be acceptable on arguments of the obtrusiveness of the mixture and the orifice-induced disturbances, which would limit the area of coverage to aft of the anticipated natural transition line. Secondly, the adherence qualities of pigment (or similar powder) to a polished metal surface at the conditions existing in a transonic pressurised tunnel are unknown. Thirdly, there is the question of tunnel contamination, in particular the contamination of the screens but also (in the writer's experience) subsequent generations of model by powder circulating the tunnel. Experience might show that the second concern (over adherence) is unfounded, but the third, that of powder contamination, cannot be ignored.

3.3 Condensing or Freezing Gases

In this surface flow visualization method, a gas is introduced to the flow just upstream of the model in the form of a discrete localised jet. With an appropriate combination of gas and model surface temperature the gas may be deposited as a solid or liquid showing the boundary layer flow direction by the pattern of deposit. There is also the possibility that the nature of the deposition, or its subsequent reliquefaction, sublimation or evaporation might show evidence of other flow properties such as transition, separation or shock position.

The phrase 'marker gas' is used to refer to the state, at normal temperature and pressure, of the substance which is to be used for surface flow visualization. When in use in a cryogenic wind tunnel the marker gas might undergo several changes of phase. The technique has been developed^{4,10*} for application to the nitrogen cryogenic wind tunnel. The marker gas is chosen to combine the possibility of showing surface flow details without permanently contaminating the model or tunnel. The intent is that once temperatures are raised sufficiently the deposits will vaporise and then be carried away in the nitrogen flow.

There is a large number of non-toxic, non-corrosive gases available for consideration, having melting or boiling temperatures in the cryogenic range at atmospheric pressure. It should be noted that the temperatures which are normally quoted apply to phase changes at atmospheric pressure in the presence of the same substance. In general the phase changes will be affected by the environment of a wind tunnel where there might exist complex combinations of phases, and gradients of partial pressure of the gas phase adjacent to the surface of the model, generally modifying the melting, boiling or sublimation temperatures. Many of the marker gases falling into this category are hydrocarbons and fluorocarbons.

A number of demonstrations has been carried out in which deposits have shown flow details over simple flat plates. The longitudinal cross section of the arrangement for these tests is shown on Figure 6, a sketch which extends from the end of the contraction to the beginning of the first diffuser.

The leading edges of the plates were radiused to discourage a separation bubble. The information in hand does not allow a claim that a bubble did not exist, or speculation on the state of the boundary layer on the plate. The plates were generally smooth.

The marker gases were introduced through a 3.6mm bore brass tube which was positioned as shown on Figure 6 for this operation, directly ahead of the leading edge. The tube was exposed to the cold flow and was uninsulated. To remove subsequent disturbance to the flow it was occasionally traversed away from the leading-edge region after depositing the gas. The supply pipe was primed with the marker gas while the tunnel was still at room temperature, the gas flow then being turned off to avoid plugging the pipe with the marker gas during the cooldown of the tunnel.

The procedure followed was to cool the tunnel to a desired temperature (and by this stage any air in the tunnel would have been purged) then to briefly inject a marker gas while observing and photographing results through the window. On the occasions when a phase change was to be induced in a deposit the temperature of the tunnel and plate usually were allowed to drift upwards with the LN₂ supply turned off. Tunnel tests were carried out with argon, CO₂ and Freon-12 (CCl₂F₂). Results are discussed only for the latter two because any argon deposits, if they were present, were not visible.

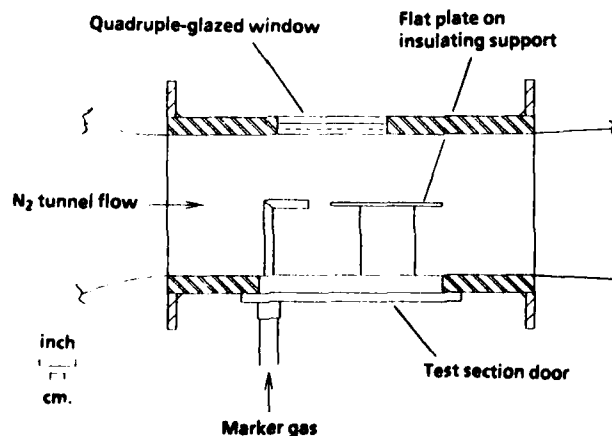


Figure 6. Arrangement for surface flow visualization demonstrations using deposits of condensing or freezing gases

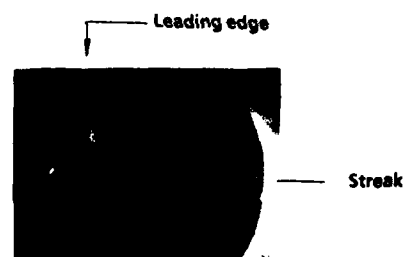


Figure 7. Streakline of CO₂ deposited at 83K on polished stainless steel plate

* The work was supported by Southampton University and by NASA under contract NAS1-17919, and currently under NASA Grant NSG-7172

CO₂

Solid deposits were made easily in the form of a streak downstream of the pipe at plate and test section stream temperatures between 83K and 220K. Under the illumination of a tungsten filament lamp their perceived colour was not always white but varied from white through grey to brown depending on the viewing angle. The contrast with the plates was always good, and the deposits remained attached to the plates (aluminium or stainless steel) and intact until sublimation occurred. Typically a streak was about 6mm wide at the leading edge of the plate, diverging to about 10mm at the trailing edge, about 100mm downstream. A relatively permanent indication of boundary-layer flow direction is thus obtained. Gradually the streak would disappear, although not uniformly, when the plate was allowed to warm. Using the aluminium plate there was a tendency for a waisting of the deposit to form just after the leading edge and the deposit to first disappear at the waist, then downstream, then finally between the waist position and the leading edge. The uneven disappearance could have arisen because of an uneven initial deposit or because of uneven sublimation, or both. A photograph is shown on Figure 7. The view is directly onto a stainless steel plate. The flow is left to right. The dispensing pipe is not visible because it has been retracted to avoid the possibility of the sublimation events being influenced by its wake. The photograph was taken just after deposition at a temperature of 83K and Mach 0.15. The streak, which is slightly divergent and generally light, is visible in the picture for only a short distance as a consequence of the camera angle. All deposits could be seen easily by eye reaching to the trailing edge of the plate. Following this deposition the tunnel and plate were slowly warmed. The deposit had completely cleared by the time the temperature reached 148K. Both of these temperatures are well below the quoted sublimation temperature of CO₂, which is about 195K. In another demonstration, slow sublimation was observed from a deposit on the stainless steel plate when the plate and test gas stream temperatures were held constant at 148K. From the accumulated experience it is beginning to appear that CO₂ deposits may be made at any temperature from about 77K to around 200K, and that sublimation will be experienced at stream temperatures well below 195K.

A word of caution is appropriate. It was noticed that the generous use of CO₂ in the tunnel could induce a general deposit of a thin layer of CO₂. This was noticed on the test section window as a clouding. The deposit completely disappeared when the tunnel temperature was raised close to 200K. While the clearing of the window does underline the fact that this marker gas will not permanently contaminate the model or tunnel, it also serves to warn of the possibility of general deposits of CO₂ forming in the tunnel or on the model, perhaps affecting the performance of both.

Freon-12

At one atmosphere the melting and boiling temperatures of Freon-12 are respectively 115K and 243.4K in the presence of Freon-12. Deposits of liquid or solid F-12 have been made in the temperature range 223K to 101K, on an aluminium plate.

In the narrow temperature range 113K to 101K the deposits of F-12 are solid, forming a streaky patch extending rearwards from the leading edge with a build up like rime ice on the leading edge. The solid deposits are white and clearly visible, but from an aerodynamic viewpoint are probably useless because of their intrusiveness. On warming the tunnel to about 115K the deposits melt and stream away.

When deposited as a liquid, in the temperature range 139K to 183K, F-12 forms a relatively uniformly wetted streak, easily visible. The wet streak dries progressively from the edges inwards at a rate which seems to increase with temperature even though this range of temperature is well below that quoted for the boiling of F-12, 243K. The evaporation was presumably a consequence of the low partial pressure of F-12 in the tunnel, but does seem to offer the possibility that the manner of the evaporation of this gas, and others similar, might show surface flow details additional to that of flow direction, for example transition or separation. The photograph of Figure 8 shows liquid Freon-12 evaporating at 148K. The edges of the streak, where evidently it was drying, are clearly seen. There was no residue left on the plate when the evaporation process was complete. Also visible are four monofilament tufts (the 0.04mm diameter fluorescent type) and their attachments.

Figure 8. Liquid Freon-12 evaporating from flat plate at 148K



3.4 The China Clay Method

This method¹¹ uses two materials deposited on the surface of the model. For use at room temperature the model is first "coated with a layer of a colourless solid of fine crystalline structure appearing white when dry. This solid deposit is then covered with a volatile oil of the same refractive index so that the layer becomes virtually transparent. As the oil is evaporated during the tunnel run the white appearance of the dry solid is once more seen, and, evaporation being more rapid in the turbulent than in the laminar region of the boundary layer, a white layer appears on the aerofoil surface aft of the transition point. ... The surface thus obtained was very smooth, the degree of roughness appearing to be no greater than that of the uncoated aerofoil surface."¹²

The method has been adapted for the cryogenic wind tunnel with some success. The principal alteration is to substitute for the volatile oil as developer. Freon-12, butane and propane have been used, with little to choose between them. Figure 9 is a photograph of a stainless steel flat plate viewed through the test section window. The plate has its surface coated with china clay to a thickness of about 0.001" (1/40 mm) which is dry and white in the light areas of this figure. The flow is left to right. The dark streak along the centre running aft from the leading edge (the vertical line just left of centre, partly in shadow and partly confused by reflections) is the area wetted by liquid Freon-12 deposited from the pipe shown in Figure 6. The tunnel conditions were Mach .15 at 122K. The contrast is very good with this developer, as it is with the others, which should allow for easy photography in a large tunnel. Evidence of the transparency of the china clay soaked with propane is the appearance of the (filled) heads of mounting screws which are quite invisible under dry china clay. One can be identified in this photograph near the centre of the propane streak to the right of the inner glazing frame.

Figure 10 is an example of a similar width of streak, again with liquid Freon-12 deposited onto china clay at the flow conditions of Mach .15 and 123K. The photograph was taken some 8½ minutes after the deposition when evaporation had begun to modify appearance. There is evidence of selective evaporation: rapid evaporation near the leading edge and again further downstream, these regions being separated by a darker patch which is still wet. The trailing edge of the dark patch is about 2cm aft of the leading edge. The photograph of Figure 11 is similar except that a broader band of Freon-12 has been painted over the surface using a sweep of the depositing tube. The band was perhaps twice as wide. The wet portion which remained when this picture was taken is similar in its streamwise extent but has a dry penetration at the centre, downstream of the depositing pipe which was deliberately left ahead of the plate to induce turbulence.



Figure 9. Light areas are dry china clay on stainless steel plate. Flow direction is shown by dark streak of liquid propane developer deposited at 122K and Mach 0.15

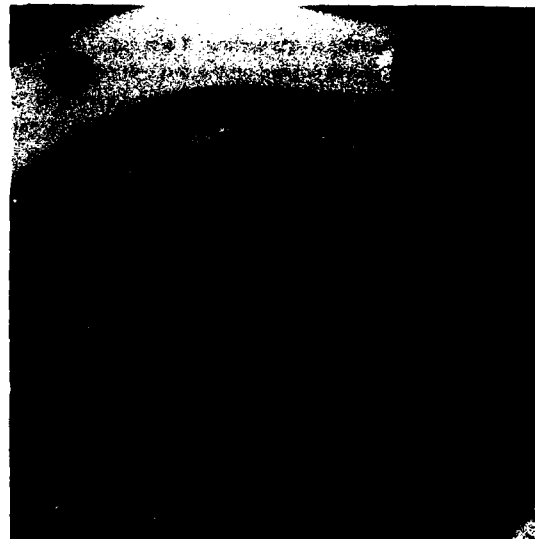


Figure 10. Evidence of varied evaporation rates 8½ minutes after depositing a Freon-12 streak onto china clay. Tunnel conditions Mach 0.15, 123K

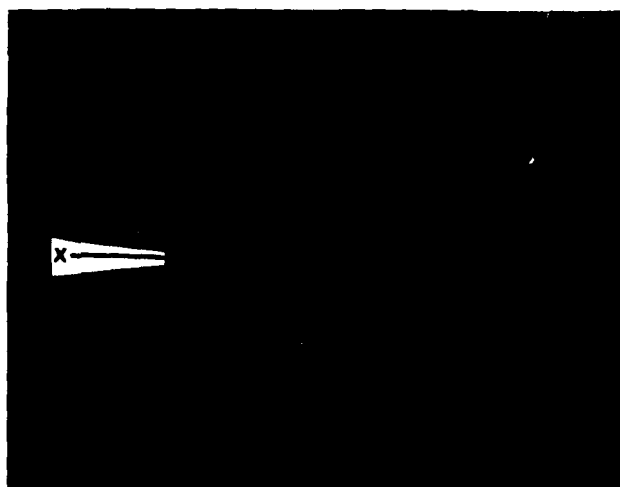


Figure 11. Several minutes after depositing a broad band of liquid Freon-12. Evidence of increased evaporation rate in wake of depositing tube, region X

These few examples serve to show that in the cryogenic wind tunnel the china clay method with an appropriate developer offers excellent contrast between its wet and dry states, showing very clearly the boundary layer flow direction by means of wet streaks. Further, it might prove capable of indicating transition but more must be done to be sure of this, emphasising the immaturity of the technology. Acceptable methods for introducing the developer to the surface must be explored, also the application of the method at high unit Reynolds numbers. Further issues can be raised relating to the china clay deposit itself: for example the surface finishes attainable, the effects of the change of model profile arising from the deposit, and the long-term durability of the deposit at high Reynolds number conditions.

3.5 Frost Deposits

ONERA has demonstrated that frosting may be turned to advantage in flow visualization. In this method a light frost deposit is induced deliberately, showing transition by means of a naturally selective pattern of deposition depending on the state of the boundary layer. The method, developed in the cryogenic tunnel T2, exploits a low level of humidity in the stream of test gas. The deposit is formed by first stabilising the stream and model temperatures, then raising the stream temperature a few degrees leaving the model cooler than the adiabatic wall temperature. The method may be regarded as a variation of that under 3.3.

Figure 12 is a photograph of a laminar flow wing model AS100 swept at 15 degrees. The light circle is a window on the far side of the test section, and the wing angles upwards in the picture from bottom left. The flow is right to left at 1.7 bar and 200K, giving a chord Reynolds number of 7 millions, at which conditions the boundary layer is laminar to around 70% chord. The dew point of water vapour in the tunnel was around 220K. Frost has formed under the turbulent boundary layer and is clearly visible. A large cone of turbulence is also visible, induced by a bad pressure tapping.

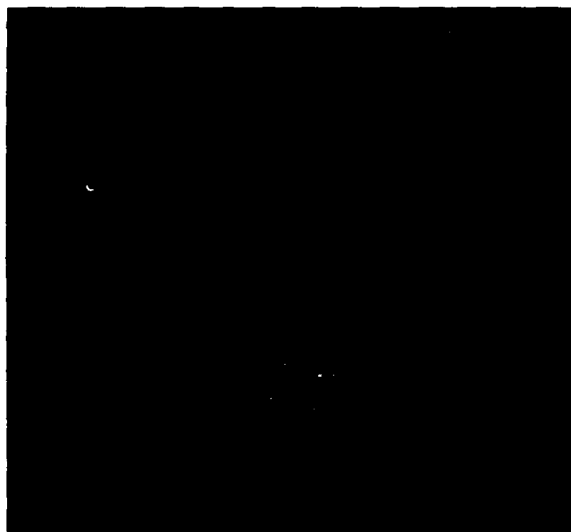


Figure 12. Boundary layer transition shown by a deliberately induced deposit of frost under a turbulent layer

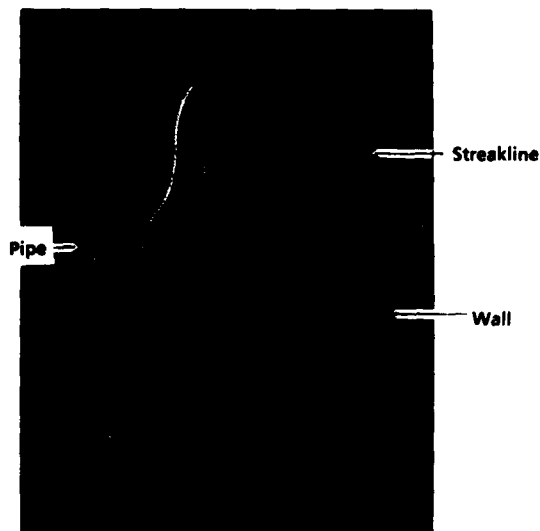


Figure 13. Smoke flow visualization in gaseous nitrogen. Streakline formed by frozen $1\mu\text{m}$ droplets in dewar at about 100K

ONERA have experience with the method down to 140K and it is expected that more photographs will be available during the lectures.

4. Visualization of Whole Flowfields

We have now moved away from the methods specially devised for surface flows and address the mostly potential flowfield in the vicinity of the model but outside its boundary layers. All techniques which are used in conventional tunnels are also available in principle for the cryogenic wind tunnel. This topic is not one in which this speaker has first-hand experience (the inputs of others will be welcome) and therefore some survey work was necessary. The most recent Bibliography¹³ has 14 different citations on the general subject of flow visualization among which only three (citations 273, 320, 449) carry results of whole-field flow visualization investigations carried out at cryogenic conditions in a wind tunnel.

The range of techniques which has been tried in the cryogenic environment with some success is very limited and includes only smoke, holography, and the vapour screen, which will now be covered individually

4.1 Smoke

Smoke has not yet been used in the cryogenic wind tunnel although there seems to be no reason for the exclusion of this method. In support of this statement is some flow visualization work carried out at Southampton in 1984¹⁴, in gaseous nitrogen convecting in a glass container above a pool of LN₂. A probe was used to introduce a stream of 1-micron frozen droplets to indicate convection currents in the nitrogen gas, which would lie in the temperature range 77K to about 125K. In Figure 13 the pipe can be seen together with the streamline formed by the smoke issuing from it. Near the pipe and away from the wall of the dewar there is a very slow downflow of gas, but as the smoke approaches the wall it is clearly seen to enter a rising current of warmer gas adjacent to the wall.

The velocities were very low (order 4cm/sec. maximum) but the principles may scale in terms of size and speed to satisfy at least some needs in the cryogenic wind tunnel. For instance a smoke probe might be developed for use with low speed high lift configurations to show flow direction, separation and vortices.

4.2 Holography

Shadowgraphs have been reconstructed successfully from holograms and one is published¹⁵, taken at the conditions of 100K, 4 atmospheres and Mach 0.77 together giving a high unit Reynolds number well into the operating areas of the new tunnels. The image is of a two-dimensional test on an aerofoil, showing a portion of the flowfield just above the model. Although the picture is very grainy the shock is clearly visible. The field of view prevents an assessment of the ability of the method to detect separated flow.

Interferograms are discussed in the same reference and it is stated that *"The lowest temperature at which interferograms have been produced is 125K at 2 atm. pressure"*. There seem to be no published examples.

4.3 Vapour Screen

A series of demonstrations has been carried out in 0.3m^{16,17} where the vortical flows over a delta wing were visualized using this method. The notion is to generate nitrogen fog in the test section by means of a suitable combination of test conditions. The angle of attack was chosen for separation vortices to be present and these were illuminated by a laser light sheet. The tunnel conditions varied up to 5 atmospheres pressure and down to 83K, and Mach numbers from 0.4 to 0.8. Recording was by a still camera and on video tape. The published photographs seem to lack detail but do show the general location of the vortex. The flow is not seeded artificially and therefore can be expected only to produce images over certain narrow ranges of tunnel conditions close to saturation. These happen to coincide with the highest Reynolds numbers, which surely is an advantage.

For a first attempt the investigation must be judged moderately successful and to promise good results with further development. Some potential users might judge the narrow range of suitable test conditions to be inhibiting.

References

1. Goodyer, M.J. The 0.1m Subsonic Cryogenic Tunnel at the University of Southampton. NASA CR-145305, Jan. 1978.
2. Goodyer, M.J. Engineering Changes to the 0.1m Cryogenic Wind Tunnel at Southampton University. NASA CR-172430, Aug. 1984.
3. Goodyer, M.J. Cryogenic Wind Tunnel Activities at the University of Southampton. NASA CR-159144, Sept. 1979.
4. Goodyer, M.J. Surface Flow Visualization in the Cryogenic Wind Tunnel. ETW second cryogenic technology review meeting, Cologne, June 1988.
5. Crowder, J.P. Aeronautics and Astronautics, Nov. 1980.
6. Crowder, J.P. Fluorescent Minitufts for Nonintrusive Surface Flow Visualization. p.667 in Flow Visualization II, Hemisphere, 1980.
7. Kell, D.M. A Surface Flow Visualization Technique for use in Cryogenic Wind Tunnels. Aeronautical Journal, vol.82, Nov. 1978.
8. Fancher, M. A transonic cryogenic wind tunnel test of a supercritical airfoil model: background and progress. AIAA paper 80-0418 at 11th Aerodynamic Testing Conference, Colorado, March 1980.
9. Fancher, M. Aspects of Cryogenic Wind Tunnel Testing Technology at Douglas. AIAA paper 82-0606, March 1982.
10. Goodyer, M.J. Preliminary experiments on surface flow visualization in the cryogenic wind tunnel by use of condensing or freezing gases. NASA CR 181634, January 1988.
11. Richards, E.J. and Burstall, F.H. The "China Clay" Method of Indicating Transition. R & M 2126, August 1945.
12. Holder, D.W. Transition indication in the NPL 20" x 8" high-speed tunnel. ARC R & M 2079, July 1945.

13. Tuttle, M.H., Kilgore, R.A., Cole, K.L. Cryogenic Wind Tunnels - A Selected, Annotated Bibliography. NASA TM 4013, September 1987.
14. Beresford, G. Laser Doppler Velocimetry Studies on Cryogenic Fluids - Ph.D. Thesis, 1984. Institute of Cryogenics, University of Southampton.
15. Burner, A.W., Snow, W.L., Goad, W.K., Helms, V.T. and Gooderum, P.B. Flow Field Studies Using Holographic Interferometry at Langley. In Flow Visualization and Laser Velocimetry for Wind Tunnels, NASA CP-2243, Sept. 1982, pp.193-204.
16. Selby, G.V. Vapor-Screen Flow-Visualization Experiments in the NASA Langley 0.3-m Transonic Cryogenic Tunnel - Final Report. NASA CR-3984, May 1986.
17. Selby, G.V. Progress in visualizing cryogenic flow using the vapor-screen technique. ICASF '87 Record, pp.233-238.

MATERIALS AND TECHNIQUES FOR MODEL CONSTRUCTION

by
D.A. Wigley

Director, Cryogenic, Marine and Materials Consultants
17 Bassett Wood Drive, Bassett
Southampton, SO2 3PT, England

SUMMARY

The problems confronting the designer of models for cryogenic wind tunnel models are discussed with particular reference to the difficulties in obtaining appropriate data on the mechanical and physical properties of candidate materials and their fabrication technologies. The relationship between strength and toughness of alloys is discussed in the context of maximising both and avoiding the problem of dimensional and microstructural instability. All major classes of materials used in model construction are considered in some detail and in the Appendix selected numerical data is given for the most relevant materials. The stepped-specimen programme to investigate stress-induced dimensional changes in alloys is discussed in detail together with interpretation of the initial results. The methods used to bond model components are considered with particular reference to the selection of filler alloys and temperature cycles to avoid microstructural degradation and loss of mechanical properties.

1. INTRODUCTION

The advent of large cryogenic wind tunnels such as the National Transonic Facility (NTF) at the NASA Langley Research Center has created many challenges for the designer of models. Optimization of the choice of material and fabrication techniques calls for fine judgment as many of the properties required are near the limits attainable with state-of-the-art technology. Furthermore, in many cases improvements in one direction seem inevitably to be accompanied by losses in others. Thus, for example, the material has to have a yield stress high enough to carry the imposed aerodynamic loadings, yet be tough enough to operate safely at cryogenic temperatures. It has to be capable of being fabricated using available machining and joining techniques to give a model with a precisely known shape and a high quality surface finish which is able to retain dimensional stability during thermal cycling between ambient and its cryogenic operating temperatures. It has to be either intrinsically resistant to, or capable of being protected from, corrosion and degradation and, if it is to be of maximum use as an aerodynamic test facility, it has to be furnished with a complex array of orifices, tubes, sensors, heaters and other components needed for data gathering. While many of these requirements have been familiar to generations of experimental aerodynamicists, it is the high Reynolds number requirement and in particular, the added cryogenic dimension that has raised the designers' challenge to its present level.

Some idea of the way information on the many factors involved in the design and construction of such models may be generated, stored and transmitted is illustrated schematically in Figure 1. At the conceptual stage the constraints set by the aerodynamic, aeroelastic and instrumental requirements require the input of data contained in the various locations shown in the "Information Sources" box. Further, more detailed, information is needed at the next stage when a general specification and design study is undertaken. These include materials properties, information on shaping and joining technologies, as well as the cost and availability of candidate materials. When fabrication of a specific model is undertaken, some information on the experience gained should start to flow back via feed-back paths to enhance the cumulative knowledge on both successful and unsuccessful techniques and materials used. Once the model has been put into service, further feed-back should enable its performance and degradation to be monitored. Modifications or the adoption of alternative configurations should also provide valuable opportunities for data feed-back. Finally, once a model has reached the end of its useful life, some form of post-mortem examination would allow comparison of the initial model design requirement with its subsequent performance. Unfortunately much useful knowledge is often lost to the technical community as a whole when pressure of work, or a change of responsibilities, prevents adequate technical documentation of both successful and unsuccessful models.

Many sources of data will need to be tapped to provide the breadth and depth of information required if models for cryogenic wind tunnels are to be fabricated efficiently. Some information on the appropriate cryogenic technology is available in references 1-4 & 22. However, designers often experience considerable difficulty in finding the data they need, partly due the fragmented location of the available information, but also due to the specific nature of the problem. Accordingly, research and development programs have been set up to investigate those areas of technology where information is most urgently needed. Three particular topics being studied at NASA Langley Research Center are: (1) Toughness Enhancement by Grain Refinement, (2) Bonding and Filler Materials and (3) Dimensional Stability and Machining-Induced Deformation in Candidate Materials for Model Fabrication. The author has been closely involved in the latter program and much of the material contained in this paper has been generated or collated under this NASA supported program. Experience generated from other models in conventional as well as cryogenic wind tunnels should be supplemented with that from other relevant technologies. For example, some of the data generated by the requirements of the nuclear fusion power generation program for very large superconducting magnets could have a direct bearing on the cryogenic model program. The rationalization and collation of relevant information from these diverse sources would be of considerable benefit to those involved in the design, fabrication and use of models in cryogenic wind tunnels, particularly if it were to be collated in a "Handbook of Cryogenic Wind Tunnel Model Technology".

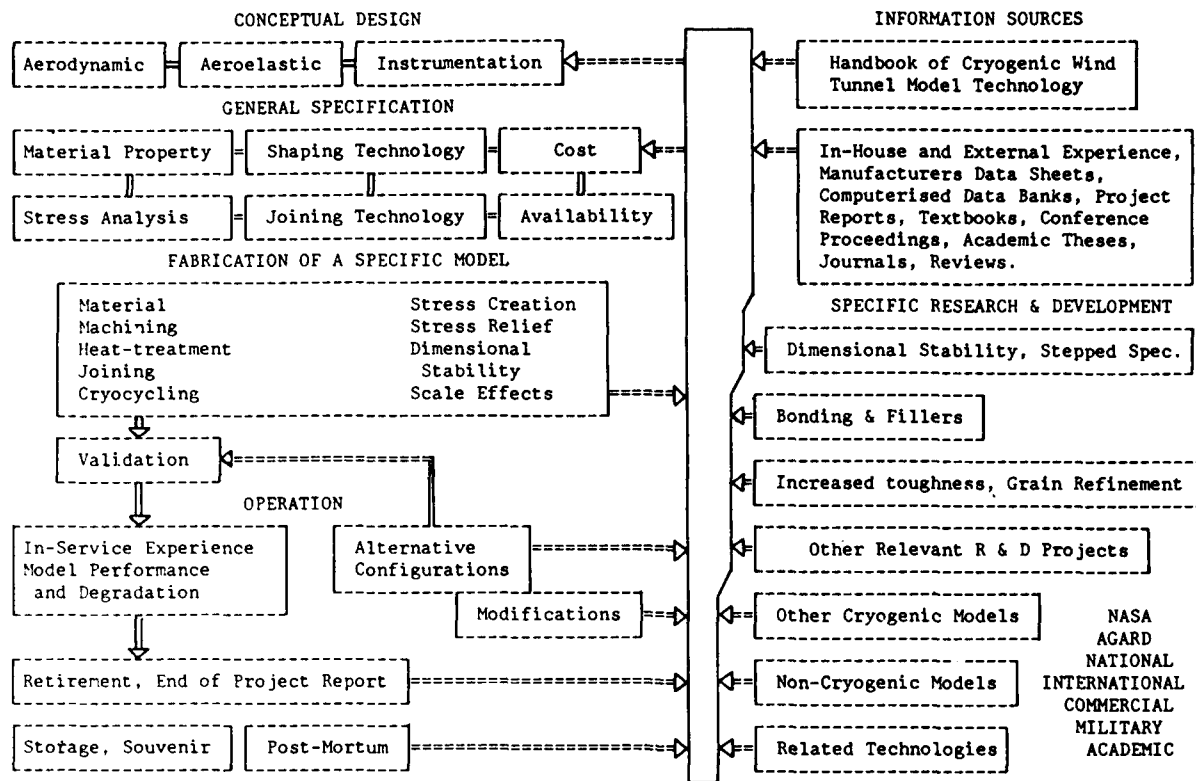


Figure 1. Schematic Representation of Information Transfer and Feedback Paths

2. FUNDAMENTAL CHARACTERISTICS OF METALS

2.1 Relationship between Strength and Toughness

The need for high strength while still retaining adequate toughness for safe operation severely limits the range of alloys that can be considered for the construction of models for large, pressurised cryogenic wind tunnels. The minimum yield stress considered acceptable for Pathfinder 1, the lead model for the NTF, is 1030 MPa. (150 ksi) at 77 K (-320 F). This is not, in fact, a high stress level and the fracture toughness requirement of at least $93.5 \text{ MPa} \sqrt{\text{m}}$ (85 ksi $\sqrt{\text{in}}$), or a Charpy V notch Impact Energy of 34 J (25 ft-lbs) is not excessively cautious. However, applied together these two design requirements combine to narrow drastically the range of candidate materials. Basically, this is because most metallurgical techniques that increase the yield stress also bring about a decrease in fracture toughness. Furthermore, as the critical flaw size in a structure is related to the crack size factor, $(K_{Ic}/\sigma_y)^2$, an increase in yield stress without a corresponding increase in fracture toughness will lower the resistance of the material to unstable, low-energy crack propagation. This toughness-versus-strength trend for structural materials is well illustrated in Figure 2, as modified by Rush (Ref. 31) from Toblers original (Ref. 22). Most materials fall between the two trend lines, those at the upper boundary having the highest toughness for a given yield stress. It should, however, be noted that these optimum properties are often not shown in the particular product form delivered for model fabrication. Considerable effort is under way to produce materials having properties which lie above the upper trend-line of Fig. 2. and there are two different basic approaches to this objective:

- Increasing Strength without Loss of Fracture Toughness as in the high nitrogen and high manganese stainless steels.
- Increasing Fracture Toughness without Loss of Strength in ferritic steels by the use of multiple stage heat-treatments through the austenite /austenite + ferrite phase transformation region.

Significant toughness improvements have been achieved by Rush (Ref. 19) in 9% Nickel, HP 9-4-20 and 18Ni 200 maraging steel using this second approach.

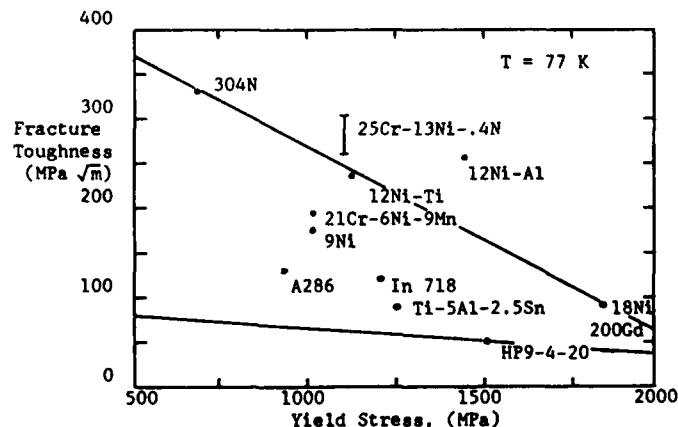


Figure 2. Toughness-vs-Strength Relationship

2.2 Dimensional Stability

In order to meet the minimum acceptable toughness requirements a number of precipitation-hardened stainless steels have to be heat-treated to a lower strength condition and it has been found that this can lead to dimensional instability. There are two basic mechanisms that can cause such instability:

- metallurgical structural instability in which one phase transforms partially or fully into a second phase which has a different crystal structure and volume.
- deformation due to the creation, or relief, of unbalanced induced or residual stresses.

Stress-induced dimensional changes will be considered further in section 4. The occurrence of severe dimensional instability in a model first came to light in 12% airfoil made from 15-5PH stainless steel and tested in the 0.3-m Transonic Cryogenic Tunnel at NASA LaRC. A post-testing co-ordinate check showed a 0.002 in. decambering of the aft airfoil section (6 in. chord) and a 0.006 in. bow over an 8 in. span. Investigation showed that the material had been heat-treated to the H1150M condition in order to achieve a Charpy impact energy in excess of the required minimum of 25 ft-lb. Table 1 shows manufacturers data on the relationship between condition, impact energy, tensile strength and contraction during the heat-treatment cycle, to which we have added comments on the structure and cryocycle stability. It can be seen that relatively little contraction is associated with the H900, H1025 and H1100 heat-treatments as these do not alter the martensitic structure of the material. The H1150M heat-treatment is accompanied by a much larger contraction as some martensite is transformed to austenite and it is the presence of this austenite that gives the material its improved toughness and impact energy. This austenite is, however, only metastable and low temperature cycling, machining or other forms of deformation trigger off a partial transformation back to martensite which is accompanied by a volume expansion. In an asymmetric section such as an airfoil, and where the effect of machining would be more pronounced in thinner sections than in the thicker parts, the volume changes show up as warpage. (Ref. 25).

Table 1: 15-5PH Stainless Steel Stability Data (Ref. 8)

Condition	77 K Charpy V Impact E (J)	Contraction H.T.-R.Temp. (%)	Cryocycle Stability	300 K UTS (MPa)	Structure
H900	-	0.045	-	1310	martensitic
H1025	2.7	0.053	good	1069	m/s
H1100	4.7	0.09	-	966	m/s
H1150	-	0.22	-	931	m/s + aust.
H1150M	44.8	0.343	poor	793	m/s + aust.

The energy required to trigger off the austenite to martensite transformation (an instantaneous shear, not a nucleation and diffusion-controlled growth mechanism) is probably provided by differential contraction during thermal cycling. Large temperature gradients would encourage such transformation, as would rapid temperature changes, and thus is is the rate of cooling and warming and the number of cryogenic cycles that determine the degree of transformation, rather than the length of time held at a particular temperature. Rapid changes of section would also exaggerate the problem as larger temperature gradients, and hence higher thermal stresses, are set up across thicker sections. In the case of the 15-5PH airfoil the dimensional changes continued over many tens of thermal cycles, the incremental change becoming gradually smaller as the amount of metastable austenite transforming decreased. As, however, the toughness decreased progressively in step with the austenite transformation, there was no point in continuing to cycle the model to achieve dimensional stability as its toughness would then become unacceptably low. In other, more stable, materials where some dimensional instability has been created by machining-induced stresses, it is possible to achieve effective metallurgical and dimensional stability by carrying out a few cryocycles prior to finish machining, providing that significant stresses are not re-introduced at this stage.

3. REVIEW OF ALLOYS USED FOR MODEL CONSTRUCTION

3.1 Austenitic Stainless Steels

3.1.1 AISI 300 series

The face-centered-cubic structure of the AISI 300 series stainless steels is rendered more or less stable at and below room temperature by the presence of austenite stabilizers such as nickel, manganese, carbon and nitrogen. The 20% nickel present in type 310 makes it particularly stable, but it has the lowest yield strength of the 300 series. In the leaner grades, particularly the readily available 304 and 304L grades, the total concentration of austenite stabilizing elements may not be high enough to prevent some transformation to martensite, with its consequent volume change. This change can be induced thermally by lowering the temperature below the Ms (martensite start) temperature, or by mechanical deformation at temperatures below the Md (martensite deformation) temperature, which is usually a few hundred degrees higher than the Ms. These temperatures may be calculated from equations given in Ref. 12 if the composition of the alloy is known. However, it is only the high-nitrogen versions of the 300 series that are likely to be strong enough for use for cryogenic models and these are some of the most stable members of the series. Of particular interest are alloys such as that developed for the Japanese Atomic Energy Research Institute (JAERI) fusion reactor program which set a target of 1200 MPa for the 4 K yield strength, together with a 4 K Charpy impact energy of 100 J. A 25Cr-13Ni-.4N alloy, YUS 170, developed by Nippon Steel (Ref. 20) has achieved this 4 K goal and its 77 K yield strength of 1130 MPa and a Charpy V energy of 243 J make it highly attractive for highly stressed cryogenic wind tunnel models.

One feature common to almost all of the austenitic stainless steels is their ability to become sensitized if they are held for a significant time in the temperature range between 590 and 920 C (1100-1700 F). This is due to the precipitation of carbides and sigma phase at the grain boundaries and it has two particularly deleterious effects on the material. At room temperature the main effect is to cause "weld-decay", a liability to inter-granular corrosion brought about by the loss of chromium adjacent to the grain boundaries. Of more significance for cryogenic applications is, however, the serious loss of toughness at liquid nitrogen temperatures due to the ease with which fracture can be nucleated and

propagated in a low energy mode in the precipitate-laden grain boundaries. Unfortunately, airfoil models are frequently cooled through this sensitizing temperature range after post-machining, stress-relieving heat-treatments at 1000 C (1900 F) or during brazing. Should sensitization occur it can be removed by reheating to 1000 C and then cooling rapidly through the sensitizing temperature range. This is, however, difficult to achieve with large, thick sections in a vacuum oven. One common method of preventing sensitization is to specify one of the "weld-stabilized" grades such as the titanium bearing AISI 321 or the niobium bearing type 347. These additional elements are strong carbide-formers and they react with any free carbon to prevent chromium depletion. An alternative approach favoured for room-temperature applications is to specify a low-carbon grade such as 304L or 316L, but as carbon is an austenite stabilizer these alloys are less stable at cryogenic temperatures. It is also worth noting that type 316 has a better corrosion-resistance, especially in marine atmospheres, due to its 2-3% molybdenum content.

3.1.2. Fe-Cr-Ni-Mn-N Alloys

Strengths higher than those of the 300 series can be obtained from these steels as their increased manganese content raises the nitrogen solubility limit. One particular material in this series, Nitronic 40, a 21Cr-6Ni-9Mn-0.4N alloy, was chosen for the construction of the Pathfinder 1 Model for the NTF and a 2 Dimensional airfoil manufactured by McDonnell-Douglas for the NASA LaRC 0.3m TCT. Some problems were encountered due to grain boundary sensitization created during fabrication, but in the 2D airfoil these were removed by heating to 1000 C and then quenching into liquid nitrogen to achieve a controlled and uniform cooling rate. Although the material was supposed to be 100% austenitic it was found to contain up to a few % delta ferrite, a body-centered-cubic phase of lower toughness than the parent metal. Remedial heat-treatments were unable to remove this stable delta ferrite and caused unacceptable grain growth. (Ref. 24). However, fracture toughness tests gave very high values at 77 K and, as the delta ferrite was aligned along the rolling axis and the span of the model wing was also in this direction, it was felt that the fracture toughness would be adequate to ensure safe operation in the NTF. Nitronic 40 can be machined using conventional techniques but care has to be taken to ensure good cooling as the material work hardens easily and tools can rapidly lose their cutting edge. Availability of the material in the form of bars and plates of the required size can also be a problem which seems to be getting more severe.

Other high manganese-high nitrogen alloys such as Nitronic 33 (18Cr-3Ni-13Mn-.2/.4N), Nitronic 50 (22Cr-13Ni-5Mn-.2/.4N) and Carpenter 18-18 plus (18Cr-18Mn-1Mo-1Cu-1Si-0.5N) are generally considered to have toughnesses too low for safe cryogenic operation. In the AISI 200 series of steels the high-manganese contents are used primarily to increase nitrogen solubility and hence strength. The earlier alloys had poor fracture toughness at cryogenic temperatures, but more recently a modified AISI 205 steel, nominal composition 18Mn-5Ni-16Cr-0.024C-0.22N, has been shown by Ogawa and Morris (Ref. 17) to give yield strengths of 1200 Mpa and Charpy impact energies of 61 J in the as-rolled condition at 77 K. However, these alloys are not yet easy to obtain, particularly in the product forms likely to be needed for model construction.

3.1.3 A286

This precipitation hardened stainless steel has become one of the state-of-the-art materials for the construction of models for cryogenic wind tunnels and it has been used for a variety of 2 and 3 D models in the NASA LaRC 0.3-m TCT with considerable success. A286 screws are frequently used to fasten together smaller components and in the 1985 paper Dr. Young discussed NASA LaRC experience with their use and the various locking systems that have been evaluated to prevent them from unscrewing under aerodynamic loading or cryogenic temperature cycling. The alloy was not considered strong enough for use in Pathfinder 1 as its yield stress at 77 K is only about 830 MPa, but more recently it has been used for the fabrication of a model of the space shuttle to be tested in the NTF. Its nominal composition is: Fe-25Ni-14Cr-2.2Ti-1.5Mn-1.2Mo-0.3V-0.2Al--0.5Si and it is the titanium, vanadium and aluminium additions that precipitation-harden the material during heat-treatment. The material is fully stable with respect to martensitic transformation both during cryocycling and deformation at cryogenic temperatures. Machining is rather difficult due to the tendency of the material to work-harden rapidly and tool wear can be excessive. Furthermore the studies of stress-induced dimensional changes to be discussed in section 5 have shown that large surface stresses are produced even during rough machining. It is a relatively expensive material and there are also often difficulties in obtaining it in the desired product forms due partially to the considerable use of the material for strategic, high-temperature applications.

3.2 Martensitic and Semi-Austenitic Stainless Steels

3.2.1 AISI 600 Series

Among this class of material are a number of materials that have had long and successful histories in the fabrication of models for use in ambient and high temperature wind tunnels due to their ease of fabrication and ability to hold a high quality surface finish. For these applications the materials were used in the fully-hardened condition but it was recognized that in this condition they would be too brittle for cryogenic applications. The H1150M heat-treatment was therefore used to bring the Charpy impact energy up to the required minimum of 25ft-lb, but, as noted earlier, this caused dimensional instability in a 15-5PH airfoil when the metastable austenite re-transformed to martensite during cryocycling. Similar problems have been found, or can reasonably be expected, to occur with 17-4PH, 17-7PH, Custom 450, AM 350, AM355, PH15-7Mo and PH14-8Mo and these materials are not recommended for cryogenic use.

3.2.2 PH13-8Mo

The picture is, however, slightly different for PH13-8Mo. From a comparison of the contraction rates that occur during the various heat-treatments shown in Table 2 (Ref. 8) for PH13-8Mo with those previously given for 15-5PH in Table 1, it is clear that austenite is reformed during the higher temperature heat-treatments. It would, however, appear that this austenite is more stable than that formed in the other alloys in this series. Perry and Jasper (Ref. 11) comment as follows:

"(After) heat-treatment at the lowest ageing temperature, in this case 482 C (900 F), the microstructure is essentially completely martensitic. As the aging temperature increases, so does the

amount of reformed austenite. The H1150M condition (the softest for these steels) has a rather complex microstructure. Heating to 760 C (1400 F) results in much of the martensite going into solution at that temperature. Upon cooling to room temperature, some of the austenite is transformed into untempered martensite. The rest of the austenite remains as austenite and the balance is highly overaged martensite. The 620 C (1150 F) ageing then ages the martensite that was formed as a result of cooling from 760 C (1400 F), together with some additional reformed austenite. Therefore, the final microstructure consists of highly overaged martensite, normal overaged martensite and reformed martensite which is completely thermally stable (authors underlining). This results in a heat-treated stainless steel with reasonably good impact strength at temperatures as low as 77 K (-320 F)."

Table 2: PH13-8Mo Stainless Steel Stability Data (Ref. 11)

Condition	77 K Charpy V Impact E (J)	Contraction H.T.-R.Temp. (%)	Cryocycle Stability	300 K UTS (MPa)	Structure
H950	2.7	0.04-.06	-	1551	martensitic
H1000	5.4	0.04-.06	-	1482	m/s
H1050	5.4	0.05-.08	good	1310	m/s
H1100	6.8	0.08-.12	-	1103	m/s
H1150	-	0.30	-	1000	m/s + aust.
H1150M	41	0.35	reasonable	896	m/s + aust.

In the H1150M condition PH13-8Mo has a yield strength of 1000 MPa at 77 K and Charpy V impact energies between 40-80 J (30-60 ft-lb) depending on the source of the data. It is therefore comparable to Nitronic 40 in its properties and its structure has been considered in so much detail because it has been used for the construction of the solid wing for Pathfinder 1 and the half-scale Pathfinder 1 model. Nevertheless there have been indications that, although the "complete thermal stability" referred to above may be true in the context of conventional applications, the very high dimensional stability demanded of models for cryogenic wind tunnels might not be met by PH13-8Mo in the H1150M condition. It was possible that deformation induced during machining might trigger off further transformation of austenite to martensite that could, in turn, create dimensional instability on cycling to cryogenic temperatures. The material was, therefore one of the first studied in the stepped specimen program to be described in section 4. Some evidence was, indeed, found for dimensional changes after 3 cryocycles into liquid nitrogen, but no further movement occurred as a result of further cryocycles, suggesting that the structure of the material had stabilized during the initial cryocycles. Experience with the two model parts made for the NTF gives further confidence for the continued use of PH13-8Mo for cryogenic models, as both proved to be completely stable. Both had been thermally cycled to liquid nitrogen temperature at the semi-finished machining stage to allow transformation of any unstable austenite and it would appear that final finishing did not further destabilize the structure. (Refs. 27 & 28).

3.3 18 Nickel Maraging Steels

Although they do not have the favoured austenitic structure, this family of high-strength steels are strengthened by precipitation hardening of the soft, low-carbon martensite to form a stable microstructure which is not adversely affected by thermal cycling to cryogenic temperatures. Furthermore they are readily machined in the annealed condition and there is very little dimensional change during the single step ageing heat-treatment which takes place at the relatively low temperature of 480 C (900 F). The higher strength members of the family have unacceptably low toughnesses for most cryogenic applications, but the lower strength 200 and 250 grades, are tough enough to find application in many high load-bearing applications in cryogenic wind tunnels. For example, the 250 grade is used for the construction of stings, while the 200 grade is the most widely used material for constructing models for the NTF. At least eight models, or substantial parts thereof, have been constructed or are still under fabrication at present. The 200 grade has a nominal composition (Fe, -17 / 19 Ni, -3 / 5.2 Co, -0.15 / 2.0 Ti, -0.05 / 0.2 Al, - 0.03 C, - 0.10 Mn, - 0.01P). Its yield strength is 1860 MPa at 77 K and it has a Charpy V notch impact strength in the region of 25-50 J (18-37 ft-lb) depending on the product form. The increasing difficulty of obtaining reliable supplies of cobalt have let the major US supplier of 18 Nickel maraging steel to introduce a series of cobalt-free alloys and the 200 grade is currently under active evaluation for possible use in the fabrication of cryogenic wind tunnel models. (Ref. 10).

As noted earlier the low-temperature toughness, as indicated by the Charpy V notch impact energy at 77 K can fall below the 25 ft-lb minimum required for NTF operation in some product forms. The grain-refinement program referred to in section 2.1 has shown that significant increases can be obtained in the toughness at 77 K. The grain-refining process consists of multiple heating and cooling cycles between the austenite and the dual-phase austenite + ferrite region, followed by rapid cooling to reduce the grain size.

3.4 Ferritic, Quenched and Tempered, and Grain-Refined Steels

In lecture 2, it was noted that the 9 Nickel steels are the only ferritic alloys considered suitable for use at 77 K and the main drive shaft for the NTF fan is made from a special grade of this alloy. The material has also been considered for use in model construction, but the more recently developed 12 Nickel alloy looks more promising. Furthermore, as both 9% and 12%Ni steels undergo a ferrite to austenite phase change they are therefore capable of grain-refinement by multi-stage heat-treatment.

3.4.1 9 Nickel Steels

Two grades of 9 Nickel steel are readily available: the double normalized and tempered A 353 and the quenched and tempered A 553 which has a slightly better toughness and about a 10% higher strength than the double normalized grade. Both grades are relatively easy to obtain, readily machined and welded, but there is no matching filler and austenitic nickel-based fillers have to be employed to give adequate strength. Unfortunately, this leads to a miss-match in the expansion coefficients and potential problems

with thermal fatigue and stability. Furthermore, the 9 Nickel steels are not very corrosion resistant and suitable coatings would need to be applied to protect the surface of a model.

3.4.2 12 Nickel Steels

Initial work by Stephens and Witzke (Ref. 21) at NASA Lewis Research Center has recently been extended by Rush (Ref. 31) at NASA Langley Research Center. Two alloy compositions, Fe-12 Ni-0.5 Al and Fe-12 Ni-0.25 Ti, have been selected for further development and this will be discussed in detail by Dr. Young. Suffice it to say that, if the results of the experimental heats are reproduced in the larger production melts, these alloys appear to offer considerable potential for use in cryogenic models. The initial data on strength and toughness of both alloys at 77 K has been included in Fig. 2 and it can be seen that the 12 Ni-Al alloy in particular has a combination of strength and toughness which places it above the upper trend line for current materials.

3.4.3 Quenched and Tempered Steels

The quenched and tempered 9Ni-4Co steels, particularly HP 9-4-20, have been used for 2 Dimensional models with some success. They have also been included in the grain refinement program and significant improvement in toughness at 77 K has been achieved. However, there are reservations about its dimensional stability and its relatively poor corrosion resistance limits its potential usefulness.

3.5 Aluminium Alloys

Aluminium alloys may be divided into two groups according to their basic metallurgical strengthening mechanisms: [1] the solution-hardened alloys which are very ductile but only of moderate strength unless cold-worked, and [2] the stronger, heat-treatable, precipitation-hardened alloys. Type 5083 is probably the most widely used of the solution hardened alloys, due in part to its excellent weldability. Even in the as-welded condition its full strength is retained, thus giving it an advantage over the nominally stronger heat-treatable alloys if post-weld heat-treatment is not possible. For example, alloy 6061 in the solution-treated-and-artificially aged T6 condition is stronger than that of 5083, but as-welded its strength drops below that of as-welded 5083. A series of six solids of revolution having the same size and shape as model bodies to be tested in the NTF have been made out of alloy 6061 in the T6 condition. Of the other heat-treatable alloys, the aluminium-copper 2014 and 2219 have been used in a number of aerospace cryogenic applications where their high strength to weight ratio is advantageous. The toughness of the very high strength 7000 series alloys is, however, too low for most cryogenic purposes.

A number of cryogenic wind tunnel models, or parts thereof, have been built from aluminium alloys and operated successfully. However, their elastic moduli and strengths are generally too low for their use in the more heavily-loaded components such as airfoils in pressurised tunnels such as the NTF. Complications can also arise when aluminium and steel components are mixed in the same model, as the two materials have significantly different coefficients of thermal expansion. Nevertheless, aluminium alloys are easy to machine and readily weldable, although brazing and soldering are not easily carried out in model fabrication. The surfaces of models also need some form of protection to prevent them from being scratched.

3.6 Titanium Alloys

Two titanium alloy have been used for cryogenic components, particularly in aerospace applications where their high strength to weight ratio is a distinct advantage. The Ti-5Al-2.5Sn alloy has a stable h.c.p. structure and can be used down to 77 K, whereas the Ti-6Al-4V alloy has a duplex h.c.p. / B.c.c. structure and is not used below 77 K because of excessive notch brittleness. For cryogenic use the special ELI (Extra Low Interstitial) grades have to be specified because the toughness of titanium is severely degraded by too many interstitial elements. As these include carbon, nitrogen, oxygen and hydrogen, great care has to be taken during fabrication, particularly welding, to prevent their pick-up. Furthermore, titanium alloys are not easy to machine, they are relatively expensive and for these reasons few, if any, models for cryogenic wind tunnels have yet been made in titanium alloys.

3.7 Nickel Based Alloys

All nickel-based alloys have the austenitic structure that makes them suitable for cryogenic applications, but relatively few have, as yet, been used for model construction. This is most probably due to a combination of their relatively high cost, poor availability and the considerable difficulties experienced in machining the high strength alloys such as the Inconels using conventional machining techniques. However, advances in chemical milling, electrical discharge machining, electron beam welding and other modern technologies have reopened the question of their possible application for model building. Nickel coatings have been used to rework model surfaces that have been undercut during machining or damaged in service, electroless nickel being used where hard finishes are required while electrolytic nickel is preferred if high ductility is needed. Nickel-copper alloys, Monels, have excellent corrosion resistance and have been used for cryogenic applications, but they do not possess any outstanding advantages that make them attractive for model building. The most promising alloys are the nickel-chromium Inconels, in particular the precipitation-hardened types 718 and X750. Inconel 718 has the higher yield strength, 1172 MPa at 300 K and 1342 MPa at 77 K, while X750 has a slightly lower strength but higher toughness.

3.8 Copper Based Alloys

Copper based alloys have limited applications for cryogenic models and are used in those applications that make use of their good thermal and electrical conductivities, their availability, or the ease with which components can be machined and joined. Commercially pure copper is used for electrical conductors and is readily available. Copper-zinc alloys, such as the 70Cu-30Zn alpha brasses and the bronzes, particularly phosphor, silicon and aluminium bronzes, tend to be used for small, lightly-loaded components that are easily machined from available product forms. Brasses are readily soldered or brazed,

although the temperatures involved in most brazing operations would anneal any cold-worked material. It is, however, the precipitation-hardened beryllium coppers that are possibly of most interest for model construction. The relatively small amount of beryllium needed to form the precipitates that allow the room temperature yield strengths to reach 1000 MPa in the fully-hardened condition do not excessively degrade the high thermal conductivity of pure copper. Beryllium copper is particularly useful in those circumstances where good thermal conductivity is needed to minimize cool-down time or temperature gradients and it is often used to form high-conductivity inserts to take heat away from particularly critical regions. The main drawback of the material lies in its very low toughness at cryogenic temperatures in the fully-hardened condition. Nevertheless a 2 D beryllium copper airfoil has been made by the Douglas Company and tested successfully in the 0.3-m TCT at NASA LARC. (Ref. 13)

4. STRESS-INDUCED DIMENSIONAL CHANGES IN METALLIC ALLOYS

4.1 Induced Stresses and their Effect on Dimensional Stability

Stress-induced deformation can produce dimensional changes of many thousandths of an inch on typical airfoil model sections. These stress systems can be of considerable magnitude and can originate from one or more of the following mechanisms:

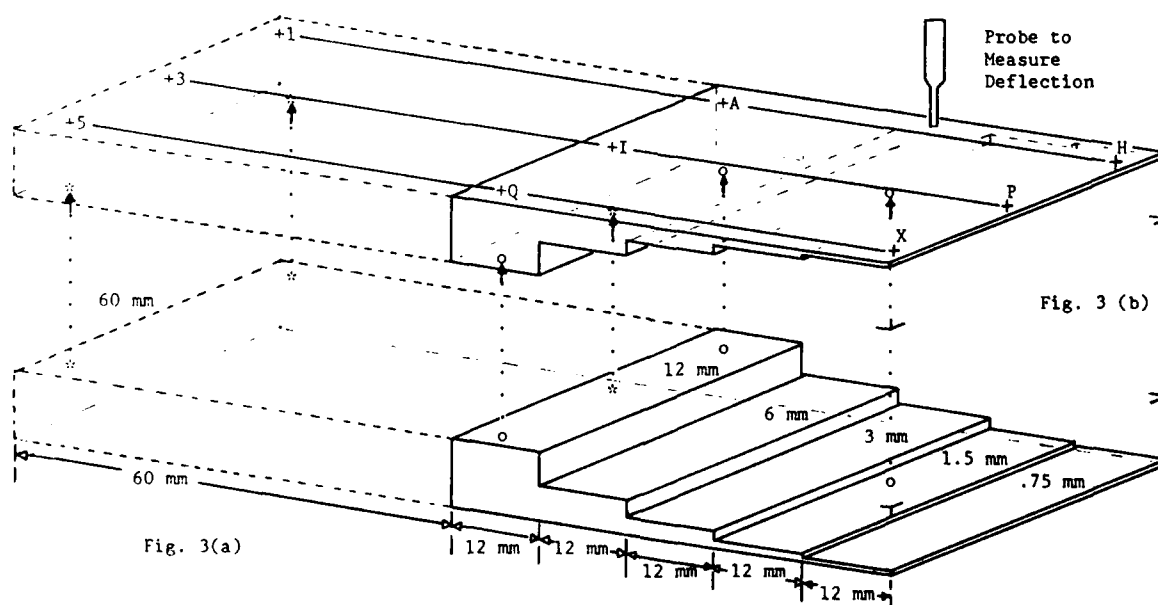
- unbalanced residual compressive and tensile stresses set-up during the original fabrication,
- quench-induced stresses generated on cooling from high temperature heat-treatments,
- compressive or tensile surface stresses induced by machining. These can be elastic or plastic depending on the degree of deformation created during mechanical working of the material and they can cause phase transformations in the surface layers,
- stresses created by temperature gradients, particularly across uneven sections.

Many different configurations were used in the initial investigations, including fully profiled airfoils and wedge shaped specimens with thin, tapered trailing edges representative of typical airfoil models. However, in view of the large number of possible combinations of material, machining technique, heat-treatment and other fabrication processes, a simplified, yet representative, stepped specimen configuration was adopted by NASA LaRC to allow these effects to be identified separated and quantified.

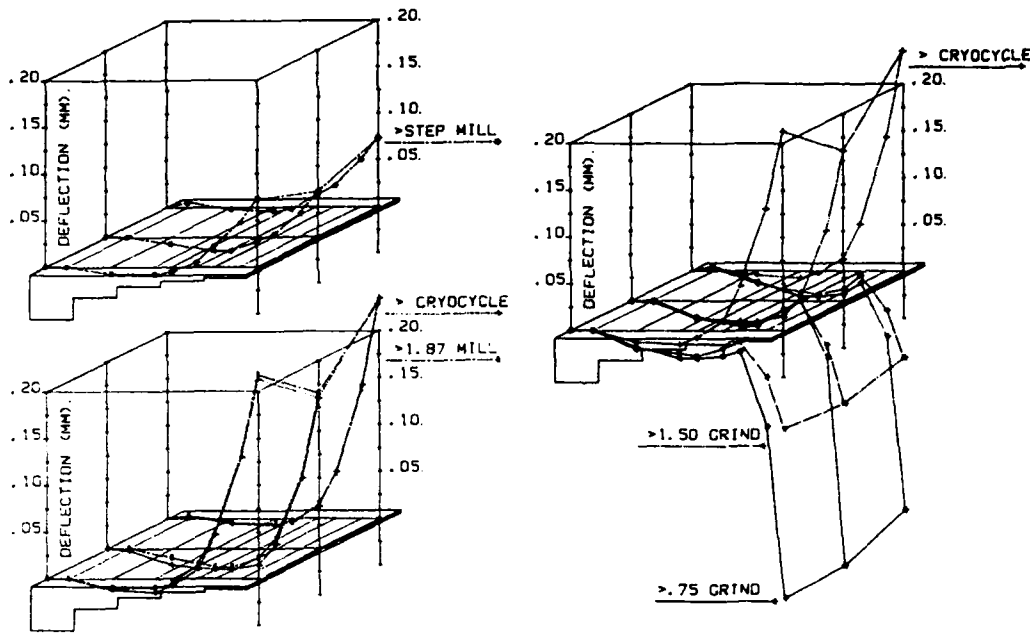
4.2 The Stepped Specimen Program

4.2.1. Specimen Configuration

The configuration used for the first 18 specimens of 18Ni 200 grade maraging steel, A286 and PH13-8 Mo stainless steel is illustrated in Fig 3(a). (Ref. 26) By limiting the maximum thickness to 12 mm, it was possible to fabricate specimens from readily available 1/2 inch plate and the choice of 60 mm width and 60 mm length minimized the amount of material required. In its final form the specimen has five steps of length 12 mm and thickness 12, 6, 3, 1.5 and 0.75 mm, the thinnest giving the most sensitive region for observing the effects of fine finishing cuts. The flat underside of the specimen provides a firm support for machining operations carried out on the top surface. It also acted as the reference surface for subsequent validation measurements when the specimens were inverted and supported at the three points marked with o symbols in Fig. 3(a). However, interpretation of the deflections of the reference surface were complicated by the fact that the 3rd support point lay within the machined region. For the latest series of specimens the configuration was, therefore, modified to increase the length to 120 mm, as indicated by the dashed lines in Fig. 3 (a), and allow the three support points marked with * symbols to be contained within the unmachined region. (Ref. 28)



Figures 3(a) and (b). Configurations of Original and Modified Stepped Specimens



Figures 4 (a), top left, (b), bottom left, and (c), right. Machining-Induced Deformation in A286

4.1.2. Initial Results and their Interpretation

Many different operations were carried out sequentially on each specimen in order to gather as much information as rapidly as possible. Milling with ball-ended cutters was used to reproduce the type of stresses induced during initial shaping on multi-axis CNC machines, with grinding used to represent the finishing stages. Feed rates, thickness of each cut and other machining details for each material were specified to be as used in actual model fabrication. For the proof-of-concept specimen made from 18 nickel 200 grade maraging steel, continuous measurements of the machining-induced deflection were made along the three lines A-H, I-P and Q-X shown in Fig. 3 (b). After milling the reference surface was found to have an upward deflection, indicating that compressive stresses were created by milling the opposite face. By treating the specimen as a cantilevered beam, it was possible to calculate the magnitude of these compressive surface stresses. These were found to increase from 36 to 62 MPa. (5 to 9 ksi) over the 4 milling cuts, each of depth 375 microns (0.015 in.), used to reduce the thickness from 3 to 1.5 mm. Subsequently, 17 similar specimens of A286, PH13-8Mo and 200 grade maraging steel were put through a similar machining sequence. Eight readings were taken along each of the three lines A-H, I-P and Q-X to give a total of 24 data points. (Ref. 27).

The effect of the different machining operations was followed by joining these points to reconstruct the appropriate reference surfaces as shown in Fig 4 (a) to (c) for an A286 specimen. The surfaces shown are: (a) after milling the 6 and 3 mm steps, (b) after milling the 1.5 mm step and after cryocycling, (c) after cryocycling, after grinding the 1.00 mm step and after grinding the 0.75 mm step. The reproducibility of the shape of the surfaces before and after cryocycling in Fig. 4 (b) is an impressive confirmation of the excellent dimensional stability of A286 at cryogenic temperatures.

4.1.3. Subsequent use of the Modified Specimen Configuration

The dip in the reference surfaces below the original reference plane in Figs. 4 is a consequence of the location of the third support point in the machined area of the specimen. As noted earlier the modified specimen configuration avoided this problem and allowed easier interpretation of the surface deflections. Improvement in the measuring technique also allowed over 360 data points to be gathered along each of the three lines 1 to H, 3 to P and 5 to X, thus effectively creating continuous traces. This increased precision allowed dimensional stability during cryocycling to be studied in more detail. Fig 5 shows how a specimen of PH13-8Mo moves during initial cryocycling, but then remains completely stable during subsequent cryocycles. This characteristic is exploited in practice by cryocycling models before finish machining to allow any necessary relaxation or phase transformation to take place before the model enters service. (Ref. 28)

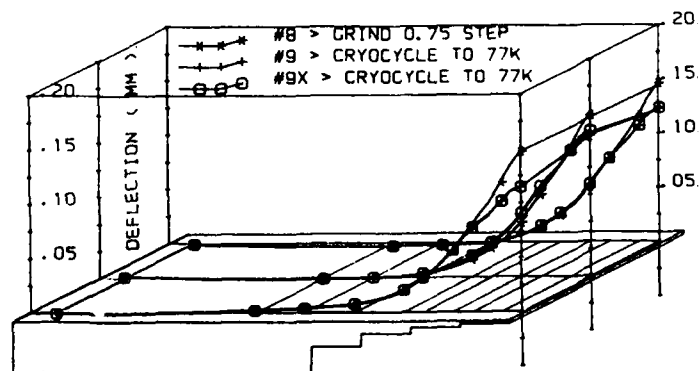


Figure 5. Machining-Induced Deformation in a PH 13-8Mo Specimen with the Modified Configuration.

The very large deflections displayed after machining the thicker steps indicate that large surface stresses are created by work-hardening during milling and grinding, a confirmation of workshop experience that the material is difficult to machine. The common practice of machining opposite faces alternately does, however, tend to balance the surface stresses created on each side and thus prevent such large deflections occurring on an actual model. The shapes of the surfaces in Fig. 4(c) indicate that grinding sets up tensile surface stresses, as the sign of the deflections created during milling was reversed by grinding.

It would, therefore, appear that if warpage occurs during rough machining of, for example, a 2 or 3 D airfoil, and if at least one surface is still over-size, dimensional fidelity could be restored by milling or grinding that surface to induce an appropriate balancing compressive or tensile surface stress.

4.1.4. Future Program

It is envisaged that the next phase of the program will involve further in-depth study of the materials most likely to be used for the fabrication of cryogenic wind tunnel models, particularly the 200 grade maraging steels. Separate specimens will be used to measure the stresses created in different machining operations such as milling, grinding, lapping and hand-finishing, as well as the supposedly stress-free techniques such as EDM and chemical milling. Stress-relieving heat-treatment cycles will also be investigated to determine their ability to remove machining-induced deformation. Scale effects will be studied using larger sized specimens, and stress-balancing investigated by developing techniques of validating specimens machined on both sides. (Ref. 29).

5. JOINING TECHNIQUES FOR METALS

Attainment of the optimum mechanical properties of materials at cryogenic temperatures requires careful control of their microstructure. In particular, the desirable combination of high strength and adequate toughness is only attainable if the grain size can be kept small and the grain boundaries free from degradation by sensitisation. Any joining technique that involves heat input must be evaluated carefully to ensure that neither the grains nor their boundaries are degraded during, or subsequent to, the joining process.

During conventional fusion welding enough heat has to be input to cause localised melting of the parent metal and this also causes annealing and modification of the adjacent heat-affected zone. For almost all wind tunnel models, the heat inputs from welding processes such as MIG, TIG, SMAW, etc. are too great and the resultant heat-affected zones too large for these processes to be acceptable. However, in the case of electron beam and laser welding, heat inputs are so low and control of the heat-affected zone so good that these techniques are becoming indispensable for joining together sub components. For example, many airfoils are designed with cover plates that allow access to the centre of the airfoil for the passage of pressure tubing from the sensing orifices on the airfoil surface. Electron beam welding has been used on many airfoils to secure fully profiled coverplates to the rest of the airfoil without damaging the tubes or their joints. It is reported by Griffin (Ref. 14) that laser welding without the use of fillers can produce strengths equal to that of the parent metal after heat-treatment. The region affected is limited to a diameter of about 0.62 mm (.025 in) and a depth of between 0.5 and 1.2 mm (.02 to .05 in) and is thus particularly useful for joining thin sections.

Austenitic stainless steels such as the precipitation hardenable A286 and Nitronic 40 (21Cr-6Ni-9Mn-0.3N) can be brazed using nickel-based fillers such as the Ni-7Cr-3Fe-4.5Si-3.2B alloy (AWS4777B, BNi3) to give ductile joints with strengths similar to the parent metal yield strength. These alloys, which are brazed at temperatures in the range 1010-1175 C (1850-2150 F), are of particular interest as they contain melting-point depressants such as boron and silicon which diffuse from the molten filler metal into the parent metal and cause the filler to solidify isothermally as the boron and silicon concentration drops. They have been used successfully in a research program to develop a fabrication technique for the construction of 2 and 3 D airfoils by bonding together two or more flat plates containing pre-machined channels that subsequently become pressure passages in the bonded airfoil. Small samples have been produced without blocked channels or cross-leaks between them and current developments are concentrating on scaling up towards airfoils large enough for use in one or other of the NASA LaRC cryogenic tunnels. For optimum bonds the gap between the two surfaces to be bonded, the faying surfaces, should be of the order of 0.025 to 0.05 mm (.001 to .002 in) and such dimensions are easy to maintain in small samples. However, as warpage out of the plane of the plates tends to increase as the square of the plate diameter, this becomes increasingly more difficult in larger samples. A better understanding of the factors controlling dimensional stability, hopefully to be obtained as a result of the stepped specimen work described earlier, will be necessary before this technique can be used routinely for airfoil fabrication.

During brazing enough heat has to be supplied to the components to allow the filler metal to flow, wet the faying surfaces and fill the gaps between them. In general, the highest strength fillers melt at the highest temperatures and there is the greatest risk of causing grain growth when they are used. It has already been noted that a special heat-treatment has been developed to reduce the grain size and thus improve the otherwise marginal cryogenic toughness of the 18 nickel 200 grade maraging steels intended for fabrication of models for the NTF. However, most of these models needed brazing and, as serious grain growth starts at temperatures above about 1000 C (1830 F) in these maraging steels, the AWS4777 type of fillers cannot therefore be utilised. Good results were, however, obtained in an experimental program using a newly developed 47Ni-47Pd-6Si alloy (Metglas MBF-1005X) and brazing temperatures in the range 900-965 C [1650-1770 F] (Ref. 31). Other maraging steel models have been brazed using the more established silver-copper alloys such as AWS BAg 3 (50Ag-15.5Cu-15.5Zn-16Cd-3Ni) which can be brazed at temperatures between 780 and 900 C (1435 to 1650 F). As the recommended solution annealing temperature for these maraging steels is about 815 C (1500 F), the two operations could be combined if so desired. Ageing takes place at between 315 and 705 C (600 to 1300 F) and it has been suggested (Ref. 14) that brazing and ageing could be combined in the same heat-treatment using an aluminium filler to produce a diffusion brazed bond. However, initial experiments at 480 C (900 F) using pressures of 28 MPa (4 ksi) failed to produce consistent bonds with adequate strengths. The instrumented wing of Pathfinder 1, which was fabricated in Nitronic 40 (21Cr-6Ni-9Mn-N) stainless steel, was brazed using an 82% Au - 18% Ni alloy melting at 955 C (1750 F).

The temperatures involved in brazing operations are often high enough to give partial or complete relief of residual stresses created during previous machining operations and, if these stresses are unevenly distributed, distortion can occur. In extreme cases cracks have been found to propagate during brazing, or subsequent cooling and the choice of heating and cooling temperature profiles is often difficult. Ideally, rapid cooling is advisable through temperature ranges that cause microstructural degradation or unwanted ageing, with slower cooling through, or periods held at, those lower temperatures that allow some degree of stress relief.

One pre-requisite for successful brazing, or soldering, is the removal of oxide films and contamination that would otherwise prevent the molten filler from wetting the two surfaces and producing a good bond between them. Thorough cleaning and degreasing is always essential and there are two principal methods of removing oxide films, the use of active fluxes, and vacuum or reducing atmospheres in furnace brazing. The main disadvantage of active fluxes is the need to ensure their complete removal after brazing in order to avoid subsequent corrosion. In contrast, furnace brazing, particularly of stainless steels, gives a clean product but can cause microstructural degradation if post-brazing temperatures cannot be reduced rapidly. It is in practice difficult to cool thick sections quickly enough through the critical temperature range in a vacuum furnace to prevent some sensitization.

Soldering is used to create joints at much lower temperatures, usually below about 330 C (620 F) and at these temperatures there are rarely, if ever, problems with microstructural or dimensional changes. Eutectic composition alloys are preferred where available as they freeze without going through a two-phase, pasty region that causes flow problems. The bond strengths attainable are also lower and in some of the stronger tin-rich alloys, brittleness can be created by phase changes in the tin. Bond strengths are strongly influenced by factors such as joint geometry and bond thickness, the highest strengths coming from the thinnest joints due to plastic constraint by the adjacent surfaces. It is also highly advisable to match as closely as possible the expansion coefficients of the solder and the metals to be joined, which need not necessarily be the same materials. This minimises the risk of failure due to thermal fatigue should the model have to undergo many temperature cycles between ambient and its cryogenic operating temperatures. The very low melting point alloys such as Woods metal (50Bi-25Pb-12.5Sn-12.5Cd) may have restricted use in tunnels such as the NTF where there is an operational requirement to withstand temperatures up to 95 C (200 F) as it melts between 62 and 70 C (144-156 F). However, their potential should not be overlooked for other applications where this restriction does not exist.

6. NON-METALLIC MATERIALS

Current state-of-the-art practice favours the use of metals for the construction of models for cryogenic wind tunnels, especially those for operation in pressurised transonic tunnels where aerodynamic loads can be quite large. Nevertheless, non-metallic materials have important roles to play in the construction of less highly loaded components or models and for particular applications where metals are unsuitable. In general, plastic materials have lower densities, moduli and strengths and higher expansion coefficients than metals, but in many cases they are easier to fabricate. Ceramics and glasses are stronger and stiffer, but more brittle and best used for compressive loads. Natural materials, particularly wood, are often overlooked, but they are cheap, readily available, easy to fabricate and possess a number of useful properties. For example, balsa wood has a very low density ranging from 90 to 190 Kg/m³, it is an excellent thermal insulator and has a reasonable compressive strength. Finally, it is worth remembering that one of the first models tested in the NASA Langley 7 x 11 in. low speed cryogenic tunnel was a simple sharp leading-edge 74 degree delta wing whose wings and fuselage were made from a single piece of mahogany. A reasonable finish was obtained by filling the wood and applying several coats of lacquer enamel and this combination stood up well to the cryogenic environment.

6.1 Thermoplastics

These plastics materials have long chain molecular structures in which the chains are held together by weak secondary bonds. The mechanical properties of the resultant material are highly temperature-dependent and below the glass transition temperature they are rigid and brittle. Lightly cross-linked elastomers are only able to show elastomeric behavior at temperatures about 20 C above their glass transition, especially when loaded dynamically. No thermoplastics have glass transitions below about 150 K, most are completely brittle at liquid nitrogen temperatures and it is only PTFE and related fluorocarbons that are of much use at low temperatures. They are used for gaskets, seals, bearings and similar applications, but unfortunately, thermoplastics have a viscoelastic nature and they are prone to creep and stress-relaxation. Consequently they are often reinforced with fibres or powders to minimise cold flow, which also has the effect of reducing their otherwise large coefficients of thermal expansion to make them more nearly match those of the metals they are used with. The low friction characteristics of PTFE are not adversely affected by low temperatures and, when mixed with graphite and bronze powder, it forms a very useful bearing material (Glacier DQ). Fluorocarbons are also LOX compatible and thus give no problems should they inadvertently be in an oxygen-rich environment.

Thermoplastics are rarely, if ever, used in thick sections as the combination of their low thermal conductivity and high thermal expansion makes them prone to thermal shock. In the form of thin films and fibres, plastics such as mylar find uses as electrical and thermal insulators, while some thermoplastics are foamed for use as insulating materials. Probably more important, however, is their use as lacquers and adhesives, often combined with thermosetting resins. For example, epoxy-nylon adhesives are stronger than unmodified epoxies.

6.2 Thermosetting Resins

Fully cured thermosetting resins form a 3 dimensional cross-linked network structure whose mechanical properties are much less temperature sensitive and prone to creep and stress-relaxation than thermoplastics. If unfilled, they generally have very high contraction coefficients and are thus almost invariably modified unless to be used in thin layers as in surface coating lacquers. Many of the fillers used to cover the heads of fasteners, to build up complex fairings and fillets and to fair up the surfaces of wind tunnel models, are loaded thermosetting resins. The fillers are generally materials such as glass,

carbon and ceramic powders that have very small expansion coefficients and the composition is chosen so as to match that of the substrate material. The rule of mixtures:

$$\text{expn. co'ft. mixture} = (\text{expn. co'ft. filler} \times \text{vol. \% filler}) + (\text{expn. co'ft. resin} \times \text{vol. \% resin})$$
can be used to give a good indication of the required composition, but experimental testing of a range of compositions that encompass to predicted value is usually necessary to optimize performance. Results of NASA LaRC experience on filler materials was given in the 1985 paper by Dr. Young.

When blown to form a closed-cell foam, many thermosetting resins form excellent insulators and some foams are also rigid enough to bear reasonable compressive loading. For wind tunnel models, foams are sometimes used in the centre of body or airfoil segments, either to fill a void or as the rigid core of a composite structure with a bonded skin of fibre-reinforced plastic forming the stressed, aerodynamically profiled surface. Probably the major uses of thermosetting resins are, however, as the matrices of the high-performance composites to be considered in the next section.

6.3 High Performance Composites

For cryogenic applications virtually all high performance composites use epoxy resins for the matrix and glass, graphite or Kevlar fibre as reinforcement. High specific strengths and moduli are obtainable using unidirectional reinforcement, while woven fibre cloths allow 2 dimensional stressed skin structures to be fabricated without too large a loss of performance compared to the unidirectional ideal. Reinforcement in 3 dimensions does, however, result in a serious lowering of the mechanical properties. The properties of a single layer of woven cloth are anisotropic, with maximum strengths and moduli along the warp and weft direction, but more isotropic properties can be obtained in laminates by varying the fibre orientations from layer to layer. Alternatively the inherent anisotropy can be utilised to enhance the mechanical and/or thermal properties in chosen directions to meet specific design requirements.

Glass fibre reinforced epoxy systems are by far the most widely used both at cryogenic and ambient temperatures where their high strengths and good toughness are desirable. Their main drawback is in their low elastic moduli and the resultant large working strains. High modulus graphite fibres can be partially or completely substituted for glass to produce stiffer composites, but their higher electrical conductivity can sometimes be a problem and even lead to galvanic corrosion if used in conjunction with more anodic metals such as aluminium. A reasonable compromise is offered by the more recently developed polyimide fibres such as Kevlar 49 which have a 45% higher modulus, a 42% lower density and similar strengths when compared to glass. This laminating cloth has a low thermal conductivity and, for a thermoplastic, a relatively low coefficient of thermal expansion, which minimises problems of differential thermal contraction between the composite and metallic alloys. Griffin (Ref. 14) has fabricated and tested a replacement forward body section for an NTF model from Kevlar/epoxy in order to compare its mechanical and thermal characteristics with those of the 18Ni 200 grade maraging steel original. Initial results appear favourable, the most serious problem involving differential thermal expansion between the dissimilar materials where the forward and main body sections join.

A prepregged epoxy resin/E glass cloth system was used successfully for fabricating the fan blades for the NTF and details of the system and the tests used in its verification are given in a report by Klich et. al. (Ref. 16). Two different types of cloth having different fibre densities in the warp and weft directions were used and stacked at varying orientations in the 19 ply thick laminate. The same system has also been used at NASA LaRC to construct a 2 D airfoil for the 0.3-m TCT. The basic shape of the airfoil core was fabricated undersize, stainless steel pressure tubes were adhesive bonded into grooves machined in the core and further plies were then pressure molded over the tubes to create the required airfoil profile. Pressure orifice holes were drilled through from the surface to pick up the buried tubes and a good surface finish was obtained by hand polishing. The airfoil was then tested safely and successfully in the 0.3-m TCT at cryogenic temperatures. A similar system is also being considered for fabricating a replacement tail fin for the Pathfinder 1 NTF model.

6.4 Glass and Ceramics

Although able to withstand reasonable compressive stresses, neither glasses nor ceramics are likely to find much application in the bulk form in cryogenic models as they are brittle when loaded in tension. Pyrex glass and pyroceram do, however, have very low expansion coefficients which renders them almost immune from thermal shock and gives excellent dimensional stability. Should windows or other optical components be needed on models, Pyrex would be the logical choice. When ground to a fine powder, advantage can be taken of their low expansion coefficients in using the powder as the filler to reduce the expansion of resins and thus make the mixture compatible with metals. The use of E glass fibres for reinforcement has already been noted, but the growing use of optical fibres for communications might lead to their use for data transmission within or from a model.

The demands for higher thermal efficiencies in high temperature gas turbines and other engines had led to considerable improvements in the strength and toughness of engineering ceramics based on oxides, carbides and nitrides. While their low temperature properties are not yet outstanding, they are improving and it would be worth keeping their development under observation. For example, machinable ceramics might have applications for lightly loaded components where their low thermal expansion and dimensional stability might be advantageous. Even state-of-the-art ceramics such as alumina could find use as bearings which can run against each other without lubrication and be stiffer than conventional metallic or polymeric systems.

7. CONCLUSIONS

Experience gained from the construction and testing of small models in the first generation of cryogenic wind tunnels, such as the 0.3m Transonic Cryogenic Tunnel at NASA LaRC, has given a valuable indication of suitable materials and fabrication techniques and highlighted some of the problems likely to be encountered. Models for the larger tunnels such as the NTF pose an even greater challenge due principally to a combination of their increased size and higher operating stresses. The required combination of high yield strength and adequate toughness at the lowest operating temperatures has severely

restricted the range of materials available. Research and development work is being carried out on improved materials to increase the strength of inherently tough alloys and to increase the toughness of strong alloys.

Earlier problems encountered with dimensional instability are now understood to have arisen due to microstructural instability in the material and the importance of choosing stable materials is now more widely understood. However, most conventional machining techniques induce surface stresses, tensile from grinding and compressive from milling, which can be quite large in alloys like A286 that work-harden rapidly. Dimensional changes can occur, particularly in thin or asymmetric sections if care is not taken to balance the surface stresses. In most model shops opposite faces are machined alternately to minimise this problem. Subsequent heat-treatment, for example as might be carried out to braze together sub-components, can upset the delicately balanced stresses and lead to warpage which could be serious enough to render the model unsuitable for testing. Furthermore, in the larger models, problems are likely to be more severe as dimensional changes, such as warpage of a wing tip, are likely to increase at least linearly with the span of the wing. The stepped specimen program has been set up to measure such dimensional changes as might be created by thermally cycling between room and cryogenic temperatures as well as to provide information on machining-induced deformation and the heat-treatments that might be used in its removal.

The development of suitable, strong bonding and joining techniques is also an area where further progress is necessary. In general, the strongest bonds are formed at the highest temperatures and in welding some of the parent metal is remelted into the fusion zone and the structure of the adjacent material in the heat-affected-zone is altered, often detrimentally. Techniques such as laser and electron-beam welding have been found useful for joining small parts such as cover plates because of their low and localised heat inputs, but they are unsuitable for many larger applications. Brazing is the most commonly utilised technique for joining model components and the correct choice of filler is very important. The highest strengths are obtained from the nickel-based alloys and they require high brazing temperatures. While this may be acceptable for alloys such as A286 which can be subsequently heat-treated to achieve their optimum properties, problems are created with their use in materials such as the 18 nickel maraging steels. These high-strength alloys must have a small grain size to ensure adequate toughness at 77 K and the grain growth that takes place at temperature above 1000 C (1800 F) would render them unsuitable for cryogenic operation. Although conventional nickel-based alloys are thus unsuitable, the recently developed nickel-palladium alloys appear to offer a satisfactory alternative. The lower temperature silver solders have been used for most model brazing operations with relative success, although some problems have been encountered due to the creation or relief of stresses during brazing or subsequent cooling.

Finally, it would appear that the use of high-performance composites such as the glass-, carbon- and Kevlar-reinforced epoxies may have an important part to play, particularly in the fabrication of the more lightly loaded parts of models. Other non-metallic materials have small, but nonetheless important, roles as seals, thermal insulation, fillers, adhesives, etc. Aluminium alloys have been used for the fabrication of simple, lightly-stressed models and copper-based alloys including bronze and beryllium copper have been used for models as well as parts such as bearings. All of these materials have different expansion coefficients and it is highly important to recognise the problems that can arise if they are used together. Tight fits can become much looser or clearances can be reduced and binding take place if dissimilar materials are cooled from room to cryogenic temperatures. Large stresses can be set up by differential thermal contraction and these stresses can lead to distortion or even failure.

It can therefore be claimed, with considerable justification, that the advances to be gained by the aerodynamicists in the attainment of high Reynolds numbers in cryogenic wind tunnels have had to be paid for in the complexity of the models to test in them. The challenges thus set to model designers and fabricators are being met and experience is accumulating on the best materials and techniques to utilize. There is still, however, much work to be done and many problems to solve and it can confidently be predicted that if a third AGARD lecture series is held on Cryogenic Wind Tunnels in another five years time, models and materials and techniques of construction will again be a major part of the programme.

8. REFERENCES

1. Cryogenic Technology. NASA-CP-2122. (1980).
2. Cryogenic Wind Tunnels. AGARD LS 111. (1980).
3. Cryogenic Wind Tunnel Models, Design and Fabrication. NASA CP 2262. (1983).
4. LNG Materials and Fluids Users Manual (1977 & Supplements), Users manual of property data in graphical format available from NBS Boulder, Colorado.
5. Metals Handbook, 8th Edition. Vol. 1 "Properties and Selection". American Society for Metals. Ohio.
6. NBS Monograph 13. Mechanical Properties of Structural Materials at Low Temperatures. (1961).
7. NBS Monograph 63. Tensile and Impact Properties of Selected Materials from 20K to 300K. (1963).
8. ARMCO Product Data Bulletins, ARMCO Steel Corporation, Stainless Steel Division, Baltimore, Maryland. Bulletin No. S-21c, 15-5 PH VAC CE.; Bulletin No. S-33e, PH 13-8 Mo.; Bulletin No. S-54a, NITRONIC 40.
9. Republic Steel Corporation Data Bulletins. "Properties of Republic HP-9-4-20 Steel". "Properties of A286 Stainless Steel".
10. Teledyne Vasco Data Bulletins, Teledyne Vasco, PO Box 151, Latrobe Pa. 15650. "Vascomax C-200, C-250, C-300, C350". "Vascomax T250".
11. Peckner, D. and Bernstein, I: M., Eds. "Handbook of Stainless Steels". McGraw-Hill, (1977). Chapter 7 "Structure and Constitution of Wrought Precipitation-Hardenable Stainless Steels".

12. Eichelman, G. H. and Hull, F. C. Trans. Am. Soc. Met. Vol. 45, pp. 77-95, (1953)
13. Fancher, M. F.: "Aspects of Cryogenic Wind Tunnel Testing Technology at Douglas [Aircraft Company]" Paper No. AIAA-82-0606. (1982).
14. Griffin, S. A.; Madsen, A. P.; McClain, A. A., et. al. "Design Study of Test Models of Maneuvering Aircraft Configurations for the National Transonic Facility (NTF)". NASA CR 3827 (1984)
15. Hudson, C. M.: "Materials Selection for the Pathfinder 1 Model". Paper 29 in NASA CP-2122. (1980).
16. Klich, P. J.; Richards, W. H.; and Ahl, E. L. Jr.: "National Transonic Facility Fan Blade Prepreg Material Characterization Tests". NASA-TM-81800, (1981).
17. Ogawa, R. and Morris, J. W., Jr. "The Influence of Alloy Composition on the Cryogenic Mechanical Properties of AISI 200 Grade High Manganese Austenitic Steels". Proc ICMC, Kobe Japan. 11-14 May (1982)
18. Reed, R. P.; and Clark, A. F.: "Materials at Low Temperatures". American Society for Metals, (1983).
19. Rush, H. F., Jr.: "Grain-Refining Heat-Treatments to Improve Cryogenic Toughness of High-Strength Steels". NASA-TM-85816, Aug. (1984).
20. Sakamoto, T.; Nakagawa, Y.; Yamauchi, I. and Zaizen, T. "Nitrogen-containing 25Cr-13Ni Stainless Steel as a Cryogenic Structural Material". Adv. in Cryogenic Eng. Vol. 30, pp 169-176. (1984).
21. Stephens, J. R. and Witzke, W. R. "Effects of Thermomechanical Processing on Strength and Toughness of Fe-12Ni Reactive Metal Alloys at 77K". Cryogenics, pp 153-160, March. (1979).
22. Tobler, R. L.: "Materials for Cryogenic Wind Tunnel Testing" NBSIR 79-1624, NBS Boulder, Colorado. (1980).
23. Wigley, D. A.: "The Structure and Properties of Diffusion Assisted Bonded Joints in 17-4PH, type 347, 15-5PH and Nitronic 40 Stainless Steels". NASA-CR-165745. (1981).
24. Wigley, D. A.: "The Metallurgical Structure and Mechanical Properties at Low Temperature of Nitronic 40, with Particular Reference to its Use in the Construction of Models for Cryogenic Wind Tunnels". NASA-CR-165097. (1982).
25. Wigley, D. A.: "The Problem of Dimensional Instability in Airfoil Models for Cryogenic Wind Tunnels". NASA-CR-16603. (1982).
26. Wigley, D. A.: "A Proposed Configuration for a Stepped Specimen to be Used in the Systematic Evaluation of Factors Influencing Warpage". NASA-CR-166004. (1982).
27. Wigley, D. A.: "The Dimensional Stability Analysis of Seventeen Stepped Specimens of 18 Ni 200 Grade Maraging Steel, PH13-8Mo and A286". NASA-CR-172168. (1983).
28. Wigley, D. A.: "Machining-Induced Deformation in Stepped Specimens of PH13-8Mo, 18 Nickel Maraging Steel Grade 200Ti and Grain-Refined HP 9-4-20". NASA-CR-172450. (1984).
29. Wigley, D. A.: "A Systematic Plan for the Continued Study of Dimensional Stability of Metallic Alloys Considered for the Fabrication of Cryogenic Wind Tunnel Models". NASA-CR-172449. (1984).
30. Wigley, D. A.: "Technology for Pressure-Instrumented Thin Airfoil Models". Final Report on Phase 1 of NASA Contract NAS1-17571, May 1984.
31. Young, C. P., Jr.; Bradshaw, J. F.; Rush, H. F., Jr.; Wallace, J. W. and Watkins, V. E., Jr. "Cryogenic Wind Tunnel Model Technology Development Activities at the NASA Langley Research Center. Paper No. AIAA 84-0586 (1984).

9. ACKNOWLEDGEMENTS

The author would like to thank all those who have assisted in the preparation of this manuscript, particularly Dr Robert Kilgore of NASA Langley Research Center who helped to determine its scope and contents, Mrs Peggy McGuire who spent many hours reading the proofs and Jackie Halliday and Carolyn Wigley for much of the typing.

TABLE 1 Properties of Alloys used in Model Construction

Property	Material	18 Ni maraging	18 Ni maraging	18Ni maraging	18Ni maraging
1 Grade		200	200 Grain-ref'd.	200Ti	250
2 Composition		8.5Co-3.25Mo-0.1Si-0.1Mn-18.5Ni 0.20Ti-0.1Al-0.01S-0.01P- 0.03C		0Co-3.0Mo-0.7Ti 18.5Ni- .03C	7.5Co-4.8Mo-.4Ti 18.5Ni- .03C
3 Structure		Martensitic	-	-	-
4 Condition		Fully aged	-	-	-
5 Strengthening Mechanisms		Precipitation of intermetallics in low-carbon martensite			
6 Corrosion Resistance		Reasonable	-	-	-
300K MECHANICAL PROPERTIES		(t) (h) (r)	(r)	(v)	(t) (v)
7 Yield (MPa)		1418 1413 1383	1414	1379	1696 1760
8 U.T.S. (MPa)		1461 1448 1411	1452	1414	1792 1895
9 Elong. (%)		12(v) 10	18	13	11
10 Reduction in Area (%)		65 38	57	68	58
11 Kc (MPa \sqrt{m})		187 187 -	-	132	110 -
12 Charpy V (J)		49 48 40	51	102-115	28 27
13 E (GPa)		193.7 180.7(v)		181	195.3 186.2
14 Poissons ratio		.311		.311	.308 -
77K MECHANICAL PROPERTIES					
15 Yield (MPa)		1861 1714	1807		2206
16 U.T.S. (MPa)		1930 1764	1883		2275
17 Elong. (%)		- 8	20		
18 Reduction in Area (%)		60			
19 Kc (MPa \sqrt{m})		86 88			44
20 Charpy V (J)		39 34 21	33	42-43.5	14
21 E (GPa)		203.0			204.8
22 Poissons ratio		.306			.304
PHYSICAL PROPERTIES					
23 Sp. Ht. (J/kg.C) [77K]		(450)	-	-	-
24 Exp. Co'ft @ 300K (106/K)		10.1 (v)	8.6 (g)	-	-
25 Exp. Co'ft @ 77K (106/K)			6.1 (g)	-	-
26 Therm. Cond. 300K (w/m.K)		19.5	-	-	25.3
27 Therm. Cond. 77K (W/m.K)					
28 Density (g/cc)		8.00	8.00	7.98	8.00
HEAT-TREATMENT INFORMATION					
29 Atmosphere		Air, Inert, Vacuum			
30 Grain Growth (C) [F]		1000 [1830]	-	-	-
31 Soln. Anneal (C) [F]		815 [1500]	-	-	-
32 " " Time (hr)		1hr per inch thickness, then air cool.			
33 Heat-Treat. Temp. (C) [F]		480 [900]	-	-	-
34 " " Time (hr)		3 to 6 hours	-	-	-
35 " " Contraction (%)		.0006mm/mm (v)	-	-	.0009mm/mm (v)
36 Sensitization (C) [F]		do not sensitize			
37 Stress Relief (C) [F]		n/a			
DIMENSIONAL STABILITY					
38 Metallurgical		Excellent	Excellent	Excellent	Excellent
39 Cryocycle (Initial)		Good	(Good)	(Good)	(Good)
40 Cryocycle (Subsequent)		Excellent	(Excellent)	(Excellent)	(Excellent)
41 Machining		Good	(Good)	(Good)	(Good)
FABRICATION					
42 Milling	Condit. A	Good	-	-	-
43 Grinding	Condit. A	Good	-	-	-
44 Surface Finish	Full Aged	Good	-	-	-
JOINING/FINISHING					
45 Welding Process		GTA MIG EBW	Sub.arc Coated electrode		
46 Weldability		Good Good Good	Good Good		
47 Brazing Process		Vacuum Inert Gas			
48 Brazing Alloy		AWS BAg1,-3	Metglas MBF 1005		
49 Solderability		Good with correct flux			
COST & AVAILABILITY					
50 Cost (\$/lb)		8 to 10	Research alloy	6 to 8	8 to 10
51 Availability Bar		Good	n/a	Good	Good
52 " Plate		Good	n/a	Good	Good
53 " Sheet		Good	n/a	Good	Good
54 Comments		200 Grade used for many NTF models. 77K Charpy often too brittle for low in thick sections, hence grain refinement progms. Co-free grade looks promising for future use.			
55 Data crossreferences		(t)=Ref. 22 (h)=Ref. 15 (r)=Ref. 19 (v)=Ref. 10 (g)=Ref. 14			

Footnotes: Comments in () brackets are authors "best guesses" where data is unavailable or unquantified

Table 1 Continued

Maraging, Ferritic and Martensitic Steels

18 Ni maraging	9 Nickel	9 Nickel	12 Nickel	12 Nickel	9 Ni-4Co-.2C	
300	A 353	A 553 type 1	0.25 Titanium	0.5 Aluminum	AMS-6523	1
9Co-.48Mo-.6Ti 18.5Ni-.03C	9Ni-0.1C-0.6Mn-0.25Si-0.01S 0.02P-0.05Al-0.05Ti		12-13Ni-0.05C- .17 to .26Ti- .025Cr-.01Si	12-13Ni-0.3C- .25 to .50Al- .025Cr-.01Si	9Ni-4.5Co-.2C .3Mn-.75Cr-.7Mo	2
martensitic	ferrite-mart'te	ferrite-mart'te	martensitic	martensitic	martensitic	3
fully aged	2x norm. & temp	Qu. & temp.	Qu. & temp.	Qu. & temp.	Qu. & temp.	4
ppt in low-C ms	tempered mart't + gr.ref	tempered mart't	very fine grain	very fine grain	tempered mart't +gr.ref	5
reasonable	bad	bad	reasonable	reasonable	poor	6
(t) (v)	(lng)	(t) (lng)	(bh)	(sw)	(rp) (r) (r)	
1903 1965	650	700 700	807		1275 1288 818	7
1982 2000	830	800 770	1076		1414 1385 1094	8
11	24	24	16		17 14 31.4	9
55 57		67	65		65 69 60.5	10
25 23	(r) 168 140	(r) 156 to 205	192		168	11
196.8 189.6	195	186			81 78 120	12
.308	.285	.286 (g)			198.6	13
					.296	14
2344	930	1000 990	1255	1300	1497 1107	15
2475	1180	1180 1140	1407		1592 1549	16
	25	24	17		12 34.5	17
40		57	61		56 41	18
12	(r) 99 65	(r) 164 to 182	225	243	50	19
206.3	138	65			18 52	20
.303	205	207				21
	.28	.279 (g)				22
	470	-				23
-	11.4 (total contract'n of 9Ni					24
-	4.95 (from 300 to 77K = .19%)					25
25.3	29	28				26
	13	12.5				27
8.00					7.83	28
Air, Vacuum	Air	-			Air, Inert, Vac	29
1000 [1830]						30
815 [1500]	n/a	n/a			900, AC; 816, WQ	31
1hr/in; AC	n/a	n/a			1 hr/in	32
480 [900]	899 788 586 AC	788, WQ; 588, AC	685	550	550 [1025]	33
3 to 6 hr	1 hr/in	1 hr/in	2hr	2hr	4 to 8 hr; AC	34
.001mm/mm		n/a				35
	temper embrittlement 370 to 540					36
	550 to 580				538 [1000]	37
excellent	(good)	-	(good)		?	38
(good)	(good)	-	-		poor	39
(excellent)	(good)	-	-		poor	40
(good)	-	-	-		?	41
good	good	-	(good)		difficult	42
good	good	-	(good)		good	43
good	good	-	(good)		reasonable	44
as 200 grade	GTA MIG SUBARC				TIG	45
"	excellent				good	46
"	?					47
"	?					48
"	?					49
8 to 10	3 to 4	3 to 4	research alloy	-	5 to 6	50
reasonable	good	good	not yet		limited	51
reasonable	good	good	available		limited	52
reasonable	good	good	commercially		limited	53
Toughness too low for most cryogenic uses.	NTF fan shaft used special 9 Ni. Poor corrosion resistance means model use unlikely.		NASA developed alloy to combine high strength and toughness		limited use in 2D airfoils	54
(v) = Ref.10	(g) = Ref.14	(lng) = Ref.4	(t) = Ref.22	(r) = Ref.19	(rp) = Ref.9	55

- symbol signifies that the entry is the same as that in the previous column

TABLE 1 Properties of Alloys used in Model Construction

Stainless Steels

Property	Material	18Cr-8Ni	18Cr-8Ni-N	18Cr-10Ni-2Mo	25Cr-20Ni
1 Grade		AISI 304L	AISI 304N	AISI 316	AISI 310
2 Composition		18/20Cr-8/10Ni-2Mn-.03C-1Si-.03S-.04P	18/20Cr-8/10Ni-2Mn-.08C-.1/.16N1Si-.03S-.04P	16/18Cr-10/14Ni-2Mn-.08C-2/3Mo-1Si-.03S-.04P	24/26Cr-19/22Ni-2Mn-.25C-1.5Si-.03S-.04P
3 Structure		metastable aust.	stable ? aust.	metastable aust.	stable aust.
4 Condition		annealed	annealed	annealed	75% cold rolled
5 Strengthening Mechanisms		solution	solution + N2	solution	solution + C.R.
6 Corrosion Resistance		excellent	excellent	excellent	excellent
300K MECHANICAL PROPERTIES		(w/1ng)	(t)	(w/1ng)	(p&b)
7 Yield (MPa)		241	315	234	470
8 U.T.S. (MPa)		641	590	584	650
9 Elong. (%)		65	51	60	35
10 Reduction in Area (%)		83	75	77	
11 Kc (MPa \sqrt{m})		430	340	400	
12 Charpy V (J)		217	336	169	
13 E (GPa)		200	190	195	191
14 Poissons ratio		.289	.289	.294	.305
77K MECHANICAL PROPERTIES					
15 Yield (MPa)		427	700	445	800
16 U.T.S. (MPa)		1600	1557	1360	1210
17 Elong. (%)		46	47	56	56
18 Reduction in Area (%)		71	63	67	
19 Kc (MPa \sqrt{m})		400	330	166	
20 Charpy V (J)		190	200	154	
21 E (GPa)		214	205	209	205
22 Poissons ratio		.278	.278	.283	.295
PHYSICAL PROPERTIES					
23 Sp. Ht. (J/kg.C) [77K]		480	[220] -	-	400 [200]
24 Exp. Co'ft @ 300K (106/K)		15.9	(total linear contraction of all 4 grades of stainless steel between 300 and 77K is .285 percent)		
25 Exp. Co'ft @ 77K (106/K)		13	14	14	11
26 Therm. Cond. 300K (W/m.K)		14	16	14	11
27 Therm. Cond. 77K (W/m.K)		8	8.2	8	6
28 Density (g/cc)		8.00(p&b)	8.00	8.00	8.00
HEAT-TREATMENT INFORMATION					
29 Atmosphere		Air, Inert, Vac.	-	-	-
30 Grain Growth (C) [F]		(1120 [2050])	--	-	(1136 [2080])
31 Soln. Anneal (C) [F]		1010/1120 [1850/2050]	-	-	1036/1149 [1900+]
32 " " Time (hr)		(few hours)	-	-	-
33 Heat-Treatm't (C) [F]		n/a	-	-	-
34 " " Time (hr)		n/a	-	-	-
35 " Contraction (%)		n/a	-	-	-
36 Sensitization (C) [F]		550 to 930C	-	-	-
37 Stress relief (C) [F]		480 [900]; slow cool. or 950 [1750]; rapid quench	-	-	-
DIMENSIONAL STABILITY					
38 Metallurgical		poor, (Ms=230K)	good, (Ms=100K)	medium, (Ms=160K)	exc., (Ms=30K)
39 Cryocycle (Initial)		(good?)	(very good)	(good)	(excellent)
40 Cryocycle (Subsequent)		(very good)	(excellent)	(very good)	(excellent)
41 Machining		poor, (Md =400K)	good, (Md=250K)	medium, (Md=300K)	exc. (Md=200K)
FABRICATION					
42 Milling		poor	-	-	-
43 Grinding		poor	-	-	-
44 Surface Finish		reasonable	-	-	-
JOINING/FINISHING					
45 Welding Process		MIG, TIG, SMAW	-	-	-
46 Weldability		excellent	-	-	-
47 Brazing Process		Vacuum or Inert Gas	-	-	-
48 Brazability Alloy		AWS BAG 1.3. AWS BNi 3.	-	-	-
49 Solderability		Good with reactive flux, for example orthophosphoric acid.	-	-	-
COST & AVAILABILITY					
50 Cost (\$/lb)		4	5	4	6
51 Availability Bar		excellent	good	excellent	good
52 " Plate		excellent	good	excellent	good
53 " Sheet		excellent	good	good	good
54 Comments		300 series stainless steels widely used for cryogenic tunnel fabric'n. Have been used for lightly stressed cryogenic models but too weak for higher loads in pressurised tunnels such as NTF.			
55 Data References		w = Ref.2	(p&b) = Ref. 11	(1ng) = Ref.4	

Footnotes: Comments in () brackets are authors "best guesses" where data is unavailable or unquantified

Table 1 Continued

Stainless Steels

21Cr-6Ni-9Mn	25Cr-13Ni-.4N	A286	PH13-8Mo	15-5PH	17-4PH	
Nitronic 40	JAERI YUS 170	AMS-5736A	UNS S13800	UNS S15500	UNS S17400	1
21Cr-6Ni-9Mn-.15/.4N-.3V-.1Si-.08C-.03S-.06P	25Cr-13Ni-.40N-.8Mo-.5Mn-.9Si-.02C-.03P-.002S	25Ni-14Cr-2.2Ti-1.2Mo-1.5Mn-.3V-.08C-.2Al-.5Si	13Cr-8Ni-.04C-1.1Al-2.2Mo-.03Mn-.03Si	15Cr-4.5Ni-.04C-3.4Cu-.4Si-.3Mn-.25Nb	16.5Cr-4Ni-.04C-3.4Cu-.6Si-.3Mn-.25Nb	2
stable? aust.	stable? aust.	stable aust.	martste + aust	ms. + rev. aust	ms. + rev. aust	3
annealed	annealed	STA	H 1150 M	H 1150M	H 1150 M	4
solutes + N2	solutes + N2	precipitates	ppt.+ temp. ms.	ppt.+ temp. ms.	ppt.+ temp. ms.	5
excellent	excellent	excellent	excellent	excellent	excellent	6
(a)	(h)	(sak)	(t) (rp) (h)	(a)	(a)	7
400	483	460	750 690 689	586 586	586	8
710	758	861	1000 1103	896 896	862	9
50		52	24	22	22	10
70		75	37	70	75	11
			114/161	165		12
294	271	477	(g) 75	162 109	136	13
197			195.8 200.6	172	196	14
.285			.330 .306	.278	.272	15
			(t)			16
1034	1034	1131	930	827	1000	17
1400	1379	1693		1482	1207	18
		46			27	19
24		63			65	20
	182					21
87	88	243				22
			202.7 (g)			23
					418	24
16.7			16.7	10.9	11	25
			12.2(g)			26
13.4			14.9	12.7	17.9	27
(5)					(15)	28
7.83			7.96	7.76	7.82	29
Air, Vac, Inert	-	-	-	-	-	30
1180 [2150]		(1180 [2150])	(1180 [2150])	1180 [2150]	1200 [2200]	31
1066 [1950]		982 [1800]	927 [1700]	1030 [1900]	1030 [1900]	32
1 hr/in; + W.Q.		1 hr then W.Q.	30 min. + A.C.	30 min. + A.C.	30 min. + A.C.	33
not relevant		734 [1350]	760,AC; 620,AC.	760,AC; 620,AC.	760,AC; 620,AC.	34
" "		16 hr then A.C.	2 hr ; 4 hr	2 hr ; 4 hr	2 hr ; 4 hr	35
			.0035	.0024	(.002-.003)	36
590/930 [1100/1700]		(- ?)	(- ?)	(- ?)	(- ?)	37
480[900],AC or 950[1750],WQ.		Solution anneal	then re-age	-	-	38
Stable		Stable	Stable ?	Unstable	Unstable	39
Good		Excellent	Some warpage	Large warpage	Large warpage	40
Excellent		Excellent	Excellent	Further warpage	Further warpage	41
High stress		V. High stress	Moderate stress	?	?	42
poor		bad	harder than 304	like 304	like 304SS	43
poor		poor	good	" "	" "	44
soft		reasonable	Very good	Excellent	Excellent	45
MIG, TIG, SMAW	-	- weld in	TIG	MIG, TIG, SMAW	-	46
Good	-	soln treat cond	Good	Good	-	47
Vacuum, Inert Gas	-	-	-	-	-	48
AWS BAg 1,3; AWS BNi 3;		soln. HT; reage	-	-	-	49
Good with reactive flux, for example orthophosphoric acid				-	-	50
5		9	7	7	7	51
Difficult	?	Long lead time	Long lead time	Reasonable	Reasonable	52
Difficult	Up to 60mm	"	"	"	"	53
Reasonable	Down to 0.3mm	Reasonable	"	"	"	54
Used for Path-finder 1 and other NTF models	Alloy developed in JAERI fusion research prog.	Many 2 & 3 D models used in La RC 0.3m and NTF tunnels	Alloy must be cooled 16 [60] before ageing NTF model use	Alloys must be cooled 32 [90] before aging to complete marten-site transformation. Unstable in H1150M, too brittle fully aged.		55
(a) = Ref. 8	(sak) = Ref. 20	(rp) = Ref. 9	(t) = Ref. 22	(h) = Ref. 15	(g) = Ref. 14	

- symbol signifies that the entry is the same as that in the previous column

TABLE 1 Properties of Alloys used in Model Construction

Aluminium and Copper Alloys

Property	Material	Aluminum	Aluminum	Aluminum	Beryllium Copper
1 Grade		AAA5083	AAA6061	AAA 2014	
2 Composition		4.5Mg-.6Mn	1Mg-.6Si-.27Cu-.25Cr	4.4Cu-.8Si-.8Mn-.4Mg	1.8Be-.2Co-.1Fe-.1Si
3 Structure		f.c.c	f.c.c	f.c.c	f.c.c
4 Condition		annealed	T6	T6	soln HT & aged
5 Strengthening Mechanisms		solution	precipitation	precipitation	precipitation
6 Corrosion Resistance		good	good	good	good
300K MECHANICAL PROPERTIES		(1ng)(m13)(asm)	(1ng)(m63)(asm)	(1ng)(m13)(asm)	(m63)
7 Yield (MPa)		150	270	420	667
8 U.T.S. (MPa)		313	306	476	702
9 Elong. (%)		23	18	13	19
10 Reduction in Area (%)		35	56		68
11 Kc (MPa.m)					
12 Charpy V (J)			22		51(U)
13 E (GPa)		71.6	70.2	73.1	131
14 Poissons ratio		.3334	.3383		
77K MECHANICAL PROPERTIES					
15 Yield (MPa)		164	330	470	819
16 U.T.S. (MPa)		434	412	565	909
17 Elong. (%)		33	24.5	14	31
18 Reduction in Area (%)		38	51		66
19 Kc (MPa.m)					47(U)
20 Charpy V (J)			22		
21 E (GPa)		80.2	77.1		
22 Poissons ratio		.3195	.3277		
PHYSICAL PROPERTIES					
23 Sp. Ht. (J/kg.K) [77]		966 [340]	966 [340]	966	420
24 Exp. Co'ft @ 300K (106/K)		23.2	23.2	23	17.8
25 Exp. Co'ft @ 77K (106/K)		9.0	9.0		
26 Therm. Cond. 300K (w/m.K)		115	118	193	218
27 Therm. Cond. 77K (w/m.K)		55			84
28 Density			2.66	2.7	2.8
HEAT-TREATMENT INFORMATION					
29 Atmosphere					
30 Grain Growth (C) [F]					
31 Soln. Anneal (C) [F]				496/507 [925/945]	
32 " " Time (hr)				1 hr (salt), air	
33 Heat-Treatm't (C) [F]				168/174 [335/345]	
34 " " Time (hr)				8 to 12 hr	
35 " Contraction (%)			none?	-	.2
36 Sensitization (C) [F]		Aluminium alloys do not sensitise		-	
37 Stress Relief (C) [F]				360/412 [650/775]	
DIMENSIONAL STABILITY					
38 Metallurgical		Excellent	Excellent	Good	Good
39 Cryocycle (Initial)		Good	Good	Good	Good
40 Cryocycle (Subsequent)		Good	Good	Good	(good?)
41 Machining		Aluminium alloys	similar to 300	series stainless	(good?)
FABRICATION					
42 Milling		Poor	Fair	Good	Poor
43 Grinding		Aluminium alloys	not normally ground		?
44 Surface Finish		Poor	Fair	Good	Fair
JOINING/FINISHING					
45 Welding Process		MIG, TIG, SMAW,	-	-	MIG, TIG,
46 Weldability		Good	Good	Fair	Excellent
47 Brazing Process		Not normally recommended for aluminium alloys			Furnace, torch
48 Brazability Alloy		"	"	"	Good, Ag-based
49 Solderability		Very aggressive fluxes needed, not recommended			Excellent
COST & AVAILABILITY					
50 Cost (\$/lb)		2-3 \$/lb	-	-	5-6 \$/lb
51 Availability Bar		Good	Good	Good	Reasonable
52 " Plate		Good	Good	Good	Reasonable
53 " Sheet		Good	Good	Good	Reasonable
54 Comments		Used in bulk in tankage. Limited model usage	Used for lightly loaded models in 0.3-m TCT & NTF	Stronger but lower toughness limits model use	Used for high thermal conductivity inserts.
55 Data References		(1ng) = Ref. 4	(m13) = Ref. 6	(asm) = Ref. 5	(m63) = Ref. 7

Footnotes: Comments in () brackets are authors "best guesses" where data is unavailable or unquantified

Table 1 Continued

Titanium, Low Expansion and Nickel Superalloys

Ti-6Al-4V	Ti-5Al-2.5Sn	Invar	Ni-Span C	Inconel 718	Inconel X750	
Ti-6Al-4V, ELI	Ti-5Al-2.5Sn, ELI	Ni1036, Ni1var	Constant Mod- ulus 42			1
6Al-4V-.1Fe-.01C	5Al-2.5Sn-.2Fe-.07C	36Ni-.1C-.36Si-.35Mn-.1Al-.015P-.015S	42Ni-5.2Cr-.5Al 2.4Ti-.06C	19Cr-18.5Fe-3Mo .9Ti-5.1Nb & Ta	15.5Cr-7Fe-.7Al 2.5Ti-.95 Nb & Ta	2
h.c.p./b.c.c.	h.c.p.	f.c.c.	f.c.c.	f.c.c.	f.c.c.	3
Annealed	Annealed	Annealed	Soln.HT & aged	Soln.HT & aged	Soln.HT & aged	4
Solute /2 phase	Solution	Solution	Precipitation	Precipitation	Precipitation	5
Excellent	Excellent	Excellent	Excellent	Excellent	Excellent	6
(g) (n) (h)	(h) (n) (t)	(lng) (h) (t)	(m63) (asm)	(t) (h) (asm)	(h) (asm)	7
951 896	724 875	276 289	774 793	1172 1034	758	8
1024 931	827 925	552 552	1202 1240	1404 1276	1241	9
17	19	55	24 18	20		10
47	44		50			11
96.9 100 (t) 90	90	101		90		12
27 37 27	34 24 34(g)	298	24 (U)	27	47.5	13
110.3	111	153 152	182	213	213	14
.330	(.330)	.2845				15
1576 1310	1207 1380	621 620	905	1207	862	16
1624 1413	1241 1437	862 862	1550	1620	1482	17
10	14	42	31.6			18
41	30		47			19
59 61 (t) 61	72 75	68		110	110	20
14 21 14	14 15 14(g)		23 (U)	27	47.5	21
121.4	(121.4)	140.4 141		227	227	22
		.307				23
		(asm)				24
(530) ([200])	530 ([200])	517 ([190])		(450 [170])		25
(9.3)	9.36 8.4/9.4	1.2 2.5		11.5		26
		0.4 .83				27
(8.17)	8.17	13.8 13.8		0.1 to 0.23		28
(4.4)	4.4	6.2 6.2		.058 to 0.16		29
4.43	4.46	8.0		(8.2)	8.3	30
Vacuum, Inert Gas		Reducing/inert atmosphere		Inert, Air	-	31
ph tr. T = 1000	760 [1400]					32
843/954 [1550]	815 [1500]	750/850 [1380] (- ?)		980, A.C.	980, A.C.	33
15/30 min; W.Q.	30 mins	30 min/in; W.Q. (- ?)		1 hr	1 hr	34
480/540 [900]	n/a	315 95 650 730		720, FC; 620, AC	870, ac; 705, AC	35
4/8 hr; A.C.	n/a	1hr, AC; 48hr, AC	5 hr 3 hr	8 hr ; 20 hr	25 hr ; 20 hr	36
n/a	n/a	n/a		0.09%	0.09%	37
do not sensitise		do not sensitise -		Do not sensitise		38
704/829; 1-2 hr	540/650; 1-2 hr	same as heat-treatment		870 for 3 hr to 980 for 7/15 min		39
(stable)	stable	stable	stable	stable	-	40
(good)	(good)	(-)	(-)	(stable)	-	41
(good)	(good)	(-)	(-)	(")	-	42
difficult	difficult	(like 304?)	(poor)	difficult, work hardens rapidly		43
fine, dry swarf is inflammable !		(" " ?)	(reasonable)	reasonable		44
poor ?	poor ?	Reasonable ?	(" ")	easily scratched		45
MIG, TIG, EBW	-	MIG, TIG	- ?	TIG, MIG, SMAW,	-	46
Excellent	-	good	- ?	good	-	47
Vacuum, Inert Gas	-	?	- ?	Vac, Inert, Air	-	48
Care needed	-	?	- ?	Copper alloys preferred to silver		49
not usual	-	active flux	- ?	Acid flux for Pb & Sn solders		50
6 to 9 depending on product form		9	10	12	12	51
reasonable	-	reasonable	poor	difficult	-	52
reasonable	-	"	"	not available	-	53
good	-	"	"	difficult	-	54
Poor low temperature toughness and difficult machinability combine to make titanium unattractive for cryogenic models		Total contraction from 300 to 77K = 0.05%, 10% of steels.	Used in springs & bellows, too brittle for general use.	High cost and extreme difficulty in machining, drilling and fabrication restrict usage to high temperature models.		55
(n) = Ref. 6	(g) = Ref. 14	(t) = Ref. 22	(asm) = Ref. 5	(m63) = Ref. 7		

- symbol signifies that the entry is the same as that in the previous column

SOME RECENT DEVELOPMENTS IN MATERIALS & TECHNIQUES FOR MODEL FABRICATION.

by
D.A.Wigley.

Director, Cryogenic, Marine and Materials Consultants Ltd,
17 Bassett Wood Drive, Bassett, Southampton, SO2 3PT, ENGLAND.

1. Introduction.

Note: On the assumption that most of the attendees at the 1989 lecture series are new to the field, Dr Kilgore and the author agreed that the first part of the lecture on Materials and Techniques for Model Construction would use the same notes as given at the 1985 lectures. These additional notes are for the benefit of those who attended the earlier lectures and would like an indication of more recent developments. The choice of material reflects those areas in which the author has a particular interest and any omissions do not imply that significant developments have not taken place in other areas during the last few years.

Three topics are considered in these notes:

- The laminated thin sheet technology used in fabrication of a model of the X29A canard that enabled a uniquely high number of pressure orifices to be placed in a thin airfoil;
- The different configurations of sample used for studies on materials and fabrication techniques for model construction, and;
- The long term objective of creating a handbook, database or expert system to bring together the information already available and indicate those areas where further work is needed.

2. Laminated Thin Sheet Technology

As part of the American Small Business Innovation Research (SBIR) program, the author and P.L. Lawing developed a radically new method of fabricating thin airfoil models that have a high density of pressure orifices. The detailed report on this programme is given in "Technology for Pressure-Instrumented Thin Airfoil Models". (Ref. 1.) An outline of the results obtained when the X29A canard model was tested in the 0.3 m TCT at NASA Langley are given in Lawings paper in this lecture series.

3. Sample Configurations for Cryotechnology Development.

In the 1985 lecture, an introduction was given to the concept of using stepped specimens to rationalise studies of warpage and machining-induced stresses. Since then, further ideas have developed and it is now possible to place the concepts into a broader framework.

3.1 Stepped Specimens.

3.1.1 The Original Purpose/Philosophy Behind the Stepped Specimen.

Essentially there were two major objectives behind the original concept of the stepped specimen: The first was to carry out a systematic study on the dimensional stability at cryogenic temperatures of the materials then being used for models. In particular it was possible to explain the warpage that had occurred in airfoil models made from the 2-phase precipitation-hardening stainless steels, such as 17-4PH and 15-5PH. The second was to develop a concept that would enable us to understand, quantify and control machining-induced stresses and the resultant dimensional changes.

The main features of stepped specimens in their original format were: the use of constant-thickness steps to allow calculation of the magnitude and sign of the surface stresses using beam theory and the restriction that all machining was carried out on one side only, the other side being used for reference.

The reasons for the modified larger format were: separation of the machined region from the support area, and closer simulation of the mounting procedure in use by NASA at that time during machining of actual airfoil models.

3.1.2 Further Developments.

A structured programme to evaluate the effect of relevant variables for range of materials of interest was curtailed when the NASA programme ceased due to financial constraints. On reflection, it would have been an almost open-ended task to complete such an ambitious project and thus selectivity is needed to define the priorities for future work.

3.1.3 Use by MBB.

Since the 1985 Agard meeting, stepped specimens have been used by Gross and Luck of MBB to investigate various aspects of the machining characteristics of materials for model applications. The MBB work (Ref. 2) was on Ph 13-8 Mo, which had been chosen for the construction of a model of the TST-demonstrator aircraft to be tested in the NTF, ETW and a number of conventional wind tunnels. Stepped specimens were used by MBB to optimise machining parameters to give the best surface finish and the smallest amount of machining-induced deformation. They also confirmed the effect of cryocycling the material in the early stages of machining to eliminate any dimensional changes on the finished model.

3.2 Wedge Specimens.

Early in the NASA programme, wedge-shaped samples, some in the form of a trailing edge cusp, were used to study warpage, but no standardised configuration was adopted. In their paper Gross and Luck developed the concept to give a sample in which the steps were replaced by a gradual taper of the machined section from an initial machined thickness of about 6mm to about 1mm at the 'trailing edge'. The purpose was to simulate more realistically machining of the thinnest part of a wing. This is a logical development of the original concept and is best used once machining parameters have been optimised, as the penalty paid for the improved realism is a loss of the ability to obtain quantitative values of the induced stresses.

3.3 Double-Sided Specimens

One limitation of the original concept of the stepped specimen arises as a consequence of the decision to limit machining to one surface only in order to have the other side available as a reference surface. In this configuration, deflections induced by machining stresses are maximised to allow the greatest sensitivity in detecting changes.

However, in machining a model airfoil, the objective is to minimise any warpage and this is achieved conventionally by the alternate machining of opposite sides in order to balance the stresses created during machining. Thus, a two-sided specimen, in which both sides are machined alternately, would be used to check how effectively the stresses in the opposite surface did, indeed, balance each other. A further use for a two-sided sample is the simulation of the adhesive hold-down procedure used increasingly for machining airfoils.

A number of different sample configurations can be used to investigate this effect, some possible concepts being given in Ref. 6. In the use of double sided samples it is important to be able to obtain measurements from both sides of the sample and to be able to relate the observed dimensional changes to the machining sequences employed.

One of the more easily analysed configurations is the simple parallel-sided block. This type of sample was used by the author and I.D Burton as part of the 'brazed-block' technique of model construction that was tried in the course of developing the 'laminated brazed sheet' concept used to fabricate the X29A canard model.

3.4 Parallel-Sided 6 mm Thick Stainless Steel Plates.

The work on machining-induced stresses was carried out to study both the basic nature of these stresses and also to develop ways of holding the plates to be machined in the later stages of the program. Initial work was carried out on 6 mm thick type 316 stainless steel plates. Various non-magnetic methods of holding down the plates were investigated and it was found that it is easier to restrain movement during milling operations than during grinding. As, however, final finishing of flat plates is conventionally carried out by grinding, it was important that dimensional changes induced by grinding, or by their relief during subsequent heat-treatment, can be controlled. Further details of this work are given in Appendix 1.

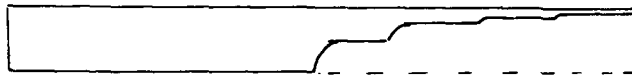
3.5 Three Dimensional Specimens.

In his lecture to the 1985 Agard lecture series entitled "Design and Construction of Models for the NTF-II", Young described a 3 dimensional 'wing spar specimen' used by NASA in the evaluation of two experimental fabrication concepts, nickel plating and fibreglass overwrapping. The specimen had a span of about 9 inches with strong attachment points built into each end so that static or dynamic loads could be applied in bending or twisting modes. A similar specimen configuration was also considered for use as a larger sized follow up to the stepped specimens for evaluation of machining stresses. In their paper referenced previously, Gross and Luck followed their stepped specimen work on machining Ph 13-8 Mo by fabrication of a 'semi-scale wing', which included a small cover plate in the bottom surface. After hand finishing, the model was validated in two sections, cryocycled 7 times and re-validated to confirm that the required accuracy could be obtained.

3.6 Future Developments.

It will by now be apparent that the author considers that a suitable series of samples can be used to develop a comprehensive understanding of the factors that determine the dimensional stability of materials used for making models. Thus, as indicated schematically in Fig 1, there is a natural progression from single-sided stepped specimens, which give the greatest sensitivity and allow calculation of the stresses involved, to wedge samples, which extend this concept to a configuration more realistic of an airfoil trailing edge. Double-sided samples, either parallel plates or with steps, then allow fixturing to be optimised and warpage minimised. Some form of idealised 3 dimensional sample wing would complete the progression. The wing should have strong points at root and tip to permit loading and it could also have sections machined away to study cover-plates, holes and slots to evaluate fillers and removable trailing edge segments to study attachment techniques.

In a NASA report (Ref. 6) the author tried to show how this approach could be extended to cover other aspects of the cryogenic technology development programme. Thus, Fig 2 is a schematic representation of how these topics could be integrated and phased, assuming that material 1 had the highest priority. An even wider over-view is suggested schematically in Fig 3, where other aspects of the programme are integrated with the dimensional stability and machining activities. In many respects, developments in the USA, Germany France and the UK are fitting into these patterns. There is, however, much that could still be added.



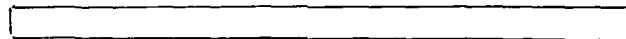
Single Sided Stepped Specimen: Maximum Sensitivity.



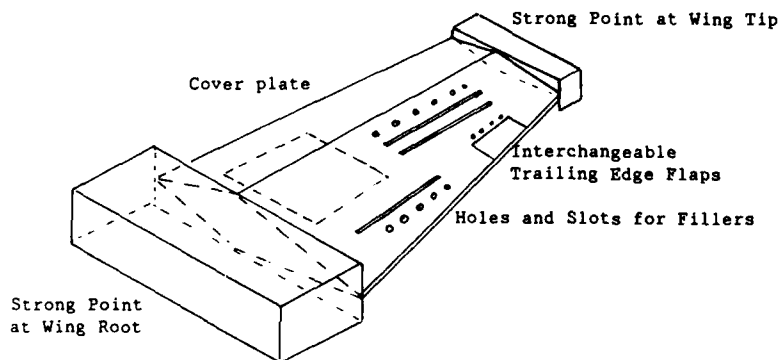
Wedge Specimen: More Realistic Machining Conditions.



or



Double-Sided Stepped or Parallel Sided Plate: Balanced Stresses.



3-Dimensional 'Wing' Specimen: Intermediate Step Before Full-Sized Airfoil.

Figure 1. Schematic Representation Sample Configurations for Cryotechnology Development.

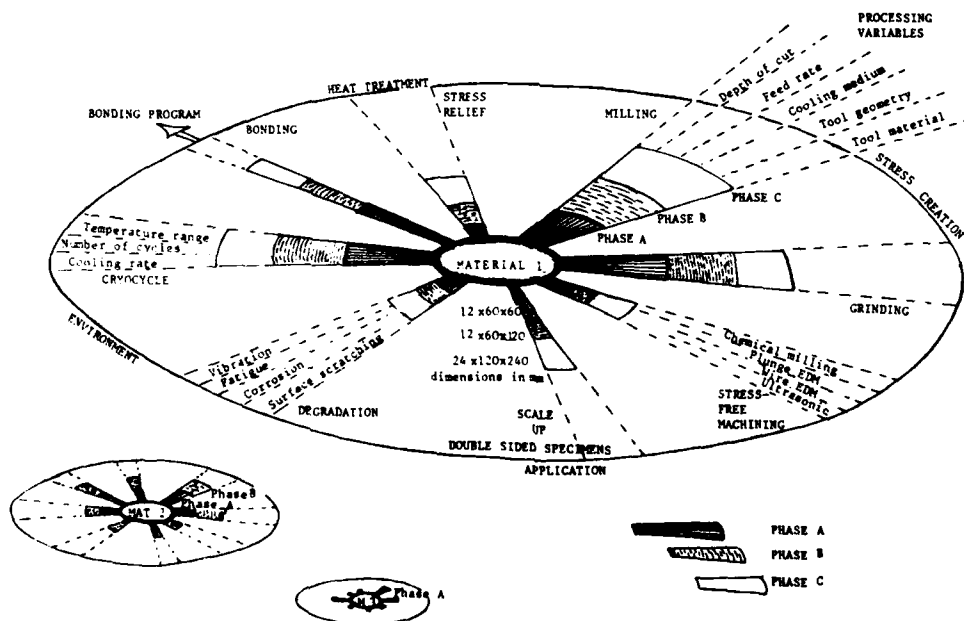


Figure 2. Phased Development of The Stepped Specimen Programme.

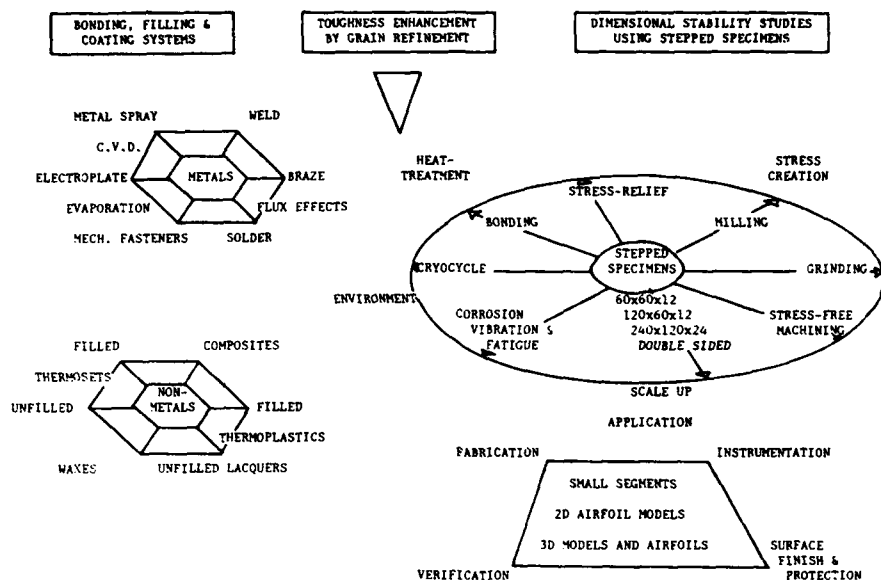


Figure 3. Schematic Representation of Inter-related Research and Development Projects to Support the NASA Cryogenic Model Programme.

4. Materials and Techniques for the Fabrication of Models for Use in Cryogenic Wind Tunnels: A Handbook, Database or Expert System?

For many years it has been recognised that there is a need for a handbook, database or expert system that will bring together the information already available and indicate those areas where further work is needed. Such a project would not only be expensive and time consuming, but its success or failure would depend on the active and willing co-operation from all the establishments where such expertise has accumulated. Assuming that such a project were to be undertaken, it would be vital to be clear at the outset where the appropriate boundaries lay between information that is clearly in the public domain and what is commercially confidential, or 'black'. Nevertheless, it should be possible to structure such a project in such a way that the information in the public domain formed the basis of the compilation, while more sensitive information was entered later by its owners.

The European programme has been extremely fortunate in having received such a free flow of information from our American colleagues. T2 and KKK are now operational, the ETW is entering its construction phase, and results are now starting to come from a number of European projects on cryogenic materials and fabrication technology. It is to be hoped that, in turn, Europe will be equally generous in sharing its data.

5. Conclusions.

The coming years should see further developments in the technologies associated with the design, fabrication and testing of models for cryogenic wind tunnels. However, many of those most experienced in this field are nearing approaching retirement and there is a danger that their experience will go with them. Financial constraints have limited the progress in consolidating the existing body of knowledge into a structured format, such as a handbook or database. An early start on such a project should be seriously considered.

6. References.

1. Wigley, D.A.: "Technology for Pressure-Instrumented Thin Airfoil Models". Final Report on Phase 2 of NASA Contract NAS1-18066, NASA CR-4173, September 1988.
2. Gross, U. and Luck.: "Design and Manufacture of a Cryogenic Wind Tunnel Model." Proc. Second Cryogenic Technology Review Meeting, DFVLR, Köln-Porz, June 28-30, 1988.
3. Wigley, D.A.: "A Proposed Configuration for a Stepped Specimen to be Used in the Systematic Evaluation of Factors Influencing Warpage". NASA CR-166004. (1982).
4. Wigley, D.A.: "The Dimensional Stability Analysis of Seventeen Stepped Specimens of 18 Ni 200 Grade Maraging Steel, PH13-8Mo and A286". NASA-CR-172168. (1983).
5. Wigley, D.A.: "Machining-Induced Deformation in Stepped Specimens of PH13-8Mo, 18 Nickel Maraging Steel Grade 200Ti and Grain-Refined HP 9-4-20". NASA-CR-172450. (1984).
6. Wigley, D.A.: "A Systematic Plan for the Continued Study of Dimensional Stability of Metallic Alloys Considered for the Fabrication of Cryogenic Wind Tunnel Models." NASA-CR-172449. (1984).

APPENDIX 1.

The Use of Nominally Parallel Sided Plates to Study Machining-Induced Deformation and the Effectiveness of Hold-Down Procedures During Machining.

A1. Specimen and Validation Details

The specimens were 120 mm [4.72 in.] long x 60 mm [2.36 in.] wide and initially 6 mm [0.236 in.] thick. Different sequences of machining operations were carried out and detailed records of the machining, validation and heat-treatment operations kept in order to enable subsequent interpretation of the observed dimensional changes.

The validation equipment used to measure dimensional changes was a developed version of that described in ref. 5., modified to cope with larger specimens. Measurement was computer-controlled and a sequence of readings were taken at pre-determined positions on the specimen surface. Eleven scans were made along the length of the specimen with height measurements made at 2 mm intervals, each scan producing 56 readings. The longitudinal scans were made at 5 mm intervals in the transverse direction, with the 6th scan carried out along the centerline of the specimen. A total of 616 height measurements were thus obtained for each surface and both surfaces were scanned. Height measurements were accurate to about 1 micron [25.4 microns = 0.001 in.] and reproducible from run to run to within a few microns.

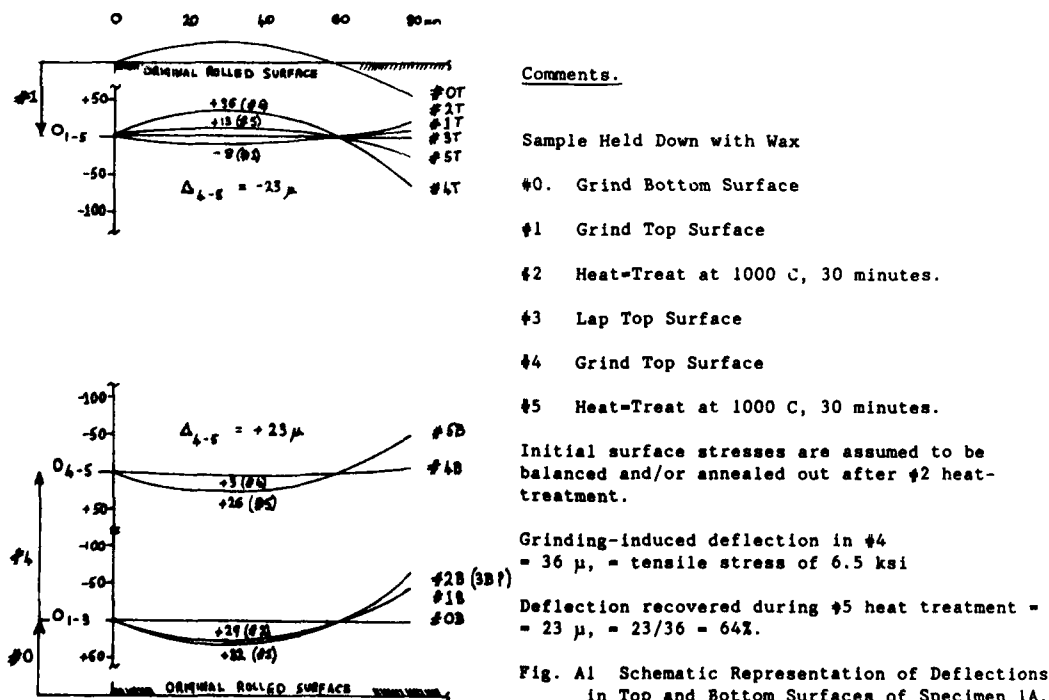
A2. Presentation and Analysis of Results

Results were initially printed out as a two-dimensional array which allowed an immediate assessment of the surface contours to be made. Subsequent processing of the data, or selected portions of it, enabled sections to be plotted and surface stresses to be calculated. Furthermore, the differences in surface stresses between two sets of conditions, for example before and after an annealing heat-treatment, could be obtained by subtracting one set of co-ordinates from the other. In this way the effects of the heat-treatment can be followed, regardless of the actual shape of the surface.

A3. Initial Specimen Preparation and Plotting Convention Used to Present the Results of Surface Profile Measurements on Parallel Sided Plates.

One of the problems in studying machining-induced stresses and strains is in getting the specimens initially prepared without inducing high surface stress levels. A second, ever-present problem is to find a method of holding specimens during machining such that the surfaces do not move as a result of the induced stresses.

The consequences of these problems can be considered with the aid of Fig. A1. The starting material for these samples was rolled plate of nominal thickness 0.312 in. [7.93 mm] and in this condition there would have been residual surface stresses created by the rolling process. The positions of the original surfaces are indicated at the top and bottom of the figure. These surfaces would normally be removed by a process such as fly cutting or end milling, but for simplicity let us assume that the first operation, #0, is to grind off the bottom surface and that this gives the flat surface with origin at O[1,3]. As a result of this machining operation, the plate now has unbalanced stresses in its two surfaces and the top surface will distort, let us assume to the position shown as #0T.



The specimen is now turned over and the rolled top surface is ground away to produce the new surface at origin O[1-5]. This is the condition in which the first measurements were made and the movement of the surfaces can be explained simply by monitoring the position of the central longitudinal scan, particularly the first 80 mm. Thus, #1T shows that the ground top surface was not, in fact, quite flat but curved, appearing to dip to a minimum of -8μ at about 30 mm before returning to zero at 60 mm then rising upwards. The surface passes through the 60 mm point because the specimen is levelled at three points, two of which lie along the zero line in the transverse direction with third 60 mm along the central scan line.

At this point, attention should be drawn to the sign convention used in plotting the surface profiles. During validation, any movement of the surface towards the capacitance measuring probe is given a positive sign and for the top surface such movements are plotted above the origin. Thus, #1T shows that the shape taken up by the top surface at the 30 mm position gave movement away from the probe.

Let us now consider the deflection of a beam of constant thickness bent in an arc. If the top surface had been bent towards the probe, the bottom surface would appear, when measured, to have moved in the opposite direction, i.e. away from the probe. The movement will therefore be recorded with a negative sign. However, in order to make it immediately apparent to the eye that the two surfaces have moved in the same actual direction, it is necessary to plot positive movements of the bottom surface downwards from the origin. Thus, as may be seen from #1B, a positive maximum central displacement of $+32 \mu$ is plotted below the origin.

Returning now to specimen 1A, it can be seen that, as a result of grinding the top surface, the ends of the bottom surface, #1B, have also curved upwards. It was known from our previous work, (refs. 5, 3 & 4), that grinding induces tensile surface stresses and that a plate free to move will curve so as to adopt a position in which these stresses are balanced by elastic tensile stresses induced in the opposite face. The double-sided tape used to hold the specimens in these initial machining stages would, indeed, have allowed such movement. Thus the profiles adopted by the two surfaces are the result of a balance between the residual tensile stresses induced by grinding both faces and any elastic bending stresses.

In order to minimise the residual stresses, the sample was heat-treated at 1000 C for 30 minutes and then oil-quenched in order to prevent any degradation of its microstructure. A further series of measurements were then taken to give the surface profiles labelled #2T and #2B. It can be seen that both the top and bottom surfaces have straightened slightly, but that there is still a pronounced curvature in the bottom surface. In order to produce a better reference surface on the specimen before starting a systematic study of machining-induced deformation, the top surface was lapped flat and the resultant profile is shown labelled #3T. It was assumed that this light lapping would not change the profile of the bottom surface and so #3B was not measured, but taken to be the same as #2B. Subsequent work casts some doubt on this assumption, but any errors thus introduced would be small.

A4. Results from Specimen 1A, Wax Held, Single Side Ground and Heat-Treated at 935 C.

The top surface, as measured in #3T after lapping, was now used as the reference surface and also the side of the specimen that was to be held down. A vacuum wax that melted at about 100 C and spread easily was used to hold the specimen to a large block of mild steel so that the next grinding operation could be carried out. Unfortunately, it was found that the specimen still 'moved' during the grinding process, indicating that the adhesion of the wax was not great enough to hold the specimen flat. The resultant ground surface had the profile shown by #4B: Note that the origin has been moved up to O[4,5] as metal was removed during the grinding process. The ground surface is reasonably flat, with a maximum central deflection of $+3 \mu$. However, validation of the top surface gave the profile shown as #4T and it can be seen that significant elastic tensile stresses have been set up to balance the residual tensile stresses created by grinding the bottom surface, the maximum central deflection of the top surface being $+36 \mu$.

When the surface from 0 to 60 mm was plotted out on a larger scale, it was found that it approximates well to a circular arc and this allows the surface stresses to be calculated from simple beam theory using the formula:

$$S = E \cdot t \cdot a / 2c, \quad \text{where,}$$

E is the elastic modulus, [2.9×10^7 psi, or 200 GPa for stainless]
 t is the beam thickness, [variable, 5.5 to 6.5 mm, .21 to .26 in.]
 2c is the chord length, [$2c = 60$ mm, thus $c = 30$ mm, or 1.181 in.]
 a is the central deflection, [variable, 5 to 100 μ , .0002 to .004 in.]

The magnitude of the extra tensile residual stresses created by grinding the bottom surface can now be calculated from the equal elastic stresses set up in the top, reference surface where the maximum central deflection was 36μ [1.417×10^{-3} in.] The beam thickness was 5.639 mm [0.222 in.] and thus,

$$\text{Stress} = \frac{2.9 \times 10^7 \times 1.417 \times 10^{-3} \times 2.22 \times 10^{-1}}{1.181 \times 1.181}$$

$$\text{i.e. Stress} = 6.54 \times 10^3 \text{ psi,} = 6.54 \text{ ksi,} = 45 \text{ MPa.}$$

The final operation carried out to this specimen was to anneal at 935 C for 30 minutes. (The original intention had been to anneal at the usual temperature of 1000 C, but problems with the furnace prevented this temperature being reached.) The resultant surface profiles are shown labelled #5T and #5B and it can be seen that the top surface has become less curved with the central deflection dropping from 36 μ to 13 μ , a decrease of 23 μ . This reduction in the elastic balancing stress in the top surface is the result of a lowering of the residual tensile stress in the bottom surface. It has also resulted in the lower surface of the specimen bending downwards, the same direction of movement as the top. Furthermore, the magnitude of the change in deflection is also the same, 26 - 3 = 23 μ , an impressive demonstration of the accuracy and reproducibility of the validation technique.

Thus, thermal annealing removed 23 / 36 = 64% of the residual tensile stress set up by grinding the bottom surface. Further annealing at higher temperatures and / or for longer times might lower the remaining stresses even further, but previous experience suggests that full recovery is unlikely.

A5. Results from Specimen 1D, Wax held, Both Sides Ground and Heat-Treated at 1000 C.

The initial preparation stages for specimen 1D were the same as those for 1A, in that both surfaces were first fly cut, then ground. The resultant surface profiles at this stage are shown by #1T and #1B in Fig. A2. However, no heat-treatment was carried out at this stage, the top was chosen as the reference surface and lapped flat to give the profile shown in #2T. Once again, it was assumed that this would have no significant effect on the profile of the bottom surface and therefore #2B was taken to be the same as #1B.

The top surface was again waxed down to the base plate and, once more it was found that movement occurred while the bottom surface was being ground. As metal was removed during #3, the origin for plotting deflections of the bottom surface has been moved upwards to O[3-5]. It can be seen that the bottom surface was, indeed, quite flat, with a maximum central deflection of +4 μ . The magnitude of the residual tensile stresses locked into the bottom surface is indicated in #3T by the very large deflections created in the top surface before the elastic stresses were large enough to balance the residual stresses in the bottom. The maximum central deflection in #3T is 76 μ and, if we subtract the 3 μ present after #2T, 73 μ [2.87 x 10⁻³ in.] of this deflection can be ascribed to the stresses set up when the bottom was ground. At this stage the beam thickness was 5.53 mm [0.22 in.] and thus, using the same formula as before,

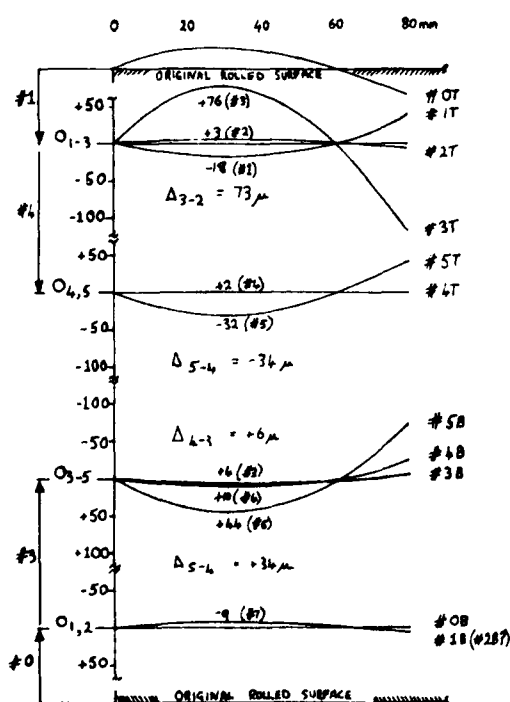
$$S = E \cdot t \cdot a / 2 c$$

the surface stress is given by,

$$\text{Stress} = \frac{2.9 \times 10^7 \times 2.87 \times 10^{-3} \times 2.2 \times 10^{-1}}{1.181 \times 1.181}$$

$$\text{i.e. Stress} = 13.1 \times 10^3 \text{ psi,} = 13.1 \text{ ksi,} = 90.5 \text{ MPa.}$$

This is double the stress induced by grinding specimen 1A, due possibly to the greater amount of metal removed or the the lack of annealing after #2.



Comments.

Sample Held Down with Wax

#0. Grind Bottom Surface

#1 Grind Top Surface

#2 Lap Top Surface

#3 Grind Bottom Surface

#4 Grind Top Surface

#5 Heat-Treat at 1000 C, 30 minutes.

Grinding-induced deflection in #3
= 73 μ , = tensile stress of 13.1 ksi

Grinding-induced extra deflection in #4
= 6 μ , = extra tensile stress of 1 ksi

Total effective deflection
= 79 μ , = total tensile stress of 14.1 ksi

Deflection recovered during #5 heat treatment =
= 34 μ , = 34/79 = 43%.

Fig. A2 Schematic Representation of Deflections in Top and Bottom Surfaces of Specimen 1D.

The specimen was now turned over and the bottom side waxed down to the base plate. The top surface was then ground flat and once again it was noticed that the specimen 'moved', indicating that the adhesion of the wax was inadequate to resist the induced stresses. As metal was removed during grinding, the origin for plotting the top surface profiles has been moved down to O[4,5] in Fig. 2. and it can be seen from #4T that the ground surface was very flat, with a maximum central deflection of $+2 \mu$. The corresponding surface of the bottom surface is given by #4B, and it can be seen that additional deflection had been created.

In order to understand the stress system at this stage, it is necessary to recall the situation at the end of #3. The bottom surface contained residual tensile stresses induced during the #3 grinding operation which were balanced by elastic tensile stresses set up in the top surface. Now, when the top surface was ground during #4, these elastic tensile stresses were replaced by residual, grinding-induced tensile stresses. Thus there are residual grinding-induced tensile stresses in both surfaces. Furthermore, comparison of #4B with #3B shows that some additional elastic tensile stress had been set up in the bottom face when the top was ground, as the central deflection had increased from $+4$ to $+10 \mu$, an addition of 6μ . Therefore, the residual stress in the top face is balanced by a residual stress equivalent to a deflection of 73μ , plus an elastic stress equivalent to a deflection of 6μ , thus giving a total stress equivalent to a deflection of 79μ .

In fact, the situation is more complicated than this as this analysis does not account for any stresses created during the initial #0 and #1 machining stages. The specimen has residual grinding-induced tensile stresses in both faces, plus elastic tensile balancing stresses in the bottom surface.

The final operation carried out on specimen 1D was to heat-treat at 1000°C for 30 minutes and subsequent validation of both surfaces gave the profiles shown as #5T and #5B. Both surfaces moved downwards, the top from $+2$ to -32 , a total of 34μ and the bottom from $+10$ to $+44 \mu$, again a total of 34μ thus confirming the consistency of the validation technique. From the direction of movement it would appear that more relaxation has taken place in the residual stresses in the bottom surface allowing the tensile stresses in the top surface to bend the specimen into a tighter arc. Assuming that the stress in the top surface was initially represented by a deflection of 79μ , the change of 34μ during heat-treatment represents a recovery of $34 / 79 = 43\%$.

These results had significant implications for the applied side of our program and the manufacture of wind tunnel models in general. Conventional practice is to machine alternate sides of an airfoil in order to balance the surface stresses thus induced. These initial results on specimen 1D suggest that if such an airfoil were to be subsequently heat-treated the residual stresses could anneal out partially to leave unbalanced stresses and distortion.

A6. Results from Specimen 1E, Epoxy held, Both Sides Ground.

Analysis of the results from this specimen suggest that much less, if any, movement took place during grinding when the specimen was held down using an epoxy resin. The results shown in Fig A3 show the latter stages of a series of machining and annealing processes carried out on this sample. Thus #6 was to heat treat at 1000°C to remove and/or balance the stresses induced by previous grinding operations. The plot of the top surface, #6T, shows that this treatment had left the top surface reasonably flat with a maximum deflection over the initial 60 mm of about 6 microns. The bottom surface is not shown, but it was similar.

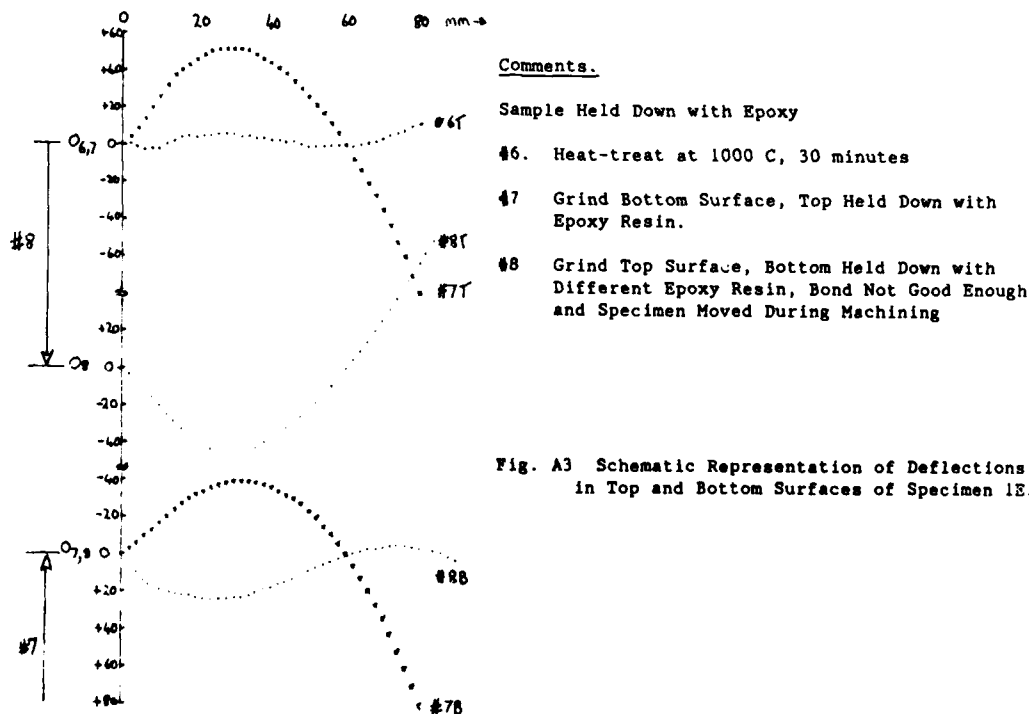


Fig. A3 Schematic Representation of Deflections in Top and Bottom Surfaces of Specimen 1E.

The sample was pressed flat into a special mounting fixture and an epoxy resin used to hold it in position. In stage 7, about 0.061 mm (0.0024 in.) was removed from the bottom surface by grinding. As material was removed, the bottom surface is shown plotted relative to a new origin O[7,8]. The hold down procedure worked perfectly and while the sample was still held in the fixture, the ground surface was essentially flat. However, when it was removed from the fixture the sample bent into an arc until the elastic stress thus created in the upper, un-machined, surface balanced the grinding-induced tensile stresses in the bottom surface. This can be clearly seen from the plots in Fig A3 in which both the top surface, #7T, and the bottom surface, #7B, have essentially the same shape. Large tensile stresses were introduced into the bottom surface during the grinding process. Subsequently, in stage 8, a different form of epoxy resin was tried, with much less success, as the specimen lifted during grinding the top surface and machining was halted. The top and bottom surfaces shown in #8T and #8B are indicative of this incomplete hold-down.

Further insight into the stress patterns after machining is given by the surface contour plots of specimen 1E after stage #7 shown in Figs. A4 and A5. Fig A4 shows the as-ground surface and it is clear that the sample had been mounted at an angle in the mounting block, leading to an off-centre effect. Nevertheless, the general effect is as expected from the central trace used to construct the surface shown previously in Fig A3, i.e. a negative deflection peaking at about -40 microns at the 30 mm line, the zero line passing centrally through the 60 mm line and increasingly large positive deflection further out.

Fig A5 shows the corresponding un-machined top (reference) surface. The bi-directional nature of the stress system is clearly shown, with the maximum positive deflection of about 50 microns located centrally and deflections reduced to between 20 and 30 microns at the edges. As the two surfaces are essentially parallel, the large negative deflections of the far end on the top surface correspond to the large positive deflection shown by the bottom. Figures A6 and A7 show a corresponding pair of contour plots for specimen 2/2 which had been held in the mounting block by a wax which melted at about 100 C. During grinding, enough heat must have been generated to soften the wax as the specimen clearly moved during machining. Thus, the as-ground bottom surface shown in Fig. A6 is very flat, while the top, reference, surface shows a distinct curvature with a maximum deflection of 39 microns at the (30 mm, 30 mm) position. Once again the bi-directional nature of the stress system is clearly demonstrated by the lower values at the edges of the specimen.

Finally, Figures A8 and A9 show some other features demonstrated by this work. The top of this specimen, 4/2, was ball-end milled while the bottom surface was held down by the better epoxy resin which did not allow the specimen to move during machining. Thus, the measured surfaces are those developed after the specimen was released from the mounting block and after elastic stresses had developed to balance the residual stresses. Evidence of the step-over pattern characteristic of ball end milling can be seen on the as-milled top surface and the deflections are quite small, suggesting that the surface stresses are low or nearly balanced. The deflections of the un-machined bottom surface, shown in Fig. A9 are quite complex. There are three 'high-spots' with positive deflections with separating and surrounding negative regions, particularly at the edges. It is believed that this stress distribution is the result of the previous machining stages in which material had been preferentially removed from those regions that were 'high-spots' at the time.

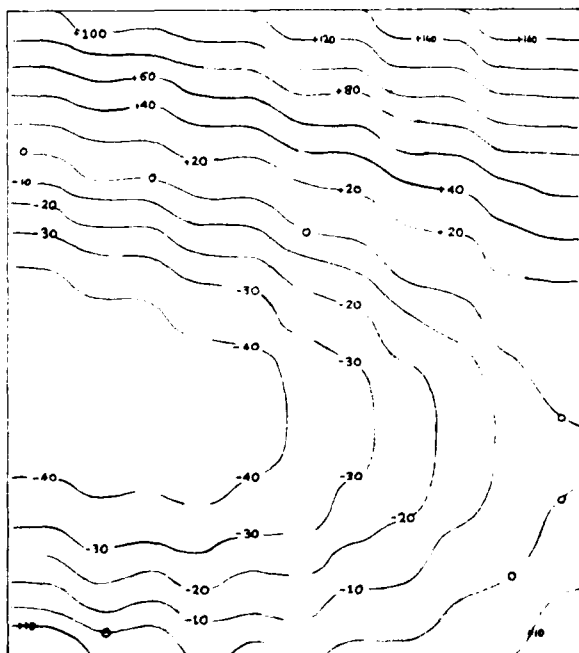


Fig. A4 As-Ground Bottom Surface of Specimen 1E (Top Surface Held with Epoxy Resin) Surface Measured After Release from Mount

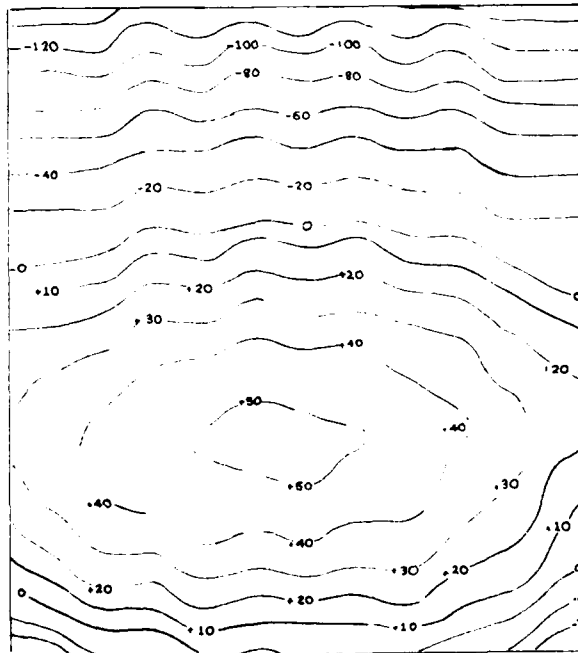


Fig. A5 Top (Reference) Surface of Specimen 1E After Bottom Surface Had Been Ground. Surface Measured After Release from Mount.

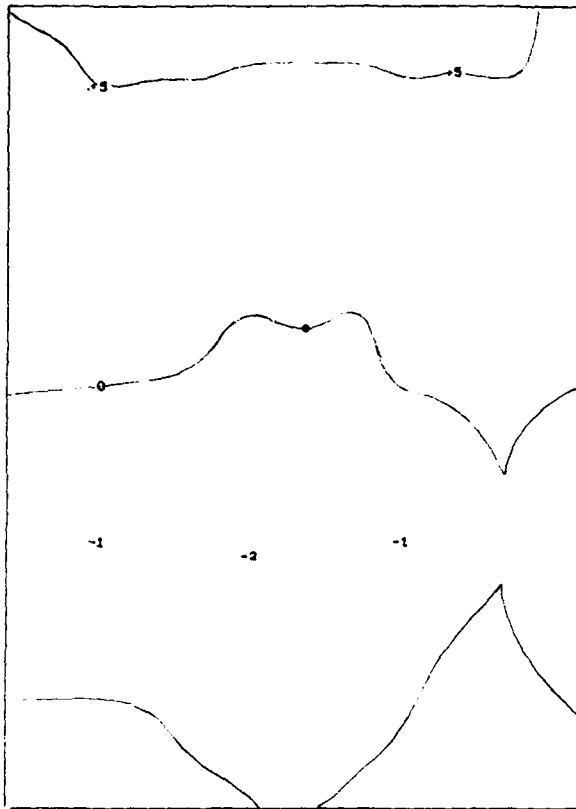


Fig. A6 As-Ground Bottom Surface of Specimen 2/2 (Top Surface Held with Wax: Bad Bond) Very Flat Surface Achieved.

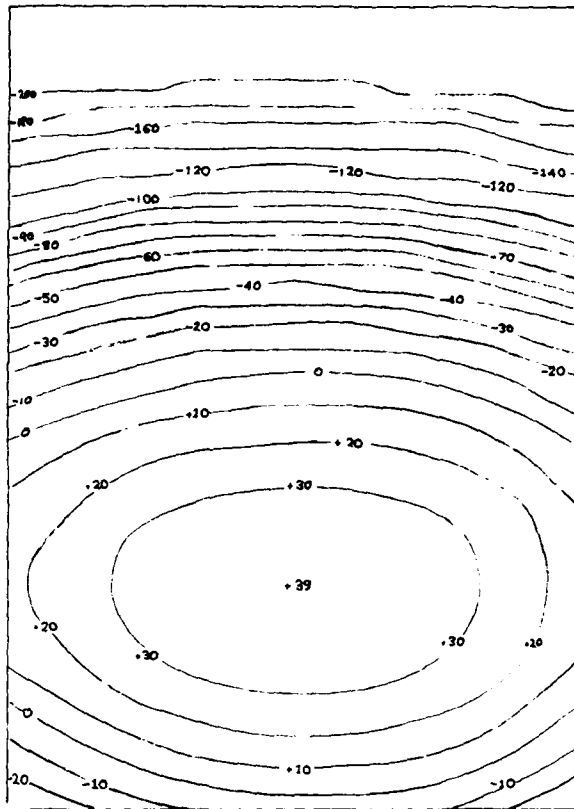


Fig. A7 Top (Reference) Surface of Specimen 2/2 After Bottom Surface Had Been Ground. Bi-Directional Stress Distribution.

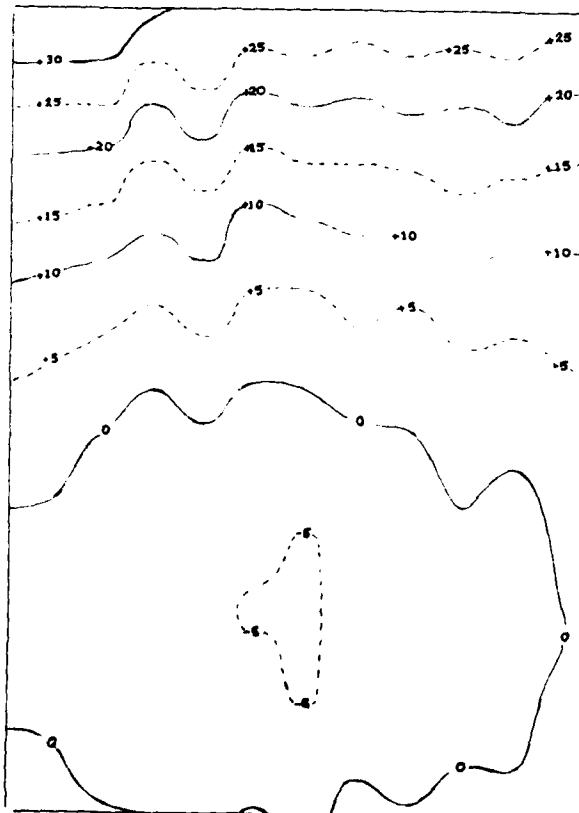


Fig. A8 As-Milled Top Surface of Specimen 4/2 (Bottom Surface Held with Epoxy Resin) Surface Measured After Release from Mount

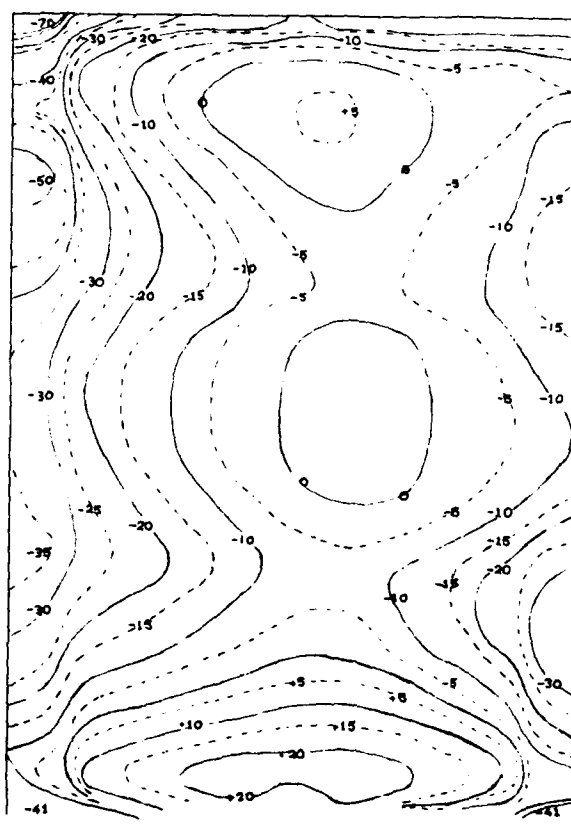


Fig. A9 Bottom (Reference) Surface of Specimen 4/2 After Top Surface Had Been Milled. Complex Stresses Created by Series of Machining Stages

MODELS FOR CRYOGENIC WIND TUNNELS

by

Pierce L. Lawing

NASA, Langley Research Center
Hampton, VA 23665-5225
U.S.A.

SUMMARY

Model requirements, types of models, model construction methods, and research in new ways to build models are the topics of this paper. The 0.3-m Transonic Cryogenic Tunnel has been in operation for 16 years and many 2-D airfoil pressure models have been tested. In addition there have been airfoil models dedicated to transition detection techniques and other specialized research. There have also been a number of small 3-D models tested. A chronological development in model building technique is described which led to the construction of many successful models. The difficulties of construction are illustrated by discussing several unsuccessful model fabrication attempts. The National Transonic Facility, a newer and much larger tunnel, has been used to test a variety of models including a submarine, transport and fighter configurations, and the Shuttle Orbiter. A new method of building pressure models has been developed and is described. The method is centered on the concept of bonding together plates with pressure channels etched into the bond planes, which provides high density pressure instrumentation with minimum demand on parent model material. With care in the choice of materials and technique, vacuum brazing can be used to produce strong bonds without blocking pressure channels and with no bonding voids between channels. Using multiple plates, a 5% wing with 96 orifices has been constructed and tested in a transonic cryogenic wind tunnel. Samples of test data are presented and future applications of the technology are suggested.

1. INTRODUCTION

The design and construction of wind tunnel models has traditionally required the highest levels of ingenuity and craftsmanship. The triple demands of high Reynolds numbers, transonic Mach numbers, and cryogenic temperatures make the task much more difficult. The need to produce high Reynolds numbers in a reasonable sized facility leads to pressurized tunnels and highly loaded models. Accurate Reynolds number simulation also requires that the surface finish of the flight article scale to the model dimensions; this can result in nearly unobtainable model surface finish requirements. The transonic requirement adds the need for high accuracy in surface contour. Finally the cryogenic temperatures add the complexities of thermal stress, differential thermal expansion, model dimension change, and fracture toughness. In return, cryogenic operation decreases the required tunnel pressurization and model loads enough to make full flight Reynolds number simulation possible.

The Langley 0.3-m Transonic Cryogenic Tunnel, reference 1, has been in operation since 1973. In the intervening years many 2-D airfoil pressure models have been built and tested as well as airfoil models dedicated to transition detection techniques and other specialized research. There have also been a number of small 3-D models tested. The early days were characterized by a success to failure ratio of less than one due to the difficulties of construction for this new tunnel. By the time of construction of The National Transonic Facility, a much larger tunnel, many of the difficulties had been solved. The NTF has been used to test a variety of models, reference 2, including a submarine, transport and fighter configurations, and the Shuttle Orbiter.

One of the advances in building pressure models was a method centered on the concept of bonding together plates with pressure channels etched into the bond planes. This provided high density pressure instrumentation with minimum demand on parent model material. With care in the choice of materials and technique, vacuum brazing can be used to produce strong bonds without blocking pressure channels and with no bonding voids between channels. Using multiple plates, it was possible to produce wings as thin as 5% with adequate numbers of pressure orifices. Samples of test data are presented and future applications of the technology are suggested.

2. NTF MODELS

2.1 Configurations

Subsonic Transports - The first transport model built for the NTF is named *Pathfinder I*. It has a representative wide-body transport fuselage and may be used to test various wing configurations. The fuselage is constructed in a conventional fashion from Nitronic 40. A photograph is shown in figure 1. Instrumentation includes a six-component strain-gage balance, 192 static pressure orifices, wing root bending gage, type-T thermocouples and angle measuring systems for pitch and roll. The major challenge is the high-aspect ratio wings typical of efficient commercial transports. Both force and pressure wings have been tested on the *Pathfinder I*. The solid, force, wing was constructed of PH13-8Mo stainless steel.

A separate lateral controls wing was also constructed with provisions for inboard and outboard ailerons and upper wing spoilers. This wing could also be tested with or without pylons and nacelles. It was instrumented to measure surface temperatures, wing-root bending moment, and aileron hinge moments. Vascomax 200 was used for the wing and A286 for the pylons and nacelles.

A one-half scale Pathfinder I model was also constructed. The material for this model was PH13-8Mo. This model has no provisions for pressure measurements but is mounted on a six-component strain-gage balance. The full and one-half scale models of Pathfinder I are shown together in figure 2.

In a NASA/Boeing cooperative effort, a model of the Boeing 767-200 has been constructed to serve as a wind tunnel to wind tunnel calibration model. It contains 48 pressure taps on wing nacelles and fuselage. Horizontal tail deflections and removable nacelles and filler blocks are model features. Figure 3 is a photograph of the Boeing 767-200 model.

Cargo Aircraft - In a cooperative program with McDonnell-Douglas, an advanced cargo aircraft model has been built. It features a high wing with winglets, including three variations in winglet geometry and wing-tips for winglet-off data. Extensive pressure instrumentation is provided including pressure taps on the winglets and gear pods for a total of over 200 pressure measurements. Demountable pylons and nacelles allow engine on and off data. Nacelles are flowthrough type. Model is on a six-component strain-gage balance and weighs 450 pounds. Model construction metal is Vascomax 200. Figure 4 is a photograph of the of the Douglas high wing cargo model with winglets and nacelles mounted.

Supersonic Transport - The wing of this model is a highly twisted and cambered arrow wing designed for cruise at $M = 2.7$. The leading edges are removable to allow variation in leading edge radius and test of leading edge deflection schemes. The model is constructed of Vascomax 200 and accommodates a six-component strain-gage balance. Figure 5 is a photograph of the supersonic transport model.

Fighters - A 1/16 scale model of the X-29 swept-forward wing fighter has been built. It accommodates a six component balance and an angle-of-attack sensor. There are 48 pressure orifices in the wing in the same locations as the flight vehicle. It has adjustable canards and several sets of trailing edge flaps, strake flaps, and rudder settings. The left canard is mounted on a 3-component canard balance. The inlets are open to allow flow-through conditions. There are two nose sections, one clean and the other having the instrumentation boom and the nose strakes. Construction material is Vascomax 200. Figure 6 shows a photograph of the model just prior to verification of ordinates.

Space Craft - A 1% scale model of the Shuttle Orbiter ascent configuration has been built for the NTF. It may be tested alone or with the external tank and the two solid boosters. Plume shapes were modeled with equivalent solid bodies and became part of the model support, as shown in figure 7. The Orbiter and stings were built from Vascomax 200. The fuselage is built in upper and lower parts. The nose and the wings are integral with the lower part. The lower part also provides the mounting surfaces for the upper fuselage, vertical tail, OMS pads, body flap and the fore and aft external tank attach structures.

The 1% Orbiter has 92 pressure taps on the left wing and elevons. There are also 8 base pressure taps and 3 taps on the lower fuselage centerline. The external tank has 11 taps on the upper centerline and 8 base pressure taps; the solid rocket boosters have 4 base pressure taps apiece. The wing and fuselage pressures are routed through the Orbiter sting to an electronically scanned pressure measurement system (ESP) mounted in the sting. The base pressures are routed through the sting assembly to an ESP unit mounted in the external tank. The external tank pressures and the booster base pressures are connected to an ESP unit mounted in the external tank nose.

The right wing of the Orbiter has an integral three component balance to measure bending, torsion and shear. A 0.030 inch metric gap between the wing and fuselage is sealed by a rolled metallic seal. The two elevon panels on the right wing are also mounted on strain gage beams to measure hinge moments. The wing elevon gap is not sealed. Brackets for 0 and 10 degrees are provided for the elevons. The rudder/speed brake on the vertical tail and the body flap are fixed at 0 degrees. A set of spoilers, deflected at 20 degrees can be installed at the elevon hinge line.

A 2% scale Orbiter was also built. Like the 1% model, the lower fuselage was machined from A286 stainless steel. It was designed to have control surfaces that were remotely actuated. The elevons, rudder, and body flap have remotely controlled electric motors and position indicators. The speed brake is set manually. The actuator mechanisms are fabricated from Armco Nitronic 60 stainless steel to prevent galling. A photograph of this model is shown in figure 8.

National Aerospace Space Plane - This model, known by the acronym NASP, is a very robust model designed to test up to 18 degrees angle of attack over the entire operating envelope of the NTF. Construction material was Vascomax 200. There was no provision for pressures and only forces were measured. The wing has a diamond-shaped airfoil cross-section of 4% thickness and a leading edge sweep of 76 degrees. This model is unique for the NTF with sharp leading and trailing edges on the wings. Edge half thickness were .005 inch and the smallest nose radius was .005 inches. There were 3 interchangeable noses with varying bluntness. The wing incidence was variable, there were high and low aspect ratio canards, 2 sizes of vertical tails, and optional vertical dorsal and ventral tails near the wingtips. A photograph of this model is shown in figure 9.

Submarine - The submarine model tested was 20 feet long. The hull was constructed of 6061-T6 Aluminum and the primary data was acquired by a survey rake aft of the sub. A photograph of this model in the NTF is shown in figure 10.

2.2 Research Models

Flat Plate - The NTF flat plate will extend from the tunnel floor to the ceiling, for a span of 2.5 m. The chord will be 5.2 m including leading edge flap. Length Reynolds numbers will approach 2 billion at 0.7 Mach number. The model will be instrumented with 107 static pressure taps, 15 thermocouples, and provision for 6 shear stress devices. There will also be provision for accelerometers, hot-wires, strain gages and a total pressure tube. The model has been designed and a sample of the hardware has been built and is being proof tested. The leading edge is a symmetric ellipse made from a solid piece of aluminum. The flat plate has a 6061-T6 Aluminum, honeycomb core which is adhesively bonded to an Aluminum skin. The honeycomb has a cell depth of 41.3 mm and a cell width of 6.4mm. A much more detailed description of the flat plate and the planned experiments can be found in reference 3.

Delta Wing Model - The delta wing has an aspect ratio 1.865, 65 degree-swept leading edges, and a 0.75 inch thick center section. There are three sets of interchangeable leading edges incorporating leading edge radii of 0.01in, 0.10 in, and 0.20 in. All have uncambered NACA-like sections and are constant spanwise. The interchangeable leading edges have a large number of surface pressure orifices. Construction material is Vascomax 200. This model will be used to investigate Reynolds number effects on upper surface vortex formation and leading edge separation. Earlier work on this problem is in reference 4.

3. 0.3-m TCT MODELS

The Langley 0.3-m Transonic Cryogenic Tunnel has been in operation since 1973. In the intervening years many 2-D airfoil pressure models have been built and tested as well as airfoil models dedicated to transition detection techniques and other specialized research. There have also been a number of small 3-D models tested. The early days were characterized by a success to failure ratio of less than one due to the difficulties of construction for this new tunnel. Much of this early experience is summarized in reference 5.

3.1 Three Dimensional Models

Shuttle Orbiter - The model of the Space Shuttle Orbiter shown in figure 11 was constructed and tested to measure the support-interference-free base pressure drag and to determine Reynolds number effects on base drag to aid in extrapolating the values of base drag measured in the wind tunnel to full flight conditions. The support-interference-free condition was obtained by supporting the model by extended wing tips attached to sidewall turn tables. The model was constructed of 9 percent nickel steel and accommodated 15 pressure orifices, 3 in the base of the vertical tail and the remaining 12 distributed over the base of the fuselage and rocket nozzles. Selected data is presented in reference 1.

Boattailed Models - A total of six models were constructed for the pressure measurements on boattailed shapes. All models were 2.54 cm in diameter. Four of the models had a length of 20.32 cm from the nose to the start of the boattail, and four different boattail geometries. Two of the models duplicated the boattails of two of the shorter bodies, but were 40.64 cm from the nose to the start of the boattail section. These models were constructed of cast aluminum with stainless steel pressure tubes cast as an integral part of the model. The tubes were placed in a sand mold in the proper position, the aluminum poured, and the model machined to the desired contour. Each of the models has 30 orifices in three rows of 10 orifices each. Figure 12 is a photograph of the models. Further information is available in reference 6.

Wing-body Interference Models - The models used in the wing-body tests, shown in figure 13, duplicated the forebody and boattail geometry of two of the short isolated boattail models. Construction of these models differed slightly from that of the isolated boattail models in that each of the models was cast around both the pressure tubes and a stainless-steel sting. By using this method, it was possible to fit each of these models with 50 pressure orifices in five rows of 10 orifices each. Provision was made for the mounting of a 10.16 cm span 60° delta wing at 0° incidence on the top of each of the models in one of three positions. Further details are in reference 7.

3.2 Two Dimensional Models

A typical airfoil construction procedure is to rough machine the contour of the airfoil and then mill out relatively large channels in the surface leading to locations where pressure taps are desired. Steel tubing is then laid into the channels to provide access to the taps and the channel filled with a suitable potting compound. Finally, the contour is finished to the final design specifications. In an environment of large temperature changes, differential thermal expansion of the metal model and the potting compound may lead to unacceptable changes in the model surface.

In an attempt to circumvent this problem for cryogenic application, a single piece metal cover plate was used to cover a scooped out lower model half. The tubing was brazed to the cover plate to provide connection to the pressure taps. When machining the cover plate to final contour, it popped up and down, or "oil-canned", leading to deviations in contour which were too large for transonic experiments.

The next evolution was to cut channels only along rows of pressure taps, and machine a strong cover plate to fit as shown in figure 14. The cover was then electron-beam welded and the surface finish machined. Successful models have been constructed by this method reference 8, but it is labor intensive, and the method is intolerant of mistakes in the fabrication process. The combination of new requirements, new materials, and the complicated solutions to these problems, led to models that were nearly complete before problems were discovered that made the model unfit to test.

A common denominator to many of these problems was the bundle of tubing which provided connection to the pressure taps. Several efforts were initiated to improve the technique; one such effort was the inclusion of the plumbing as an integral part of the model. This was done by cutting channels on the face of a metal plate, and then sealing the channels by bonding a second plate. Details of this method are discussed in the next section.

4. A NEW METHOD OF BUILDING PRESSURE INSTRUMENTED MODELS

4.1 Model Construction Using Two Plates

Fabrication of Samples - Many small samples were constructed to investigate the bonding technology necessary to seal the integral pressure channels. Results from the sample construction programs are contained in references 9 and 10. A typical example of the bonding investigation is shown in figure 15, where a sample has been sectioned to show a bond obtained using brazing foil and a vacuum brazing oven. Also shown in this figure are the triangular pressure channels, several of which have been cut in the face of each plate. Since the sandwich of plates was laid flat in the brazing oven this becomes a test of gravitational effects; if gravity is a factor in the flow of metal during the braze foil melt, then the channels on the bottom plate would be expected to fill with molten metal. As shown in the figure, this does not happen. The dominant force is the capillary attraction from the narrow gap between the plates. This belief is reinforced when it is realized that the brazing foil was a single thin sheet which also covered the grooves. Close examination shows that during the melt, the portion of the foil covering the grooves partially melted and was drawn away into the adjacent narrow gap.

Construction of Model - After developing a successful bonding technique, the next step was to construct an airfoil model suitable for test in the 0.3-m TCT. The airfoil design chosen was a 12% thick symmetrical supercritical shape. One of the reasons for constructing a test article was to learn of problems in building a model rather than samples. Therefore, an ambitious pressure orifice layout was proposed to fully exercise the new capabilities of the bonded plate method.

Figure 16 is a photograph of the two halves of the model showing the surfaces to be bonded. The channel layout shown is for 94 orifices. Most of the orifices have been pre-drilled at the proper angle and depth to erupt the model surface during contour machining. At the ends of the model, where the channels are parallel, alternate channels end in a hole drilled normal to the mating surface. The other half of the channels will mate with holes drilled in the mating plate. Each of the holes intercepts a connector hole drilled from the end of the plate. Tubes brazed in these connector holes provide the connection with the wind tunnel pressure instrumentation system. This method is used to avoid overcrowding, since the larger connector holes would be too closely spaced if drilled side-by-side in the bond plane.

Figure 16 shows the plates arranged with the channels at the trailing edge matching. The channels will combine to form the orifice. There are eight trailing edge orifices shown. The left and right hand edges of the plates will become the model leading edge. The right hand edge is the upper model surface. The fan shaped channel configurations are the top and bottom leading edge orifice rows. Note that room is provided at the leading and trailing edge for an offset after brazing. Thus, the dowel holes at the trailing edge will be removed; the smaller dowel holes near mid-chord will have the dowel pins brazed in and will remain in the model; the larger holes near the ends of the plate at mid-chord will remain open and will secure the model during testing.

Figure 17 is a photograph of the model halves, two of the four sheets of brazing foil, two of the alignment dowels, and all of the connector tubes. Figure 18 shows the model in the vacuum brazing oven. The cylindrical weights on top of the model provide a moderate pressure to force the two pieces together as the brazing foil melts. Figure 19 is a photograph of the model after brazing. The model has been rough machined to cut off the excess material from the leading and trailing edges and to form the mounting tangs. At this point it is possible to check the integrity of much of the internal plumbing before the relatively more expensive contour work is performed. Figure 20 shows the model as completed and ready for test.

Results With Two Plate Model - The model was successfully machined to contour, validation measurements taken, tests run in the 0.3-m TCT, and the data published (5). The next sections will list the capabilities demonstrated by this model, discuss the problems encountered, and present typical aerodynamic data.

New Research Capabilities - Capabilities offered by this new model construction technology and not routinely available on other 2-D airfoil models are as follows:

1. A spanwise row of trailing edge pressure orifices is easy to install. Installing even a single trailing edge orifice was difficult with previous methods, and often impossible on thin airfoils.
2. An orifice row at the wing stagnation line-test section wall juncture is provided. This capability is extremely difficult to provide with normal methods.
3. Less than 0.1 percent of the model volume is used for pressure passages. There are no large voids in the model to cause structural irregularities during mechanical or thermal stress. Also, the models inherently have higher strength and can take larger loads.
4. Bonds of near parent metal strength and toughness offer improved margins of safety. The bond line acts as a crack stopper. Failure in one half of the model will not easily propagate to the other half.
5. The expense due to fabrication failure is less since all of the pressure channels can be checked for leaks and blockage before any contour machining.
6. Construction costs are less because of the reduction in time to install pressure orifices and related internal tubing.

Problems Encountered - The first problem encountered in the construction of this model was warpage of the plates during the vacuum brazing process. This was unexpected since there had been no detectable warpage during the extensive sample construction program. The warpage was primarily spanwise and resulted in a dip in the bond plane at mid-span of about 0.010 inches. Although small, this deflection was sufficient to prevent some of the upper surface pressure orifices from appearing. They had to be located and drilled externally. This was accomplished by taking an x-ray photograph with the film in contact with the model surface. After development, the film was taped to the surface and the orifices were drilled directly through the film. This technique was successful about 80 percent of the time on the first try. It was necessary to drill a second time on the remaining orifices, and all orifices were eventually recovered.

Because of the warpage, leakage between channels was detected in approximately 30 channels. Since some of the leaks were on groups of 3 channels, this meant that there were approximately a dozen cases of small bonding voids. These leaks were detected by the channel's failure to hold a vacuum. The actual size of the cross leak was not determined. At the present stage of data analysis, there have been no anomalies in the data attributable to leaks between channels.

There were 30 channels that were blocked. The cause of the blockage is suspected to be from the use of "stop-off" compound during the brazing process. This is standard practice in normal brazing procedure when there is a portion of the work that is not to be brazed. There was no indication that the stop-off was required based on the results of the sample program. However, due to a break-down in communications, it was used to insure that the brazing metal did not run into the channels. The stop-off compound is suspect primarily because it was possible to free some channels of blockage with a pressurized can of liquid Freon, which would not have been possible had they been blocked with the brazing metal.

Aerodynamic Data on Airfoil Model - Figure 21 shows pressure coefficient data at transonic conditions and a moderate lift coefficient. This data shows the presence of a shock wave on the upper surface between 30 and 38 percent chord. There are two sets of data superimposed. One is for the model at an angle of attack of 2° , corresponding to a lift coefficient of 0.31. The other is for -2° , lift coefficient of -0.31. Since this is a symmetrical airfoil, the pressure distributions at positive and negative angle of attack should match with the upper and lower symbols changing places. The pressures coefficients are very nearly the same. This agreement demonstrates good top and bottom symmetry of model construction. It also demonstrates good testing technique and shows that some cross-leakage between channels may be tolerated without significant error. Reference 11 gives additional aerodynamic data for this airfoil.

Extensions of the Two Plate Method - The previous sections have demonstrated the success of the bonded plate technology in producing a useful airfoil model to test. However, there are only a limited number of interesting airfoils which can be produced with flat bond planes. Therefore, research was initiated to extend the technology to other shapes. The effort was slanted somewhat by a desire to produce a "thin" airfoil model not possible with current methods. A thin airfoil is roughly defined in terms of the maximum thickness to chord ratio. In terms of fabrication difficulty, any airfoil with a ratio of less than 10 % is considered thin. However, there are aircraft in service with wings and other components much thinner, and so a goal of 5 % has been set. Obviously a small absolute value of chord length is more difficult to construct than a larger one, and the thinness ratio used here must be accepted as only a loose criteria of fabrication difficulty.

Bonding Technology - A persistent handicap met during this program is the lack of reliable vacuum brazing methods. This problem has many facets, but for the current application a principal problem is control over the gap between the two plates being brazed. The gap changes as residual machining stresses in the plates relieve themselves as we heat the plates in the brazing oven. One possible solution is brute force loading to suppress any relative movement between the two plates. However, use of low stress machining may eliminate relative movements due to relaxing mechanical stresses imposed primarily by the various machining processes. One low stress machining technique is electron discharge machining. Another approach is to use stacked thin sheets which require only light loading to overcome warpage, since each sheet experiences the entire load.

Photoetched Channels - An early advance in this model construction technique was using photoetching rather than milling to form the pressure channels. The desired channel layout is drawn at a conveniently large scale and then photographically reduced to the size of the model. Figure 22 shows chemically etched channels on a stainless steel surface. The orifice holes are drilled at the end of the channels. Note the dimples etched at the end of the channel to help locate the drill bit.

Curved Bond Planes - Figure 23 shows the results of using the photoetching technique on curved surfaces, in this case one convex and one concave. An electrical discharge milling machine cuts the matching surfaces. The machine uses a small wire as the electrode, somewhat in the fashion of a wire cheese slicer. This process is known as wire cutting. The sample shown in figure 24 is the trailing edge cusp section of a 6 % supercritical airfoil. After brazing the matching surfaces together, the wire cut process was once again used to cut upper and lower contours. The left side of figure 25 shows various size orifices as exposed by the wire cut. It also shows a trailing edge orifice. The right side shows magnified views of 1.0, 0.5, and 0.32 mm diameter orifices. This figure clearly shows the high quality of the orifice after being machined by the wire cut technique. Further details of two plate construction are documented in reference 12.

4.2 Model Construction Using Multiple Plates

Although the two plate method has the potential to solve a number of our model building problems, it has at least two limitations. One is the increasing thermal warp (due to uneven stress relief) as larger plates are used, thus limiting us to small models. The other limit is the physical room available for channels. This will occur when a high aspect ratio wing, such as a commercial transport wing, is pressure instrumented. If the wing has six spanwise stations of fifty orifices each, the bond

plane at the fuselage juncture would contain 300 channels.

Multiple bond planes, with each plane serving one of the 6 spanwise stations, will allow 0.015 inch wide channels with 3-channel-width lands separating them. This would require at least 7 thin sheets to be brazed together. These thin sheets are much easier to flatten than thick plates, and the problems due to warpage are greatly reduced. The next sections tell of the development of the multiple sheet method.

Fabrication of Samples - Figure 26 shows a stack of thin sheets and the sheets of brazing foil for each bond plane. Each sheet has numerous parallel pressure channels so that all channels exit both ends of the sample. This allows easy diagnosis of blocked or cross leaking channels. The material shown here is A286 stainless steel. This material has excellent fracture toughness properties at cryogenic temperatures, but is difficult to machine (as compared to the 300 series stainless steels). It was chosen because it is readily available in 0.032 inch sheets and it brazes readily. The brazing foil is the same as that used in the two plate model.

Bond Strength and Toughness - The bond strength was determined by 3-point bend tests on simple two piece bonds, reference 12. For toughness testing, Charpy bars were cut from multi-sheet samples with no internal channels. These were then broken at room temperature and at liquid nitrogen temperature. The multiple sheets and their bonds were always parallel to the long axis of the bars, but they were notched to break either through the sheets or parallel to the sheets. Figure 27 shows the Charpy bars. Charpy V Notch impact energies were reduced by 6 percent to 42 percent depending on orientation and temperature. The remaining toughness of this material was adequate in all of the tested situations. Details are reported in reference 12. The partially broken bar in the foreground was a cryogenically tested sample.

Construction of Model - The canard of the X29a fighter aircraft was chosen as a proof-of-concept model to build. This configuration was only 5% of the chord thick at the point of maximum thickness. Also it is highly tapered from root to tip, making pressure instrumentation even more challenging. The choice of actual model size to test resulted in a root chord of 14.5 cm and a 4.6 cm tip chord. This gives a corresponding maximum thickness of only 0.725 cm (0.285 in.) and 0.23 cm (0.091 in.).

Figure 28 is a photograph of the top sheet of the stack of thin plates. The outline of the model is chemically etched on the sheet along with reference points for machining purposes. Ten thin plates were bonded together to build this model. The airfoil contour is the NACA 64A-105, which has a design lift coefficient of 0.1. What this means to the model builder is that the airfoil is cambered and requires more plates for the top than the bottom. The next photograph, figure 29, is of the innermost of the top plates near the center of the model. Channels have been etched in this plate to go and return to many orifice locations. This will allow checking for blockage or crossleaks before machining. The bond plane shown will serve some of the orifices on each of the three spanwise rows. Other planes will serve the rest, but the bond planes nearer the surface will have less room and fewer channels.

Figure 30 is a photograph of the upper surface of the completed model. Pressure orifices may be seen in three spanwise rows. The orifices are deliberately staggered to minimize any build-up of boundary layer instabilities. There are three rows of orifices with a total of 56 orifices on the upper surface. Six thin plates form the upper surface of the airfoil. The outcrop of the five bond planes is clear on the photograph. There are 37 additional orifices on the bottom surface. Figure 31 shows the model assembled with its fairing and mounting block, ready for testing in the 0.3-m Transonic Cryogenic Tunnel. Reference 13 contains a full account of the construction of this model.

Research Testing of Model - The primary purpose of the test was to verify the model construction technique, but also the test provided the opportunity to take unique aerodynamic data and to exercise the solid adaptive wall test section(8) for 3-D testing. The airfoil was tested over nearly the full range of conditions available with the adaptive wall test section. This included both ambient and cryogenic operation at pressures up to 6 bars at Mach numbers up to 1.3. For testing this semi-span 3-D model, the method of Rebstock was used to adapt the solid test section walls for minimum interference.(9)

Aerodynamic Data - Aerodynamic data was taken for the airfoil (surface pressures and wake survey) at Mach numbers from 0.3 to 1.2. The tests covered angles of attack from -4° to $+15^{\circ}$. At most Mach numbers a 10 to 1 range of Reynolds number was covered and flight values of Reynolds number were easily obtained. Figure 32 shows an example of the airfoil data at an angle of attack of 8° , a Mach number of 0.9, and a Reynolds number (based on root chord) of 43 million. This was a very recent test (May 1988), and a full data set is not yet available for reference.

4.3 Potential New Wind Tunnel Applications

New Wing Configurations - The thin sheet technique has also been applied to the construction of twisted sections. Figure 33 shows two blocks of metal which were wire cut from a single block for use as platens. They were cut with a twist on the mating surfaces. The platens, thin sheets, and brazing foil were all clamped together by corner bolts in the platens. The sheets formed to the twist at the same time they brazed, leaving open channels with no cross leaks. The twisted stack of thin plates were then wire cut to the propeller blade shape shown. Twisted wing sections with pressure or cooling channels can be made in a similar fashion.

Success has also been achieved with small-scale samples of exotic configurations such as gull-wing airfoil sections, typical of some designs for supersonic transports. At this stage in the development of the technique, further effort in fabricating small models of these more advanced configurations could produce results unachievable by any other technique. Figure 34

shows a very thin gull wing sample with internal channels. It is resting on a generic fuselage and represents a span wise cross section of a supersonic transport type wing.

Ambient Temperature Models - Thus far the discussion has centered around problems peculiar to cryogenic tunnels. These are primarily differential thermal expansion encountered when dissimilar materials are used, and fabricating the often unfamiliar materials required to meet the combined strength and fracture toughness criteria demanded by the cryogenic environment. The requirement for high fidelity of surface contour is typical of transonic tunnels at any temperature. The requirements for high strength is characteristic of high Reynolds number tunnels, and becomes more severe as the operating temperature of the tunnel increases from cryogenic. The constraint of limited instrumentation volume is a function of model configuration and tunnel size. Therefore, the multiple plate method should find application in ambient temperature tunnels at all speed ranges.

Hypersonic Models - Hypersonic configurations designed for efficient cruise performance tend to have thin, highly swept wings and control surfaces with nearly sharp leading edges. These components have small volumes, and when pressure distributions are required, they present an ideal opportunity for application of the multiple plate method. Due to its high strength and excellent dimensional stability during the thermal cycling that accompanies hypersonic testing, 17-4 ph stainless steel is one of the metals of choice for hypersonic models. Even though its very low fracture toughness at cryogenic temperatures prevents its applications in cryogenic tunnels, it was used in the early stages of the bonded plates program because of its good dimensional stability in the brazing oven and the familiarity of the shop personnel with its fabrication characteristics. Using electroplated copper between the plates as an assist, parent metal strength bonding was easily obtained. The process is particularly interesting because the resulting bond was partially brazed and partially diffusion bonded. Figure 36 shows a sample airfoil constructed of 17-4 ph. Since it had no cryogenic application, further development of the technique using 17-4 ph was discontinued, and the research was directed to other metals. The data accumulated using 17-4 ph stainless steel is documented by Wigley (4).

Technology Spinoff - The technology of using embedded passages could be applied to other areas of aerodynamic research other than pressure measurements. Possibilities include, boundary layer control by ducting flow through internal passages, seeding devices for flow visualization studies, surface cooling studies, optical position indicators using fiber optics, etc. Finally, it is believed that the laminated thin sheet technology could be applied in non-aerodynamic applications, for example in building small heat-exchangers, fluid control devices and other devices that need the formation of complex channel geometries within a confined space.

5. CONCLUSIONS

Models for cryogenic wind tunnels have been addressed by describing the models built during the 16 years of experience at NASA Langley with cryogenic tunnels. Both models for the 0.3-m TCT and the much larger NTF have been described. Also a research and development program for a new method of building pressure models has been described leading to these specific conclusions:

1. A sophisticated airfoil model has been constructed by brazing together two plates containing pressure channels; it has been successfully tested in an advanced cryogenic transonic wind tunnel.
2. Photographic "masking" combined with chemical milling is a reliable and cost effective method of providing pressure channels suitable for high density pressure instrumentation with minimum demand on parent model material.
3. Small diameter high quality pressure orifices (i.e., round holes with smooth edges) are economically produced when pre-drilled holes are cut at the model surface by the wire-cut process.
4. With care in the choice of materials and technique, vacuum brazing can be used to produce strong bonds without blocking pressure channels and with no bonding voids between channels.
5. Using multiple plates, a 5% thick wing with 96 orifices has been constructed and tested in a cryogenic wind tunnel.

6. REFERENCES

1. Ray, E. J.; Ladson, C. L.; Adcock, J. B.; Lawing, P. L.; and Hall, R. M.: **Review of Design and Operational Characteristics of the 0.3-Meter Transonic Cryogenic Tunnel.** NASA TM-80123, September 1979.
2. Gloss, Blair B.: **Initial Research Program for the National Transonic Facility.** Presented at the AIAA 13th Aerodynamic Test Conference, San Diego, California, March 5-7, 1984. AIAA Paper No. 84-0585.
3. Saric, W. S. and Peterson, J. B. Jr.: **Design of High-Reynolds-Number Flat-Plate Experiments in the NTF.** AIAA 13th Aerodynamics Testing Conference, March 5-7, 1984/San Diego, California. AIAA paper # 84-0588.
4. Henderson, William P.: **Effects of Wing Leading-Edge Radius and Reynolds Number on Longitudinal Aerodynamic Characteristics of Highly Swept Wing-Body Configurations at Subsonic Speeds.** NASA TN D-8361, December 1976.
5. Lawing, P. L. and Kilgore, R. A.: **Model Experience in the Langley 0.3-m Transonic Cryogenic Tunnel.** Presented at the Workshop on High Reynolds Number Research, NASA CP-2183, December 1980.

6. Reubush, Davis E.; and Putnam, Lawrence E.: **An Experimental and Analytical Investigation of Effect on Isolated Boattail Drag of Varying Reynolds Number up to 130×10^6** . NASA TN D-8210, May 1976.
7. Reubush, Davis E.: **Effect of Reynolds Number on the Subsonic Boattail Drag of Several Wing-Body Configurations**. NASA TN D-8238, July 1976.
8. Young, C. P.; Bradshaw, J. F.; Rush, H. F., Jr.; Wallace, J. W.; and Watkins, V. E., Jr.: **Cryogenic Wind Tunnel Model Technology Development Activities at the NASA Langley Research Center**. AIAA Paper No. 84-0586, 1984.
9. Wigley, D. A.; Sandefur, P. G., Jr.; and Lawing, P. L.: **Preliminary Results on the Development of Vacuum Brazed Joints for Cryogenic Wind Tunnel Aerofoil Models**. ICMC preprint, San Diego, CA, August 10-14, 1981.
10. Wigley, D. A.: **The Structure and Properties of Diffusion Assisted Bonded Joints in 17-4PH, TYPE 347, 15-5PH and Nitronic 40 Stainless Steel**. NASA CR 165745, July 1981.
11. Mineck, Raymond E. and Lawing, Pierce L.: **High Reynolds Number Tests of the NASA SC(2)-0012 Airfoil in the Langley 0.3-Meter Transonic Cryogenic Tunnel**. NASA TM-89102, July 1987.
12. Wigley, D. A.: **Technology For Pressure-Instrumented Thin Airfoil Models**. NASA CR 3891, Contract NAS1-17571, May 1985. (Phase I SBIR)
13. Wigley, D. A.: **Technology For Pressure-Instrumented Thin Airfoil Models**. NASA CR 4173, Contract NAS1-18066, August 1988. (Phase II SBIR)



Figure 1.- Photograph of the Pathfinder I transport model for the NTF.

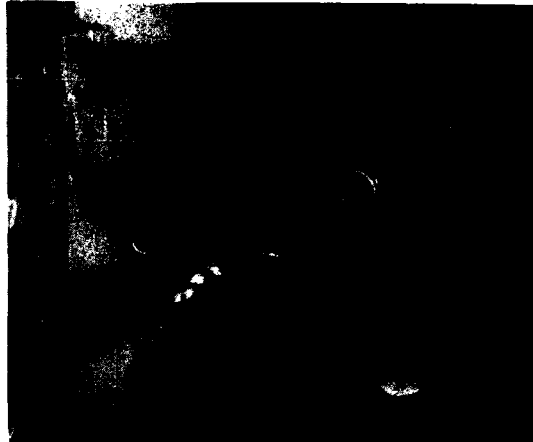


Figure 4.- Photograph of the Douglas high wing cargo model with winglets.

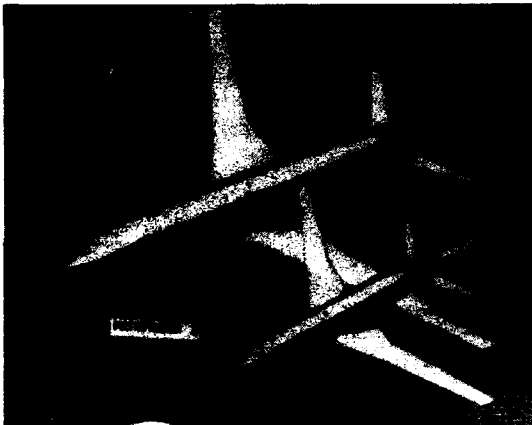


Figure 2.- Photograph of full and one-half scale models of Pathfinder I.



Figure 5.- Photograph of the supersonic transport model.

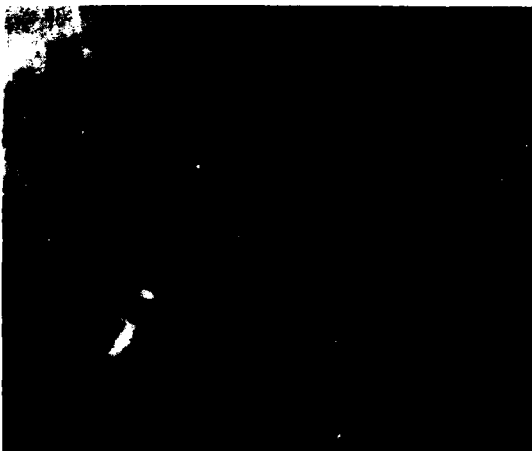


Figure 3.- Photograph of the Boeing 767-200 model.



Figure 6.- Photograph of the X29 fighter model.

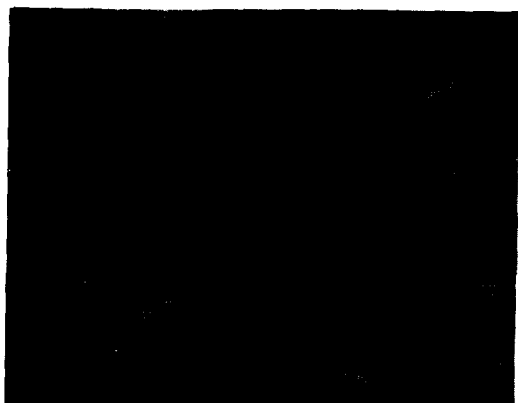


Figure 7.- The 1% Shuttle Orbiter model with external tank, boosters, and plume shapes.

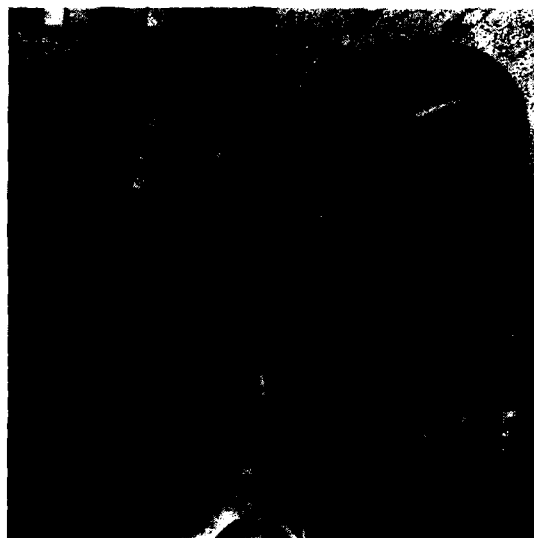


Figure 10.- Photograph of a submarine model tested in the NTF.



Figure 8.- The 2% Shuttle Orbiter model for the NTF.



Figure 11.- A Shuttle Orbiter model tested in the 0.3-m TCT.

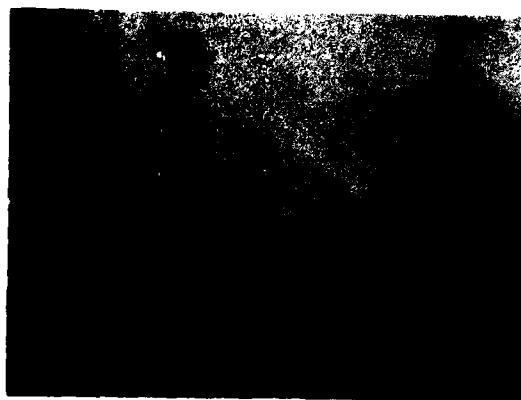


Figure 9.- Research model for the National Aerospace Plane.



Figure 12.- Six models for research on boattailed shapes.



Figure 13.- Wing-body interference models.

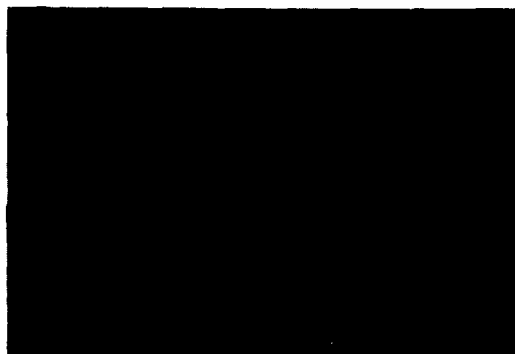


Figure 16.- Plates for symmetrical airfoil model shown prior to brazing to illustrate pressure channel layout.

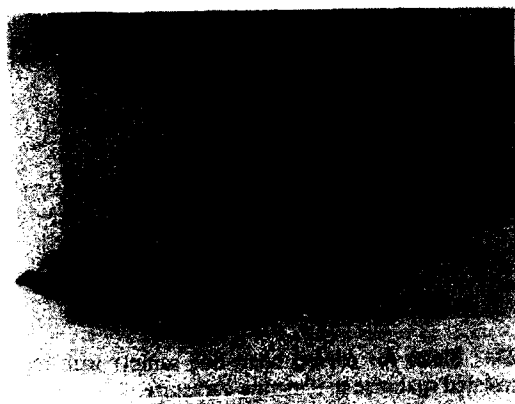


Figure 14.- Photograph of two dimensional airfoil body and cover showing complex void for pressure orifice tubing.

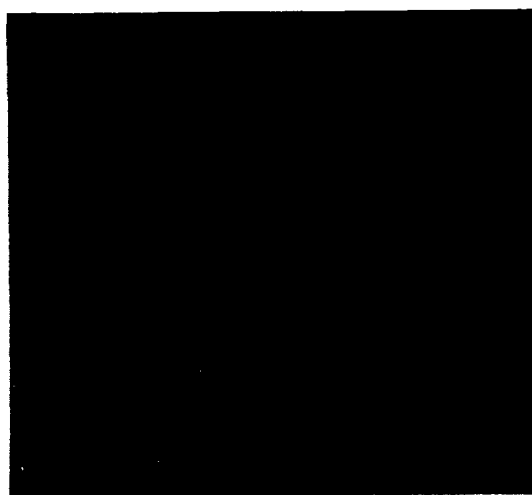


Figure 17.- Plates, connector tubing, and 2 of 4 pieces of brazing foil for symmetrical airfoil model.

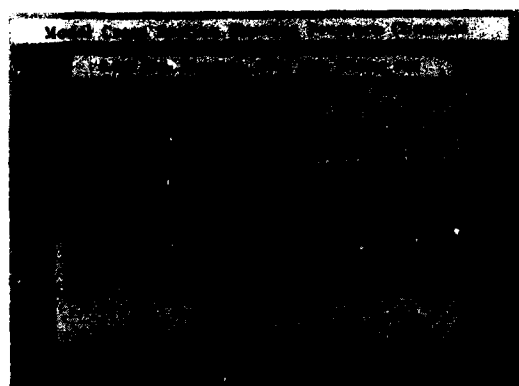


Figure 15.- Cross section through sample showing brazed joint and pressure channels.

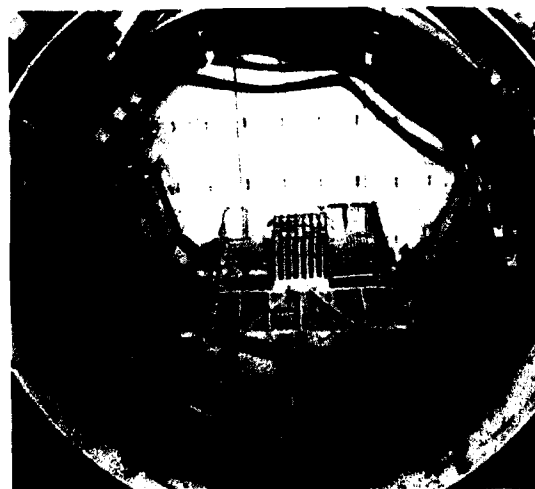


Figure 18.- Symmetrical airfoil model positioned in vacuum brazing furnace, with vertical cylindrical weights in place.

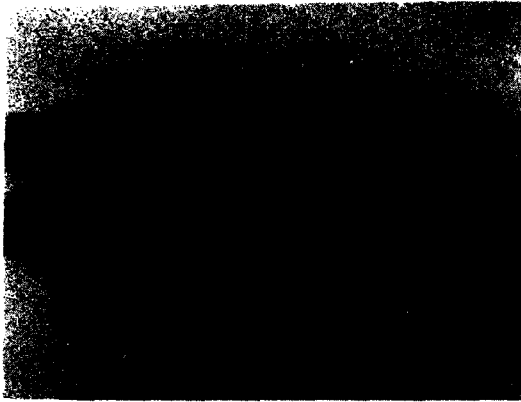


Figure 19.- Airfoil model after vacuum brazing; model now ready for leak check.

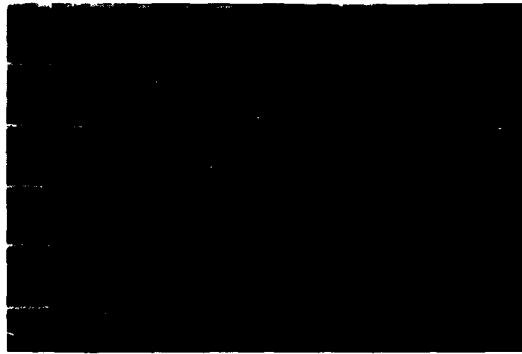


Figure 22.- Photoetched pressure channels.

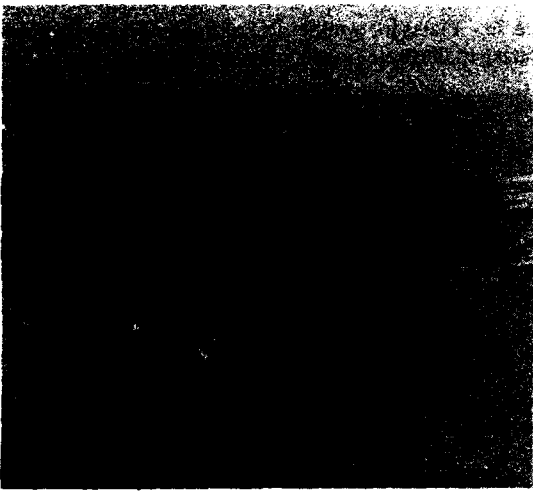


Figure 20.- Completed symmetrical airfoil model fabricated by the bonded plate method.



Figure 23.- Plates for curved bond line sample with top plate translated spanwise to illustrate curvature.

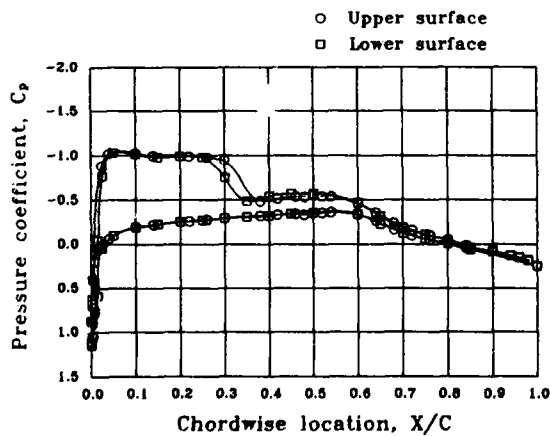


Figure 21.- Symmetrical airfoil pressure distribution for Mach number of 0.76, Reynolds number of 30 million. Positive and negative lift superimposed.



Figure 24.- Sample of a cusped, thin, wirecut, airfoil trailing edge sample together with cutoffs.



Figure 25.- Airfoil trailing edge sample; arrow at left points to trailing edge orifice, inset at right shows orifice quality for 1.0, 0.5, and 0.32 mm (0.040, 0.020, and 0.013 inch) orifices.

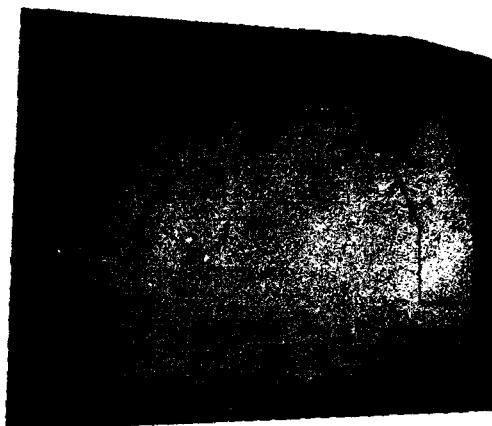


Figure 28.- Top sheet of multiple sheet stack. Photoetched outline is planform of X29 canard.

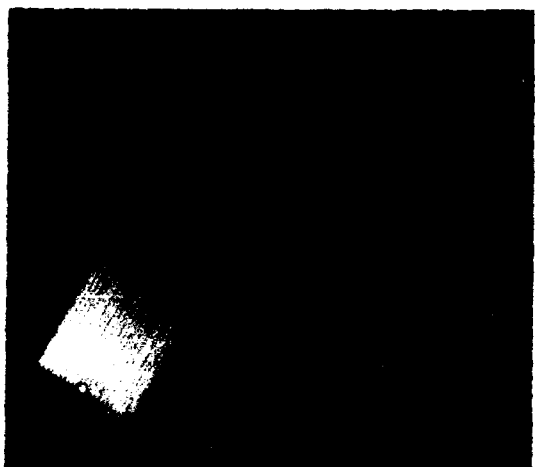


Figure 26.- Multilayer thin sheet concept proposed for high aspect wings to provide additional pressure channels.

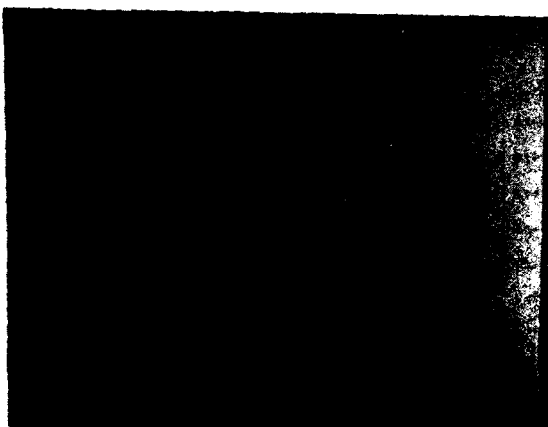


Figure 29.- Center bond plane of the X29 canard model stack showing channel layout.

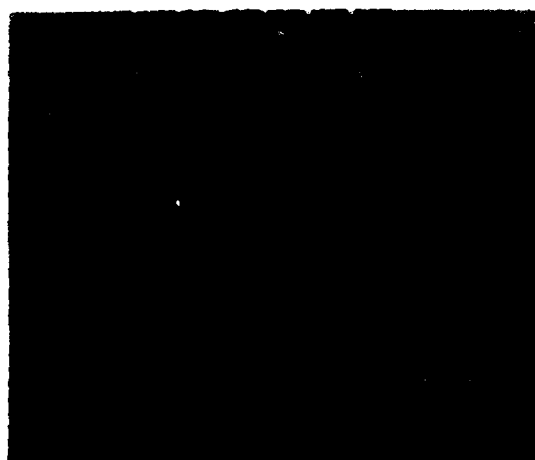


Figure 27.- Charpy bars cut from multiple sheet samples. Bars are broken normal to, and through the bond planes.

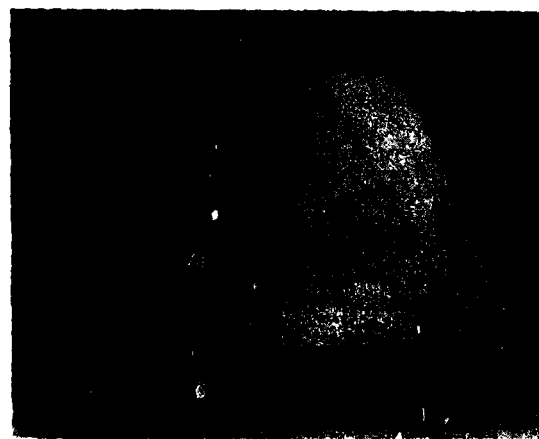


Figure 30.- Upper surface of X29 canard model showing bond planes and orifice rows.



Figure 31.- X29 Canard model and mounting hardware ready for cryogenic testing.

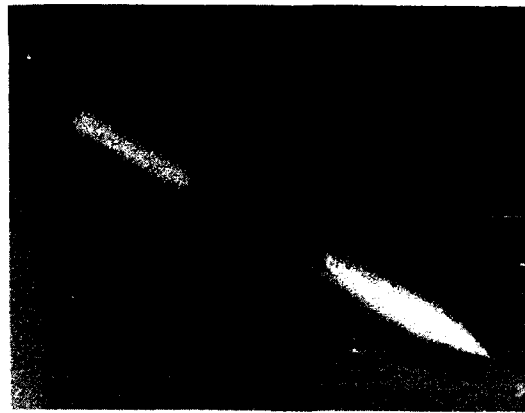


Figure 34.- "Gull wing" sample mounted on generic fuselage. Sample represents a very thin wing section with a three-dimensional wing shape. Pressure channels run spanwise.

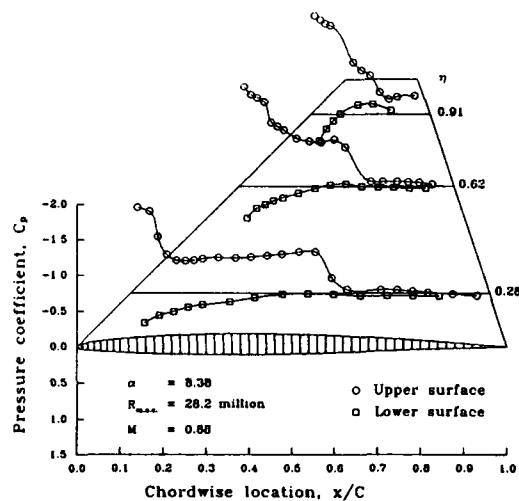


Figure 32.- Sample test result showing high Reynolds number, transonic pressure distribution.



Figure 35.- Sample airfoil model constructed by the bonded plate method using 17-4 ph steel.



Figure 33.- Twisted multiple plate sample and platens. Wire cut propeller blade shape in the twisted sample. Channels run spanwise.

AUTOMATIC CONTROL OF CRYOGENIC WIND TUNNELS

S. Balakrishna
NASA Langley Research Center
Hampton, Virginia 23665-5225
U.S.A.

SUMMARY

Inadequate Reynolds number similarity in testing of scaled models affects the quality of aerodynamic data from wind tunnels. This is due to scale effects of boundary-layer shockwave interaction which is likely to be severe at transonic speeds. The idea of operation of wind tunnels using test gas cooled to cryogenic temperatures has yielded a quantum jump in our ability to realize full scale Reynolds number flow similarity in small transonic tunnels. In such tunnels, the basic flow control problem consists of obtaining and maintaining the desired test section flow parameters. Mach number, Reynolds number and dynamic pressure are the three flow parameters that are usually required to be kept constant during the period of model aerodynamic data acquisition. In this lecture, the series of activity involved in modeling, control law development, mechanization of the control laws on a microcomputer, and the performance of a globally stable automatic control system for the 0.3-m Transonic Cryogenic Tunnel (TCT) are discussed. The lecture covers description of a lumped multi-variable nonlinear dynamic model of the cryogenic tunnel, generation of a set of linear control laws for small perturbation and nonlinear control strategy for large set point changes including tunnel trajectory control. The details of mechanization of the control laws on a 16 bit microcomputer system, the software features, operator interface, the display and safety are discussed. The controller is shown to provide globally stable and reliable temperature control to ± 0.2 K, pressure to ± 0.07 psi and Mach number to ± 0.002 of the set point value. This performance is obtained both during large set point commands as for a tunnel cooldown, and during aerodynamic data acquisition with intrusive activity like geometrical changes in the test section such as angle of attack changes, drag rake movements, wall adaptation and sidewall boundary-layer removal. Feasibility of the use of an automatic Reynolds number control mode with fixed Mach number control is demonstrated.

LIST OF SYMBOLS

Names

A	area, m^2
\bar{c}	mean aerodynamic chord, m
C_m	specific heat of structural material, kJ/kg K
C_p	specific heat at constant pressure, kJ/kg K
C_v	specific heat at constant volume, kJ/kg K
e	error or exponential
h	enthalpy
K	constant
\dot{m}	mass flow rate, kg/s
M	Mach number
N	fan speed, rpm
P	pressure, atm
q	dynamic pressure
Q	heat rate, kJ/s
r	fan pressure ratio
R	universal gas constant
Re	Reynolds number
S	Laplace operator
t	time constant, s
T	temperature, K
U	internal energy, kJ
V	volume, m^3
v	velocity
W	mass, kg
y	heat transfer coefficient $J/m^2/s/K$
ϕ	test direction parameter
Δ	small variation
ρ	density of nitrogen, kg/m^3
μ	viscosity of nitrogen gas
θ	rheostat position
γ	ratio of specific heat for nitrogen

Subscripts

bl	boundary-layer
c	circuit
d	diffuser
F	fan
G,Gv	gas and gas valve
i	integral
l	cross section
L,Lq	liquid nitrogen
m	structural material
M	Mach number
N	fan speed
o	reference
p	proportional
P	pressure
q	dynamic pressure
r	pressure ratio
Re	Reynolds number
s	static
t	test section
T	temperature
max	maximum
set	set point

1. INTRODUCTION

Closed circuit tunnels provide an efficient means by which uniform flow velocity can be generated over aerodynamic models. The test section flow in any tunnel is usually characterized by a set of flow parameters - Mach number, Reynolds number per unit length and dynamic pressure. The non-dimensional flow parameters, Mach number, and Reynolds number form the basis on which results from a subscale aerodynamic model can be extrapolated to a full-scale aerodynamic equivalent. The wind tunnel control problem consists of precise realization and regulation of flow parameters during the period of aerodynamic model articulation in the test section and during data acquisition. Ambient

temperature closed circuit tunnels use atmospheric air and have a long history of successful usage since the beginning of this century. Initially, in such tunnels, the flow velocity alone could be varied while there was no control over Reynolds number. With the advent of tunnel pressurization concept, the stagnation pressure and the velocity could be independently varied. This provided the ability to control Mach number and dynamic pressure independently which was associated with a dependent Reynolds number. High Reynolds number was always associated with high dynamic pressures and large tunnel fan power consumption. Independent control of all the three flow parameters is not feasible in an ambient temperature wind tunnel.

The idea of using nitrogen gas at cryogenic temperatures in closed circuit fan driven pressure tunnels allows independent control of all the three flow parameters. In a cryogenic tunnel, the gas temperature is controlled by injection of liquid nitrogen which evaporates to the tunnel resident gas while cooling and building up the mass. The difference in the cooling capacity of injected liquid nitrogen mass and the tunnel fan induced heating dictates the direction and the rate of change of tunnel temperature. It can be used to control the temperature precisely to any desired operating point in the gas phase. The cryogenic tunnel pressure is controlled by discharging warmer tunnel gas to atmosphere. Under equilibrium conditions, the discharge gas mass flow equals the injected liquid nitrogen mass flow. Bipolar pressure control is feasible as long as non zero liquid nitrogen input mass flow exists. The cryogenic tunnel Mach number is controlled by fan pressure ratio using either fan speed or the inlet guide vane angle as the control input. An engineering demonstration of this concept at transonic speeds was first made by the 0.3-m Transonic Cryogenic Tunnel (TCT) at NASA Langley Research Center in 1973.

Initially, the 0.3-m TCT was operated manually using fan speed for Mach number control, liquid nitrogen mass flow rate for temperature control and gas discharge mass flow rate for pressure control. The effects of these three control inputs on the tunnel states are highly coupled. Skilled manual effort was required to manipulate the three inputs to hold or vary the tunnel conditions precisely. Use of model attitude changing systems, drag rake traversing mechanisms, adaptive flexible wall systems, and sidewall boundary-layer removal systems and other intrusive data acquisition devices increased the complexity of maintaining the tunnel equilibrium. It requires an inordinately long time to obtain equilibrium conditions during typical model aerodynamic data acquisition. The quality of manual control of the tunnel was always very subjective and generally resulted in uneconomical use of liquid nitrogen and uncertainty in aerodynamic data quality. A strong need for closed loop control of the tunnel conditions was keenly felt during the initial phases of development of cryogenic tunnels. This need for closed loop control has been generally recognized and accepted as a basic necessity for all major cryogenic tunnel facilities now under design.

The theory behind the design of closed loop control system for any process is well established through principles of classical and modern control theory. It is based on availability of a validated mathematical model of the physical system which relates the process states to the control inputs. The cryogenic tunnel is a multi-input multi-output dynamical process. Serious efforts to obtain a mathematical model to represent the dynamics of cryogenic tunnels have been made for 0.3-m TCT and NTF at Langley Research Center in USA and the DFYLRs KKK tunnel in Europe.

The cryogenic tunnel dynamic models express the thermodynamic interaction involved in motion of the gas in the tunnel for inputs due to fan pressure ratio, the liquid nitrogen injection and gas discharge, both spatially and temporally. Such a model can be expected to be time invariant in parameters due to deterministic and causal nature of the tunnel process. The model is nonlinear since the mass enthalpy interactions are nonlinear. The local tunnel pressure, temperature and velocity at any point in time can be mathematically analyzed by duct flow equations of state, continuity, momentum, energy, and the thermophysical properties of nitrogen. This representation is to be further complemented by liquid nitrogen injection at one segment of the tunnel involving the phase transition of liquid nitrogen to nitrogen gas state, the adiabatic fan compression at a second segment of the tunnel and the enthalpy-mass disturbances caused by gas discharge at a third segment of the tunnel. Yet another major factor to be considered is the spatial and temporal convective heat transfer from the internal surface of the tunnel, such as the metallic parts of the tunnel structure, which are exposed to tunnel gas. The mathematical formulation of this process in a closed circuit cryogenic tunnel has been looked at as a problem of modeling a single volume lumped parameter system (ref. 1), a 16 volume dynamical system (ref. 2) and a distributed parameter system (ref. 3). Experimental validation of a lumped multi-variable mathematical model has been reported for the case of 0.3-m TCT (ref. 4).

The closed loop control system design for cryogenic tunnels involves use of the mathematical model to synthesize a set of control laws to provide small perturbation stability and large set point trajectory control. A fully validated model and its real time simulation provides an excellent method of synthesizing and evaluating control law designs. The mathematical model should include the dynamics of sensors and actuators as well as other ancillary systems. The model should also account for flow dynamics due to geometrical changes in test section due to aerodynamic model attitude change, flexible wall streamlining systems, and drag rake. In the closed loop control system design, which is an iterative process, a guess on the closed loop bandwidth is necessary. This leads to choice of minimum required accuracy and bandwidths for the sensors and actuators. In many cases, a custom built actuator or sensor may be necessary and has to be experimentally modeled. For the 0.3-m TCT an explicit nonlinear multi-variable model and a real time hybrid simulator has been used to analyze the closed loop stability and control (ref. 5). A linear closed loop control design at specific operating point is made for small perturbation. A series of such designs covering the full tunnel envelope leads to control laws having nonlinear gain schedules and use of feed forward. Once the control laws for the automatic control of cryogenic tunnels are available, their implementation on an appropriate controller is an important issue. With the revolution that has occurred in the area of real time numerical computation both in speed and volume, many choices of microcomputers are available for a low cost. The choice of real time input/output devices and the computational cycle time are made based on design accuracy and bandwidth.

This lecture presents the chain of activities involved in modeling, small perturbation control law analysis, large set point nonlinear control laws, simulation, choice of actuators and sensors, controller hardware and software design, commissioning of the automatic control system, response of the control system to set point changes and to disturbances concerning the 0.3-m TCT.

2. CRYOGENIC TUNNEL DYNAMICS AND MODELING

The dynamics of any conservative physical system is governed by the laws of conservation of mass and energy. The cryogenic tunnel process can be analyzed from such an energy and mass conservation view point.

2.1 Energy Storage in the Cryogenic Tunnel System

Consider a well insulated closed-circuit cryogenic nitrogen pressure-tunnel with a volume of V , having a typical geometrical disposition involving a settling chamber, test section, diffuser, return leg leading to a fan and a liquid nitrogen injection illustrated in figure 1.

Nitrogen as a gas has basic thermophysical properties which can be expressed as:

$$\rho = 338.9 P/T (1 + 250(P/T^2))$$

for saturation $T < 400$ K and $1 < P < 8$ atm

$$W_G = \rho V$$

Most cryogenic tunnels have an internal metal structure which will generally be at the same temperature as the tunnel gas under equilibrium conditions. The metal stored energy at any temperature under steady state conditions can be estimated assuming it to be in equilibrium with gas temperature and that the system is ideally insulated from the ambient.

$$\text{Enthalpy in the structural mass} = W_m \int_0^T C_m \delta T \text{ assuming nonlinear } C_m \text{ vs } T.$$

The gas internal energy due to molecular motion is a function of the temperature and can be expressed as $W_G C_v T$ in kilojoules. Using the steady state spatial pressure and velocity profile for the tunnel flow based on the local cross sectional area, the kinetic energy of the flow can be estimated as:

$$\text{Kinetic energy in motion of gas} = \int_{\text{circuit}} \frac{1}{2} \rho v^2 \propto \int_{\text{circuit}} P M^2, \quad \text{kilojoules}$$

Utilizing the area profile, volume, and structural mass details of 0.3-m TCT, the energy state of the tunnel gas has been evaluated. A plot of the tunnel resident gas mass versus the gas internal energy as a function of pressure and temperature is shown in figure 2.

Figure 3 provides a second energy state diagram which shows mass of tunnel gas versus the combined energy in metal mass and the gas under equilibrium conditions.

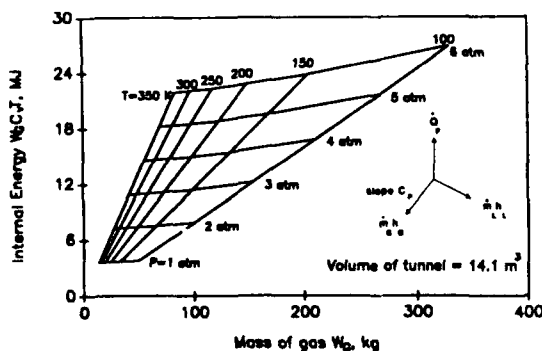


Fig. 2 0.3-m TCT energy state diagram, ideal internal insulation.

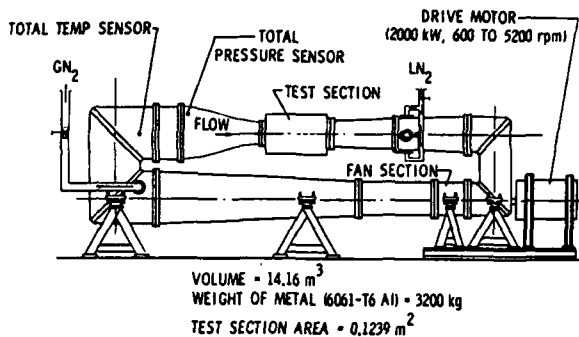


Fig. 1 Schematic of Langley 0.3-meter Transonic Cryogenic Tunnel.

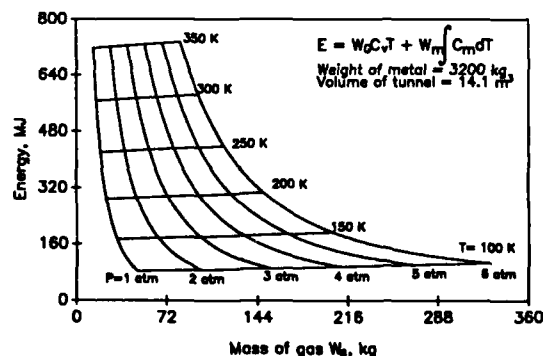


Fig. 3 0.3-m TCT energy state diagram, ideal external insulation.

Figure 4 shows a plot of the kinetic energy of the moving gas as a function of test section Mach number and tunnel total pressure. The kinetic energy has been estimated by integrating local kinetic energy using the local gas mass and velocity around the circuit. The total energy breakup in the system at 300 K, 6 atm pressure, and Mach 1 is 600 megajoules in the metal, 24 megajoules in gas enthalpy and 200 kilojoules as kinetic energy. At 100 K, 6 atm pressure, and Mach 1 the energy breakup is 80 megajoules in the metal structure, 28 megajoules in gas enthalpy and 200 kilojoules as kinetic energy. It is evident that metal stored energy dominates the energy scene, and the kinetic energy even at Mach 1 is less than 1% of the gas internal energy.

2.2 Total Temperature Dynamics

Ignoring for the moment the spatial density and velocity variations due to motion of the fluid, the cryogenic tunnel can be looked up on as a closed thermodynamic system illustrated in figure 5. Assuming uniform mixing and evaporation of the liquid nitrogen, and ignoring the work done by the system the following identities can be written.

$$h_L = U_L + P_L V_L \quad \text{and} \quad h_G = U_G + P_G V_G$$

$$-\dot{Q}_m + \dot{Q}_F + \dot{m}_L h_L = \dot{m}_G h_G + d(W_G C_V T)/dt = \dot{m}_G h_G + C_V T(\dot{m}_L - \dot{m}_G) + W_G C_V dT/dt$$

which can be simplified to

$$W_G C_V dT/dt = \dot{m}_L (h_L - C_V T) - \dot{m}_G (C_P - C_V) T - \dot{Q}_m + \dot{Q}_F \quad \text{isothermal model} \quad (1)$$

The lumped energy model of equation (1) shows an isothermal interaction of the control input energy terms from liquid nitrogen injection, gas discharge, fan operation and metal wall release of heat with the tunnel resident gas mass. In certain other cryogenic tunnel modeling efforts (ref. 6), an adiabatic interaction of the energy terms with the tunnel resident gas mass is proposed. Such an adiabatic model typically takes the form:

$$W_G C_P dT/dt = \dot{m}_L (h_L - C_P T) - \dot{m}_G (C_P - C_P) T - \dot{Q}_m + \dot{Q}_F = \dot{m}_L (h_L - C_P T) - \dot{Q}_m + \dot{Q}_F \quad \text{adiabatic model}$$

This temperature model of a cryogenic tunnel postulates that gas discharge from the cryogenic tunnel has no affect on the temperature of the tunnel for small perturbation. Naturally, a question arises as to which of the two mechanisms of thermodynamic interaction is valid for a cryogenic tunnel. Experimental evidence from 0.3-m TCT performed under open loop operating conditions point to an isothermal like behavior of the cryogenic tunnel since gas discharge does change the temperature.

Figure 6 illustrates the effect of an incremental pulse mass flow discharge to 0.3-m TCT which is being run manually under equilibrium conditions. The mass removal results in a temperature drop to the tunnel gas. The temperature slowly recovers to original value, after equilibrium flow has been established, due to heat release from the tunnel walls. If the adiabatic model is true, a pulse removal of mass from the tunnel would not affect the total temperature, where as an isothermal model does predict this behavior.

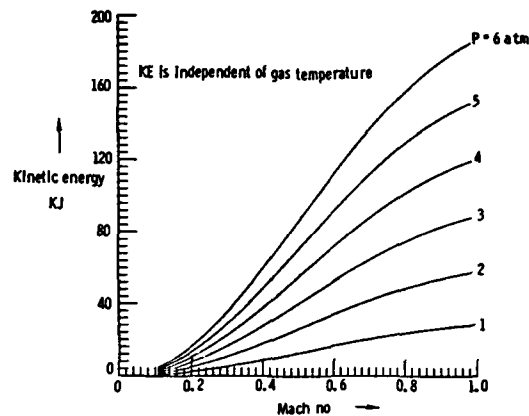


Fig. 4 Kinetic energy of moving gas, 0.3-m TCT.

The lumped temperature model of the cryogenic tunnel process is nonlinear and coupled by effects of tunnel pressure dynamics, fan heat and the tunnel wall heat release. In postulating this simple tunnel temperature model, the spatial effects caused by momentum and transport effects have not been considered. Since the tunnel gas temperature is dictated by the energy mechanics of the system, ignoring the kinetic energy contributions which form a very small part of the total energy scene is a reasonable approximation.

2.3 Tunnel Pressure Dynamics

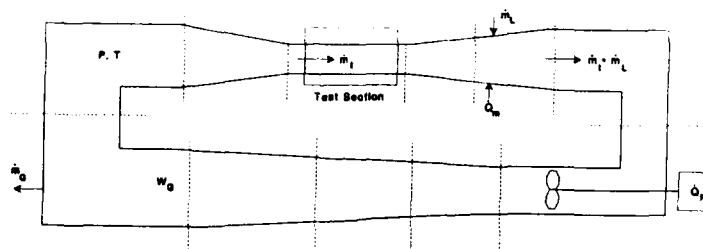
Using the equations of state we have $P = \rho RT = kW_G T$

$$\text{By differentiating } dP/dT = kW_G dT/dt + kT dW_G/dt = P/T dT/dt + P/W_G (\dot{m}_L - \dot{m}_G) \quad (2)$$

This simple model postulates that the tunnel total pressure is a function of time rate of gas temperature and tunnel mass variation rate. In a cryogenic tunnel, the mass variation is caused by control inputs due to the injection of liquid nitrogen and gas discharge. The time rate of change of tunnel total temperature is caused by energy terms of the control inputs described in equation (1).

2.4 Tunnel Flow Continuity

The equations (1) and (2) provide the pressure and temperature dynamics of a cryogenic tunnel in which the effects of spatial variations of pressure and temperature are ignored. The spatial variation of the flow in a closed circuit pressure tunnel can be studied by continuity and momentum equations.



First Law of Thermodynamics:

$$-\dot{Q}_m - \dot{Q}_F + \dot{m}_L h_L - \dot{m}_G h_G + W_G C_V dT/dt = u(\dot{m}_L - \dot{m}_G)$$

Assumptions:

perfect gas
uniform temperature
zero work done

Fig. 5 Thermodynamic model of cryogenic tunnel.

Consider a cryogenic tunnel circuit represented by several sections 'T', where liquid nitrogen is added at the downstream diffuser segment, a fan with its inlet/outlet guide vanes is located in the second corner and gas discharge occurs at the third corner shown in figure 5. Under steady state equilibrium conditions, the spatial profile of the tunnel flow can be expressed using one dimensional representation of the continuity equation with isentropic assumptions. At any section 'T':

$$\begin{aligned} \dot{m}_t &= \rho_t V_t A_t = K P_t M_t A_t \sqrt{\gamma/R T_t} \\ P_t &= P_i / (1 + 0.2 M_t^2)^{3.5} \\ T_t &= T_i / (1 + 0.2 M_t^2) \\ (1 + 0.2 M_t^2)^3 - K \sqrt{\frac{1.4}{R}} \frac{P_i M_t A_t}{\dot{m}_t \sqrt{T_i}} &= 0 \end{aligned} \quad (3)$$

This description of the steady state tunnel flow relates the local area, Mach number, total pressure and total temperature to the mass flow around the circuit, except through the fan segment. Under equilibrium conditions, the mass flow \dot{m}_t between liquid nitrogen injection point and the gas discharge point is $\dot{m}_t + \dot{m}_i$ and in the rest of the tunnel circuit the mass flow is \dot{m}_t .

In a test section with time varying geometry, the relation of area change in A_t on the flow Mach number under steady state conditions can be expressed in a one dimensional approximation, based on continuity as:

$$dA_t/A_t = -dv/v - d\rho/\rho = -dM/M (1-M^2)$$

One solution to tunnel dynamic modeling is to use the energy equation, continuity equation, momentum equation, equation of state for each segment of the tunnel, and generate a numerical real time simulator for the tunnel dynamics. Such a tunnel simulator provides a tool on which control law validation can be made. Alternately, in a lumped modeling approach, the continuity equation can be looked upon to provide spatial description of a tunnel in which the total pressure and temperature at the settling chamber are dictated by the averaged dynamical equations described in equations (1) and (2). This approximation is based on the bulk of the tunnel losses occurring in the high speed diffuser and the corners near the fan, which have very low volume.

In a closed circuit tunnel with known total pressure at settling chamber, the pressure profile around the circuit is dependent on the circuit loss characteristics and the fan pressure rise. The circuit loss in a tunnel is typically represented by a loss factor which relates the static pressure drop in any given segment to the flow dynamic pressure, $K_t = (\Delta P_t/q_t)(q_t/q_o)$. The maximum circuit pressure loss for the 0.3-m TCT is such that a fan pressure ratio of about 1.14 is necessary at about $M=0.9$. This accounts for a total pressure variation of about 10% from the fan inlet to outlet. For known stagnation temperature at settling chamber, total temperature profile shows a drop in the segment downstream of the liquid nitrogen injection point which is equal to the total temperature rise through the fan due to adiabatic compression. Once the local temperature and total pressure profile is known, the local Mach number can be estimated using equation (3).

The tunnel circuit typically carries the flow continuously around, and a circuit can be defined for a cryogenic tunnel as:

$$\text{Tunnel circuit time, } t_c = W_G/\dot{m}_t = 0.0486V/(A_t M_t \sqrt{T_i}) (1 + 0.2 M_t^2)^3$$

2.5 Metal Wall Temperature Dynamics

Consider a cryogenic tunnel which is ideally insulated to ambient, and in which an internal structural material of weight W_m and surface area A_m is exposed to nitrogen gas. Under steady state temperature conditions, the structural material is at the same temperature as the tunnel gas. The rate of the heat exchange between the gas and the tunnel structure is a function of the convection heat transfer occurring at the turbulent boundary-layer throughout the surface of the tunnel. This heat transfer coefficient is a function of the local velocity, density and temperature of tunnel gas. A simple first order model description of this heat transfer is:

$$\int_{\text{surface}} \dot{Q}_t = W_m C_m TS / (1 + t_m S) = (T - T_m) A_m y_m; \quad T_m = T / (1 + t_m S) \text{ and } t_m = (T - T_m) / \dot{T}_m \quad (4)$$

This model describes heat transfer in the tunnel through a heat transfer coefficient y_m from a structural mass whose average temperature is T_m . Parameter t_m represents an equivalent time constant of heat transfer. Both y_m and t_m are complex functions of the tunnel pressure, temperature and flow Mach number. The heat transfer rate y_m can be estimated using principles of convection heat transfer through turbulent boundary layer and integrating it for the total internal surface of the tunnel, as in reference 4. It can also be experimentally determined by using equation (4) where T , T_m and \dot{T}_m can be measured while performing a cooldown from which the structural heat release time constant t_m

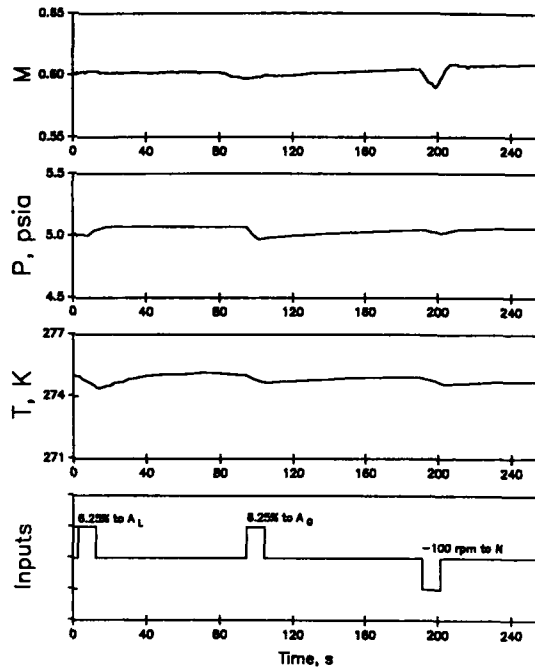


Fig. 6 0.3-m TCT open loop response to pulsed inputs under equilibrium.

can be estimated. For the 0.3-m TCT cooldown experiments conducted with a fixed $(T-T_m)$ of 40 K confirm the first order description of the heat transfer and have yielded the following estimate for the metal time constant based on the external wall temperature at the settling chamber. In a specific cooldown of the tunnel at a constant $M=0.440$ and $P=30$ psia, t_m has been estimated to be about 530 s. The general expression for time constant based on analysis and later reconciled to experimental data is:

$$t_m = 943/(T^{0.12}(PM)^{0.8})$$

2.6 Fan System

The single stage axial flow fan creates the pressure ratio in a closed circuit tunnel to generate the necessary tunnel flow. The fan pressure ratio control, over the large range of mass flows, is obtained by fan speed variation and is sometimes complemented by inlet guide vane angle control. For the 0.3-m TCT the fan consists of 12 blades with its 7 fixed inlet guide vanes. Speed control between 600-5600 rpm provides a stall free pressure ratio-mass flow control.

The fan pressure ratio $r = 1 + k_f M^2$ where $k_f = 0.8205 \text{ Re}^{-0.096}$

The pressure ratio r in any axial flow fan is related to fan speed normalized to temperature; hence the cryogenic tunnel test section Mach number can be expressed as $M = f(N/\sqrt{T})$. For the 0.3-m TCT, this relation has been obtained experimentally in the range $M=0$ to 0.95 as:

$$N/\sqrt{T} = k_N M(1 - 0.3M); \quad M = 1.667 \left\{ 1 \pm \sqrt{1 - \frac{1.2N}{k_N \sqrt{T}}} \right\}$$

The constant k_N is a function of the test section geometry. The Mach number dynamics can be expressed as a simple first order time constant to account for pressure buildup time delays in the plenum. The fan pressure rise is accompanied by a temperature rise and all the mechanical energy into the fan manifests itself as heat transferred to the tunnel gas. This heat release is an adiabatic process and can be estimated by the identity $\dot{Q}_F = \dot{m}_F C_p \Delta T$. This can be simplified to a form:

$$\dot{Q}_F = K_F P M^3 \sqrt{T}/(1 + 0.2 M^2)^3 \quad (5)$$

2.7 Lumped Multi-Variable Model of Closed Circuit Cryogenic Tunnel

From the set of identities discussed, the cryogenic tunnel lumped nonlinear model can be summarized using the following equations.

$$\frac{dT}{dt} \left\{ 1 + \frac{1}{W_G C_v} \frac{W_t C_m}{(1+t_m S)} \right\} = \frac{\dot{m}_L}{W_G C_v} (h_L - C_v T) - \frac{\dot{m}_G}{W_G C_v} (C_p - C_v) T + \frac{1}{W_G C_v} \frac{K_F P M^3 \sqrt{T}}{(1 + 0.2 M^2)^3}$$

$$dP/dT = (P/T) dT/dt + P/W_G (\dot{m}_L - \dot{m}_G)$$

$$M = \frac{1.667}{(1+t_1 S)} \left\{ 1 \pm \sqrt{1 - \frac{1.2 N}{k_N \sqrt{T}}} \right\}$$

$$\text{and } dA_t/A_t = -dM/M(1 - M^2)$$

In these nonlinear coupled equations, the tunnel pressure, temperature and Mach number are expressed as functions of the input control variables \dot{m}_L , \dot{m}_G , N and test section area disturbance. These equations describe the global behavior of the tunnel states in the full envelope of tunnel operation.

3. CONTROL LAWS

Classical and modern control theory are well established for stability and control analysis of linear and multi-variable systems. Nonlinear control analysis methods are usually problem dependent and defy easy global analytical solutions. The highly nonlinear and coupled nature of the cryogenic tunnel process does not allow easy multi-loop control analysis. Hence a small perturbation stability and control analysis has been performed analytically by treating the temperature, pressure and Mach number dynamics as a set of single input-output systems. An inspection of the tunnel model reveals very few energy storage elements and these are also of a low order. The tunnel control problem appears to be dominantly one of a quasi-static balance of large nonlinear

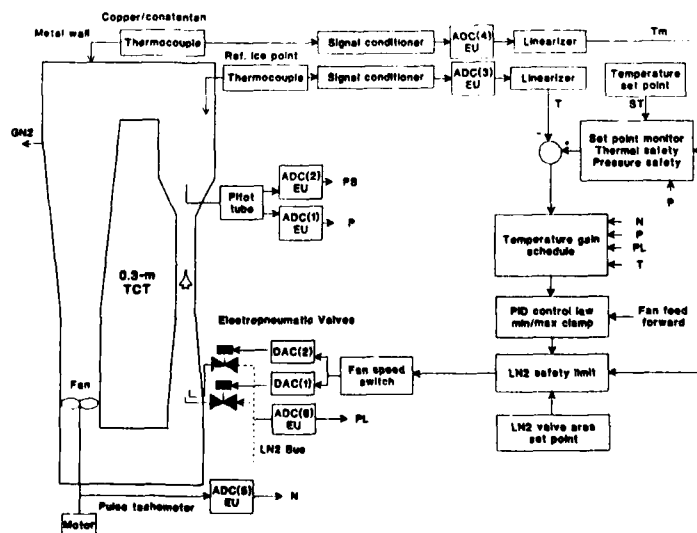


Fig. 7 0.3-m TCT temperature control schematic.

terms. In the following analysis, control laws have been generated based on small perturbation analysis using the dynamic model generated and assuming typical sensors and actuators.

3.1 Temperature Control

A study of the temperature equation reveals that the tunnel gas temperature rate is sensitive to liquid nitrogen mass flow, gas discharge, fan induced heating and metal wall. Liquid nitrogen mass flow can be chosen as the main temperature control input while treating other sensitivities as disturbances. Figure 7 shows a schematic diagram of the temperature loop. A small perturbation control analysis, assuming linear behavior, for a given set of operating points near equilibrium, shows that the temperature control sensitivity varies by a large range. A gain schedule of the type $M/(P/T)$ has been found to provide adequate stability and accuracy through a PI control law. A feed forward of the fan power cancellation is necessary. The control law for 0.3-m TCT is:

$$\dot{m}_L = M/(P/T) \{ K_{TT} e_T + K_{PT} e_T \} + FF \dot{Q}_F / (h_L + C_p T) \quad \text{where } e_T = T - T_{set}$$

For large set point changes, the metal temperature does not follow the gas temperature because of the thermal inertia of the system and limitations of heat transfer rate. With linear control laws, the resultant error integrates to large nitrogen flow commands more than the rate of evaporation. This generally results in liquid nitrogen accumulation in the tunnel. To overcome this, a nonlinear control law is necessary to limit large error. This nonlinear control is based on the model of the metal temperature dynamics. Under steady metal cooling conditions, with a fixed \dot{T} , the heat release from tunnel metal is $W_t C_m \dot{T}_m$. Given the cooling capacity of liquid nitrogen as $(h_L + C_p T)$, the maximum liquid nitrogen flow should be limited to:

$$\dot{m}_{Lmax} = (W_t C_m \dot{T}_m + \dot{Q}_F) / (h_L + C_p T) = (W_t C_m (T - T_m) / t_m + \dot{Q}_F) / (h_L + C_p T)$$

This limiting nonlinear control term can be estimated either from a measured structural cooling rate or from metal to gas temperature difference. Location of metal temperature measurement point decides the local metal time constant and should be chosen from thermal stress considerations.

In the case of 0.3-m TCT the nonlinear control law used for large set point cooldown commands is a simple clipping of the linear control law output.

$$\begin{aligned} \dot{m}_{Lmax} &= 100 \% \text{ of flow} & \text{for } (T_m - T) \leq T_{max}/2 \\ \dot{m}_{Lmax} &= 100 \{ 1 - [(T_m - T) - T_{max}/2] / 2/T_{max} \} & \text{for } (T_m - T) > T_{max}/2 \\ \dot{m}_{Lmax} &= 0 & \text{for } (T_m - T) > T_{max} \end{aligned}$$

This algorithm keeps the metal-gas temperature difference at a value very near T_{max} during a cooldown and prevents accumulation of liquid nitrogen in the tunnel circuit.

For tunnel warmup with large set point commands, it is desirable to switch the fan feed forward off. This is obtained by a hysteresis type nonlinear law where FF is a feed forward logic variable.

$$\begin{aligned} \text{IF } T - T_{set} < -5 \text{ K} & \quad \text{THEN } FF=0 \\ \text{IF } T - T_{set} > 0 & \quad \text{THEN } FF=1 \end{aligned}$$

3.2 Pressure Control

The tunnel gas pressure is controlled by the incoming mass flow as commanded by the temperature loop, the gas discharge mass flow rate and the tunnel gas temperature rate. Typically, in a closed circuit cryogenic tunnel the pressure control is obtained by varying the gas discharge mass flow while treating the temperature loop liquid nitrogen injection and the tunnel temperature rate of change as disturbances to the pressure loop. Figure 8 illustrates a schematic of the pressure control loop. A linear control analysis of the pressure loop shows the need for a gain scheduling of the type $1/T$ to the mass discharge control law and is a fairly weak gain scheduling. The small perturbation PI control law is:

$$\dot{m}_G = 1/T \{ K_{PP} \int e_P + K_{PT} e_P \} \quad \text{where } e_P = P - P_{set}$$

This control law is globally stable and can accept large set point command changes. The tunnel pressure buildup rate is dictated by the temperature loop commanded mass flow rate of \dot{m}_L , where as the tunnel pressure drop rate is limited only by the valve full opening flow. It may be desirable to control the rate of pressure drop by programming

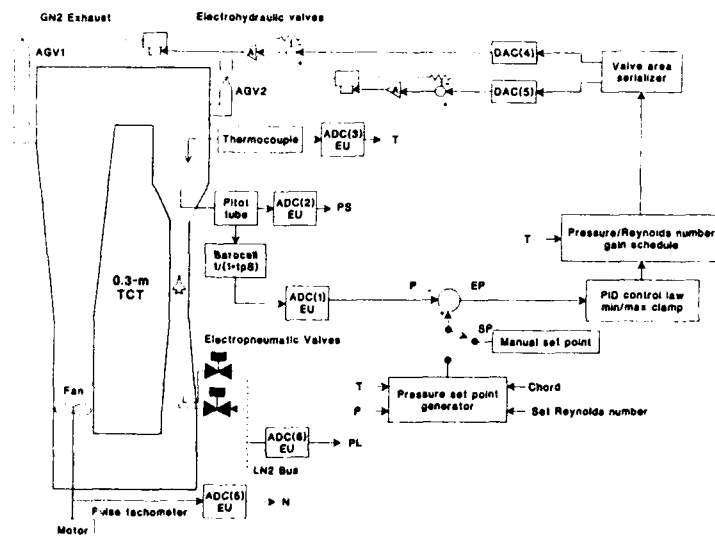


Fig. 8 0.3-m TCT pressure-Reynolds number control schematic.

Fig. 9 0.3-m TCT fan speed and Mach number control schematic.

change, and only the momentum of the moving gas mass is changed. Consider the tunnel operating at P_1-T_1 located on a line of constant gas mass. The trajectory control problem is one of taking the tunnel to an arbitrary point P_2-T_2 . Four zones can be identified relative to the starting point on the P-T plane. The final gas mass in the tunnel is equal to or lower than the starting mass in zones 1 and 2. The final mass is higher than the starting mass in zones 3 and 4. In zones 2 and 3, the final temperature is lower than starting temperature, implying a cooldown of the tunnel which is associated with liquid nitrogen mass addition. Zones 1 and 4 are areas where the final temperature is higher than the starting temperature, requiring fan heat and no cooling. In zone 4, additional mass is required to build the pressure, but the temperature control law does not provide additional nitrogen mass. For set point commands where both higher temperature and pressure are simultaneously commanded, the temperature and pressure loops shut the control valves close. In theory, the fan heat should result in a slow pressure and temperature rise. However, the rates are usually very slow due to leakages; hence, a nonlinear control algorithm is proposed which identifies the final tunnel resident mass and takes the tunnel to the final point quickly. The control law is:

$$\text{IF } P_2/T_2 \geq P_1/T_1 \text{ AND IF } T_2 > T_1 \text{ THEN } T_{\text{use}} = T_1 - \Delta T \text{ ELSE } T_{\text{use}} = T_2$$

This law checks the final mass desired in a large set point change, and whenever there is a shortage in the extrapolated mass flow, the temperature set point is temporarily brought down to add some liquid nitrogen to build up the mass.

3.6 Minimum Energy Test Direction

An aerodynamic test of a model involves operation of the cryogenic tunnel at various Reynolds numbers, Mach numbers, and dynamic pressures. The tunnel pressure, temperature, Reynolds number, Mach number, and dynamic pressure are related (equation 6) through a number which is defined as test direction parameter ϕ .

$$\phi = R_e/M (1 + 0.2 M^2)^{2.1} = K_{Re} P \bar{C}/T^{1.4} \text{ and } q = K_q P M^2 \gamma$$

Figure 11 shows loci of constant ϕ in the tunnel P-T plane. When choice tunnel dynamic pressure q is left open, for any given Mach number and Reynolds number, a number of P_n-T_n combinations are feasible as shown by a typical locus DE. The locus ABC provides a minimum energy test direction design for any series of tests (ref. 7) and can be designed by choosing monotonically decreasing test direction parameter ϕ_n . This locus is also associated with minimum dynamic pressure. If all of the three flow parameters are fixed, they uniquely translate to tunnel pressure and temperature, and the test direction for such a case is more difficult to obtain (ref. 8).

4. SENSORS AND ACTUATORS FOR THE CRYOGENIC TUNNEL

Closed loop control of the cryogenic tunnel requires a number of tunnel variables to be measured continuously, and a set of actuators of adequate performance are necessary. In this section, typical requirements of the tunnel sensors and actuators are presented.

4.1 Temperature Measurement

The gas temperature in the cryogenic tunnel settling chamber is representative of the tunnel total temperature. For closed loop control purposes, accuracy of measurement required is about 0.05 to 0.1 K, based on the sensitivity of the flow parameters to change in nitrogen temperature. The speed of response required is a function of the temperature control loop bandwidth and the sensor delay should account for less than a few degrees of phase margin. The speed of response of a temperature sensor is a function of heat transfer to surrounding medium. It varies with the gas density, and velocity of flow. Typically a Copper constantan thermocouple of wire diameter 0.028 inches provides a response time of 0.5 to 3 seconds depending on flow conditions in the settling chamber. The output of the thermocouple ranges from -5.6 to +2.9 millivolts for 78 to 340 K, and is a nonlinear function of temperature. It is necessary to linearize the sensor output in real time. A polynomial type linearization fit to obtain linear voltage-temperature relationship is easy to implement. Further, the thermocouple output needs to be referred to a cold junction compensator for accuracy and repeatability of measurement.

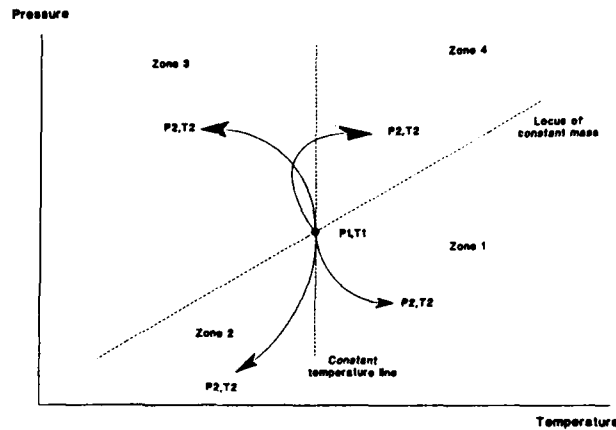


Fig. 10 Tunnel trajectory in pressure-temperature plane.

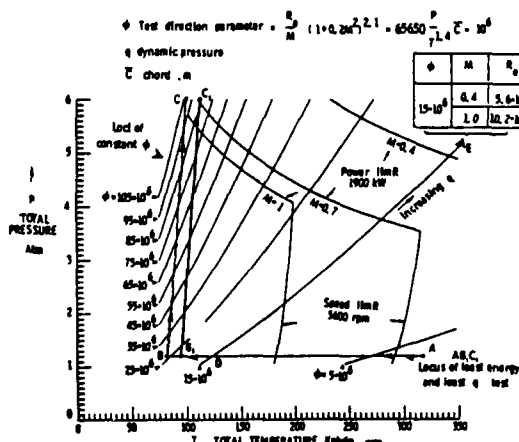


Fig. 11 Test direction design in cryogenic wind tunnel-locus of least liquid nitrogen consumption and least q in P-T plane.

It is also necessary to measure the tunnel structural temperature at a representative point for feedback control to be used in nonlinear control law mechanizations. A similar thermocouple can perform this task and again the signal needs to be linearized.

4.2 Pressure Measurement

The tunnel total pressure in the settling chamber and the static pressure in the uniform part of the test section should be very accurately measured for correctly estimating the tunnel flow Mach number. At a low Mach number of 0.200, an error in pressure measurement of about 0.01 psia in 20 psia causes an uncertainty in the Mach number of 0.002. The Mach number measurement accuracy dominates the accuracy requirement of the pressure transducers needed for cryogenic tunnel control. Typically a repeatability of 0.003 psia and an accuracy of 0.01 psia is necessary for a tunnel like 0.3-m TCT. Many transducers which use quartz-bourdon type elastic elements provide the kind of accuracy planned, but suffer from very slow response. For the purposes of cryogenic tunnel pressure and Mach number control, a quick response time constant of 0.20 seconds including the tube time delays is desirable. The 0.3-m TCT uses a capacitance type pressure transducer which is maintained at a constant temperature. In measuring the liquid nitrogen pressure, an accuracy of about 0.5% is adequate for use in control laws. Mass flow measurement of either gaseous flow or liquid flow requires measurement of pressure drop across venturi or similar devices. Liquid nitrogen mass flow measurement is difficult and its accuracy limited to 5 - 10% likely due to two phase flow. It is desirable to avoid use of measured mass flow rates in the control of cryogenic tunnels.

4.3 Fan Speed/Guide Vane Measurement

The fan drive speed is measured using a magnetic or an optical pulse counting device which is differentiated to provide the fan speed accurately. The industrial quality devices provide an accuracy of speed measurement to better than 0.02% very easily. In cases where inlet guide vane angle control is also used, the angle is measured usually by potentiometric devices.

4.4 Gas Vent Valve

Butterfly valves, plug valves or gate valves operated by electrohydraulic actuators are usually used for controlling the mass flow out of the cryogenic tunnel. The mass flow is a function of the pressure drop across the valve, the temperature, and the valve area and can be expressed as:

$$\dot{m}_G = K_G A_{Gv} P / \sqrt{T} \quad \text{for a pressure ratio in excess of 0.528}$$

$$\dot{m}_G = K_{G1} A_{Gv} \sqrt{(P \Delta P / T)} \quad \text{for unchoked conditions}$$

The valve area-stroke relation tends to be somewhat nonlinear for butterfly valves. The speed of response of the valve is a function of the control command rate for disturbances occurring in the pressure control system. For the 0.3-m TCT a full stroke response time of 0.3 seconds is used. The valve is driven in a position feedback and dynamics can be represented by a second order system of 5 Hz natural frequency and a damping of 0.5 with a transport lag term of about 5 milliseconds. For large size cryogenic tunnels this response time can be scaled by circuit time as a design pointer.

4.5 Liquid Nitrogen Supply System and Injection Valve

The liquid nitrogen is pumped from a vacuum jacketed source tank and is returned back to the tank through a back pressure valve such that when no demand for liquid nitrogen from the tunnel exists, the pumped fluid returns back. The tunnel is supplied from the pressurized leg of the pumping line. In the case of 0.3-m TCT the constant speed impeller type pump generates the pressure which varies from 90 to 150 psia depending on the back pressure setting. This back pressure control is a PI control loop with very slow integration and can accommodate tunnel flow ranging from zero to about 8 kg/s. The liquid nitrogen injection into the tunnel is through three diaphragm operated liquid flow control valves capable of about 0.02 kg/s up to 6 kg/s depending upon the area of opening. The control valve has a repeatability of 0.5% and a nonlinear area-stroke behavior. The spring loaded diaphragm is actuated by a pneumatic power booster signalled from a 4-20 mA driven flapper-nozzle transducer. The air to open type control valve has a velocity limit of 130%/s corresponding to about 0.72 s for full stroke. The valve response is about 4-5 rad/s bandwidth for small perturbations and has a transport lag associated with it.

$$A_L / \text{current} = e^{-0.103 S / (1 + 0.230S)} \quad \text{and} \quad \dot{m}_L = K_L C_{Lq} \sqrt{(P_{Lq} - P)} A_L$$

For large size cryogenic tunnels this response time can be scaled by circuit time normalizing factor as a design guide.

4.6 Fan Speed Control

The 0.3-m TCT is driven by a water cooled 2 pole induction motor fed from a 10-120 Hz electrical supply 35 Vrms/Hz sensitivity. The fan motor speed control is obtained by varying the speed of the electrical alternator driven by a DC motor. The DC motor supply is controlled by a DC generator whose field supply rheostat is the control element. The stability of speed control through these many rotating devices is about 5 rpm around the set speed. The rheostat is driven by a position servo whose set point can be controlled through 0-5 VDC signal to realize full range speed control. The dynamics of the speed control system has been modeled as a second order system of a natural frequency of 2 radians and a damping of 0.55. The system has a velocity limit of 300 rpm/second.

5. DESIGN OF CLOSED LOOP CONTROLLER

For precise closed loop control of the cryogenic tunnel states, the control laws provide the necessary feedback and feed forward of measured tunnel variables to the various actuators. These control functions are realized in an integrated manner on a microcomputer based system. In this section, the details of the functions of the 0.3-m TCT controller, its mechanization and its performance are discussed.

5.1 Functions of the Controller

The temperature control has three modes of operation; Manual, Auto, and Emergency. In the Manual mode the liquid nitrogen valve area is set by the operator. In the Auto mode, the temperature is under closed loop control. The loop gain, feed forward and control estimations are made from existing tunnel states. The tunnel temperature set point commanded by the operator is managed through thermal restrictions of 20 K/minute gas cooling rate, 10 K/minute metal cooling rate, maximum gas-metal temperature difference restriction of 40 K and tunnel trajectory mass management algorithm. There are no restrictions on the tunnel warming rate since there is a natural limit of about 10 K/minute based on fan power. The gas cooling rate restriction has been imposed so that fine protruding devices like thermocouples, pressure probes and turning vanes are not exposed to thermal shocks which can reduce their life. Further, this reduced gas cooling rate aids in better evaporation of the liquid nitrogen droplets. The metal cooling rate restriction prevents thermal stresses and leakage at flanges due to uneven thermal contraction. These thermal restrictions of rate of cooling apply even during Manual mode of temperature control. In the Emergency mode, the liquid nitrogen valves are closed shut immediately.

The pressure control loop of the 0.3-m TCT has four modes of operation; Manual, AutoPressure, AutoReynolds number and Emergency. In the Manual mode, the gas discharge valve area is under manual control of the operator with no restrictions on opening authority. In the AutoPressure mode, the pressure is under closed loop control. The tunnel pressure set point commanded by the operator is managed through a ramp function generator to command a pressure maximum rate of 3 psia/s in a downward direction. This is to prevent a rapid pressure drop associated with the vent valves fully open. This pressure drop creates loading on the thin flexible walls due to poor plenum/test section ventilation in the 0.3-m TCT flexible wall test section. In the AutoReynolds mode, the pressure set point for the tunnel is estimated using the existing tunnel gas temperature, test section Mach number and model chord. This set point for pressure is estimated continuously. In the Emergency mode, the vent valve 1 is fully opened to relieve the tunnel of all the pressure.

The fan control loop has three modes of operation Speed and Mach number and Emergency. In the Speed control mode, the operator commands a desired fan speed which is the set point for the speed control loop. This control works in the range 600-5600 rpm with a restriction of 100 rpm/s ramp rate limitation. In the Mach number control mode, the speed control loop set point is generated by the Mach control law. In an automatic Mach number control mode, tunnel choking results in a runaway condition due to loss of pressure ratio control by the fan. Choking is a probable occurrence at transonic speeds and high angles of attack with the flexible solid wall configuration of the 0.3-m TCT. Tunnel choking is identified through the temperature control loop and the Mach mode reverts to Speed control mode with a reduced fan speed command. In the Emergency mode, the control reverts to Speed mode with a fixed set point of 600 rpm which corresponds to the idling speed.

The liquid nitrogen pressure control loop is permanently on an Automatic mode. The liquid nitrogen pressure set point is either from the operator or an automatic choice of about 60 psia higher than tunnel pressure.

5.2 Controller Mechanization

The control functions have been realized on a Personal Computer type 16 bit 16 MHz clock microcomputer working on DOS operating system. The microcomputer uses an analog to digital conversion (ADC) input card with 8 channels of floating inputs, and digitizes the signals to 16 bit resolution which is considered essential for cryogenic tunnel use. The system output is through a digital to analog conversion (DAC) device with 8 channels output based on a 12 bit resolution. The standard keyboard constitutes the tunnel operators input and the standard color monitor provides the continuous display of the tunnel control status. Figure 12 illustrates the schematic diagram for a microcomputer based tunnel controller. All the sensor outputs are signal conditioned for 0-5 VDC inputs to be connected to ADC. For nonlinear signals like the outputs from the thermocouples, the linearization is at the software level. Control laws are estimated in the computer. The controller output commands are generated as 4-20 mA for the pneumatic valves and 0-5 VDC for electrohydraulic valves and the fan rheostat position servo set point drive.

The software is written in a higher level language and is compiled to generate an executable code. The software is in seven modules. The initialization module is used when the controller is powered, and it reads all the control constants, initializes recursive estimators

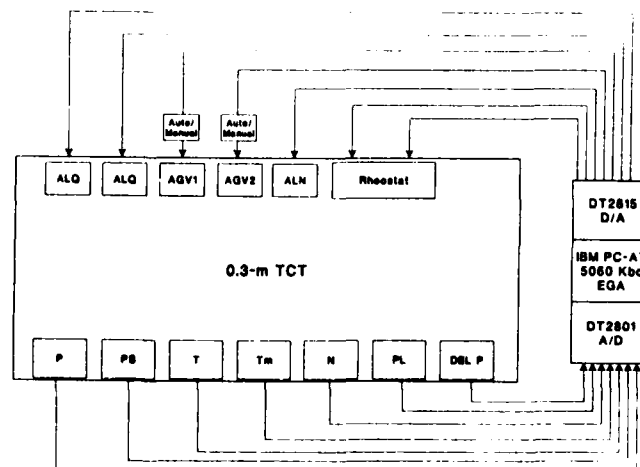


Fig. 12 Schematic for IBM PC-AT based temperature, pressure-Reynolds number and Mach number controller.

and creates a data display format on the monitor. It is executed only once. The ADC module measures the tunnel data and converts to engineering units. If the sensor outputs are out of normal range, the system generates a sensor failure emergency command. The keyboard module looks for operator commands from the keyboard. If any one of the 10 numeric and 12 alpha commands exist, one command per cycle of computation is serviced. The first alpha command defines the control mode or the input variable. This is followed by five numerical commands constituting the four digit and decimal inputs. Six such commands in the proper order allow loading the numerical inputs to the control loops. Provision exists for deleting any input at an intermediate stage. The set point management module executes shaping of all the set point commands based on safety considerations. The control module computes the control law and drives to the various actuators. The display module writes the status of the tunnel states, set points currently used, and the keyboard data as it is loaded. The DAC module generates the commands to the various actuators. The total software of nearly 800 lines of code is executed in about 98 milliseconds for all the five loops. The timing varies by a few percent depending on the software routing, control mode and keyboard activity. The software is in an endless loop and has been tested for more than 5000 hours of continuous operation without numerical failures. All the possible divide by zero and overflow situations have been trapped to prevent computational shutdown. The details of this system are available in reference 9.

6. CONTROL PERFORMANCE

The microcomputer based tunnel controller has been exhaustively tested and operated for over 5000 hours. The system has globally stable control and accepts set point commands of all combinations and magnitude within the operating envelope of the tunnel.

6.1 Controller Performance for Large Set Point Commands

Figure 13 illustrates an automatic cooldown of 0.3-m TCT from 300 to 100 K at a constant pressure of 30 psia and constant Mach number of 0.440. The set point for temperature is changed from 300 to 100 K at 50 seconds. Initially the gas cools at a rapid rate of about 20 K/minute till the metal-gas temperature difference grows to about 40 K.

Then the gas temperature automatically follows the metal cooling rate of 3.6 K/minute and reaches 100 K in about 3000 seconds. The pressure and Mach number are held to ± 0.07 psia and ± 0.002 of the set points, throughout the period of cooldown. The fan speed is continuously adjusted automatically to hold the Mach number. Once the tunnel conditions are stabilized at 100 K, aerodynamic test activity involving large pressure changes to 50, 75, 40 psia, and Mach number changes to 0.800, 0.250, and 0.500 are shown during next 2000 seconds. The aerodynamic testing includes angle of attack changes, drag rake traverse and flex wall movement. The controller performance demonstrates very little cross coupling and very stable behavior. At 5200 seconds the tunnel has been warmed up at two Mach numbers of 0.600 and 0.700. The tunnel pressure has slowly leaked away during warmup. The mass control algorithm has not been invoked during this period.

6.2 Controller Performance for Small Set Point Changes and Geometrical Disturbances

In figure 14, the closed loop response of the tunnel to temperature step from 231 to 227 K and back to 233 K is illustrated. The temperature response time is about 15 seconds, and during this period the tunnel pressure is held stable to ± 0.07 psia of the set value of 68 psia. The flow Mach number remains within ± 0.002 of the set value of 0.760.

Figure 15 shows the closed loop tunnel response to a pressure step from 68 to 64 psia and back to 68 psia. The pressure control faithfully follows the set point command. The tunnel temperature shows a transient coupling of about 1.5 K and a Mach number change of 0.03 during the period of pressure change. The measured Mach number disturbance is most likely due to delays in the pressure sensors used in pressure measurement than to the actual process response. In any case, the Mach number settles down to within ± 0.002 of the set value within about 8 seconds.

Figure 16 shows the response of the tunnel to Mach number set point step from 0.760 to 0.730 while the tunnel is on Reynolds number hold mode. The tunnel Mach number responds to within about 10 seconds and settles to within ± 0.002 of the set value. The tunnel pressure set point is automatically changed from 68 to 70 psia, based upon an estimated set point for pressure loop as in equation (7). The tunnel flow Reynolds number is held to within ± 0.03 of set value of 20 million/chord. The fan speed is automatically adjusted to achieve the set point Mach number.

The tunnel control response to geometrical disturbances in the test section caused by angle of attack change and drag rake movement in the wake of a CAST 10 model is shown in figures 17, 18 and 19. The angle of attack change from 2° to 0° of a 9 inch chord model in the 0.3-m test section is quickly corrected by the controller as illustrated in figure 18. The Mach number shows a transient increase which is adjusted by fan speed reduction to correct for the reduced blockage. A drop of 200 rpm occurs for the 2° change of angle of attack. For drag rake movement in the

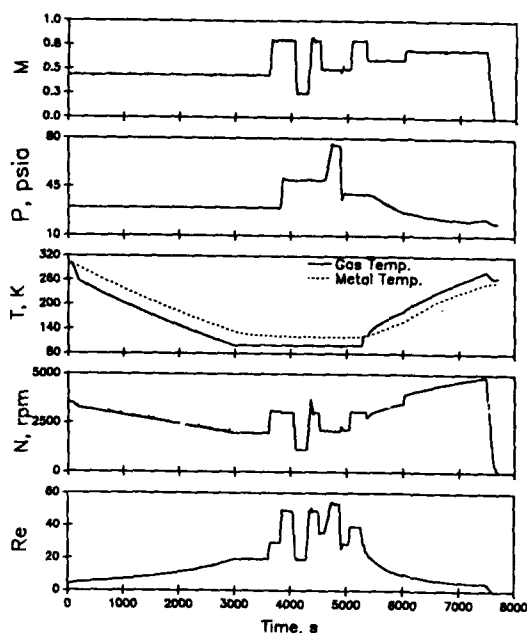


Fig. 13 Response to large set point change during cooldown and warmup at constant Mach number.

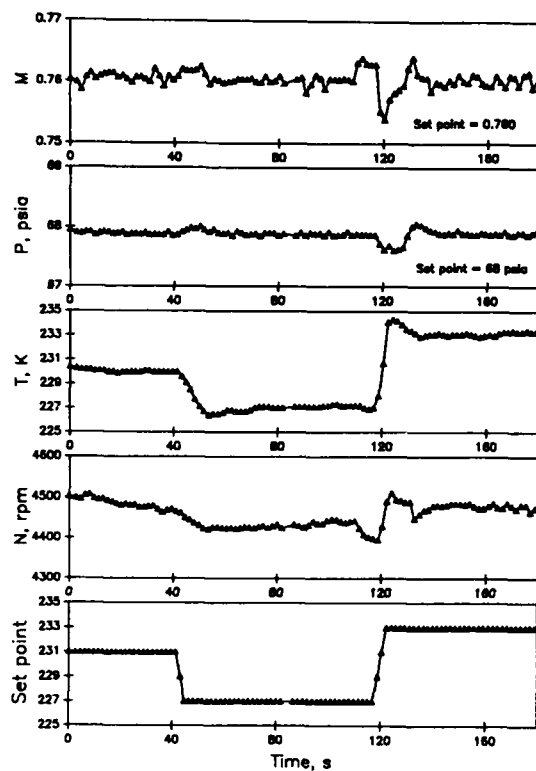


Fig. 14 Tunnel response while in closed loop control to temperature set point command change. Drag rake traverse. (4.4 to -2.8 inches) CAST 10 model, $\alpha=0^\circ$.

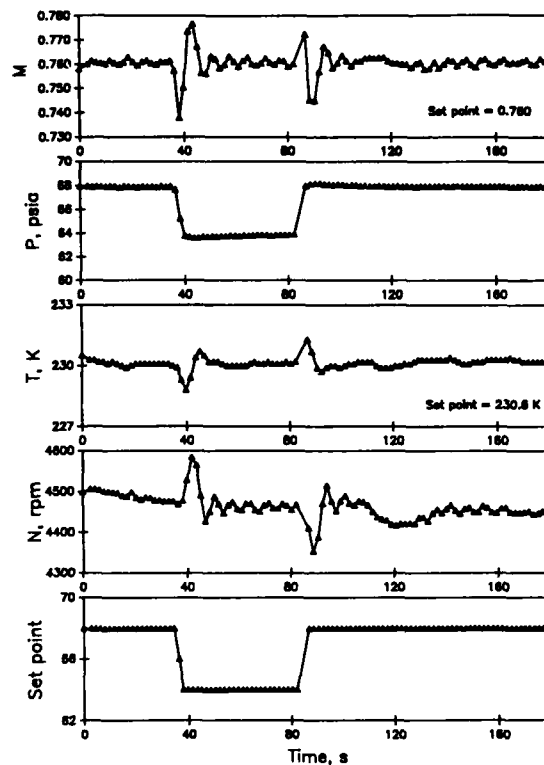


Fig. 15 Tunnel response while in closed loop control to pressure set point command change. Drag rake traverse. (4.4 to -2.8 inches) CAST 10 model, $\alpha=0^\circ$.

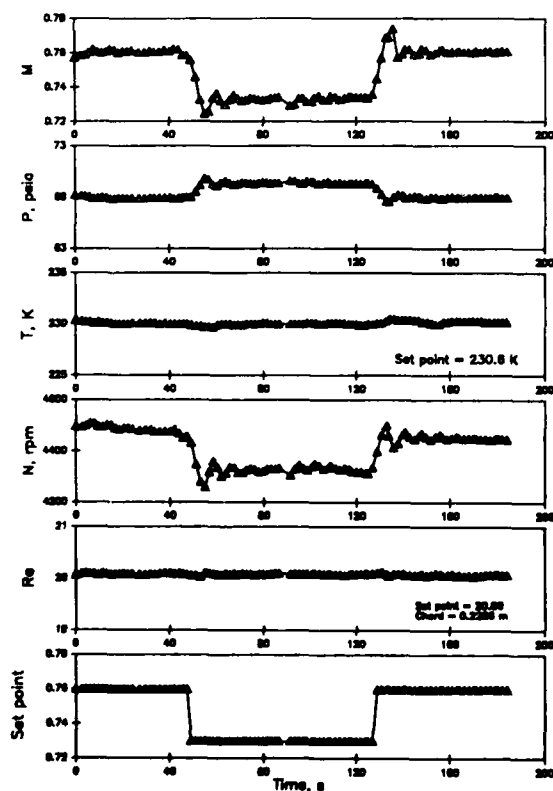


Fig. 16 Tunnel response while in closed loop control to Mach number set point change. Drag rake traverse. (4.4 to -2.8 inches) CAST 10 model, $\alpha=0^\circ$.

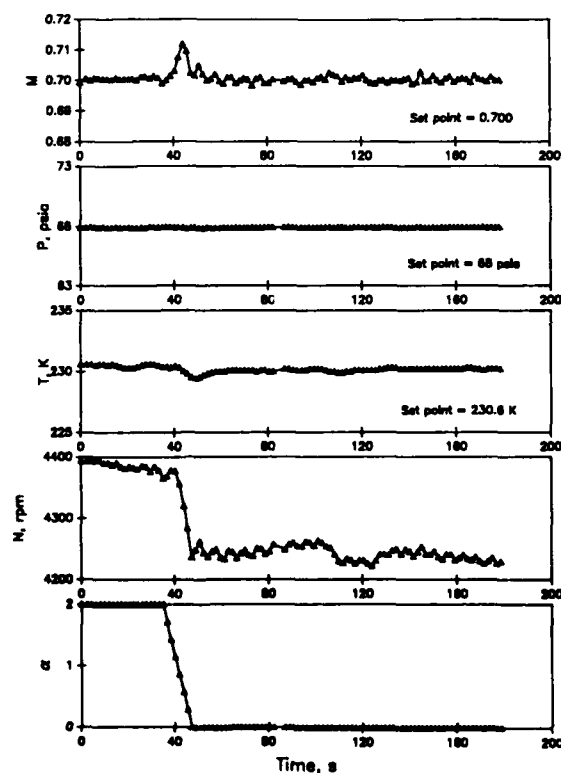


Fig. 17 Tunnel response while in closed loop control to changes in angle of attack. Drag rake traverse. (4.4 to -2.8 inches) CAST 10 model.

wake of the model, the rake blockage effect is reduced when in the wake flow of the model. The resultant Mach number increase is corrected by reduction of fan speed and this shows up as a trough in the fan speed vs time plot of figure 18. This feature has been found to repeat in all the transonic drag rake traverse conditions.

Figure 19 shows the tunnel response to solid top and bottom flexible wall movement from an unstreamlined condition to streamlined condition involving nearly 1 inch adjustment of the wall near the model. The decreased blockage due to streamlining is evident in the reduction of the fan speed by nearly 300 rpm to hold the Mach number. The tunnel controller is thus able to correct dynamically all the disturbances caused by the geometrical variation in the test section due to intrusive data acquisition based mechanisms.

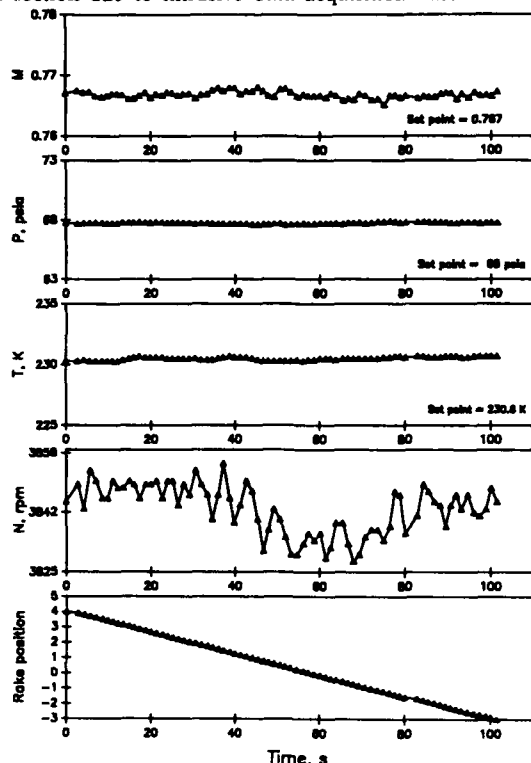


Fig. 18 Tunnel response while in closed loop control to disturbances caused by drag rake traverse. CAST 10 model, $\alpha = 1.8^\circ$, walls streamlined.

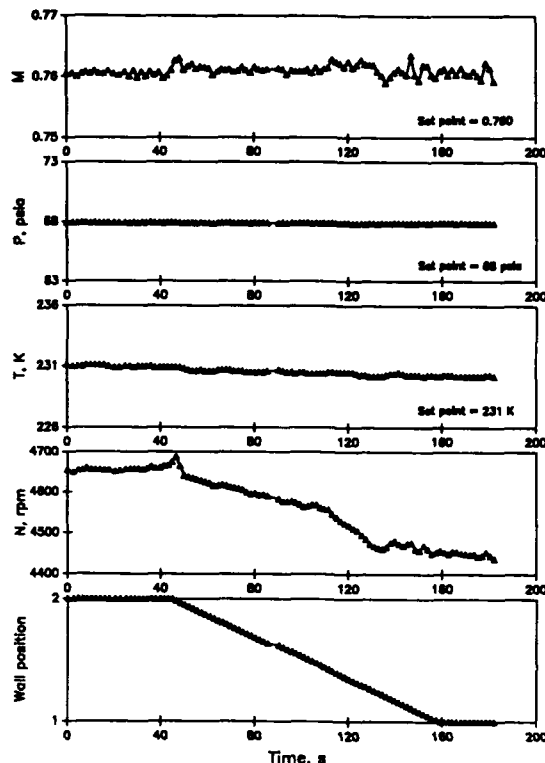


Fig. 19 Tunnel while in closed loop control to disturbances caused by wall shape change. Drag rake traverse. (4.4 to -2.8 inches) CAST 10 model, $\alpha = 0^\circ$.

6.3 Effect of Sidewall Boundary-Layer Removal on Control

The 0.3-m TCT has an active sidewall boundary-layer removal system capable of removing 4 to 10% of the test section mass flow from the sidewall and reinjecting the same back to the tunnel circuit at the diffuser as illustrated in figure 20. This sidewall flow treatment assists in delaying the onset of separation both at the tunnel walls and the model. The mass flow removal and reinjection require a pressure rise through the external compressor and is associated with temperature rise. The compressor pressure ratio required is a function of the tunnel flow Mach number and the sidewall mass flow and can be expressed as (ref. 10):

$$\text{compressor pressure ratio} = \frac{P_d}{P_s} \left\{ 1 - k \left(\frac{\dot{m}_{bl}}{\dot{m}_t} \right)^2 M^2 (1 + 0.2 M^2) \right\}^{-1}$$

The compressor energy manifests itself as an enthalpy disturbance to the tunnel control. The 0.3-m TCT tunnel temperature control law can adequately compensate for this disturbance without the need for an extra cooling in the compressor circuit. Figure 21 illustrates a time trajectory of tunnel purge, cooldown of the tunnel, and sidewall boundary-layer removal compressor operation with Mach numbers varying from 0.8 to 0.3 in steps of 0.1. In each Mach number step, \dot{m}_{bl} has been varied from 0.5% to 10% of the test section mass flow. Clearly, the quality of tunnel control is not affected by the active sidewall boundary-layer removal.

7. CONCLUSION

In this paper, the modeling and control issues associated with closed circuit fan driven transonic cryogenic nitrogen pressure tunnel with specific reference to 0.3-m TCT has been discussed. The 0.3-m TCT is modeled as a nonlinear coupled dynamical system dominated in pressure and temperature by isothermal like slow thermodynamic interaction and by the tunnel structural enthalpy within the insulation shell. The pressure and temperature dynamics are shown to be dominantly a quasi-static process with strong cross coupling. The flow Mach number dynamics of a cryogenic tunnel is not very different from any other closed circuit tunnel and is sensitive to test section geometry. Combination of small

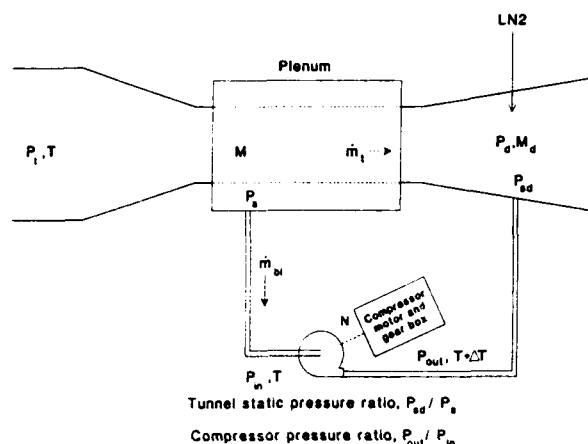


Fig. 21 Response to large set point changes during cooldown and boundary layer system mass-enthalpy disturbances.

1. Balakrishna, S. and Thibodeaux, J.J.: Modeling and Control of a LN₂-GN₂ Operated Closed Circuit Cryogenic Wind Tunnel : Paper No. 23 ; First International Symposium on Cryogenic Wind Tunnels. Southampton. UK. April 3-5, 1979, pp 23.1 to 23.11.
2. Gumas, G.: System Analysis - A dynamic Model of the National Transonic Facility. Pennsylvania State University. December 1976.
3. Tripp, J.: Development of a Distributed-Parameter Mathematical Model for Simulation of Cryogenic Wind Tunnels. NASA TP 2177, September 1983.
4. Balakrishna, S.: Synthesis of a Control Model for a Liquid Nitrogen Cooled, Closed Circuit, Cryogenic Nitrogen Wind Tunnel and its Validation. NASA CR 162508. February 1980.
5. Thibodeaux, J.J. and Balakrishna, S.: Development and Validation of a Hybrid-Computer Simulator for a Transonic Cryogenic Wind Tunnel. NASA TP 1695, September 1980.
6. Palancz, B.: Analysis of the Performance of a Liquid Nitrogen Cooled, Closed Circuit, Cryogenic Nitrogen Wind Tunnel and its Application to DFVLR's 3 M-Tunnel in Cologne. DFVLR IB-WKT 8/80.
7. Balakrishna, S.: Minimum Energy Test Direction Design in the Control of Cryogenic Wind Tunnels. NASA CR 163244. June 1980.
8. Tripp, J.: An Algorithm for Minimum-Cost Set Point Ordering in a Cryogenic Wind Tunnel. NASA TP 1923. November 1981.
9. Balakrishna, S. and Kilgore, W. Allen: Microcomputer Based Controller for the Langley 0.3-m Transonic Cryogenic Tunnel. NASA CR 181808, March 1989.
10. Balakrishna, S.; Kilgore W. Allen and Murthy, A.V.: Performance of the Active Sidewall Boundary-layer Removal System for the Langley 0.3 - Meter Transonic Cryogenic Tunnel. NASA CR 181793, February 1989.

9. ACKNOWLEDGEMENTS

The author is grateful to NASA for permission to present this lecture. He also wishes to thank Dr. Robert A. Kilgore and Mr. Edward J. Ray for their support in the 0.3-m TCT work. In particular, the author is indebted to W. Allen Kilgore for help in documentation of this work.

EXPERIENCE WITH STRAIN-GAGE BALANCES FOR CRYOGENIC WIND TUNNELS

M. Susan Williams
NASA Langley Research Center
Hampton, Virginia 23665-5225, U.S.A.

Introduction

The U.S. National Transonic Facility (NTF) is a cryogenic wind tunnel built to meet the United States' needs for high Reynolds number testing. The facility was declared operational in August 1984, and since that time numerous models have been tested in the NTF using unheated strain-gage balances to measure aerodynamic forces.

The difficulty in accurately measuring forces and moments of models in conventional wind tunnels becomes more challenging at cryogenic conditions. The Force and Strain Instrumentation Section of the Instrument Research Division at NASA Langley Research Center designed and fabricated the balances to measure forces at cryogenic temperatures without thermally controlling the balance temperature. Presented in this paper are balance results from a recent cryogenic test program in the NTF. The data indicated the accuracy with which aerodynamic forces are determined using current instrumentation and test methods as well as identified areas for future research.

Accuracy Requirements

To achieve the largest range of Reynolds numbers, the NTF operates at temperatures from cryogenic to ambient (from about 100 K to 300 K) and pressures from atmospheric up to 130 psia. When the higher Reynolds numbers are achieved (Re up to about 120 million at Mach 1.0) through increases in pressure, there are accompanying increases in balance loads. Under these conditions it is not feasible to have a single balance with the strength to match the maximum loads and the sensitivity required for accurate data at the minimum loads.

With the current balance technology, the accuracy quoted for NTF balances is $\pm 0.5\%$ of maximum balance design loads. It is necessary to have the axial force design loads to be at least 10% of the normal force design loads in order to achieve calibration repeatability.¹ However, when the balance is sized for normal force requirements, it is impossible to obtain drag resolution on the order of one drag count, which is desired by some users of the NTF.

A recent test of a transport airplane model in the NTF expected loads as high as 6500 lb of normal force and 13,000 in-lb of pitching moment. The NTF-113 balance was chosen since its design loads met these load requirements and also offered the most sensitive axial section available (400 lb maximum load). With an accuracy level of $\pm 0.5\%$ of design load, the axial force uncertainty was ± 2 lb. In the wind tunnel test of this model at the flight cruise Mach number and Reynolds number test condition, this uncertainty was equivalent to ± 3 drag counts.

To better understand and define the operating characteristics of an NTF balance, an extensive study was undertaken using the NTF-113 balance to identify accuracy associated with cryogenic testing in the NTF. Before completing this study, the NTF-113 balance was damaged as a result of an equipment failure in the model preparation area. The NTF-113 balance was replaced with the NTF-101B balance. The NTF-101B balance has the same design loads except for the axial component, which is rated at a maximum load of 700 lb. Axial force resolution is ± 3.5 lb or approximately ± 5 drag counts for the same transport model at the cruise test condition. Maximum design loads for both NTF-113 and NTF-101B are presented in Table 1. The following text outlines the method used for acquiring force data in the NTF and the results of the study.

Temperature Compensation Algorithms

The strain-gage balances used in the NTF are not thermally controlled. Therefore, the bridge outputs change not only with applied aerodynamic loads but also with thermal loads. Temperature affects apparent strain, sensitivity, and causes false output due to balance mechanical deformation resulting from thermal gradients. The Instrument Research Division at NASA Langley Research Center developed a method to minimize thermally-induced outputs of the bridges.² Corrections for residual apparent strain output of the six bridges are applied in the NTF data reduction program.

The philosophy of the temperature compensation algorithm is to correct all balance readings (wind-off zero, weight tare, and wind-on data) to a reading that would have been measured at the calibration temperature (295 K).³ The general bridge voltage at any temperature is defined in equation 1,

$$V_T = V_{EZ,295} + \Delta V_{EZ,T} + (V_{TARE} + V_{AERO})_T \quad (1)$$

where V_T = measured voltage at temperature T

$V_{EZ,295}$ = bridge electrical zero at 295 K

$\Delta V_{EZ,T}$ = change in bridge electrical zero from 295 K to temperature T

$V_{TARE,T}$ = voltage output due to model weight

$V_{AERO,T}$ = voltage output due to aerodynamic loads

The measured voltage, V_T , is corrected to a value that would have been measured at 295 K ($V_{T,295}$). Equation 1 assumes no interaction changes with temperature, which is supported by the findings of the Instrument Research Division.

The bridge electrical zero at 295 K, $V_{EZ,295}$, is measured for the balance alone prior to model build-up. The change in electrical zero with balance temperature is measured as the balance is cooled from ambient to cryogenic temperatures in a laboratory cryogenic chamber at the NTF. NTF balances are moment type balances with six bridges that are correlated with balance surface temperatures as shown in figure 1. A second order fit is applied to the data obtained during the temperature cycle, and the change in the electrical zero is calculated by the equation,

$$\Delta V_{EZ,T} = C_0 + C_1 T + C_2 T^2 \quad (2)$$

where C_0, C_1, C_2 = second order coefficients

T = balance temperature, K

The load terms in equation 1 are corrected also for gage sensitivity changes with temperature. Laboratory balance loadings indicated that the thermally compensated bridges have a sensitivity shift with temperature, i.e., maximum reduction in gage output is approximately 1.5% for a given load over a temperature range from ambient to near liquid nitrogen temperature. Currently, the sensitivity correction with temperature is a linear term. Future work is needed to determine if a higher order correction better defines the sensitivity change with temperature. The load terms from equation 1 are related to their ambient temperature value in the following manner,

$$(V_{TARE} + V_{AERO})_T = (V_{TARE} + V_{AERO})_{295} * S_C \quad (3)$$

where $S_C = S_T/S_{295}$, ratio of bridge sensitivity at any temperature to bridge sensitivity at 295 K

$S_C = 1 + SS(T-295)$

$SS = [(S_T - S_{295})/S_{295}] [1/(T - 295)], 1/K$

T = balance temperature, K

S_T = bridge sensitivity at temperature T, volts/lb or volts/in-lb

S_{295} = bridge sensitivity at 295 K, volts/lb or volts/in-lb

The SS value for each balance bridge is supplied from the laboratory balance calibration.

A force or moment is calculated from a measured voltage by first calculating the load terms at the measurement temperature from equation 1,

$$(V_{TARE} + V_{AERO})_T = V_T - V_{EZ,295} - \Delta V_{EZ,T} \quad (4)$$

V_T is the measured voltage, $V_{EZ,295}$ is updated with each wind-off zero data point, and $\Delta V_{EZ,T}$ is calculated from equation 2.

$(V_{TARE} + V_{AERO})_{295}$ is calculated using equation 3. The voltage that would have been measured at 295 K is determined by the equation,

$$V_{T,295} = V_{EZ,295} + (V_{TARE} + V_{AERO})_{295} \quad (5)$$

After temperature corrections are applied to both wind-on and wind-off data points, the force (or moment) is calculated by the equation,

$$F \text{ (or } M) = (V_{T,295,\text{wind-on}} - V_{T,295,\text{wind-off}}) * K \quad (6)$$

where F = force, lb

M = moment, in-lb

K = bridge sensitivity at 295 K, lb/volt or in-lb/volt

These values are further corrected for interactions, model weight tares, and base and chamber pressures.

Pre-Test Balance Check-Out

Before a model is tested in the NTF, it undergoes an instrumentation check-out at ambient and cryogenic temperatures in a model preparation area. The model and balance are cooled to temperatures as low as 115 K in the cryogenic chamber (see figure 2) where they are loaded statically to check that the balance is functioning properly through the NTF data acquisition and reduction system.

Prior to model build-up, the balance is cooled from ambient temperature to 115 K and warmed back to ambient temperature. The balance temperature is stabilized at 115 K and also at ambient temperature. During the cryogenic cycle, the outputs of the six balance bridges are recorded and plotted against balance temperature. These data are the basis for the electrical zero corrections discussed in the previous section.

Balance measurement requirements for testing models of the transport type in the NTF led to an investigation of NTF balances to identify and quantify balance measurement errors associated with cryogenic testing. Two NTF balances, NTF-113 and NTF-101B, were used in the study. Data obtained in the cryogenic chamber were used to determine the error due to strain gage electrical zero shift with respect to both the temperature and the balance longitudinal thermal gradients.

Different temperature cycles of the NTF-113 balance indicated that the electrical zero shift for the axial bridge was repeatable to within $1 \mu\text{V/V}$ (0.4 lb.). The NTF-113 balance was cooled at different rates in the various temperature cycles. In temperature cycle 1 as shown in figure 3a, the balance temperature was stabilized at intermediate temperatures between ambient and 115 K. The resulting second order curve fit through the data represented the bridge electrical zero shift once the balance had reached thermal equilibrium. During temperature cycles 2 and 3 as shown in figures 3b and 3c respectively, the balance temperature was stabilized only at ambient temperature and 115 K, and the second order curve fit was applied to these two points and was weighted toward the top curve in order to be representative of the curve in figure 3a. It was determined that a temperature cycle where the balance was brought to thermal equilibrium at ambient and 115 K was sufficient to define the curve for electrical zero shift since the resulting curve fit of the bridge output versus balance temperature was repeatable to within $1 \mu\text{V/V}$ for the different cycles.

When the balance was not at thermal equilibrium, the bridge output deviated from the correction that was calculated by the second order equation. This was particularly true of the axial component because of the balance design.² The result was an error, which either overcorrected or undercorrected the gage output change with temperature. An attempt was made to correlate this error with balance longitudinal thermal gradient. An example is shown in figure 4. The axial bridge output is shown in figure 4a for the NTF-113 balance as it was cooled from 295 K to 130 K, brought to thermal equilibrium at 130 K, and then warmed from 130 K to 295 K. Gradients as large as 17 K were measured between the middle and rear thermocouples during the cycle. The correction for electrical zero shift rotated the curve about the x-axis but did not eliminate the hysteresis loop as shown in figure 4b. Error or difference between bridge output and calculated output is plotted against temperature difference from the middle to the rear of the balance in figure 4c. A third order curve fit was applied to the data such that,

$$\Delta V_{EZG} = C_0 + C_1 \Delta T + C_2 \Delta T^2 + C_3 \Delta T^3 \quad (7)$$

where ΔV_{EZG} = change in bridge electrical zero due to balance thermal gradient, volts

C_0, C_1, C_2, C_3 = third order coefficients

ΔT = balance temperature gradient, $T_2 - T_3$, K

This correction was applied then to the measured balance output and collapsed the original loop to within $\pm 1 \mu\text{V/V}$ of the value that would have been measured at 295 K as shown in figure 4d. This method was tried using the temperature gradient from front to rear on the balance also. For any given temperature cycle, this method collapsed the data to within $\pm 1 \mu\text{V/V}$. However, the error correction varied from one cycle to the next and was configuration dependent. The longitudinal balance temperatures that were measured did not provide adequate information to correlate temperature gradient effects with balance output. At this time, a correction for balance temperature gradient is not being used at the NTF.

Balance error resulted if the instrumentation leads across the balance were not carefully installed. Earlier unpublished balance research at the NTF by Peter F. Jacobs and Alice T. Ferris showed that by using wiring with thinner insulation as well as minimizing the number of wires across the balance, apparent strain curves were achieved for the model/balance with instrumentation wires that were nearly identical to those for the model/balance alone. Much care was taken when installing the wires across the balance to insure sufficient slack for contraction with cold temperatures. When the model, balance, and instrumentation build-up was completed, the entire configuration was put through another temperature cycle to insure that the wiring and instrumentation had a minimal effect on the electrical zero shift of the gages. Shown in figure 5 are the changes in the six balance bridges versus balance temperature for the NTF-101B balance alone and again in figure 6 with the model on the balance and the instrumentation wiring and pressure tubing spanning the balance.

In a separate temperature cycle, the model was loaded statically after the balance temperature had stabilized at 115 K. The data from the static loading of the NTF-101B indicated that the balance accuracy was within $\pm 0.5\%$ of the balance design loads.

After the temperature compensation information for the balance had been collected and all instrumentation systems had been shown to work satisfactorily, the model was moved to the NTF test section. The pre-test check-out in the test section was limited to ambient conditions.

Balance Characteristics in the NTF

Since the variation in the electrical zero shift from one temperature cycle to another in the cryogenic chamber was on the order of the required accuracy for the axial bridge and the attempt at correcting bridge output as a function of temperature instability was unsuccessful, the following approach was taken for testing in the NTF:

1. Wind-off zero data points were taken before and after a series of runs with the three balance temperatures at the required test temperature and with the difference between any two of these temperatures less than 1.7 K.
2. Balance wind-off and wind-on data were corrected for electrical zero shift and sensitivity change with temperature but not for temperature gradient.

With the procedure of taking wind-off zero and wind-on data points at the same temperature, the temperature correction for zero shift was voided, and the only temperature correction was for sensitivity shift.

The disadvantage to this approach was that it was costly. Generally, it took an additional 1.5 hours and many tons of liquid nitrogen to stabilize the balance at the test temperature once the airstream total temperature had reached the test condition. This reduced the number of polars that were obtained per tank of liquid nitrogen. However, this approach provided wind-off data taken during the test program for comparison with data taken in the cryogenic chamber. It also provided information on the stability of the electrical zeroes taken before and after a series of polars.

Shown in figure 7 are the outputs of the six balance bridges versus balance temperature for the NTF-101B. These data were taken in the tunnel over a two month period, which began after the model was moved from the preparation area to the test section. In each case, the difference between any two of the three balance temperatures was less than 1.7 K. The data points were taken both before and after a series of data runs at a given temperature. With the exception of the rolling moment, all gage outputs followed the same trend as the temperature correction curve established during model build-up and check-out (see figure 6 for comparison). However, there was significantly more scatter in the tunnel data. For an unknown reason, the rolling moment bridge was the mirror image of the data obtained during testing in the cryogenic chamber. The normal1 bridge actually shifted levels over the two month period, which is not obvious from the plot. The data taken in the 300 to 320 K range were taken early in the test program; the ambient electrical zero had actually shifted to a level shown by the dashed circle on the graph by the end of the test program. The post-test inspection of the balance in the laboratory found a resistance to ground with the normal1 bridge, which accounts for the large voltage shift.

An examination of the change in bridge electrical zeroes from an initial wind-off point taken prior to a series of polars to a final wind-off point taken at the conclusion of a set of runs showed shifts that were in the same direction and fairly repeatable throughout the entire test. The average change for each bridge of the NTF-101B is presented in Table 2. Duration of data runs, Mach number, or test temperature did not appreciably influence the change. Reducing the data with an initial or final wind-off zero had an effect that is shown in figure 8. A difference of approximately 5 drag counts existed when each of the four consecutive runs in figure 8 were reduced using initial and final wind-off zeroes. The reason for the shift was unknown. However, the shift must have occurred between the initial wind-off zero and the first run or between the last run and the final wind-off zero; since, there was no evidence of a gradual change over the four runs.

It is not known which wind-off point is more accurate or representative of the wind-on data. Instinctively, it is felt that the final wind-off zero is better because of the testing method used at the NTF. Typically, the balance is not heavily loaded while cooling to test temperature. After the initial wind-off zero is taken, the tunnel is brought on line and stabilized at test conditions. This process takes on the order of 30 minutes, and during this time the balance is heavily loaded for 5 to 10 minutes. Typically, the final wind-off zero is taken within 5 minutes of the last polar; and therefore, may be more representative of the balance electrical zero during test runs. However, at this time unless a wind-off point is obviously in error, the method for data reduction is to reduce the first half of a run series with the initial wind-off zero and the second half with the final wind-off zero.

Balance repeatability was within the quoted accuracy of $\pm 0.5\%$ of balance design load. Shown in figure 9 are repeat runs over a large Reynolds number range. The repeat runs were taken on different days, and the worst offset was in the order of 5 drag counts between runs 161 and 175. This offset would not have existed if run 175 was reduced with the final wind-off zero rather than the initial wind-off zero.

After the test program, the model was moved to the preparation area for post-test check-out. Shown in figure 10 are the balance outputs versus temperature during a post-test temperature cycle in the cryogenic chamber. With the exception of the normal1 bridge, there was good repeatability with the pre-run data (see figure 6). The normal1 bridge output was similar to the pre-test value except for a level shift, which was attributed to the grounding problem.

Concluding Remarks

Unheated strain-gage balances are being used in the NTF for testing of models at cryogenic conditions. Recent test programs indicated that with current balance technology and temperature compensation methods, model forces and moments are measured to within $\pm 0.5\%$ of maximum balance design loads. Many users of the NTF desire measurement accuracy in the range of $\pm 0.1\%$ of maximum balance design loads, especially in the axial direction.

In an effort to obtain more accurate balance data, additional research is needed to:

1. Establish better electrical zero stability of the bridge at any given temperature.
2. Establish better repeatability of the apparent strain curves as determined at different times and locations (i.e., tunnel, cryogenic chamber in the model preparation area, and balance laboratory).
3. Further check linearity of bridge sensitivity with temperature.
4. Determine if there are better balance temperature gradient measurement locations and corresponding corrections.
5. Obtain a data base in the NTF tunnel of balance output at cryogenic temperatures without instrumentation leads spanning the balance and develop better ways to carry instrumentation leads across the balance without appreciably loading the balance.

References

1. Ferris, A.T.: Status Report on Cryogenic Force Balances for the U.S. NTF, Lecture No. 19 presented at AGARD lecture series Advances in Cryogenic Wind Tunnel Technology, Rhode-Saint-Genèse, Belgium, June 5-9, 1989.
2. Ferris, Alice T.: Cryogenic Strain Gage Techniques Used in Force Balance Design for the National Transonic Facility. NASA TM 87712, May 1986.
3. Foster, Jean M.; and Adcock, Jerry B.: User's Guide for the National Transonic Facility Data System. NASA TM 100511, December 1987.

Table 1.- Balance design loads.

<u>Maximum Design Loads</u>	<u>NTF-113</u>	<u>NTF-101B</u>
Normal Force (lbs)	6,500	6,500
Pitching Moment (in-lbs)	13,000	13,000
Axial Force (lbs)	400	700
Rolling Moment (in-lbs)	9,000	9,000
Yawing Moment (in-lbs)	6,500	6,500
Side Force (lbs)	4,000	4,000

Table 2.- Average Change in Initial and Final Wind-off Zeroes for NTF-101B.

<u>Balance Bridge</u>	<u>Average Change in Wind-off Zero</u>		
	<u>μV/V</u>	<u>lbs</u>	<u>in-lbs</u>
Normal1	4.7	15	43
Normal2	1.5	5	14
Axial	2.6	2	-
Rolling Moment	1.3	-	16
Side1	2.6	5	16
Side2	4.7	10	28



Balance Component	Temperature Correlation
Normal1	T3
Normal2	T1
Axial	T2
Rolling Moment	T3
Side1	T3
Side2	T1

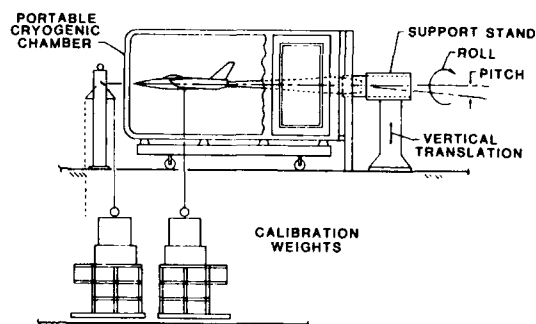


Figure 1.- NTF balance temperature measurement location.

Figure 2.- Model checkout equipment and cryogenic chamber.

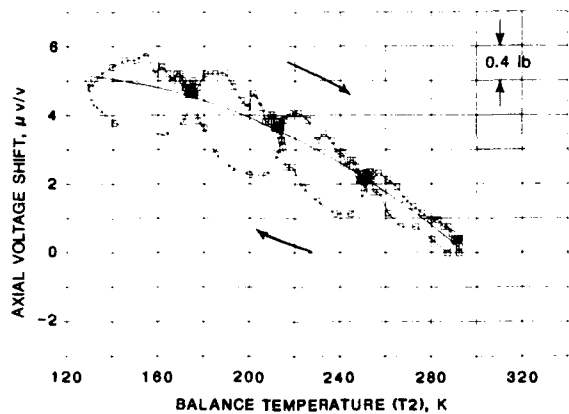


Figure 3a.- Temperature cycle 1.

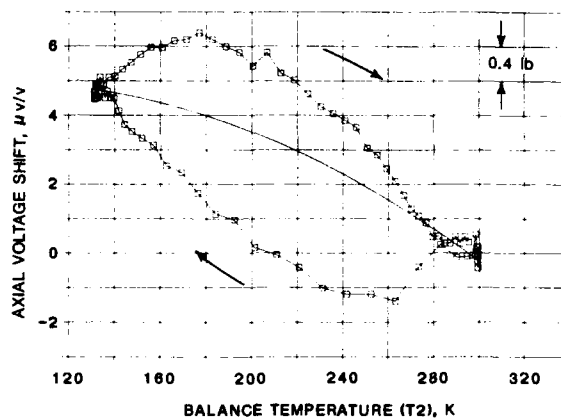


Figure 3b.- Temperature cycle 2.

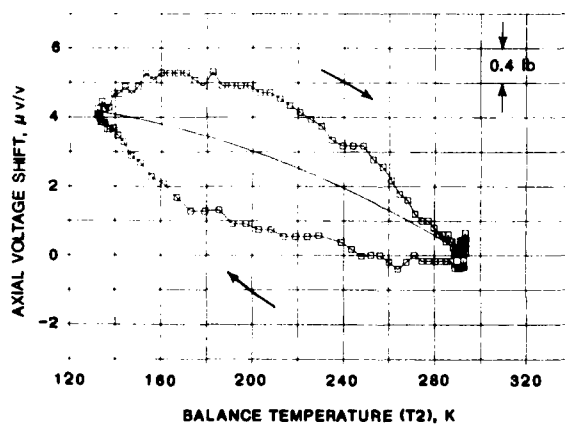


Figure 3c.- Temperature cycle 3.

Figure 3.- NTF-113 balance axial voltage versus balance temperature for three temperature cycles.

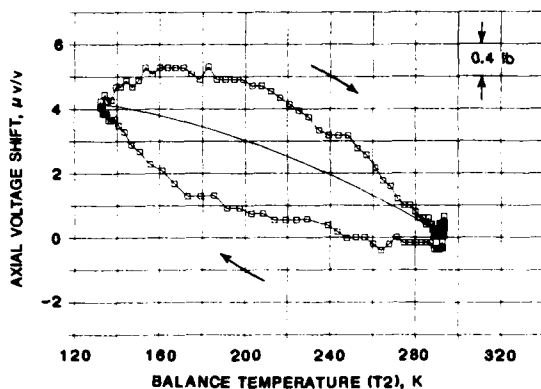


Figure 4a.- NTF-113 balance axial voltage shift versus balance temperature.

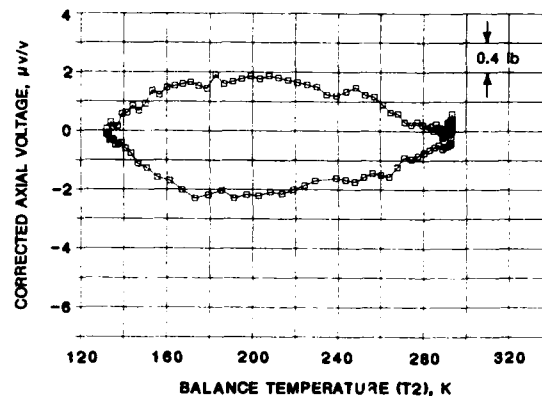


Figure 4b.- Axial voltage corrected for zero shift.

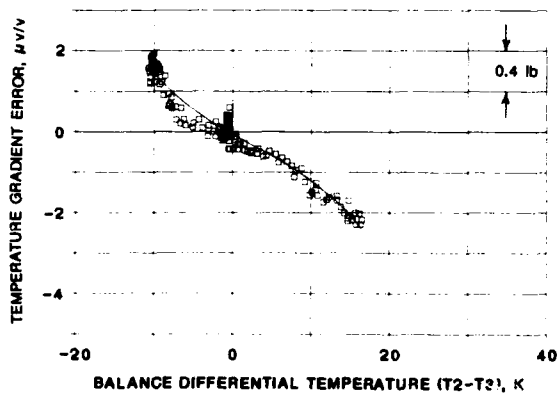


Figure 4c.- Axial output due to balance temperature gradient.

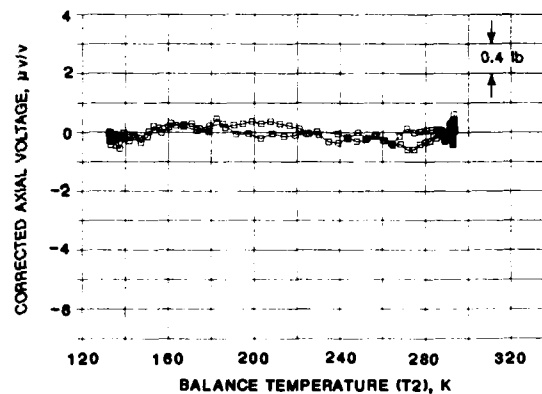


Figure 4d.- Axial voltage corrected for zero shift and balance temperature gradient.

Figure 4.- Correction of axial voltage for balance temperature gradient.

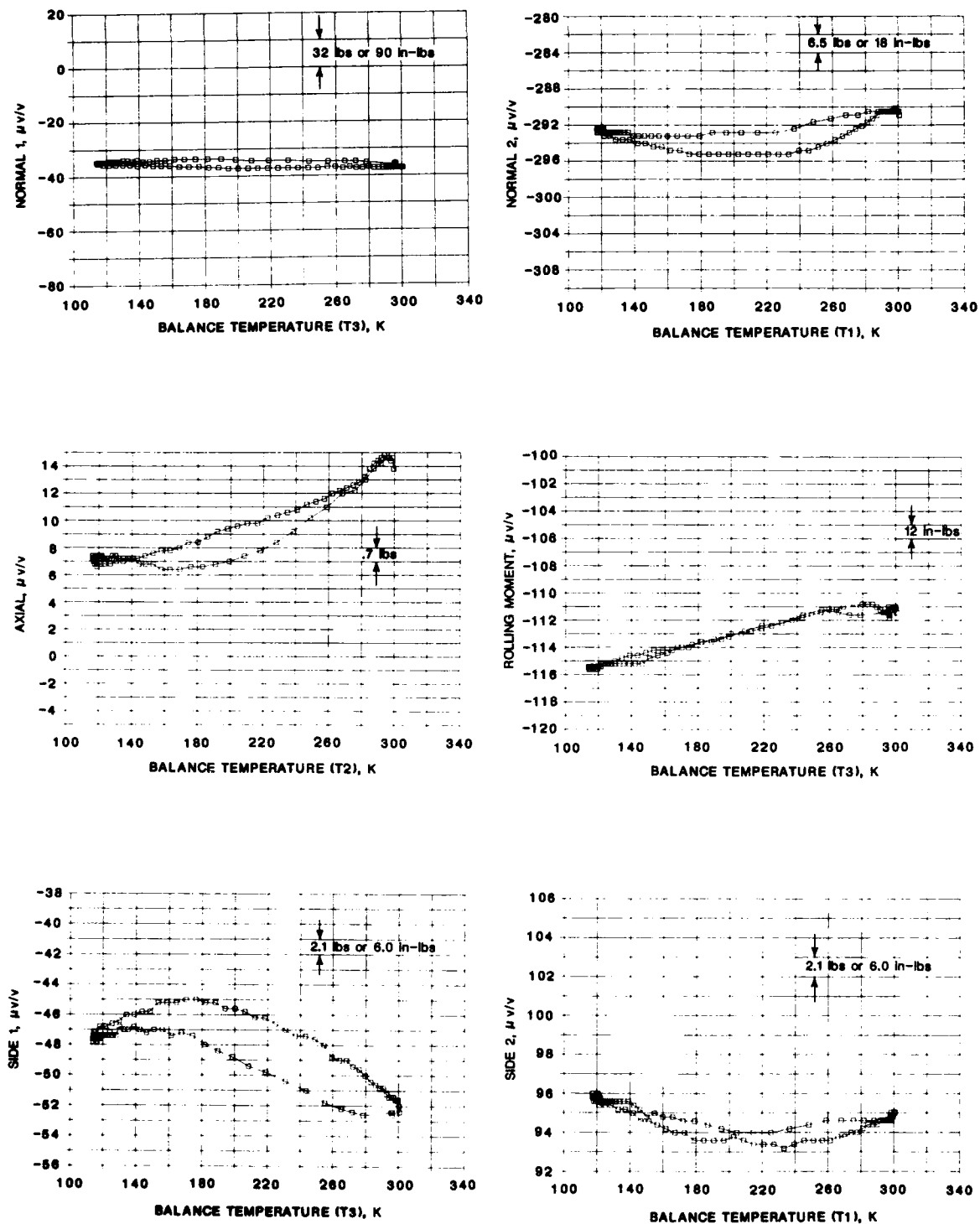


Figure 5.- NTF-101B balance temperature cycle.

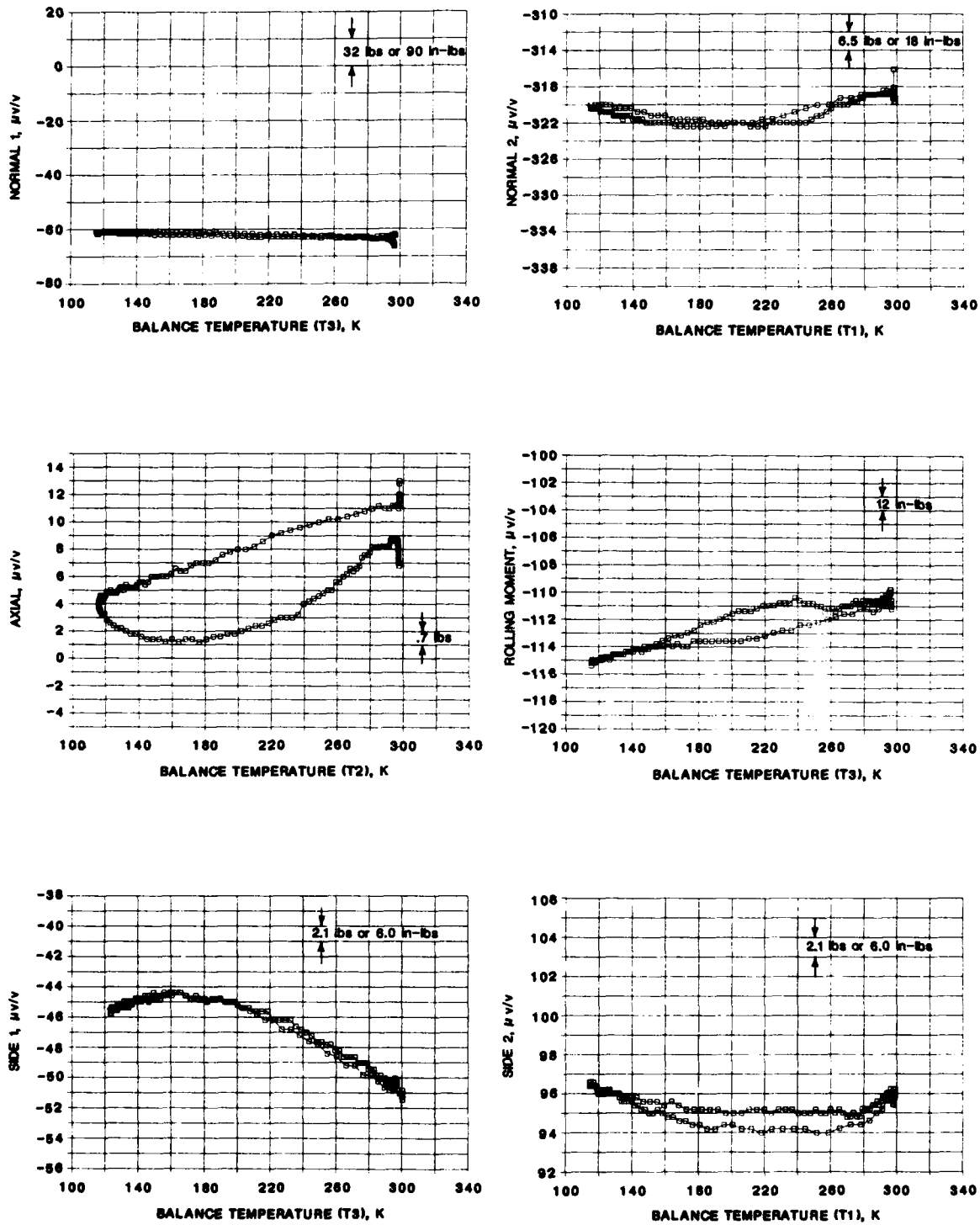


Figure 6.- NTF-101B balance temperature cycle with model on balance and all instrumentation leads across balance.

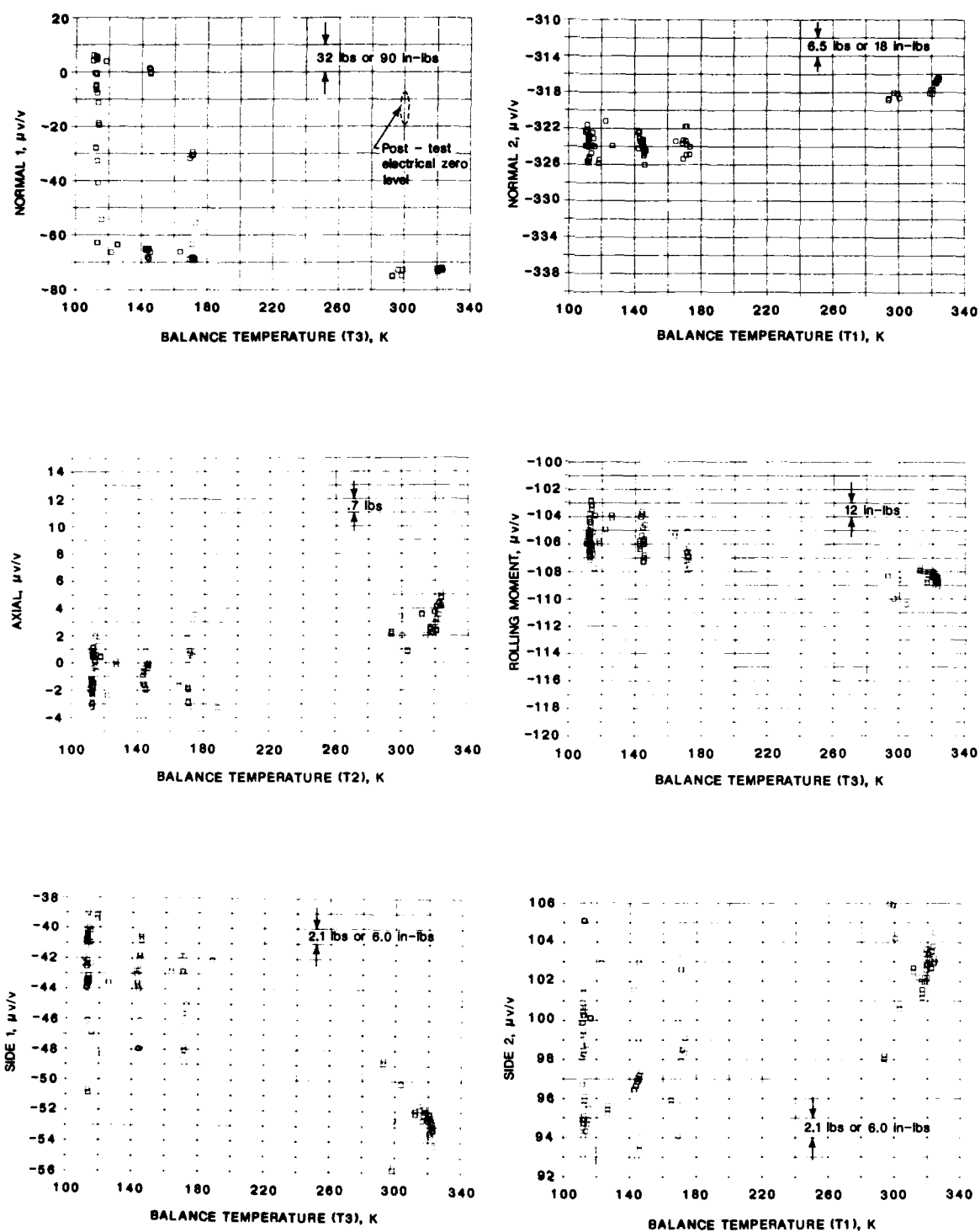


Figure 7.- NTF-101B balance wind-off zeroes taken during test program.

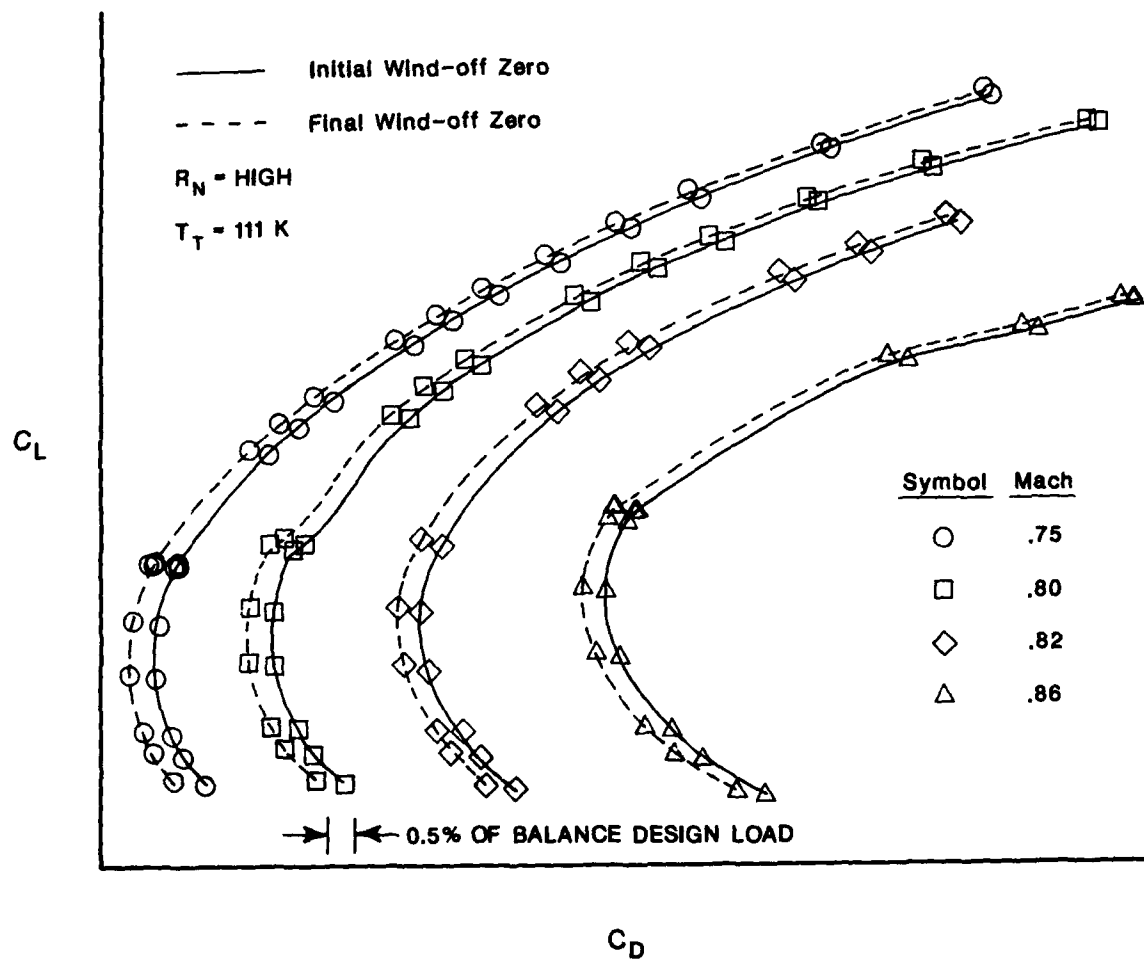


Figure 8.- Effect of reducing data with initial and final wind-off zeroes.

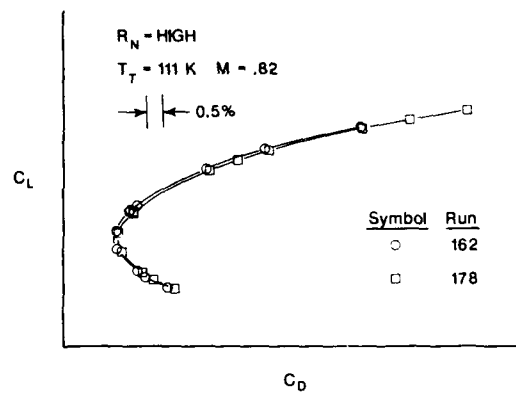
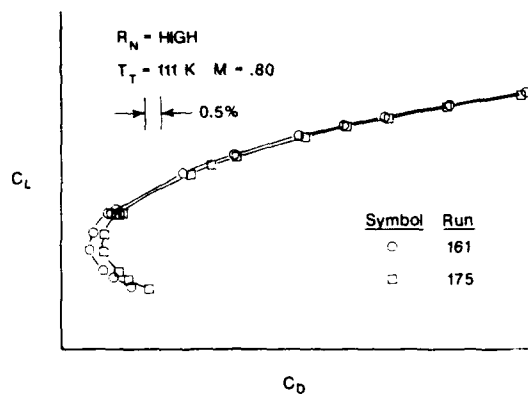
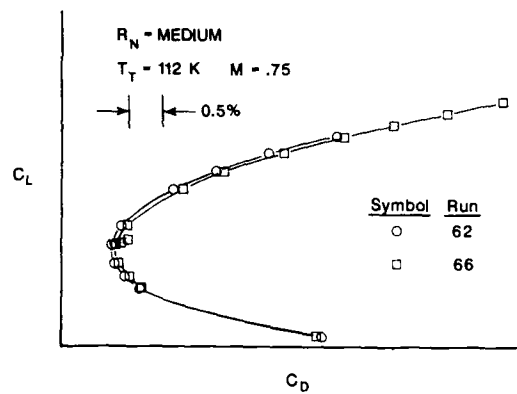
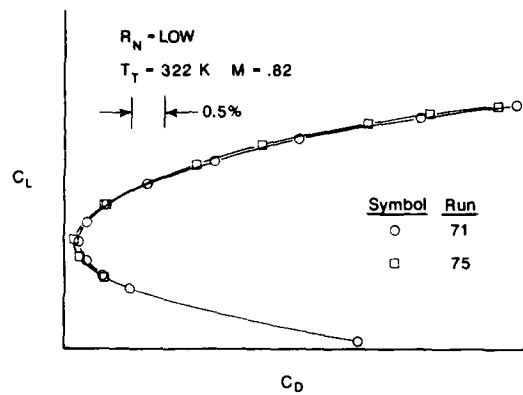


Figure 9.- Balance repeatability over a temperature and Reynolds number range.

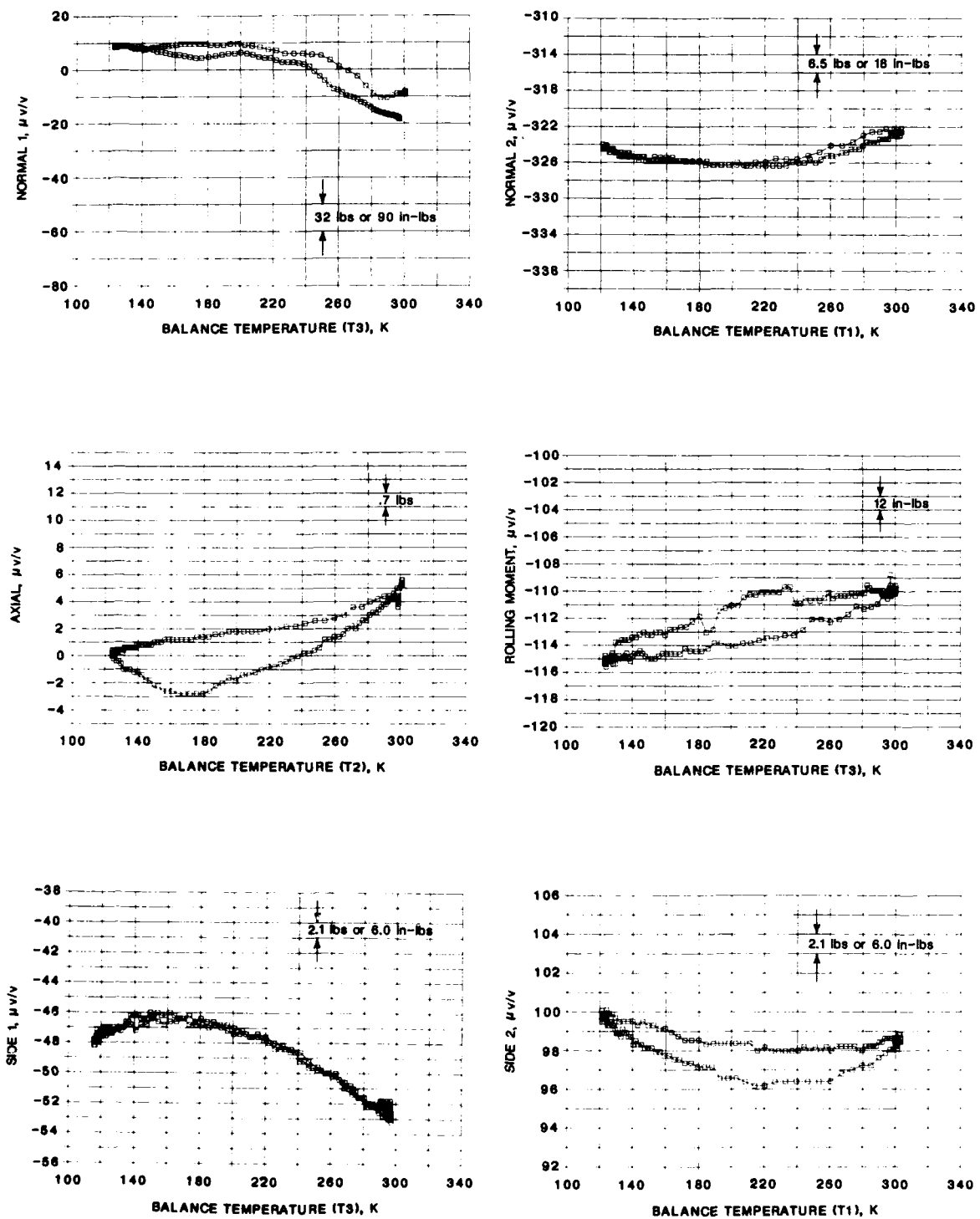


Figure 10.- NTF-101B balance post-test temperature cycle.

STATUS REPORT ON CRYOGENIC BALANCES FOR THE U. S. NTF

Alice T. Ferris
Senior Engineer
NASA - Langley Research Center
Hampton, VA

ABSTRACT

Force balances have been used to obtain aerodynamic data in the National Transonic Facility (NTF) wind tunnel since it became operational in 1983. These balances were designed, fabricated, gaged, and calibrated to Langley Research Center's specifications to operate over the temperature range of -320°F to $+140^{\circ}\text{F}$ without thermal control. This paper will review some of the materials and procedures developed to obtain a balance that would perform in this environment, report on the degree of success in using these balances thus far, specify some of the problem areas that need additional work and describe some of the progress addressing these problems.

INTRODUCTION

Since the early 1970's the cryogenic wind tunnel has been one of the primary approaches toward achieving higher Reynolds numbers for better flow simulation especially in the transonic range (reference 1). However, operating a wind tunnel at cryogenic temperatures presents additional problems of getting both tunnel and model systems to work reliably and accurately in this severe environment. This lecture will address the problem of getting accurate data from the force balance used to measure the aerodynamic forces and moments on the model.

The aerodynamic forces and moments of models in conventional wind tunnels are usually measured using a strain-gaged force balance. Early tests in cryogenic wind tunnels used conventional balances that were heated with water-jackets or resistance heaters (reference 2). Some of these tests allowed the balance to follow the ambient stream temperature. In these tests, even though there were large zero and sensitivity shifts, the balance did not cease to function. A 0.3 meter pilot cryogenic wind tunnel was built and placed into operation at NASA Langley Research Center in Hampton, VA, in 1973. It was requested that the Force and Strain Instrumentation Section of the Instrument Research Division at NASA Langley Research Center research methods to accurately measure forces at cryogenic temperatures. Since the balance can be smaller and simpler if it is used without thermal control and the early tests indicated that this was a viable course, the initial effort was along this path. This approach entailed determining the effect of temperature on each of the components of the force balance and finding methods of alleviating or compensating for any undesirable thermally-induced output. These studies were quite productive. The results have been previously reported in references 3, 4, and 5.

Briefly, the results of these tests were as follows:

The force balances should be fabricated from high-quality high-strength steels that do not become brittle at cryogenic temperatures. An 18% Nickel, Grade 200 maraging steel was chosen.

Solder for cryogenic use should contain antimony to prevent 'tin' disease.

The wiring should be insulated with TFE Teflon insulation to resist cracking and shrinking at cold temperatures.

Moistureproofing compounds should not be applied over the grid of the strain gages. An acceptable, removeable, 100% effective moistureproofing compound was not established. All of the tested 100% waterproof compounds tended to affect the apparent strain curve (unloaded zero output with temperature) when applied over the exposed thermal compensation wires and jumper wires. A Teflon spray coating originally applied over the entire balance (except the fitting surfaces) to protect against corrosion was found to also provide adequate protection for the exposed thermal compensation wire and jumpers with minimal apparent strain effect.

The strain-gages selected were commercially available karma gages used for conventional room-temperature balances. The self-temperature-compensation (STK) number of the gage was chosen to minimize apparent strain output and sensitivity shift over the temperature range -320°F to $+140^{\circ}\text{F}$. (See figure 1). A gage matching procedure was developed to match the four strain gages prior to permanent installation so inherent thermal characteristics would cancel when placed in a conventional four-active-arm bridge. The gages were installed in a Poisson Ratio configuration (tension and compression gage at 90 degrees adjacent to each other) to minimize thermal gradient effects.

A large axial output was generated when the axial section deformed during thermal gradients. Temperature sensitive wires or grids were placed at each corner of the axial section and incorporated into the axial bridge (Figure 2). The room-temperature resistance of the four wires was adjusted until the differential resistance change in these wires caused by the temperature gradients across the axial section were equal and opposite to that induced by the thermal gradient deformation thus cancelling the effect.

Calibration at cryogenic temperatures was accomplished using flexible hoses to pass liquid nitrogen through passages in cryogenic loading fixtures and supporting stumps (Figure 3). Using this technique, calibrations could be performed using standard calibration labs, equipment, and techniques.

Tests were conducted in the 0.3 meter pilot tunnel using 3-component balances that incorporated these new features. The results of these tests as indicated in figure 4 show that the unheated balance data was as good as that obtained using electric resistance heaters. These test results are presented in reference 6.

In 1978, France, Germany, Great Britain, and the Netherlands joined efforts to develop a cryogenic wind tunnel. Development of cryogenic force measurement techniques was undertaken in Europe by ONERA, NLR, DFVLR, and RAE headed respectively by Messrs. M. Bazin, K. Breman, W. Lorenzmeier, and M. Wood. Generally NLR, DFVLR, and RAE have approached the thermal compensation problem by measuring the thermal gradients and using mathematical algorithms to correct the output. ONERA has taken the same approach as NASA and uses temperature sensitive elements incorporated in the balance circuitry to do the compensation. In the past few years a great deal of work has been done by

Professor Bernd Ewald, recently retired from the MBB and now a professor at the Technical University of Darmstadt (reference 7).

EXPERIENCE IN THE NTF

The NTF has been operational since 1983. There are fourteen balances available for use in the NTF, four of which have been used in models tested in that facility. Ten of these balances are shown in figure 5. With each balance and test considerable knowledge has been gained through experience.

Temperature induced changes in the length and/or stiffness of the wires and tubes passing over the balance to instrumentation in the nose of the Pathfinder I model was measured to be approximately 11 pounds by the balance axial output during early check-out tests (Reference 8). By using thin insulation on the wiring and careful routing of these wires the temperature induced loads were reduced to less than one pound (figure 6).

The ready-bay procedures used to check out the model-instrumentation combination has been covered by my colleague Susan Williams. The repeatability of the balance output during successive thermal cycles in the ready bay is very good when no model or instrumentation changes are made. If a component's output does not have thermal hysteresis the output will repeat within a few microvolts over the entire temperature range under rather severe and different temperature conditions. When thermal hysteresis is present, allowing the balance to soak at temperature shows the output converges to a median value as expected. If the instrumentation is properly selected and installed, if thermal hysteresis is not present in the balance output, and if the data acquired during this check-out remains unchanged when taken into the wind tunnel, then corrections could be applied to the wind tunnel data that could be within the tolerance needed to acquire aerodynamic data of the desired accuracy of one drag count.

Strain gage bridges have always had a small amount of electrical zero drift with time. Because of this drift, wind-off zeros are typically taken at the beginning and at the end of a series of runs during the course of wind tunnel tests. In the NTF this drift as well as the apparent strain, thermal hysteresis, and varying stiffness of wires and tubes over the balance as defined during the ready bay may change during the tests; consequently taking frequent wind-off zeros becomes even more desirable. Cryogenic tunnel conditions, especially pressure and temperature, must be maintained dynamically. When a wind-off zero is taken the tunnel temperature and pressure change rapidly. Therefore the wind-off zero is not taken at a steady state condition nor is it at the desired wind-on conditions. Additionally, the productivity of the tunnel is severely impacted by the amount of time and nitrogen used to get back to set-point after stopping to take a wind-off zero.

The balance used in the Pathfinder I check-out tests was designed and built before the Pathfinder model was built. Thus the design full scale loads of the balance were not chosen to fit a particular test envelope. The 700 pound design axial load was much too large for the Pathfinder test program. One drag count fell inside the noise and calibration accuracy. Later tests of the Pathfinder model used another balance with a 400 pound axial design load. If the design axial load is less than 10% of the design normal force, balance deformation makes calibration repeatability very difficult. Some balances at Langley Research Center do have axial design loads as low as 5% of that of normal force but in all cases these balances are difficult to calibrate and are sensitive to very small misalignments. Because of the large load range of the NTF tunnel the most accurate data would be obtained if several balances were used, each covering a different range of loads.

PROBLEM AREAS THAT NEED IMPROVEMENT

Compensation tolerances will need to be more exacting. The directive given to the strain gage technicians for temperature compensating balances thus far is to correct the apparent strain output to be within ± 25 microvolts of the room temperature zero over the entire temperature range (-270°F to $+140^{\circ}\text{F}$). Experience has shown that the resulting apparent strain curve is repeatable and can be used for correcting the output if it does not exhibit thermal hysteresis i.e. output that is dependent on temperature and time. The cost of the nitrogen used by the NTF in one day waiting for the balance temperatures to stabilize exceeds the estimated cost of the additional gaging effort needed to obtain balance bridges that do not have thermal hysteresis. A new directive will be issued that the apparent strain curve must still be within ± 25 microvolts of the room temperature zero but the thermal hysteresis must be within 10 microvolts of the fit through that curve. This will be accomplished through continuing the compensation procedure until the hysteresis falls inside this tolerance or to regage if further compensation efforts are non-productive.

In order to obtain more accurate force data in the NTF without the necessity of taking frequent wind-off zeros, the effect of each of the following factors on any component should be reduced to less than 2 microvolts/volt.

- 1) The stability of the balance electrical zero in an eight hour period at a constant temperature
- 2) The repeatability of the apparent strain curves (especially predicting the tunnel zero from the apparent strain curve obtained in the ready bay)
- 3) The thermal hysteresis of the balance output with thermal gradients as large as 50°F .
- 4) The thermal hysteresis induced by the instrumentation wires and tubes passing over the balance as well as the changes that occur in these wires and tubes under varying tunnel conditions such as vibration, temperature, and internal air flow.
- 5) The effect of model configuration such as seals, baffles, etc.

If this tolerance cannot be met, the acquired data will not be accurate enough to detect some of the small differences in aerodynamic performance sought by aerodynamicists. Figure 7 shows that the wind-off zeros taken on Boeing's 635H balance during a recent test in the NTF (no cryogenic testing) and the NTF101B balance in the same model over the temperature range -250°F to 80°F do not differ greatly. In either case the data accuracy would be compromised if this shift in wind-off zeros was not taken into account. To obtain accurate data will require reducing the amount of wind-off zero shift or developing a method to obtain wind-off zeros more efficiently.

Sensitivity shift with temperature for the NTF balance bridges typically falls between -0.7% and $+0.4\%$ over a 375°F temperature range for the N1, N2, S1, and S2 bridges and between -1.5% and -0.8% for axial and roll. Currently the correction for sensitivity shift seems to be very good. However the current calibration technique only allows for calibration at two temperatures, 75°F and -300°F and assuming a linear change between these two points. Greater accuracy can be achieved by calibrating at two or three intermediate temperatures and using a second order fit. Two balances were calibrated for sensitivity and first and second interactions at both 75°F and -300°F . These calibrations indicated that most of the first and second order interactions did not change enough with temperature to warrant performing full cold calibrations. However as accuracy requirements become tighter it may be necessary to determine the temperature effect on large interactions.

Recently, a phenomenon was observed that has not as yet been explained. If a four-active-arm strain gage bridge in bending undergoes a temperature excursion while loaded, the apparent strain output differs from the unloaded case by more than that accounted for by sensitivity shift. The amount of this unexplained apparent strain shift varies directly with load and temperature. Since this phenomenon was first observed approximately twenty-five bridges have been tested. About three-fourths of them have exhibited the unexplained shift. Cold sensitivity is unaffected regardless of whether the balance was cooled loaded or unloaded. Figure 8 shows the apparent strain curves of a bridge loaded and unloaded. The third curve shows the loaded output with sensitivity shift correction. As can be seen the corrected curve is not the same as the unloaded apparent strain curve. This apparent strain shift has occurred in strain gage bridges mounted on 17-4 PH stainless steel, beryllium copper, and 300 grade maraging steel. There appears to be little effect when the strain gages are mounted on aluminum. It is present in the N1, N2, S1, S2 bridges of a balance designated NTF 113 but not on the axial and roll bridges. Additional tests indicated that it did not matter whether the bridge was in single or double bending. Constant moment test beams of maraging 200 steel were gaged with multiple bridges in order that comparisons could be made. These test beams included 1) one poisson ratio and non-poisson ratio bridge, 2) four bridges where each bridge was from one of the four different lots of gages we have used since we have been using cryogenic gaging, and 3) two bridges using two different types of adhesive. In all cases all the bridges exhibited the unexplained apparent strain shift.

Moistureproofing the balance may need to be improved. Since 1983 there have been two balances that have experienced slight grounding problems during wind tunnel tests. While the TFE spray has minimal apparent strain effect and is easy to remove for access for bridge repairs it is not 100% effective against moisture and offers little protection for delicate bridge components during handling.

WORK IN PROGRESS

A series of tests have just been completed to study the effects of gradients. While the results are not complete figures 9a, 9b, & 9c indicate that the present compensation techniques are very good even in the presence of large and vastly different temperature gradients. A complete analysis of this data remains to be accomplished. With the closer tolerance imposed on hysteresis error, the results should be even better. To further investigate the gradient effects on axial force, an existing test balance was chosen that is similar in design to the current NTF balances for the purpose of researching alternate axial design configurations. A large number of thermocouples have been placed throughout the axial section and half-bridges have been placed on each of the four sets of flexures. The balance will be tested with the center measuring beam in place then the center beam will be cut out so a comparison can be made to see if the design of the axial section can be improved to eliminate the deformation induced axial output. Reference 7 describes how this modification should cause temperature induced deformation output to cancel.

In order to calibrate at intermediate temperatures, a cryogenic heat-exchanger is being designed that will use liquid nitrogen to control the cooling of freon which will then be circulated through the calibration loading fixture and supporting stump.

Additional studies are planned to further investigate the unexplained apparent strain shift of a strain gage bridge that is loaded while being cooled. The tests conducted up to this point have failed to determine the bridge component responsible for the loaded shift. It may be necessary to start over using a step-by-step plan that will pinpoint the cause. In the meantime since a balance is usually not heavily loaded during tunnel cool-down this effect should be quite small.

SUMMARY

Accurate wind tunnel data is being obtained from one-piece strain-gaged force balances in the NTF that have been designed, fabricated, strain-gaged, and calibrated for cryogenic use. However to reliably detect a one drag count difference between models or configurations a number of actions need to be taken to obtain even greater accuracy.

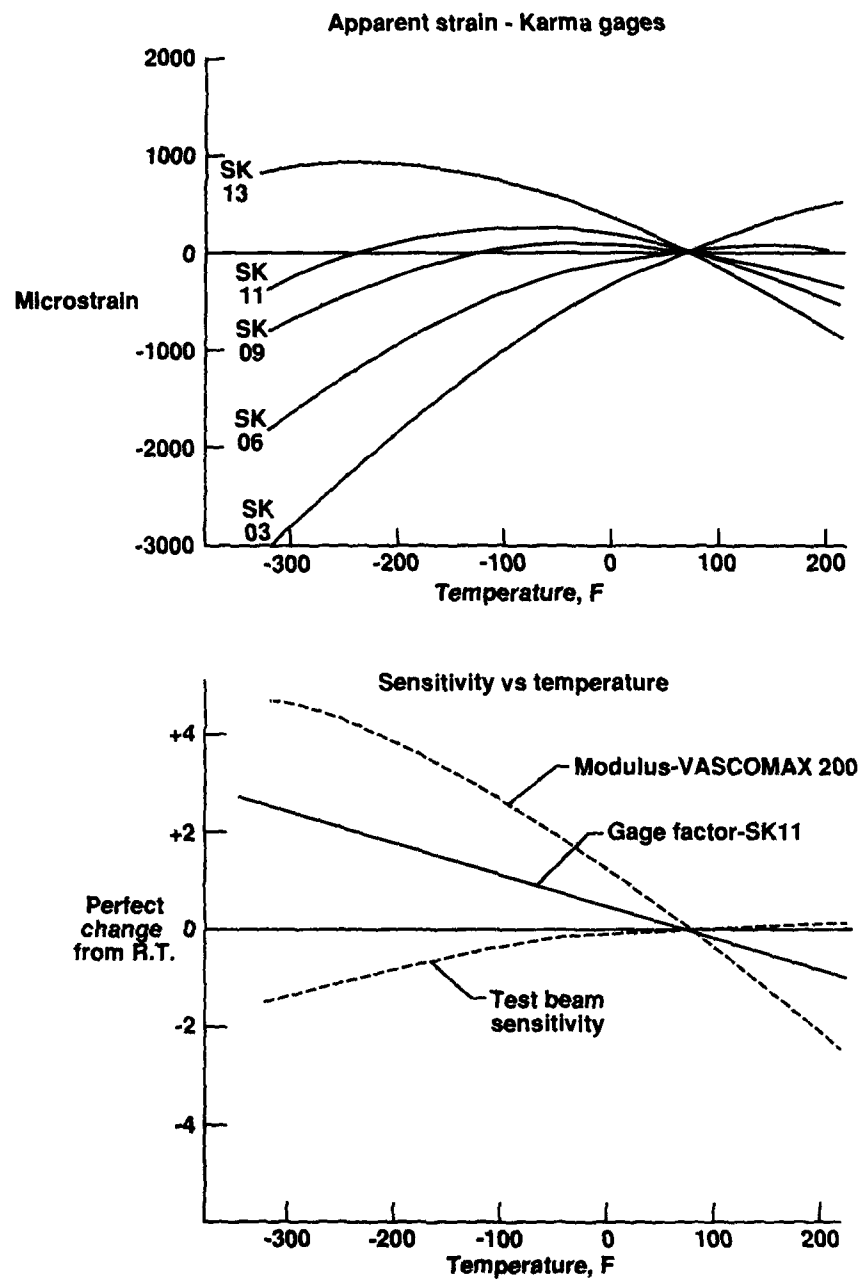
These actions include:

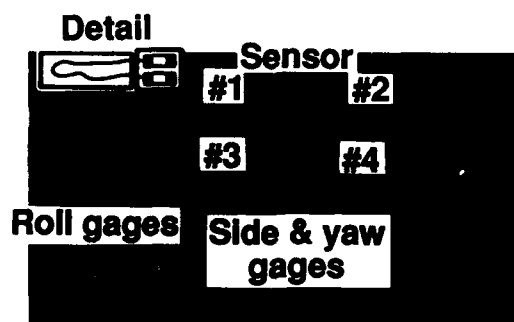
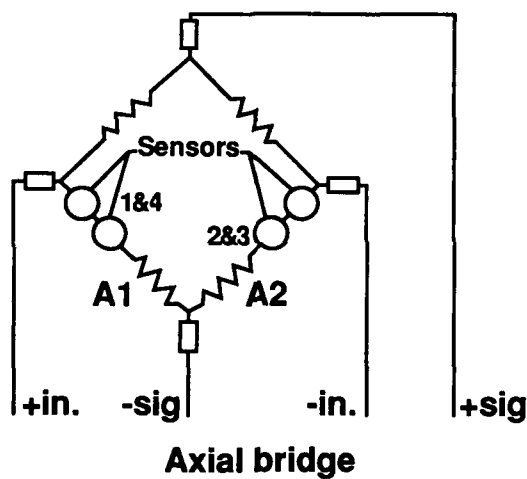
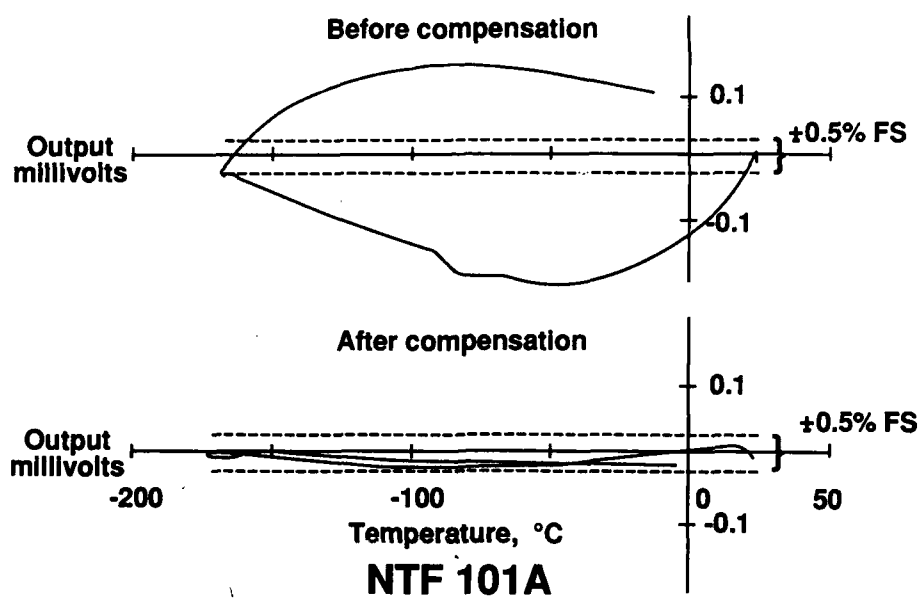
- 1) impose closer tolerances on temperature compensation;
- 2) acquire the ability to calibrate at intermediate temperatures;
- 3) find a better moistureproofing agent to reduce the chances that the balance will develop grounds if it is subjected to moisture or rough handling;
- 4) find methods to eliminate loads being imposed on the balance by wires or tubes that pass over the balance;
- 5) determine why the apparent strain data obtained in the test section does not repeat that established in the ready bay;
- 6) establish a research program to eliminate the unexplained shift in the apparent strain curve in the loaded as opposed to the unloaded condition;
- 7) pursue alternate force balance design to minimize temperature induced output;
- 8) improve the stability of the electrical zero or take frequent wind-off zeros;
- 9) select the appropriate balance or family of balances for the expected loads in the test envelop.

REFERENCES

1. Kilgore, Robert A.; Goodyer, Michael J.; Adcock, Jerry B.; and Davenport, Edwin E.: The Cryogenic Wind-Tunnel Concept for High Reynolds Number Testing. NASA-TN-D-7762, Nov. 1974.
2. Kilgore, Robert A.; and Davenport, Edwin E.: Static Force Tests of a Sharp Leading Edge Delta-Wing Model at Ambient and Cryogenic Temperatures With a Description of the Apparatus Employed. NASA-TM-X-73901, June 1976.
3. Ferris, Alice T.: Cryogenic Wind Tunnel Force Instrumentation. Paper no. 32, 1st Int. Symp. on Cryogenic Wind Tunnels, Southampton, U.K., Apr. 3-5, 1979.
4. Ferris, Alice T.: Force Instrumentation for Cryogenic Wind Tunnels Using One-Piece Strain-Gage Balances. NASA-TM-81845, June, 1980.

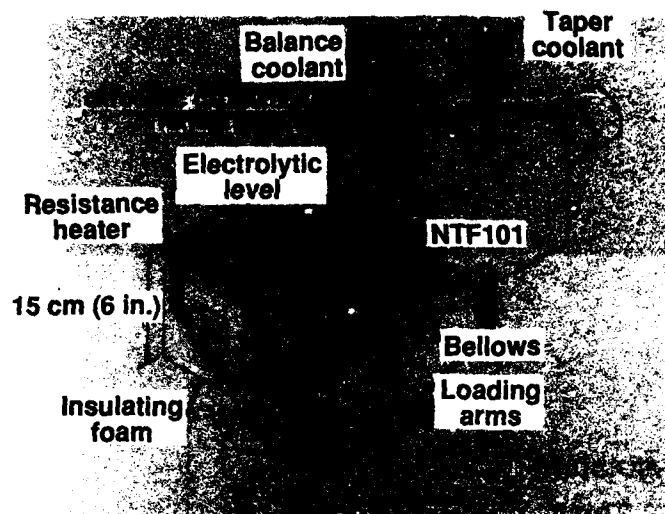
5. Ferris, Alice T.; and Moore, Thomas C.: Force Instrumentation for Cryogenic Wind Tunnels. Presented at the 27th International Instrumentation Symposium, Indianapolis, Indiana, April 27-30, 1981, pp. 149-160.
6. Boyden, Richmond P.; Johnson, William G. Jr.; and Ferris, Alice T.: Aerodynamic Force Measurements With a Strain-Gage Balance in a Cryogenic Wind Tunnel. NASA-TN-2251 December, 1983.
7. Ewald, B. and Krenz, G.: The Accuracy Problem of Airplane Development Force Testing in Cryogenic Wind Tunnels. Technical University of Darmstadt and MBB Transport Division, AIAA Paper 86-0776.
8. Jacobs, Peter F. and Ferris, Alice T.: Testing Experience with Unheated Strain-Gage Balances in the NTF. 66th Semiannual STA Meeting, Albuquerque, New Mexico, October, 6-7, 1986.

**Figure 1**



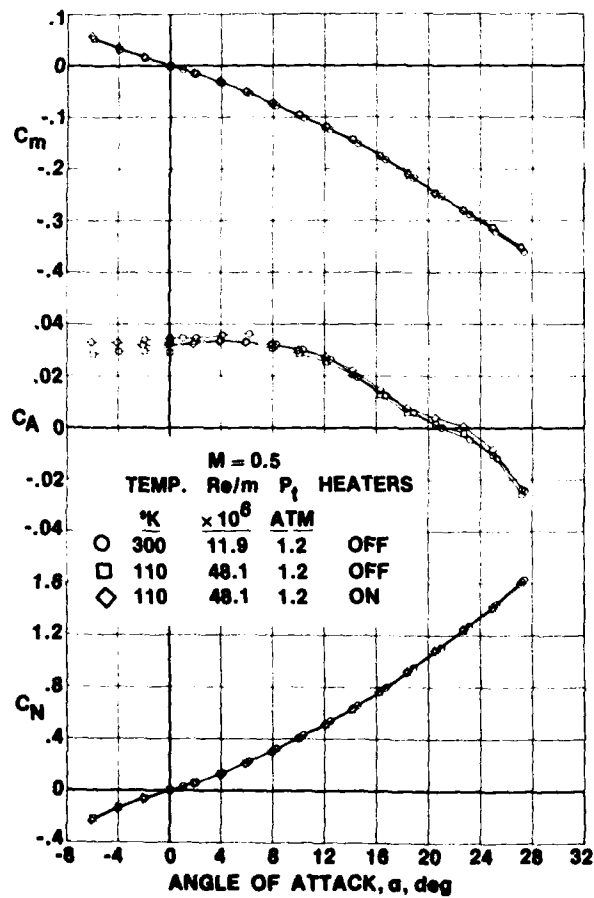
Axial Transient
temperature compensation

Figure 2



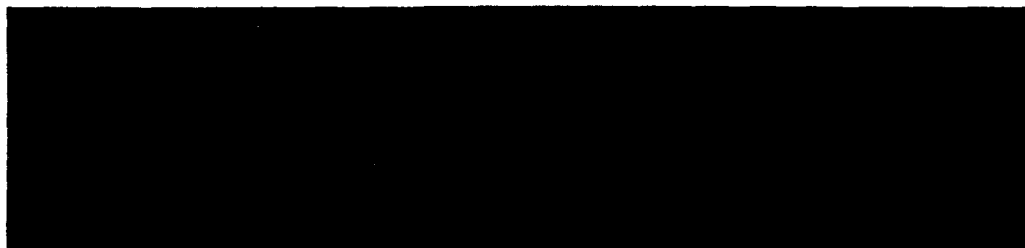
Cryogenic calibration fixture

Figure 3



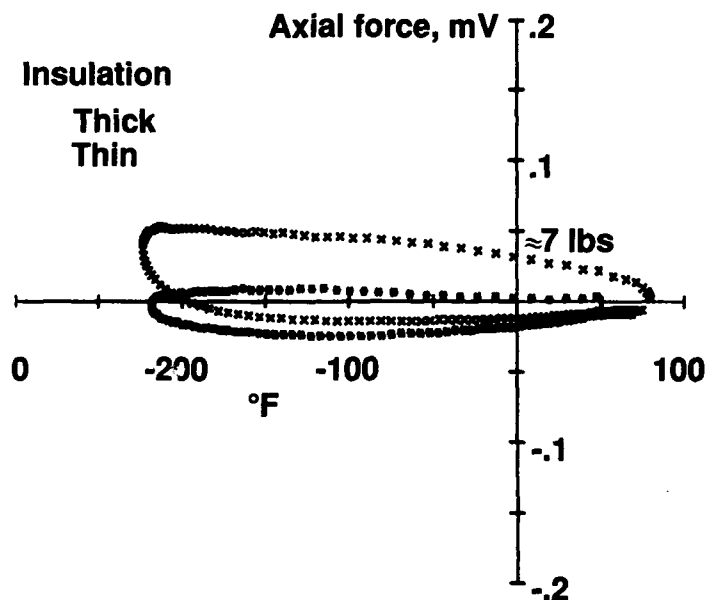
0.3 Cryogenic wind tunnel test results

Figure 4



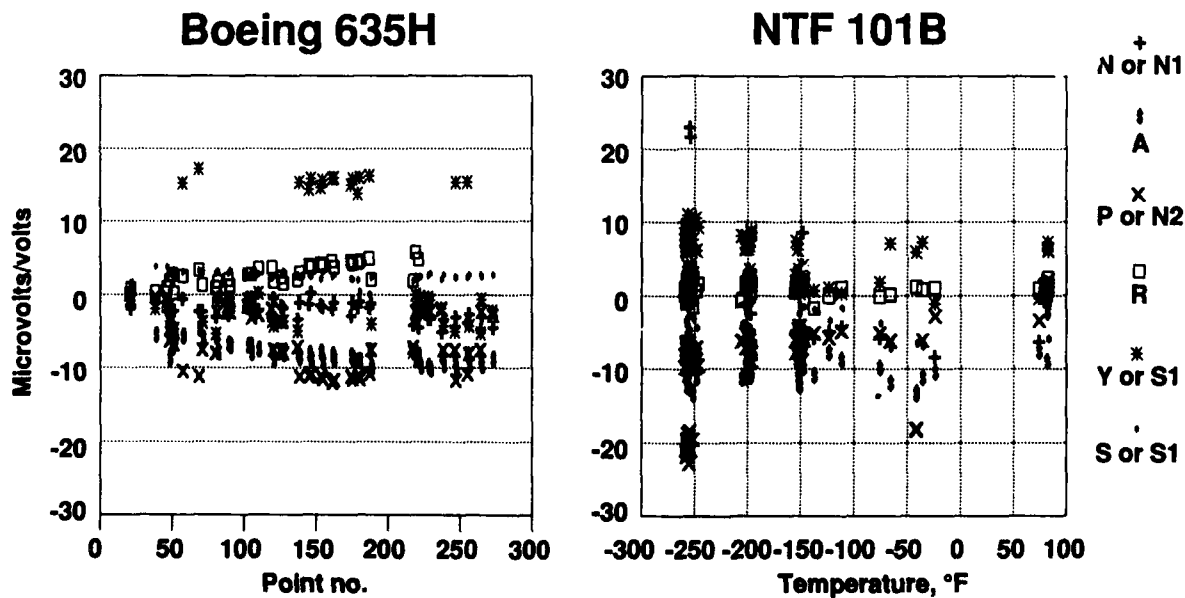
Balances for NTF

Figure 5



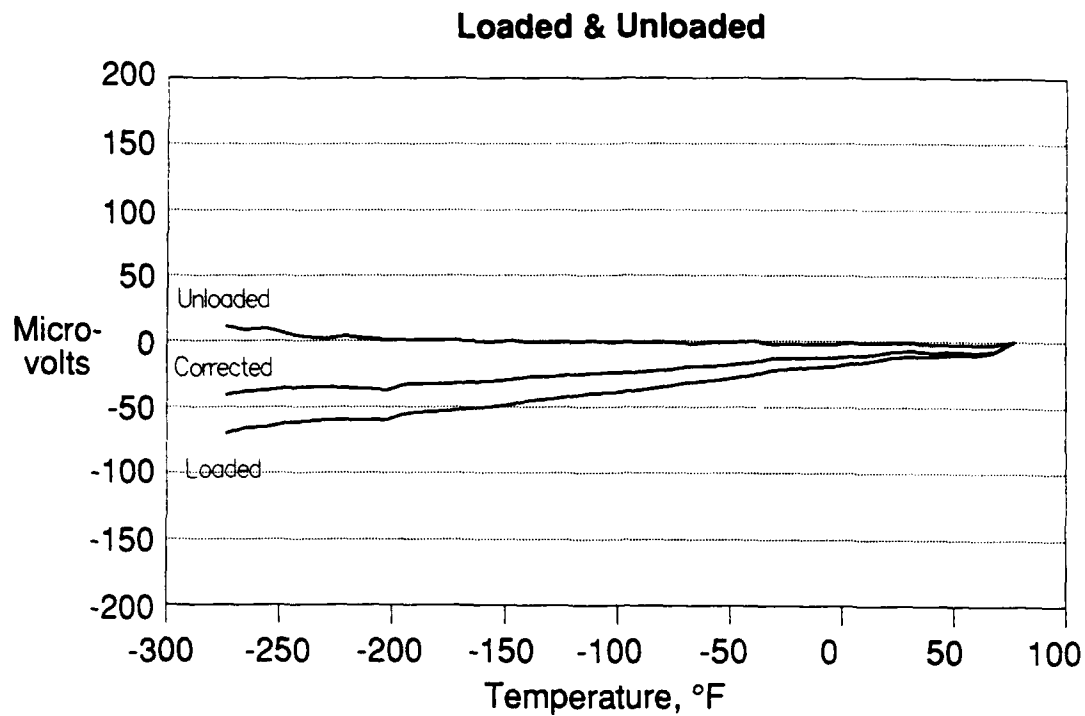
Effect of Wires Across Balance

Figure 6

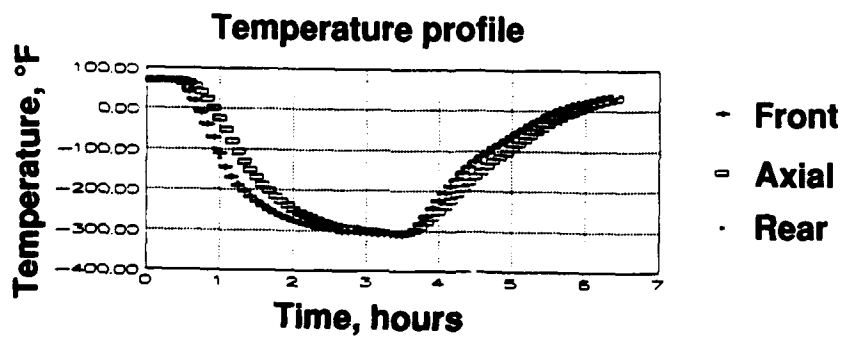
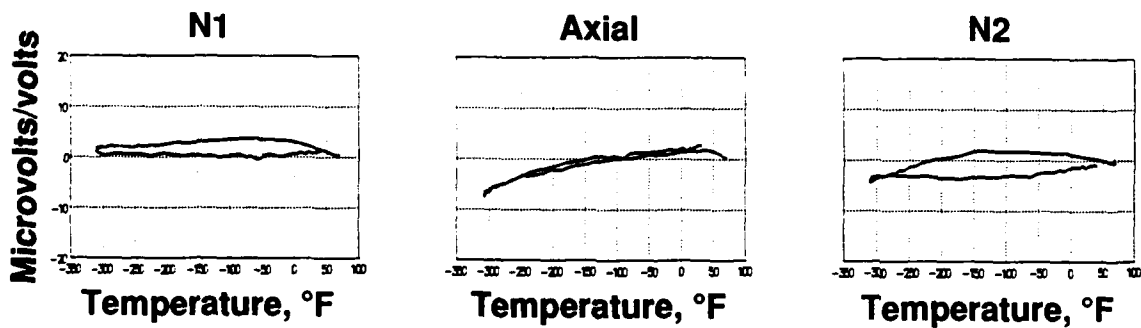


Wind-off zero stability Boeing 767 test

Figure 7

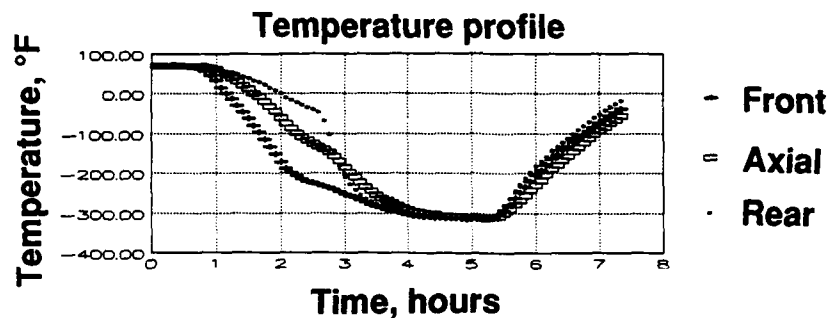
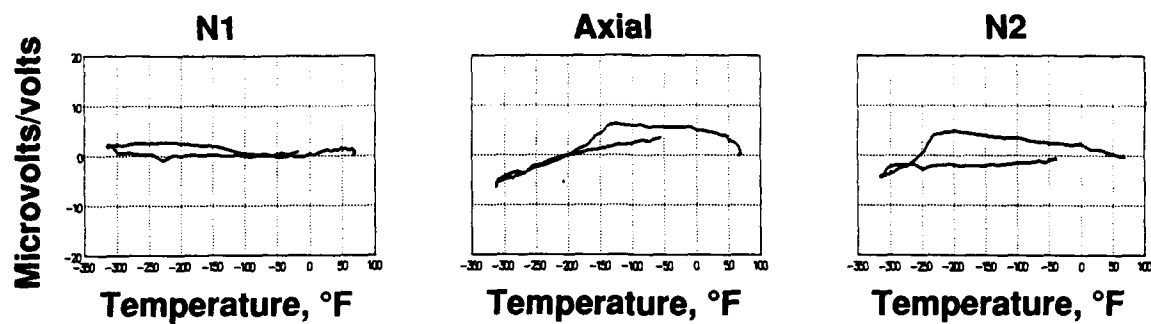


Apparent strain curve
Figure 8



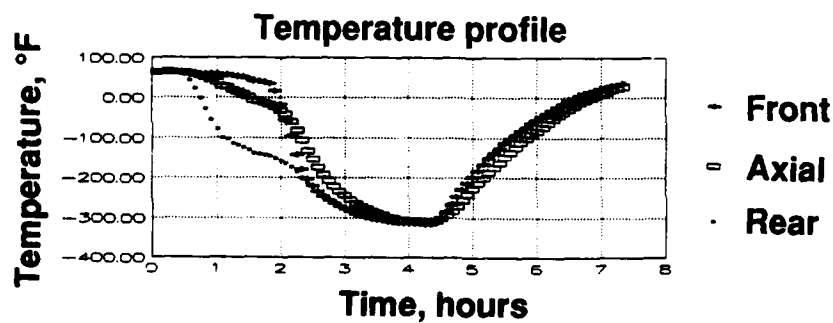
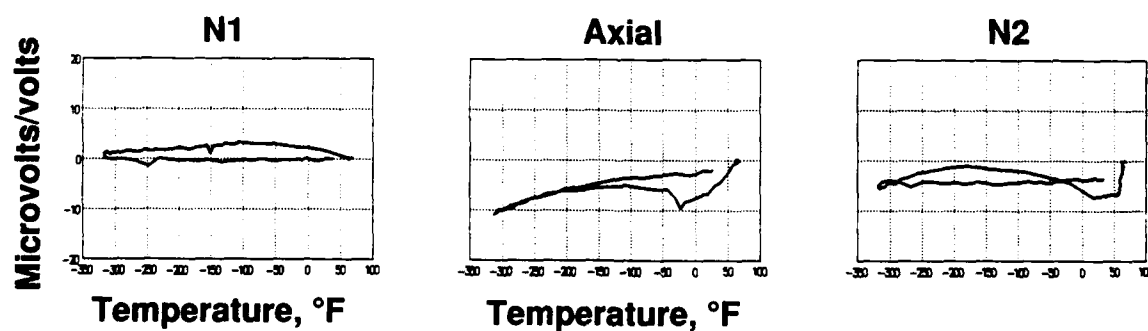
NTF 103 APPARENT STRAIN
Front and back of balance cooled simultaneously

Figure 9a



NTF 103 APPARENT STRAIN
Front of balance cooled first

Figure 9b



NTF 103 APPARENT STRAIN
Rear of balance cooled first

Figure 9c

SAFETY AND CRYOGENIC WIND TUNNELS

by

Edward J. Ray

NASA, Langley Research Center
Hampton, VA 23665-5225
U.S.A.

SUMMARY

The Langley 0.3-Meter Transonic Cryogenic Tunnel (0.3-m TCT) was placed in operation at NASA's Langley Research Center in 1973 as the world's first cryogenic pressure tunnel. The 0.3-m TCT can operate from ambient to cryogenic temperatures over an absolute pressure range from about 1 to 6 atmospheres. Three major test section concepts have been developed and refined in this unique facility. The 0.3-m TCT has been a leader in the development of various cryogenic pressure wind tunnel experimental techniques, instrumentation, control, model technology and safety standards.

This paper concentrates on the safety experience gained by the author who has acted as the 0.3-m TCT facility safety head during the facility's 15 years of existence. During this period of advanced research, new operating techniques, training policies, and procedures had to be established. The paper deals with the "Do's" and "Don'ts" of cryogenic wind tunnel testing. Hazards and safety requirements which are unique to cryogenic testing are discussed. Highlights of experience and "lessons learned" with the 0.3-m TCT are reviewed.

1. INTRODUCTION

From the earliest days of the 0.3-m TCT, beginning with the design of the tunnel, safety has been an ever present concern. Not only was there a great respect for the potential hazards involved with cryogenic pressure operations, but there was also a constant awareness that a mishap would probably doom the concept. In addition, the tunnel was designed and built in haste and was not intended to be used for more than 60 hours of operation. Originally classified as a pilot tunnel its first and only envisioned role was to verify the validity of the cryogenic wind tunnel concept at transonic speeds.

The role of the 0.3-m TCT has obviously changed during the 15 years of operational experience. Rather than the original estimate of 60 hours of operation, the facility has actually operated for about 6000 hours. Most of these thousands of hours have been spent at cryogenic temperatures and at stagnation pressures up to 6 atmospheres. Many additions and modifications have been made to the basic facility along with an ever changing array of experimental techniques, models, and instrumentation. There has been a continual program to train operators, document and validate equipment, establish operating procedures, refine the safety organization, "fail-safe" the facility, and control test models and apparatus. Throughout these years of changing technology, attempts have been made to encourage independent safety reviews^{2,3}.

As might be expected in the early days of operations of the 0.3-m TCT, as the first cryogenic pressure tunnel, many mistakes were made during its evolution to an operational status. Fortunately, none of these mistakes have resulted in serious consequences and the frequency of our mistakes continue to diminish. It is the intent of this paper to review these experiences in an effort to minimize mistakes of others in the future.

This paper will first review the typical hazards of cryogenic pressure tunnel operations. Familiarity with these hazards is an essential starting point for cryogenic pressure tunnel "users." Next, the paper will identify a safety organization which has evolved over the many years of 0.3-m TCT testing. The basic elements of the facility's safety program will be reviewed along with selected "lessons learned" which are related to the safety program elements. Finally, this paper provides a brief review of today's 0.3-m TCT safety equipment, procedures, and features.

2. TYPICAL HAZARDS OF CRYOGENIC PRESSURE TUNNELS

The operation of a cryogenic pressure wind tunnel involves both the familiar hazards associated with high pressure, electrical shock, and moving parts while opening up a relatively new dimension in operational concerns associated with the utilization of both liquid and gaseous nitrogen. Experience with the 0.3-m TCT has vividly illustrated that the extremely low temperatures and the tremendous liquid-to-gas expansion rates associated with nitrogen present unforgiving hazards which require special equipment and materials, highly trained personnel, and constant vigilance. The operations associated with the nitrogen storage, transfer, change of state, and exhaust would be expected to lead to the possible exposure of personnel and equipment to the following hazards:

- (1) Asphyxiation or loss of orientation due to oxygen deficiency
- (2) Freezing of human tissue due to excessive cold

- (3) Failure of metals or other materials which are not suitable for use at low temperatures
- (4) Over-pressurization ruptures due to the vaporization of trapped liquid nitrogen
- (5) Failures due to differential contraction and expansion
- (6) Fires and explosions caused by condensed atmospheric air coming in contact with combustible materials
- (7) Fogging, spraying and/or icing due to escape or intermittent release of liquid or cold gas
- (8) Exposure to excessive exhaust or release noise
- (9) Incorrect installation of cryogenic equipment
- (10) Inadequate training and staffing of personnel for cryogenic operations
- (11) Inadequate provisions for warning, emergency, and rescue equipment

Descriptions are presented in the following sections to indicate "lessons learned" examples and approaches taken at the 0.3-m TCT to avoid the hazards listed above.

3. ORGANIZATION

It should be pointed out at the beginning of this discussion that the safety organization which will be described was not completely in place during the early 1970's at the beginning of the 0.3-m TCT operations. This organizational structure, as with test procedures and other related subjects, has been an evolving process based on many years of experience and "lessons learned."

Two very important concepts at Langley directly related to safety are "quality assurance" and "configuration control." Quality assurance may be loosely defined as a set of procedures that insure you are using what you think you are using, whether it be a complete model with critical design dimensions or a bolt which must be of a specific material produced in a prescribed manner. Configuration control is loosely defined as having records, such as a set of drawings, which reflect the true up-to-date situation with respect to the tunnel hardware, electrical wiring, plumbing, etc.

As mentioned earlier during the initial period of operation with the Langley 0.3-m TCT, several safety-related incidents occurred which may have been caused by our inexperience combined with a lack of a proper quality assurance program and an organizational structure suitable for cryogenic wind tunnels. However, soon after the classification of the 0.3-m TCT was changed from a pilot tunnel to an operational wind tunnel facility, it was decided that all materials, models, and test equipment used in cryogenic tunnels at Langley would be "flight rated." Flight rated is a generic term which implies that there is a special concern with the overall operating environment, design criteria, safety factors, and quality assurance of the article.

As might be expected, the subsequent development of the U.S. National Transonic Facility (NTF) at Langley added momentum to these concerns and hastened the evolution of new quality assurance standards and review procedures for cryogenic testing. New positions of responsibility, such as "Cryogenic Practice Engineer," appeared in the organization structure, and handbooks dealing specifically with cryogenic model criteria⁴ and a quality assurance plan⁵ were incorporated in the Langley Safety Manual.

The system which has evolved at Langley is obviously too complicated to be considered for every cryogenic wind tunnel. This is especially true where competent researchers are running their own small cryogenic tunnels and the results of an accident would not be catastrophic. Most small cryogenic tunnels operating at atmospheric pressure can be safely operated without any formal safety program. However, for the larger cryogenic tunnels, especially those that are pressurized, there are certain basic elements of a formal safety program which provide the necessary organizational structure for the safe and efficient operations of the cryogenic tunnel. It is essential that these basic elements are considered and covered by someone or by some type of organized team, whether its two or ten people.

At Langley, it has been found that a Facility Safety Head (FSH) and a Facility Coordinator (FC) should be formally assigned to manage the day-to-day safety program. These two positions, described in Reference 5, provide the foundation for an acceptable safety program. The FSH is usually a research engineer, familiar with the operation of the cryogenic tunnel, who serves as the on-site manager of the safety program. The primary function of the FSH is to assess and control hazards and thereby minimize the possibility of an accident. The FC is normally the senior technician in charge of the tunnel operation team who assists the FSH in configuration management and the safe operation of the facility. In large facilities, particularly in ones that incorporate significant auxiliary equipment or complicated software, alternate FSHs are appointed to monitor specialized areas of concern.

In addition to the FSH and the FC, the impartial "third party" within the organization is the Cryogenic Practice Engineer (CPE) with the responsibility of providing a constant check on approach of designs for baseline configuration changes, models, and test equipment. The CPE has an up-to-date collection of information on subjects related to the selection of materials, design, and fabrication techniques for cryogenic wind tunnel devices.

At Langley, any significant changes or additions to the original, "baseline," facility configuration is processed and supervised by a Technical Project Engineer (TPE) who is responsible for coordinating the effort with the FSH to insure that all facility drawings are corrected and operational procedures are updated if required.

Finally, each research project in the tunnel, such as a buffet or flutter test, is sponsored and supervised by a Research Project Engineer (RPE) who has a thorough knowledge of the details of the individual research project and a basic familiarity with the major characteristics and safety concerns of the facility.

The key safety elements concerning this or any other cryogenic pressure tunnel organizations are:

- (1) Define, document, and validate the "baseline" facility configuration.
- (2) Control and document all changes to the baseline facility configuration.
- (3) Operate the facility properly.

In the following three sections of this paper, each of these safety elements will be examined in more detail. Examples will be presented to illustrate **what can happen** when these safety elements are not considered. The relationships between these elements and the previously described **hazards of cryogenic pressure tunnels will be described.**

4. DEFINE, DOCUMENT, AND VALIDATE "BASELINE" CONFIGURATION

A brief description of a process to comply with this first safety element is as follows:

- (1) Considering all of the "HAZARDS" of the operation, incorporate a design which will avoid or protect against all undesirable events throughout the entirety of the operating envelope.
- (2) Inspect and insure that the configuration is constructed as designed and that documentation and records reflect "as built" characteristics.
- (3) Conduct controlled, well planned, conservative, and systematic validation trials of the "baseline" configuration. Whenever possible, subsystems as well as major systems should be cooled slowly and evenly before applying any degree of rotational velocity or other force to the individual systems. The individual systems should be monitored and recorded as closely as possible during the build-up of applying energy. This conservative approach will minimize damage if malfunctions occur and provide a reference for future consideration.

In simplified terms, this safety element dictates that the "baseline" configuration must be designed and built properly, recorded accurately, and proven safe and effective throughout the operating envelope. The following accounts reveal several 0.3-m TCT "lessons learned" in dealing with this first, crucial safety element.

4.1 Basic Tunnel Structure and Internal Apparatus

In retrospect, the operation of the pilot tunnel as the first transonic cryogenic tunnel was very successful and relatively trouble-free. Considering the haste of the original construction, installation, and initial "proof-of-concept" tests, there were surprisingly few major deficiencies. The basic tunnel pressure vessel withstood the many cryogenic pressure cycles during the initial validation tests. There was however, one general class of internal structural damage which occurred in cases where "spoke-like" aluminum struts were rigidly attached to the tunnel pressure vessel (see figure 1). Although not shown in this photograph, all four turning vanes have indicated repeated minor damage due to problems associated with differential contraction and expansion. Remember hazard number 5 which was listed in the preceding HAZARDS Section 2. This class of failures was later reduced with a redesign which provided for polytetrafluoroethylene cushioned "T" slots at the central hub attachment points (see figure 2). The four turning vanes of the 0.3-m TCT still experienced minor damage of this type, but they will be replaced in a forthcoming facility update. Although a mishap occurred because of overlooking a **HAZARD**, the organizational "safety net" noticed the mishap during a prescribed periodic (procedure) inspection before it became a serious threat to the facility. During those early days of operation, the 0.3-m TCT team became very familiar with **HAZARDS** (5) Failure due to differential contraction and expansion (7) Loss of visibility due to fog formation and (9) Incorrect installation of cryogenic equipment.

One of these incidents almost ended our young cryogenic pressure tunnel career. Shortly after the original airfoil validation tests⁶ the support strut for the long Mach distribution calibration probe failed and a large portion of this apparatus "went down the tunnel." The various parts of this assembly after the mishap are shown in figure 3. The rather large bullet shaped fairing shown at the left of the photograph made it past turn number 1, dropped down and lodged in a corner of turn number 2 just "ahead" of the propeller. The author has often wondered what would have happened to Langley's cryogenic pressure tunnel career if that fairing had gotten through turn 2. While collecting the "missing" parts it was determined that about 20 to 30 bolts had "backed" out of their intended locations. A strong "lesson learned" is; never expect any bolt or pin or whatever to stay put in a cryogenic tunnel unless it is retained with safety wire, or by some other manner.

The covering (spacer) on the fan assembly hub was originally featured from core assembly which was covered with epoxy and fiberglass materials with a foam core. This spacer was retained on the fan hub assembly by a circular series of aluminum retainer device (see figure 4). The dissimilar material of the fan hub covering, expanding and contracting at a different rate than the aluminum may have caused initial cracking. Therefore, centrifugal force probably led to its total destruction. Again, there was no serious damage and the covering was replaced with an aluminum plate.

4.2 Nitrogen Storage, Exhaust and Relief Systems

A severe fogging problem existed with the original exhaust stack design during periods of high humidity and low wind velocities. A very simple and effective solution to this problem has been the incorporation of exhaust driven ejectors (see figure 5). However, it should be mentioned here that fogging has been a continual problem with secondary and auxiliary exhaust stacks and inadvertent LN_2 spills. The 0.3-m TCT's close proximity to roadways (see figure 6) aggravates this situation due to the fact that fogging can impose a hazard to nearby traffic. The occurrence of this type of happening is very infrequent but periodic updates are being made to reduce this type of occurrence. Usually the fogging occurs because of an inadvertent "spill" during transfer of LN_2 or fog is emitted out of a low velocity auxiliary system such as the boundary layer removal stack shown in figure 7. It is planned to eventually route all of the 0.3-m TCT and NTF auxiliary system and relief gas to a controlled accumulator system.

During the 0.3-m TCT experience, several incidents of piping failure in the LN_2 delivery and return systems and in GN_2 vent systems have indicated that this is an area of concern that requires constant diligence. Proper standards of design, fabrication, installation, and inspection must be adopted. Relief devices, both valve and rupture disc and associated vent lines, need to be properly designed to eliminate pipe twisting (torque) by installation of "T" vent caps, as shown in figure 7. Vent pipes must be retained while allowing for thermal expansion and contraction. The design approach should make every attempt to eliminate the possibility of venting liquid nitrogen to an uncontrolled area. As mentioned above, vents and reliefs should be routed to a controlled area to avoid the possible HAZARDS of cryogenic operation.

One of the closest "calls" we have ever had with a possible personnel mishap was with a nitrogen vent system. This vent system area was the type shown in the schematic of figure 8. This particular vent located in the LN_2 storage area was designed to provide an overpressure relief for the LN_2 tunnel supply line near the liquid nitrogen pump station. The right angle relief exit was about 10 feet above an operator working platform and was directed away from the working station towards the storage tanks. Three errors were made in the design of this system. First, a relief vent should never be located in an area near working personnel. The vent should be isolated in a controlled situation away from apparatus, or operators should be restricted from those areas. Secondly, the rupture characteristics of the disc were calculated improperly. It was assumed that the disc would always be at cryogenic temperatures when it was actually nearer to ambient temperatures. This misapprehension resulted in the disc rupturing at a pressure of about 50 percent less than had been assumed. Lastly, when the disc ruptured, the vent system was not supported properly and the asymmetric loading at the exit caused the vent to torque and turn towards the working platform. Fortunately, other than a bad scare, there were no injuries. Inspections of other facilities, which have been made by this observer, have indicated that this type of error with vents and reliefs is often repeated.

4.3 Insulation System

Hazard number 6, fires and explosions caused by condensed atmospheric air coming in contact with combustible materials can present one of the most hazardous aspects of the cryogenic tunnel operation. Several catastrophic accidents have occurred in industrial situations with liquid nitrogen systems because of this hazard. Fire or explosion cannot normally occur without the presence of the following three factors: the ignitor, the material for combustion, and the oxidant. It must be recognized that if any of the above factors are present or can be present, a situation might arise where the other two factors could coincide.

In the late 1970's during the 0.3-m TCT recertification period, the original external insulation system, which was described in an earlier paper on the 0.3-m TCT, was removed. Large areas of corrosion were discovered on the exterior walls of the aluminum pressure vessel. This evidence of moisture condensation was taken as proof of leaks in the vapor barrier and suggested the possibility of condensing oxygen on the external tunnel walls at the low operating temperatures.

Since the original insulation material, polyurethane foam, is not an oxygen compatible material, the evidence of moisture condensation was regarded as a serious safety hazard. The original insulation was replaced with a relatively simple and inexpensive insulation concept which facilitates rapid, uncomplicated modifications and repairs. This new system features fiberglass insulation, outer vapor barrier and an internal gaseous nitrogen purge system. Mr. Lawing has described this system in detail in an earlier paper. If installed and operated properly, this system provides a perfectly safe and inexpensive external insulation system.

4.4 Tunnel Controls, "Fail-Safe" Failure Strategy, and Low O_2 Warning System

During the early years of 0.3-m TCT operation, the tunnel control was primarily a manual system. It was a difficult task for three operators to individually control three different tunnel parameters, with all of these parameters responding to changes in the other two. Control of the tunnel required a great deal of skill and training, and it was not at all uncommon for the operators to vary from the most acceptable approach to a given set of tunnel conditions. The original control devices had no automatic protection against large temperature differentials between structural members in the flow stream and the pressure vessel. This control weakness may have attributed to the internal structural damage discussed earlier.

In order to avoid several of the hazards previously noted, the facility was "failsafed" to a rather high degree. The term "failsafed" here means that if an undesirable event occurs, such as a bearing overheating, the tunnel will automatically shut down. The tunnel fail-safe systems incorporate features to provide protection against overcurrent, low oil, overtemperature,

excessive vibration, excessive thrust, overpressurization, LN_2 supply hazards, and low O_2 situations.

An overall failure strategy or philosophy has been adopted at Langley which professes that there will be **no single order failures**. A single order failure would be a situation where one undesirable happening could result in a mishap. To illustrate the concept of having several levels of protection, let us examine a typical LN_2 system. HAZARD number 4 implies that LN_2 systems can be hazardous due to "over-pressurization ruptures due to the vaporization of trapped liquid nitrogen." In the 0.3-m TCT facility, for all LN_2 systems where there is a possibility of "trapping" LN_2 , the system will incorporate both a rupture disc and a relief valve thereby providing two levels of protection.

The original low O_2 warning system and emergency response procedure at Langley were developed by the 0.3-m TCT team. These systems and procedures have undergone many changes and updates during the 15 years of operational experience. The general philosophy, however, has always been that in case of a seriously low O_2 situation (below 16.5 percent), the tunnel system would be shut down automatically, outside rescue specialists would be called to the scene automatically, and all facility personnel would evacuate by specified escape routes and assemble at predesignated areas for mustering. After the arrival of the rescue team with specialized equipment and completion of musters, selected facility technicians would be made available to assist the rescue team in entering the facility with breathing apparatus to perform rescue, evaluation, casualty control, and repair functions. The NTF has adopted a similar approach and the current Langley low O_2 procedure is based on a two-phase alarm system. Phase I audio and visual alarms are activated at O_2 levels from 19.0 to 16.5 percent of a standard atmospheric environment at sea level. The 19.0 percent level is referred to as the **low level alert condition** and the 16.5 percent condition is termed as the **low hazard warning level**. A summary table of the 0.3-m TCT low O_2 procedures is shown in figure 9. A photograph of the O_2 monitoring panel in the 0.3-m TCT control room is shown as figure 10. About 13 various O_2 sensors are monitored throughout the facility. These sensors are located in strategic positions to provide an early warning of low O_2 conditions in any area of the facility. As shown in the table of figure 9, if a Phase I situation is measured in any of 13 monitored areas, a blue light and a "wobbler" audio warnings will be activated. The control panel will indicate the area where the alarm has been activated. The Phase I audio and visual alarms differ from the general alarm system and, in this condition, only the concerned area or areas are evacuated. If the O_2 level drops below the low hazard warning (16.5 percent) condition in any space in the facility, the general audio and visual alarms are activated, a low O_2 alert (indicating location) is automatically "tripped" in the Langley fire and rescue station, the tunnel automatically goes to "fail-safe," and the facility is completely evacuated.

A study conducted several years ago on the O_2 monitoring system installed in the NTF and the 0.3-m TCT indicated that there is a significant difference in the quality of the replaceable O_2 sensor cells currently available. One or possibly two of the cells have been shown to be vastly superior to the other available products. In addition, an O_2 sensor analysis (reference 9) has shown that it is not advisable to continually reset the O_2 monitors to an arbitrary percent level due to the design features of the sensors and the influence of local environmental conditions on the "real" O_2 level of concern.

4.5 Inspections

Periodic inspections have been designed and refined during the 0.3-m TCT experience to insure that the baseline configuration is surviving as predicted. The frequency of these inspections varies from daily inspections, to other specialized areas, which are only inspected every 6 years. Inspections should be established for a facility which are based on the design life of the various components. The 0.3-m TCT was originally inspected on a frequent basis due to inexperience with aluminum welding technology and methods for estimating the effects of combined temperature-pressure cycles. The basic inspection procedure for the 0.3-m TCT is now established on a semiannual basis and includes the nondestructive examination of critical areas such as the fan, turnvanes, pressure shell, bolts, and flanges. Inspection plays an important role in the control and safety of the baseline configuration. As mentioned in previous sections of this paper, several potentially serious mishaps have been avoided through our inspection procedure.

5. CONTROL AND DOCUMENT CHANGES TO BASELINE CONFIGURATION

After the facility baseline has been established and validated, the tunnel configuration and test apparatus can be controlled by utilizing a form of the management structure suggested in the preceding organization.

5.1 Control Tunnel Updates and Other Facility Changes

As mentioned earlier, changes that impact the facility baseline, such as the addition of a boundary layer control system, should be processed by a Technical Project Engineer, TPE, through a Cryogenic Practice Engineer, CPE. The TPE would coordinate the effort with the Facility Safety Head (FSH) and Facility Coordinator (FC) to insure that all "affected" drawings and procedures are updated. Before construction these facility modifications are reviewed in a preliminary design review, PDR, and then later a critical design review, CDR. The new system, which changes the "baseline" should not be operated before considering an integrated systems review, ISR, and/or an operational readiness review, ORR. If this system is followed then the "baseline" configuration is protected and operating procedures and inspection plans should be established for the new systems. Again, as mentioned earlier, the safety plan does not always have to be this formal, but the basic safety elements discussed before should be followed.

5.2 Control of Research Projects

Prior to each research investigation, a pretest meeting should be conducted among the FSH, FC, Research Project Engineer (RPE), data acquisition, and data reduction personnel to address an agenda that includes model (or apparatus) design, safety analysis, test requirements, test conditions, and test procedures. Reference 4 presents the criteria for the design, analysis, quality assurance, and documentation of wind tunnel model systems to be tested at the Langley facilities. The pretest meeting has proven to be an effective safety net available to the FSH and the FC for controlling the facility after the "baseline" has been established and validated. At the time of the pretest the facility configuration now consists of a baseline configuration which hopefully is totally defined, documented, and validated and any other facility modifications, such as the boundary layer control system, which also should be defined, documented, and validated. The only variable then is the installation of the research model and/or apparatus. If the researcher RPE has complied exactly with the provisions of reference 4, then the model and apparatus is totally defined, certified, and analyzed for all of the test conditions proposed for the project.

During the early 1980's, the 0.3-m TCT was heavily involved in an extensive airfoil research program, Advanced Technology Airfoil Test (ATAT) Program¹⁰. At the beginning of this period the model failure rate while in the fabrication process was over 50 percent. During this period of intense testing of new model technology there was never a serious model failure. The 0.3-m TCT has always been involved with the testing of advanced model designs. It is believed that many mishaps were avoided by this pretest process.

5.3 "Lessons Learned" During Several Research Projects

There were, however, several vivid "lessons learned" during the early days of "controlling and documenting changes to the baseline configuration." During the 1970's, a .0045-scale model of the space shuttle orbiter was tested in the original octagonal test section¹⁰. A photograph of this model installed in the test section is shown as figure 11. In order to eliminate possible sting interference effects on the base, the model was supported by slender wing tip extensions which were covered with stainless steel cover plates. The cover plates were removable to accommodate the routing of base pressure tubes. The cover plates were to be held in place by small stainless steel bolts which are suitable for cryogenic testing. However, after the first series of tests most of which were conducted at cryogenic temperatures, it was found that most of the bolt heads had broken off and the cover plates were approaching a failure condition. After investigating this "near miss" it was found that someone in the shop had installed carbon steel bolts to temporarily hold the cover plates in place. Unfortunately, the model was shipped to the facility with the carbon steel bolts still in place after the discrepancy was missed by the quality assurance team who inspected the model. The pretest process did not detect this problem because the bolts had been certified to be a proper stainless steel selection. **Hazard** number 3, "failure of metals or other materials which are not suitable for use at low temperatures."

Another interesting incident, which also occurred back in the 1970's presents another example of what can happen when an unsuitable test apparatus is installed in the test section. This incident occurred in the two-dimensional test section of the 0.3-m TCT. Stagnation pressure probes were installed through the slotted ceiling of the test section to measure possible condensation effects on the stagnation pressure results. A photograph of typical probes installed in one of the slotted walls is shown as figure 12. After a short period of testing at cryogenic temperatures, it was discovered that two probes had failed and gone "down" the tunnel circuit. A major portion of the tunnel circuit had to be dismantled to find the missing probes. When the probes were found, an investigation by a structures specialist concluded that the probes had failed because they had been brazed at high temperatures which had changed the ductility of the normally suitable stainless steel material. The base of the probes then became extremely brittle at cryogenic temperatures and could not withstand the vibrations imposed by the flow through the test section. A photograph of the probes, after they were recovered, is shown in figure 13. The amazing thing with this incident is that when the front probe failed it apparently "flew" downstream and "clipped" the after second probe off at its brittle base. **Mishap** 3: "Failure of metals or other materials which are not suitable for use at low temperatures." The "lesson learned" here is that you cannot shortcut the system and always get by with it.

One final example illustrates a classic situation of improper selection of cryogenic model material. During the ATAT program mentioned earlier, a large number of advanced, highly cambered supercritical wings were tested for the first time at flight equivalent Mach and Reynolds numbers. Due to the very high Reynolds number conditions of the tests, the models were required to be extremely accurate. Model contour accuracies were held to $\pm .001$ in. ($\pm .0025$ cm). These very accurate models were measured before and after being tested in the 0.3-m TCT. During the testing of a supercritical airfoil model, it was noticed that there was a dramatic shift in the normal force angle of attack results. Upon removing the model it was found that the model was actually "bowed" downwards at the midspan station. The after test measurements showed a drastic change in the model ordinates (see figure 14). It can be seen from this figure that the model at the midspan station had been bowed downward by about .008 in. (.020 cm) and had decambered by about .006 in. (.015 cm) at the trailing edge of the airfoil. At that time there was a similar supercritical model which had been constructed from identical material that was awaiting tests. This "never tested" model was cryocycled in a dewar and then measured. The measurements revealed that after the static cryocycle, the model distorted in an almost identical manner as the airfoil actually tested. Here was another case of improper selection of materials. This particular happening, however, was very instrumental in the establishment of the now standard policy of cryocycling all Langley cryogenic models before final machining.

6.0 PROPER OPERATION OF THE FACILITY

Before operating the facility safely, it must be insured that two key safety elements have been accomplished. These elements, as previously discussed, dictate that:

- (1) The baseline configuration has been defined, documented, and validated.
- (2) All changes to the baseline have been controlled and documented.

If these two essential elements have been met and a facility operating envelope has been defined, then the facility should be safe to operate by a trained staff. If the user stays within the confines of the prescribed limits, then the system is responsible and accountable for the facility. Operation outside of the prescribed limits, however, would require a waiver by the FSH or higher authority.

6.1 The Operational and User Teams

The operational team is considered to be the group of trained technicians required to operate the facility safely and efficiently. This operational team for the 0.3-m TCT consists of four to five technicians. This operation does not include the conduct of a research investigation. Each research project in the tunnel, such as an airfoil test, is sponsored and supervised by a Research Project Engineer (RPE) who should have a thorough knowledge of the details of the individual research project and a basic familiarity with the major characteristics and safety concerns of the facility.

6.2 Operational Procedures

The development and maintenance of operational procedures and check sheets represent a continuing task at the 0.3-m TCT. After many years of operation, we are still updating and modifying our procedures and check sheets to reflect modifications to equipment or improvements in operating procedures.

The operational procedures establish a set procedure for all major recurring functions and tasks, such as system start-up, purging, cooldown, operation, warm up, operational limits, protective clothing, "buddy" system, communications, re-oxygenation, tunnel entry, emergency reactions, low O_2 response, evacuation of facility, and system shutdown. The operational procedures also provide guidance to avoid the **hazards** associated with restricted areas, low temperatures, low O_2 levels, high voltage sources, moving parts, O_2 enrichment, moisture in the tunnel, excessive fogging at the tunnel exhaust, rupture of tunnel or nitrogen systems, and "puddling" of LN_2 in the tunnel.

Check sheets are used each time the 0.3-m TCT is being prepared for a test. The check sheets are arranged by system and provide both start-up, operational, and shutdown steps which are checked off by a qualified tunnel technician as they are performed. In the 0.3-m TCT, check sheets which have been developed for tunnel operations include: cooling water system, hydraulic system, tunnel control systems, fan drive shaft lubrication system, fan drive motor lubrication system, instrumentation, LN_2 system, and test section.

6.3 Training

Training is a vital part of any safety program. A proven and acceptable method for training and qualifying the tunnel technicians is to address the training by facility system categories identical to the categories used for the facility check sheets. For example, if a technician is qualified on the drive system, then that technician is authorized to prepare the drive system for operation and "sign off" on the drive system start-up and shutdown check sheets. The FSH and the FC share responsibility for qualifying the technicians on the various facility and tunnel control systems.

It is essential that the operators of pressurized cryogenic tunnels be provided with training that leads to a good understanding of the interaction between the various tunnel control parameters. Such training and knowledge enable the technicians to control the tunnel properly and respond quickly and accurately to undesirable events such as LN_2 "puddling" in the tunnel circuit. Periodic meetings devoted to safety and briefings by visiting specialists, as well as self-graded achievement tests, have proven to be very helpful in training the operating personnel at the 0.3-m TCT.

In the safety program for the 0.3-m TCT, advantage is always taken of available resource material and information related to safety and cryogenic systems. References 7 through 11 are examples of sources of safety related information that are required reading for all tunnel operating personnel.

Training represents a key element in the safe operation of these relatively new and rather complex cryogenic wind tunnel facilities. As such, the training program should be periodically reviewed and updated as required to meet changing needs. During 1989, the 0.3- TCT research group plans to hold two 1-week training courses for potential research "users."

7. BRIEF TOUR OF TODAY'S 0.3-M TCT

Having reviewed the **Hazards of Cryogenic Tunnels**, a safety organization, and several important safety elements, it might be helpful to present a "tour" of today's 0.3-m TCT systems. Some of the information presented here will

be redundant. However, if you will keep the **Hazards of Cryogenic Tunnels** in mind, you will probably benefit from this review. There are still several areas in the various systems that need further improvement. My experience has been that it takes a considerable amount of exposure to this relatively new testing concept to really start thinking **cryogenic**. The various systems will be reviewed in the following order:

- (1) LN₂ supply, transfer, and storage
- (2) Test cell and exhaust
- (3) Control, data acquisition, and monitoring

7.1 LN₂ Supply, Transfer, and Storage

The majority of the LN₂ used by the 0.3-m TCT today is produced in this plant (see figure 15) which is only a short distance away. The plant is owned by a private corporation and it supplies LN₂ to our facility, the NTF, and other local users. The LN₂ is transferred to the 0.3-m TCT and NTF through a vacuum insulated pipe system. The pipe crosses the state highway here (see figure 16) and then comes back down to the ground on Langley property. The supply line from that point runs in a protected trench (figure 17) until it reaches the 0.3-m TCT and NTF sites. At that point, one line runs to the large NTF storage tank (figure 18). Just before this point, slightly to the right of figure 18, the supply pipe, as shown in figure 19, runs along the 0.3-m TCT building towards our two 20,000-gallon storage tanks. The 0.3-m TCT is located behind the large door with the **Caution** sign. Notice the pipe "hangers" which have been placed to avoid problems with contraction and expansion. It will also be noticed that the supply line is now conventionally insulated. The other lines shown here are various supply and return lines to our LN₂ storage area. Several cryogenic safety features are evident in this photograph. The louvers on the tunnel building provide protection against a tunnel pressure vessel failure. Notice the blue, Phase I, light which, if activated, would provide a warning that the O₂ level in that part of the facility is below 19 percent. The "T" vent on top of the building is a boundary layer removal system vent which has in the past caused problems with "fogging." One of the other small "T" vents is located above a rupture disc on a nitrogen return line. This roof is restricted when operating. In addition to the supply method from the plant, we have a truck delivery station (figure 20) which can service both the NTF and the 0.3-m TCT.

Our nitrogen storage area is on the opposite side of the building from the plant supply trench. Figure 21 shows the entrance to the restricted area. Again, notice the low oxygen, blue warning light. This is considered as one of the most potentially hazardous areas in the facility. Start-up and shutdown still require that technicians "man" this area. In this location, personnel are encouraged to wear protective equipment (located in the yellow locker) and they must be accompanied or monitored by another qualified technician. There is a TV monitor in this area which can scan the operators platform which is located just behind the door. To the right of the door there is a shower and eye wash station. During this coming winter, the LN₂ systems will be automated which will eliminate the necessity of having technicians in this area during operations.

The two storage tanks are located just inside the controlled entrance (figure 22). These are double walled, vacuum insulated tanks which were originally used for hydrogen storage. Figure 23 shows the operators' working station and controls. As mentioned before, an operator is required to be in this area very briefly during start-up and shutdown, but this station is not normally manned during tunnel operations. The cryogenic transfer pumps, which supply LN₂ to the facility, are located near the base of the storage tank on the right. As you might guess from the blue pump, it is a continuing project to keep the vacuum at a proper level. The "close call" that I described earlier, with the relief vent, occurred on this platform.

All of the vents in this area are now routed to the back corner of the storage area to a vent accumulator (see figure 24). This has taken care of the type of mishap that I described earlier; however, we have had fogging and spraying problems with this system which also needs to be updated. There are tentative plans to route all of the 0.3-m TCT and NTF vents to a common controlled system.

7.2 Test Cell and Exhaust

Moving back towards the tunnel we will enter the test cell through the control room. The test cell is separated from the control room by two controlled doors. The outer door (figure 25) is not locked during operations, but it is normally closed to reduce the noise level in the control room. Again, notice the Phase I visual and warning devices. The Phase II low O₂ alarm is shown at the top right of this photograph.

The second door to the test cell is controlled during operations (see figure 26). The test cell can only be entered after the facility has been brought to "reduced" test conditions. Ear protection is available at this entrance. It is the opinion of this observer that there is no risk to facility personnel if everyone remains in the control room area during tunnel operations. In this situation, all of the potentially hazardous areas are restricted.

The tunnel main vent valves (figure 27), which protect the tunnel structure against over pressurization are located on the top of the tunnel near the low velocity end of the facility. The tunnel is also protected by a rupture disc relief system which provides an additional level of protection. In this case, at least three things would have to go wrong before the tunnel exceeded its validated test envelope.

Since the tunnel is insulated externally, the tunnel structure actually shrinks. At cryogenic test conditions its length is reduced about 1.5 in. (3.8 cm) and it becomes shorter by about 0.5 in. (1.3 cm). This characteristic is taken care of in several different ways. Having an "upright" facility alleviates some of the problems that might be associated with a tunnel that "shrinks." The tunnel is fixed (anchored) at the fan section and is free to move on sliding joints relative to the fan section to account for contraction and expansion. One of the sliding joints with the teflon pad is shown in figure 28. These sliding joints and an alignment device (figure 29), which is mounted under the tunnel, at the end away from the fan, prevent side-to-side movement during contraction and expansion of the tunnel.

Clearance is provided through the roof for exhaust stacks. Constant load spring hangers (figure 30) compensate for the weight of the upper leg and allow the test section to move vertically.

Low O_2 sensors (figure 31), which are tied into the low O_2 warning and tunnel fail-safe system, are strategically located throughout the test cell. These sensors are usually located near the floor to provide an early warning of decreasing O_2 levels. A large exhaust fan (figure 32) can, when required, pull in fresh outside air around the base of the tunnel. The fan will start automatically if there is low O_2 alarm. As mentioned before, the test cell room was designed with louvered windows (figure 33) which will relieve an overpressure situation in the test area.

The fan, drive, and motor systems of the 0.3-m TCT are protected against overheating, loss of lubrication, vibration and other failures with a variety of instrumentation which are all considered in the fail-safe system. Figure 34 shows some of the vibration detection equipment which is located near the base of the fan section. Pressure reliefs and rupture discs (figure 35) are provided in all nitrogen lines if there is any possibility of "trapping" liquid nitrogen.

Figure 36 shows a lower leg, tunnel circuit, section which was removed during an annual inspection of the fan. The insulation has been cut to provide access to the flange, but can be easily repaired. This recent inspection, which was conducted in April 1989, did not reveal any moisture under the external insulation material. This relatively inexpensive, easy to repair, positive purge insulation system has been described in previous papers. It appears that this system has been significantly improved by the addition of a second generation warm nitrogen supply and distribution system shown in figure 37.

Sudden asphyxia can occur at oxygen levels below 6 percent. As reference 7 states: "The man falls as if struck down by a blow on the head and he may die in a few minutes." At oxygen levels ranging from 10 to 14 percent by volume "He may realize that he is dying but he does not greatly care." Asphyxia, explosion, and fires are the most frightening hazards of cryogenic operations. Special procedures regarding purging the tunnel circuit with ambient air before re-entry protect personnel against low O_2 situations when working in the test section. The 0.3-m TCT is small and technicians are normally outside of the test section. Asphyxia is still a concern though, and warning signs are posted at the test section entrance. In addition, it is a requirement that a portable O_2 sensor is used to check the test section before working near it. Additional protection in the test section area, to further insure that personnel are not subjected to low O_2 situations, is provided by a double block and vent system shown in figure 38. These devices and other safeguards insure that nitrogen cannot enter the test section when the access door is open.

Figure 39 presents a very recent photograph of the AWTS with the test section and plenum walls removed. The angle of attack, rake driver, and AWTS stepping motors are shown on the top of the test section plenum. The flexible ceiling wall drive rods are shown inside the plenum area. All of these drive mechanisms are protected against overdriving the various systems.

Just outside of the test cell, the primary tunnel exhaust system is visible (see figure 40). Entrance to the building from this side of the facility is also protected with low O_2 warning devices. A TV monitor is located on the roof to observe exhaust behavior and warn the operators if there is a fogging hazard. Instrumentation is also provided on the roof to indicate wind direction and velocity in the control room. Access to this roof area is tightly controlled (figure 41).

7.3 Control, Data Acquisition, and Monitoring

The control room provides readouts of all the information required to operate the facility safely and efficiently. The operators are warned in advance of any undesirable situation. The new controller automatically runs the facility in a completely safe and effective manner. The O_2 situation at 13 different locations throughout the facility is constantly monitored. The tunnel fail-safe system protects the facility from a mishap and will automatically shut down if there is a hazard. Our O_2 alarm system (figure 42), having evolved over many years of experience, is an excellent system. As with the NTF, an emergency "knockdown" phone (figure 43) system is available in the control room. If the receiver is lifted or "knocked" from the hook, it automatically calls the Langley fire department and rescue team. In addition, if there is one Phase II low O_2 alarm in the facility, the fire department will be notified automatically in addition to the tunnel failsafing. If the tunnel failsafed due to a low O_2 situation, all areas of the facility will be evacuated and all personnel will assemble in predetermined safe areas. Assigned technicians will bring rescue equipment (figure 44) to the assembly areas and await further instructions.

8. CONCLUDING REMARKS

Since the beginning of the 0.3-m TCT operations in 1973, safety has been an ever present concern. The facility was originally designed and built as a pilot facility and was intended to be used for only a short period of time. Later the facility was reclassified as a permanent facility and has actually operated for about 6000 hours. During these thousands of hours of operation, many changes have been made to the original configuration. Three major test section configurations have been evaluated and refined in the basic 0.3-m TCT tunnel circuit. The 0.3-m TCT has been a leader in the development of cryogenic pressure tunnel experimental techniques, model construction techniques, and advanced instrumentation. These constant changes have increased the difficulty of the overall safety operation.

Throughout the evolution of the 0.3-m TCT, there has been a continuing effort to improve safety standards and procedures. The **hazards** of cryogenic pressure tunnels have been defined and a viable safety program has been established which provides for a relatively safe operation. Many mistakes have been made during this evolution. However, the 0.3-m TCT has demonstrated that cryogenic pressure tunnels can be operated safely.

The facility has been completely "failsafed" to avoid the most serious **hazards**. An excellent low O₂ warning system has been established which virtually eliminates low O₂ **hazards** to personnel during normal operations. The majority of problems with expansion and contraction have been solved. A good LN₂ exhaust system has been installed and fogging problems have been reduced. There are still problems with auxiliary system vents, but a solution has been identified and will be incorporated in the near future. Cryogenic model technology has improved dramatically and complex model and instrumentation systems have been tested successfully. The 0.3-m TCT experience has shown that there are no unsolvable safety problems associated with cryogenic pressure tunnel operations.

9. REFERENCES

1. Ray, Edward J.; Kilgore, Robert A.; and Adcock, Jerry B.: **Analysis of Validation Tests of the Langley Pilot Transonic Cryogenic Tunnel**. NASA-TN-D-7828, 1975.
2. Voth, R. O.; and Strobridge, R. T.: **Cryogenic Design and Safety Review**. NASA Langley Research Center 0.3-Meter Transonic Cryogenic Tunnel. NASA-TM-74767, NBSIR-77-857, 1977, 28 pp.
3. Webster, T. J.: **A Report on Possible Safety Hazards Associated with the Operation of 0.3-m Transonic Cryogenic Tunnel at the NASA Langley Research Center**. NASA-CR-166026, 1982, 12 pp.
4. **Wind-Tunnel Model Systems Criteria**. NASA Langley LHB 1710.15, 1986.
5. **Wind-Tunnel Model Systems Quality Assurance**. NASA Langley LHB 5330.3, 1984.
6. Ray, Edward J.; Kilgore, Robert A.; Adcock, Jerry B.; and Davenport, Edwin E.: **Analysis of Validation Tests of the Langley Pilot Transonic Cryogenic Tunnel**. NASA TN-D-7828, 1975.
7. Safety Panel British Cryogenics Council: **Cryogenics Safety Manual - A Guide to Good Practice** - Second ed., Mech. Eng. Pub., Ltd. 1982.
8. **Facility System Safety Analysis and Configuration Management**, LHB 1740.4, June 1987.
9. Wyle Laboratories: **NTF O₂ Monitoring System Sensor Analysis**. Report to NTF Files, 1984.
10. Ray, Edward J.: **A Review of Reynolds Number Studies Conducted in the Langley 0.3-m Transonic Cryogenic Tunnel**. AIAA Paper 82-0941, presented at the AIAA/ASME 3rd Joint Thermophysics, Fluids, Plasma and Heat Transfer Conference, St. Louis, MO, June 1982.
11. Webster, T. J.: **Latest Developments in Cryogenic Safety**. NASA-CR-166087, 1983.

10. ACKNOWLEDGMENTS

The safe record of the first cryogenic pressure tunnel could not have been accomplished without the 0.3-m TCT Research Group and the support of the Operations Support Division. The advice and assistance of two highly qualified cryogenic pressure tunnel technicians, Patrick T. Bauer and K. Leon Parrish, were essential to this success.

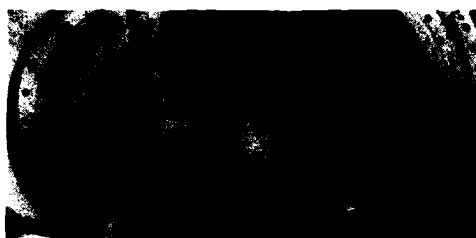


Figure 1. - Internal structure damage.

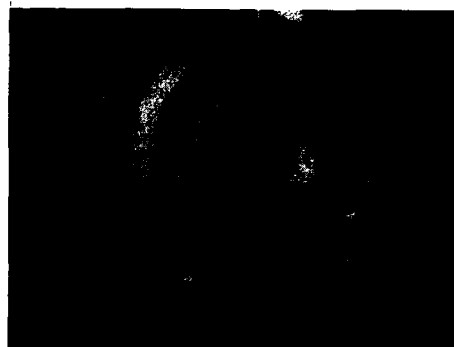


Figure 2. - Structural modifications of nacelle section.

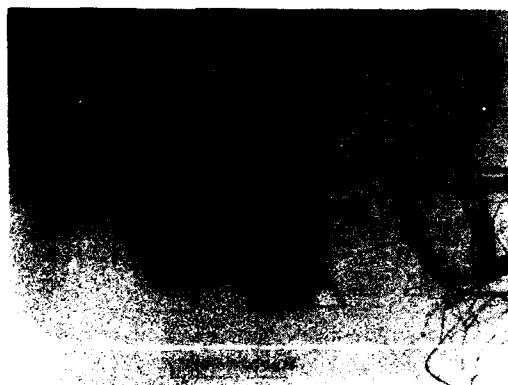


Figure 3. - Damaged calibration probe and support assembly.



Figure 4. - Original fiberglass fan hub assembly.
Damaged during testing.



Figure 5. - Nitrogen exhaust with ejector stacks.



Figure 6. - Aerial photograph of 0.3-m TCT and NTF sites.



Figure 7. - Auxiliary exhaust system for Boundary Layer Control.

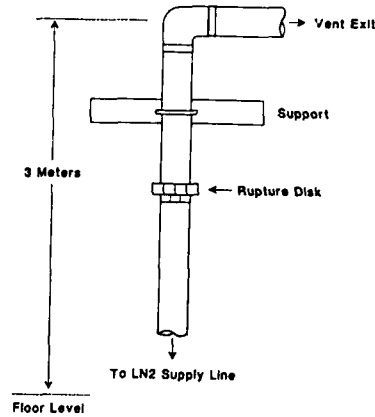


Figure 8. - Schematic of an early 90° nitrogen vent.

Low O₂ Procedure for 0.3-m TCT

Phase I O ₂ Level 19.0 to 16.5%		Phase II O ₂ Level 16.5% or lower	
<u>Warning and Alarms</u>		<u>Warning and Alarms</u>	
<ul style="list-style-type: none"> • AREA O₂ Warning Panel - 0.3-m TCT • AUDIO - Area Wobbler - 0.3-m TCT • VISUAL - Blue Area Lights - 0.3-m TCT 		<ul style="list-style-type: none"> • AREA O₂ Warning Panel - 0.3-m TCT • AUDIO - Wobbler (All Areas) - 0.3-m TCT - Fire Alarm - 0.3-m TCT - Low O₂ Alarm - Fire Station • VISUAL - All Blue Area Lights - 0.3-m TCT • TUNNEL - Fail Safe 	
<u>Actions Taken</u>	<u>Responsibility</u>	<u>Actions Taken</u>	<u>Responsibility</u>
<ul style="list-style-type: none"> • Alarm Assessment • Evacuate Low O₂ Area • Casualty Control • General Announcement 	0.3-m TCT	• Evacuate Facility	0.3-m TCT
	0.3-m TCT	• Hot Line Info. & General Announcement	0.3-m TCT
	0.3-m TCT	• Fire Station Team (Dispatched to Scene)	Fire Station
	0.3-m TCT	• Survey Facility (Assistant Survey)	Fire Station (0.3-m TCT)
		• Reset Alarm	Fire Station
		• Rescue (Assistant Rescue)	Fire Station (0.3-m TCT)
		• Casualty Control	0.3-m TCT
		• Re-Man Facility	0.3-m TCT

Figure 9. - Low O₂ procedures for the 0.3-m TCT.



Figure 10. -Photograph of monitoring panel.



Figure 11. - Photograph of space shuttle model installed in the original test section of the 0.3-m TCT.

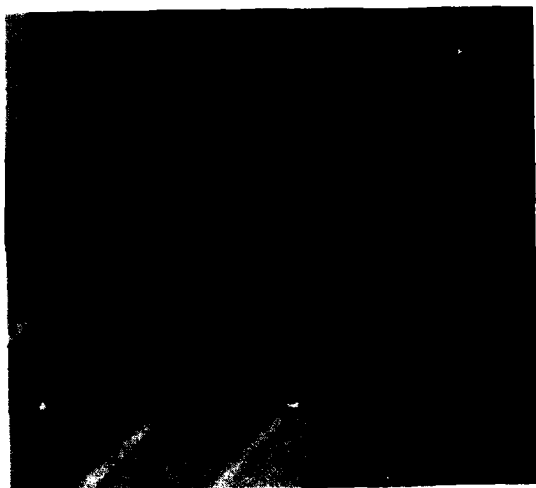


Figure 12. - Photograph of condensation study probes mounted with slotted wall.



Figure 13. - Photograph of damaged probes.

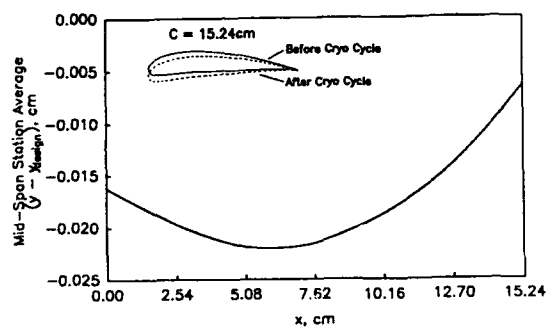


Figure 14. - Airfoil coordinate changes during cryogenic testing.



Figure 15. - Photograph of LN₂ plant.



Figure 16. - LN₂ lines crossing highway.



Figure 17. - LN₂ supply line.

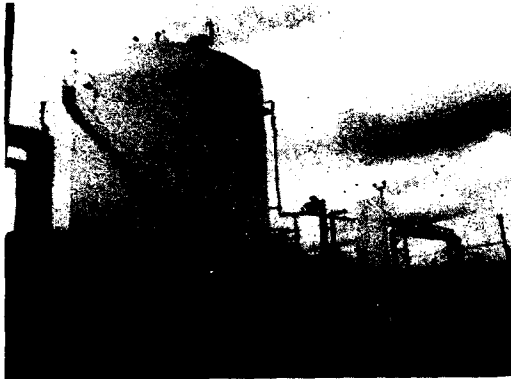


Figure 18. - NTF LN_2 storage tank.



Figure 19. - LN_2 supply line to 0.3-m TCT storage area.



Figure 20. - LN_2 track off-loading stations.

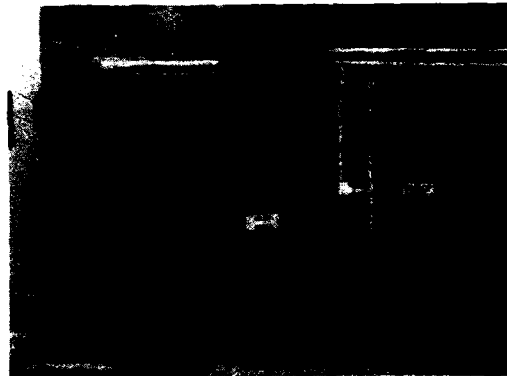


Figure 21. - Entrance to 0.3-m TCT LN_2 storage area.



Figure 22. - 0.3-m TCT LN_2 storage tanks.



Figure 23. - Working platform and vacuum pump in LN_2

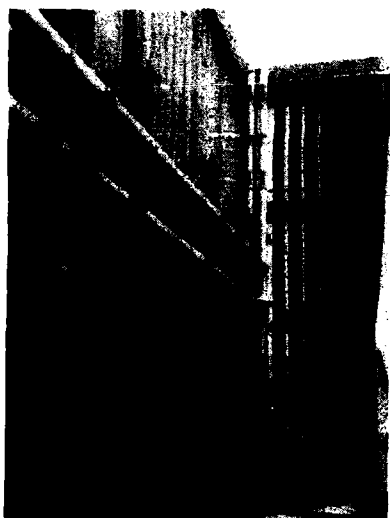


Figure 24. - Accumulator for nitrogen subsystem venting.

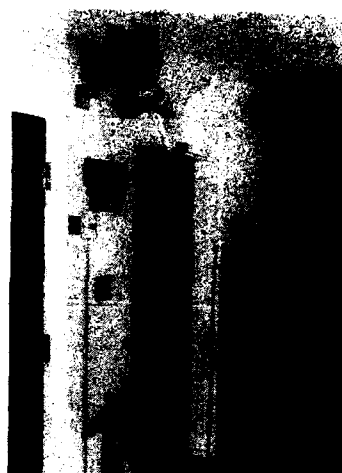


Figure 25. - First entrance to test cell area from control room.

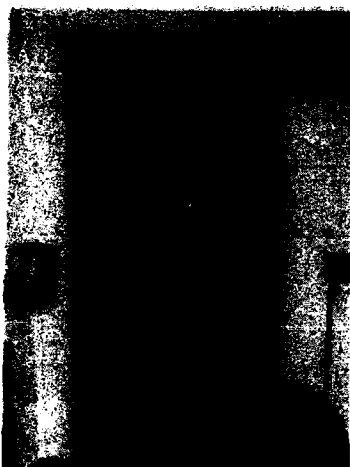


Figure 26. - Controlled entrance to test cell area.



Figure 27. - Vent system for 0.3-m TCT pressure vessel.

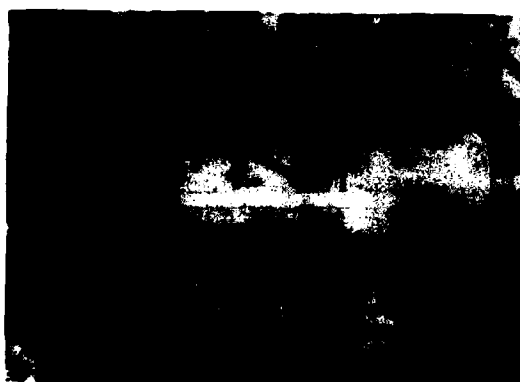


Figure 28. - A sliding joint for the 0.3-m TCT.



Figure 29. - Alignment device for 0.3-m TCT.



Figure 30. - Spring hanger for 0.3-m TCT.



Figure 31. - Typical low O₂ alarm installation.

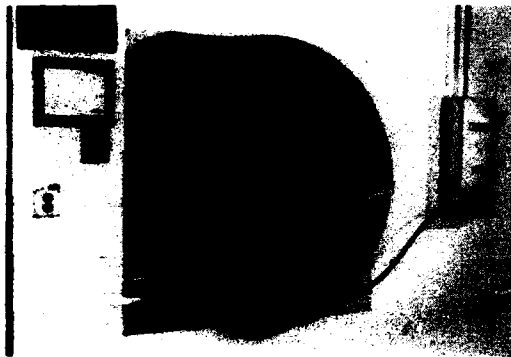


Figure 32. - Exhaust fan for test cell area.

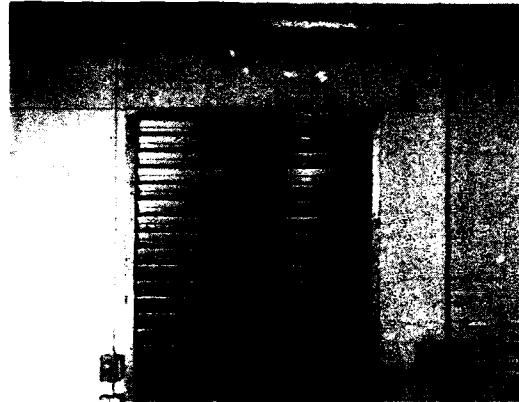


Figure 33. - Louvers in the test cell area.

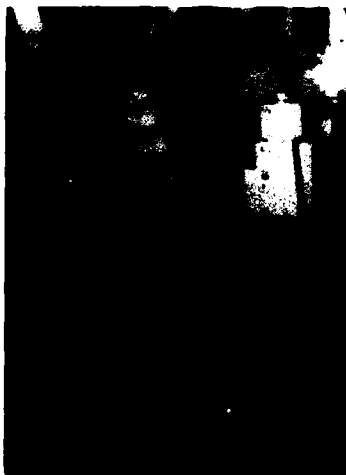


Figure 34. - Vibration detection instruments for 0.3-m TCT.



Figure 35. - Typical relief devices for 0.3-m TCT.



Figure 36. - Typical insulation system for the 0.3-m TCT.



Figure 37. - Supply and distribution devices for 0.3-m TCT insulation system.



Figure 38. - Double block and vent system protecting the 0.3-m TCT.

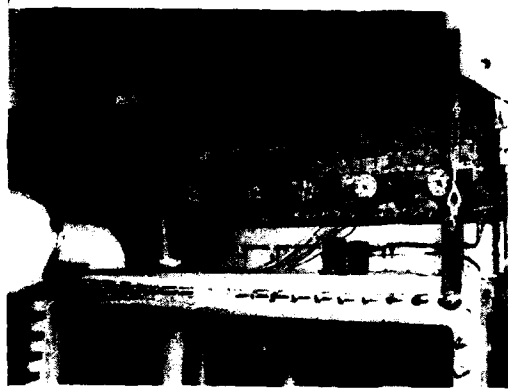


Figure 39. - AWTS with plenum and test section wall removed.

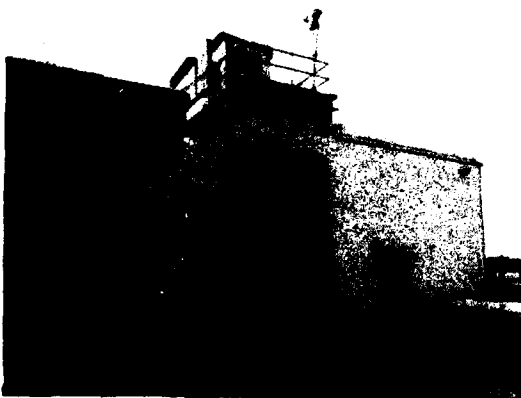


Figure 40. - Primary nitrogen exhaust area for 0.3-m TCT.



Figure 41. - Controlled entrance to 0.3-m TCT roof area.



Figure 42. - O₂ monitoring panel in control room.

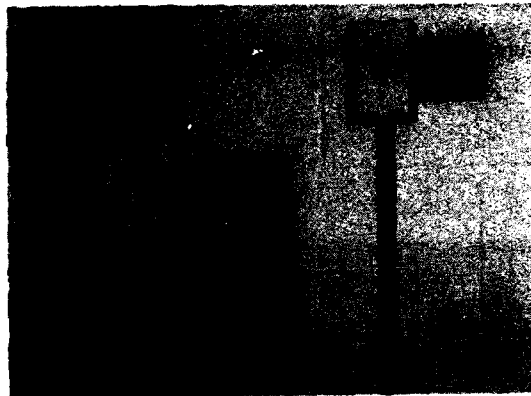


Figure 43. - Emergency phone system in control room.



Figure 44. - Rescue equipment available in 0.3-m TCT control room.

PRODUCTIVITY AND CRYOGENIC WIND TUNNELS

J. CHRISTOPHE

Office National d'Etudes et de Recherches Aéronautiques
29, Avenue de la Division Leclerc
92320 Châtillon, France

ABSTRACT

After a brief review of the situation of existing cryogenic wind tunnels, the thermal balance of five wind tunnels is discussed.

This discussion of the thermal balance is then generalized to suggest guidelines for the designers of future cryogenic wind tunnels.

Finally, with the same concern, unconventional schemes are examined.

1. NOTATIONS

M		Mach number
Re		Reynolds
k	W/mK	Conductivity
ρ	kg/m ³	Density
C	J/kg.K	Specific heat
$a = k/\rho C$	m ² /s	Diffusivity
$\sqrt{k \rho C}$	J/m ² .K. s ⁻¹	Effusivity
e	m	Thickness of a wall
x	m	Distance to the wall
$t_c = e^2/a$	s	Characteristic time
t	s	Time
h	W/m ² K	Transfer coefficient between a fluid and a wall
$h\sqrt{at}/k = h\sqrt{t/k\rho C} = A$		Dimensionless coefficients
$x/\sqrt{at} = B$		"
$h x/k = AB$		"
T	K	Temperature
T_t or T_i	K	Total temperature in the test section
P_t or P_i	bar	Total pressure
T_{tJ} or T_{tR} or T_o	K	Total temperature of the injected gas
QJ or QG	kg/s	Injected gas flow rate
QTS or QV	kg/s	Flow rate in the test section
QLN ₂ or QN ₂	kg/s	Liquid nitrogen flow rate
$Q_o = QV \sqrt{T_i/T_R}$	kg/s	Flow in the test section at temperature T_R
W	W	Fan power
QGN ₂	kg/s	Ejected gas flow rate
E	MJ/m ² .K	Energy transferred from the gas to a wall
H	J/kg = m ² /s ²	Enthalpy
S	J/kg K	Entropy
T, T _G , T _I , T _i	K	Temperatures (for definitions, see section 4)

2. INTRODUCTION

The first test of NASA Langley to check the validity of the cryogenic wind tunnel concept, in a subsonic wind tunnel with a test section measuring $0.18 \times 0.28 \text{ m}^2$, go back to 1972 [1]. Since that time, much work has been done on the subject, as can be seen from the bibliography kept up to date by R.A. Kilgore [2] and of figure 1 taken from document [3] which gives the list of the existing large and small cryogenic wind tunnels.

In this paper, special attention will be given to the ONERA-CERT T2, NASA Langley 0.3 m TCT, DFVLR KKK, NTF wind tunnels and the future ETW. The key dates concerning these wind tunnels are: start of operation of 0.3 TCT in 1973, first cryogenic tests in T2 in September 1981, inauguration of NTF on December 3, 1983, inauguration of KKK on July 9, 1987. The genesis of the ETW project, whose beginning is recounted in document [4], already has a long history, leading to the creation of the European Transonic Wind Tunnel GmbH on April, 28, 1988 for construction of ETW.

It should be noted that these wind tunnels have internal thermal insulation except 0.3 m TCT which has external insulation. The particularity of T2 with a quasi-integral internal insulation and short runs should be noted.

In all these wind tunnels, cooling of the moving gas is achieved by injecting liquid nitrogen and the resulting cold gas mixture is rejected to atmosphere.

The high cost of liquid nitrogen leads to paying particular attention to the energy balance of a cryogenic wind tunnel and investigating its productivity [5].

An excerpt from the work of G. Claude "liquid air, oxygen, nitrogen, rare gases" [6] shows the characters of liquid air used as coolant.

"... As concerns the amount of cold it contains, liquid air is in no way unusual, far from it; its vaporization heat is very close to 50 calories per kilogram, compared with more than 600 for the vaporization heat of water; thus, the evaporation of 1 kilogram of liquid air produces substantially less cold than the melting of 1 kilogram of ice, which absorbs 79 calories! It is true that by proper procedures, it is possible to add the heat produced by heating the gas, approximately 50 calories, to the vaporization heat to increase the total cooling effect of 1 kilogram of liquid air to that of 1.25 kg of ice...

Thus, what is remarkable with liquid is not the amount of cold it involves but the quality of this cold, the extraordinarily low temperature which can be achieved with it; however, by its very quality, the cold contained in liquid air is much more costly to obtain than that obtained with ice. A horse-hour, as was seen, supplies about 100 frigories as liquid air whereas it can supply more than 2000 as ice!"

This can be summarized in another way by noting that 2 600 kJ/kg are necessary to produce liquid nitrogen and that the frigories obtained after vaporization are at 77 K: 200 kJ/kg; they are at 120 K: 245 kJ/kg and at 300 K: 434 kJ/kg.

The nitrogen consumption of a wind tunnel can be classified in various ways: cooling, losses through the walls, change of temperature level and in steady state cancellation of the thermal energy contributed by the entrainment system. These factors are examined from a numerical standpoint for the five wind tunnels discussed and more generally by reviewing and supplementing the outstanding points of document [5].

From this study, we will suggest guidelines for the designers of future cryogenic wind tunnels.

Finally, we examine the solutions proposed by various authors using means other than liquid nitrogen injection alone and attempting not to exhaust the cold gas to atmosphere. The limited time we were able to spend on this study did not allow us to draw any conclusions, except to invite our colleagues to devote more time to these reflections.

3. NITROGEN CONSUMPTION - CHARACTERISTIC VALUES

3.1. NTF

Figure 7 of document [5] shows, from NASA documents, the NTF nitrogen expense in dollars per second during continuous operation of the wind tunnel in steady state during which the nitrogen flow compensates for the power dissipated by the fan into the circuit. For instance, at Mach 1, the expense is \$ 10 per second for a Reynolds number of 40×10^6 and \$ 20 per second for 80.10^6 . This corresponds to a nitrogen cost of \$ 70/ton.

The internal insulation of this wind tunnel is such that the loss through the walls represents a power of 315 kW, i.e., 85 W/m^2 for an internal surface area of 3700 m^2 . Cooling from 300 K to 120 K appears to be carried out at a rate of 45 K per hour.

Document [7] very clearly summarizes the way in which operation of such a wind tunnel should be considered:

"The NTF has the general appearance and is often talked about as a typical continuous operating fan-driven wind tunnel that has the potential to mass produce data on a continuous basis. Although in principle the potential exists, it is somewhat misleading to think about a large cryogenic tunnel in this context. In reality, the operation must be viewed much as a blow-down tunnel with efforts directed toward minimizing run time and maximizing data gathering rates. The main constraints with regard to run time are liquid nitrogen logistics and costs, and model access."

3.2. ETW

The ETW project has advanced from the cold box concept to the internal insulation concept. The insulation specifications require a loss of less than 60 W/m^2 .

The annual liquid nitrogen consumption, according to Sverdrup (January 1986) is approximately 72,000

metric tons, including 34,000 metric tons for testing (500 rotations), 7,000 metric tons for repressurization and restarting of the fan and 31,000 metric tons for conditioning.

Conditioning includes, for instance, 20 pallet coolings from 290 to 120 K, each costing 30 metric tons of nitrogen, and 35 coolings of the circuit, each requiring an average of 300 metric tons. The weight of the uninsulated internal metal parts of the circuit is approximately 500 metric tons.

The operating cost includes 48 percent electricity and 33 percent payroll. The share of electricity required for the nitrogen plant is 90 percent, i.e., 43.5 percent of the operating cost.

3.3. KKK [8, 9, 10]

The KKK wind tunnel has very good internal insulation with a thickness of 320 mm, for which the estimated loss is 15 W/m².

Cooling of the wind tunnel from 300 K to 100 K at a rate of 10 K per hour leads to a liquid nitrogen expense of 90 metric tons. The hold at 100 K for 24 hours involves an expense of 24 metric tons nitrogen (Fig. 2).

3.4. 0.3 m TCT

The TCT wind tunnel is made of aluminium and has external insulation.

Cooling of the wind tunnel consists of cooling the walls and internal components. During the tests, the liquid nitrogen injected compensates for the power dissipated by the fan. Figure 3 shows that using an insulation with a conductivity $k = 0.33$ W/mK and a thickness of 0.08 m, the ratio between the energy loss by conductivity and that required to compensate for the power dissipated by the fan is only 1.5 percent.

3.5. ONERA-CERT T2

The transonic T2 wind tunnel with adaptive walls is a blowdown wind tunnel with runs lasting approximately 60 seconds. The ordinary parts are made of carbon steel and the areas most exposed to cold of austenitic steel. The internal insulation is mainly polyurethane foam with a thickness of 10 mm [11, 12]. Except for the honeycomb and gratings, all the internal parts are insulated.

Figure 4 shows the variation of the total temperature and pressure, T_t and P_t , the Mach number, the liquid nitrogen flow rate $QLN2$ and the injected air flow rate QJ during a typical run as well as the cooling, model introduction, wall adaptation, wake exploration phases. Cooling from 300 K to 150 K takes place in 10 seconds [13]. Figure 5 shows both the injector efficiency, characterized by the ratio of QJ to the test section flow rate QTS and the nitrogen consumption characterized by ratio $QLN2/QTS$, for conditions $M = 0.8$ and a total pressure of 1.8 bar. Ratio QJ/QTS decreases at T_t decreases, confirming the increased efficiency of the injector when ratio T_t/T_i increases, where the injection temperature T_i is ambient temperature, near 300 K. The experimental $QLN2/QTS$ curve shows that at 120 K, the liquid nitrogen flow rate is equal to 8 percent of the flow rate in the test section. The dotted-line computed curve exhibits a difference of 15 percent at 120 K, representing the losses through the walls.

The integration of curve $QLN2 = f(t)$ of figure 4 leads to a nitrogen consumption of 720 kg. Over a large number of runs, the consumption is 1000 to 1200 kg per run (including the transfer, storage and model cooling losses).

4. THERMAL BALANCE

The nitrogen consumption is the sum of the consumptions for various operations:

- Initial cooling for time t_i with an average flow rate $QN2i$. Changes of test conditions: M , p_i , T_i . The consumption is:

$$QN2i \cdot t_i + \sum QN2c \cdot t_c$$

- Test time t_e during which the nitrogen compensates for the heat $QN2w$ dissipated by the drive component and the thermal losses $QN2p$, giving:

$$(QN2w + QN2p)t_e$$

- Cooling during periods outside the useful test periods to compensate for the heat losses through the insulation:

$$(QN2m \cdot t_m)$$

The importance of the time can be seen. In effect, if, for instance, $QN2m$ is small compared with $QN2w$ but t_m is large compared with t_e , the consumption during the idle times will become predominant. All the operations are affected by the energy transferred through the insulation which, for long periods in steady state, is proportional to time t . It will be seen below that in transient state, the energy transferred is proportional to \sqrt{t} .

4.1. Power $QN2w$ Dissipated by the Drive

Figures 6 and 7 from document [5] show the characteristic terms as a function of T_i and the compression ratio ω :

W/Q_0 and $QLN2/Q_0$ for a fan-driven wind tunnel
 QG/Q_0 and $QLN2/Q_0$ for an induction-driven wind tunnel.

When the wind tunnel is in steady state, the liquid nitrogen flow compensates in one case for all the power W dissipated by the fan and converted to heat and in the other case for the heat dissipated by the injected flow QG at ambient temperature T_0 .

4.2. Cooling - Changes of Condition

Section 3 showed very different cooling rates: 10 K per hour for KKK, 45 K per hour for NTF, 15 K per second for T2.

In the T2 wind tunnel, cooling concerns only the idle gas in the circuit, the filters, the honeycomb and the power dissipated to the insulation in transient state. In effect, except for the filters and the honeycomb, all the internal parts of this wind tunnel are insulated like the walls of the shell withstanding the internal pressure.

These concepts of "integral insulation" and "transient state" will be discussed in greater detail below.

On the contrary, for KKK and NTF and also for ETW, the weight of the internal uninsulated components to be cooled is high, for instance 500 metric tons for ETW. Cooling such weights requires a large expense of liquid nitrogen. In addition, the risk of excessive thermal stresses in more or less hyperstatic structures led to limiting the cooling rate.

The orders of magnitude of the energies involved are given by KKK, for which cooling to 100 K requires 90 metric tons of nitrogen, and by ETW, for which cooling to $\Delta T = 180$ K of 500 metric tons of steel at $C = 0.63$ kJ/kgK with a nitrogen cooling capacity of 245 MJ/t requires 230 metric tons of liquid nitrogen. Similarly, cooling of an ETW pallet requires 30 metric tons of nitrogen and cooling of the part of the sting-holder sector located in the test section (3 metric tons) requires approximately 1.5 metric tons of nitrogen.

These phases of cooling and changes of conditions mainly involve consecutive cooling and heating operations of internal structural parts. This is why in 1979, then in 1982, 1984 and 1985 [14, 15, 11, 5] we drew the attention, although apparently unsuccessfully, to the very different response times of the components which are sources of thermal stresses and deformations, the necessity of decreasing the heat capacity of internal parts, the advantage of insulating the internal parts, the requirement of not cooling parts which can be kept at ambient temperature using suitable technological solutions [5, pages 8, 16].

Figure 8, drawn from [5], shows the variation of the gas temperature T_G and the temperature of the internal components T_I for a fixed liquid nitrogen flow rate under various conditions concerning the internal parts and walls, in a wind tunnel completely insulated externally. The variation of T_G , rapid for a wind tunnel without internal parts and with internal wall insulation, is slower with an internal parts and with internal insulation of the walls; it is much slower with internal parts and walls without internal insulation.

4.3. Insulation

After considering the effect of the heat dissipated by the drive element in the wind tunnel and the effect of the heat capacity of internal parts, we now examine factors related to wall insulation which determine both the temperature hold conditions outside useful periods and the thermal losses during various operations.

Approximate amounts of nitrogen required to hold the temperature are given by KKK: 24 metric tons of nitrogen for 24 hours at 100 K for this wind tunnel, with an excellent insulation (15 W/m²) and by NTF: loss of 325 kW, i.e., approximately 27,000 MJ or roughly 110 metric tons of nitrogen per 24 hours (with 245 MJ/t for nitrogen).

After reviewing the results already given concerning comparison between internal and external insulation [15, 11, 5], the behavior of semi-infinite body will be studied more completely.

4.3.1. Review

Figures 9 and 10 show the heat transfer from a fluid to the wall for a steel wall 10 mm thick with either an internal foam insulation with thickness e_I or the same external insulation. The heat transfer coefficient h_1 between gas and wall is assumed to be ∞ , i.e., the internal wall temperature is the same as the gas temperature. The energy E transferred at time t after a temperature step ΔT is expressed in MJ/m²K, i.e., for a unit area of 1 m² and a step $\Delta T = 1$ K. Figure 9 shows that for internal insulation with infinite thickness, the quantity of heat transferred is proportional to \sqrt{t} (1/2 slope in logarithmic coordinates). The same is true for relatively short times and a finite insulation thickness. After a certain time, steady state is reached and the energy is proportional to time t (slope 1 in logarithmic coordinates). For zero insulation thickness, the relation between E and t is of the form $E = a + bt$ (where a represents the heat capacity of the metal wall).

Figure 10 compares the internal and external insulation. It can be seen that for long times, the curves approach the same limit. For an insulation thickness of 25 mm, this time is approximately 1 week; for 250 mm it is approximately 1 month. For short times, only the internal insulation is to be considered. The 1/2 slope lines graduated at $n = 1.25 - 1.6 - 2 - 2.5$ represent n times the energy transferred for $e_I = \infty$.

4.3.2. Semi-Infinite Body

For a semi-infinite body, initially at $T = 0$, subjected on the wall to an exchange h with a fluid at temperature T_G , the analytic solution [16, 17] giving the temperature T in the body versus the depth x and the time t is written:

$$T/T_G = \operatorname{erfc} \frac{B}{2} - e^{(AB + A^2)} \operatorname{erfc} \left(\frac{B}{2} + A \right)$$

On the wall, $x = 0$ and we have:

$$T/T_G = 1 - e^{(A^2)} \operatorname{erfc} A$$

if $h = \infty$ or, which amounts to the same thing, if the wall temperature of the body is imposed, we have:

$$T/T_G = \operatorname{erfc} \frac{B}{2}$$

where $A = h\sqrt{at/k} = k\sqrt{t/k\rho C}$
 $B = x/\sqrt{at}$

The wall temperature depends only on A. If A is large, $T_{x=0}$ approaches T_G and, in this case, the temperature in the body depends only on B.

Figure 11 summarizes these results. It can be seen that for $A \geq 32$, the curves are practically identical to the curve $A = \infty$.

If we consider a foam defined by :

$$k = 0.025 \text{ W/mK} \quad \rho = 100 \text{ kg/m}^3 \quad C = 1000 \text{ J/kg K}$$

$$\sqrt{k \rho C} = 50 \quad a = k/\rho C = 2.5 \times 10^{-7}$$

The table below shows the values of A:

kW/m ² K	100	400	1000
t = 1 s	2	8	20
t = 16 s	8	32	80
t = 64 s	16	64	160
t = 256 s	32	128	320

The limit curve $A = \infty$ is reached very rapidly. Thus, considering only this limit curve, it is possible to plot the body temperatures versus x and t (Fig. 12) (these values are overestimated for short times). The notation T/T_G is replaced here by $(T-T_i)/(T_G-T_i)$ (which is only a change of origin), where T is the local temperature, T_i is the initial wall temperature, T_G is the gas temperature. The integral $\int_0^x \rho C (T-T_i)_x dx$ represents the energy transferred to the wall expressed as J/m² at time t. The area located between the T axis and the curve at time t is proportional to \sqrt{t} (in effect, for a given value of $(T-T_i)/(T_G-T_i)$, x is proportional to \sqrt{t}). The proportionality of the transient transfers to \sqrt{t} , already seen at the beginning of section 4, is found here again.

4.3.3. Semi-Infinite Body Covered by a Thin Metal Plate

The above computation is repeated numerically after adding to the surface of the insulation an aluminium plate of 1 mm thick and with the following characteristics:

$$k = 140 \text{ W/mK} \quad \rho = 2800 \text{ kg/m}^3 \quad C = 850 \text{ J/kg K}$$

$$\sqrt{k \rho C} = 18000 \quad a = k/\rho C = 60.10^{-6}$$

The computation made for $h = 63, 100, 160, 250, 400, 630, 1000 \text{ W/m}^2\text{K}$ supplies the temperature tables and curves for $x = 0, 10, 20, 50$ and 100 mm versus the time. For the same values of x and t, the differences between the values of $(T-T_i)/(T_G-T_i)$ for $h = 100$ and $h = 1000$ are only sensitive for $x < 20 \text{ mm}$ and for short times. Above 400 seconds, the differences are very small.

The points corresponding to $h = 1000$ are plotted in figure 12. The differences are small.

However, the wall temperatures vary more slowly (Fig. 13). For $h = 1000$, the difference is negligible at around 10 seconds.

This aluminium plate does not affect computation of the energy transferred from the fluid to the foam-insulated wall during a transient state.

Figures 9 and 10 and the integration of figure 12 show that the energy transferred to the foam-insulated wall is approximately equal to $0.0035 \text{ MJ/m}^2\text{K}$ in one hour and $0.0022 \text{ MJ/m}^2\text{K}$ in 0.5 hour. This can be compared to the losses through the walls insulated with 160 mm of foam, approximately equal to $0.1 \text{ MJ/m}^2\text{K}$ in one week (Fig. 9 and 10).

However, the 1 mm aluminium foil is relatively costly, $0.00238 \text{ MJ/m}^2\text{K}$, but it would eliminate any problems of contamination by the humidity contained in the insulation.

5. GUIDELINES

From the above discussion, it could be concluded that the search for nitrogen savings leads to a T2 type wind tunnel with integral insulation (walls and internal components) and relatively short runs, with no foregone conclusions as to the entrainment mode. The insulation would have to be much thicker than in T2 since the run times would be longer. It will be necessary to study the optimum run time with the greatest care.

The insulation would only function in transient state so as to preserve a heat transfer proportional to \sqrt{t} . Therefore, between runs, the wind tunnel would not remain cold so as to avoid losses in steady state. This would amount to cooling only what must absolutely be cooled.

Like T2, this wind tunnel would be very flexible as regards the change of test conditions.

As concerns the compensation for the thermal energy dissipated by the entrainment system, the use of liquid nitrogen can be questioned. For instance, in a T2 type wind tunnel, if the entrainment airflow QJ were cooled first (at the cost of a slight loss of efficiency of the injection, certainly acceptable, Fig. 5), injection would be unnecessary. This will be examined in section 6.

It first appears necessary to mention two other guidelines which will be discussed in section 6.

First of all, it is possible to recover the frigories obtained at high cost instead of rejecting them to atmosphere?

In addition, is cooling by nitrogen injection the best method? As indicated by document [1], the first cryogenic test facility appears to be the compressor test facility of D.C. MacPheil and C.K. Rush [8] dating back to 1962. In this facility, an air temperature of 125 K was obtained using a liquid nitrogen exchanger.

The idea of a cryogenic exchanger was also suggested by Lieng Chi Chiang in 1980. With this suggestion, a high pressure gas, adiabatically expanded, cooled a "regenerator" then crossed by air at moderate pressure which was cooled in the regenerator [20].

6. OTHER SCHEMES

The essential part of a wind tunnel is the test section part, preceded upstream by a settling chamber and a convergent and followed downstream by a diffuser. To place the air in motion, it is necessary to create a difference in pressure between upstream and downstream. This can be achieved by a fan or a compressor located in the circuit (conventional wind tunnel) or by compressed air injection (induction-driven wind tunnel) or by a pressure difference between an upstream receiver and a downstream receiver (blow-down wind tunnel). For the last two types, it is also necessary to use a compressor to compress the air, but the compression plant is external to the wind tunnel. For the compressor, internal or external, the energy it receives is rejected as waste by the coolants but, for the last two types, this is done by an external system which does not affect the wind tunnel. However, for the fan-driven wind tunnel, the water cooler (air/water exchanger) is located in the wind tunnel circuit. This exchanger introduces a large pressure loss and affects the design of the forms of the aerodynamic circuit. An induction-driven wind tunnel operating at ambient temperature does not have this problem, since the inductor air QG is introduced at ambient temperature.

This distinction between internal and external components of the aerodynamic circuit appears very important in investigating unconventional schemes.

6.1. Pan Ruikang Scheme [10]

Figure 14 shows the scheme proposed by Pan Ruikang in 1984. The existence of a large supply (1290 m³) of air at 220 bar allowed this ambitious project for a blow-down transonic wind tunnel with a test section size of 2.4 × 2.4 m² to be suggested. The main principle consists of isenthalpic expansion (iso H) from 150 bar to 5 bar through a valve. This would bring the air to a total temperature of 154 K.

At the compressor outlet, the air is precooled to 215 K as shown in Figure 14. After the test section, the air flows into a receiver with a capacity of approximately 3 × 10⁴ m³. The document [20] does not discuss insulation of the various components.

6.2. Nelander's Scheme

Figure 15 shows the scheme proposed by Nelander in 1979 [27] then in 1983 and 1984 [21, 22] for a wind tunnel with a test section size of 2 × 2 m². A supply of 36 × 10³ kg of air at 120 bar drives an expansion turbine which drives a fan. The cold air from the expansion turbine supplies the circuit then flows into a low pressure receiver after cooling the turbine feed air in an exchanger. The total temperature in the test section could be as low as 140 K.

6.3. Remarks on the Two Above Schemes

In these two schemes can be recognized both the expansion without work at constant enthalpy of Linde (in which cooling is due to the shape of the iso H in the TS diagram) and the expansion with work of Claude. This is summarized in Figure 16 [26]. However, as the purpose is only to cool the gas but not to liquefy it, the expansion process does not reach the critical curve, contrary to what occurs in Figure 16 which describes the liquefaction processes. The essential importance of the exchangers in liquefaction cycles, clearly visible in Figure 16, also led to precooling in the Pan Ruikang and Nelander schemes.

The blow-down wind tunnel proposed by Pan Ruikang suggests a very interesting alternative to the conventional blow-down wind tunnel (supplied with the air at ambient temperature) cooled by nitrogen injection, which is economically unfeasible (see [5], page 8.8).

For a given mass of high pressure air in a wind tunnel at room temperature, the test time increases from a blow-down wind tunnel to an induction-driven wind tunnel and perhaps to a wind tunnel with compressor driven by an expansion turbine as suggested by Dobrohotov [23]. But the concern for mechanical simplicity would lead to choosing an induction-driven wind tunnel. The choice is even more difficult if it is desired to create part of a liquefaction plant with the "external" components of the wind tunnel.

In spite of the advantages of an expansion turbine, is it wise to drive with it a fan which dissipates all its power as heat into the circuit to be cooled and which additionally must be built to work at low temperature?

6.4. Amecke's Scheme [25]

Amecke's scheme, proposed in 1985, is shown in Figure 17. The idea proposed and the scheme summarizing it show a clear separation between "internal" and "external" components.

The fan operates at ambient temperature and the heat it dissipates is evacuated by a water cooler. The fan provides the differential pressure required across the exchanger.

The cold air, at temperature T_i , from the wind tunnel itself loses its frigories in the exchanger which it leaves at ambient temperature. The air at ambient temperature from the compressor crosses the exchanger where it is cooled down to T_i .

If the exchanger efficiency were perfect (frigories lost by the cold fluid completely transmitted to the fluid to be cooled) no additional energy would be required. If this is not the case and if a difference ΔT is assumed, the frigories to be supplied are equal to :

$$w = Q_V \cdot C_p \cdot \Delta T$$

i.e. where

$$C_p = 1 \text{ kJ/kg.K}$$

$$w/Q_V \text{ kJ/kg} = \Delta T$$

According to Figure 17, these frigories are supplied by injecting nitrogen.

Figure 6 shows the values of W/Q_0 , where W represents the energy to be compensated for by injecting liquid nitrogen, versus T_i and the fan compression ratio. It is necessary for w to be much smaller than W . As an example, it can be noted that for $T_i = 200 \text{ K}$, $W/Q_0 = 15$, with $T_R = 300 \text{ K}$ $W/Q_V = 15 \sqrt{T_i/T_R} = 12.24$.

The exchanger must therefore be very efficient and with a low ΔT .

During private conversations, Mr. Nicolas of Air Liquide suggested the same solution of a compressor operating at ambient temperature and cooled by a water exchanger. But, not having found the separation into "internal" and "external" components of Figure 17, it was not seen how the exchangers could be located in the wind tunnel circuit without an excessive pressure loss.

6.5. Scheme Suggested by P. Contensou [24]

An appendix describing a scheme for a cryogenic induction wind tunnel was attached to a letter from Mr. Contensou of January 1977 relative to the European cryogenic wind tunnel project.

The compressed gas supply crosses a previously cooled A-B accumulation heat exchanger and supplies the injector. The gas is exhausted from the wind tunnel by another C-D accumulation heat exchanger where it loses all its frigories and is exhausted to atmosphere at ambient temperature. This type of exchanger is called "regenerator" in the document [26, pp. 169-175]. In the scheme considered, cylinders with a length of 15 m and a diameter of 0.6 m filled with 35 metric tons of steel balls with a diameter of 50 mm were considered. This dimensioning was relative to a wind tunnel with a test section size of $0.85 \times 0.85 \text{ m}^2$, a volume of 250 m^3 , $p_i = 4.4 \text{ bar}$, $T_i = 130 \text{ K}$, for which $M = 0.9$; $Q_V = 1120 \text{ kg/s}$ and $Q_J = 134 \text{ kg/s}$. The weight of gas was 5360 kg for a 40-second run at 4.4 bar and 130 K. The mass of air contained in the wind tunnel was 2960 kg.

Figure 18 shows the general arrangement, the distributions of the ball temperatures T_b along the axis after cooling, after the run and after regeneration, the variation of T_a versus time during the run.

A cooler supplied by the supply of high pressure air and a path B, A, C, D was considered for cooling, with no other details. Regeneration by circulation in direction D, C, A, B was obtained by a water-cooled blower (as in Amecke's scheme) to carry off the heat due to the power supplied to the blower. To return to the initial state, this regeneration could be supplemented by a contribution from the cooler.

The author pointed out that the blower and the control valves were at ambient temperature.

Accumulation heat exchangers with a moderate cost and low pressure loss are of particular interest [26, p. 170] as is the possibility of recovering all the frigories at exhaust.

The "external" components of the wind tunnel, with simple geometric shapes, can be made using conventional cryogenic techniques allowing, for instance, the use of the superinsulation technique, much more difficult on an aerodynamic circuit with complex shapes.

6.6. Remarks

The above schemes either completely avoid or considerably reduce the injection of liquid nitrogen.

Should part of a liquid nitrogen plant be built to make the cooler (see sections 6.1 and 6.2)? This depends on local availabilities, in particular compressed air. However, it can be noted that in the two cases mentioned, the minimum temperatures are 154 K and 140 K whereas it is desired to go down to 100 K. It would appear more logical to have a liquid nitrogen plant providing a supply of nitrogen at 77 K but with a cycle specially designed to supply both liquid nitrogen (cost 2800 kJ/kg) and gaseous nitrogen (cost 860 kJ/kg).

The gas in the wind tunnel would be cooled by exchangers requiring a thorough study (accumulation exchanger, plate exchanger (two gases or liquid nitrogen gas), heat exchanger with coolant, etc.). It is not yet certain whether the gas in the wind tunnel should be nitrogen or air.

It is necessary to avoid introducing the heat dissipated by the drive system into the wind tunnel circuit.

An accumulation exchanger would allow the cold contained in the gas exhausted from the wind tunnel to be recovered without using large receivers. The requirement for such receivers wrongly led to rejection of the idea of recovery in document [4].

Again, we note that cryogenic wind tunnels, even those called continuous, have the character of blow-down wind tunnels (with runs of varying duration).

7. CONCLUSIONS

The future development of cryogenic wind tunnels will certainly be determined by economic considerations. Therefore, we would not like to draw any conclusions for the time, to avoid choices made without sufficient comparisons and likely to be reversed. We would especially like to invite our colleagues to investigate the ideas discussed.

Along these lines, we wish to draw attention to the concept of "internal" or "external" components. The external components are not subjected to the contingencies related to the shape of the aerodynamic circuit and can be implemented with customary industrial technologies, for instance water cooling, or conventional cryogenic technologies (insulation, exchangers, liquefaction plant).

In our opinion, a future wind tunnel should have an integral internal insulation operating in transient state. The choice of the desired test time is a very important point.

Considering the success of T2, an induction-driven wind tunnel cooled by exchanger with recovery of the frigories appears to be an attractive solution. The absence of mechanical parts in the circuit introduces a large degree of simplification. It can thus be hoped that work will only be required rarely in the circuit, where it will be possible to keep the gas uncontaminated. The test section area where work is necessary will be treated to eliminate any contamination from the circuit.

But as we said, we do not wish to draw any conclusion.... Before going any further, many comparisons and figures are still necessary.

8. ACKNOWLEDGMENTS

I would like to thank my colleague, Mr. François, for our long and friendly thermal and thermodynamic conversations and for all the time devoted over many years to cryogenic wind tunnels.

REFERENCES

- [1] R.A. Kilgore and D.A. Dress: The application of cryogenics to high Reynolds number testing in wind tunnels. *Cryogenics*, August 1984, September 1984.
- [2] M.H. Turtle and R.A. Kilgore: Cryogenic wind tunnels. A selected, annotated bibliography ; NASA Technical Memorandum 8634, April 1985.
- [3] D.A. Dress and R.A. Kilgore: Cryogenic wind tunnel research : a global perspective. *Cryogenics* 1988, Vol. 28, January.
- [4] J. Christophe: Genèse du projet de soufflerie transsonique européenne à grande nombre de Reynolds. *L'Aéronautique et l'Astronautique* n° 72, 1978.
- [5] J. Christophe: Productivity: the economic aspects of cryogenic wind tunnel design and use. Special Course on Cryogenic Technology for Wind Tunnel Testing. Rhode Saint-Genèse, 22-26 April 1985, AGARD Report n° 722.
- [6] G. Claude: Air liquide, oxygène, azote, gaz rares. Deuxième édition Dunod 1926.
- [7] W.E. Bruce, B.B. Gloss and L.W. Mc Kinney: Testing and checkout experiences in the national transonic facility since becoming operational. Second Cryogenic Technology Review Meeting, DFVLR Köln/Porz, 28-30 June 1988.
- [8] G. Viehweger: The cryogenic wind tunnel Cologne. AGARD CP 348, Cesme, 26-29 September 1983.
- [9] G. Viehweger: The Kryo-Kanal-Köln project KKK. Special Course on Cryogenic Technology for Wind Tunnel Testing. Rhode Saint-Genèse, 22-26 April 1985. AGARD Report n° 722.
- [10] G. Viehweger: The Kryo-Kanal-Köln project KKK. Second Cryogenic Technology Review Meeting DFVLR Köln/Porz, 28-30 June 1988.
- [11] J. Christophe, M. Bazin, P. Broussaud, G. François, P. Paci, M. Dubois: Développement des travaux suscités par les réalisations et les projets de souffleries cryogéniques. *Recherche Aéronautique* n° 1984-2.
- [12] A. Mignosi, J.B. Dor: La soufflerie cryogénique à parois autoadaptables T2 de l'ONERA-CERT. AGARD CP 348, Cesme, 26-29 September 1983.
- [13] J.B. Dor: The T2 cryogenic induction tunnel in Toulouse. Special Course on Cryogenic Technology for Wind Tunnel Testing. Rhode Saint-Genèse, 22-26 April 1985. AGARD Report n° 722.
- [14] J. Christophe and G. François: Thermal insulation of pressurised cryogenic wind tunnels. Paper n° 25, First International Symposium on Cryogenic wind tunnels, Southampton, 1979.
- [15] G. François: Thermal behaviour and insulation of a cryogenic wind tunnel. Réunion technologie cryogénique. Amsterdam, 15 septembre 1982. TP ONERA 1982-89.

- [16] H.S. Carslaw and J.C. Jaeger: Conduction of heat in solids. Clarendon Press (second edition), 1959.
- [17] C.C. Lin: Turbulent flow and heat transfer. High Speed Aerodynamics and Jet Propulsion, Vol. V, Princeton University Press, 1959.
- [18] C.K. Rush: A low temperature centrifugal test rig (Mech. Eng. Report). Nat. Res Council of Canada, Rep. MD-48 NRC-776, 1963.
- [19] R.A. Kilgore and D.A. Dress: A survey of cryogenic wind tunnels. Presented at Department di Ingegneria Aeronautica e Spaziale Politecnico di Torino. April 14, 1986.
- [20] Pan Ruikang: A cryogenic high Reynolds number transonic wind tunnel with precooled and restricted flow. Acta Aerodynamica Sinica, n° 2, 1984.
- [21] C.A. Nelander: Quasi continuous transonic wind tunnel for cryogenic operation. Rollab Memorandum RM 096, 1983.
- [22] C.A. Nelander: Ett Unik drivsystem för Vindtunnlar; FFA Memo 126, 1984.
- [23] A.N. Dobrohotov: Opisani izobretenijak avtorskomu svidetel "stvu" brevet CDU 629.7.018 (088.8). Traduction EDF du 1er juin 1988.
- [24] P. Contensou: Etude d'une soufflerie à rafales cryogénique. Document non publié, janvier 1977.
- [25] J. Amecke: Energieparender Kreislauf für kontinuierliche Kryo-Windkanäle ; DGLR Jahrestagung Bonn Bad Godesberg 30 sept 2 okt 1985.
- [26] G.G. Haselden: Cryogenic Fundamentals. Academic Press 1971.
- [27] C.A. Nelander: Proceedings of the First International Symposium on Cryogenic Wind Tunnel, 3-5 April 1979.

Organization	Tunnel	Test gas	Test section size, h,w,l (m)	Speed or Mach range	Stagnation pressure (bar)	Stagnation temperature (K)	Running time
RAE - Bedford	Closed circuit, centrifugal fan	Nitrogen	0.3 × 0.3 × 1.5	Up to 25 m s ⁻¹	Atmospheric	90-ambient	Typically 1 h
University of Southampton	Closed circuit, fan	Nitrogen	0.11 × 0.11 × 0.25 (regular) 0.14 × 0.11 × 0.41 (MSBS)	14-72 m s ⁻¹	Atmospheric	79-380	Typically 1 h
ETW Group	PETW, closed circuit, fan	Nitrogen	0.23 × 0.27 × 0.78	0.35 - 1.0 continuous 1.2, 1.35 fixed nozzles	1.25-4.5	90-313	Typically 1 h
ONERA-CERT	T2, closed circuit, induction driven	Nitrogen rich air	0.37 × 0.39 × 1.32 (solid adaptive walls)	0.3-1.0	1.6-5.0	95-ambient	Up to 100 s +
ONERA-CERT	T3, closed circuit, fan	Nitrogen	0.1 × 0.12 × 0.6 (solid adaptive walls)	0.05-0.8	1.0-4.0	95-ambient	Up to 25 min
DFVLR - Köln	KKK, closed circuit, fan	Nitrogen	2.4 × 2.4 × 5.4	Up to 0.38	Up to 1.12	100-300	Up to several hours
NAL (Japan)	Closed circuit, fan	Nitrogen	0.1 × 0.1 × 0.3	Up to 1.02	Up to 2	90-ambient	More than 2 h
University of Tsukuba	Closed circuit, fan	Nitrogen	0.1 × 0.1 × 0.3	Up to 30 m s ⁻¹	Up to 2	100-ambient	Up to 2 h
University of Tsukuba	Closed circuit, fan	Nitrogen	0.5 × 0.5 × 1.2	7-65 m s ⁻¹	1.22-8.10	118-ambient	30 min at maximum R
NDA (Japan)	Closed circuit, centrifugal compressor	Nitrogen	0.30 × 0.06 × 1.0	Up to 157 m s ⁻¹	Up to 1.77	108-ambient	Up to 30 or 40 min
University of Illinois	Closed circuit, fan	Nitrogen	1.22 × 0.60 × 1.0	0-8 m s ⁻¹	Atmospheric	80-300	Several minutes
NASA Langley	0.3 m TCT closed circuit, fan	Nitrogen	0.33 × 0.33 × 1.42 (solid adaptive walls)	0.05-1.0+	1.1-6.2	78-340	Up to several hours
NASA Langley	NTF, closed circuit, fan	Nitrogen or air	2.5 × 2.5 × 7.62	0.2-1.22	1.0-8.9	78-340	Up to several hours

Fig. 1. Current cryogenic wind tunnels.

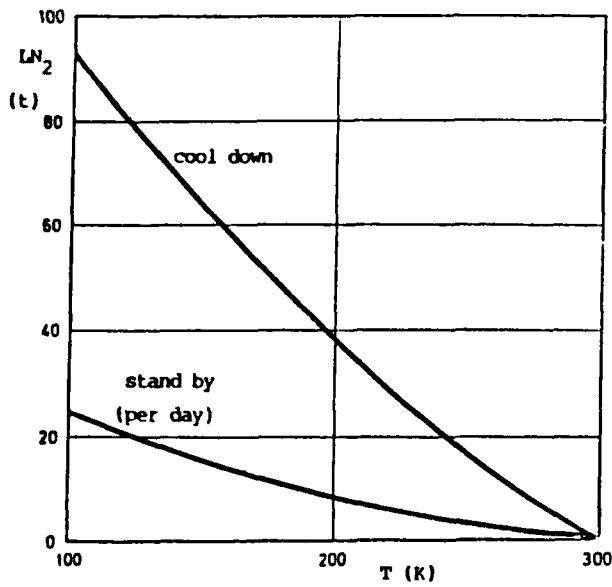


Fig. 2. Consumption of LN₂ during the cool down and stand-by phases.

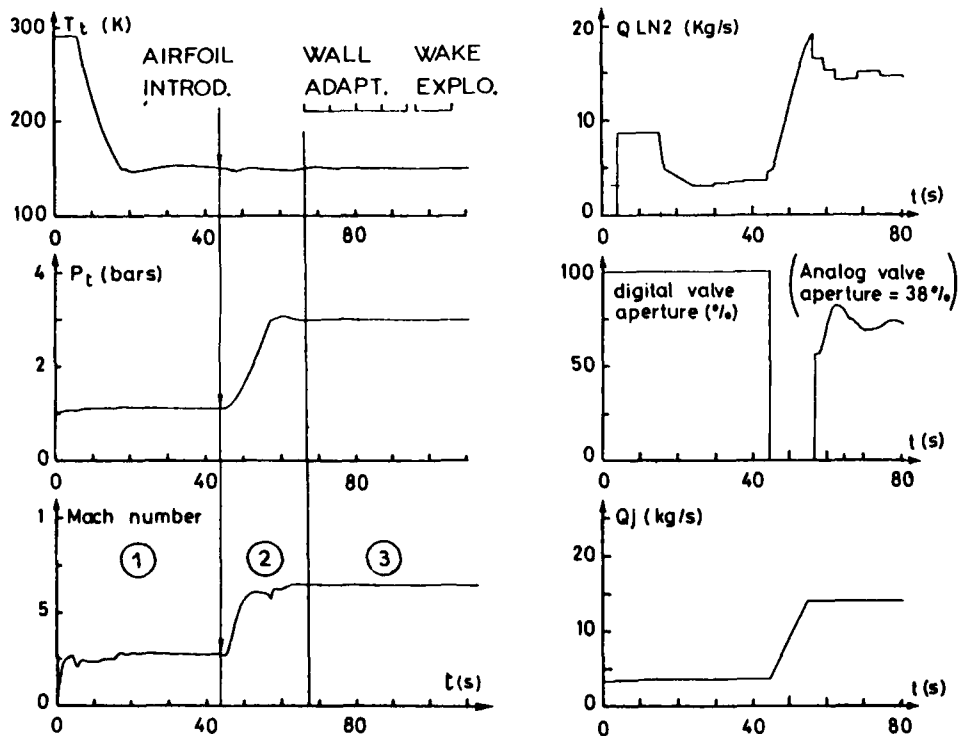
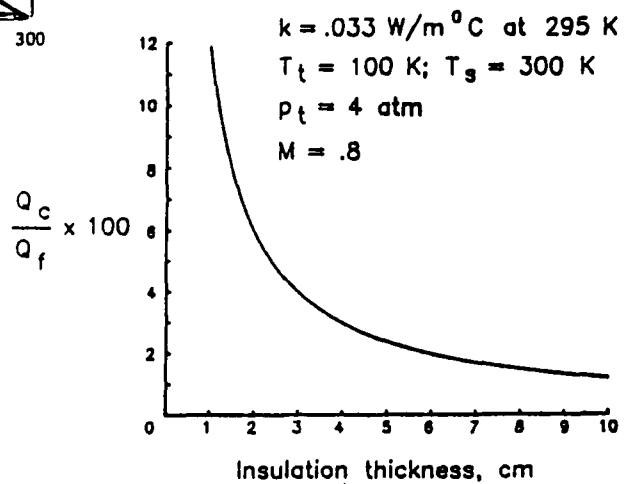
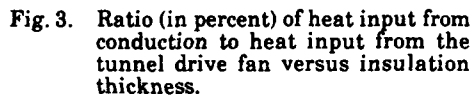


Fig. 4. Typical cryogenic run: $M = 0.7$, $P_t = 3\text{bar}$, $T_t = 150\text{ K}$.

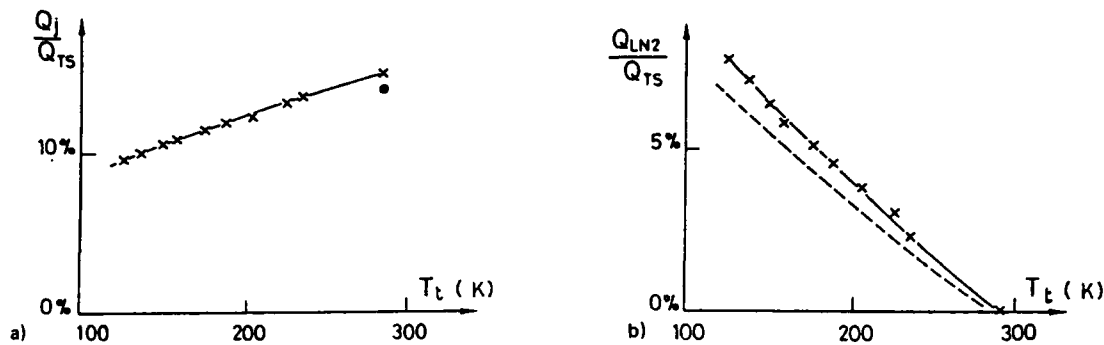


Fig. 5. a) Induction efficiency variation with flow temperature; b) Liquid nitrogen consumption.

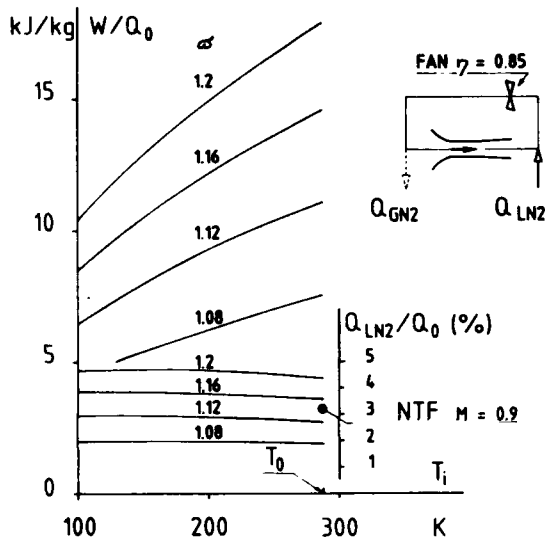


Fig. 6. Fan power and liquid nitrogen consumption for a wind tunnel driven by fan.

Fig. 7. Nitrogen consumption for an air driven wind tunnel.

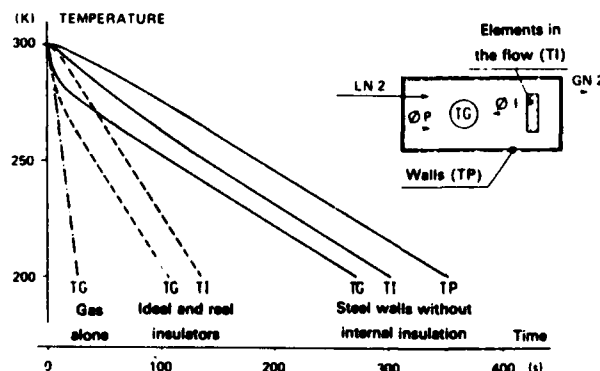
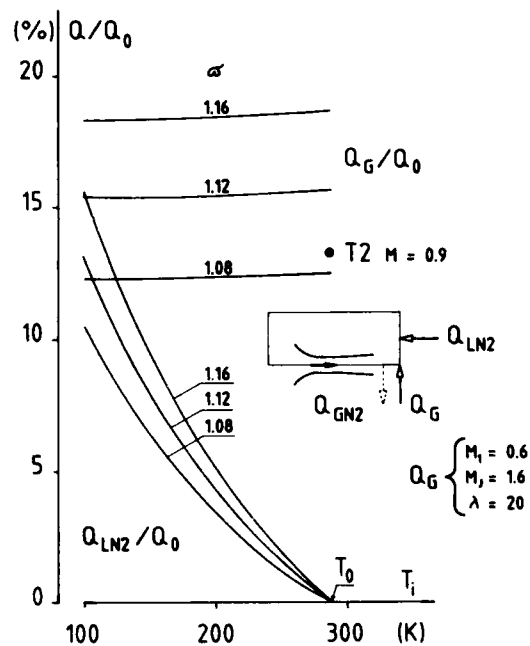


Fig. 8. Temperature variation of the fluid T_G , of the internal element T_I and of the walls T_P under the following conditions: liquid nitrogen flow: 50 kg/s; fluid heat capacity: 5 MJ/K; heat storage capacity of the internal element: 21 MJ/K; time constant for these elements: 30 s; wall heat storage capacity: 40 MJ/K; time constant of these elements: 80 s.

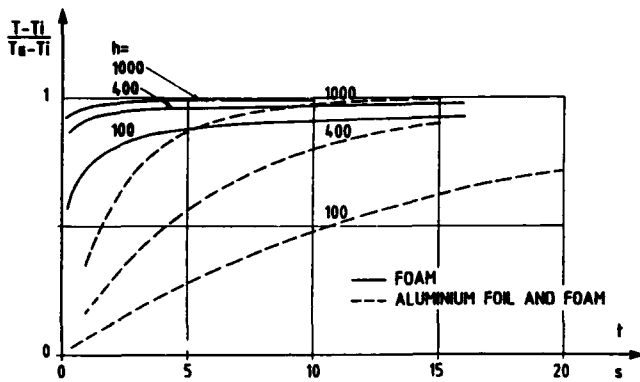


Fig. 13. Variation of surface temperature with time.

Fig. 14. CARDC 2.4×2.4 m high Reynolds number transonic wind tunnel.

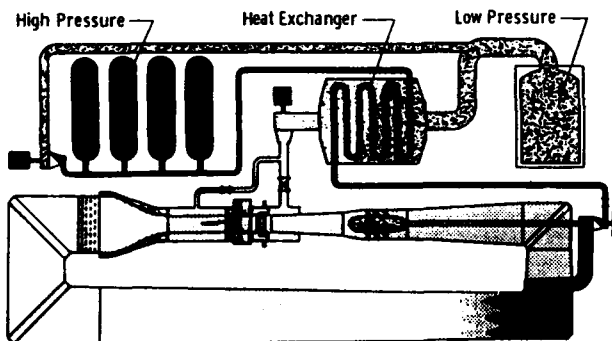
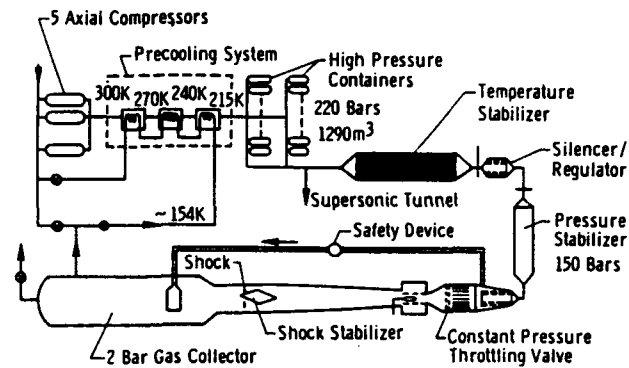


Fig. 15. High Reynolds number transonic wind tunnel (Nelander).

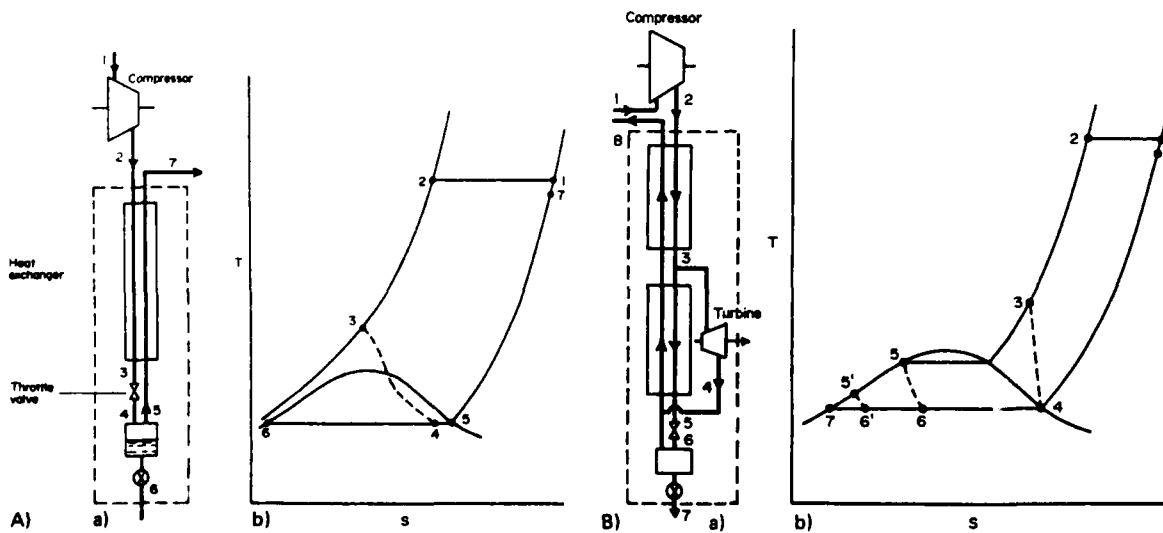


Fig. 16. (A) a) Flow diagram for a simple Linde liquifier; b) T-S diagram for the same cycle. (B) a) Flow diagram for the Claude cycle; b) T-S diagram for the same cycle.

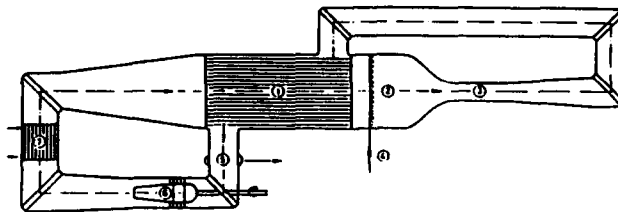


Fig. 17. Proposal of Amecke: 1) Heat exchanger; 2) Stilling chamber; 3) Test section; 4) LN₂ Entry; 5) GN₂ Exhaust; 6) Compressor; 7) Water cooler.

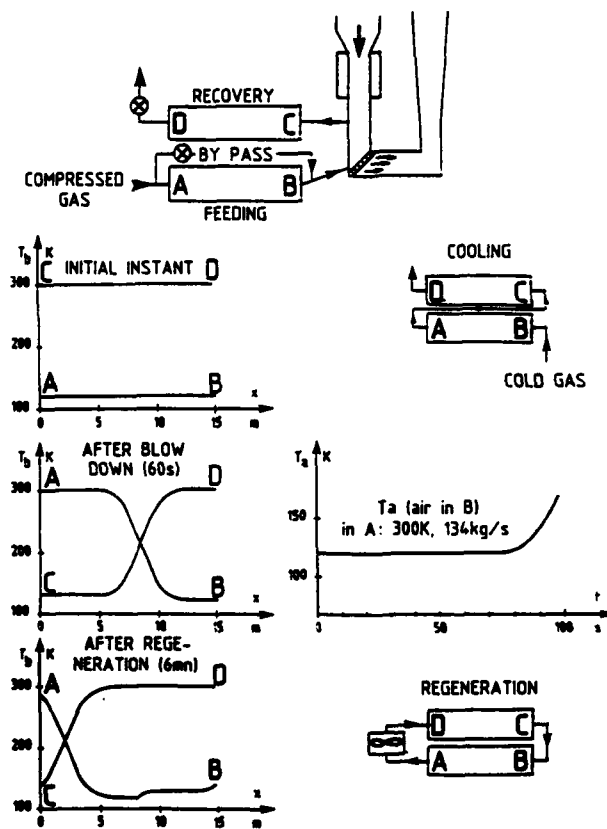


Fig. 18. Air driven wind tunnel with regenerators.

ENERGY MANAGEMENT AND RECOVERY

by

Pierce L. Lawing

NASA, Langley Research Center
Hampton, VA 23665-5225
U.S.A.

SUMMARY

Energy management is treated by first exploring the energy requirements for a cryogenic tunnel. The requirement is defined as a function of Mach number, Reynolds number, temperature, and tunnel size. A simple program and correlation is described which allow calculation of the energy required. Usage of energy is also addressed in terms of tunnel control and research operation. The potential of a new wet expander is outlined in terms of cost saved by reliquefying a portion of the exhaust. The expander is described as a potentially more efficient way of recovering a fraction of the cold nitrogen gas normally exhausted to the atmosphere from a cryogenic tunnel.

The role of tunnel insulation systems is explored in terms of requirements, safety, cost, maintenance, and efficiency. A detailed description of two external insulation systems is given. One is a rigid foam with a fiber glass and epoxy shell. The other is composed of glass fiber mats with a flexible outer vapor barrier; this system is nitrogen purged. The two systems are compared with the purged system being judged superior.

1. ENERGY USAGE IN A CRYOGENIC TUNNEL

In a closed circuit tunnel, energy is used to turn the fan which drives the flow around the tunnel circuit. This energy is converted into heat by the various dissipative processes around the circuit. More energy is used in cooling the flow to maintain a constant temperature. If the tunnel is operated at an elevated pressure, energy is used to compress the working fluid. Each tunnel system has its own unique array of energy usages. Cryogenic tunnels use energy differently from ambient temperature tunnels. The next sections primarily describe the energy usage in the 0.3-m TCT, and to a lesser extent, the NTF.

1.1 Tunnel Circuit Losses

Figure 1 presents fan pressure ratio (which represents circuit pressure loss) as a function of test section Reynolds number for a range of Mach number values. The pressure ratio required to overcome the circuit losses is seen to rise with increasing Mach number and decrease with increasing Reynolds number. Although these data are for test section empty, and do not include the additional loss of a model mounted in the test section, they provide a basis for estimating power requirements and the associated liquid nitrogen consumption. Since fan power has a strong effect on tunnel noise, understanding of the circuit loss characteristics can lead to reduction in the losses and thus the noise. Also this information in turn is useful in tunnel scheduling and in feed forward tunnel control logic. Attempts to characterize the data by simple curve fits was tedious and produced a clumsy set of equations. Modeling the circuit loss by a global "skin friction law" in terms of Reynolds number to an inverse power was much more successful and produced the correlation shown in figure 2, allowing the circuit losses over a wide range of conditions to be expressed by a single function of test section Mach number and Reynolds number. Details may be found in reference 1.

1.2 Test Parameters and Energy

The energy required for a cryogenic tunnel is a function of a large number of parameters. This makes understanding system requirements difficult. To aid the researcher, the staff of the 0.3-m TCT has, over the years, developed a computer program that performs the flow parameter calculations for cryogenic wind tunnels which use nitrogen as a test gas. The program has been rewritten for the personal computers in BASIC language. Reference 2 has a program description, listing, and instructions for obtaining a floppy disk of the program.

The flow parameters calculated include the following: static pressure, static temperature, compressibility factor, specific heat ratio, dynamic viscosity, total and static density, velocity, dynamic pressure, mass flow rate, and Reynolds number. Simplifying assumptions have been made so that the calculations of Reynolds number as well as the other flow parameters can be made on personal computers. The program, which also includes various power calculations, has been developed to the point where it has become a very useful tool for the users and possible future designers of fan-driven continuous flow cryogenic wind tunnels.

Output from the program is listed in four categories: physical tunnel parameters, tunnel flow parameters, power parameters, and LN_2 flow parameters. The program can be used in conjunction with a graphics routine to generate plots of various parameters. For example, since a cryogenic wind tunnel has independent control of q , R , and M , operating envelopes

in terms of two of these parameters can be generated while holding the third parameter constant. Samples of these plots are shown in figures 3, 4, and 5. In addition, plots involving power parameters can be generated as shown in figures 6 and 7. Also, performance charts, similar to the ones shown in figures 8 and 9, can be made by using this program.

1.3 Power Predictions

Figures 8 and 9 contain a few data points from the 0.3-m TCT and the NTF which are used to compare with the values calculated from the program. An overall drive-motor system and fan efficiency of 80% is assumed for both tunnels. The values plotted on figures 8 and 9 include the efficiency. Note that the fan power curves in these figures were generated using the fan pressure rise correlation from reference 1 which is based on the 0.3-m TCT. In the case of the 0.3-m TCT data, the comparison is very good. All three values calculated using the program are within 16% of their respective data values. Also, the percent difference decreases as the power level increases.

In the case of the NTF data, the calculated values are within 33% and 9% of their respective data values. A more accurate comparison with the NTF data may be obtained if a fan power correlation for the NTF is used. Note that the assumed overall efficiency of 80% for the drive-motor system and fan resulted in all five data values for P_f being higher than their respective calculated program values. This may imply that an overall efficiency of 80% is too high for both tunnels.

2. LIQUID NITROGEN RECOVERY

Although cryogenic tunnels offer the best solution to acquiring high Reynolds number transonic data, they are expensive to operate due to the relatively high cost of LN_2 used for cooling. Some of this cost could be recovered by taking advantage of energy contained in the GN_2 exhausted into the atmosphere. Reference 3 shows that recovery of the LN_2 by the usual Joule-Thompson effect expansion is not economical. However, an energy recovery proposal has been explored in reference 4 for an expansion turbine. Turbines are not operated down to the condensing region to avoid cavitation damage. A new device known as a Turgine is more robust in design and may be capable of recovering energy as well as liquid nitrogen. The turgine is described as a "wet expander". Figure 10, from reference 5, shows performance predictions for the expander as a function of tunnel operating parameters. We believe that for overall operations, we may be able to convert 10 percent of the GN_2 usually exhausted from the tunnel into LN_2 , which can then be re-injected into the tunnel for cooling. This unique performance is due to the adaptation of the Turgine to cryogenic operation. Its efficiency is much greater than the more usual Joule-Thompson effect expansion valves, reference 5.

The concept is to be constructed and demonstrated on a relatively small scale where engineering changes necessary for optimizing the system can be simply accomplished. This size device will be immediately adaptable to small jobs such as scavenging the NTF storage tank boiloff. The resulting design will then be available for application to NASA tunnels such as the 0.3-m TCT or the larger NTF. Payback time for the 0.3-m TCT is estimated at less than 3 years. For tunnels such as the U.S. NTF or the proposed European Transonic Windtunnel (ETW), an average recovery of only 10 percent will likely translate into an annual savings of at least \$1,000,000 per year.

A Turgine for liquid nitrogen recovery is being constructed under a Small Business Innovators Research program, or SBIR. This work has progressed to a Phase II effort and has funding of about \$500,000. The Turgine is a nutating machine similar in approach to a rotatory engine. Figure 11 shows the machine in cross section. Figure 12 is a photograph taken during construction showing the crankshaft and other parts. Initial trials are expected in a few months.

3. THE 0.3-m TCT INSULATION SYSTEM REQUIREMENTS

3.1 Economic Requirements

Insulation efficiency. Many cryogenic systems require highly efficient thermal insulation for economical operation (ref. 11). However, in a transonic cryogenic wind tunnel such as the 0.3-m TCT, the major usage of liquid nitrogen is to remove from the flow an amount of heat equal to the amount of heat added by the fan. Using the simple insulation system described in this paper, the liquid nitrogen required to offset the heat due to conduction from the ambient room air into the tunnel circuit at 100K tunnel operating temperature is estimated to be only about 1.5 percent of the liquid nitrogen used to offset the fan heat. Thus, a perfect insulation system for the 0.3-m TCT could save no more than 1.5 percent of the liquid nitrogen and only then during the time when the tunnel is operating at the lowest temperatures. It should be noted, however, that these requirements are pertinent only to tunnels very similar in size and type to the 0.3-m TCT; for example, if a particular tunnel had a very limited thermal cycle life, and it was desired to keep it cold even when not in use, then a more efficient insulation system might be very cost effective. In a similar vein, very large tunnels which require large amounts of liquid nitrogen for cooldown of the tunnel structure may also require more efficient insulation if it is desired to maintain a low temperature between work shifts.

System cost. Factors contributing to the cost of a thermal insulation system are: materials and labor required to install the system, system operation and control, and the cost of opening and closing the system as required for maintenance, inspection, modification, and repair to the structure of the tunnel. Based on experience with the original insulation system for the 0.3-m TCT, of the factors listed above, the installation cost, which is a fixed cost, may be far outweighed by the rest of the costs which recur throughout the life of the tunnel. Materials for the thermal insulation system should be readily available,

conventional, materials that are compatible with liquid nitrogen temperatures. Conventional materials tend to require less labor to install and do not require highly skilled technical specialists for their installation. The cost factor that is possibly unique to cryogenic wind tunnel insulation systems arises from the necessity for relatively frequent access to the tunnel structure, thus requiring opening and closing of the insulation system. The selection of conventional materials minimizes this cost.

One potentially costly feature unique to purged insulation systems is the operation and control of the purging system. Purging costs are minimal for the 0.3-m TCT due to the availability of a practically unlimited supply of dry nitrogen as storage tank boil-off gas which is normally lost to the atmosphere in a cryogenic storage facility. Purging costs may be further reduced at the 0.3-m TCT by the use of simple, readily available automatic components for the purge control system.

Productivity.- Since the construction of a wind tunnel typically requires a large capital investment, it is desirable to maintain productivity at a high rate in order to maximize the return on the investment. An efficient thermal insulation system can aid productivity by making it possible to stop the tunnel at the end of the work day and restart the tunnel at the beginning of the next work day with a minimum of cooldown and stabilization time. In keeping with the general desire to maximize productivity, an additional requirement for a thermal insulation system is that it can be returned to operational status after being opened with minimum lapsed time.

3.2 Safety Requirements

Reference 6 contains an extensive discussion of safety requirements for working with cryogenic fluids or devices. Among the basic safety requirements is the need to prevent contact between personnel and extremely cold surfaces. In the case of cryogenic systems operating below the temperature required to condense oxygen from the atmosphere, there is an additional requirement for isolating the cryogenic surfaces from the atmosphere in order to avoid creating an explosion hazard due to the formation of liquid air. A lesser hazard is also avoided if the thermal insulation is sufficient to prevent the condensation of water vapor from the atmosphere which can lead to slick, unsafe working conditions.

In the case of the 0.3-m TCT, which is constructed of aluminum, it is also a requirement that the insulation not trap water or oxygen-rich condensed air in such a manner as to corrode the surface of the pressure shell. Additionally, the material used for insulation must not chemically attack the surface or degrade the integrity of the pressure shell in any manner. The 0.3-m TCT could operate for many years without the need to remove the insulation from some sections. Thus, damage to the pressure shell due to even slow rates of corrosion might go undetected for long periods of time, leading, in the worst case, to rupture of the pressure shell.

3.3 Operational Requirements

Test section access.- The 0.3-m TCT thermal insulation system must allow free and repeated access to the test section area for model and instrumentation changes and maintenance. In a typical model change, the test section is opened by removing an aluminum plenum lid which serves as a portion of the pressure shell. The relatively large size of the components and the frequency of test section entrance (approximately three times each week) leads to a requirement of rugged durability for the insulation in this region.

Modification.- As mentioned earlier, the 0.3-m TCT is the first of its kind and continual modification to the tunnel is the rule. For this reason, the thermal insulation system should be easily removed and replaced or modified with the minimum of downtime or special equipment. Clearly, a vacuum jacketed thermal insulation system is not a viable candidate for the insulation of this facility.

Auxiliary equipment.- In addition to test section access and facility modifications, a cryogenic wind tunnel thermal insulation system must also accommodate the numerous pressure shell penetrations required for a wide variety of auxiliary equipment. For the 0.3-m TCT, pressure shell penetrations are required for electrical power leads, instrumentation leads, liquid nitrogen supply lines, gaseous nitrogen exhaust pipes, drive systems for angle-of-attack struts, wake momentum survey rakes, windows for visual access, tunnel supports, the fan drive shaft, and any future innovations required in the performance of the facility's research function.

4. Description of the Insulation System

The thermal insulation system presently used on the 0.3-m TCT was selected based on the aforementioned requirements as well as experience gained with an earlier foam system. The present insulation system is actually a combination of insulation subsystems as required by the particular section of the tunnel being insulated. The main insulation system for the tunnel is a simple glass fiber wrap covered by a vapor barrier and slightly inflated by a continuous dry nitrogen purge. The following sections describe each part of the thermal insulation system.

4.1 Insulation of Cylindrical Sections

Insulation material.- The cylindrical sections of the tunnel were wrapped with four successive mats of spun glass fiber insulation (Pittsburgh Corning's "Temp-Mat" or equivalent). In the uncompressed state, each mat had a thickness of approximately 2.5 cm and a density of approximately 176 kg/m³. The mats contained no material other than the glass fiber.

Each mat is held together by fiber interlocking which was accomplished during manufacture by repeatedly punching blunt needles through the thickness of the mat. This type of material was selected rather than the more conventional bonded glass fiber mats in order to avoid the introduction of any combustible material into areas cold enough to condense oxygen from the atmosphere.

The insulation was supplied in rolls of 122 cm width, which is less than the length of a typical tunnel section, thus necessitating circumferential butt joints as well as the butt joints parallel to the axis of the cylinders. Since there were four layers of insulation, it was possible to stagger the joints to avoid having more than one joint at any given location. Each layer of insulation was held in place by copper wire or thin aluminum bands. A sketch of a typical installation is shown in figure 13. In addition to the four layers of glass fiber mat, an outer layer of woven glass fiber cloth was applied and secured by a tightly wrapped spiral of a 15 cm wide strip of woven glass fiber cloth. The combined compressive action of the copper wire or aluminum bands and the cloth strips resulted in a total insulation mat thickness of approximately 7.6 cm and, with the added woven cloth, a total insulation system thickness of approximately 8 cm.

Vapor barrier.- The woven glass cloth layer and spiral wrapped strip described above formed a stable foundation for the vapor barrier system. The vapor barrier covering the insulation, as sketched in figure 13, consists of three separate layers applied as a liquid by brush to the spiral wound glass fiber cloth. The first layer is a two component urethane elastomer (Eagle Picher/Plas-Chem Coatings "Chem-Elast 2819R," or equivalent) which serves as a flexible, tough, impact resistant coating which bonds well to the glass fiber cloth. This layer is reasonably impermeable to water vapor and serves as a base for subsequent layers of the vapor barrier system. The second layer, which serves as the main impermeable membrane of this vapor barrier system, is a two component butyl rubber which has very low water vapor transmission rates, but is soft and has low toughness. The third, and outermost, layer is chloro-sulfonated polyethylene which serves mainly as a protective coating for the butyl rubber layer.

Purge system.- The entire glass fiber thermal insulation system is maintained at a positive pressure of about 1.007 atm (0.1 psig) by a purge system to preclude entry of outside air or moisture. The purge gas is dry nitrogen from the normal boil-off of the liquid nitrogen storage tanks. The dry nitrogen gas is supplied to a pressure regulator at the purge system supply manifold through an uninsulated copper pipe approximately 30 m long and 5 cm in diameter. Because of the relatively low mass flow rate of the nitrogen purge gas, the heat transfer from the atmosphere to the nitrogen gas through the uninsulated copper pipe is sufficient raise the gas temperature to ambient by the time it reaches the supply manifold at the tunnel. From the supply manifold, the purge gas is delivered to each section of the tunnel insulation through small (9.5 mm o.d.) flexible plastic tubing.

The purge gas flows through a perforated copper tube (9.5mm o.d.) buried in the insulation and running the full length of each of the tunnel sections. In this way, the it is introduced relatively evenly into the glass fiber insulation. The purge gas is collected in a similar perforated tube located 180° around the tunnel section. The flow area provided by the perforations is larger in the outlet tube than the inlet tube in order to guard against any malfunction of the purge gas supply system applying an overpressure to the vapor barrier system. In a manner similar to the inlet flow, the outlet flow is collected from each of the tunnel sections through flexible tubes which are connected to an exhaust manifold vented to the atmosphere.

When operating at the lowest temperatures, portions of the tunnel pressure shell can approach within a degree or so of the temperature of boiling liquid nitrogen at one atm, 77.35 K. For this reason, the purge gas pressure must be selected with some care. For example, should a purge gas pressure of 1.07 atm (1 psig) be used, the purge gas will start to condense when the pressure shell wall temperature reaches 78.0 K. By reducing the purge gas pressure to the design pressure of 1.007 atm (0.1 psig), the wall temperature must be below 77.47 K for the purge gas to condense. This is only slightly higher than the boiling temperature of liquid nitrogen at one atm, 77.35 K, thus greatly reducing the likelihood of collecting liquid nitrogen due to condensation of the purge gas within the insulation layer.

Insulation of Flanges. - A typical flange insulation scheme is shown in figure 14. The glass fiber insulating mats have been terminated in a staggered fashion to minimize heat leakage at the joints and the remaining distance to the flange has been fitted with smaller pieces of insulation for the first three layers. Although terminated in the same fashion as the first three layers, the fourth layer of the insulation is carried across the flange. An additional fifth layer of insulation is bridged across the flange and is long enough to overlap the vapor barriers of each of the tunnel sections. Finally, the three layer vapor barrier system is applied over the fifth layer of insulation and carefully joined to the vapor barrier on either side of the flange. Thus, the volume of the insulation in the region of the flange is unified with the purge system on both sides of the flange.

Flanges or other breaks in the tunnel pressure shell which are likely to be opened for maintenance, alternate equipment placement, instrumentation installation, etc., are insulated differently. In these locations the vapor barrier has been brought down through the insulation on one side of the flange and adhesively bonded to the tunnel pressure shell. Purge gas is supplied by pipes from the purge gas manifold to both sides of this type of joint. This deviation from the flange insulation scheme described previously allows the insulation system to be opened without disturbing the insulation on at least one side of the joint.

4.2 Insulation of Special Areas

There are many small areas of the 0.3-m TCT which are not insulated as previously described, but rather given special insulation treatment as requirements dictate. Three examples of such areas are provided in the following sections.

Test section.- Typically, an airfoil model mounted in a special turntable module is installed in the two-dimensional test section by using an overhead crane after removing the plenum cover and the ceiling of the test section. To accommodate this type of activity, the thermal insulation system used in the region of the test section must be more rugged than that employed for the bulk of the tunnel. Ruggedness is achieved by bonding a 5.8 cm thick rigid urethane foam insulation directly to the aluminum pressure shell and sealing it with a mastic coating adhesive, Crest Products Corporation's "Crest 391 A & B". The various components of the test section are then wrapped with four layers of woven glass fiber cloth which is subsequently sealed with "Crest." Because of the relatively thin thermal insulation, the test section area eventually becomes covered with frost after long periods of cryogenic operation. Thus, thermal efficiency and low installation cost have been traded for durability in the region of the test section.

Tunnel supports.- A typical tunnel support is shown in figure 15. The combination of temperature extremes and the high thermal expansion coefficient of aluminum lead to substantial horizontal movement of the tunnel pressure shell on its supports, typically 4 cm or so in changing from ambient to 100 K. The aluminum support surfaces of the 0.3-m TCT are welded directly to the pressure shell. These support surfaces rest on 2.5 cm thick pads of Teflon which, in turn, rest on a buffer support of stainless steel. The stainless steel buffer is bolted directly to "A" frame supports made from ordinary structural steel.

The aluminum part of the tunnel support is insulated by a thin elastomeric covering except where it rests on the Teflon pad, and even this part becomes reasonably well insulated when frost forms. The Teflon pad provides high thermal resistance between the aluminum tunnel support and the stainless steel. In addition, the Teflon pad provides a relatively slippery surface to allow easy sliding of the aluminum support surface with respect to the fixed support structure. There is sufficient heat transfer from the tunnel through the Teflon to form frost on the upper portion of the stainless steel support after extended operation at low temperatures. If structural steel were used here instead of stainless steel, the frost and subsequent moisture on warming would possibly result in excessive corrosion and, more importantly, the low temperature could place the ordinary structural steel in a dangerously low fracture toughness condition. In addition to resisting corrosion and providing fracture toughness, the uninsulated stainless steel section gains heat rapidly from the surroundings, thus avoiding placing the adjoining structural steel support at an unfavorably low temperature. Some additional thermal resistance is also introduced by the contact resistance at each joint between the various components of the support system. Thus, the tunnel supports represent a carefully planned part of the overall thermal insulation system.

Momentum rake and angle-of-attack actuators.- The actuators which drive the momentum (wake survey) rake and the angle-of-attack mechanism are located outside the tunnel pressure shell in an ambient temperature and pressure environment. Because of the relatively high heat transfer through the actuator drive rods, the heat available inside the heated sheet metal enclosure was not sufficient to prevent moisture in the air from forming ice on the rake actuator drive rod. The ice would cause the rod to bind in the drive-rod pressure seal rendering it inoperable. Rather than attempt to solve the problem by increasing the size of the heater, a purge-gas line was attached to the sheet metal enclosure to keep it filled with dry nitrogen. This eliminated all moisture from the enclosure which, in turn, eliminated the problem with icing. A small duct is provided to allow recirculation of the dry nitrogen through the heater inlet.

4.3 Foam External Insulation System

Since the 0.3-m TCT was the first wind tunnel designed and built specifically for cryogenic operation, there was a tendency toward a very conservative design. This conservatism led to the rather complex and expensive early thermal insulating system. Basically, the insulation system consisted of two separate layers of polyurethane foam, separated by two layers of glass fiber cloth. The combined thickness of the foam and the glass cloth was approximately 13 cm. The outer layer of foam was covered with a hard shell vapor barrier of glass fiber reinforced polyester. Operational experience with the original insulation system soon demonstrated that in order to temporarily remove and reinstall even a small portion of the insulation for inspection, tunnel modification, or repair, the services of skilled technicians had to be procured at considerable expense and tunnel down time.

Upon removal of the original insulation system during a major modification to the tunnel, large areas of corrosion were discovered on the exterior walls of the aluminum pressure shell. This evidence of moisture condensation was taken as proof of leaks in the vapor barrier and demonstrated the possibility of condensing oxygen on the external tunnel walls at the lower tunnel operating temperatures. Since polyurethane foam is not an oxygen compatible material, the evidence of moisture condensation was regarded as a serious safety hazard which should be corrected. As a result, the new thermal insulation system described in section 4 of this paper was designed and tested on an unused section of the original 0.3-m TCT. It and performed well under conditions typical of those that would be encountered during the operation of the 0.3-m TCT, and led to the present system.

4.4 System Performance

Operation of the insulation system described in this paper over the past five and a half years has proven it to be a practical system. It has been possible to pursue vigorous operational schedules as well as frequent tunnel modification, inspection, and repair with no significant delays or problems traceable to the insulation system. Since only two types of thermal insulation systems have been used with the 0.3-m TCT, it is difficult to judge how near the present system might be to an optimum insulation system. Compared to the previous insulation system, the present system was almost an order of magnitude lower in initial installation costs. However, the major advantage of the present system is related to improvements

in productivity. The time required to reactivate the insulation system after it has been opened for some tunnel function typically has been reduced from a few days for the previous system to a few hours for the present system.

If faced with the task of replacing the insulation system for the 0.3-m TCT at the present time, the design would remain essentially unchanged. Although insulation system requirements are highly dependent on the type, size, and operational cycles for a particular cryogenic wind tunnel, the information provided herein may serve as a helpful guide to the tunnel designer facing for the first time the problem of providing a cryogenic tunnel with a suitable thermal insulation system. Additional details are in reference 7.

5. ADDITIONAL TOPICS IN ENERGY MANAGEMENT

Controls. - An instant savings in energy results from a shortened test program. Experience in the 0.3-m TCT and the NTF has shown that a tunnel controlled manually requires much more time than one that has automatic controls. The 0.3-m TCT has gone through several generations of control systems. The latest of these is personal computer based and is described in reference 8. The NTF is also steadily improving its control capabilities. It is estimated that since the initial, manually operated operations, LN₂ consumption during testing has decreased by a factor from 3 to 5.

Adaptive Walls. - This is the latest major innovation being developed in the 0.3-m TCT. Logically, it will save energy because it does not circulate mass flow through slots to operate at transonic conditions. The magnitude of these savings cannot be determined because a very inefficient diffuser was improved in the same installation with the adaptive walls. However, the improved blockage situation allows testing of models 50% to 100% larger at the same energy usage. Thus for the same model Reynolds number the tunnel total pressure and energy requirements can be reduced by 50% to 100%. Adaptive wall technology is summarized in reference 10.

Liquid Nitrogen Storage. - Pumping large amounts of LN₂ from storage to the tunnel is frequently made difficult by cavitation in the pump. A typical solution is to pressurize the system, as is done in the 0.3-m TCT. Pressurizing the LN₂ over a period of time stores energy in the liquid, thus penalizing its cooling capacity. Reference 9 shows the reduction in cooling capacity due to storage as a function of pressure. For a tunnel test at 5 atmospheres pressure, storing the LN₂ at 5 atmospheres results in a 15% loss in cooling capacity, or a 15% increase in LN₂ usage and cost. The NTF avoids this penalty by immersing the pump in a well and making use of the elevation of the stored LN₂ to provide the necessary pressure at the pump entrance. The NTF storage is only at enough pressure to insure proper venting.

REFERENCES

1. Lawing, P. L.; Adcock, J. B.; and Ladson, C. L.: **A Fan Pressure Ratio Correlation in Terms of Mach Number and Reynolds Number for the Langley 0.3-Meter Transonic Cryogenic Tunnel.** NASA Technical Paper 1752, November 1980.
2. Dress, David A.: **Computer Program for Calculating Flow Parameters and Power Requirements for Cryogenic Wind Tunnels.** NASA TM 87609, November 1985.
3. Voth, R. O. and Strobridge, T. R.: **Cryogenic Design and Safety Review, NASA-Langley Research Center 0.3-m Transonic Cryogenic Tunnel.** NBSIR 77-857, April 1977.
4. Goodyer, M. J.: **Introduction to Cryogenic Wind Tunnels..** *Cryogenic Technology for Wind Tunnel Testing*, AGARD-R-722, July 1985.
5. McIntosh, Glen E.; Lombard, David S.; Martindale, David L. and Dunn, Robert P.: **Cost Effective Use of Liquid Nitrogen in Cryogenic Wind Tunnels.** NASA CR 178279, April 1987.
6. Webster, T.J.: **Latest Developments in Cryogenic Safety.** NASA CR-166087, 1983.
7. Lawing, Pierce. L.; Dress, David. A.; and Kilgore, Robert A. : **Description of the Insulation System For the Langley 0.3-Meter Transonic Cryogenic Tunnel.** NASA TM - 86274, January 1985.
8. Balakrishna, S. and Kilgore, W. Allen: **Microcomputer Based Controller for the Langley 0.3-Meter Transonic Cryogenic Tunnel.** NASA CR-181808, March 1989.
9. Kilgore, Robert A., and Adcock, Jerry B.: **Specific Cooling Capacity of Liquid Nitrogen.** NASA TM X-74015, February, 1977
10. Wolf, Stephen W. D.: **Adaptive Wall Technology for Minimization of Wall Interferences in Transonic Wind Tunnels.** NASA CR 4191, November 1988.

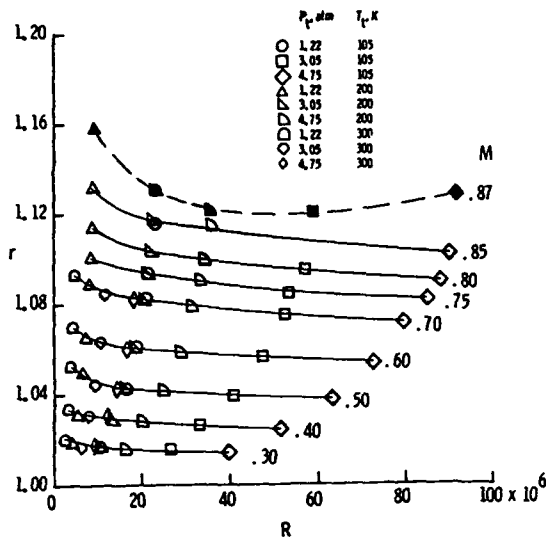


Figure 1.- Fan pressure ratio as a function of Reynolds number for a set of Mach numbers.

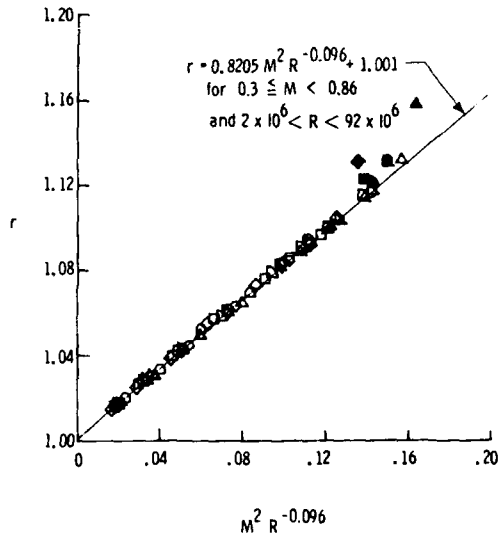


Figure 2.- Fan Pressure ratio correlation in terms of Mach number and Reynolds number.

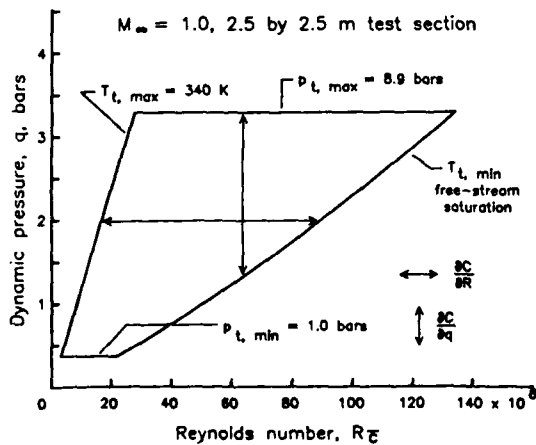


Figure 3.- Constant Mach number operating envelope.

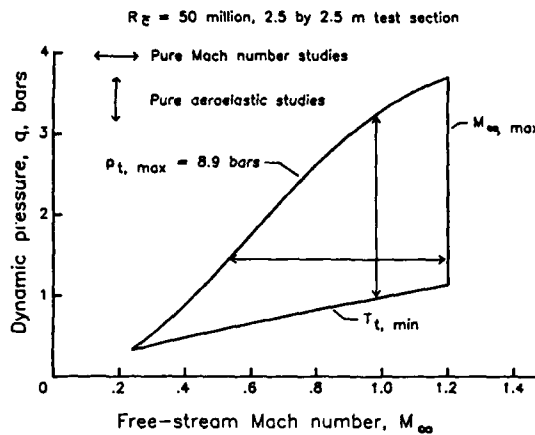


Figure 4.- Constant Reynolds number operating envelope.

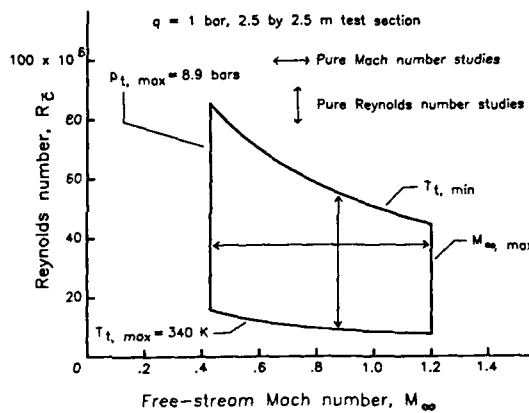


Figure 5.- Constant dynamic pressure operating envelope.

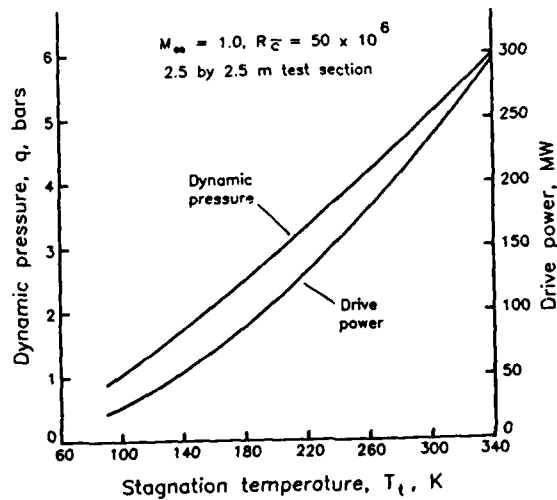


Figure 6.- Dynamic pressure and drive power as a function of tunnel operating temperature.

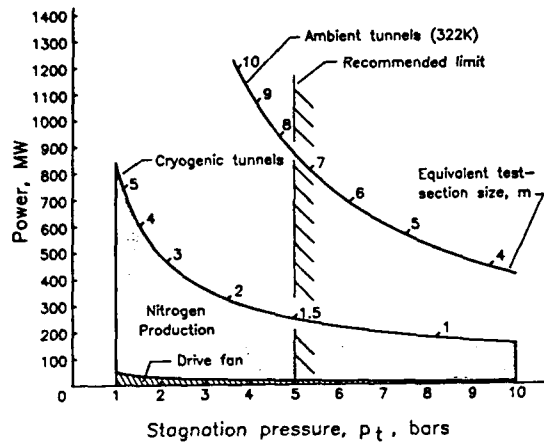


Figure 7.- Comparison of total power requirements for ambient and cryogenic fan-driven tunnels.

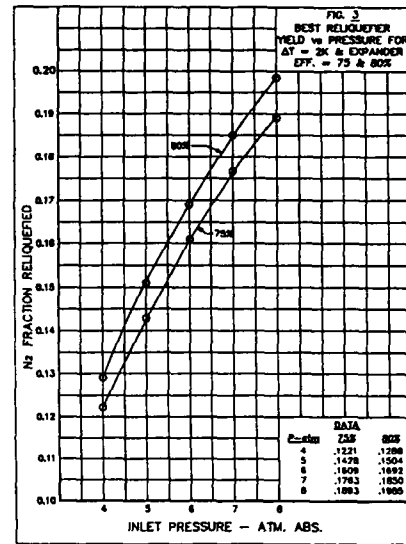


Figure 10.- Fraction of exhausted nitrogen liquefied as a function of pressure.

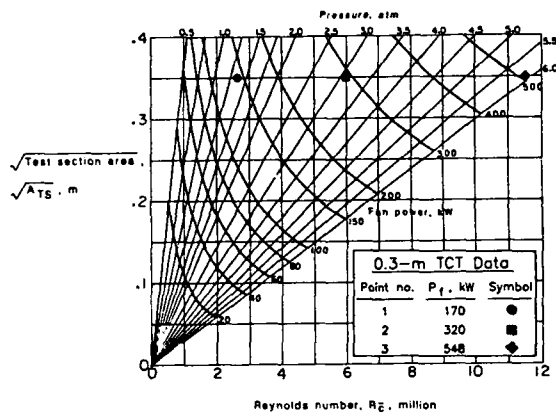


Figure 8.- Program predictions compared with 0.3-m TCT data; Mach number of 0.70, and temperature of 105 k.

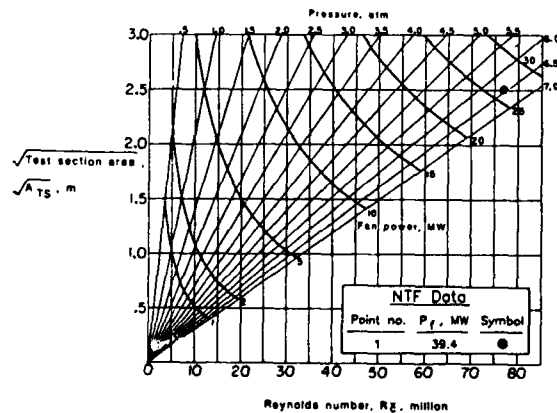


Figure 9.- Program predictions compared with NTF data; Mach number of 0.712; temperature of 117 k.

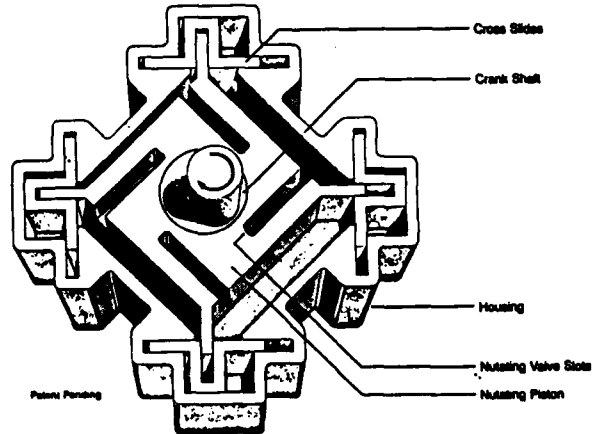


Figure 11.- Cutaway diagram of "Turgine" wet expander.

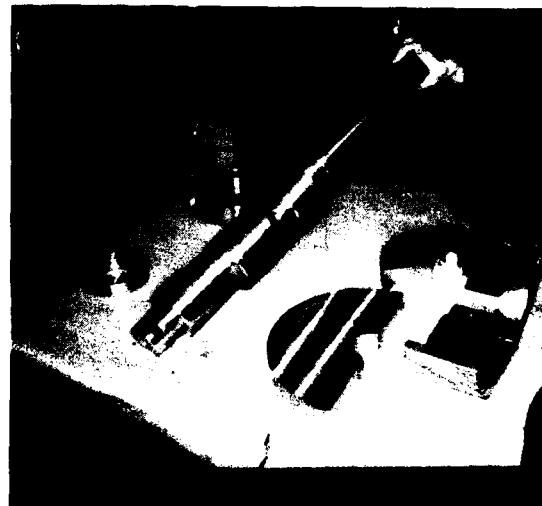


Figure 12.- Photograph of crankshaft and other parts during construction of expander.

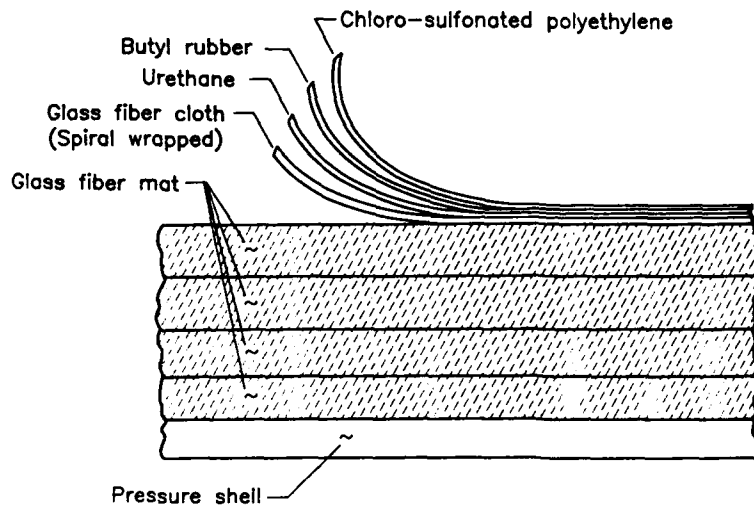


Figure 13.- Details of insulation and vapor barrier system for the 0.3-m TCT.

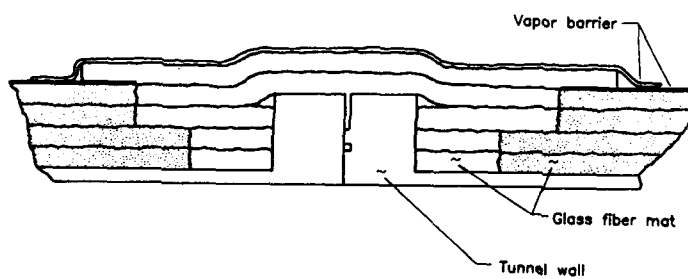


Figure 14.- Typical flange insulation scheme.

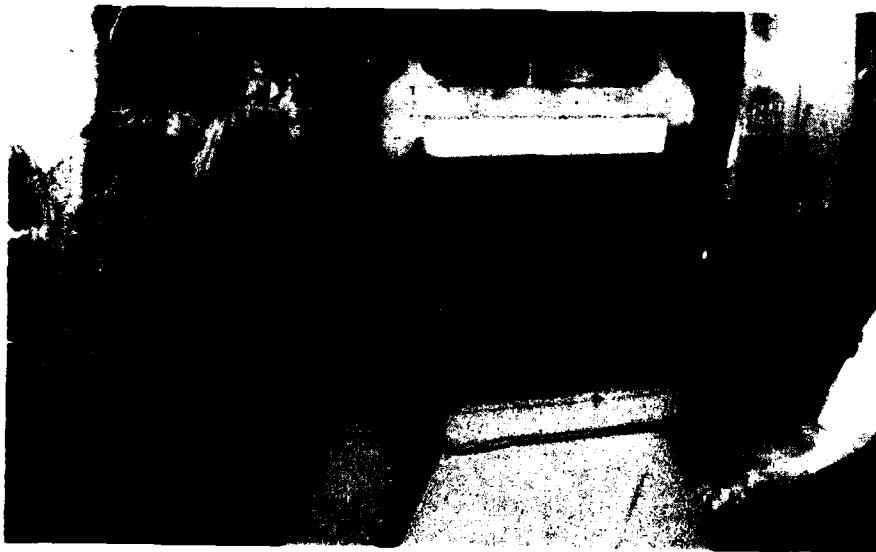


Figure 15.- Tunnel support for the 0.3-m TCT.

Round Table Discussion

At the end of the Special Course we had a Round Table Discussion (RTD) where the lecturers responded to written questions submitted during the week. At the coffee break before the RTD, I distributed the written questions to the lecturers. I have copied the questions below. The questions are followed by a slightly edited transcription of a tape recording of the comments and discussions.

To:

From: *Bill Hirst, ARA*

Question: *The question still to be addressed before we will be able to readily predict flight performance from high Reynolds number (cryogenic) wind tunnel tests are varied. Many of them are similar to those of ambient temperature tunnels but compounded by the effects of variable temperature and high pressure, and include --*

- *wall interference*
- *support interference*
- *force measurement accuracy*
- *flow quality*
- *knowledge of the model geometry under test*
-

Which of these (or others) is considered to be the most critical and if we are gathered together 4 years from now, which would we expect to have progressed to a satisfactory level of knowledge?

Mike Goodyer: [Goodyer reads the question to the audience.] "... compounded by the effects of various temperatures and high pressure."

And he lists a set of those questions to be addressed. The first of them is *wall interference*. It happens that of the set of maybe four or five questions raised here, *wall interference* seems to me to be -- unless I've missed something -- no more severe in the environment that we are going to find ourselves in -- people already finding themselves in -- in the pressurized cryogenic wind tunnel than in any conventional tunnel. So, unless I've missed something, the issues are not compounded in the new tunnels. Is that fair comment?

Bill Hirst: What I am trying to say is that some of the questions that need to be addressed, wall interference maybe is not compounded by variations in temperature and pressure. But I've tried to list some of the things I've thought of that need to be addressed and among them are wall interference and support interference.

Mike Goodyer: That's further down the list. I'm not trying to suggest in the case of support interference that this is not compounded by the cryogenic wind tunnel. I just felt that wall interference was probably no different.

I'll run through the rest of the question then. The wall interference has been mentioned, carrying on with the list, the next one is *support interference*, the next one is *force measuring accuracy*, then *flow quality*, then *knowledge of model geometry under test*. That's significant, I think. And any others. There's a blob suggesting the list may be longer than that.

The final part of this question is: "*Which of these questions or others is considered to be the most critical? And if we are gathered together four years from now, which would we expect to have progressed to a satisfactory level of knowledge?*"

Trying to partially answer your question, *support interference* could be a bigger problem, simply because in the case of some wind tunnels we're using higher pressures than are normally experienced (although not exclusively so) in ambient temperature tunnels. And I don't think anything special is being done to alleviate the problem. So again, as a personal opinion, and I am quite willing to hear other opinions, the problem is not going to go away. What can you do about it? Not much, unless you have a really radical solution like magnetic suspension... And that could come along, conceivably.

The next topic is *force measurement accuracy*. I spoke to Judy about this just now and she feels that the issue of accuracy has been addressed properly, and as long as you do the job properly, you can get the kind of accuracy that people have specified. If the specifications are wrong, that's a different matter. But a lot of effort has been put in on improving accuracy and the problem, surely in four years time, if not cracked now -- and it may be -- surely will be in four years time.

Flow quality. At least the 2 large wind tunnels are being designed to specifications laid down. Now if it turns out that the specifications were wrong, then there is a problem. But we're stuck with following a particular route and again there is nothing much that we can do to influence the quality that has been decided upon.

Knowledge of model geometry. That might be a more difficult one. Of course, people are proposing schemes for measuring deformation under load, of the wings in particular. There are schemes around intended to address that problem and they probably will yield to the efforts that are being put on them right now. That's my feeling.

There are other areas -- this is gone on to your last blob -- your last question, which is open, "*Are there any other things?*" I think there are some other things. Some of the non-intrusive measurement methods may not yield to effort. They may not have enough effort being put on them. There may be a management problem and my feeling is that there probably

is. That is, decisions are being taken which are wrong. Correct decisions have to be made very early on in the project, not late on. Coming up with possible solutions late on quite often proves to be too late.

I am going to leave it there and let other people comment if they want to add to what I've said or contend a statement.

Bill Hirst: From what we've heard this week and from what we've read in the past, it seems that flow quality and balance accuracy are the two things that we have to get right to start with. If you specify the endpoint of what you require from the balance properly, I would think four years from now that will have been progressed satisfactorily.

Flow quality I am not so sure about. Flow quality in terms of variable temperature, variable pressure, and how the tunnel will react to the change of temperature, and the spatial distribution of temperature, flow angle, Mach number, and whether that will still be as tightly controlled as we would expect it to be to achieve this half a drag count accuracy that we expect out of large high Reynolds number facilities, I'm not so sure of that.

Bob Kilgore: That question of doubt is a good way to leave it, perhaps. Let's move on. Mike, thank you. Judy, you are next in line so we might as well just take this in rotation.

To: Judy Ferris, and others.

From: David G. Coulton, ARA, UK.

Question: *In our ongoing search for improved data accuracy it becomes essential to consider those items once thought of as being only of second order importance. Considering the large temperature difference between the strain gauge balance in the model and the instrumentation used to measure the micro-volt signals developed by it, what precautions have been taken i) to insure that thermocouples naturally developed in the tunnel to the control room connecting wires are correctly accounted for, and ii) to correctly measure the actual, as distinct from source, bridge excitation voltage required for the ratiometric measurements?*

Judy Ferris: O.K., I have a question here from David Coulton, is that correct? And the question is: *"In our ongoing search from improved data accuracy it becomes essential to consider those items once thought as being as only of second order of importance. Considering the large temperature difference between the strain gauge balance and the model, and the instrumentation used to measure the microvolt signals developed by it, what precautions have been taken: 1. To insure that the thermocouples naturally developed in the tunnel to the control room connecting wires are correctly accounted for."*

This might be better addressed to Ed Bruce because he's the one that takes the signals from the back of the sting on in to the control room. But he can correct me if I'm wrong. Most of our thermocouples are the type T, copper constantan, and we maintain the copper constantan through the pressure wall all the way back to the control room to an ice point reference junction back there. And we try to maintain the quality of that and not come into any discontinuities in material.

David Coulton: Sorry, that was not the question. The question regards the actual wiring from the strain gage balance. Not thermocouples. Do thermocouples form ...

Judy Ferris: Oh, in the wiring. That question has been posed to me before. And in the early days, I did find one wire that did have a thermocouple effect. It was in only one roll of wire. And since that time, I have to admit that we have not been checking for that but have just been including it as part of the thermally-induced output and compensating for it which is somewhat different. But I plan to do that. As soon as I get back home I plan to take all of my balances cold and check the thermocouple effect without any power applied. But I have not been doing that. The other thing is that we hope that if we correct closely enough for temperature gradients that the small temperature differences that you might see there won't affect the output. So that's the ultimate right there. If you have no effect from temperature then you don't have to measure it. Do you have any further comment on that portion?

David Coulton: On a normal transonic tunnel at temperatures ... we've found it absolutely essential in order to get a good quality of data to take care of thermocouple effects within the connecting wires.

And if that is required of from a tunnel which is running maybe up to 40 degrees C, to control over about 20 degrees C, then surely the problems must be much larger at the cryogenic temperatures in tunnels to control than at the normal ambient temperatures. These problems must be far larger and therefore much more care is required in order to look into these problems.

Bob Kilgore: Ralph Scurlock should be here. He would be ever so happy to hear this. Of course Ralph would propose conditioning the signal and turning it into digital information at the balance...

Judy Ferris: So that you eliminate the microvolts...

Bob Kilgore: ...to avoid the potential problem. One question that we might propose to André: Have you seen problems in your setup of the sort described where ordinary wires, and not thermocouple wires, developed an emf because of gradients or plugs in the wrong place?

André Mignosi: We have not enough experience with the balance but we have experience with the pressure transducers and we have not really observed ...

Bob Kilgore: You are being quizzed. It sounds like the kind of thing that if it is a major problem we would have stumbled over it. It may be a part of a general problem within the noise, and as Judy says, she found one roll of wire which did give her this effect.

Judy Ferris: And I'm sorry. I keep reverting back to thermocouples instead of addressing the problem that you have been telling me because my thinking is in the wrong thing. But at any rate, you're right, we need to check that and I think that we should be very conscious of it and I plan to be. That's the reason we have these meetings, I suppose.

Bob Kilgore: The other part ...

Judy Ferris: Yes. The second part is: *"To correctly measure the actual, as distinct from source, bridge excitation voltage required for the ratiometric measurements."* And, yes, we do that by monitoring our input voltage on the balance itself so that we don't have any losses there. Professor Ewald, you had a comment.

Bernd Ewald: Yes, I would like to make a comment to the last item. We agree that there may be big problems with thermocouple effects on the wiring. And that's the reason why we have used, for a long time, an advanced carrier frequency measuring system which completely eliminates these problems.

Bob Kilgore: There is a way around the problem.

To: Mrs. Judy Ferris
 From: Klaas Breman (NLR)
 Question: Did you already work on cryogenic hinge moment* balances, and if so, did you encounter problem areas? Were the balances sufficiently accurate, and did you calibrate under 'cold' conditions?

* (I think I saw hinge moment balances on a Shuttle Orbiter model photograph of Pierce Lawing.)

Judy Ferris: The second question I have here is from Klaas Breman, and his question is: *"Did you already work on cryogenic hinge moment balances, and if so, did you encounter any problem areas? Were the balances sufficiently accurate, and did you calibrate under 'cold' conditions?"*

And the answers to those are yes, we have done it. We have encountered some problem areas and we feel that we conquered them to a certain degree. First of all, in conventional tunnel you can pot over the top of hinge-moment gages. You can fill them in to get your contour back. You cannot do that in a cryogenic environment because it affects the gage output. So the only time that we've been able to do it is when it is either enclosed inside the model, and does not have anything more than the green Teflon spray moisture proofing, or if it is thick enough so you can put a cover plate over the top of it. So we did have to make the concession that we cannot put them in such thin areas that they have to be filled over.

The second one is, *"Were they sufficiently accurate and did we calibrate under cold conditions?"* We did. But as many of you probably know, there usually such small ones that you have to be very careful about your connection and so we won't do it unless we can actually put it on the model using proper torques to torque it down because the end where you mount it is very sensitive to the mounting torque of the bolts and so forth. And so we do do that and we don't quote half percent accuracy though. We have not been able to get that, and we think it's mostly because of the small size and the difficulty in getting good mounting. And so I think that the ones we've been getting have fallen in the range of about 2 to 5 percent instead.

Has anyone else here that works with force balance measurements had any experience with that? So we've had several and I think in the talks you also heard about three component balance in the canard. We've worked with that also and we're having pretty good success with it.

Bob Kilgore: We'll speed right along. I know that David speaks fast so ...

David Wigley: He speaks even faster right now with the rush to get outside ... If you move this back to the end and if we've got time we will talk generally about it. But this is a specific question so I'll pass.

Bob Kilgore: You are given a temporary pass.

To: Mr. Ed Bruce
 From: Klaas Breman (NLR)
 Question: Suppose the NTF blades would have been made of Carbon Fibre Composite.

Would the blade damage be comparable to your "glass fibre" blades?

Ed Bruce: That was the easy way out. [Referring to David Wigley passing on his question.] Klaas Breman, his question is: "Suppose the NTF blades would have been made out of carbon fiber composites. Would the blade damage be compared to your fiberglass blades?"

I'm not a carbon fiber person so I can't really answer the question exactly. But I would suspect it would, being a composite blade and considering the type of failure that we had, where metal came loose and when it came loose, it went down and acted like a chisel or an axe against the leading edge of the fan blade and cut it off or abraded it off. I would expect at least the same thing would have happened. At least there would have been damage done to the leading edge of it whether the whole thing breaks off or not though, in a carbon type, I don't know.

Klaas Breman: You didn't look at going with a different material such as kevlar ...

Ed Bruce: You mean changing material? Our position here was we were really satisfied with the way these fiberglass blades were holding up -- performing -- the life cycle going with them. Since we already had procedures on how to make these blades, and the QA process, we didn't want to get back into another development process at this time.

To: Dr. G. Viehweger + W. E. Bruce

From: T. Balden, MBB, Germany

Question: The KKK fan blade material is "simple" stainless steel. The NTF constructors used - as mentioned - an extremely expensive composite material construction.

Which reasons led you to such different solutions of nearly the same technical problem?

The second question here is from Mr. Balden, MBB: "The KKK fan blade material is 'simple stainless steel.' The NTF constructors used, as mentioned, an extremely expensive composite material. Which reasons lead you to use such different solutions to nearly the same technical problem."

[Looking at Günter Viehweger] I'll let you speak to the KKK but I can tell you how we arrived at the NTF fan blades. In the early days there was a study made of the type of fan blades to use in the NTF. There was a committee put together for that. They looked at steel blades, they looked at aluminum blades, I think they looked at titanium blades, and composite blades. And when they considered that the NTF blades were going to be under very high loading -- horsepower loading, aerodynamic loading -- very high centrifugal force to go along with it for the speed we had to go to to get the aerodynamic requirements, and at the same time for the extreme environment -- high temperature and low temperature -- and wanting a blade that would be forgiven if small particles would go through it, which we've had. We've had things -- even up to the size of a pair of scissors that were left in the tunnel -- that went through the fan system -- it didn't actually go through the blade -- and it nicked it.

We've had a case where a nail about that long went through the fan blade and it actually went through it and hung in there. We've been able to make those repairs right in place in the tunnel. It leaves a nick in it. People come in and they patch that and we go right on and make our run. So we are very happy with the forgiveness that a fiberglass blade has -- at least up to this time -- for those nominal things that could be left in the tunnel and go through them. Not for the type of situation that we had in January. So that's the basis that ours was picked on.

To: Ed Bruce

From: Bernd Ewald

Question: Wind tunnel users agree, that in a good conventional transonic tunnel a repeatability of a drag count or less is achievable and used by transport airplane designers.

Cryogenic tunnels are designed to improve simulation.

Do you agree that we need a 1 drag count cryogenic balance to get benefit from the cryogenic tunnel at all?

Let me answer the other one I have here then I'll give this to Mr. Viehweger to address his part when he comes across it. Mr. Ewald's question: "Wind Tunnel users agree that in a good conventional transonic tunnel a repeatability of a drag count or less is achieved and used by transport airplane designers. Cryogenic tunnels are designed to improve situations. Do you agree that we definitely need a one drag count cryogenic balance to get benefits from the cryogenic tunnel at all?"

I guess if I start with the end question and answer that yes or no, I'd say no we don't need a one drag count balance to get any benefits at all. Let me elaborate on that and I will come back to the balance

I see two big goals that a cryogenic tunnel has. One is understanding aerodynamics of high Reynolds number, and how do we apply that back to the conventional type transonic tunnels that we have so the many users that have those can do the high Reynolds numbers studies. There is no way we in the United States are going to be able to use one tunnel and do everybody's testing at high Reynolds number. So we have goals to understand various configurations, various shapes, and see how they behave at high Reynolds number. That will go into code fitting and also how you do tests back at the low Reynolds number to be applicable. We intend to do things like transition trips. How does that affect drag as a function of Reynolds number to get the transition to occur where we want it with the minimum height or spacing to go with it?

And we have fluid dynamic studies lined up. In other words, using delta wings with various types of leading edges on them -- round, sharp, and so forth -- looking at just basic fluid dynamic studies. That's not highly dependent on drag components at all. So there is a lot of technology development that we have lined up to be looked at when proving technology overall.

I recognize you are going to validate or look at a wing configuration, or aerodynamic configuration -- and this is applicable say to an aircraft company or a company that is going to design a new aircraft or re-wing an aircraft -- then you want to get the best measurement that you can. And we recognize that every drag count counts because you want to get performance out of it. I believe, if you are talking about what you have indicated here, repeatability, that we can get good repeatability in the NTF.

If you look back at the figure Susan Williams had in her report -- I forget the figure number, figure 9, I think -- the repeatability that we had from day to day was very good. And if that had been strictly just a drag type run that we were going to make, and we had picked the right balance, which gives us the most sensitivity in axial force, we would be down in that range. I think that we could be doing about the best we can. And the other thing... I see the work going on with the balances. Over the next years that's going to be improving as we go along. I don't know if that answers your question or not.

Bob Kilgore: I'd like to add to that just a bit. Anytime the Reynolds number effect exceeds the accuracy of the balance effects -- if the Reynolds number effect is 5%, and you go from a 1/2% balance to 1% balance -- you are still better off with the cryogenic tunnel because you've seen the 5% effect although you can't define quite as accurately. Many of the affects of separation on bluff bodies are fairly gross with angle of attack, and the ability to accurately define on a subscale model where they will occur usually overrides the lack of ability to define the precise level because of the accuracy of balance. That's an argument that I will make for keeping the cryogenic tunnels running. But at the same time that we keep them running, we must put more effort into not only achieving the accuracy that we presently enjoy but achieving the kind of accuracy that we would really like to have. There is no reason to stop a 1/2 percent or a 1/4 percent. The goal is perfection.

[Returning to T. Balden's question about fan blades.]

Günter Viehweger: You must know that the requirements and the loading of the blades of the NTF are remarkably higher than in the case of the KKK.

During the design phase of the tunnel, we looked for blades of the fan and for blades of composite and the prices we got from the bidders for composites were significantly higher than for metal blades. The type of the material we used for the blades -- it is the type 4541 -- is in accordance with the requirements of the loads on blades. That is the answer to your question.

Bob Kilgore: I think to illustrate they are the same generic problem but not the same specific problem, ...

Günter Viehweger: That is right.

Bob Kilgore: ... what is your maximum horsepower into the fan?

Günter Viehweger: The load is smaller. The forces as a result of the high circumference velocity is remarkably smaller in the case of our fan.

Bob Kilgore: And the size of your motor is what in terms of megawatts?

Günter Viehweger: One megawatt. [KKK]

Ed Bruce: Up to 100. We've had 102. [NTF]

[Günter trips and almost falls leaving the podium.]

Bob Kilgore: I think we had better get Ed Ray up here to consider *what if* someone falls off there and kills himself.

All right. I put Ed Ray up here because this is a safety problem and I want you to consider this, Ed.

To: Mr. Ed Ray
From: Klaas Breman (NLR)
Question: What - if Question

- I - What happens if a model is blown out of the test section?
 - a) To the circuit and the LN₂ system?
 - b) To the client (Does he get his damage to the model paid?)
 - c) To the Facility Safety Head?
- II - What factor of safety is applied on models and stings in 0.3 m TCT and NTF?

Ed Ray: I've got some *what if* questions. And someone was listening to my lecture because my friend Klaas from Amsterdam has said *what if?* These are very interesting questions.

"What if the model is blown out of the test section?" And then under that he has three parts to it:

Part A: *"... to the circuit and the LN₂ system."* I think the answers to all these questions are fairly individual.

I have been fortunate in being able to put in a catch screen in front of our [0.3-m TCT] fan which has saved me many hours of horror. However, ...

Unidentified speaker: You have a catch screen?

Ed Ray: Yes. I have a stainless steel screen that lays on the number two turning vanes, and we've been able to capture almost all the missing parts except for parts that were less than a centimeter square.

We've had some hits on the propeller. Those probes that I showed you got all the way around the circuit. But all the big pieces we've been able to catch. The other advantage that we have is that we have the turn vanes in turn one and I've caught several parts there before it got down to the second turn. I think that's a question that would be individual to each tunnel and I hesitate to answer in a very broad sense. But I love the way you are playing your game and I would invite anyone that is in the businesses to "What if the loss of a model?"

Another part to the same question. *"... to the client."* Very good question. *"Does he get his damage to the model paid?"* Again I don't want to answer too broadly. The losses that we've had at NASA -- and I don't think we've lost any client's models yet -- unless Ed knows something that I don't -- but I would say generally, is that they probably would suffer the loss with the Government. I don't think the Government, if the tunnel was damaged, would try to press the client for any return money. I just can't see them doing that.

We've had some major model losses in ambient tunnels. For instance, not too long ago in our 16-ft tunnel they lost, I think from the same client, three models in a row. And one of them happened to go through the fan, and you know, multi, multi big bucks, and they just took their loss.

Peter Fuijkschot: But, for instance, you tested our balance in your tunnel. Suppose the sting broke and our balance was lost. Would we be insured?

Bob Kilgore: Not by us.

Peter Fuijkschot: Or would you say to us, "I'm sorry, we had a little mishap."

Ed Ray: If it were insured it would be a special case for that one balance. That sounds like a real dodge to your question but I'm sorry about avoiding specifics because I think that I could mislead you.

"What would happen to the facility safety head?" It depends. There have been cases at Langley where the facility safety head has suffered a great embarrassment.

"What factor of safety is applied on models or stings in the 0.3-meter TCT?" Again, I don't have a specific answer. It varies. It varies with the material from one extreme -- glass and quartz -- NASA just doesn't know how to apply a safety standard to it. They have assumed that it has got to be more than ten. But legally as a Facility Manager or Safety Head, I could judge each case individually. Play *what if*. *What if* I lost this model and ... Sorry, again but no specifics. I refer you to the NASA Langley Handbook, reference 4, and in there that deals directly with it.

A related answer that I am going to tack on here -- and I think it might even be more appropriate to another question -- but the one distinction -- and this is something I think that the ETW people need to look at -- is that through our persistence at Langley the cryo pressure tunnels have been listed as a special case facility. And in that handbook, if I'm not mistaken, are 8 or 9 special facilities at Langley that need special attention. And so we have this generic type of category where our models are flight rated. In other words, it's not man rated but it indicates that special attention has to be given to them. And with that special attention, the facility safety heads can require certain things be given to them such as metal certifications and things like that during the pretest, so you should certainly try to get a special category because it takes special talents to control the safety.

To: Mr. X Bouis and Mr. E. J. Ray

From: J. Krengel, DLR

Question: Would an AGARD activity like a personal consultancy or a Working Group be considered as helpful in the field of cryogenic safety and operation bearing in mind that there are no officially accepted standards available in NATO countries?

Ed Ray: O.K. this is to you [X. Bouis] and I both. I think we agree. *"Would an AGARD activity like a personal consultant or a working group be considered as helpful in the field of cryogenic safety and operation, etc."*

What I would recommend there is that -- and we've done this before -- I would recommend that all of us consider maybe periodically exchanging facility safety heads and swapping around a bit. I think that is a good way to gain experience throughout the community. The ETW and Langley have done that on two occasions. J. P. Hancey came to Langley for six months and I think he benefited from it. And then I went to PETW and gave them my opinion. I don't like committee types of decisions and again these safety aspects of the cryogenic pressure tunnel are individual for that facility. For instance, the safety that would have to do with internal insulation as opposed to external would be completely different. So I would avoid trying to categorize this subject and keep it specific and keep it as objective as possible.

That comment that I made with regards to flight rating -- or maybe you want to call it say cryo rated, I don't know, whatever -- but in my opinion the pretest meeting is where it all gets done. We've done a real good job there. Never really lost a model. Because of the pretest meeting we've caught 99% of the things right there between the safety head and the user.

To: Mr. E. J. Ray

From: J. H. Kregel, DLR

Question: You pointed out that LN₂ should be supplied to test installation by direct piping from LN₂ plants rather than by car tanker.

Could you give the critical distance for pipe supply please, assuming that a vacuum insulated line is used and supply would be intermittent only.

Are there any implications for operation and maintenance of such lines?

Ed Ray: Last question came from DLR. Oh, I can understand how this happened. It is from Mr. Kregel, DLR. *"You pointed out that LN₂ should be supplied to the test installation by direct piping from a plant rather than by a tanker. Could you give the critical distance of the pipes supplied assuming the vacuum installation alone, etc. Are there any implications of operation in making such line?"*

I didn't mean to imply that you were out of tune or off base if you did not have a continuous supply line. The point I was trying to make was that there are certain aspects regarding safety and the purity of the nitrogen that are affected by that situation and it's my opinion that safety goes up and purity goes up if you have or are fortunate enough to enjoy that. But I'm sure that many of us can never probably expect to do this. For instance, the German facility at Göttingen, it wouldn't be practical for the amount of LN₂. So again, I think it's an individual case. In our case we're about -- what would you say, about a thousand meters from the plant?

Bob Kilgore: I don't know the exact distance. Ed Bruce, how far is it? How long is the pipe?

Ed Bruce: 3600 feet.

Ed Ray: O.K., pretty close. But anyway, the expense of that pipe is horrible. I don't know exactly what it is but we are talking about megabucks per foot. So you would have to consider that. I think again it's up to the individual. And also the trucking thing could be greatly improved. It doesn't have to be as bad as I've seen it at times. That's all.

Bob Kilgore: Günter Viehweger is going to tell you the ratio in Germany of the expense of vacuum insulated pipe to ordinary pipe. A factor of 2?

Günter Viehweger: No more. Only a factor of 2.

Ed Ray: [Carefully stepping down from the podium.] As a safety specialist, you watch your step.

To: Mr. Pierce Lawing

From: Klaas Breman. (NLR)

Question: - You mentioned costs of "1/2 million \$s" for NTF models. Is this a minimum or an average?
(If minimum, what is an average?)

- In the past someone expected that the design of cryo models would be 3X, manufacture 1.5 - 2X the time/cost of conventional models. What is your impression after all of these models you have experience with?

- What is the present delivery time of NTF models? (Are they made in shifts?)

- Do customers generally bring their own models?

Pierce Lawing: I'm Pierce Lawing and my question is from Klaas Breman of NLR. *"You mention the cost of half a million dollars for NTF models. Is this the minimum or an average?"*

It is an average for an average model and I'll define an average model as a transport with pressure distributions on one wing and with a six component internal balance.

"In the past someone expected that the design of cryo models would be three times the manufacture and 1 1/2 to two times the cost of conventional models. What is your impression after all these models you have had experience with?"

In the early days it looked that way but as the experiences have been gained, as the manufacturers have become used to working with the materials, the cost has steadily come down and it's still highly variable, but we believe that the average increase in cost overall for a cryogenic model as compared to the same loaded model, that is, high pressure tunnel type model, is about 30%.

And, *"What is the present delivery time of NTF models?"*

If you don't want to give somebody extra money for building it in a hurry, about a year and a half. A good part of that is ordering material and getting it in hand and getting it certified. If you have your own material... There are a lot of ways to cut this down, I'm sure.

"Do customers generally bring their own models." Yes they do. Our shops only build one of a kind research type models that haven't been built before.

These questions beg one more question and I would like to offer a recommendation, that if you are going to spend the money to build, and test, and analyze the data for a cryogenic model, that you certainly assign a person to follow that model and to baby-sit it through every part of the process from ordering the material right on.

Peter Fuijkschot: Do you mean that if the customer builds the model one of your people guides him all the time?

Pierce Lawing: No, the customer should supply a person to be with that model. You don't want to trust somebody else to build your model and keep track of it. Ed, do you want to ...

Ed Ray: May I please add to that?

Pierce Lawing: Sure.

Ed Ray: I think that's a very important part that I know that I'm going to slip by somehow. Pierce picked up on it in a couple of places but these models ... the quality assurance and the documentation is so important ... a lot of expenses is actually shifted up forward. And if you put enough emphasis into a good design, good QA, it will end up being cost effective because you won't end up doing the wrong thing to the models.

But the documentation is essential and I would recommend that you have a traveler with each one of these models and then you avoid the possibility of heat treating it twice -- and that's happened -- you've got to know every process that this model or this apparatus goes through and it's got to go right with them and you've got to have ... to avoid large costs and losses you have to be very very careful in the management of these special tools that we have.

Bob Kilgore: Pierce, are there any other parts to that?

Pierce Lawing: No.

Bob Kilgore: The one outstanding question that I know of is Dave Wigley's and again if you want to ... what? Three or four minutes? Pick a time.

To: D. A. Wigley or P. L. Lawing

From: A. Mignosi, ONERA/CERT

Question: *Do you have information about insulating materials which can be used for optical purposes: Plastic, glass or anything else? For Example, can we protect a window at the wall of a cryogenic wind tunnel to avoid fluxes at the wall and reduce deformation due to thermal expansion and frosting?*

Dave Wigley: The question was from André Mignosi and it was specifically about do we know anything about insulating materials that might be capable of giving a decent optical window.

Now, there are a number of people here that know much more about optical windows than I do, but between André and I, we at least went through a generic way of how you might look at this because if you look at the type of materials that you can see through you come back to either glasses or ceramics -- and particularly pyrex glasses -- and the possibility of some of the more modern two phase ceramic materials. The essential thing is that there you try and minimize the expansion coefficient.

When you come to plastics, the ones that you can see through and might be tough enough at low temperatures, would be, for example, mylar and polycarbonate. PMMAs, are almost certainly going to be a bit brittle. But there you also have high contraction coefficients. So with plastic materials you've got both a high contraction, poor thermal conductivity, and therefore very strong potential for thermal shocks. And then, if you are really seriously looking at windows, you really have got to know exactly the pressures, whether you are trying to equalize pressures either side of the window, thermal inertias...

Now in their tunnel they have only got a 60 second run times so how you would design potentially a low thermal inertia model would possibly have very thin components in it so that you got temperature equalization. Equally you might go to completely the other extreme and look for something that was so thick that you would have a large thermal mass. In which case if you went to take that approach you have really got to make certain that you have very small expansion coefficients. Otherwise you are going to lose it from thermal shock. So it's a very specific problem and you've really got to go through all the subsets of constraints and variables.

Now you [nodding toward Bob Kilgore] know about windows, and when we talked at coffee you said purge them. You've had good experience purging them. Now when André... when we talked about that he said one of things he wants to do is to put a laser through it. And if you put a laser ... if you get diffusion in the plastic, you might melt the plastic. So you have to iterate around the loop to get into a very specific answer. That's why I dodged it the first time.

Bob Kilgore: Good. I wasn't going to let you get by with that. Thank you David. Do we have any other written questions outstanding?

I almost forgot to respond to a question I was holding, asking if there were any others. Yes, there is one other.

To: Auditorium

From: B. Ewald

Question: The question is risen by the contribution on Helium tunnels.

Compared to air the specific heat ratio of exotic wind tunnel media (Helium, heavy gases) is wrong. So simulation of compressible flow will be wrong.

In what respect are the results wrong?

How wrong are they? (as a function of Mach number)

Exists a similarity rule for the specific heat ratio?

No comments in literature!

Any comments from audience?

Bob Kilgore: When Mike Smith gave his talk on the helium tunnel, there was the implication that this would be a wonderful way to avoid such big tunnels as the NTF or the KKK or whatever. And Bernd points out quickly that the specific heat ratio of exotic wind tunnel media, helium or heavy gases such as sulfur hexafluoride (SF_6), is wrong, so simulation of compressible flow will be wrong. And therein lies the stumbling block that most of us see with things like helium for transonic testing.

If you are attempting to get information to use ... say by Boeing to make their next transport better, if it's got to simulate flight, according to our present knowledge, it has to have the proper ... not necessarily the ratio of specific heats ... but it is going to have to act like air when you do what you are going to do to it.

So Bernd has raised the question, "In what respect are the results wrong?" Well, the one I know about, Mike, is the pressure rise across a normal shock. That's wrong. And this leads to things like pitching moments being wrong. And if the pitching moment is wrong and you are trying to design a C-141, you put 800 pounds of lead up front and you make the pitching moment right.

"How wrong are they?" Eight hundred pounds wrong, that is how wrong they are.

"Does there exist a similarity rule for the ratio of specific heats?" For Freon 12, I think they have tried to come up with adjustments on Mach number when they would run, and some other fixes. But in 1946, when many smart people put Freon 12 in a NASA [NACA] Langley tunnel, they worked for several years and never published the data, so far as we can find.

In the future, someone may go back and find that there are several reports published and all the data is good. But we can't find it. So I think there are not satisfactory ways of correcting ... as if it were a general purpose tunnel. If it is specific to do buffet and flutter and dynamic testing, where any answer is better than no answer, then you use things like Freon 12.

"No comments in literature." That's a statement by Bernd. There are some comments and we'll dig those out and I will try to get you copies.

"Any comments from the audience?" Well, I'm not sure. If I mention sulfur hexafluoride, as I've done to Ted Carter at ARA, it may become a religious experience. Ted simply said, "Jesus."

It [using SF_6] is not the kind of thing that people who had a lot of thought about it really want to go to. But, if you want to use sulfur hexafluoride or helium or anything else to get extremely high Reynolds numbers to do fundamental fluid dynamics or to do things at low speed where there are no compressibility problems, it is a wonderful way to do it and should be encouraged.

Well. Decision time. I've made a decision. That's the end of the question and answer period.

Concluding Remarks

Bob Kilgore: You should remember this chart from Monday morning.

Goals of the Special Course

- * Review the development of cryogenic wind tunnels
- * Describe advances in cryogenic wind tunnel technology
- * Provide sources of information
- * Help establish technical contacts
- * Promote informal discussions
- * Identify problem areas

These were our goals and at least some of them we've met by reviewing the development of cryogenic tunnels.

You've heard some advances in cryogenic wind tunnel technology. Whether the advances are as far as you would like to see depends upon your special interest and your interpretation of what you have heard.

The sources of information ... several new references have come to light.

You've met some people. Established technical contacts. I've heard informal discussions going on even during the lectures, which is not to be discouraged. It's like going to sleep in church. The preacher should be happy because he has put you at such ease with yourself that you can just go to sleep.

And to identify problem areas... we still have some problem areas. Again, which ones you think are the real problem areas will depend upon what knotty problem you're up against right now. I think we all agree that we would like to do better with strain gage balances than we think we're doing, not because we're doing worse than before, but because our desires continually increase. There could be other examples.

Well, having done that, it's really time to wind things up. And for that, I won't put my jacket on but I will carefully step up here and go down the list of people to thank for making all of this possible.

Normally, you thank the attendees last and say wonderful things about them. Actually, you have been an ornery [difficult, contrary, wayward, balky] lot of attendees because you seldom returned from coffee breaks or lunch in a timely manner. But we still thank you for being here. If you weren't here, there would be no excuse for the large number of lecturers who have assembled. There are 17 of us and 50 of you.

Finally, coming to the thanks that are due to the AGARD Fluid Dynamics Panel and VKI ... They funded some of the lecturers. And AGARD will bind the final lecture notes and mail them out to all the attendees. So you will eventually get a complete set of lecture notes.

Thanks certainly to the lecturers, some of whom were paid for their efforts, not all. DLR did a good thing by sending people beyond the call of duty. They funded people to come and talk, as did ONERA, as did ETW GmbH. And the Donnelly Group at the University of Oregon. They suffered doubly. They had to pay the fee for Mike Smith and then we let him also give a lecture.

NASA Langley comes in for thanks because they funded both Dr. Goodyer and Dr. Balakrishna. And then Dr. Wigley comes out really last in all of this. David funded himself, for which we thank him. But I told him he owed me one. He didn't know why, but he agreed.

The final thanks... and I look back to Professor Carbonaro to do this... goes to Mario Carbonaro for providing an ideal location and a perfect staff to carry all of this off. And we all thank you for that.

And if there are no further comments, observations, or outcries, we'll leave and have lunch and try to stay in touch.

The End

NASA Technical Memorandum 4013

Cryogenic Wind Tunnels -- A Selected, Annotated Bibliography

INTRODUCTION

This Informal Supplement to NASA TM 4013 was prepared especially for the AGARD-FDP/VKI Special Course *Advances in Cryogenic Wind Tunnel Technology*. It contains 58 citations selected from the papers related to cryogenic wind tunnels that we have found since we published TM 4013 in September 1987.

The reader is requested to call to our attention errors or omissions since we are likely to include these citations in the next formal up-date of the continuing NASA series of bibliographies on cryogenic tunnels.

Marie H. Tuttle

Robert A. Kilgore

Deborah L. Moore

May 22, 1989

ORDERING INFORMATION

The following table lists the various kinds of accession numbers used. It also lists the type of material each indicates and the sources for each type.

Accession Number	Type of Material	Source
AXX-XXXXX Example: A75-25583	AIAA papers and published literature available from AIAA or in journals, conferences, etc., as indicated	American Institute of Aeronautics and Astronautics Technical Information Service 555 West 57th Street, 12th Floor New York, NY 10019
NXX-XXXXX Example: N67-37604	Report literature having no distribution limitation	National Technical Information Service (NTIS) 5285 Port Royal Road Springfield, VA 22161
XXX-XXXXX Example: X72-76040	Report literature having some type of distribution limitation	NASA Scientific and Technical Information Facility (STIF) P. O. Box 8757 B.W.I. Airport, MD 21240
AD Numbers Example: AD-A162351	Report literature with or without distribution limitation	Defense Technical Information Center Cameron Station Alexandria, VA 22314
Order number (when given)	Theses	University Microfilms A Xerox Company 300 North Zeeb Road Ann Arbor, MI 48106
Library of Congress numbers Example: TL570.P48	Books, conference proceedings, etc.	Libraries

For any other type of material, contact your library or the NASA Scientific and Technical Information Facility (see address above), and include any information given.

A "#" after an acquisition number indicates that the document is also available in microfiche form.

ISSN is an acronym for International Standard Serial Number. This is an internationally accepted code for the identification of serial publications; it is precise, concise, unique, and unambiguous.

ISBN is an acronym for International Standard Book Number. This is a number given to every book or edition of a book before publication to identify the publisher, the title, the edition, and volume number.

BIBLIOGRAPHY

1 *Baals, D. D., Ed.: **High Reynolds Number Research**. NASA CP-2009, 1977. A workshop, sponsored in part by George Washington Univ., held at Langley Research Center, Hampton, VA, Oct. 27-28, 1976, 192 pp.

N77-27139#

This report discusses the fundamental aerodynamic questions for which high Reynolds number experimental capability is required. It also reviews the operational characteristics and design features of the U.S. National Transonic Facility (NTF).

*NASA, Langley Research Center, Hampton, VA 23665-5225, USA

2 *Prieur, J.; and *Dor, J. B.: **Estimation des pertes Thermiques et Calculs des Caracteristiques de l'Ecoulement dans une Soufflerie a Rafales Cryogeniques**. (Estimating heat losses and calculating flow characteristics in an intermittent cryogenic wind tunnel), DCAF F070143, June 1978, 44 pp., in French.

(Contact the NASA Langley Technical Library for information about possible translations of this paper.)

This paper discusses the heat flux transmission phenomena of the various elements of the aerodynamic system of the T2 wind tunnel at ONERA/CERT. It is possible to estimate the thermal losses and make a comparison with the theoretical thermal balance. The internal insulation is found to be quite effective.

*ONERA/CERT, 2, Ave. Edouard Belin, 31055 Toulouse Cedex - FRANCE

3 *Clausing, A. M.: **Advantages of a Cryogenic Environment for Experimental Investigations of Convective Heat Transfer**. In: International Journal of Heat and Mass Transfer, vol. 25, no. 8, Aug. 1982, pp. 1255-1257.

Experimentalists studying convective heat transfer phenomena often have difficulty in obtaining sufficiently large Reynolds numbers, *Re*, and/or Grashof numbers, *Gr*. A cryogenic environment, such as in a cryogenic wind tunnel, provides a means of obtaining, simultaneously, large increases in both the Reynolds number and the Grashof number; hence, it provides an excellent tool for forced, natural, and combined convective heat transfer research. The Reynolds and Grashof numbers are increased with an ambient temperature of 80 K by factors of approximately 14 and 200, respectively, over those obtainable in a room temperature facility. The cryogenic environment virtually eliminates the influences of radiative heat transfer. The ability to vary the temperature in the test section greatly increases the range in the Reynolds and Grashof numbers that can be studied with fixed model and test section dimensions. The cryogenic facility also provides an excellent environment for the study of the influences of property variations across the boundary layers.

*University of Illinois at Urbana-Champaign, Urbana, IL 61801, USA

4 *Shchelkunov, V. N.; *Rudenko, N. Z.; and *Fdfelov, M. A.: **Cryogenic Wind Tunnel of Variable Density at low Reynolds Numbers**. In: Pribery i Tekhnika Eksperimenta, no. 5, Sep. - Oct. 1982, pp. 230-?, in Russian.

5 *Archambaud, J. P.: **Calcul de L'Evolution du Champ des Temperatures dans un Element Metallique Paroi-Raidisseur au Cours d'une Rafale Cryogenique**. (Computation of the evolution of the temperature field in the metal piece wall-stiffener during a cryogenic run). RTOA no. 25/3075 AND (DERAT n° 8/5015 DN) - Dec. 1982, 17 pp., 9 figs., 3 refs., in French.

This paper deals with the theoretical behavior of classical flexible walls (metallic, not insulated) during a cryogenic run carried out at the T2 wind tunnel of the ONERA/CERT. This is an unsteady coupling calculation: boundary layer on the internal side - heat transfer throughout a piece of wall involving a stiffener. This calculation allows us to get as a function of time the following: - the local variations of the thermal fluxes at the wall; - the temperature field into the wall; - and the boundary layer which will be taken into account by the wall adaptation process.

*ONERA/CERT, 2, Ave. Edouard Belin, 31055 Toulouse Cedex - FRANCE

6 *Sawada, H.: **NAL TCWT Status - Cryogenic Operation**, NAL News, no. 229, 1984-3, 8 pp., in Japanese.

ISSN 0023-2726

This paper describes the 0.1 x 0.1 m Transonic Cryogenic Wind Tunnel at the National Aerospace Laboratory (NAL). It also describes the use of the original manual control systems for typical purging, cooldown, running, and warm-up operations.

*National Aerospace Laboratory, Tokyo, JAPAN

7 *Blanchard, A.; *Seraudie, A.; *Plazenet, M.; and *Payry, M. J.: **Essai de la Balance Probatoire Cryogenique ONERA dans la Soufflerie T2**. Rept. no. DERAT-TR-22/5007-DN, July 1983, 47 pp., in French.

Note: For an English translation of this report see no. 31 in this bibliography.

A three component cryogenic balance designed and built by ONERA, was fitted with a light alloy model and tested at the end of 1984 in the T2 wind tunnel in flows at temperatures down to 120 K. The tests were to determine the effect of cryogenic operation on the behavior of balance while cooling the balance-model system mounted in the conditioning device and during tests with models in the test section. A few tests with thermal disequilibrium between the flow and balance made it possible to confirm proper operation in the range 120 K - 300 K. These tests showed that the balance, which was well compensated thermally, may be used in T2 with or without precooling. For any thermal gradient, the analysis was always made with the same matrices and the aerodynamic coefficients were obtained with the same precision.

*ONERA/CERT, 2, Ave. Edouard Belin, 31055 Toulouse Cedex - FRANCE

8 *Lawing, P. L.: **The Construction of Airfoil Pressure Models by the Bonded Plate Method: Achievements, Current Research, Technology Development and Potential Applications**. NASA TM-87613, Sept. 1985, 34 pp.

N86-16234#

This paper describes a method of building airfoils by inscribing pressure channels on the face of opposing plates, bonding them together to form one plate with integral channels, and machining this plate to the desired contour. The research and development program to develop the bonding technology is described as well as the construction and testing of an airfoil model. Sample aerodynamic data sets are presented and discussed. Also, work currently under way to produce thin airfoils with camber is presented. Samples of the aft section of a 6 percent airfoil with complete pressure instrumentation, including the trailing edge, are pictured and described. This technique is particularly useful in building models for transonic cryogenic testing, but it should find use in a wide range of model construction projects, as well as the fabrication of fuel injectors, space hardware, and other applications requiring advanced bonding technology and intricate fluid passages.

*NASA Langley Research Center, Hampton, VA 23665-5225, USA

9 *Sawada, H.: **Automatic Operation of the NAL Cryogenic Wind Tunnel.** NAL News, no. 321, 1986-1, 8 pp., in Japanese.

ISSN 0023-2726

This paper describes the 0.1 x 0.1 m Transonic Cryogenic Wind Tunnel at the National Aerospace Laboratory (NAL). In a previous paper, [no. 6 in this bibliography], I describe the operation of this tunnel using the original manual control systems. In 1985 we installed automatic controls for liquid nitrogen injection, gaseous nitrogen exhaust, and fan speed. Under manual control, changing from one test condition to another took from 5 to 10 minutes. The same changes in test conditions now take only about 1 minute under fully automatic control. The automatic controls are implemented using a NEC microcomputer.

*National Aerospace Laboratory, Tokyo, JAPAN

10 *McKinney, L. W.; and *Fuller, D. E.: **Preliminary Calibration and Test Results from the National Transonic Facility.** In: Langley Symposium on Aerodynamics, N88-14926, vol. 1, Dec. 1986, pp. 311-331, paper presented Apr. 23-25, 1986.

N88-14941#

The U.S. National Transonic Facility (NTF) was operated to design condition of 120 million Reynolds number at a Mach number of 1.0. All systems were checked out except plenum isolation valves; modifications are being made to heaters on the actuators. Initial steady-state calibration indicates excellent steady flow characteristics. The first test of the Pathfinder 1 model indicated significant Reynolds number effects. Some effect of temperature on instrumentation were obtained. The cause of these effects is being evaluated.

*NASA Langley Research Center, Hampton, VA 23665-5225, USA

11 *Ewald, B.; and **Graewe, E.: **The Development of DMS-Scales for Cryogenic Wind Tunnels.** (Ueber die Entwicklung von DMS-Waagen fuer Kryo-Windkanalee). Presented at the BMFT, Statusseminar ueber Luftfahrtforschung und Luftfahrttechnologie, Munich, West Germany, Apr. 18-30, 1986, 18 pp., in German.

The development of a DMS scale for use in a cryogenic wind tunnel is discussed. The accuracy of power measurements in wind tunnels is reviewed, and attainable accuracies for DMS scales are compared with those required for cryogenic wind tunnels. The main sources of inaccuracy in DMS scales are described, and methods to overcome them are indicated.

*Technische Hochschule Darmstadt, Darmstadt, FRG

**Messerschmitt-Bölkow-Blohm Bremen, FRG

12 *Supplee, F. H., Jr.; and *Tcheng, P.: **A Miniature Remote Deadweight Calibrator.** Presented at the 32nd International Instrumentation Symposium, Seattle, Wash., May 5-8, 1986. In: Proceedings (A87-45101) Instrument Society of America, 1986, pp. 65-85.

A87-45104#

A miniature, computer-controlled, deadweight calibrator was developed to remotely calibrate a force transducer mounted in a cryogenic chamber. This simple mechanism allows automatic loading and unloading of deadweights placed onto a skin friction balance during calibrations. Equipment for the calibrator includes a specially designed set of five interlocking 200-milligram weights, a motorized lifting platform, and a controller box taking commands from a microcomputer on an IEEE interface. The computer is also used to record and

reduce the calibration data and control other calibration parameters. The full-scale load for this device is 1,000 milligrams; however, the concept can be extended to accommodate other calibration ranges.

*NASA Langley Research Center, Hampton, VA 23665-5225, USA

13 *Daryabeigi, K.; *Ash, R. L.; **Dillon-Townes, L. A.: **Thermal Sensing of Cryogenic Wind Tunnel Model Surfaces - Evaluation of Silicon Diodes.** Presented at the 32nd International Instrumentation Symposium, Seattle, Wash., May 5-8, 1986. In: Proceedings, (A87-45101), Instrument Society of America, 1986, pp. 203-217, 16 refs.

A87-45111#

Different sensors and installation techniques for surface temperature measurement of cryogenic wind tunnel models were studied. Silicon diodes were selected for further consideration because of their good inherent accuracy. Their average absolute temperature deviation in comparison tests with standard platinum resistance thermometers was found to be 0.2 K in the range from 125 to 273 K. Subsurface temperature measurement was selected as the installation technique to minimize aerodynamic interference. Temperature distortion caused by an embedded silicon diode was studied numerically.

*Old Dominion University, Norfolk, VA 23508-0369, USA

**NASA Langley Research Center, Hampton, VA 23665-5225, USA

Contract NASA 1-17099

14 *Hoenlinger, H.; and *Sensburg, O.: **Aeroelastic Models in Aircraft Design.** Rept. MBB/LKE-294/S/PUB/249; ETN-88-9-91439; DCAF E070087, June 1986, 10 pp., in German.

N88-20298#

The use of aeroelastic model tests in aircraft design is outlined. Aeroelastic models are economical for the development and testing of novel active-control technologies and measuring methods for aircraft vibration tests. The linearized dynamic calculation model of a flying elastic aircraft was realized in a wind tunnel using aeroelastic models. The validity domain of an aeroelastic model was substantially extended in a cryogenic wind tunnel.

*Messerschmitt-Bölkow-Blohm GmbH, Ottobrunn, FRG

15 *Heinzerling, W.: **Der zukünftige Einsatz des Europäischen Transschall-Windkanals ETW bei der Entwicklung fortschrittlicher Flugzeuge.** (The future use of the European Transonic Wind Tunnel ETW in the development of advanced aircraft). In: Yearbook 1986 II; DGLR, Annual Meeting, Munich, West Germany, Oct. 8-10, 1986, Reports (A87-48154 21-01). Bonn, Deutsche Gesellschaft für Luft- und Raumfahrt, 1986, pp. 700-711. 18 refs., in German.

DGLR Paper 86-140

A87-48162

*Messerschmitt-Bölkow-Blohm GmbH, Munich, FRG

16 *Seraudie, A.; *Blanchard, A.; and *Dor, J. B.: **Description of Tests Run in the T2 Cryogenic Wind Tunnel.** Presented at the Association Aeronautique et Astronautique de France, Colloque d'Aérodynamique, 23rd, Modane, France, Nov. 12-14, 1986, 44 pp., in French.

AAAF Paper NT 86-07

A87-38033#

Note: For an English translation of this report see no. 17 in this bibliography.

Test methods and measurement techniques of the high-Reynolds-number (up to 30 million), high-pressure, cryogenic T2 wind tunnel are discussed. Velocity and pressure fluctuation measurements are obtained with high-bandpass pressure probes

and hot-film probes. Stagnation and static pressure probes with short response times are used to investigate wakes, and unsteady static pressure measurements, with sensors placed at the profile boundary, are obtained to study buffeting. Transition positions are detected using IR thermography, stagnation-pressure and longitudinal sounding, thermocouple measurements of boundary temperatures, and oil-film parietal visualizations. The measurement of aerodynamic coefficients of a model using a five-component balance is also discussed.

*ONERA/CERT, 2, Ave. Edouard Belin, 31055 Toulouse Cedex - FRANCE

17 *Seraudie, A.; *Blanchard, A.; and *Dor, J. B.: **Description of Tests Run in the T2 Cryogenic Wind Tunnel.** Rept. PB87-170296; and NOTE-TECHNIQUE-86-07; Nov. 1986, 51 pp., in English.

ISBN-2-7170-0855-1

N88-16672#

Note: For an earlier form of this report see no. 16 in this bibliography.

Research done on the testing techniques and measurement methods to be used in the T2 pressurized cryogenic wind tunnel is described. It was found that the model temperature must be established before measuring the gust. Several rounds of cryogenic tests provided valuable experience in conducting cold flow measurements. Cross checking was done to validate the tests. However, some experimental snags related to high unit Reynolds numbers were encountered during natural transition tests. It was found necessary to take the level of flow turbulence into account and to improve the condition of the model surface to maintain a laminar state in the boundary layers of most of the airfoils.

*ONERA/CERT, 2, Ave. Edouard Belin, 31055 Toulouse Cedex - FRANCE

18 *Schnerr, G.: **Homogene Kondensation in Stationären Transsonischen Strömungen Durch Laval-Düsen und um Profile,** In German, 1986, 135 pp., 57 refs.

*Universität Karlsruhe (TH), Karlsruhe, FRG

19 *Johnson, C. B.; *Carraway, D. L.; *Stainback, P. C.; and **Fancher, M. F.: **A Transition Detection Study Using a Cryogenic Hot Film System in the Langley 0.3-Meter Transonic Cryogenic Tunnel.** Presented at the 25th AIAA Aerospace Sciences Meeting, Reno, Nev., Jan. 12-15, 1987, 23 pp.

AIAA-87-0049

N87-22380#

Note: For a later paper on this work see no. 25 in this bibliography.

A transition detection study was made in the Langley 0.3-m Transonic Cryogenic Tunnel (TCT) using a specialized hot film system designed specifically for use in cryogenic wind tunnels. Quantitative transition location data obtained at near cryogenic conditions, represent the first definitive transition Reynolds numbers obtained in a cryogenic wind tunnel. The model was tested at both adiabatic and nonadiabatic wall conditions with a wall-to-total temperature ratio as low as 0.47. Test results indicate an improved technique for hot-film installation and a modified data acquisition system would allow the on-line determination of the location of boundary layer transition in cryogenic wind tunnels, such as the U.S. National Transonic Facility.

*NASA Langley Research Center, Hampton, VA 23665-5225, USA

**Douglas Aircraft Co., 3855 Lakewood Blvd., Long Beach, CA 90846, USA

20 *Sawada, H.: **Heated External Balance for Cryogenic Wind Tunnel.** In: NAL News, no. 333, 1987-1, 8 pp., in Japanese.

ISSN 0023-2726

This paper describes a heated external balance used with the 0.1 x 0.1 m Transonic Cryogenic Wind Tunnel at the National Aerospace Laboratory (NAL). It also describes tests of a 30 mm span AGARD-B model at cryogenic temperatures using the heated balance. The results show the heated balance works well.

*National Aerospace Laboratory, Tokyo, JAPAN

21 *Kraft, Dieter: **Optimal Control: A Systematic Device for the Computer-Aided Exploration of the Dynamic Possibilities of a Cryogenic Wind Tunnel.** ESA-TT-1016, Mar. 1987, 228 pp., (Translation into English of the German report DFVLR-FB-86-23, ETN-87,90014, which is no. 452 in TM 4013). The original language document is available from DLR, Cologne, FRG.

N87-27676#

The dynamic systems behavior of a cryogenic wind tunnel was analyzed for an automatic control system which meets the safety requirements and operating specifications in a wide domain of operations. For cost, safety, and availability reasons this analysis cannot be performed on the real tunnel, but must be made using a mathematical model. The dynamic behavior of the wind tunnel is characterized by strongly coupled nonlinear differential equations; therefore optimal control was applied for analysis. The boundary values of the system are the basis of comparison for the different steps of the analysis, while the control and state constraint and their variations resulting from the operating specifications represent systematic step sizes along which the dynamic spectrum was explored. This procedure yields statements about the robustness of nonlinear systems. Direct numerical methods for the solution of optimal control problems are described. ESA

*DFVLR, Oberpfaffenhofen, D-8031 Wessling/Obb, FRG

22 *Boyden, R. P.; *Ferris, A. T.; *Johnson, W. G., Jr.; *Dress, D. A.; and *Hill, A. S.: **Aerodynamic Measurements and Thermal Tests of a Strain-Gage Balance in a Cryogenic Wind Tunnel.** NASA TM-89039, April 1987, 85 pp.

N87-20517#

An internal strain-gage balance designed and built in Europe for use in cryogenic wind tunnels has been tested in the Langley 0.3-meter Transonic Cryogenic Tunnel (TCT). Part of the evaluation was made at equilibrium balance temperatures. It consisted of comparing the data taken at a tunnel stagnation temperature of 300 K with the data taken at 200 K and 110 K while maintaining either the Reynolds number or the stagnation pressure. We used a sharp-leading-edge delta-wing model to provide the aerodynamic loading for these tests. We found the results obtained with the balance during the force tests to be accurate and repeatable both with and without the use of a convection shield on the balance. An additional part of this study involved obtaining data on the transient temperature response of the balance during both normal and rapid changes in the tunnel stagnation temperature. We measured the variation of the temperature with time at three locations on the balance near the physical locations of the strain gages. The use of a convection shield significantly increased the time required for the balance to stabilize at a new temperature during the temperature response tests.

*NASA Langley Research Center, Hampton, VA 23665-5225, USA

23 *Blocher, R.; and *Weiss, E.: **Design Study - Manipulator Systems for Model Handling in European Transonic Wind Tunnels.** (Konzeptstudie, Manipulatorsystem fuer Modelhandhabung im Europaeischen Transschall-Windkanal), ETN-88-91944, May 25, 1987, 199 pp., in German.

N88-24651#

Electrical master-slave manipulators in cryogenic temperatures and under pressure are proposed for remote model handling. Economy of time and energy can be achieved without thermal stresses in model and wind tunnel. Manipulator design consists of two arms and seven degrees of freedom. Control is achieved by frequency regulated asynchronous motors. Digital electronics procures total automation for the study of collision protection and special handling cycles. Viewing and associated audio-systems are provided by stereo and monosystems giving optimal global view of the operating field. Mechanical properties of construction parts in cryogenic environment are studied.

ESA

*Blocher-Motor, GmbH and Co. K.G., Metzingen, FRG

24 *Rao, M. G.; and *Scurlock, R. G.: **A Silicon Diode Thermometer, With Integrated Circuit Instrumentation Package, for Operation Between 77.5 K and 290 K.** In: ICIASF '87 - International Congress on Instrumentation in Aerospace Simulation Facilities, 12th, Williamsburg, VA, June 22-25, 1987, Record (A88-36483 14-35). New York, Institute of Electrical and Electronics Engineers, Inc., 1987, pp. 92-94.

A88-36492

The use of cold electronic systems for processing transducer signals is studied. In particular, the development of a single-channel cold electronic system interfacing with a silicon diode thermometer, in which the whole instrumentation package operates at any temperature between 77.5 K and 290 K is described. The electronic system includes a constant current source, signal conditioning amplifiers and a 12-bit A/D converter. The thermometer package has a resolution of 0.2 K and an absolute accuracy of 0.5 K.

*The University of Southampton, Southampton, SO9 5NH, Hampshire, UK

Research supported by the Department of Trade and Industry

25 *Johnson, C. B.; *Carraway, D. L.; *Hopson, P., Jr.; and *Tran, S. Q.: **Status of a Specialized Boundary Layer Transition Detection System for Use in the U.S. National Transonic Facility.** In: ICIASF '87 - International Congress on Instrumentation in Aerospace Simulation Facilities, 12th, Williamsburg, VA, June 22-25, 1987, Record (A88-36483). New York, Institute of Electrical and Electronic Engineers, Inc., 1987, pp. 141-155, 15 refs.

A88-36500#

Note: For an earlier paper on this work see no. 19 in this bibliography.

This paper reports on an improved deposition technique for cryogenic hot films used for transition detection in cryogenic wind tunnels. Tests of the hot films in a low-speed tunnel demonstrated the ability to obtain online transition data. The capability of an enhanced hot film data acquisition system was also demonstrated. A comparison of data from the new system with stability theory shows the detection of Tollmein-Schlichting waves at transition onset.

*NASA Langley Research Center, Hampton, VA 23665-5225, USA

26 *Burner, A. W.; *Snow, W. L.; *Goad, W. K.; and *Childers, B. A.: **A Digital Video Model Deformation System.** In: ICIASF '87 - International Congress on Instrumentation in Aerospace Simulation Facilities, 12th, Williamsburg, VA, June 22-25, 1987, Record (A88-36483 14-35). New York, Institute of Electrical and Electronics Engineers, Inc., 1987, pp. 210-214.

A88-36508#

This paper discusses the use of solid-state array cameras and a PC-controlled image acquisition system to measure model deformation in a wind tunnel. This digital system improves an earlier video model deformation system that used high-resolution tube cameras and required the manual measurement of targets on video hardcopy images. The new system

eliminates both the vibration-induced distortion associated with tube cameras and the manual readup of video images necessary in the earlier version. Camera calibration and data reduction procedures necessary to convert pixel image plane data from two cameras into wing deflections are presented. The paper also describes laboratory tests to establish the uncertainty of the system with the geometry to be used. I.E.

*NASA Langley Research Center, Hampton, VA 23665-5225, USA

27 *Selby, G. V.: **Progress in Visualizing Cryogenic Flow Using the Vapor-Screen Technique.** In: ICIASF '87 - International Congress on Instrumentation in Aerospace Simulation Facilities, 12th, Williamsburg, VA, June 22-25, 1987, Record (A88-36483 14-35). New York, Institute of Electrical and Electronics Engineers, Inc., 1987, pp. 233-238, 10 refs.

A88-36511

We visualized the vortical flow on the leeward side of a delta-wing model at several different tunnel conditions in the NASA Langley 0.3-m Transonic Cryogenic Tunnel (TCT) using a vapor-screen flow-visualization technique. Vapor-screen photographs of the subject flow field are presented and are interpreted relative to phenomenological implications. Results indicate that the use of nitrogen fog in conjunction with the vapor-screen technique is feasible.

*Old Dominion University, Norfolk, VA 23508, USA

28 *Ewald, B.; and **Graewe, E.: **Development of Internal Balances for Cryogenic Wind Tunnels.** In: ICIASF '87 - International Congress on Instrumentation in Aerospace Simulation Facilities, 12th, Williamsburg, VA, June 22-25, 1987, Record (A88-36483 14-35). New York, Institute of Electrical and Electronics Engineers, Inc., 1987, pp. 274-282.

A88-36517

The construction of large cryogenic wind tunnels will be of little benefit for aircraft development, if force measurements in such tunnels are not possible with at least the same accuracy as in conventional tunnels. Up to now this target is still far away due to severe thermal effects in the strain gage balance. For two of these effects novel approaches are outlined in the paper. The effect of apparent strain over the whole temperature range is minimized by a compensation of each individual gage. With respect to temperature gradients a novel arrangement of the axial force systems allows a correct separation of thermal effect and force measurement.

*Technische Hochschule Darmstadt, Darmstadt, FRG

**Messerschmitt-Bölkow-Blohm GmbH, Bremen, FRG

Funded by the German Ministry of Research & Technology

29 *Sawada, H.: **Cryogenic Wind Tunnels.** In: Journal of the Japanese Society of Aeronautical and Space Sciences, vol. 35, no. 401, June 1987, pp. 285-293, in Japanese, 36 refs.

This paper describes the 0.1 x 0.1 m Transonic Cryogenic Wind Tunnel built at the National Aerospace Laboratory (NAL) in 1982. It describes the fully automatic control system implemented using a NEC microcomputer. It also describes a heated external balance successfully used in tests with the tunnel at cryogenic conditions. Finally, the author presents the need for a large cryogenic transonic wind tunnel for Japan.

*National Aerospace Laboratory, Tokyo, JAPAN

30 *Lassiter, W. S.: **Plume Dispersion of the Exhaust from a Cryogenic Wind Tunnel.** NASA TM-89148, June 1987, 29 pp.

N87-25545#

An analytical model was developed to predict the behavior of the plume exhausting from the cryogenic U.S. National Transonic Facility. Temperature, visibility, oxygen

concentration, and flow characteristics of the plume are calculated for distance downwind of the stack exhaust. Negative buoyancy of the cold plume is included in the analysis. Compared to photographic observations, the model predicts the centerline trajectory of the plume fairly accurately, but underpredicts the extent of fogging. The diffusion coefficient is revised to bring the model into better agreement with observations.

*NASA Langley Research Center, Hampton, VA 23665-5225, USA

31 *Blanchard, A.; *Seraudie, A.; *Plazenet, M.; and *Payry, M. J.: *Test of a Trial Cryogenic Balance in the ONERA T2 Wind Tunnel*. English translation of "Essai de la Balance Probatoire Cryogenique ONERA dans la Soufflerie T2." NASA-TT-20078, July 1987, 106 pp.

N87-24485#

Note: For the original French version of this report see no. 7 in this bibliography.

The three component cryogenic balance designed and manufactured by the ONERA Large Means Directorate, was equipped with a light alloy schematic model and tested at the end of 1984 at the T2 wind tunnel in gusts at low temperatures up to 120 K. The tests pertained to the impact of the cryogenic conditions on the behavior of extensometric bridges while cooling the balance-model system mounted in the conditioning device and during gusts with models in the test section. A few tests with thermal disequilibrium between the flow and balance made it possible to confirm the proper operation in the range 120 to 300 K. This gust system showed that the balance, which was well compensated thermally, may be used in T2 with and without precooled. For any thermal gradient, the analysis was always performed with the same matrices and aerodynamic coefficients were obtained with the same precision.

*ONERA/CERT, 2, Ave. Edouard Belin, 31055 Toulouse Cedex - FRANCE

32 *Bonnet, J. L.; *Seraudie, A.; *Archambaud, J. P.; and *Mignosi, A.: *Mise en Oeuvre d'une Chaîne Anémométrique Laser Bi-Composantes à la Soufflerie T2*. (Implementation of a two-component laser anemometer at the T2 wind tunnel.) RTOA no. 28/5006 AND (DERAT N° 28/5006 DN), July 1987, 34 pp., 55 figs., 3 refs., in French.

A series of tests for perfecting the velocity measurement with a two-component laser anemometer has been carried out on a 180 mm chord RA16SCI airfoil at the T2 wind tunnel, in September 1986. Measurements have been made on boundary layers, wake, and shock probing on the upper side of the model, mainly for two Mach number values (0.6 and 0.725) at 2° angle of attack, corresponding respectively to a steady shock and to a buffeting configuration. This experimental study allowed to test the anemometer system, to know its limitations and practical problems of its use: theoretical limitations due to the operating mode (with or without Bragg cells), limitations due to the filter, to the wall approach, to the density gradients, and so forth. In conclusion, good velocity measurements are reliable with this laser anemometer at the T2 wind tunnel, with respect to the use limitations.

*ONERA/CERT, 2, Ave. Edouard Belin, 31055 Toulouse Cedex - FRANCE

33 *Ladson, C. L.; and *Ray, E. J.: *Evolution, Calibration, and Operational Characteristics of the Two-Dimensional Test Section of the Langley 0.3-Meter Transonic Cryogenic Tunnel*, NASA TP-2749, Sept. 1987, 170 pp.

N87-28570#

This paper presents a review of the development of the world's first cryogenic pressure tunnel, the Langley 0.3-Meter Transonic Cryogenic Tunnel (TCT). Descriptions of the instrumentation, data acquisition systems, and physical features of the two-

dimensional 8- by 24-in. (20.32-by 60.96-cm) and advanced 12- by 12-in. (33.02-by 33.02-cm) adaptive-wall test-section inserts of the 0.3-m TCT are included. Basic tunnel-empty Mach number distributions, stagnation temperature distributions, and power requirements are included. The Mach number capability of the tunnel is from about 0.20 to 0.90. Stagnation pressure can be varied from about 1.2 to 6.1 atm, and the stagnation temperature can be varied from about 80 K to 327 K.

*NASA Langley Research Center, Hampton, VA 23665-5225, USA

34 *Ewald, B.: *Balance Accuracy and Repeatability as a Limiting Parameter in Aircraft Development - Force Measurements in Conventional and Cryogenic Wind Tunnels*. Presented at the AGARD Fluid Dynamics Panel Symposium "Aerodynamic Data Accuracy and Quality: Requirements and Capabilities in Wind Tunnel Testing", AGARD-CP-429(N89-16846#), held in Naples, Italy, Sept. 28 - Oct. 1, 1987; Paper no. 27, 12 pp., 16 refs.

N89-16873#

The success of a commercial transport development is heavily influenced by the accuracy of drag measurements during the aerodynamic development in the wind tunnel. It is shown that the internal balance is one factor limiting accuracy. The accuracy standard of modern internal balances is compared to the accuracy and repeatability requirement of the aerodynamicist. The comparison with high precision single component load cells promises a large improvement potential in multi-component balance design and calibration. The following fields of improvement are discussed in the paper: Balance design, Balance material selection and treatment, Calibration methods, Calibration software, and Thermal effects. Perfect correction of the thermal effects is the key to the successful use of cryogenic tunnels. An approach for the crucial problem of balance body distortion due to temperature gradients is demonstrated.

*Technische Hochschule Darmstadt, Darmstadt, FRG

35 *Mabey, D. G.: *Some Aspects of Aircraft Dynamic Loads Due to Flow Separation*. Presented at the 65th Meeting of the Structures and Materials Panel of AGARD, Cesme, Turkey, Oct. 4-9, 1987. AGARD-R-750, Feb. 1988, 33 pp.

ISBN-92-835-0445-3

N88-18588#

This AGARD paper discusses various topics associated with the study of Aircraft Dynamic Loads due to Flow Separation. Topics discussed include the need for consistent definitions of buffet and buffeting, the advantages of consistent notation for all the papers, buffeting due to wings and other components, the alleviation of buffeting, the special difficulties of flight tests, and the special advantages of buffeting measurements in cryogenic wind tunnels.

*Royal Aircraft Establishment, Bedford, MD4 16AE, UK

36 *Dor, J. B.; *Archambaud, J. P.; and *Breil, J. F.: *Etude des Couches Limite: Laterales, Avec et Sans Aspiration, pour le Profil CAST 7 de Corde 150 mm, à la Soufflerie T2*. (Sidewall boundary layer study, with and without suction, for the 150 mm chord CAST 7 airfoil at the T2 wind tunnel). RTOA n° 40/3075 AND (DERAT n° 14/5015 DN) - Dec. 1987, 19 pp., 80 figs., 4 refs., in French.

This paper presents tests about sidewall effects realized at the T2 transonic wind tunnel equipped with top and bottom adaptive walls. The model is the 150 mm chord CAST 7 airfoil tested with fixed transition at 0.5° angle of attack. The flow field is studied near the solid sidewall, above the downstream part of the model upper side and in the wake, at Mach number 0.705 and 0.755: directional boundary layer probing, static pressure measurements, wall visualizations. Suction rate ($Q_{suction}/Q_{flow}$) of about 4/1000 is achieved on sidewalls, on the downstream part of the model upper side and around the trailing edge. The velocity distribution on the airfoil, the lift coefficient and the modifications of the sidewall boundary layers

(measurements, visualizations) allow to analyzed the suction effect.

*ONERA/CERT, 2, Ave. Edouard Belin, 31055 Toulouse Cedex - FRANCE

37 *Bitter, R. E.: *Assessment of the Use of Cold Gas in a Windtunnel to Investigate the Influence of Thermal Effects on the Dispersion of LNG Vapour Clouds*. Cambridge Univ., Rept. No. CUED/A-Aero/TR14, 1987, 64 pp.

ISSN-0309-7293

N87-24436#

The accidental spillage of liquefied natural gas (LNG) from sea-going transport vessels or land storage tanks may lead to clouds of a cold gas of lower molecular weight than the ambient air. The size of the cloud out to the lower flammability limit and the distance travelled by the cloud from the source are required for estimation of the potential hazard posed. The possibility of using cold gases in a wind tunnel to correctly model heat transfer to the plume and subsequent plume density changes was assessed. A literature survey of the previous modeling of dense-gas dispersion including heat transfer effects was summarized. The scaling laws for the physical modeling of the dispersion of dense gases in the transfer effects are developed. As a result of the scaling laws developed, it is found that the modeling of flows in which free convective heat transfer is important at full-scale, is not possible. The application of the scaling laws to possible release scenarios is undertaken. When forced convection heat transfer is dominant at full-scale physical modeling is feasible. However, the resulting model will have heat transfer dominated by free convection, and, therefore, be unacceptable.

*Cambridge University, Cambridge, UK

38 *Dress, D. A.; and *Kilgore, R. A.: *Cryogenic Wind Tunnel Research: A Global Perspective*. In: *Cryogenics*, vol. 28, Jan. 1988, pp. 10-21.

Personnel at the NASA Langley Research Center built the first cryogenic wind tunnel in 1972. Following the development of this low-speed tunnel, various research establishments around the world also built cryogenic wind tunnels. This paper describes some of these tunnels in England, France, Germany, Japan, and the USA.

*NASA Langley Research Center, Hampton, VA 23665-5225, USA

39 *Goodyer, M. J.: *Preliminary Experiments on Surface Flow Visualizations in the Cryogenic Wind Tunnel by Use of Condensing or Freezing Gases*. NASA CR-181634, Jan. 1988, 21 pp.

N88-18602#

Cryogenic wind tunnel users must have available surface flow visualization techniques to satisfy a variety of needs. While the ideal from an aerodynamic standpoint would be non-intrusive, until an economical technique is developed there will be occasions when the user will be prepared to resort to an intrusive method. One such method is proposed, followed by preliminary evaluation experiments carried out in environments representative of the cryogenic nitrogen tunnel. The technique uses substances which are gases at normal temperature and pressure but liquid or solid at cryogenic temperatures. These are deposited on the model in localized regions, the patterns of the deposits and their subsequent melting or evaporation revealing details of the surface flow. The gases were chosen because of the likelihood that they will not permanently contaminate the model or tunnel. We identified twenty-four gases as possibly suitable and four of these were tested from which we concluded that surface flow direction can be shown by the method. Other flow details might also be detectable. The cryogenic wind tunnel used was insulated on the outside and did not show signs of contamination. Author

*ViGYAN Research Associates, Inc., 30 Research Drive, Hampton, VA 23666-1325, USA

40 *Yamaguchi, Y.; *Kuribayashi, N.; and *Kaba, H.: *Characteristics for Ambient Conditions of NDA Cryotunnel Cryogenic Operation*. Paper presented at the 19th Annual Meeting of the JSASS, Apr. 5-6, 1988, pp. 73-74.

The National Defense Academy (NDA) built the 2-D cryogenic tunnel in 1985 for basic aerodynamic research using the cooling method which was developed by the NASA Langley Research Center. The tunnel calibration tests and improvement of the cryogenic operation method have been conducted. The velocity distribution, turbulence level, and boundary layer thickness of the side wall were measured at several cross sections. The test section for ambient conditions, and the original manual control system was modified to one of a limited automatic cryogenic operation to maintain more accurate cryogenic conditions. The calibration and operational tests show that the present tunnel has sufficient capability for a 2-D tunnel, and that the new control system works well. The time for cryogenic operation increased about 1.5 times as long as that of the original system.

*National Defense Academy, Yokosuka, Japan.

41 *Kilgore, R. A.; *Dress, D. A.; **Wolf, S. W. D.; and ***Britcher, C. P.: *Test Techniques: A Survey Paper on Cryogenic tunnels, Adaptive Wall Test Sections, and Magnetic Suspension and Balance Systems*. Presented at the Transonic Symposium held at NASA Langley Research Center, Hampton, VA, April 19-21, 1988, In: NASA CP-3020, vol. 1, pt. 2, pp. 705-715.

Our ability to get good experimental data in wind tunnels is often compromised by things seemingly beyond our control. Inadequate Reynolds number, wall interference, and support interference are three of the major problems in wind tunnel testing. Techniques for solving these problems are available. Cryogenic wind tunnels solve the problem of low Reynolds number. Adaptive wall test sections can go a long way toward eliminating wall interference. A magnetic suspension and balance system (MSBS) completely eliminates support interference. We are beginning to realize the potential of these techniques. This survey paper covers cryogenic tunnels, adaptive wall test sections, and MSBS. We give a brief historical overview and describe the present state of development and application in each area. Finally, we attempt to predict future developments and applications of these test techniques.

*NASA Langley Research Center, Hampton, VA 23665-5225, USA

**NRC Associate, NASA Langley Research Center, Hampton, VA 23665-5225, USA

***Old Dominion University, Norfolk, VA, 23508, USA

42 *Ng, W. F.; *Gundappa, M.; and **Peterson, J. B., Jr.: *Turbulence Measurements in a Cryogenic wind Tunnel*. Presented at the 15th Aerodynamic Testing Conference, May 18-20, 1988, San Diego, Calif., 10 pp.

AIAA-88-2026

A high-frequency combination probe was used to measure dynamic flow quality in the test section of the NASA Langley 0.3-m Transonic Cryogenic Tunnel. The probe measures stagnation (total) temperature and pressure, static pressure, and flow angles in two orthogonal planes. Simultaneous unsteady temperature and pressure measurements were also made in the settling chamber of the tunnel. The data show that turbulence intensities increase by almost a factor of four as the flow accelerates from the settling chamber to the test section. In the test section, the maximum rms values of the normalized fluctuating Mach number and flow angle are 2.0 percent and 0.5 degrees, respectively.

*Virginia Polytechnic Institute and State University, Blacksburg, VA 24060, USA

**NASA Langley Research Center, Hampton, VA 23665-5225, USA

43 *Wolf, S. W. D.; and **Ray, E. J.: **Highlights of Experience With a Flexible Walled Test Section in the NASA Langley 0.3-Meter Transonic Cryogenic Tunnel.** In: *AIAA Aerodynamic Testing Conference*, 15th, San Diego, Calif., May 18-20, 1988. Technical Papers (A88-37907), 1988, pp. 321-330, 18 refs.

AIAA Paper 88-2036

A88-37938#

Note: This paper was published later as NASA TM-101491. See no. 50 in this bibliography.

This paper describes the unique combination of adaptive wall technology with a continuous flow cryogenic wind tunnel. This powerful combination allows wind tunnel users to carry out two-dimensional (2-D) tests at flight Reynolds numbers with wall interferences essentially eliminated. Validation testing was made to support this claim using well tested symmetrical and cambered airfoils at transonic speeds and high Reynolds numbers. The test section hardware has four solid walls, with the floor and ceiling flexible. The paper outlines the method of adapting/shaping the floor and ceiling to eliminate top and bottom wall interference at its source. Data comparisons for different size models tested and other in several sophisticated 2-D wind tunnels are made. In addition, the effects of Reynolds number, testing at high lift with associated large flexible wall movements, the uniqueness of the adapted wall shapes, and the effects of sidewall boundary layer control are examined. The 0.3-m TCT is now the most advanced 2-D research facility anywhere.

*ViGYAN Research Associates, Inc., 30 Research Drive, Hampton, VA 23666-1325, USA

**NASA Langley Research Center, Hampton, VA 23665-5225, USA

44 *Macha, J. M.; *Landrum, D. B.; **Pare, L. A.; and ***Johnson, C. B.: **Heating Requirements and Nonadiabatic Surface Effects for a Model in the NTF Cryogenic Wind Tunnel.** In: *AIAA Aerodynamic Testing Conference*, 15th, San Diego, Calif., May 18-20, 1988. Technical Papers (A88-37907), 1988, pp. 372-381, 20 refs.

AIAA Paper 88-2044

A88-37944#

A theoretical study has been made of the severity of nonadiabatic surface conditions arising from internal heat sources within a model in a cryogenic wind tunnel. Local surface heating is recognized as having an effect on the development of the boundary layer, which can introduce changes in the flow about the model and affect the wind tunnel data. The geometry was based on the NTF Pathfinder I wind tunnel model. A finite element heat transfer computer code was developed and used to compute the steady state temperature distribution within the body of the model, from which the surface temperature distribution was extracted. Particular three dimensional characteristics of the model were represented with various axisymmetric approximations of the geometry. This analysis identified regions on the surface of the model susceptible to surface heating and the magnitude of the respective surface temperatures. It was found that severe surface heating may occur in particular instances, but could be alleviated with adequate insulating material. The heat flux through the surface of the model was integrated to determine the net heat required to maintain the instrumentation cavity at the prescribed temperature. The influence of the nonadiabatic condition on boundary layer properties and on the validity of the wind tunnel simulation was also studied.

*Sandia National Laboratories, Albuquerque, NM 87185, USA

**Lockheed Missiles and Space Co., Inc., Sunnyvale, CA 94086-3504, USA

***NASA Langley Research Center, Hampton, VA 23665-5225, USA

Grant NAG1-417

45 *Bruce, W. E., Jr.; *Gloss, B. B.; and *McKinney, L. W.: **Testing and Checkout Experiences in the National Transonic Facility Since Becoming Operational.** Paper

presented at the 2nd ETW Cryogenic Technology Review Meeting, held at Cologne, FRG, June 28-30, 1988, 24 pp.

A88-49378#

The U.S. National Transonic Facility, built by NASA to meet the national needs for High Reynolds Number Testing, has been operational in a checkout and test mode since the operational readiness review (ORR) in late 1984. During this time, there have been problems centered around the effect of large temperature excursions on the mechanical movement of large components, the reliable performance of instrumentation systems, and an unexpected moisture problem with dry insulation. The more significant efforts since the ORR are reviewed and NTF status concerning hardware, instrumentation and process controls systems, operating constraints imposed by the cryogenic environment, and data quality and process controls is summarized.

*NASA Langley Research Center, Hampton, VA 23665-5225, USA

46 Borisov, S. Yu.; Kulesh, V. P.; and Naumov, A. M.: **ISSLEDOVANIYE KACHESTVA POTOKA V EZHEKTORNOY KRIOGENNOY AERODINAMICHESKOY TRUBE.** (Study of the Quality of the flow in an ejector cryogenic wind tunnel). Presented at the Institute of Theoretical & Applied Mechanics of the USSR International Seminar, Novosibirsk, USSR, July 25-29, 1988, 8 pp.

(Contact the NASA Langley Technical Library for information about possible translations of this paper.)

47 Kozlov, V. V.; Omelayev, A. I.; and Ramazanov, M. P.: **Issledovaniya Struktury Potoka i Voprosov Modelirovaniya v Dozvukovoy Aerodinamicheskoy Trube pri Kriogennykh Temperaturakh.** (Studies of the Flow Structure and Problems of Modeling in a Subsonic Wind Tunnel at Cryogenic Temperatures.) Paper presented at the International Seminar "Problems of Simulation in Wind Tunnels" and held at Inst. of Theoretical & Applied Mechanics of the USSR, Novosibirsk, USSR, July 25-29, 1988, pp 1-18.

(Contact the NASA Langley Technical Library for information about possible translations of this paper.)

48 *Wolf, S. W. D.: **Application of a Flexible Wall Testing Technique to the NASA Langley 0.3-m Transonic Cryogenic Tunnel.** Paper presented at the ICAS 16th Congress, Jerusalem, Israel, Aug. 18-Sept. 2, 1988. In: *Proceedings*, vol. 2, (A89-13501), Washington, D.C., AIAA, Inc., 1988, pp. 1181-1191, 24 refs.

ICAS-88-3.8.2

A89-13820#

Wind tunnel wall interference can be minimized by means of a flexible wall technique, whose application to the NASA Langley 0.3-m Transonic Cryogenic Tunnel (TCT) is presently discussed. The adaptable test section of the TCT has four solid walls, of which only the floor and ceiling are adaptable; these are computer-controlled to minimize wall contour-definition times, and can operate at cryogenic temperatures and high pressures despite large wall deflections. This paper presents both two- and three-dimensional test data illustrative of the experience gained with the TCT system over the course of two and a half years of operation.

*ViGYAN Research Associates, Inc. 30 Research Drive, Hampton, VA 23666-1325, USA

49 *Kilgore, R. A.; and *Lawing, P. L.: **Cryogenic Wind Tunnels for High Reynolds Number Testing.** Paper presented at the ICAS 16th Congress at Jerusalem, Israel, Aug. 28-Sept. 2, 1988. In: *Proceedings*, vol. 2, (A89-13501), Washington, D.C., AIAA, Inc., 1988, pp. 1199-1209, 36 refs.

ICAS-88-3.8.4

A89-13622#

This paper begins with a brief review of cryogenic wind tunnels and their use for high Reynolds number testing. Emphasis is on operational experience and recent aerodynamic testing in the NASA Langley 0.3-m Transonic Cryogenic Tunnel (TCT). Specific areas covered in this paper include development of test techniques and aerodynamic testing in cryogenic tunnels. This paper also gives details of research experience in developing model construction techniques, including airfoils as thin as 5 percent, are given. The use of advanced testing techniques to increase the value of cryogenic tunnels to the research community is recommended. These include adaptive wall test sections using solid but flexible top and bottom walls and magnetic suspension and balance systems.

*NASA Langley Research Center, Hampton, VA 23665-5225, USA

50 *Wolf, S. W. D.; and **Ray, E. J.: **Highlights of Experience with a Flexible Walled Test Section in the Langley 0.3-Meter Transonic Cryogenic Tunnel.** NASA TM-101491, Sept. 1988, 11 pp.

N89-10061#

Note: For an earlier presentation see no. 43 in this bibliography.

The unique combination of adaptive wall technology with a continuous flow cryogenic wind tunnel is described. This powerful combination allows wind tunnel users to carry out two-dimensional (2-D) tests at flight Reynolds numbers with wall interferences essentially eliminated. We highlight validation testing to support this claim using well tested symmetrical and cambered airfoils at transonic speeds and high Reynolds numbers. We briefly describe the test section hardware which has four solid walls, with the floor and ceiling flexible. We outline the method of adapting/shaping the floor and ceiling to eliminate top and bottom wall interference at its source. The highlights of our testing experience involve discussion of data comparisons for different size models tested by us and others in several sophisticated 2-D wind tunnels. In addition, we examine the effects of Reynolds number, testing uniqueness of the adapted wall shapes and the effects of sidewall boundary layer control. Our 2 years of operational experience with the adaptive wall test section hardware and its associated control system has taught us important lessons about design and operating procedures. We conclude that the 0.3-m TCT is now the most advanced 2-D research facility anywhere.

*ViGYAN Research Associates, Inc., 30 Research Drive, Hampton, VA 23666-1325, USA

**NASA Langley Research Center, Hampton, VA 23665-5225, USA

51 *Wigley, D. A.: **Technology for Pressure-Instrumented Thin Airfoil Models. Final Report.** NASA CR-4173, Sept. 1988, 44 pp.

N88-28933#

A novel method of airfoil model construction has been developed during this program. This "Laminated Sheet" technique uses 0.8 mm thick sheets A286 containing a network of pre-formed channels which are vacuum brazed together to form the airfoil. A 6.25 percent model of the X29A canard, which has a 5 percent thick section, has been built using this technique. The model contained a total of 96 pressure orifices, 56 in three chordwise rows on the upper surface and 37 in three similar rows on the lower surface. It was tested in the NASA Langley 0.3-m Transonic Cryogenic Tunnel. Unique aerodynamic data was obtained over the full range of temperature and pressure. Part of the data was at transonic Mach numbers and flight Reynolds number. A large two dimensional model of the NACA 65a-105 airfoil section was also built. Scale-up presented some problems, but the airfoil was testable.

*Applied Cryogenics and Materials Consultants, Inc., 15 Cantamar Court, Hampton, VA 23664, USA

Contract NAS1-18066

52 *Lawing, P. L.; **Wigley, D. A.; and **Glaab, L. J.: **Construction of Airfoil Pressure Models Using the Multiple Plate Method.** Presented at SAE AEROTECH 88, Anaheim, Calif., Oct. 3-6, 1988, 9 pp.

A research and development program to build wind tunnel pressure models is described. The program is centered on the concept of bonding together plates with pressure channels cut into the bond planes. Photographic "masking" combined with chemical milling is a reliable and cost effective method of providing pressure channels suitable for high density pressure instrumentation with minimum demand on parent model material. Small diameter high quality pressure orifices (that is, round holes with smooth edges) are economically produced when pre-drilled holes are cut at the model surface by the wire-cut process. With care in the choice of materials and technique, vacuum brazing can be used to produce strong bonds without blocking pressure channels and with no bonding voids between channels. Using multiple plates, a wing with a thickness of 5 percent of chord and having 96 orifices has been constructed and tested in a transonic cryogenic wind tunnel.

*NASA Langley Research Center, Hampton, VA 23665-5225, USA

**Applied Cryogenics and Materials Consultants, Inc., 15 Cantamar Court, Hampton, VA 23664, USA

***Joint Institute for the Advancement of Flight Sciences, George Washington University, Hampton, VA 23665-5225, USA

53 *Yamaguchi, Y.; *Kaba, H.; *Kuribayashi, N.; and **Yoshida, S.: **Preliminary Test Results of NDA Cryogenic Wind Tunnel and its System.** Presented at the SAE Aerospace Technology Conference and Exposition, Anaheim, Calif., Oct. 3-6, 1988, 16 pp.

SAE Paper 881449

A89-28219#

This paper presents the major design specifications of the National Defense Academy (NDA) cryogenic wind tunnel, together with the results on the preliminary calibration tests of the tunnel. The NDA tunnel, designed for two-dimensional airfoil testing, was constructed using the SUS 304 stainless steel as the material for the pressure shell. The results of the operational and the calibration tests at ambient and cryogenic temperatures demonstrated that the NDA cryogenic tunnel has sufficient potential as a tunnel for performing low-temperature transonic flow experiments.

*National Defense Academy, Yokosuka, JAPAN

**Japan Defense Agency, Tokyo, JAPAN

54 *Baljeu, J. F.: **Development of a Multi-Component Internal Strain-Gauge Balance for Model Tests in a Cryogenic Wind Tunnel.** NLR TR 88157 U, Oct. 30, 1988, 96 pp., 9 refs.

NLR order number 563.607

A three-component internal strain-gauge balance for use in a cryogenic wind tunnel has been developed by NLR. With the balance, model tests were made in the NASA Langley 0.3-m Transonic Cryogenic Tunnel. The results are discussed with a view to the development of strain-gauge balances for the ETW.

*National Aerospace Laboratory NLR, Anthony Fokkerweg 2, 1059 CM, Amsterdam, THE NETHERLANDS

55 *Schmitt-von Schubert, B.: **Gas Cooling by Droplet Evaporation.** In: Ingenieur-Archiv, vol. 58, no. 3, 1988, pp. 205-214, in German.

ISSN 0020-1154
44583#

A88-

The cooling of the parallel flow of a gas by injection of droplets of the same material (as in a cryogenic wind tunnel) is investigated theoretically by means of numerical simulations,

with a focus on the equalization processes which take place when the temperature, velocity, and vapor pressure of the droplets (considered as a continuum) differ from those of the gas. The derivation of the balance, material, and interaction equations is explained; the final state of the gas after all droplets have evaporated is characterized; and the flow process is described in detail. Numerical results for nitrogen under various initial pressure and density nitrogen under various initial pressure and density conditions and for different droplet radii are presented in extensive graphs and discussed.

*DFVLR, Institut fuer Theoretische Stroemungsmechanik, Goettingen, FRG

56 *Gloss, B. B.; and *Bruce, R. A.: A Solution to Water Vapor in the National Transonic Facility. Presented at the 27th AIAA Aerospace Sciences Meeting, Reno, Nev., Jan. 9-12, 1989, 9 pp., 5 refs.

AIAA Paper 89-0152

A89-25135#

As cryogenic wind tunnels are used, problems associated with the low temperature environment are being discovered and solved. Recently, water vapor contamination was discovered in the U.S. National Transonic Facility. The source was shown to be the internal insulation which is a closed-cell polyisocyanurate foam. After a study of the absorptivity characteristics of the NTF thermal insulation, the most practical solution to the problem was shown to be the maintaining of a dry environment in the circuit at all times. Using a high aspect ratio transport model, it was shown that the moisture contamination effects on the supercritical wing pressure distributions were within the accuracy of setting test conditions and as such were considered negligible for this model.

*NASA, Langley Research Center, Hampton, VA 23665-5225, USA

57 *Balakrishna, S.; *Kilgore, W. A.; and *Murthy, A. V.: Performance of the Active Sidewall Boundary-Layer Removal System for the Langley 0.3-Meter Transonic Cryogenic Tunnel. NASA CR-181793, Feb. 1989, 24 pp.

A performance of an active sidewall boundary-layer removal system for the Langley 0.3-m Transonic Cryogenic Tunnel (TCT) was evaluated in 1988. This system uses a compressor and two throttling digital valves to control the boundary-layer mass flow removal from the tunnel. The compressor operates near the maximum pressure ratio for all conditions. The system uses a surge prevention and flow recirculation scheme. A microprocessor based controller is used to provide the necessary mass flow and compressor pressure ratio control. Initial tests on the system indicated problems in realizing smooth mass flow control while running the compressor at high speed and high pressure ratios. An alternative method has been conceived to realize boundary-layer mass flow control which avoids the recirculation of the compressor mass flow and operation near the compressor surge point. This scheme is based on varying the speed of the compressor for a sufficient pressure ratio to provide needed mass flow removal. The system has a mass flow removal capability of about 10% of test section flow at $M=0.3$ and 4% at $M=0.8$. The system performance has been evaluated in the form of the compressor map, and compressor tunnel interface characteristic covering most of the 0.3-m TCT operational envelope. A simple analytical model which describes the compressor-tunnel interface flow mechanics has been proposed and validated.

*ViGYAN Research Associates, Inc., 30 Research Drive, Hampton, VA 23665-1325, USA

Contract NAS1-17919

58 *Balakrishna, S.; and *Kilgore, W. A.: Microcomputer Based Controller for the Langley 0.3-M Transonic Cryogenic Tunnel. NASA CR-181808, March 1989, 148 pp.

Flow control of the Langley 0.3-meter Transonic Cryogenic Tunnel (TCT) is a multivariable nonlinear control problem. In this work, globally stable control laws have been generated to

hold tunnel conditions in the presence of geometrical disturbances in the test section and precisely control the tunnel states for small and large set point changes. The control laws are mechanized as four inner control loops for tunnel pressure, temperature, fan speed, and liquid nitrogen supply pressure, and two outer loops for Mach number and Reynolds number. These integrated control laws have been mechanized on a 16-bit microcomputer working on DOS. This document details the model of the 0.3-m TCT, control laws, microcomputer realization, and its performance. The tunnel closed loop responses to small and large set point changes are presented. The controller incorporates safe thermal management of the tunnel cooldown based on thermal restrictions. The controller is shown to provide control of temperature to ± 0.2 K, pressure to ± 0.07 psia, and Mach number to ± 0.002 of a given set point during aerodynamic data acquisition in the presence of intrusive geometrical changes like flexwall movement, angle-of-attack changes, and drag rake traverse. The controller also provides a new feature of automatic Reynolds number control. The controller provides a safe, reliable, and economical control of the 0.3-m TCT.

*ViGYAN Research Associates, Inc., 30 Research Drive, Hampton, VA 23665-1325, USA

Contract NAS1-17919

AUTHOR INDEX

A	Entry
Archambaud, J. P.	5, 32, 36
Ash, R. L.	13

B	
Baals, D. D.	1
Balakrishna, S.	57, 58
Baljeu, J. F.	54
Blanchard, A.	7, 16, 17, 31
Blocher, R.	23
Bonnet, J. L.	32
Borisov, S. Y.	46
Boyden, R. P.	22
Breil, J. F.	36
Britcher, C. P.	41
Britter, R. E.	37
Bruce, R. A.	56
Bruce, W. E., Jr.	45
Burner, A. W.	26

C	
Carraway, D. L.	19, 25
Childers, B. A.	26
Clausing, A. M.	3

D	
Daryabeigi, K.	13
Dillon-Townes, L. A.	13
Dor, J. B.	2, 16, 17, 36
Dress, D. A.	22, 38, 41

E	
Ewald, B.	11, 28, 34

F	
Fancher, M. F.	19
Fdfelov, M. A.	4
Ferris, A. T.	22
Fuller, D. E.	10

G	
Glaab, L. J.	52
Gloss, B. B.	45, 56
Goad, W. K.	26
Goodyer, M. J.	39
Graewe, E.	11, 28
Gundappa, M.	42

H	
Heinzerling, W.	15
Hill, A. S.	22
Hoenlinger, H.	14
Hopson, P., Jr.	25

J	
Johnson, W. G., Jr.	22
Johnson, C. B.	19, 25, 44

K	
Kaba, H.	40, 53
Kilgore, R. A.	38, 41, 49
Kilgore, W. A.	57, 58
Kozlov, V. V.	47
Kraft, D.	21
Kulesh, V. P.	46
Kuribayashi, N.	40, 53

L	Entry
Ladson, C. L.	33
Landrum, D. B.	44
Lassiter, W. S.	30
Lawing, P. L.	8, 49, 52

M	
Mabey, D. G.	35
Macha, J. M.	44
McKinney, L. W.	10, 45
Mignosi, A.	32
Murthy, A. V.	57

N	
Naumov, A. M.	46
Ng, W. F.	42

O	
Omelayev, A. I.	47

P	
Pare, L. A.	44
Payry, M. J.	7, 31
Peterson, J. B., Jr.	42
Plazanet, M.	7, 31
Prieur, J.	2

R	
Ramazanov, M. P.	47
Rao, M. G.	24
Ray, E. J.	33, 43, 50
Rudenko, N. Z.	4

S	
Sawada, H.	6, 9, 20, 29
Schmitt-von Schubert, B.	55
Schnerr, G.	18
Scurlock, R. G.	24
Selby, G. V.	27
Sensburg, O.	14
Seraudie, A.	7, 16, 17, 31, 32
Shchelkunov, V. N.	4
Snow, W. L.	26
Stainback, P. C.	19
Supplee, F. H., Jr.	12

T	
Tcheng, P.	12
Tran, S. Q.	25

W	
Weiss, E.	23
Wigley, D. A.	51, 52
Wolf, S. W. D.	41, 43, 48, 50

Y	
Yamaguchi, Y.	40, 53
Yoshida, S.	53

REPORT DOCUMENTATION PAGE

1. Recipient's Reference	2. Originator's Reference AGARD-R-774	3. Further Reference ISBN 92-835-0532-8	4. Security Classification of Document UNCLASSIFIED
5. Originator	Advisory Group for Aerospace Research and Development North Atlantic Treaty Organization 7 rue Ancelle, 92200 Neuilly sur Seine, France		
6. Title	ADVANCES IN CRYOGENIC WIND TUNNEL TECHNOLOGY		
7. Presented at	the von Kármán Institute, Rhode-Saint-Genèse, Belgium, on 5—9 June 1989		
8. Author(s)/Editor(s) Various	9. Date November 1989		
10. Author's/Editor's Address Various	11. Pages 382		
12. Distribution Statement	This document is distributed in accordance with AGARD policies and regulations, which are outlined on the Outside Back Covers of all AGARD publications.		
13. Keywords/Descriptors <div style="display: flex; justify-content: space-between;"> <div> Wind tunnels Cryogenics Automatic control equipment Data acquisition </div> <div> Flow visualization Wind tunnel models Expenses </div> </div>			
14. Abstract <p>Since 1980, the AGARD Fluid Dynamics Panel and the von Kármán Institute for Fluid Dynamics have sponsored three series of lectures on cryogenic wind tunnels. The lectures of this Special Course are, in many ways, updates of the lectures given in 1980 and 1985. These lectures reflect the progress made in building and using cryogenic tunnels in recent years. The course was conducted at the von Kármán Institute for Fluid Dynamics from June 5—9, 1989.</p> <p>The purpose of this Special Course was to address as specifically as possible current concerns with trying to build and use cryogenic wind tunnels. It was designed for engineers and managers wishing to obtain in concentrated form the most up-to-date information on cryogenic wind tunnels. This course covered both the theory and practice of cryogenic wind tunnel design, operation, and use.</p> <p>The course provided a brief review of the development and early use of cryogenic tunnels and then covered all aspects of the design and operation of cryogenic tunnels. Among the areas covered were: cryogenic engineering and safety, properties of materials at cryogenic temperatures, tunnel design requirements, model design and construction, automatic tunnel control, data acquisition, data accuracy, flow visualization, productivity, and costs of models and operation. The status of cryogenic wind tunnel projects in AGARD countries and in the rest of the world was also presented.</p> <p>This bound volume of lecture notes also includes a transcription of a question and answer session held at the end of the Special Course.</p>			

<p>AGARD Report No. 774 Advisory Group for Aerospace Research and Development, NATO ADVANCES IN CRYOGENIC WIND TUNNEL TECHNOLOGY Published November 1989 382 pages</p> <p>Since 1980, the AGARD Fluid Dynamics Panel and the von Kármán Institute for Fluid Dynamics have sponsored three series of lectures on cryogenic wind tunnels. The lectures of this Special Course are, in many ways, updates of the lectures given in 1980 and 1985. These lectures reflect the progress made in building and using cryogenic tunnels in recent years. The course was conducted at the von Kármán Institute for Fluid Dynamics from June 5-9, 1989.</p> <p>P.T.O</p>	<p>AGARD-R-774</p> <p>Wind tunnels Cryogenics Automatic control equipment Data acquisition Flow visualization Wind tunnel models Expenses</p>	<p>AGARD Report No. 774 Advisory Group for Aerospace Research and Development, NATO ADVANCES IN CRYOGENIC WIND TUNNEL TECHNOLOGY Published November 1989 382 pages</p> <p>Since 1980, the AGARD Fluid Dynamics Panel and the von Kármán Institute for Fluid Dynamics have sponsored three series of lectures on cryogenic wind tunnels. The lectures of this Special Course are, in many ways, updates of the lectures given in 1980 and 1985. These lectures reflect the progress made in building and using cryogenic tunnels in recent years. The course was conducted at the von Kármán Institute for Fluid Dynamics from June 5-9, 1989.</p> <p>P.T.O</p>	<p>AGARD-R-774</p> <p>Wind tunnels Cryogenics Automatic control equipment Data acquisition Flow visualization Wind tunnel models Expenses</p>
<p>AGARD Report No. 774 Advisory Group for Aerospace Research and Development, NATO ADVANCES IN CRYOGENIC WIND TUNNEL TECHNOLOGY Published November 1989 382 pages</p> <p>Since 1980, the AGARD Fluid Dynamics Panel and the von Kármán Institute for Fluid Dynamics have sponsored three series of lectures on cryogenic wind tunnels. The lectures of this Special Course are, in many ways, updates of the lectures given in 1980 and 1985. These lectures reflect the progress made in building and using cryogenic tunnels in recent years. The course was conducted at the von Kármán Institute for Fluid Dynamics from June 5-9, 1989.</p> <p>P.T.O</p>	<p>AGARD-R-774</p> <p>Wind tunnels Cryogenics Automatic control equipment Data acquisition Flow visualization Wind tunnel models Expenses</p>	<p>AGARD Report No. 774 Advisory Group for Aerospace Research and Development, NATO ADVANCES IN CRYOGENIC WIND TUNNEL TECHNOLOGY Published November 1989 382 pages</p> <p>Since 1980, the AGARD Fluid Dynamics Panel and the von Kármán Institute for Fluid Dynamics have sponsored three series of lectures on cryogenic wind tunnels. The lectures of this Special Course are, in many ways, updates of the lectures given in 1980 and 1985. These lectures reflect the progress made in building and using cryogenic tunnels in recent years. The course was conducted at the von Kármán Institute for Fluid Dynamics from June 5-9, 1989.</p> <p>P.T.O</p>	<p>AGARD-R-774</p> <p>Wind tunnels Cryogenics Automatic control equipment Data acquisition Flow visualization Wind tunnel models Expenses</p>

<p>The purpose of this Special Course was to address as specifically as possible current concerns with trying to build and use cryogenic wind tunnels. It was designed for engineers and managers wishing to obtain in concentrated form the most up-to-date information on cryogenic wind tunnels. This course covered both the theory and practice of cryogenic wind tunnel design, operation, and use.</p> <p>The course provided a brief review of the development and early use of cryogenic tunnels and then covered all aspects of the design and operation of cryogenic tunnels. Among the areas covered were: cryogenic engineering and safety, properties of materials at cryogenic temperatures, tunnel design requirements, model design and construction, automatic tunnel control, data acquisition, data accuracy, flow visualization, productivity, and costs of models and operation. The status of cryogenic wind tunnel projects in AGARD countries and in the rest of the world was also presented.</p> <p>This bound volume of lecture notes also includes a transcription of a question and answer session held at the end of the Special Course.</p> <p>ISBN 92-835-0532-8</p>	<p>The purpose of this Special Course was to address as specifically as possible current concerns with trying to build and use cryogenic wind tunnels. It was designed for engineers and managers wishing to obtain in concentrated form the most up-to-date information on cryogenic wind tunnels. This course covered both the theory and practice of cryogenic wind tunnel design, operation, and use.</p> <p>The course provided a brief review of the development and early use of cryogenic tunnels and then covered all aspects of the design and operation of cryogenic tunnels. Among the areas covered were: cryogenic engineering and safety, properties of materials at cryogenic temperatures, tunnel design requirements, model design and construction, automatic tunnel control, data acquisition, data accuracy, flow visualization, productivity, and costs of models and operation. The status of cryogenic wind tunnel projects in AGARD countries and in the rest of the world was also presented.</p> <p>This bound volume of lecture notes also includes a transcription of a question and answer session held at the end of the Special Course.</p> <p>ISBN 92-835-0532-8</p>
<p>The purpose of this Special Course was to address as specifically as possible current concerns with trying to build and use cryogenic wind tunnels. It was designed for engineers and managers wishing to obtain in concentrated form the most up-to-date information on cryogenic wind tunnels. This course covered both the theory and practice of cryogenic wind tunnel design, operation, and use.</p> <p>The course provided a brief review of the development and early use of cryogenic tunnels and then covered all aspects of the design and operation of cryogenic tunnels. Among the areas covered were: cryogenic engineering and safety, properties of materials at cryogenic temperatures, tunnel design requirements, model design and construction, automatic tunnel control, data acquisition, data accuracy, flow visualization, productivity, and costs of models and operation. The status of cryogenic wind tunnel projects in AGARD countries and in the rest of the world was also presented.</p> <p>This bound volume of lecture notes also includes a transcription of a question and answer session held at the end of the Special Course.</p> <p>ISBN 92-835-0532-8</p>	<p>The purpose of this Special Course was to address as specifically as possible current concerns with trying to build and use cryogenic wind tunnels. It was designed for engineers and managers wishing to obtain in concentrated form the most up-to-date information on cryogenic wind tunnels. This course covered both the theory and practice of cryogenic wind tunnel design, operation, and use.</p> <p>The course provided a brief review of the development and early use of cryogenic tunnels and then covered all aspects of the design and operation of cryogenic tunnels. Among the areas covered were: cryogenic engineering and safety, properties of materials at cryogenic temperatures, tunnel design requirements, model design and construction, automatic tunnel control, data acquisition, data accuracy, flow visualization, productivity, and costs of models and operation. The status of cryogenic wind tunnel projects in AGARD countries and in the rest of the world was also presented.</p> <p>This bound volume of lecture notes also includes a transcription of a question and answer session held at the end of the Special Course.</p> <p>ISBN 92-835-0532-8</p>